Prevention of CO_2 Leakage From Underground Storage Reservoirs

By

Pedram Mahzari

BSc., Msc.

Submitted for the Degree of Doctoral of Philosophy
In Petroleum Engineering

Institute of Petroleum Engineering
Heriot-Watt University
Riccarton, Edinburgh
August 2015

ABSTRACT

The risk of leakage from CO_2 storage sites is recognised as one of the challenging aspects of large scale implementation of geologic sequestration of CO_2. Uncertainties in characterizing a geologic reservoir and the current lack of a complete understanding of possible interactions between rock and fluids involved in CO_2 storage have resulted in concerns over contingent leakages. The debate on the allowable rate of leakage has led to different perspectives among the CCS stakeholders; some believe that, by analogy to natural CO_2 reservoirs, risk of having leakage of less than 1 %/year is dispensable and on the other side, some state that "Any non-zero leak-rate from a stored carbon system means that eventually the entire inventory will be released to the atmosphere". There is also the issue of public acceptance which would be adversely affected by the non-zero potential of leakage of CO_2 back to the surface. This negative impact on the members of the public has proved to be very powerful as it has resulted in the delay and even cancellation of some CCS (carbon capture and storage) projects.

To the best of our knowledge, no practically viable techniques existed for prevention of CO_2 leaks from unknown leakage paths. Our technique is based on in-situ precipitation of an appropriate solute dissolved in the stored super-critical CO_2. Supercritical CO_2 ($SCCO_2$) has a distinct characteristic that its density changes from gaseous-like to liquid-like monotonically and uniformly. This allows $SCCO_2$ to act as manageable solvent for various solid solutes. Thus, once the solution of $SCCO_2$ + solid solutes departs from the equilibrium conditions, the solute will appear in the form of crystallized particles. Based on this unique behaviour of the supercritical solutions, we have developed a novel technique for tackling contingent CO_2 leakage from storage sites as a preventive method. The sealing process takes place in-situ at the exact location of the leak without the need for identifying the leak target area and the exact nature of the leak.

In this study, an integrated research methodology was designed and employed to comprehend the physics behind our leakage prevention technique and also, to deliver the required package, i.e. suitable solutes and reliable simulator, for larger scale implementation of this technique. It was aimed firstly to demonstrate the performance of our proposed leakage prevention technique at different leakage scenarios and secondly, to put forward a number of solutes efficient in tackling contingent leakages. In order to identify the underlying mechanisms and the pertinent parameters controlling the efficacy of this technique, a good number of direct visualisation experiments were performed

where the kinetics behind solute solidification and precipitation were visually investigated. Three different ranges of potential solid solutes were used in visualisation experiments to cover a wide spectrum of solute solubility in supercritical CO_2, which would enable us to draw more general and consistent conclusions. The understandings acquired from the direct visualisations were employed to design efficiently a few yet adequate number of coreflood experiments in which the performance of our technique was studied in more realistic reservoir cores. Having attained the adequate information from the experimental part of this investigation, the findings was subsequently utilised to develop an in-house simulator to fundamentally model the kinetics of solid solute precipitation and consequently, the pertinent parameters of the semi-empirical equations were tuned to match and predict the coreflood experiments.

In experimental part of this investigation, a series of visualisation experiments using transparent porous media (micromodel) to physically simulate CO_2 leakage under conditions typical of geologic storage sites. In these experiments, degree of "supersaturation" was identified as an important parameter behind effectiveness of solute precipitation. In addition to evaluating the behaviour of different solutes, the impacts of resident water existing in storage reservoir and impurities in CO_2 stream were taken into account in visualisation experiments. Utilising the findings from the visualisations, 6 coreflood experiments were carried out, which revealed that a strong and durable blockage was formed in the core and the flow (leakage) of CO_2 was effectively sealed. Practically speaking, there should not be any premature precipitation as the solution travels inside the storage reservoir; therefore, apart from the performance of this technique in the vicinity of contingent leakages, the integrity of the solution (as it flows in the simulated storage reservoir) was also investigated in visualisation and coreflood experiments.

From the findings revealed by the coreflood and micromodel experiments, it was identified that the solution made with solid-solute and $SCCO_2$ may not be responsive in some scenarios. Therefore, the desire to better control the onset of blockage formation has triggered investigation of developing a complementary method to be able to adjust the response of the solution. It was rationalised that adding another solutes (co-solvent) to the solution would enable us to modify the response of the solution. Sandpack, micromodel visualisations, and coreflood experiments were performed to evaluate influence of co-solvent on the response of the solution to various leakage types.

On the modelling the precipitation process in the leakage path, it was first demonstrated that conventional reservoir simulators could not adequately capture the physics leading to the blockage formation and the results of lab-scale coreflood experiments could not be correctly simulated. Therefore, there is a need for developing models, which can predict the performance of the LPT at different cases. Based on the experimental information, we have attempted to develop the relevant equations that describe the mechanisms behind particle formation due to pressure drops. After matching one coreflood experiment, the resultant model was used to predict another coreflood experiment performed at similar conditions, which demonstrated an encouraging performance for the developed mathematical model.

The results and findings of this study have primarily verified that our leakage prevention technique, which is developed here through extensive experimental and modelling investigation, is well-capable of tackling various contingent leakages. A number of economically feasible solid solute has been found with positive responses to physically simulated leakage paths, which would be considered as the potential solutes for large scale implementation of our technique. Moreover, an in-house simulator was developed based on the finding observed in the different experiments. The simulator can successfully predict the results of coreflood experiments, which implies that it captures the underlying mechanisms adequately. Having developed the necessary equipment, i.e. appropriate solutes and reliable simulator, our proposed leakage prevention technique is ready to be incorporated in demonstration and pilot trials.

ACKNOWLEDGEMENTS

I would like to express my sincere gratitude to my supervisors, Prof. Mehran Sohrabi and Prof. Mahmoud Jamiolahmady for providing the opportunity and financial support to pursue my ambitions. Without their expertise and mentoring, it would have been impossible to complete my thesis.

Also, I would like to thank my wife and my parents for their unreserved encouragement, support, and understanding.

ACADEMIC REGISTRY
Research Thesis Submission

Name*:*	Pedram Mahzari		
School/PGI:	School of Energy, Geoscience, Infrastructure, and Society		
Version: *(i.e. First, Resubmission, Final)*	Final	Degree Sought (Award **and** Subject area)	PhD in Petroleum Engineering

Declaration

In accordance with the appropriate regulations I hereby submit my thesis and I declare that:

1) the thesis embodies the results of my own work and has been composed by myself
2) where appropriate, I have made acknowledgement of the work of others and have made reference to work carried out in collaboration with other persons
3) the thesis is the correct version of the thesis for submission and is the same version as any electronic versions submitted*.
4) my thesis for the award referred to, deposited in the Heriot-Watt University Library, should be made available for loan or photocopying and be available via the Institutional Repository, subject to such conditions as the Librarian may require
5) I understand that as a student of the University I am required to abide by the Regulations of the University and to conform to its discipline.

* *Please note that it is the responsibility of the candidate to ensure that the correct version of the thesis is submitted.*

Signature of Candidate*:*		Date:	

Submission

Submitted By *(name in capitals):*	
Signature of Individual Submitting:	
Date Submitted:	

For Completion in the Student Service Centre (SSC)

Received in the SSC by *(name in capitals):*			
Method of Submission *(Handed in to SSC; posted through internal/external mail):*			
E-thesis Submitted (mandatory for final theses)			
Signature:		Date:	

TABLE OF CONTENT

LIST OF TABLES

LIST OF FIGURES

INTRODUCTION

Underground storage of anthropogenic CO_2 has been recognized as a viable solution to the global climate changes (Metz, et al., 2005). CO_2 can be stored under different trapping mechanisms such as structural sealing, dissolution in the resident water, and mineralisation due to reactions with water and rock (Shik Han, et al., 2010). The dissolution and mineralisation processes would retain the CO_2 safely in geological time scales (Bachu, et al., 2007). However, amongst the CO_2 trapping mechanisms, structural sealing plays a predominant role in efficient storage of CO_2 as its volumetric capacity would outperform the efficiency of other two mechanisms (Shik Han, et al., 2010). Therefore, the main target for CO_2 storage is the structural sealing which may be prone to contingent leakages. Pathways such as abandoned wells, faults, and network of fractures are the conceivable source of leaks that could jeopardize the integrity of the storage sealing. The risk of leakage from CO_2 storage sites is recognised as one of the challenging aspects of large scale implementation of geologic sequestration of CO_2 [(He, et al., 2011), (Nelson, et al., 2005)]. Uncertainties in characterizing a geologic storage reservoir and the current lack of a complete understanding of possible interactions between rock and fluids involved in CO_2 storage have resulted in concerns over contingent leakages. The debate on the allowable rate of leakage has led to different perspectives amongst the CCS (carbon capture and storage) stakeholders; some believe that, by analogy to natural CO_2 reservoirs, risk of having leakage of less than 1 %/year is dispensable (Metz, et al., 2005) and on the other side, some state that "Any non-zero leak-rate from a stored carbon system means that eventually the entire inventory will be released to the atmosphere" (Hawkins, 2004). There is also the issue of public acceptance which would be adversely affected by the non-zero probability of CO_2 leakage back to the surface. This latter negative impact on the members of the public has proved to be very powerful as it has resulted in the delay and even cancellation of some CCS projects [(Tokushige, et al., 2007), (Pietzner, et al., 2011), (TNS Opinion & Social at the request of Directorate-General for Energy, 2011)].

Potential undetected CO_2 leakage pathways including natural (e.g. faults, fractures and sand streaks through caprock) and manmade (e.g. wells) can exist in any geologic formation as evident by natural oil, gas and CO_2 seeps in many parts of the world (Kvenvolden & Cooper, 2003). Although CO_2 storage sites will be studied and selected

carefully to minimise CO_2 leakage risks, identifying potential leakage locations and effective remedies would inherently possess a huge problem and comes with a great degree of uncertainty. The difficulty of detecting all potential leakage paths in natural underground reservoirs raises concerns about safety and reliability of CCS without a proper leakage prevention strategy. There is a very recent finding on one of the well-known CO_2 storage project (Sleipner CCS project (Arts, et al., 2008)) where the injected CO_2 has been detected on the seabed surface (Monastersky, 2013), which has led to a substantial degree of concerns around CCS success. Therefore, any insignificant CO_2 leakage can cast some doubt on the entire process of CCS, which may not be healed for decades. Indeed, the CCS project in Sleipner can be considered as a valuable experience in the large scale implementation of CCS; not only it has demonstrated CO_2 scape back to the surface, but also, the CO_2 plume was evolved in a manner that is different from the predictions (Boait, et al., 2011).

Similar to the incident reported from Sleipner project, there has been an allegation about the Weyburn CCS project (Malik & Islam, 2000) in which the appearance of CO_2 in a farmland has raised concerns among the residents living around this CCS-EOR project (The Canadian Press, 2011). It should be mentioned that the subsequent investigation for finding the source of the CO_2 appeared in surface has indicated no clear link between the CO_2 injected in Weyburn project and CO_2 bubbles detected in the farmland (Boyd, et al., 2013). Although the evidences behind the allegation were somehow debatable, the overall outcome of the reported incident has notified the local people around the planned CCS projects that the probability of upward CO_2 leakage is not negligible. Furthermore, these controversial reports can put some doubts on the safe and secure storage of CO_2 globally, which would produce bad publicity on the concept of CCS (The Globe and Mail, 2011).

Hence, the current status of geological characterisation methods would not suffice to assure zero probability of leakage in the reservoirs. Even a leak-proof formation can develop leakage over the very large time-scale needed for permanent storage of CO_2 in geologic formations. Natural movements of the earth, tectonic activities and earthquakes can break these formations and cause multiple leakage locations through faulting and fracturing. Therefore, if CCS is to be accepted as an effective and reliable measure to combat increased CO_2 concentrations and the global warming, the risk of leakage of stored CO_2 will have to be properly addressed by putting in place effective methods to intervene in case of a leakage.

There are a good number of natural analogous of underground CO_2 reservoirs that have exhibited leaky behaviour at various leakage rates (Lewicki, et al., 2007). Some of these leakages have occurred due to tectonic movements, which led to catastrophic consequences (Zhang, 1996). Leakage examples can be found in natural reservoirs where activation of the sealing fault accommodated the migration of CO_2 upwards (Shipton, et al., 2004). On the other hand, pressurisation of an underground storage reservoirs would change geo-mechanical characteristics of the formation, which may undermine the sealing integrity of the formation. Therefore, occurrence of leakage "after" CO_2 storage would not be inconceivable and its associated risk can be reduced by preventive techniques.

Large scale deployment of CCS projects is crucially dependent on the favourable economics of the entire chain of capture, transportation, and storage (van der Zwaan & Gerlagh, 2009). A leaky storage reservoir would adversely risk the economics of CCS (Hawkins, 2004). The cost of CO_2 storage would be increased in short and long terms if the stored CO_2 started to leak (Ha-Duong & Keith, 2004). The problem would not be alleviated if a leak occur and no post-injection remedy can target the leaking point and cease the leakage. Therefore, if one aims to address the issues around contingent leakages, any remedied should be employed as a preventive method to reduce the risk of leakage, which would bring down the insurance costs and hence overall cost of CCS. Thus, any preventive technique would inherently reduce the cost of CCS.

Another concern about geologic storage of CO_2 is that injected CO_2 may leak out of the intended storage formation, migrate to the near-surface environment, and eventually flow out of the ground. This is a concern because such leakage may contaminate existing energy, mineral and groundwater resources and it may pose a hazard at the ground surface. It has been reported that the leaking CO_2 would bring about the release of metal constituent of aquifers, which would be hazardous (Kirsch, et al., 2014). Besides the metal release, the leaked CO_2 would contaminate the overlying formation resulting into acidification of the near surface waters, which would reduce the quality of drinking water. This event can take place in the offshore storage reservoir (Eiken, et al., 2011); leakage of CO_2 would lead to carbonation of marine environments, which would destabilise pH of the water and endanger marine lives (Queirós, et al., 2014). Therefore, even small but continued leakage is undesirable and would undermine the purpose of CCS and contribute to increased concentrations of CO_2 by releasing large quantities of the greenhouse gas back into the atmosphere.

Therefore, there is an outstanding need for developing preventive measures to tackle the risk of leakages. Some methods have been proposed to reduce the risk of leakage (Grataloup, et al., 2009). Also, a couple of methods was put forward as preventive approaches to tackle upward migration/escape of CO_2 (Emeka Eke, et al., 2011). There are mainly based on injection of CO_2-enriched water into the storage reservoir instead of plain CO_2 injection. Since the carbonated water would have higher density compared to the in-situ brine, the injected CO_2-enriched water would move downwards and settle in the storage reservoir. This method seems interesting but, there is a big problem attached to CO_2-enriched water injection; the solubility of CO_2 in water is less than 10 percent (Duan & Sun, 2003), which would make 90% of the storage reservoir filled with water. Thus, employing this method would undermine the storage capacity of any site, which would be a damaging factor for the whole concept of CCS.

To the best of our knowledge, no practically viable techniques existed for prevention of CO_2 leaks from unknown leakage paths. Here in this work, the proposed technique is based on in-situ precipitation of an appropriate solute dissolved in the stored super-critical CO_2. Supercritical CO_2 ($SCCO_2$) has a distinct characteristic that its density changes from gaseous-like to liquid-like monotonically and uniformly. This allows $SCCO_2$ to act as manageable solvent for various solid solutes. Thus, once the solution of $SCCO_2$ + solid solutes departs from the equilibrium conditions, the solute will appear in the form of crystallized particles. Based on this unique behaviour of the supercritical solutions, a novel technique for tackling contingent CO_2 leakage from storage sites was developed as a preventive method. The sealing process takes place in-situ at the exact location of the leak without the need for identifying the leak target area and the exact nature of the leak.

The broad objective of this investigation is to examine a preventive technique proposed to tackle contingent leakages and develop the necessary tools for large scale implementation of the Leakage Prevention Technique (LPT). These objectives were attempted to achieve by conducting a comprehensive set of flow visualisation experiments, core/sand pack flow studies, numerical modelling and simulation. The approach is to conduct flow visualization studies in the transparent micromodels to investigate pore scale mechanisms controlling the efficiency of our leakage prevention technique. The micromodel observations are used to design and perform representative core/sand pack flow studies. The quantitative results from coreflood tests will be used in an in-house mathematical model to check if the experimental results can be properly

reproduced. The results obtained from pore scale and core scale experiments can be utilised to define the pertinent parameters of the in-house model and tuning of the parameters. Subsequently, the trained simulator will be used for scaling-up purposes and prediction of the performance of the proposed LPT at larger scales.

This thesis reports the findings attained from the experimental and theoretical works performed to identify fundamentally the phenomena taking place in the proposed leakage prevention technique. The central achievement of this investigation was to find an efficient solid-solute for stopping leaks at reasonable costs. Also, a tool should be developed in order to simulate the performance of LPT in large scales based on the laboratory findings. Furthermore, a method was put forwards to control/enhance the performance of solid-solutes at different leakage scenarios, which would enable us to design practical strategies for specific storage reservoir conditions. Various solid-solutes were used and they were classified base on their solubility and blockage efficiency. Hence separate set of experiments were required for different solutes.

In this thesis, the concept of the proposed leakage prevention technique is presented in c*hapter 1*. The involving physics, which control the performance of LPT, will be given in this chapter to gives a broad overview of the theoretical aspects of the proposed leakage prevention technique. *Chapter 2* describes the experimental facilities used for this work including micromodel, coreflood, and sandpack rigs. The results of visualisation experiments including micromodel and sightglass are all presented in the *chapter 3*. The results of coreflood and sand pack experiments are given in c*hapters 4*. In *chapter 5*, the experimental results verifying the effectiveness of a novel method to control the response of LPT is discussed, which is based on adding a slight amount of a liquid solute. Chapter 6 describes the simulation exercises and mathematical modelling attempts that were carried out to fine-tune the pertinent parameters in LPT. Chapter 7 explains two methods of delivering solid solute into the storage reservoir and solubility measurements performed for constructing the solubility profile along the injection wellbore. *Appendix A* presents the Visual Basic.Net script of the in-house software developed for mathematical modelling of how leakage prevention technique works. Below, summary of the experiments performed in this investigation can be found;

Visualisation experiments (Micromodel)

For visual investigation of the underlying mechanisms, a unique high-pressure micromodel facilities available in laboratories in the Institute of Petroleum Engineering of Heriot-Watt University was used. The unique advantage of the visualisation

experiments over conventional laboratory techniques is that the complex dynamic process of CO_2 leakage and the subsequent formation of solid particles and blockage of the leakage can be directly seen and studied. Following visualisation experiments were performed to observe the formation of particles and consequent precipitations (28 experiments in total);

1. Highly soluble solute (1 solute)
    a. 4 different scenarios of pressure drop were imposed.
2. Moderately soluble solutes (2 solutes)
    a. 5 different pressure drop conditions were investigated for each solute
3. Marginally soluble solutes (1 solute)
    a. 4 conditions of pressure drop were tested.
4. Impact of impurities (Nitrogen)
    a. Using 2 solutes at 3 different pressure drop regimes.
5. Impact of presence of Water
    a. 1 pressure drop scenarios were applied.
6. SightGalss (a high pressure viewing cell) experiment for nucleation study;
    a. 2 experiments for the time of particle formation.
    b. 1 experiment in presence of water.

SandPack Experiment (high leak rates)

Sandpack facility can be used to quantify the pressure response of the solution to high leakage rates and also as a reliable tool for fast screening of the solutes suitable for a particular application. The main feature of the sandpack experiments is its capability to determine the pressure at which the blockage can form in a rather short period of time. Following experiments were carried out for identifying the performance of the technique in high leakage rates:

1. Using 4 different solutes (low and moderately soluble solutes)
    a. 6 sandpack experiments in total.

Coreflood Experiments (Slow leakage rates)

Coreflood experiments are mainly carried out for two purposes; first, to simulate slow rate of leakage and, second, to apply leakage prevention method in real porous rocks. The following coreflood experiments were designed and performed;

1. Test #1: performance in slow leakage rates through cap rocks
2. Test #2: effect of leakage rate

3. Test #3: effect of length of leakage path
4. Test #4: process of re-blockage.
5. Test #5: effect of solute type (Using another moderately soluble solute)
6. Test #6: effect of length of leakage path on the performance of latter solutes
7. Test #7: degree of adsorption as our solution flows through a porous medium
8. Test #8: investigating integrity of our solution as it flow through the storage reservoir (possibility of premature precipitation is negligible)

Controlling the response of the solution to various leakage rates

One observation made in some of the experiments was existence of a time lag in formation of solid blockage when only solid solute had been dissolved in the CO_2 solution. Therefore, to better control and speed up the onset of blockage formation, we suggested using appropriate liquid solutes (co-solvent) in the solution. We reported a series of visualization, sandpack, and coreflood experiments demonstrating an improved efficiency for our solution in the presence of a liquid solute. Following experiments were performed for this purpose;

1. 8 visualisation experiments,
    a. formation of co-solvent,
    b. better response of primary solute in the presence of co-solvent
    c. impact of presence of water on co-solvent behaviour
2. 3 sandpack tests,
    a. effect of co-solvent on the pressure drop, particle size, and blockage durability were investigated
3. 2 coreflood experiments.
    a. Effect of co-solvent content on improving the response of our solution.

Solubility measurements

The solubility of the solid solutes in supercritical CO_2 was measured at various reservoir conditions to be able to produce the sufficient information required for modelling the leakage prevention technique:

5 sets of solubility data were measured for three different solutes.

CHAPTER 1 Concept of HW Leakage Prevention Technique

1.1 Introduction

Under geological sequestration conditions CO_2 is stored as a supercritical fluid. Supercritical fluids have liquid-like (high) density which gives them high solvent power (i.e. able to dissolve relatively large quantities of solid solute) (Gupta & Shim, 2006). Gases have very low solvent power. Therefore, as CO_2 passes from a supercritical fluid to a gas, its ability to dissolve solutes decreases dramatically (CO_2 Critical Pressure, Pc=73.8 atm & Critical Temperature, Tc=31.1 °C).

For example, Dissolution of solid Solute-9 (just an example, this would not be used as an actual solute due to environmental and costs issues) in CO_2 would vary with respect to temperature and pressure as illustrated in Figure 1-1. As pressure falls below the critical point of CO_2, the Solute-9 solubility would decrease to effectively zero. Once a solution becomes saturated with a solid solute, the solid will therefore precipitate out of the solution at a pressure below the critical point. The high pressures correspond with typical CO_2 storage reservoir conditions and the low pressures with the surface.

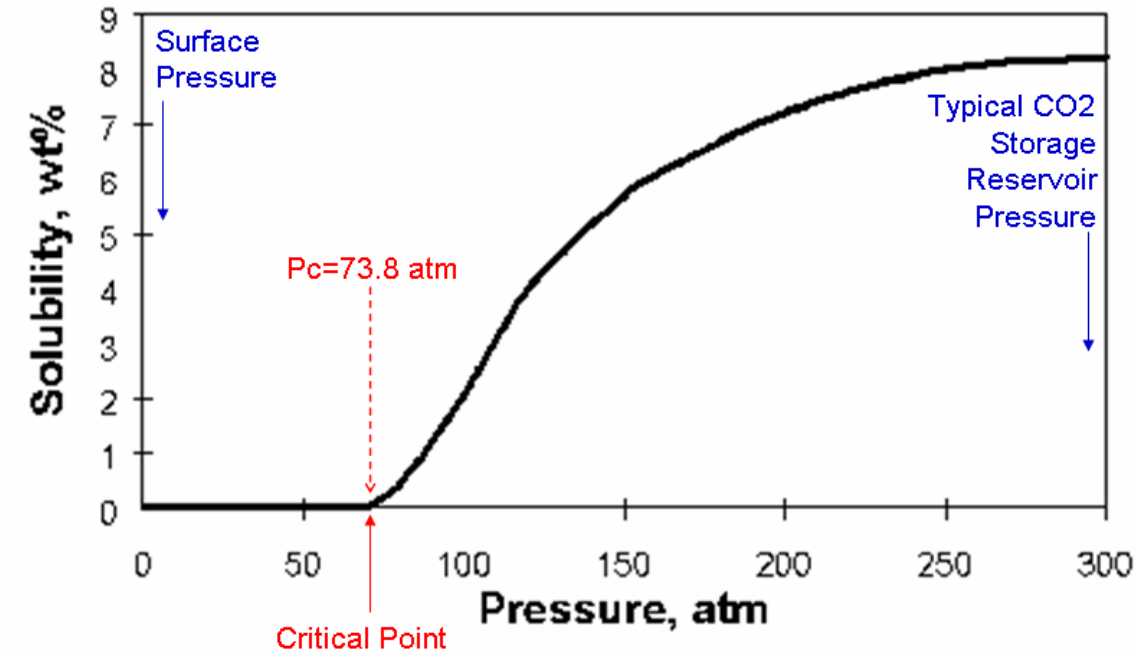

Figure 1-1: Isothermal solubility of Solute-9 in CO_2 at 45°C (Gupta & Shim, 2006).

Utilising the abrupt change in solvent power of CO_2 at the critical point, a self-diagnosis and self-sealing method for stopping CO_2 leakage was developed by dissolving an appropriate solid solute(s) in injected supercritical CO_2 at the time of storage. When a leak occurs, the pressure drops and so does the solvent power of the CO_2. This results in the solid solutes precipitating out of the CO_2 where the pressure drop is taking place (leakage paths). As this precipitation continues, a solid blockage builds up and ultimately blocks the leak.

The unique advantage of this novel technology is the automatic detection and effective sealing of CO_2 leakage from both known and unknown leakage paths in geological storage reservoirs by the precipitation of a solid sealant. This eliminates the need for information on the type, extent and location of the leaks, which are generally not available. The sealing process takes place in-situ, automatically, when the leak occurs and at its exact location. without the need to monitor or intervene and without any particular equipment. In practice, the CO_2 would be pumped for storage into a subsurface reservoir containing a dissolved solid solute (Figure 1-2). If a leak occurs (through an existing leakage path or due to a geo-mechanical activation), the CO_2 saturated with a solid-solute flows along the leak, which associates with a pressure drop and hence solvent power of the CO_2 decreases that would trigger solid solute precipitation out of the CO_2. The precipitation continues building up a blockage which ultimately seals the leak (Figure 1-3):

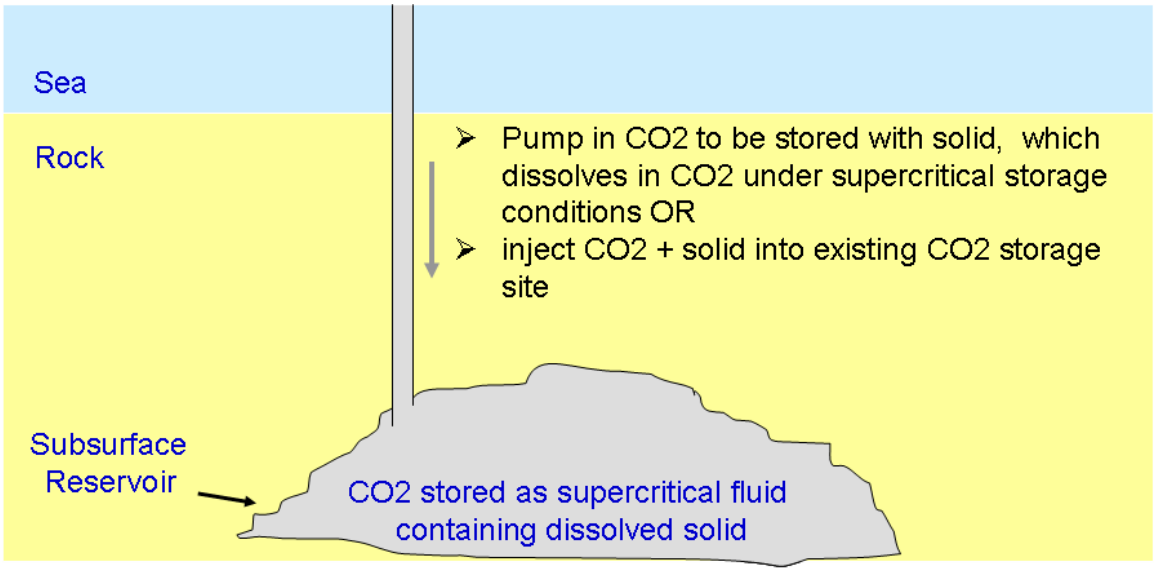

Figure 1-2: General schematic of CO_2 storage process in an underground storage reservoir.

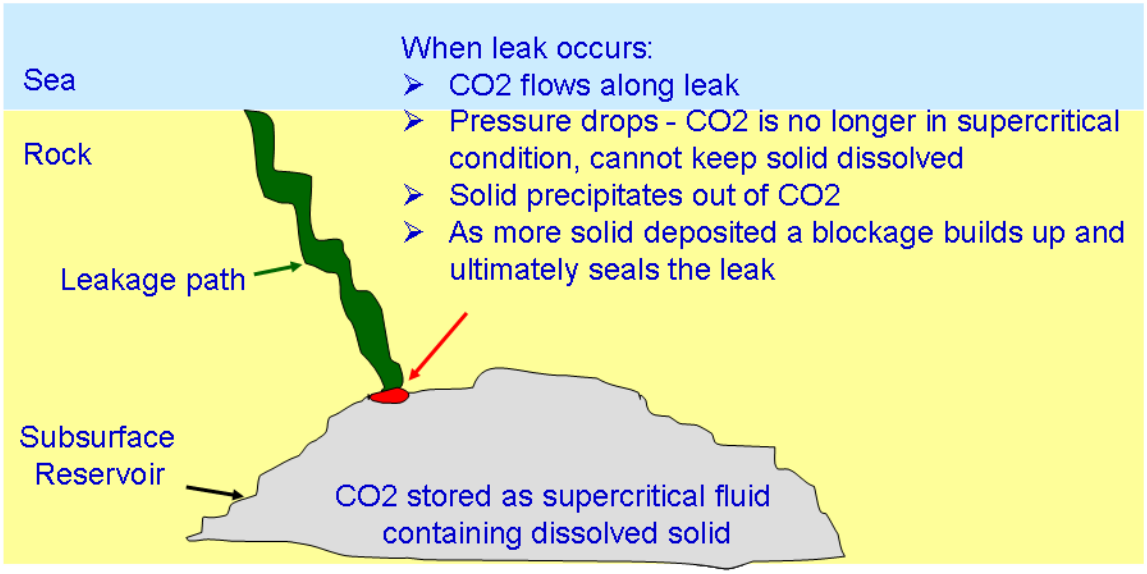

Figure 1-3: Schematic description of how hypothetically leakage prevention technique works.

In order to understand the processes under which the precipitation occurs and consequent blockage forms, the underlying mechanisms invloving in the blockage formation should be elaborated for proper designing of the experiments. Pressure drop is the main cause

behind the new phase formation, i.e. solidification of the solutes, which is controlled essentially by kinetics of nucleation. This complex physical phenomenon expresses the kinetics and amount of solid solute formation. Having formed the solid particles out of the solution, the other mechanism kicks in, i.e. solid precipitation/deposition, which controls the building up the blockage. In the following part of this chapter, the mechanisms invloved in the blockage fromation will be discussed.

1.2 Mechanisms involved in LPT

1.2.1 Nucleation Kinetics

The process of nucleation and precipitation of a solute from a solution is a dynamic process that requires supersaturation (solution containing more of the solute that it can dissolve under equilibrium conditions) as well as a critical body of the solute that represents the first nucleus. This dynamic process has to be considered as a time-dependent mechanism rather than an instantaneous thermodynamically equilibrated process (Debenedetti, 1990). The molecular gathering in assembly of the critical nucleus is not fully understood. However, theoretically, based on the condensation of a vapour to a liquid, phase change would occur by minimisation of the Gibbs free energy (G) with Equation 1.1 describing the critical nucleus size (Mullin, 2001).

$$r^* = \frac{2\sigma v_m}{k.T.lnS}, \qquad \text{Eq. 1.1}$$

Where σ is the interfacial tension, T is the temperature, v_m is the molecular volume, k is the Boltzman constant. *S* represents the supersaturation and its definition based on the assumption of ideal gas and ideal solution as follows:

$$S = \frac{y^*(P_{up},T)}{y^e(P_{down},T)} \qquad \text{Eq. 1.2}$$

In this Equation $y^*$is the solute mole fraction at the upstream conditions of P_{up} and y^e is defined as the solubility at the downstream condition of P_{down}. The definition of supersaturation can be extended to non-ideal conditions by including the fugacities at each relevant mole fraction. However for the present case the assumption of ideal solution could not be irrelevant due to low solubility of the solutes.

The rate of nucleation, J, the number of nuclei formed per unit time per unit volume, can be expressed by the following equation:

$$J = A.exp\left(\frac{-\Delta G}{k.T}\right) \qquad \text{Eq. 1.3}$$

In Equation 1.3, the constant A (same unit as J) is a characteristic of solute and is between 10^{20} and 10^{27} as a generic approximation.

Substituting the expression of the critical nuclei size (Eq. 1.2) into the Eq. 1.3 gives the formula for predicting the rate of nucleation in terms of solute properties and working conditions;

$$J = A.exp\left(-\frac{16\pi\sigma^3 v_m^2}{3k^3.T^3(\ln S)^2}\right) \qquad \text{Eq. 1.4}$$

According to this equation, three main variables control the kinetics of nucleation; *temperature, degree of supersaturation and interfacial tension* (Römer & Kraska, 2010). Supersaturation will have the critical influence on the nucleation rate; Figure 1-4 schematically shows the theoretical prediction of a rapid rise in the nucleation rate after a critical level of supersaturation attained. Therefore, determination of the critical level of supersaturation plays a fundamental role in the selection of suitable solutes for leakage prevention technique.

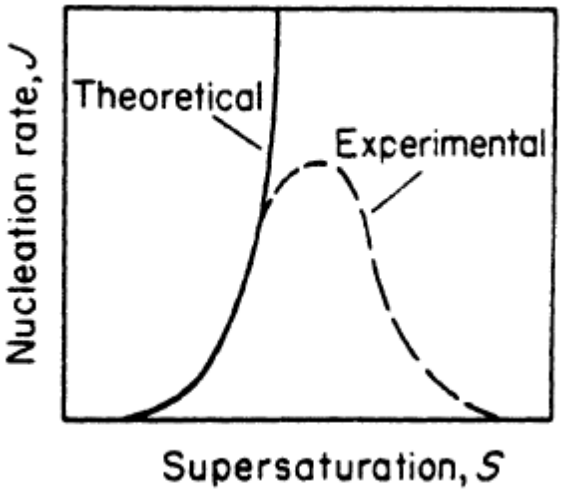

Figure 1-4: Effect of supersaturation on nucleation rate (Mullin, 2001).

The dominant effect of the degree of supersaturation on the time required for the spontaneous appearance of nuclei in supercooled water vapour was calculated by Volmer

(1925) and has been presented in Table 1-1 (Volmer & Schultz, 1931). In this special case, a critical supersaturation exists in the region of S ~ 4.0, but it is clear from the data that nucleation would also occur at any value of supersaturation if sufficient time had been allowed.

Table 1-1: Nucleation time in supercooled water as function of supersaturation.

Supersaturation, S	Time
1.0	∞
2.0	1062 years
3.0	10^3 years
4.0	0.1 s
5.0	10^{-13} s

If the critical supersaturation is chosen to correspond to a nucleation rate of one nucleus per second per unit volume, then equation 1.4 could be rearranged to:

$$\ln S_{crit} = \left[\frac{16\pi\sigma^3 v_m^2}{3k^3.T^3 \ln A}\right]^{1/2} \qquad \text{Eq. 1.5}$$

Figure 1-5 shows the relationship between the critical supersaturation for nucleation, interfacial tension and molecular volume.

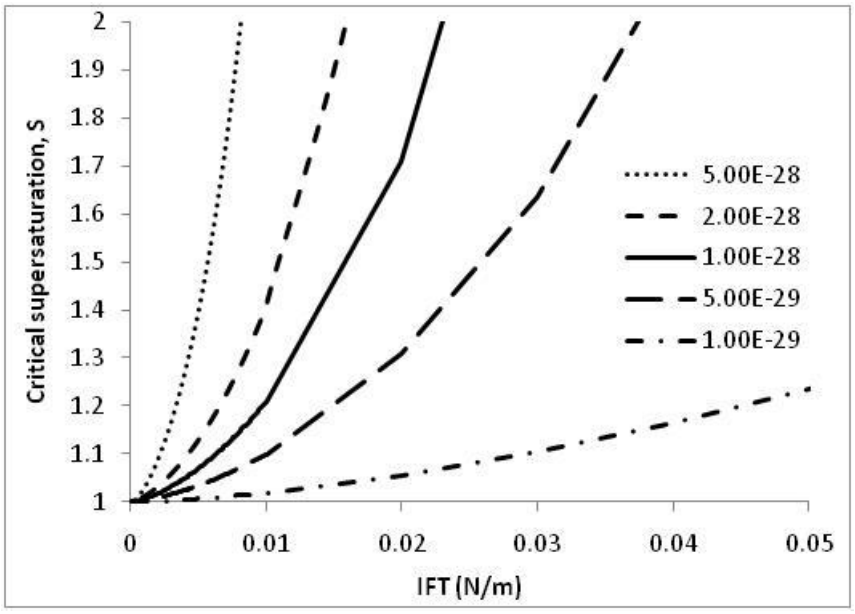

Figure 1-5: Critical supersaturation as function of interfacial tension at different molecular volume. The label of this figure on the right is molecular volume.

Based on Figure 1-5, in order to design a leak prevention system which would be sensitive to slight pressure drops (small and slow leaks), the interfacial tension between CO_2 and the solute should be engineered as the main selecting criterion. In this Figure an IFT of 0.01 N/m can be considered as one of the selection criteria to ensure critical supersaturation of greater than one. The effect of temperature, which affects the interfacial tension of gas-solid mixtures should also be considered. Türk (2000) attempted to determine the relationship between the interfacial tension of Solute-9 supercritical CO_2 and temperature (Türk, 2000). The results showed that, temperature does not affect IFT strongly. Equation 1.6 expresses their relationship.

$$\sigma(T) = \sigma_0 + C(T - 273.15) \qquad \text{Eq. 1.6}$$

σ_0, in N/m, is the interfacial tension at the base temperature which, in this case, is 0 ^oC and C is the thermal constant (T is in Kelvin). In order to have numeric sense of the variation of IFT with respect to temperature, Table 1-2 illustrates the value of σ_0 and C for three solutes dissolved in supercritical CO_2.

Table 1-2: Typical values for IFT dependency on temperature (Türk, 2000).

Solute	σ_0 (N.m^{-1})	C (N.m^{-1}.K^{-1})
Solute-9	0.04347	-1.109×10^{-4}
Benzoic acid	0.03757	-8.709×10^{-5}
Cholesterol	0.04105	-7.224×10^{-5}

The range of interfacial tension between solid solutes and supercritical CO_2 in Table 1-2 for different solutes is not wide. Furthermore because of low C value it can be confirmed that its dependency on temperature is minimal. This is consistent with the findings in the literature (Debenedetti & Kumar, 1986) that IFT does not vary significantly unless the working temperature elevates close to the solid solute melting point. Full coverage of the behaviour of the solute in contact with supercritical CO_2 in such conditions is not available to study the solubility and nucleation kinetics of solid solutes in that region and hence, experiments are required to obtain such information.

1.2.2 Deposition (filtration) of Solid Particles

Inertial Impaction

After the particles have been formed, they are required to precipitate to cause blockage. One of the main mechanisms of particle precipitation for particles with diameter greater than 1μm is inertial impaction. In this process, the fluid streamlines closer to the point of precipitation (collector) begin to change direction, as shown in Figure 1-6 (Tien & Ramarao, 2011). These streamlines as they turn away from the spherical collector, in order to conserve the no-slip flow condition, cause a change of velocity which in turn results in deposition. In other words, because of their inertia and deviation from the corresponding streamline, some of the particle trajectories may intersect with collector surface leading to deposition. The discussion here will be a qualitative and aimed at an understanding of the physical significance of the inertial impaction.

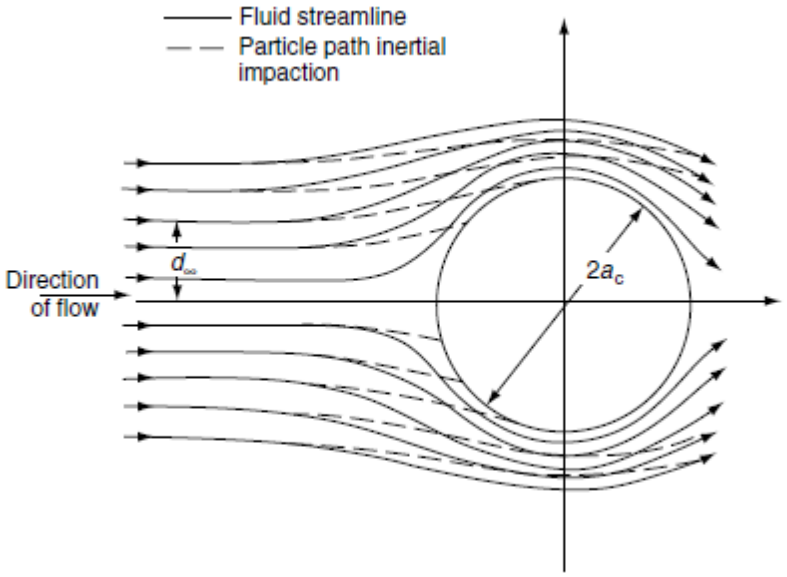

Figure 1-6: Particle deposition by inertial impaction (Tien & Ramarao, 2011).

The parameter which governs the extent of the inertial impaction is the Stokes number (Tien & Ramarao, 2011), N_{st}, defined as;

$$N_{st} = \frac{2\rho_p \bar{U} a_p^2}{9\mu a_c} \qquad \text{Eq.1.7}$$

Where a_p is the particle radius; a_c the characteristic length of the collector; $\bar{U}$ the average velocity of the flow; and ρ_p particle density and μ is the fluid viscosity. The physical meaning of the Stokes number can be explained as the ratio of the inertial force to the

drag force which can be further expressed as the particle's stopping distance if it was multiplied by the characteristics length of the collector. For the case of the single isolated-sphere model, the numerical results shows that the efficiency of precipitation (η_i) can be approximated by the following relationships (Beizaie, 1977);

$$\eta_i = \frac{\beta_4}{1+\beta_4} \qquad for\ N_{st} \geq 1.2130 \qquad \text{Eq.1.8}$$

$$\beta_4 = 0.2453(N_{st} - 1.2130)^{0.955} \qquad \text{Eq.1.9}$$

Which states that there exists a critical value of the Stokes number below which particle deposition by inertial impaction is minimal. Figure 1-7 shows dependency of inertial impaction on the Stokes number with a critical value for activation of this mechanism, which depends on the flow regime.

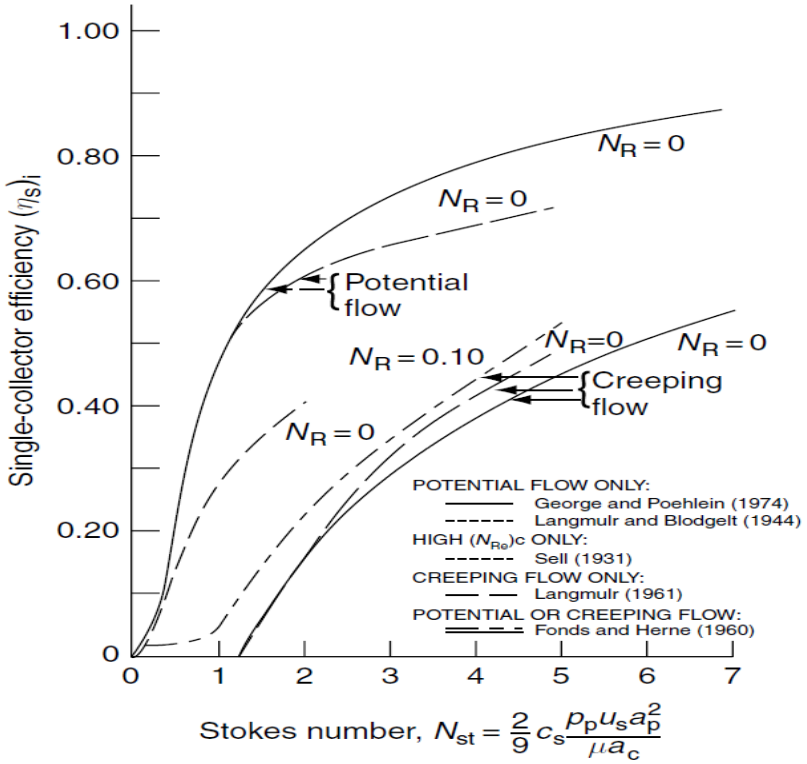

Figure 1-7: Calculated single collector efficiency by inertial impaction as the function of Stokes number (Beizaie, 1977).

Interception

Particle retention by interception occurs because particles are finite in dimension and collide as they move along the streamline that is deviated due to the presence of the

collector. This mechanism is directly related to the size of the particle and the radius of the collector. Indeed, the ratio of particle diameter to the grain diameter is the governing factor to determine the significance of the interception deposition. Pendse obtained the collector efficiency in term of interception of particle as expressed by Equation 1.10 (Pendse, 1979).

$$\eta_I = \frac{3}{2}(N_R)^2 \qquad \text{Eq. 1.10}$$

In which N_R is defined as the ratio of diameters of the simplest form of the spherical particles and the completely rounded collector. In general, interception is an important deposition mechanism only if inertial impaction's effect is negligible. Thus, interception plays an important role in the filtration of liquid like fluids where inertial effects are negligible due to lower flow velocities.

Sedimentation

In the presence of density difference between particle and the carrier fluid, the gravitational force causes the particles to settle down. The speed of the sedimentation in dilute suspension of solid particles with diameter (a_p) can be approximated by the Stokes law (Payatakes, et al., 1974):

$$V_t = \frac{2}{9}\frac{a_p^2 g \Delta\rho}{\mu} \qquad \text{Eq. 1.11}$$

Consequently the single collector efficiency can be described by

$$\eta_G = \frac{2a_p^2 g \Delta\rho}{9\mu\bar{U}} = N_G \qquad \text{Eq. 1.12}$$

Equation 1.12 implies that for sedimentation to take place, either large particles or low superficial velocity would be needed. The influence of the direction of the velocity would modify the efficiency of capturing the particulates by sedimentation. Paretsky proposed the following correlations for the single collector efficiency due to gravity (Paretsky, 1972)

$$\eta_G \uparrow = 0.0375 {N_G}^{0.5} \qquad \text{Eq. 1.13a}$$

$$\eta_G \downarrow = \eta_G \uparrow + 0.21 N_G^{0.78} \qquad \text{Eq. 1.13b}$$

In these two equations, the arrows show the direction of the vertical suspension flow of the suspended particles. However, it should be noted that the difference of the two corresponding equations is not considerable for practical purposes.

1.3 Solute Selection

1.3.1 Selection Criteria

There is a wide range of materials, both natural and synthetic (primarily and extensively used in food and pharmaceutical industries), that is soluble in supercritical CO_2 and would precipitate out as the CO_2 pressure drops. However, the selected solutes for CO_2 leakage prevention purposes should meet certain criteria.

The selection criteria for the optimised CO_2 solute include:

1. Be at the right concentration to remain soluble within the injected stream and only precipitates if a leakage scenario within the well stream or reservoir was developed.

2. Stability at the pressure and temperature storage conditions, i.e. the solid solute melting point should be above the storage site temperature.

3. Being environmentally friendly abiding the regulations including those related to the injection of chemicals into subsurface geological reservoirs.

4. Being inexpensive in bulk quantity to make its implementation in an already costly operation viable. This can be partially be addressed by selecting lower solubility solute requirements.

5. Should be durable at reservoir conditions, That is, the blockage does not lose its integrity with time.

These factors ensure that this technique is practically economical, solute remains in the solution, it provides a blockage when it precipitates out in response to a leak and remains in its desired solid state at the temperature typical of underground geological storage site for long period of time. 17 potential solutes, listed in Table 1-3, were considered in this study. In Table 1-3, number of crosses (×) represents the severity of the unfavourable property of the solute. If three crosses are assigned for that particular solute, the solute is considered unsuitable and is rejected. Solutes with one x are

acceptable for this study but needs to be re-considered with respect to that property and for the particular application.

Table 1-3: List of potential solutes (HWS stand for **H**eriot **W**att **S**olute)

Index	Solute	Reservoir conditions	Environmental constraints	Cost
1	Solute-1	×××	×××	×
2	Solute-2			×××
3	Solute-3	×××		
4	Solute-4	×××		
5	Solute-5		×××	×××
6	Solute-6 **(HWS-7)**	×××		
7	Solute-7		×××	
8	Solute-8			×××
9	Solute-9		×××	
10	Solute-10		×××	
11	Solute-11		×××	
12	Solute-12			×××
13	Solute-13 **(HWS-3)**		×	
14	Solute-14 **(HWS-2)**			×
15	Solute-15 **(HWS-4)**		×	
16	Solute-16 **(HWS-5)**			×
17	Solute-17 **(HWS-6)**		×××	
18	Solute-18	××		
19	Solute-19 **(HWS-1)**			

Considering that the experiments were designed based on the prevailing reservoir conditions of 3000 psig and 45^{o}C, only solid solutes that have a suitable solubility signature for those conditions are desirable. Here particular attention was paid to the reservoir temperature as melting point of the solid solute must be above this value. For instance, HWS-7 melts at 39^{o}C and in-fact most conventional storage conditions; consequently, is considered unsuitable for our leakage prevention method but it was

included in the table for other purposes; in later stages of this research, it was identified that there would be a desire to better control the response of the solution and improvement method would be adding a secondary co-solvent. HWS-7 would be considered for these purposes.

Next environmental considerations were considered. For instance, Solute-7 was considered as a good candidate, but because this solute is not allowed to be injected into underground storage reservoirs due to environmental concerns, it was excluded from this experimental and theoretical study. The next criterion is that the potential solute should be inexpensive in bulk quantity, which strongly depends on the target pressure of storage site as well as its temperature, both affecting the amount of solute needed. An example of this category is Solute-2. It is noted that some of the solutes are unsuitable for more than one reason. After shortlisting a number of solute, these solute should be experimentally examined and then more fine-tuning should be done for further assessing of the solute for the field applications. It should be pointed out that the range of solutes should not be limited to the substances listed in Table 1-3. Since our proposed leakage prevention technique is still in verification stages (laboratory studies), the window for the selected solutes should be opened for new solutes.

CHAPTER 2 EXPERIMENTAL FACILITIES AND FLUIDS

2.1 Micromodel Rig

Studying the solute transport through porous media requires thorough understanding of two main physics which govern this technique; (1) kinetics of nucleation and (2) precipitation of the suspended particles. For visual investigation of the physics involved in the process of leakage prevention, we have utilised unique high-pressure micromodel facilities available in our laboratories in the Institute of Petroleum Engineering of Heriot-Watt University which is one of the world pioneers in the area of high pressure flow visualisation. The unique advantage of the visualisation experiments over conventional laboratory techniques is that the complex dynamic process of CO_2 leakage and subsequent formation of particles and blockage of the leakage can be directly seen and studied. However, it should be noted that glass micromodels are not real rocks and inevitably minor idealization have been made.

Figure 2-1 shows a schematic diagram of the high-pressure micromodel rig used for the experiments. For all the experiments reported here, the micromodel orientation was vertical with the inlet of the porous medium located at the top and the outlet at the bottom. A high-pressure cylinder with a capacity of 300 cc was used as a CO_2 reservoir which supplied CO_2 to the micromodel. A set of very accurate pumps were used to inject the fluids and also collect the effluent. The pumps are capable of delivering fluid at an ultra-low flow rate of 0.001 cc/hr. In order to control the temperature of the fluids and the micromodel, two oil baths were used with one housing the fluid cylinder and the other

one housing the micromodel. The pressure of the micromodel can be accurately measured and monitored by two pressure transducers located at either sides of the porous medium.

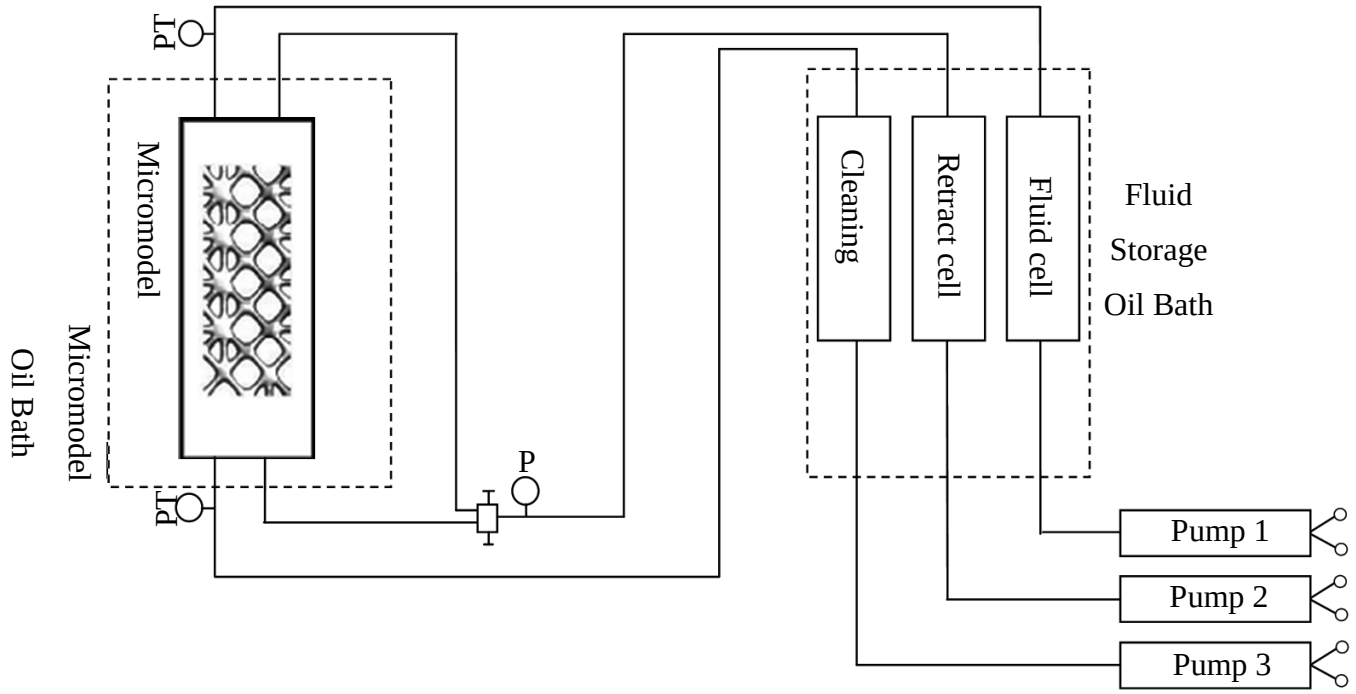

Figure 2-1: Schematic diagram of the micromodel rig.

In the micromodel experiments, pore network patterns which are etched on glass provide realistic flow conduits and allow flow visualisation at reservoir conditions. The available experimental facilities and expertise developed over many years of research in these areas have been employed to investigate the water-CO_2 injection process visually. Figure 2-2 shows the photo of the high-pressure high temperature micromodel rig which was used in this study. The rig consists of the following major components:

Fluid Storage Tank: A temperature-controlled oil bath is used to house injection fluids, lines and connections at constant temperature. In this part of the rig, five fluid storage cells exist. Three of them are for injection of different fluids, e.g. pure CO_2, water, solution (CO_2+soloutes), N_2 and one cell is used to collect the effluent of the micromodel.

Micromodel Tank: A separate temperature-controlled oil bath is considered, which is used to maintain the overburden and micromodel-housing chamber at constant temperature. Micromodel is loaded vertically in its housing chamber.

Injection and Retraction Pumps: To inject and retract fluids around the flow system (micromodel and overburden chamber) two highly accurate pumps are used. A third pump is used to keep the overburden at fixed pressure well above the working pressure. The pumps are capable of working at pressures up to 6000 psia with a flow rate in the range 0.0001 to 900 cm^3/hr.

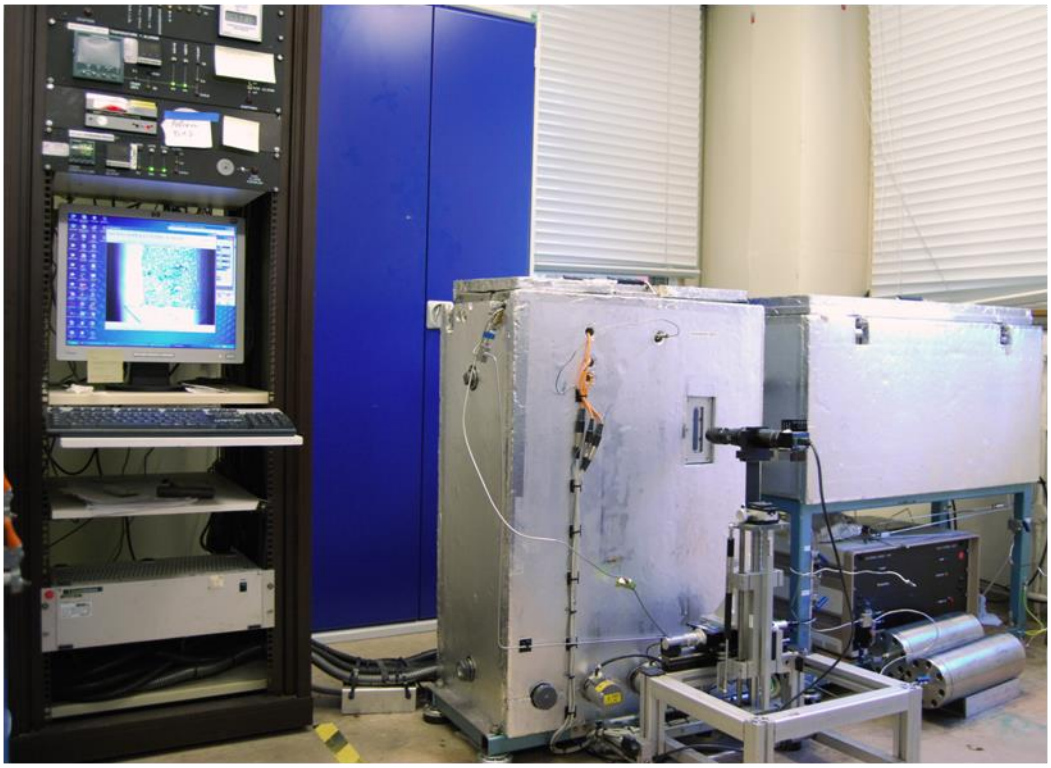

Figure 2-2: The high-pressure high-temperature micromodel rig used for the visualization tests in this study.

Glass Micromodels: Micromodels are made of a two-dimensional pore structure, which is etched onto the surface of a glass plate, which is otherwise completely flat. A second glass plate is then placed over the first, covering the etched pattern and thus creating an enclosed pore space. This second plate, the cover plate, has an inlet hole and an outlet hole drilled at either end, allowing fluids to be displaced through the network of pores (Figure 2-3). Because the structure is only one pore deep, and the containing walls are all glass, it is possible to observe the fluids as they flow along the pore channels and interact with each other. It is also possible to observe how the geometry of the pore network affects the patterns of flow and trapping.

In this study two micromodels with heterogeneous pattern were used. One of the patterns was rock look-alike and the other one was more synthetic representation of rock, as

depicted in Figure 2-4 and Figure 2-5, respectively. Table 2-1 shows dimensions of the selected section of the glass micromodels used for the experiments reported here.

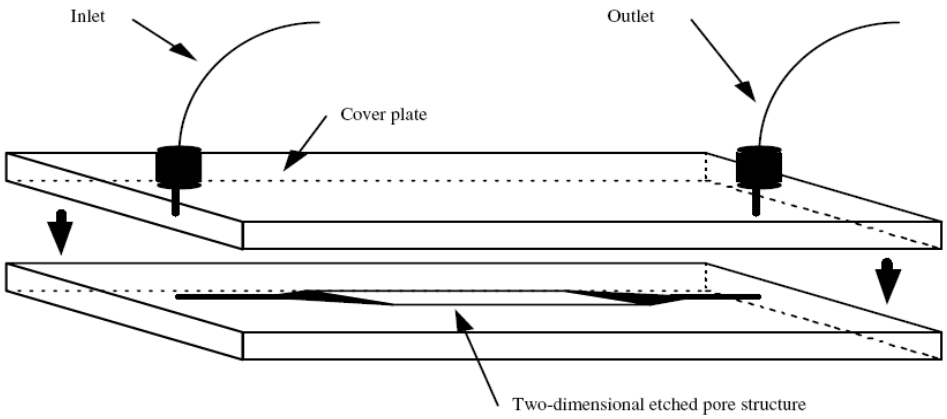

Figure 2-3: Schematics of a glass micromodel.

Table 2-1: Dimensions of the glass micromodels and their pore.

MM	Length cm	Width cm	Micromodel pore volume Cm^3	Ave. depth μm	Pore Dia. Range μm
Rock Look alike Pattern (heterogeneous)	4	0.7	0.01	50	30-500
Synthetic Pattern of Rock (heterogeneous)	4	0.7	0.01	50	30-500

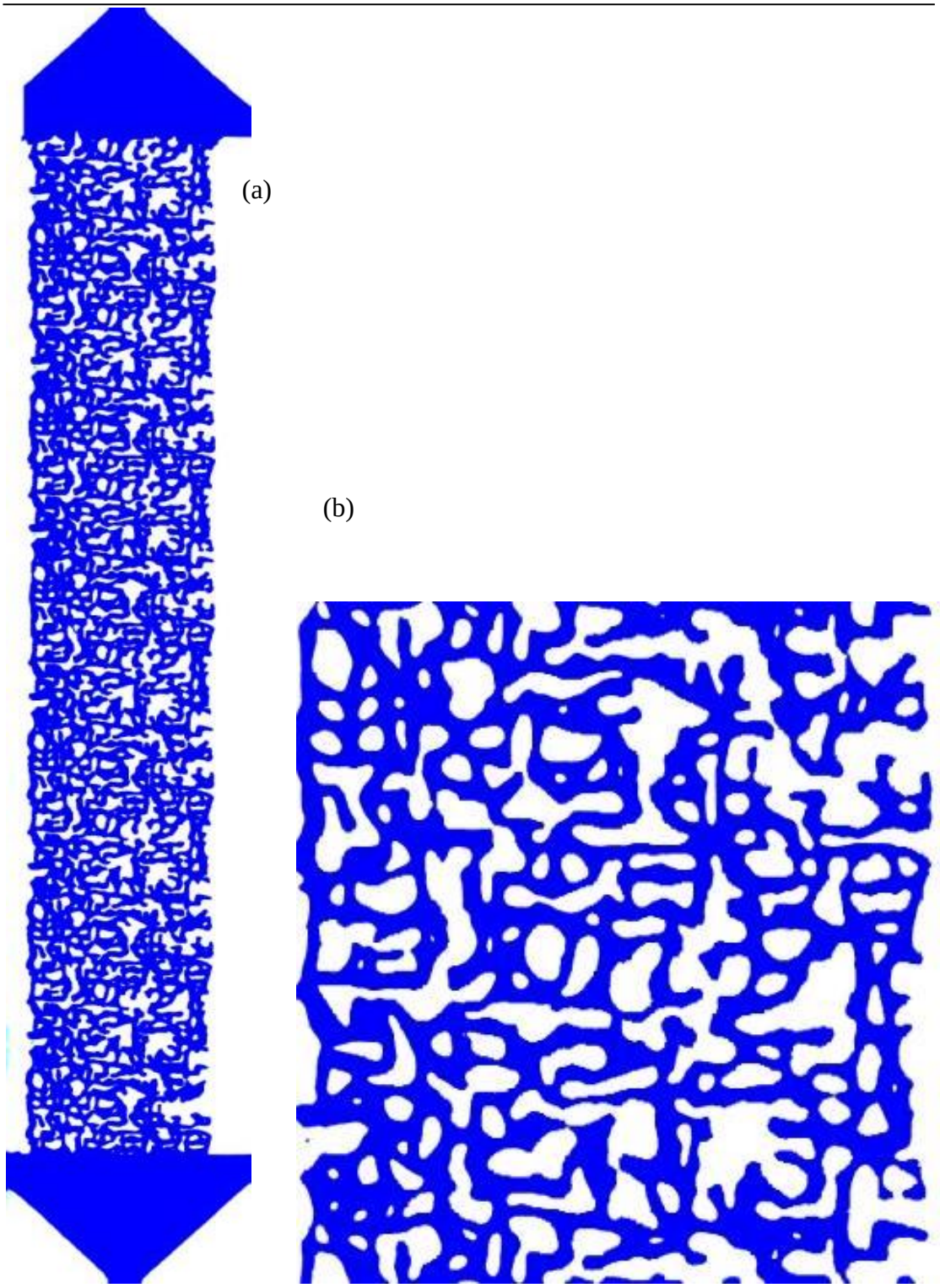

Figure 2-4: Pictures of the heterogeneous rock-look-alike micromodel which is fully saturated with blue-dyed water. Pores are shown in blue and un-etched glass in white. A magnified section of the pore pattern is shown in right image.

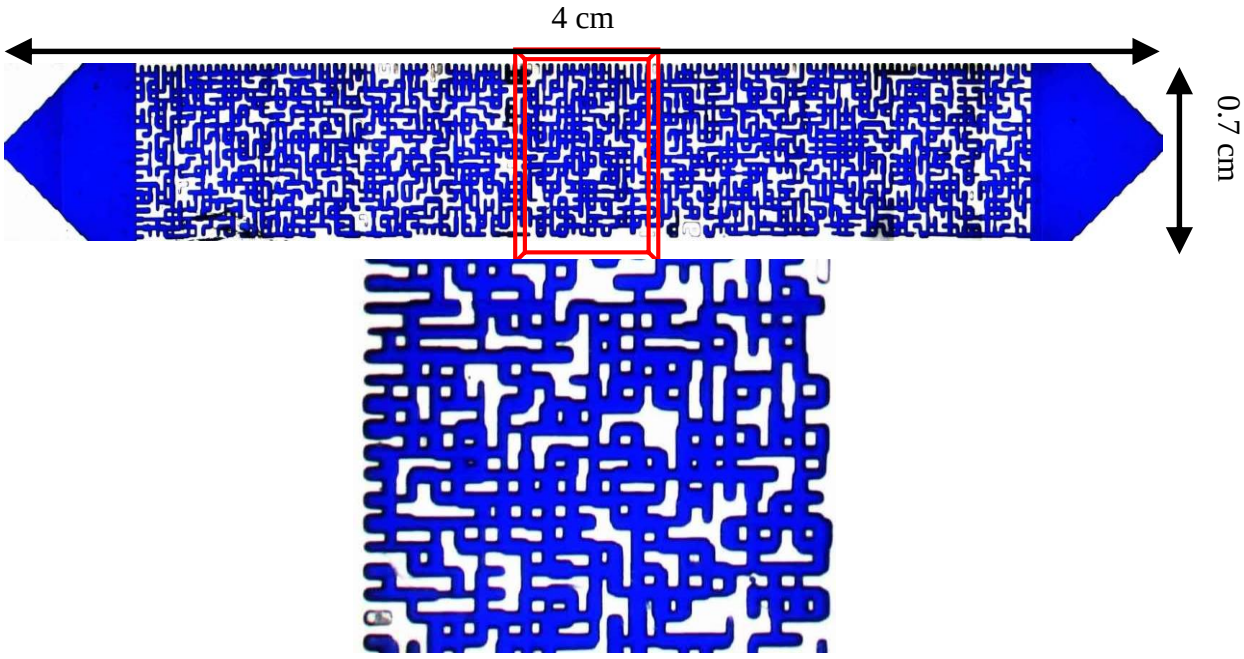

Figure 2-5: Pictures of the heterogeneous synthetic pattern micromodel which is fully saturated with blue-dyed water. Pores are shown in blue and un-etched glass in white. A magnified section of the pore pattern is shown in the below image.

Computer Controlled Linear Drive System: A computer controlled linear drive system is used in the tests, which allows a camera equipped with a magnifying lens to be positioned automatically at any part of the micromodel, or sequentially sweep the micromodel for digital recording. These digital records can then be used in image analysis to determine fluid saturation. The optical system can provide magnifications of up to 200 times.

2.2 Visual cell (Sightglass)

Figure 2-6 shows a schematic of the visual cell rig and its essential parts. The objective of the sightglass visualization tests was to quantify the kinetics underlying particle formation in terms of supersaturation and induction time for nucleation and precipitation of the solutes. The setup is equipped with a high resolution camera that can detect appearance of very small fines. The volume of the sightglass is 3 cm^3, which makes very sensitive to any volume or pressure change in the setup.

To carry out the tests, first, the solution of CO_2 and solute has to be prepared in the CO_2 storage cell whilst the visual cell is pressurized to the test pressure by solvent

(acetone/methanol mixture) injection. Then, the solvent in the sightglass is displaced by injection of the CO_2 solution which continues until no interface between fluids can be seen. The volume of the sightglass is relatively small and is around 3 cm^3; therefore it does not require the injection of a large volume of the CO_2 solution to ensure that all the solvent inside the cell has been displaced. However, an additional volume of 10 cm^3 was injected into the cell to vaporize any residues of the solvent. Then the pressure of the sightglass is adjusted and set to the pressure at which the test will be conducted. The final step of the experiment involves simultaneous closing and opening two valves; closing the valve connecting the sightglass to the CO_2 solution cell and opening the valve from sightglass to the retract cell. At the same time, the images will be recorded to analyse the time required for first batch of particle to appear in the sightglass. The main output of the test is the induction time for appearance of particles.

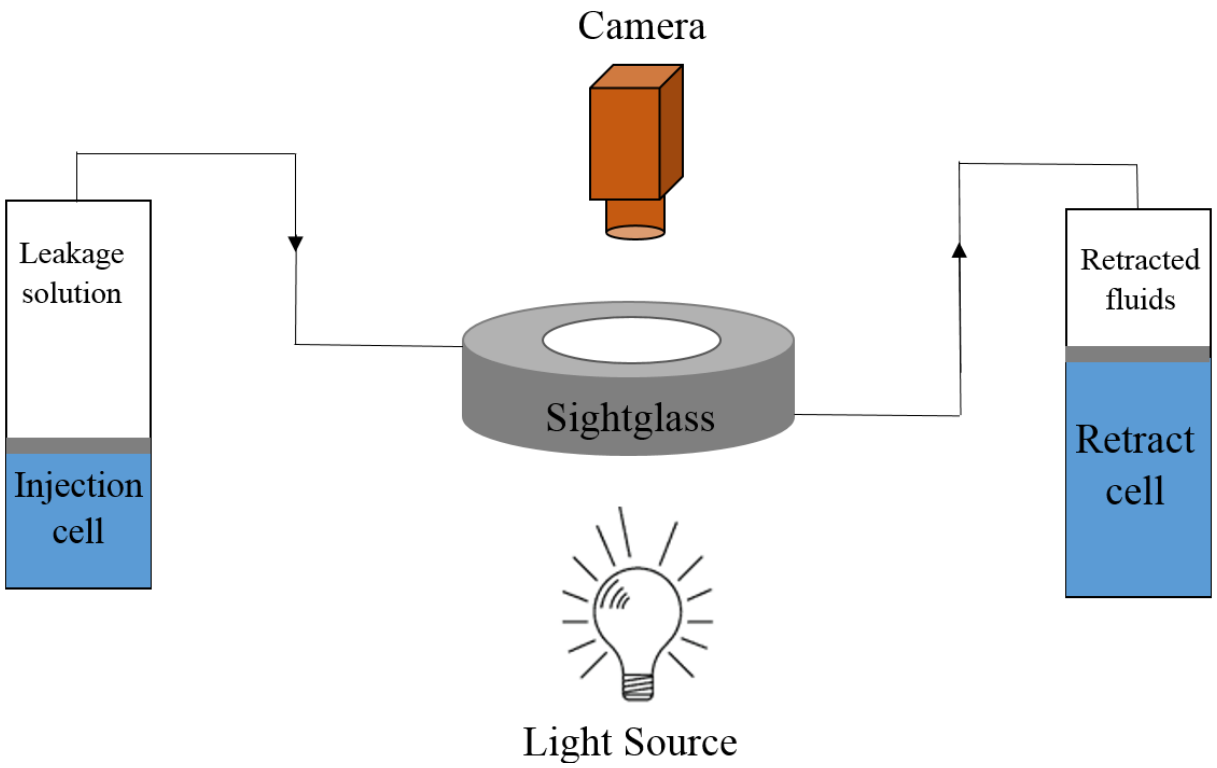

Figure 2-6: Simplified diagram of the visual-cell (sightglass) setup.

Image Analysis System: To analyse the results of the sightglass experiments, it is necessary to detect and measure the changes in image colours within the viewing cell.

Using image analysis software, slight and very tiny changes in the darkness and also appearance of a dust-like particles would be detected.

2.3 Sand Pack

Figure 2-7 illustrates the experimental setup of the sandpack rig, which has been specifically developed for investigating the proposed leakage prevention method. Three high-pressure cells were placed in the constant temperature oven; one pure CO_2 cell to pressurize and prepare the sandpack for the test, one leak cell at the outlet end of the flow for imposing the leakage condition, and one CO_2 + Solute cell to prepare the solution. The connections and the plumbing for the solution cell have been designed to be flexible to allow shaking of the mixture in order to equilibrate the solution prior to injection. A ¼" pipe was filled with glass beads as the sandpack. The length of the porous medium (sandpack) is 80 cm. The other distinct feature of the system is the incorporation of a visualization cell (SightGlass) at the outlet end of the sandpack in order to observe the solute particles moving out of the simulated leak path. Using sightglass has two advantages; first, it would show the influence of suspension flow of the particles and second, the visualization would reveal some qualitative information about the size of the solid solutes after they were formed. Two low-rate Quizix pumps were connected to the injection and leak cells to adjust the working pressures at both ends of the sandpack.

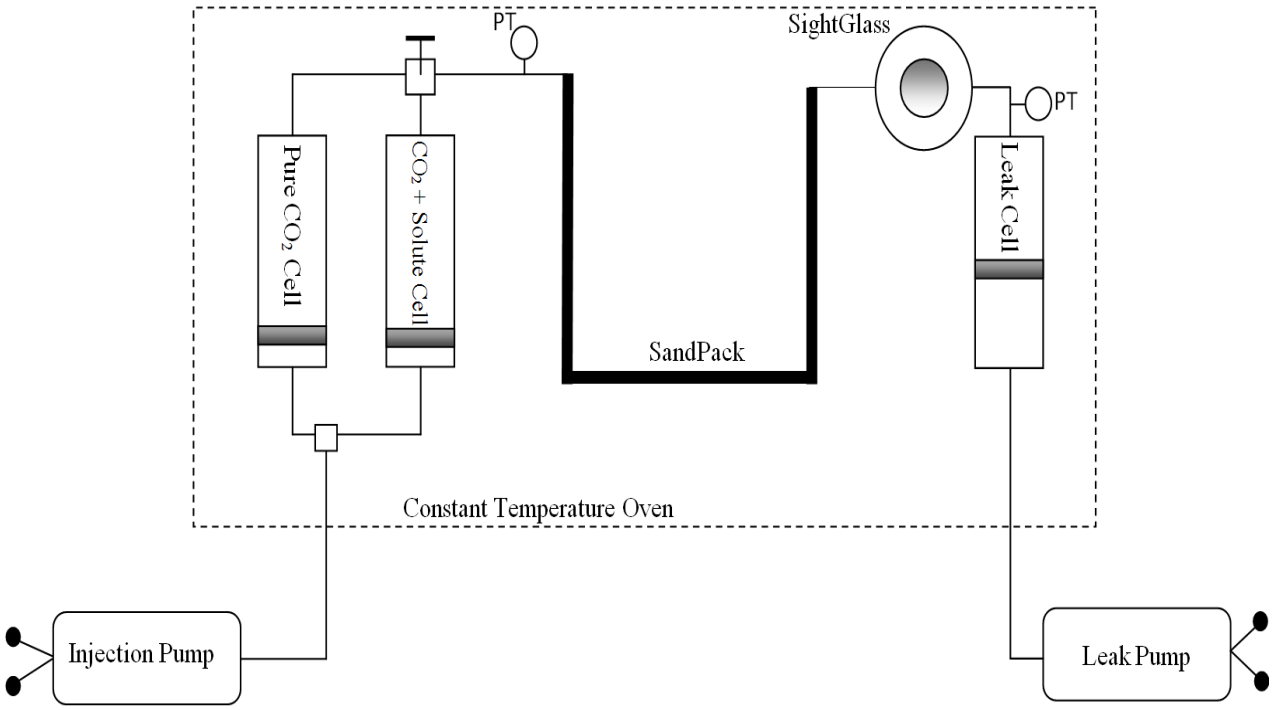

Figure 2-7: Experimental setup of Sandpack tests.

Two Quartzdyne pressure transducers (PT) were utilised to measure accurately the pressures. Therefore, the reported pressures would be the readings from these Quartzdyne transducers rather than the recorded data of the pumps. The pressure at which the solution is prepared for all tests reported here is 3000 psig. In summary, this facility is adequately equipped to capture the sequence of stages of the process of blockage, i.e. formation of particles and deposition of solid solute where the solution meets the applied pressure drop.

2.4 Coreflood Rig

Figure 2-8 and Figure 2-9 and respectively show the real photo and the schematic diagram of the high-pressure/high temperature coreflood rig which was used in this study. Two high pressure cells one filled with CO_2 + solute solution and the other with pure CO_2 are placed in the temperature-controlled oven near the inlet side of the coreholder. Two pressure transducers have been employed to accurately measure the pressure of both ends of the core. Two pumps are connected to the cells in order to flow the fluids at high pressure. In these experiments, no back pressure regulator (BPR) utilised since the precipitation in BPR would block the flow lines.

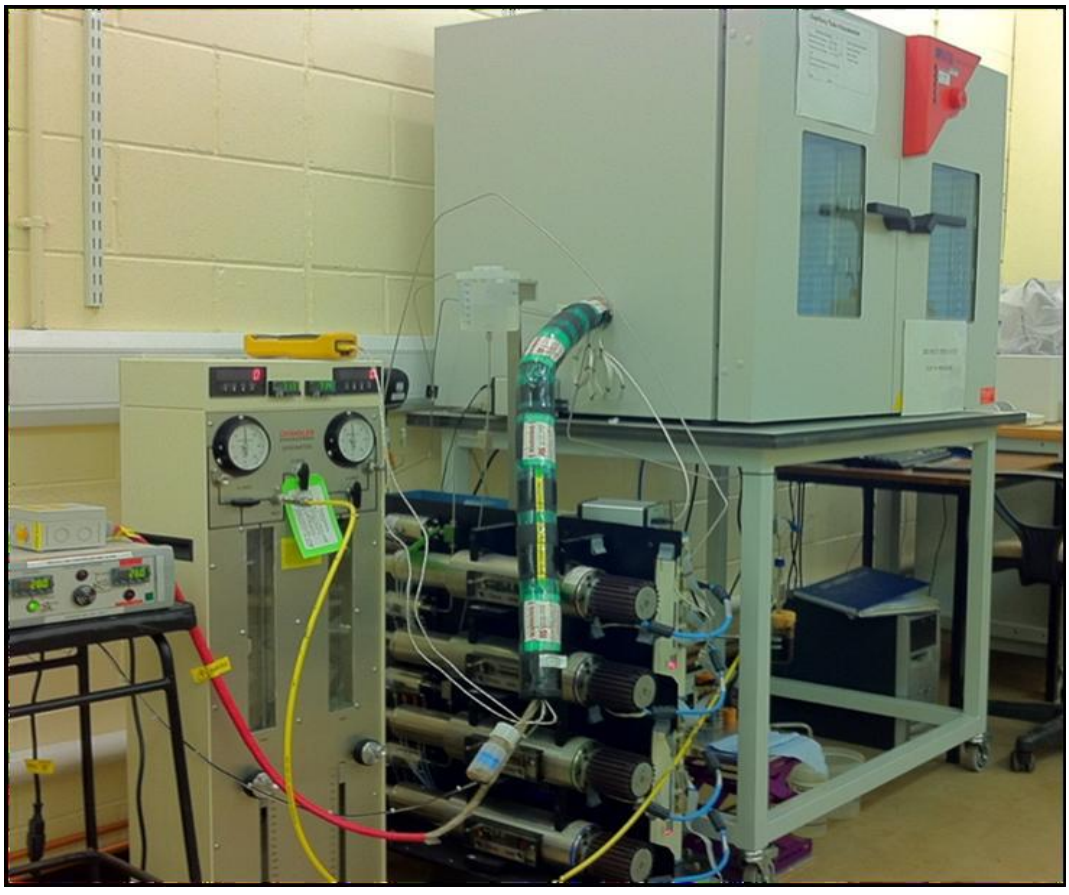

Figure 2-8: The coreflood setup used in this study

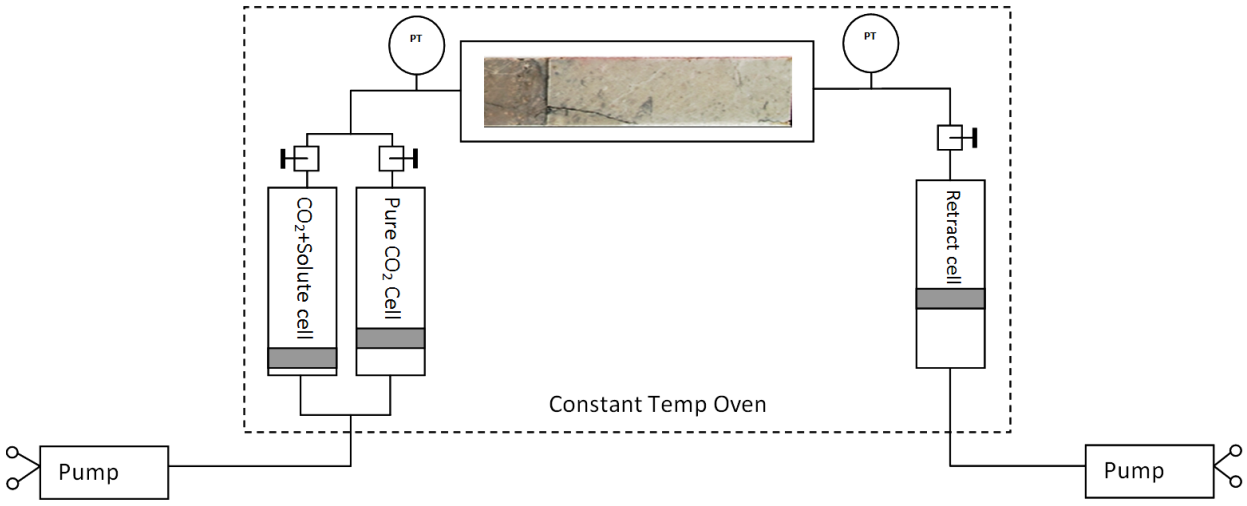

Figure 2-9: Experimental setup of the coreflood rig; the solution cell and CO_2 cell are located in inlet side of the coreholder.

Two leak types, (i) constant pressure and (ii) constant flow rate, were considered in these experiments. That is, in some experiments, the leak was physically simulated in the form of constant leakage rate at the inlet and the outlet of the core was set to remain at constant pressure mode. However, in order to have a more consistent and fixed analysis of the solute solubilities at the inlet and outlet conditions, some coreflood experiments have been conducted at the constant pressure mode at either ends of the core ends to give fixed solubility values.

Two methods for preparing the solution were utilised. (i) Surface mixing: the method for preparation of the solution (CO_2 + Solute) was based on mixing the supercritical CO_2 and the solid solute in a high pressure cell which simulates the process of surface mixing in the field. However, sometimes due to unfavourable thermodynamic behaviour of injected CO_2, surface mixing of the solute and CO_2 may not be a suitable option for applying the leakage prevention method in the field. Therefore, another approach was used in the coreflood experiments, i.e. (ii) downhole mixing: The modified setup represents a downhole mixing process in which the solute is added to the injected CO_2 stream at the bottom-hole conditions of an injection well. That is, pure CO_2 picks up the amount of solute that it can dissolve as it travels through the solute batch. For this purpose, a ¼" pipe with length of 80 cm, which was packed with the solute, was placed just before the core inlet. Figure 2-10 illustrates the modified setup of the coreflood rig that is used for

bottomhole mixing representation. It should be pointed out that two filters have been placed at either ends of the pipe to prevent free flow (suspension flow) of the solute particles through the porous media. The solution at the end of the pipe (or inlet of the core) is assumed to be fully saturated with the solute.

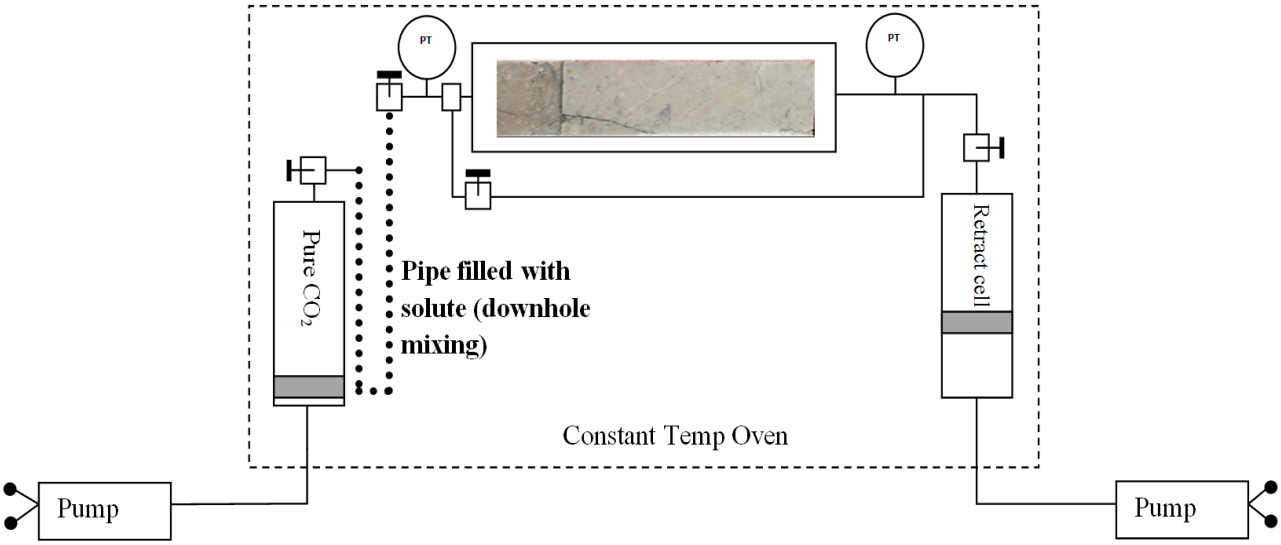

Figure 2-10: Experimental setup of coreflood experiments, which has been modified to simulate downhole mixing technique for delivering the solute into storage reservoir.

CHAPTER 3 VISUALIZATION OF SOLUTE FORMATION AND PRECIPITATION

3.1 INTRODUCTION

Studying solute transport through porous media requires understanding of two main mechanisms which govern our proposed leakage prevention technique (LPT); (1) kinetics of nucleation and (2) precipitation of the suspended particles. The current understanding of these mechanisms in evolution of blockage is inadequate and it's obvious that without consolidating our understanding, implementing of such technique is hardly practical.

For visual investigation of these mechanisms, a unique high-pressure micromodel facilities available in the Institute of Petroleum Engineering of Heriot-Watt University was utilised (Riazi, et al., 2011). The unique advantage of the visualisation experiments over conventional laboratory techniques is that the complex dynamic process of CO_2 leakage and the subsequent formation of solid particles and blockage of the leakage can be directly observed and studied. However, it should be noted that glass micromodels are a small 2D representation of a porous medium and hence, their results may not be directly and quantitatively extend to real rocks.

The progress and growth of a blockage against a leak in porous media requires two sequential and spontaneous phenomena; formation of solid particles and filtration of particles out of the CO_2/solute solution. Two sets of visualisation experiments have been designed and carried out to capture the evolution and formation of the blockage and to

obtain better understanding of solute precipitation kinetics. In the first set of experiments, mixtures of CO_2 and solutes were used in transparent micromodels undergoing an imposed pressure drop to investigate the precipitation of solutes and formation of a blockage inside a porous medium. The process of formation of solid particles and the mechanism of particle retention in a porous medium are expected to be different than those taking place in a vessel or pipe.

Results of the micromodel tests also reveal the mechanism of solid precipitation and whether the particles attach to the surface of the porous medium or accumulate inside the pore spaces of the rock, as a result of increased population of the particles, and eventually block the leakage path of CO_2. The evolution of blockage body is an important process through which the efficacy and feasibility of leakage prevention technique can be evaluated; for instance, our technique would not be feasible in field scales if it is to fill the leakage path completely, i.e. massive amount of solid particles would be needed to pack the path, like cementation (Bachu & Bennion, 2009). However, it would be more desirable to tackle the leakages more smartly and target the main pores involving the leak, which would in turn lead to less solid particles needed and hence, a more cost-effective technique. Therefore, the outcome of micromodel visualisations would shed some lights on whether the blockage would evolve in a smart manner.

In the second type of visualisations, the solution made with CO_2 + solid-solute was placed in a high pressure sightglass which would enable us to visualise with very high resolution and then, a finite pressure drop was imposed on the solution to observe the kinetics of particle formation. This type of experiments would result in quantifying the kinetics of particle formation through measuring the time required for the first solid particle detected during the experiment. The valuable information attained from this experiment can be input into the nucleation equations for the mathematical modelling purposes. Using the same experimental setup, another experiment was performed to investigate whether the CO_2+solid-solute would adversely interact with brines. It has been well-established that CO_2 dissolves into brines (Duan & Sun, 2003) and this phenomenon can disturb the equilibrium conditions of our proposed solution made with CO_2 and solid-solute. On the other hand, storage of CO_2 in underground aquifers involves a substantial level mutual interactions between injected CO_2 and the resident brine (Metz, et al., 2005), which may lead to premature particle formation in the storage reservoir instead of desirable precipitation in contingent leakage paths. Therefore, the integrity of the solution should

be studied as the pre-requisite of the performance of our proposed leakage prevention technique.

In this chapter, first the experimental setup and procedures followed in the micromodel and visual cell (sightglass) tests will be discussed. Then the results of the micromodel tests for the binary/ternary/quaternary systems of solid solute, CO_2, nitrogen (as an impurity), and water will be presented. These experiments were carried out in order to investigate possible effects of different solute types and presence of nitrogen contamination in the CO_2 stream on the performance of the leakage prevention techniques. Moreover, the impact of resident water was investigated. The main findings in the visualisation experiments would enable us to infer the dynamism behind solute precipitation, which then would be used in developing a mathematical model.

3.2 EXPERIMENTAL PROCEDURE

Figure 3-1 shows a simplified schematic diagram of the high-pressure micromodel rig used for the experiments. Dimensions of the micromodel are provided in Figure 3-1. For all the experiments reported here, the micromodel orientation was vertical with the inlet of the porous medium located at the top and the outlet at the bottom. A high-pressure cylinder with a volume of 300 cc was used as a CO_2 storage reservoir which supplied the LPT solution (CO_2 + solutes) to the micromodel. A set of very accurate pumps were used to inject the fluids and collect the effluent. The pumps are capable of delivering fluid at an ultra-low flow rate of 0.001 cc/hr. In order to control the temperature of the fluids and the micromodel, two oil baths were used with one housing the fluid cylinder and the other one housing the micromodel. The pressure of the micromodel can be accurately measured and monitored by two pressure transducers located at either sides of the porous medium.

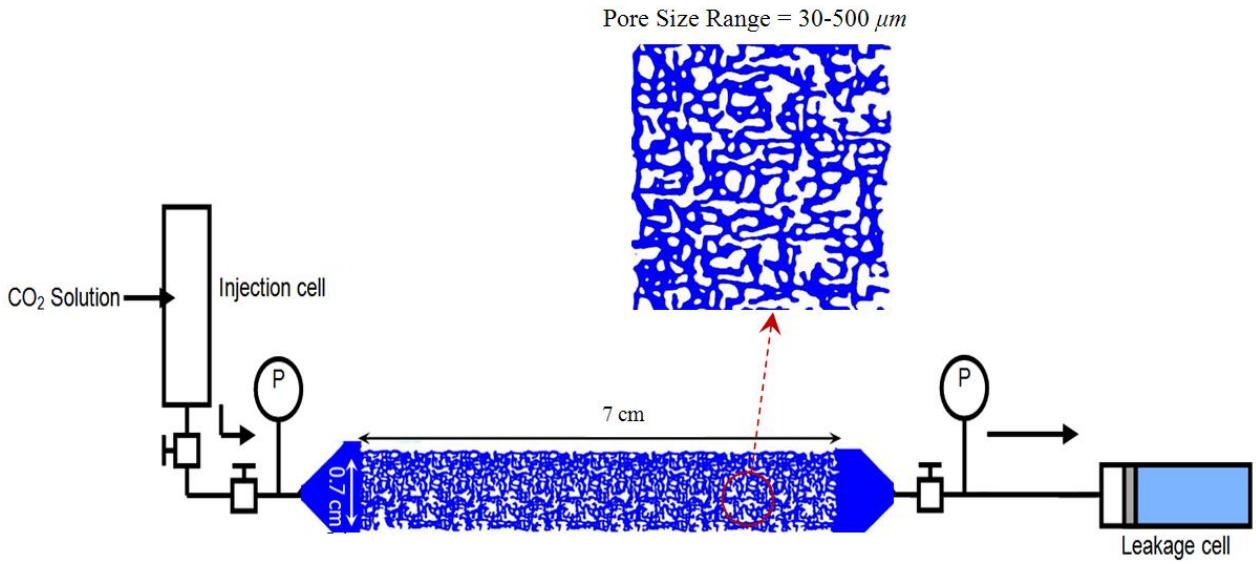

Figure 3-1: Experimental setup of the micromodel illustrating the basic dimension of the porous medium. On the magnified section of the micromodel, the pore size distribution range is shown. Two cells in the both ends of the micromodel establish the pressure conditions across the leakage path.

Experimental procedure for each test involves three parts; (1) preparation of the solvent, (2) preparation of micromodel and (3) performing the leak test. The overall procedure is as follows (more details can be found in Chapter 2):

(1) In order to prepare the LPT solution of CO_2 and solid solutes, an amount of solid solute is added into a cell. Then, the cell is filled with CO_2 and the cell's pressure is increased to the desired pressure of the test. To establish equilibrium conditions between CO_2 and solutes, the solution is allowed to mix for 10 hours at constant pressure and temperature. During this period, the cell is rocked to facilitate mixing.

(2) To prepare the micromodel, first, solvent (Toluene/Methanol mixture) is injected at the test pressure and temperature to thoroughly clean the micromodel. Then, the prepared solution displaces the solvent miscibly and the micromodel becomes saturated with the CO_2 solution. The inlet valve connecting the micromodel to the solution cell is then shut and the leak pressure is established by adjusting the pressure of the leak cell.

(3) After establishing the micromodel pressure at the desired leak pressure, the inlet valve of the micromodel is opened to allow flow of the solution through the

micromodel. During the flow of the solution, the camera is focused on one section of micromodel taking still images as well as recording videos for further analysis.

The details of the experimental procedure followed in each particular test may vary slightly depending on the specific conditions of that test and it would be explained accordingly.

3.3 Highly Soluble Solute (*HWS-5*)

HWS-5 is white crystalline powders insoluble in water but highly soluble in alcohols. It molar mass and density are 152.15 g/mol and 1.385 g/cc, respectively. This solute stays solid up to 185^{o}C, which is favourable for almost all of underground reservoir temperature. Figure 3-2 shows the molecular structure of *HWS-5*.

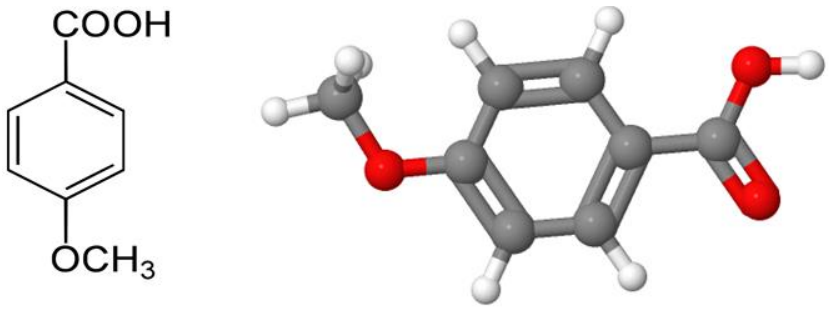

Figure 3-2: Planar (left) and 3D (right) images of *HWS-5*.

In terms of solute solubility, *HWS-5* (here referred to as high solubility solute) has a maximum solubility of 0.0383 mole fraction at 2900 psig and 45^{o}C (prevailing test conditions). It should be pointed out that no experimental measurement exists for solubility of this solute at the above conditions and hence, a correlation was utilised to interpolate and estimate the solid-solute solubility.

Solubility Estimation

Figure 3-3 shows the solubility of *HWS-5* at supercritical CO_2 at constant temperature of 45°C. The main criterion for selecting the solutes has been a limited published solubility data. According to the data the solubility of *HWS-5* in supercritical CO_2 is 15 times more than that of moderately soluble solutes (discussed in next section). The resulting regression of the available data resulted in the following equation (Mendez-Santiago & Teja, 2000);

$$\ln(y_2 P) = \left(\frac{1}{T}\right)\left(-7180 + 134150\rho_{CO_2} + 17.1T\right) \qquad \text{Eq. 3.1}$$

Where, y_2 represents the molar solubility of the solute in CO_2 and P and T are pressure in bar and temperature in Kelvin and ρ_{CO2} is the CO_2 density of in mole/cc. This type of correlation has been used throughout this thesis to estimate solubility of solutes in supercritical CO_2.

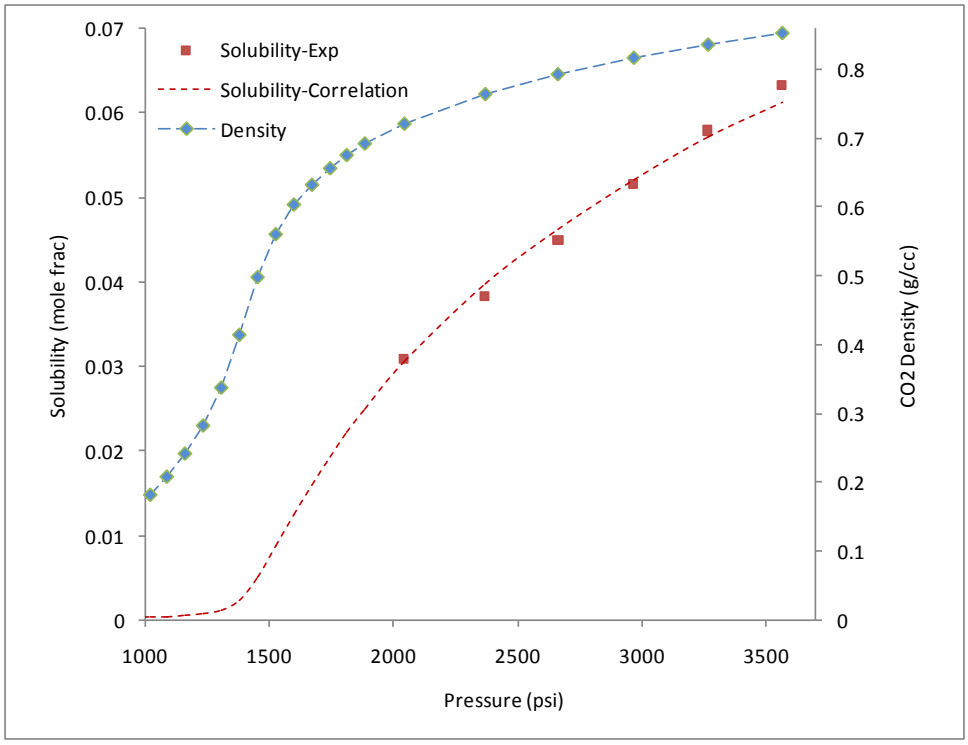

Figure 3-3: Solubility of *HWS-5* in supercritical CO_2 at 45°C. (Gupta & Shim, 2006)

Experiment 1, HWS-5, from 2966 psig to 2400 psig

It is important to study the impact of solute type on the performance of the leakage prevention method to identify the extent by which the process is affected by solute type. For this purpose, a series of experiments were carried out using *HWS-5* which is a high-solubility solute compared to moderately soluble solutes. Having observed in our preliminary observations, the behaviour of *HWS-5* and, in particular, its tendency to attach to the surface of the porous medium is of great importance and interest since this characteristic directly affects the required concentration of the solute.

In Experiment 1, the CO_2 storage pressure was 2966 psig and the leakage pressure was 2400 psig and the concentration of the solute was 0.0383 mole fraction. Figure 3-4 shows the image of the micromodel during the test. As can be seen, as a result of the leakage and the activation of the leakage prevention mechanisms, precipitation of the solute has taken place in some of the pores. One very interesting observation is the significant difference between the patterns of precipitation of *HWS-5* compared to other solutes (subsequent solutes used in experiments performed with moderately and low soluble solutes). While some solutes precipitation would be concentrated around the outlet of micromodel (where the solution experienced highest degree of supersaturation), in this experiment, precipitation of *HWS-5* is more scattered. This is an indication of the differences in the mechanisms of precipitation depending on solute type.

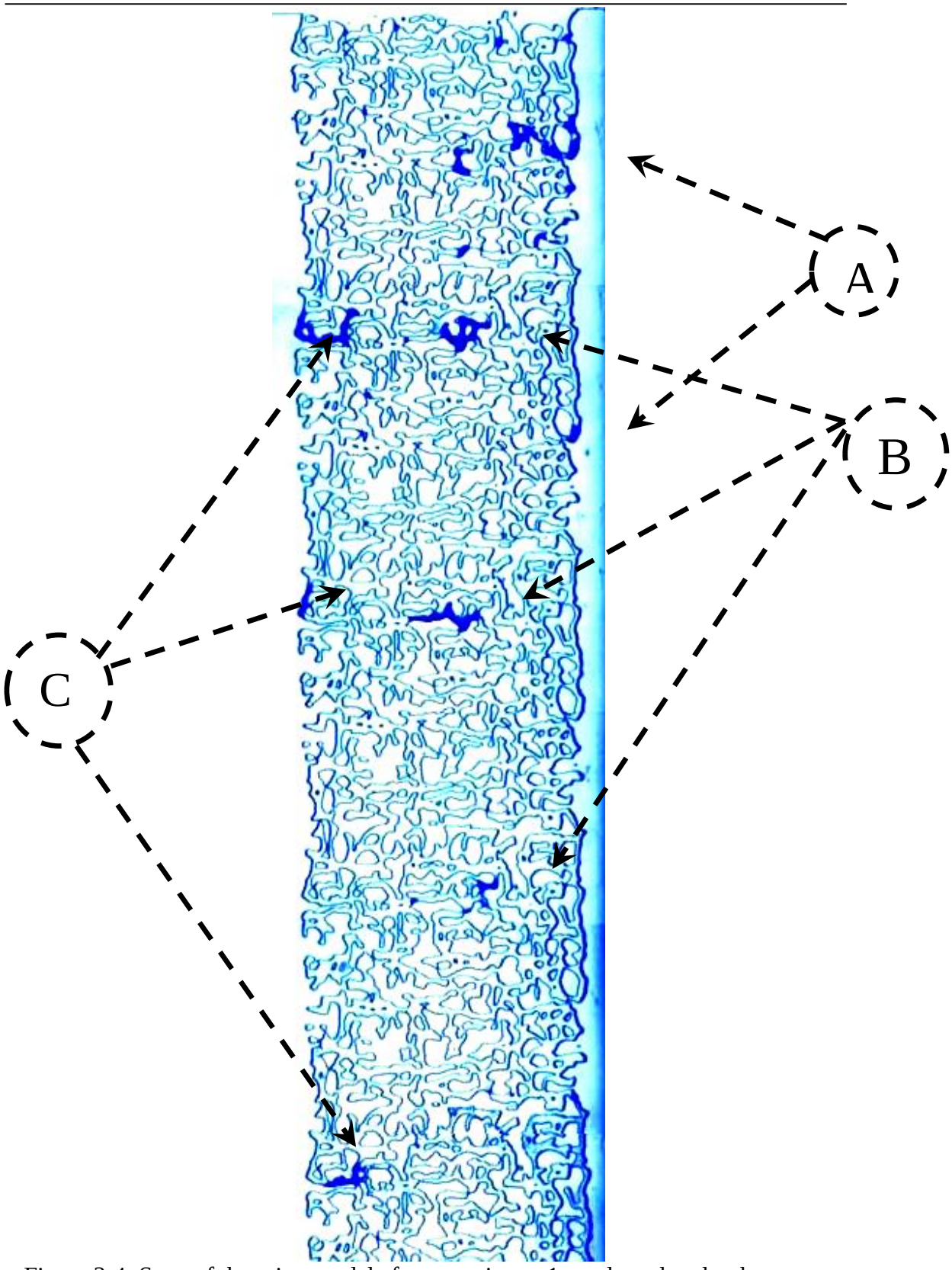

Figure 3-4: State of the micromodel after experiment 1 conducted under the pressure drop of 566, i.e. 2966 psig (inlet pressure) minus 2400 psig (outlet pressure).

Figure 3-5 shows a sequence of images of one spot in the micromodel taken during Experiment 1. In this sequence of images, time increases from left to right and from top

to bottom. As can be seen, the size of the blockages formed during the experiment increased with time and the leak was completely sealed.

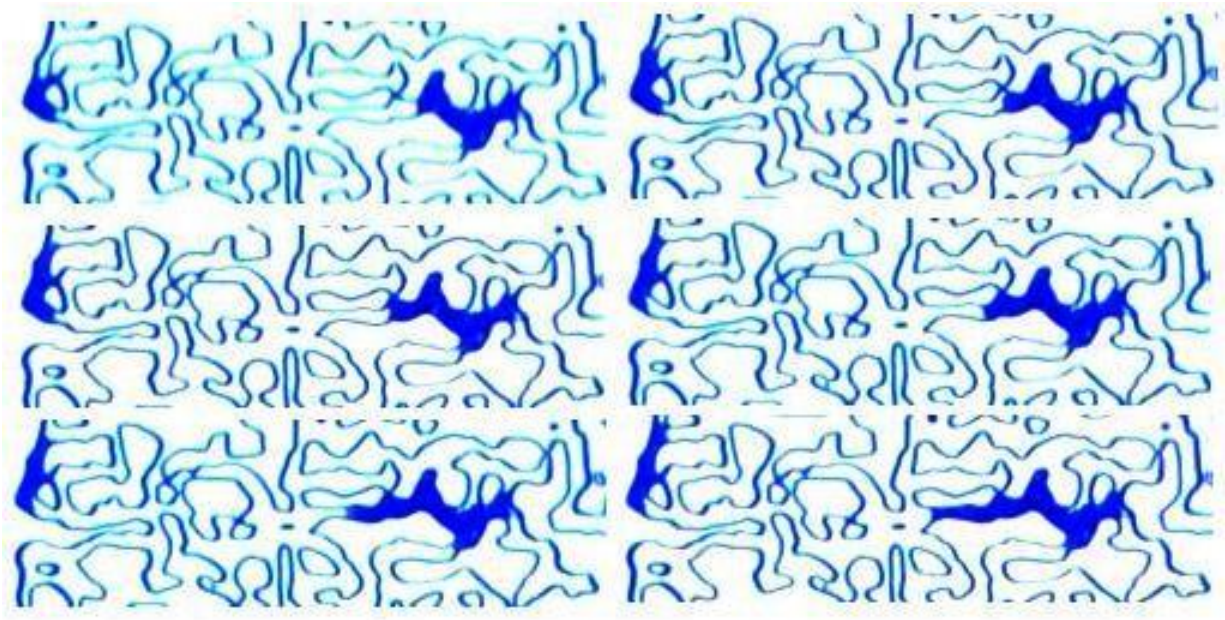

Figure 3-5: Development of complete plugging during Experiment 1 conducted under the pressure drop of 566, i.e. 2966 psig (inlet pressure) minus 2400 psig (outlet pressure).

Experiment 2 and 3, HWS-5, from 2966 to 2600 and 2700 psig

After successful sealing of the leakage of CO_2 at 2400 psig, it was aimed to test the performance of *HWS-5* at a lower pressure difference. In Experiment 2, the initial CO_2 storage pressure was again 2966 psig but the leakage happened at 2600 psig (366 psig pressure difference). As it is the case for the other experiments in micromodel visualisations here, the temperature of the test was 45 ^{o}C. The final scan of the micromodel taken in this test is presented in Figure 3-6. It can be identified that the amount of deposition is relatively lower in this test than that of the previous test (Experiment 1). Although precipitation of *HWS-5* took place at a pressure difference of 366 psig, however, the amount of precipitation was not enough to completely seal the leak. Magnified images of evolution of the particles and trapping of them have been demonstrated in zoomed snapshots shown in right side of Figure 3-6.

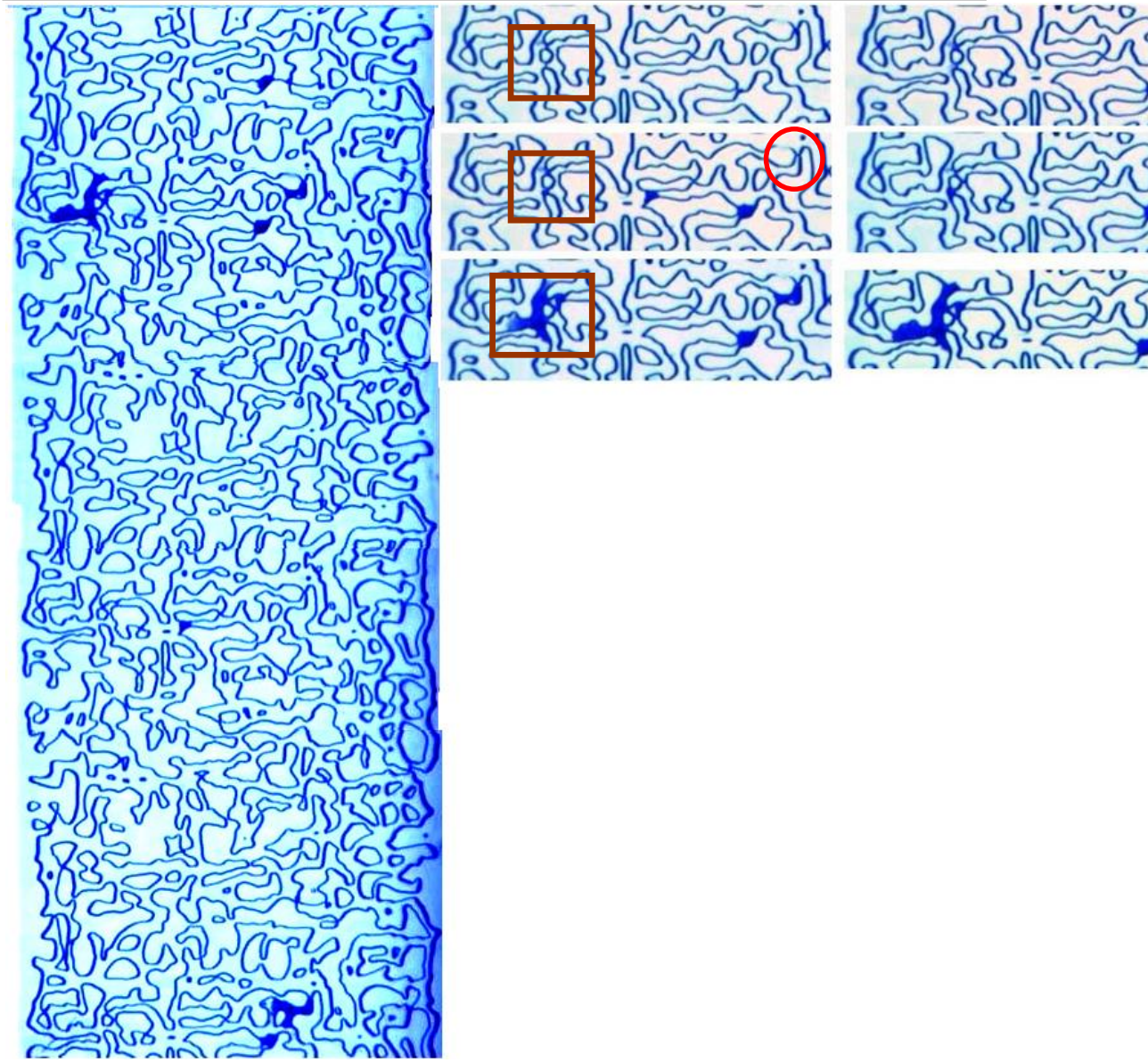

Figure 3-6: The progressive development of the precipitation inside the micromodel during experiment 2 conducted under the pressure drop of 366, i.e. 2966 psig (inlet pressure) minus 2600 psig (outlet pressure).

In the next attempt with of *HWS-5* (Experiment 3), the leakage pressure was increased to 2700 psig which reduced the pressure difference to 266 psig (difference between storage pressure of 2966 and leakage pressure of 2700 psig). The interest in lower pressure difference is to evaluate the performance of the leakage prevention method at low differential pressure that represents "creeping" flow which happens at low flow rates in the reservoir.

Figure 3-7 highlights formation of particles by "jet like" particle formation mechanisms in which, particles are formed when passing through a narrow pore (highlighted by the red circle) and subsequently adhere to an adjacent collector causing partial precipitation

and blockage. This finding indicates that the process of particle formation is a quasi-smart phenomenon which would target the main pores rather than filling the leakage path completely to stop the leakage.

Figure 3-7: Particle generation and filtration during Experiment 3 conducted under the pressure drop of 266, i.e. 2966 psig (inlet pressure) minus 2700 psig (outlet pressure).

3.4 Moderately Soluble Solutes

Two solutes, HWS-3 and HWS-2, with similar level of solubility have been used to investigate the impact of solute properties in similar range of solute solubilities. Table 3-1 shows some physical properties of the two solutes. After testing with HWS-3, HWS-2 (another solute) was used in order to investigate how chemical structure of solutes would affect nucleation of particles. Although the solubility of these two solutes is in a similar range, the interfacial properties are intrinsically different.

Table 3-1: Physical properties of the moderately soluble solutes used in the micromodel tests

	Molecular Weight (g mol^{-1})	Density (g/cc)	Melting Point (^oC)
HWS-3	152.15	1.056	81
HWS-2	136.23	1.08	270

3.4.1 HWS-3

Solubility Estimation

Figure 3-8 illustrates the solubility of the HWS-3 as a function of pressure. Also shown in Figure 3-8 is the density of CO_2 versus pressure. As expected, solubility of the solute in CO_2 increases as the CO_2 density increases. In fact, change of density with respect to

pressure is the basis of our CO_2 leakage prevention method. Regression of experimental data on the CO_2 density is known as the most applicable method for correlating the solubility data (Mendez-Santiago & Teja, 2000). Equation. 3-2 correlates solubility of HWS-3 in terms of CO_2 density and temperature.

$$\ln(y_2 P) = \left(\frac{1}{T}\right)\left(-7270 + 136700\rho_{CO_2} + 14.59T\right) \qquad \text{Eq. 3-2}$$

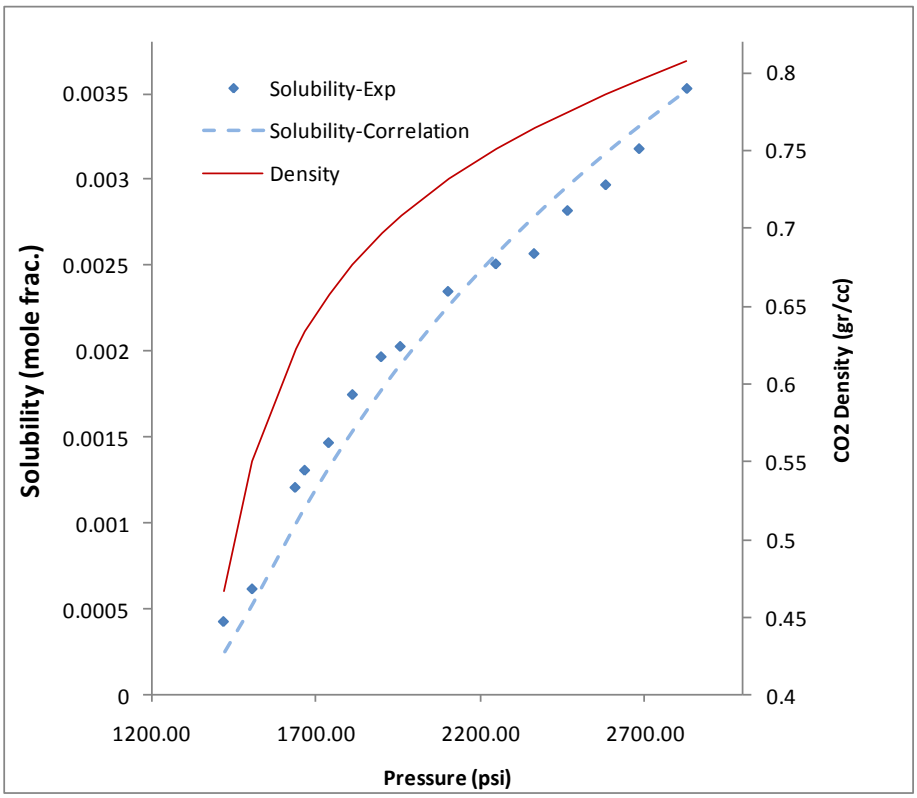

Figure 3-8: Solubility of HWS-3 and density of CO_2 at 45°C. (Gupta & Shim, 2006)

Preliminary Test

For first trial, with HWS-3, the mid-point of its solubility curve was selected at the pressure of 1800 psia corresponding to a solute mole fraction of 0.00175. This solute generally exhibits low solubility in CO_2 and hence, the concentration used in the test represents a dilute solution.

The mixture of CO_2 and the solute was kept in a cylinder at 1800 psia and 45°C while the micromodel was kept at 1200 psia and the same temperature as the CO_2 storage cell (45°C). In order to simulate the leakage, the valve connecting the CO_2 storage cell to the

micromodel was slowly opened allowing the CO_2 to flow through the micromodel and therefore imposing a pressure drop of 600 psi on the solution of CO_2 and the solute.

Figure 3-9 shows a sequence of three images of the micromodel taken during this test. As the pressure dropped, solute particles appeared in the form of cloudy suspensions and the colour of the CO_2 changed from initial clear and colourless (left image) to dark grey (middle image). However, it was observed that the particles had no tendency to attach to surface of the pores to form a blockage. Due to nature of the solute used, no precipitation occurred and the particles stayed in suspension form and moved through the pores. In this type of solute which exhibits no attachment, the main two parameters that govern the precipitation are concentration and particle size and evidently the particles are not sufficiently formed to get captured by the porous medium,

Figure 3-9: The appearance of HWS-3 during the preliminary test at which the pressure dropped from 1800 psig to 1200 psig. Initial state (left), suspension flow (middle), and final state (right).

Experiment 4, HWS-3, High ΔP

HWS-3 was used in this test with a concentration of 0.00353 mole fraction (double the concentration used in the preliminary test) at 2820 psig and temperature of 45^{o}C. The leakage pressure was kept at 1200 psig.

A series of five pressure drop shocks were applied in this test. Figure 3-10 shows the particle deposition as a result of the imposed pressure drop in the first pressure drop shock. It illustrates two clean (left) and the precipitated (right) images of the micromodel. The particles appeared in the vicinity of the outlet end of the porous medium. The main points where the precipitation has taken place in this image are highlighted by the dashed circles. According to Figure 3-10, the mechanism of precipitation at spot-A is related to

high aspect ratio between the pore and corresponding pore throat. It can also be attributed to high relative pressure drop in this particular pore-throat adjacent to the outlet end of the micromodel.

Figure 3-11 to Figure 3-14 show the image of the micromodel during the subsequent 2nd, 3rd, 4th and 5th pressure drop shocks, respectively. As can be seen, solute precipitation has significantly increased and has resulted in total blockage of the leak. In addition to the visual observation of the blockage formation, examination of the inlet and outlet pressure of the micromodel also confirmed that there was no pressure communication and the micromodel was fully blocked.

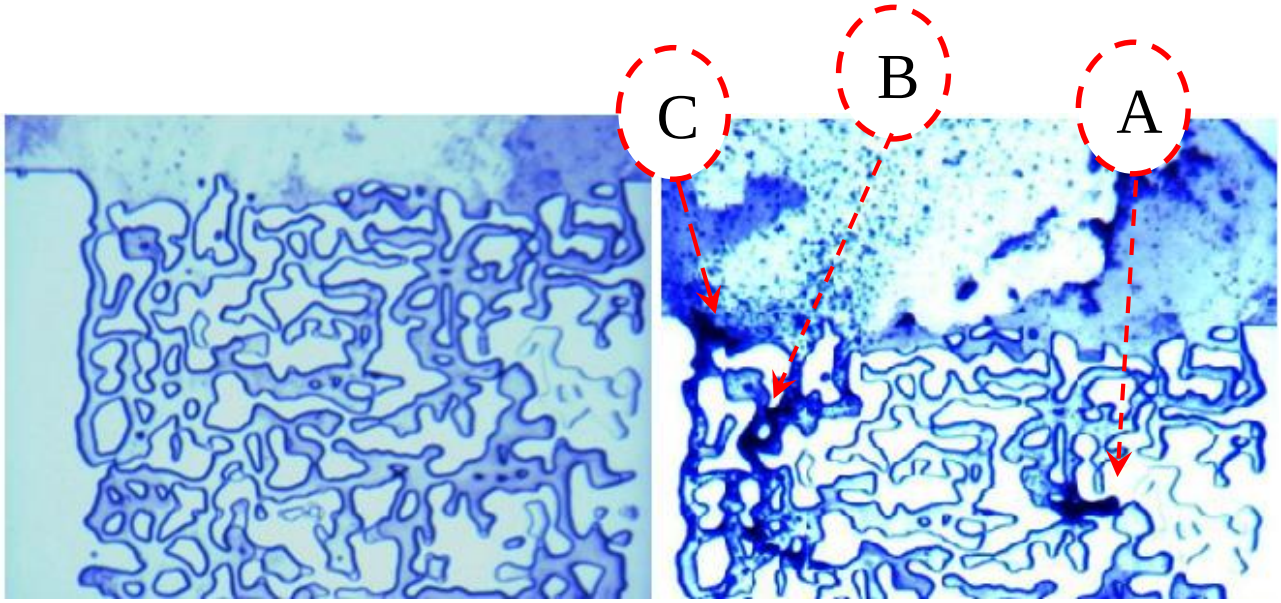

Figure 3-10: First pressure pulse of1620=2820-1200 psig during Experiment 4; A, B, and C are the main collector spots.

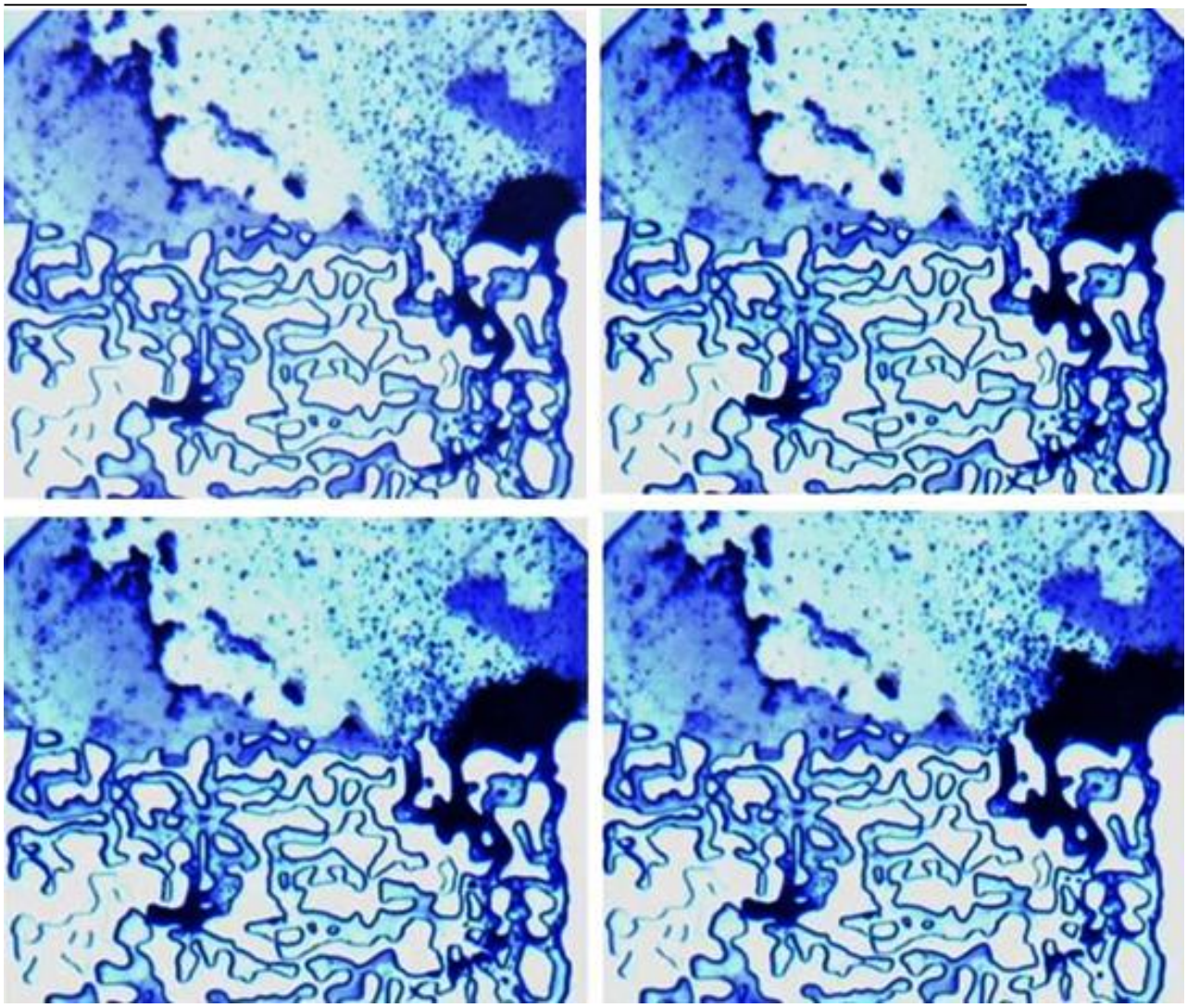

Figure 3-11: Second pressure pulse of 1620=2820-1200 psig during Experiment 4; evolution of precipitants from upper left to bottom right images.

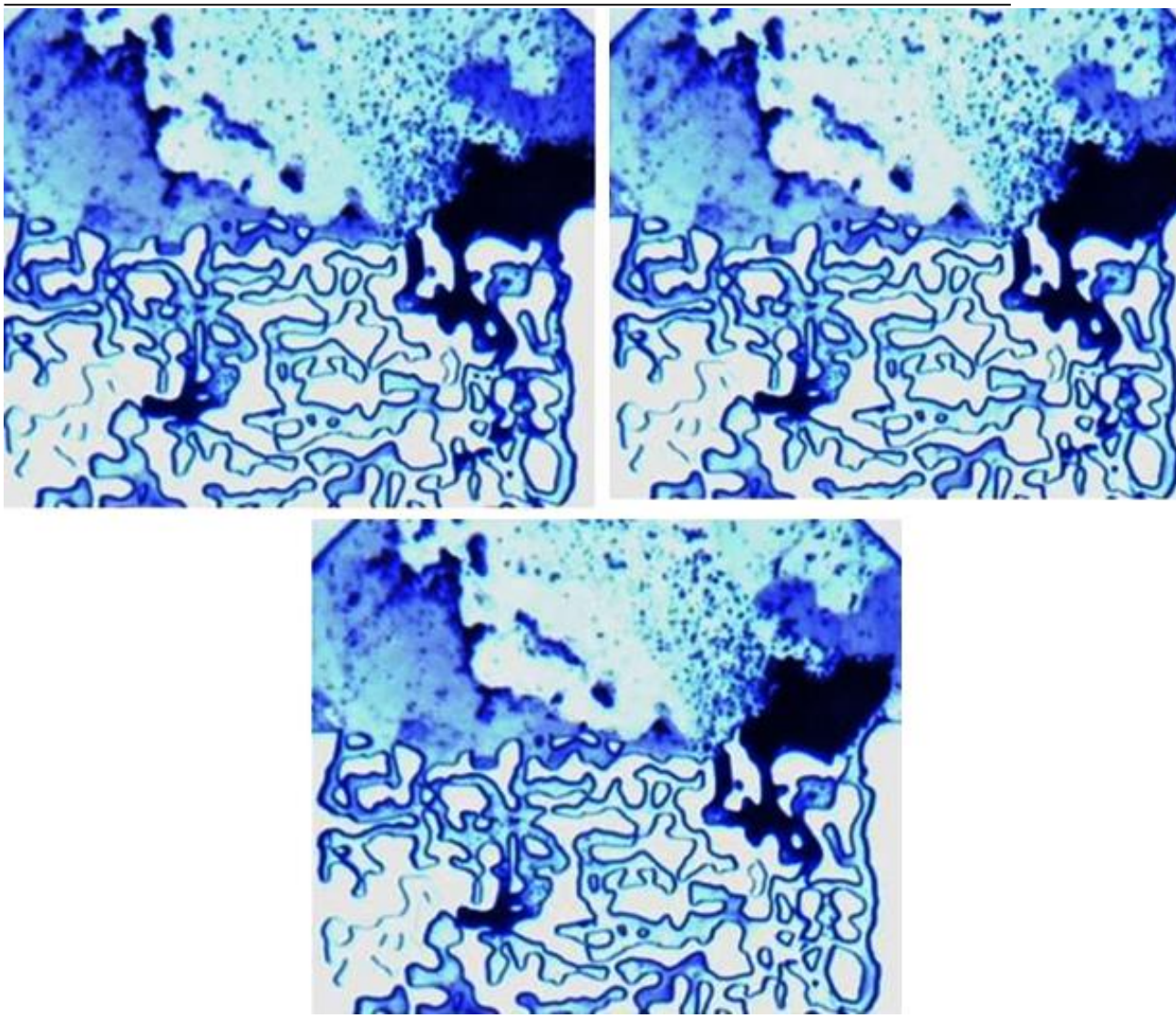

Figure 3-12: Third pressure pulse of 1620=2820-1200 psig during Experiment 4; washing out the deposits because of sudden flow.

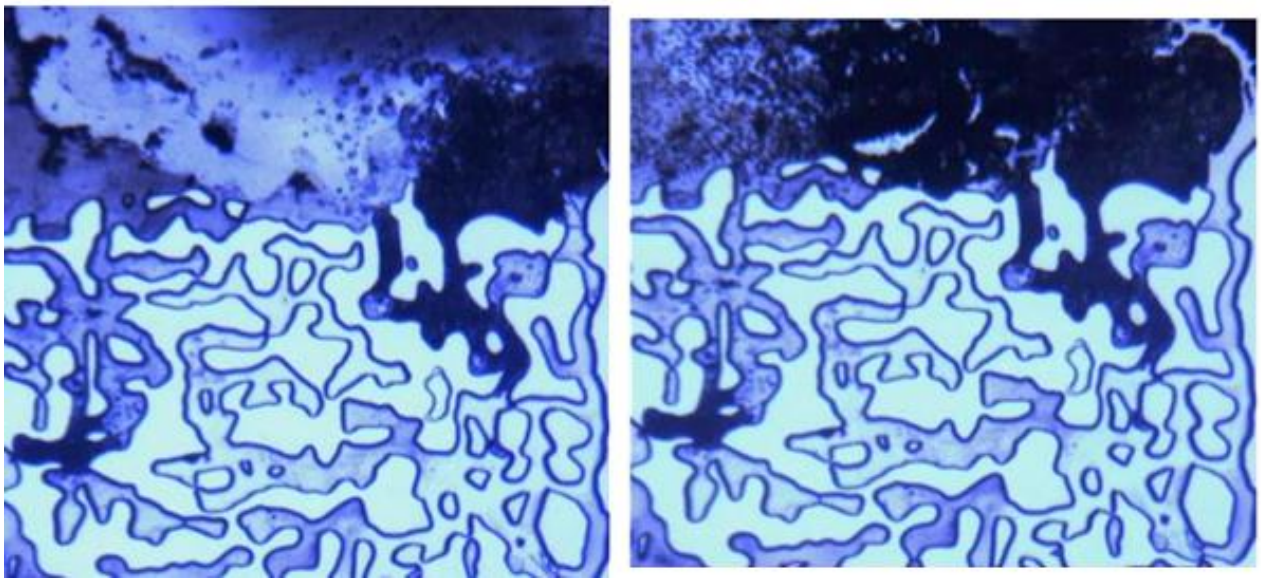

Figure 3-13: Fourth pressure pulse of 1620=2820-1200 psig during Experiment 4; growing the precipitation and establishing reclogging.

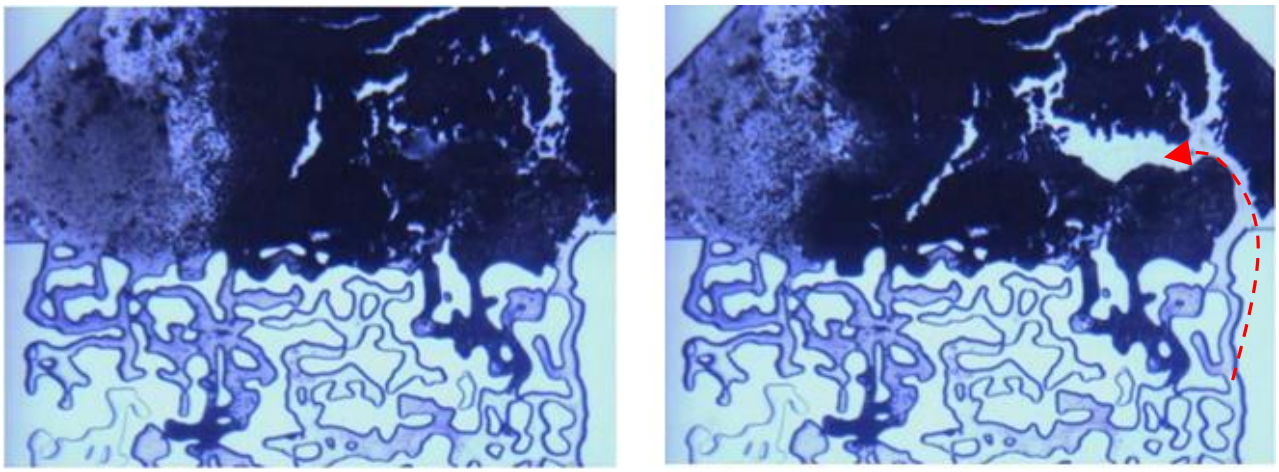

Figure 3-14: Fifth pressure pulse of 1620= 2820-1200 psig during Experiment 4; moving the particles as results of shock.

Figure 3-15 shows a visible tube connected to the porous medium downstream of the lockage which can be thought of a fracture in a real reservoir. It was observed that even after the blockage was formed in the leakage point, precipitation of solute continued in the tube. This favourable particle generation can be attributed to either the diffusion mass transfer between phases at the lower pressure region or negligible flow of the solution through the blockage body.

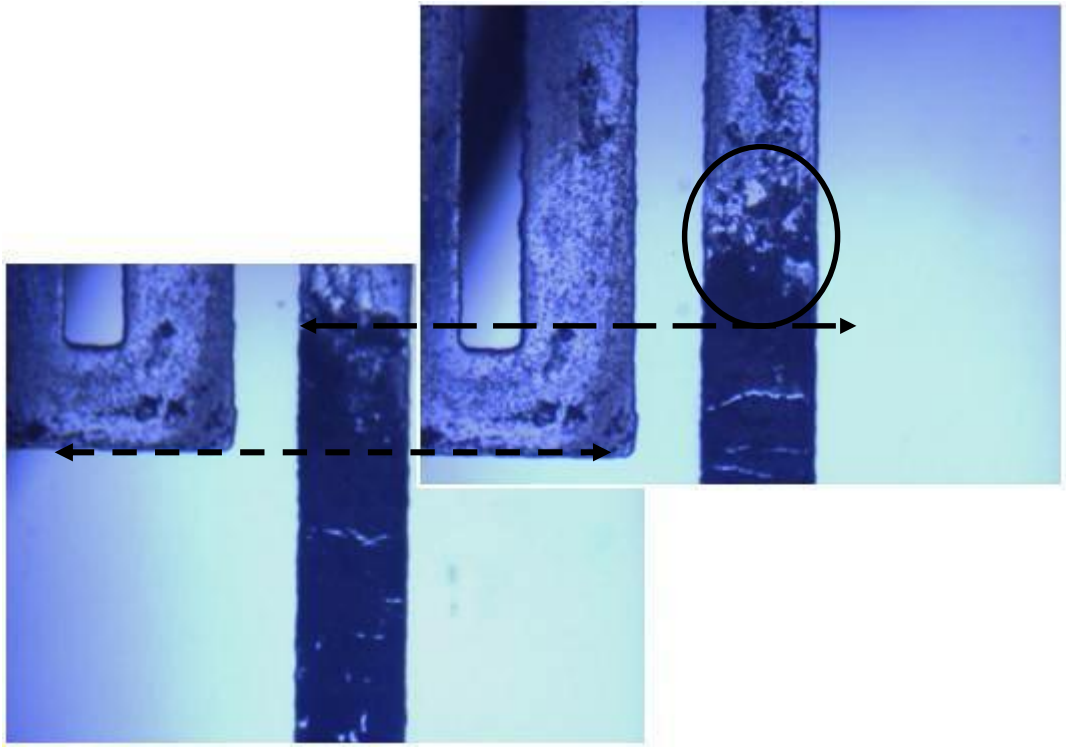

Figure 3-15: Spontaneous advancement of the blockage interface during Experiment 4. The black circle highlights the advancement of HWS-3 precipitants after 5 hours.

In summary, this test highlighted that the thermodynamic equilibrium cannot be assumed for such dilute system of fluids and the process of nucleation should be considered as a dynamic process rather than independent from time.

Experiment 5, HWS-3, High ΔP

In this test, an identical set of initial conditions was employed compared to Experiment 4 (previous test), i.e. same solute (i.e., HWS-3) and same pressure and temperature (2820 psia and 45^{o}C). The only difference between this test and Experiment 4 was the outlet leakage pressure, which was 1400 psig in this test as opposed to the previous test, which was 1200 psig. The aim was to gradually reduce the differential pressure (Dp) between storage pressure and leak pressure and to approach the conditions of creeping flow (low velocity) in the reservoir.

Figure 3-16 shows a sequence of images taken during this test. The process of the precipitation and blockage as function of time can be clearly seen in these image. It took only about one minute for the blockage to form and for the leak to stop fully after introducing the leakage.

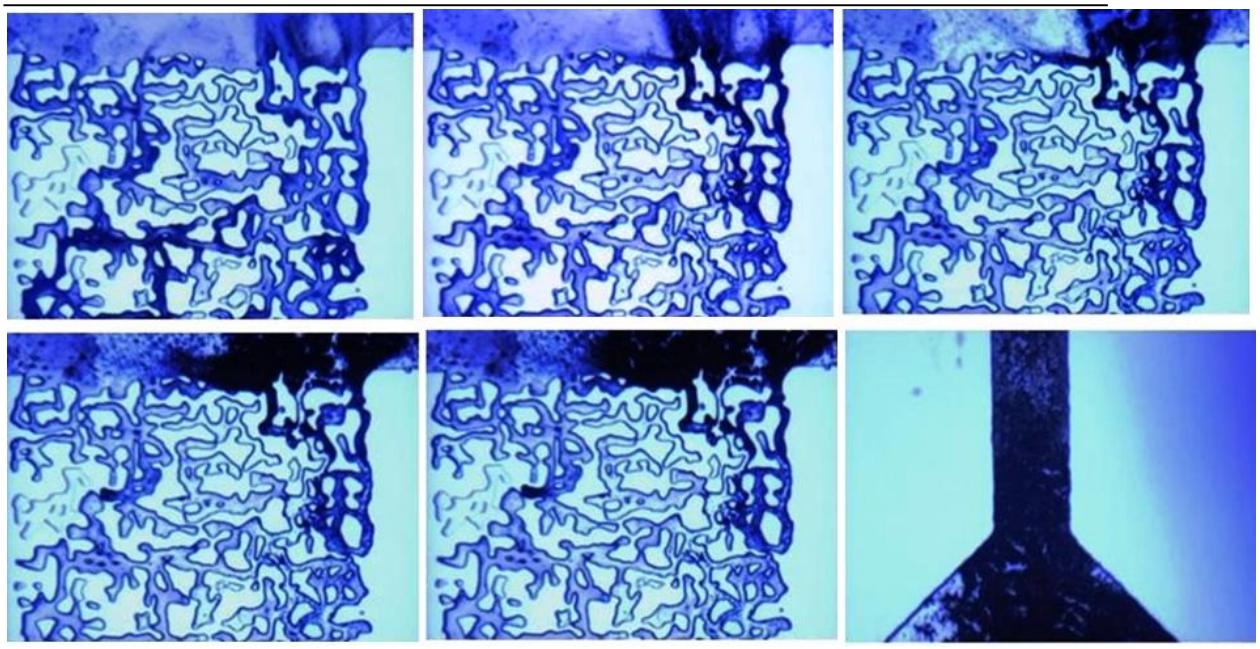

Figure 3-16: The process of blockage formation for HWS-3 in 2820 (inlet) – 1400 (outlet) psig.

Comparing the images from the previous test and Figure 3-16 shows that the same locations in the micromodel have been targeted by the solute and the progress and evolution of the blockage is also similar to the previous test. Spontaneous generation (advancement) of particles downstream of the blocked leakage was also observed in this test as demonstrated in Figure 3-17.

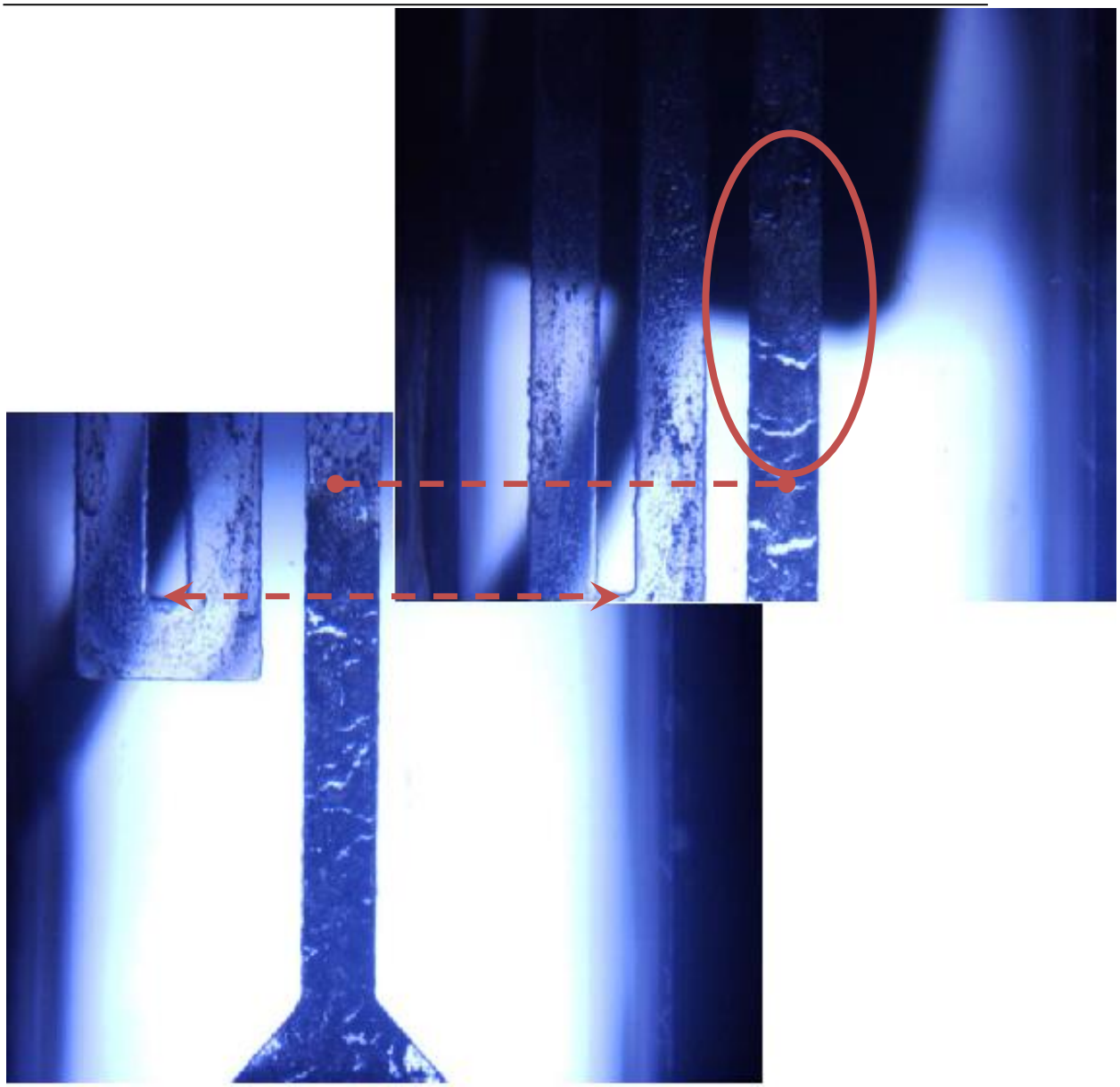

Figure 3-17: Spontaneous advancement of the blocked point after 5 hours during Experiment 5 conducted under the pressure drop of 1420 psig, which is highlighted by orange circle.

Experiment 6 and 7, HWS-3, Moderate ΔPs

The successful blockage of the leaks simulated with HWS-3 in the first two experiments at 1200 and 1400 psig was encouraging. In Experiment 6 and 7, the conditions of the tests were very similar to the previous two tests with the only difference being the leakage pressure which was raised to 2000 psig (as opposed to the previous tests which were carried out at 1200 and 1400 psig). Similarly to the previous two experiments, in these tests again the CO_2 storage cell was at 2820 psig. Figure 3-18 exhibits the log of pressure during Experiment 6. As can be seen, as soon as the leak was introduced, the pressure

dropped but it became quickly (2 minutes) stabilised (blocked) at 2778 psig as a result of particles precipitation due to activation of the leak prevention technique. Examination of the pressure of the inlet and the outlet of the micromodel also proved total blockage of the micromodel as no pressure communication between inlet and outlet could be detected. However, the blockage was not formed in the micromodel as it could "not" be seen in visible part of the physically simulated leakage path. Therefore, the blockage happened in the connecting flow lines. Inspection of the flow lines after the test confirmed that the lines were blocked by the precipitation of the solute. However, as can be identified from Figure 3-18, in this test, the blockage was not permanent and it reopened judged by the pressure drop at the late stage of the test after 40 minutes.

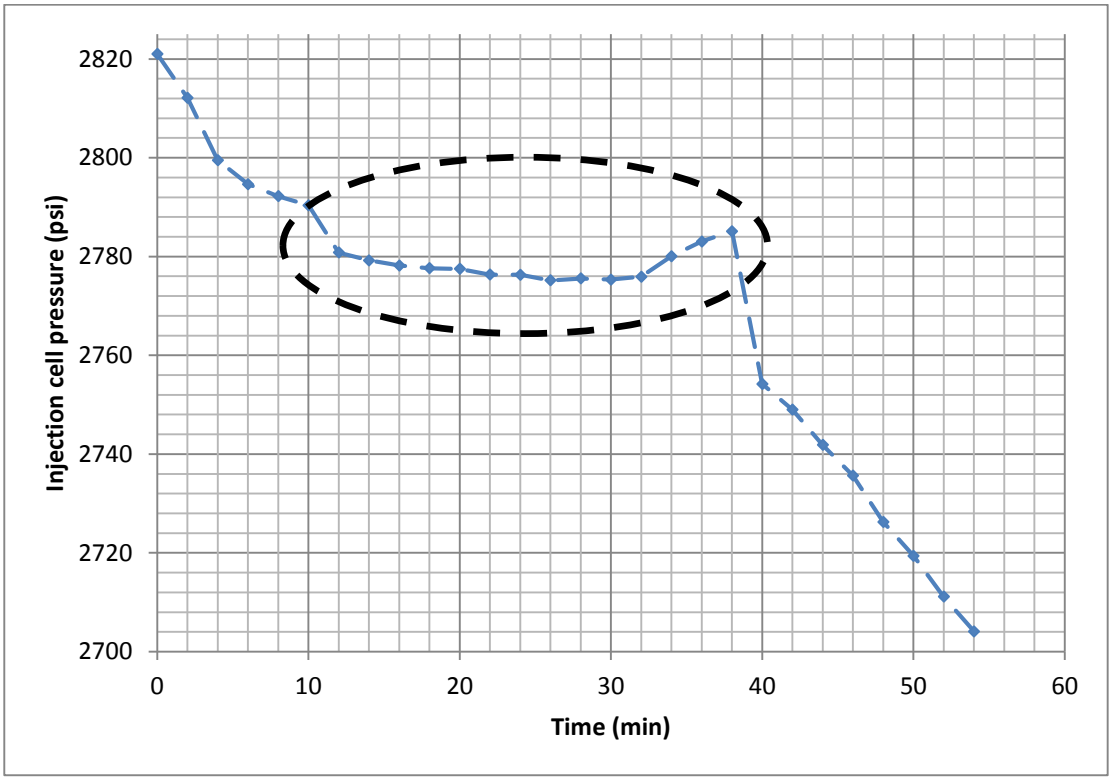

Figure 3-18: Pressure of injection cell during Experiment 6 conducted under the pressure drop of 820=2820-2000 psig.

Performing the test at the outlet leakage pressure of 2000 psig was partially successful since the blockage formed in response to leakage but it was not permanent. In the next test (Experiment 7) all conditions of the test was kept the same as the previous test apart from leakage pressure which was reduced from 2000 psig to 1600 psig. The log of pressure recorded in this test is illustrated in Figure 3-19. It is focussed in very early stages to better feature the pressure behaviour. The Figure shows that as soon as the leak is introduced, the pressure drops slowly and then stays constant which indicates formation

of a blockage and sealing of the leak. The strength of this blockage was tested for a few hours and no drop could be identified which reconfirms the presence of a strong and permanent blockage.

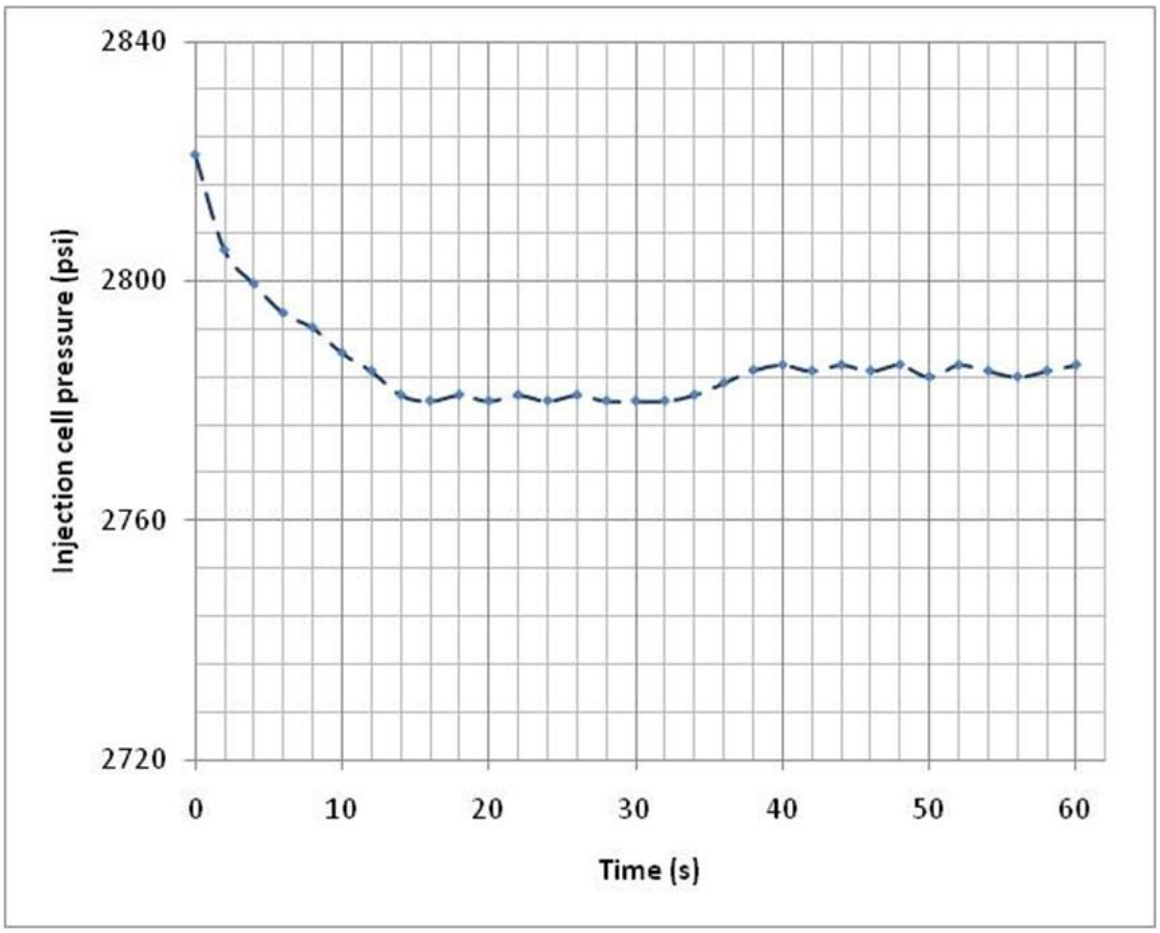

Figure 3-19: Pressure log of the injection cell during Experiment 7 conducted under the pressure drop of 1220psig.

3.4.2 HWS-2

In the previous tests, HWS-3 was used as a moderately soluble solute, which was effective. The previous tests demonstrated the effect of the kinetics of solute precipitations and the effects of solute structure on particle formation in terms of particle size and critical supersaturation. In this test a different solute, HWS-2, has been used to evaluate its performance in comparison with HWS-3.

Solubility correlation

In order to be able to compare the performance of HWS-2 with that of HWS-3, this test was carried out under similar conditions of pressure and temperature and also solubility as the previous test with HWS-3 was carried out. However, no experimental data on the solubility of HWS-2 at temperature of 45 ^{o}C is available in the literature. Using the published data at 60 ^{o}C and 70 ^{o}C and using the general solubility correlation**,** the solubility data at 45 ^{o}C was predicted.

Figure 3-20 and Figure 3-21 depict the correlation between CO_2 density and the solubility of HWS-2 at temperatures of 60 ^{o}C and 70 ^{o}C along with the fitted correlation in dashed blue line. Due to constraints on regression parameters, it is necessary to tune the correlation with at least two different isothermal solubility curves. The mean square errors of the correlation at 60 ^{o}C and 70 ^{o}C are 0.0006 and 0.00158 respectively which reveals that the regression is biased toward lower temperature.

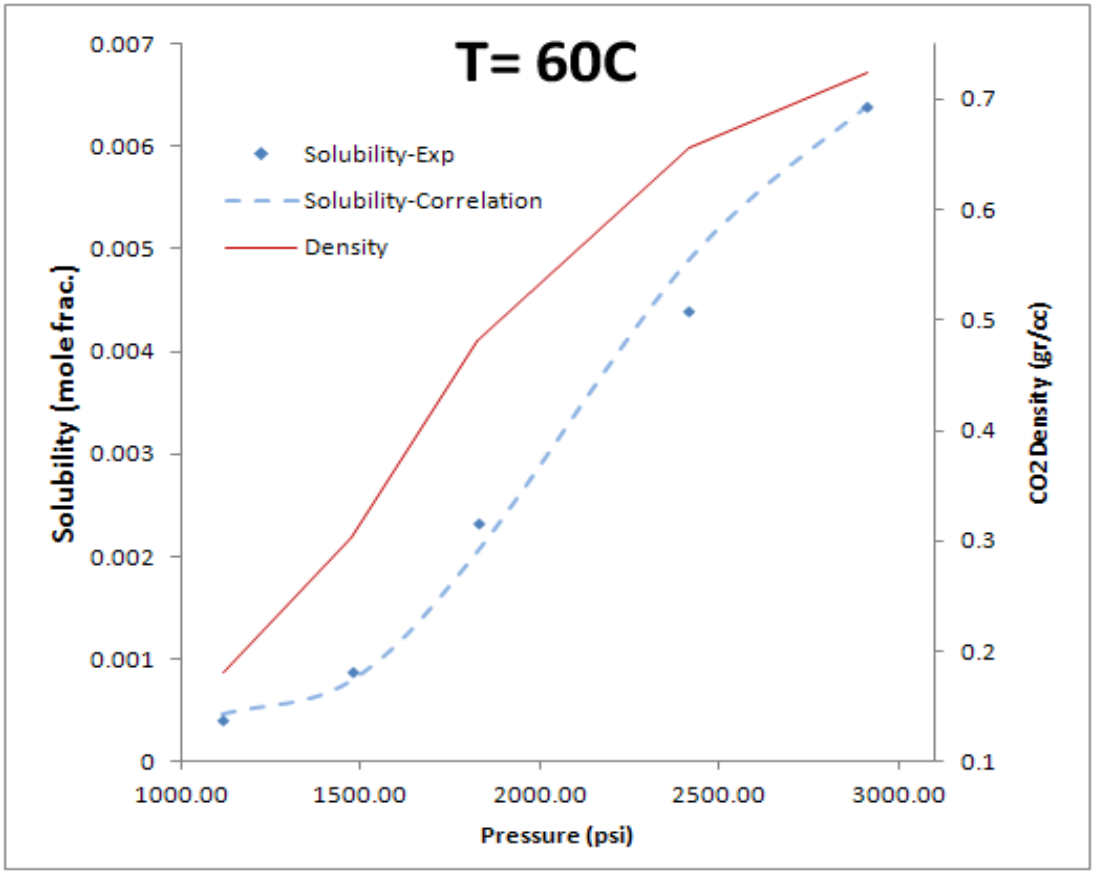

Figure 3-20: Isothermal solubility correlation of HWS-2 at 60 ^{o}C.

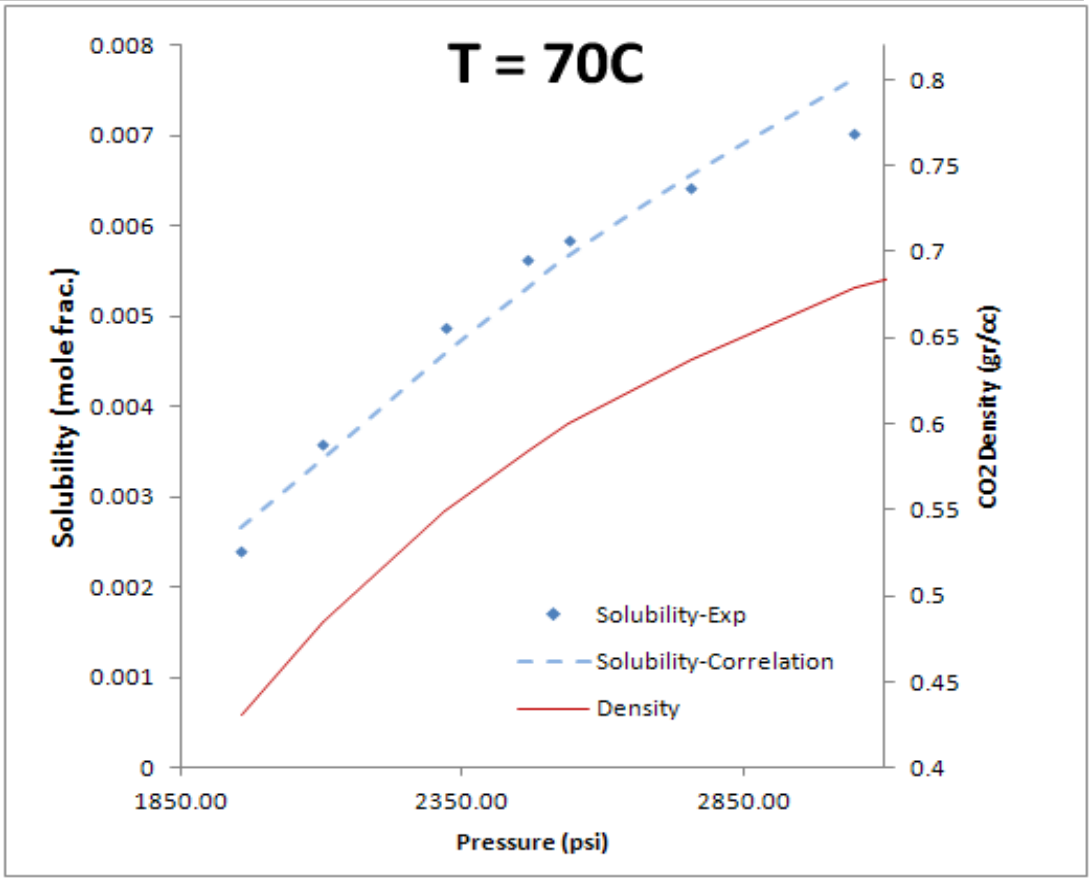

Figure 3-21: Isothermal solubility correlation of HWS-2 at 70 °C.

Results of the prediction of the solubility data for HWS-2 at the temperature of 45 °C are presented in Figure 3-22 and represented by Equation 4-3. The trend of the solubility correlation resembles that of CO_2 density. Nevertheless, the solubilities of HWS-3 and HWS-2 are different resulting in higher degree of supersaturation for HWS-3. Figure 3-22 (right) also shows the supersaturation degree of HWS-3 and HWS-2, which can be considered as an indication of the driving force of the nucleation in both solutes and hence it is higher for HWS-3. Up to this point, it would be interpreted that HWS-3 would nucleated faster than HWS-2 but considering nucleation theory, other parameters are also involved such as interfacial properties which makes the phenomenon to be case dependent.

$$\ln(y_2 P) = \left(\frac{1}{T}\right)\left(-10066.12 + 96153.75\rho_{CO_2} + 25.72279T\right) \qquad \text{Eq. 3-3}$$

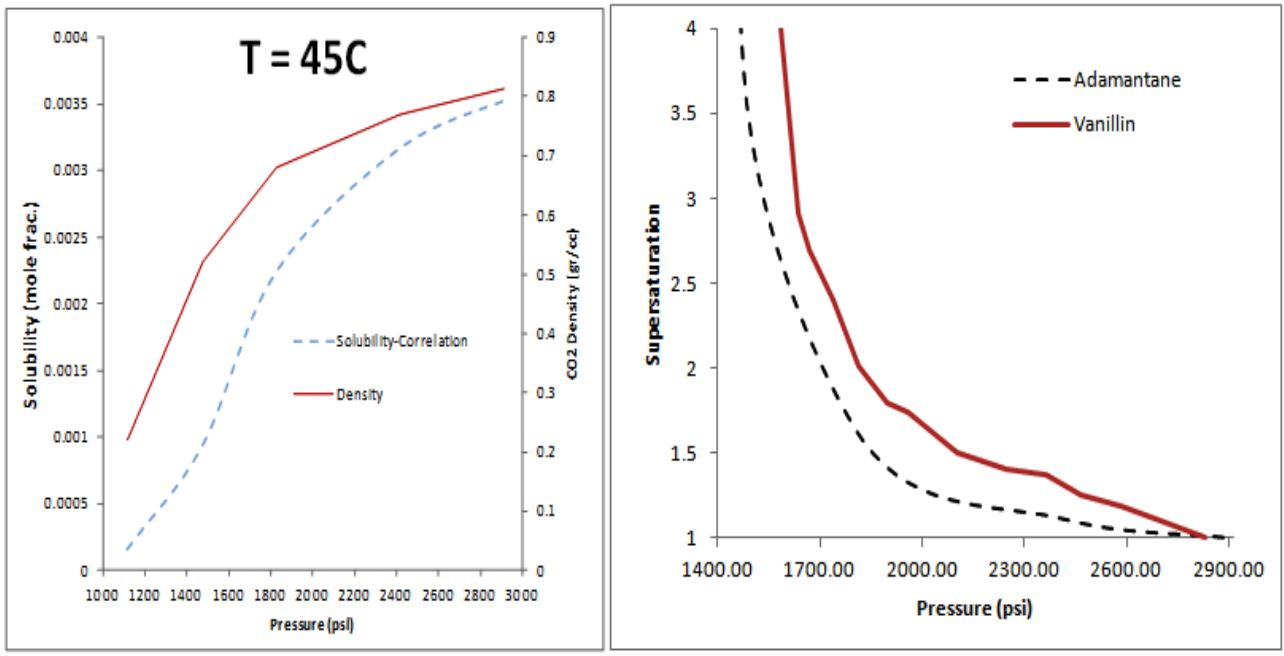

Figure 3-22: Left graph; prediction of isothermal solubility of HWS-2 at 45C. Right image: isothermal supersaturation of HWS-3 and HWS-2.

Experiment 8; HWS-2, high ΔPs

The first trial test with HWS-2 was carried out with a high DP (differential pressure. In this test (Experiment 8), the CO_2+solute sample was prepared at 2905 psig and 45ºC and the downstream (leakage) pressure was set at 1200 psig which was very close to subcritical conditions of CO_2. Figure 3-23 presents a sequence of images showing the state of the micromodel during this test and as solute precipitates in the pores in the micromodel. The blockage has taken place at the end face of micromodel and efficiently blocked the leakage path. The blockage was stable and lasted for about 20 hours with a pressure difference of 1705 psig applied between the micromodel ends.

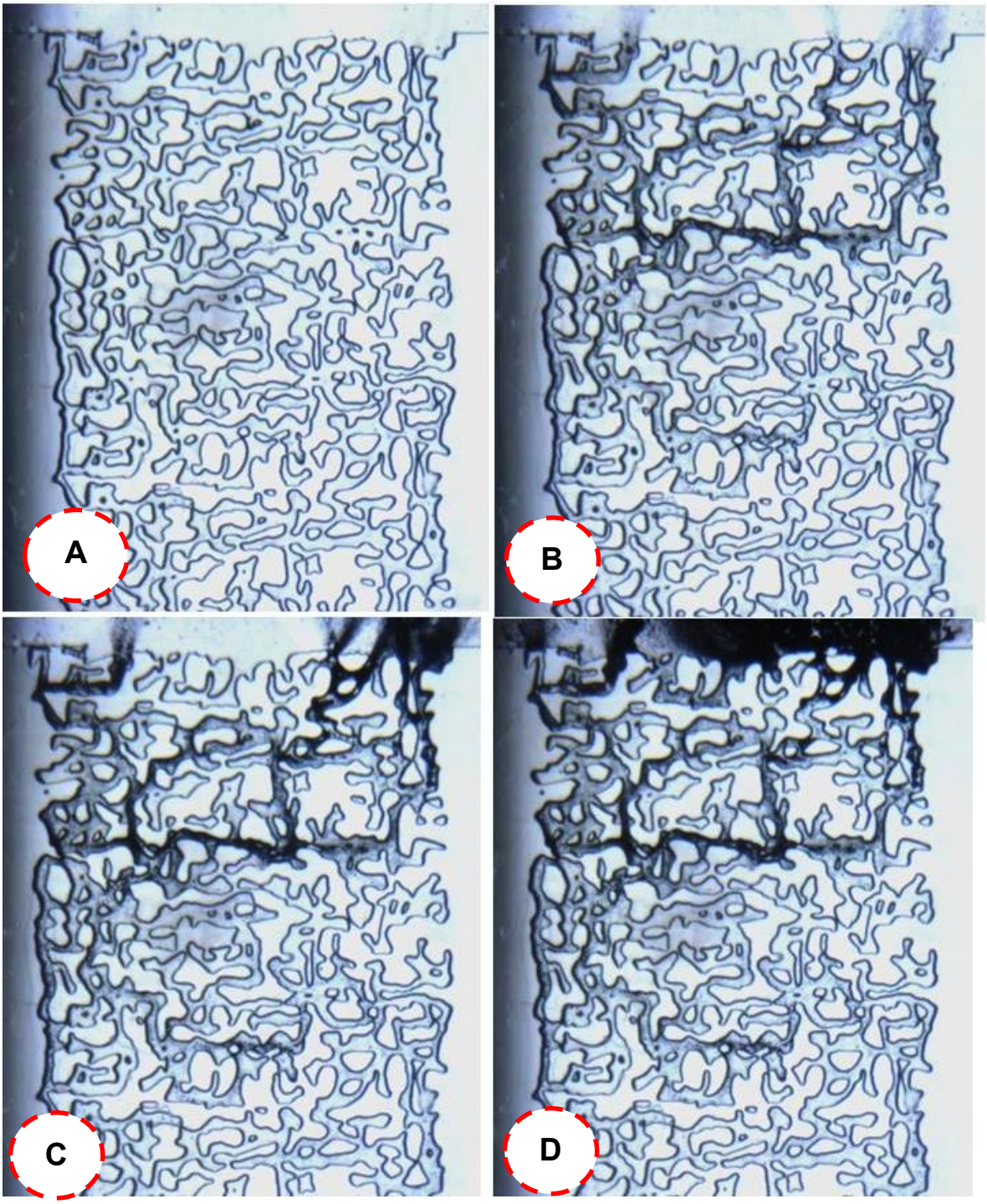

Figure 3-23: Leaking at Dp=1200 psig; (A) clean state of the micromodel at the beginning of the test, (B) start of particle formation, (C) particle precipitation, and (D) formation of a full blockage.

As can be visualised, HWS-2 particles started to form at the outlet end of porous pattern as manifested like dark powders. Also, HWS-2 particles did not fully pack the entire length of micromodel. In other words, it can be identified that the particles have targeted the main flow path smartly. Therefore, once this technique becomes activated in real storage reservoirs due to encountering a leakage path, it is not necessary to completely

fill the leakage path; the proposed leakage method would smartly precipitate its solids in main pores.

Experiment 9: HWS-2 with pressure drop of 1000 psig

This experiment was carried out similarly to the previous experiment using HWS-2 as solute. The pressure and temperature at which the CO_2 was stored was also the same as the previous test. The test was carried out with the aim of observing the performance of HWS-2 at lower pressure drops. While the pressure of the stored CO_2 was 2900 psig, the pressure at which leakage took place was 1900 psig resulting in a differential pressure (DP) of 1000 psig as opposed to the previous test with a DP of 1700 psig. Figure 3-24 presents a sequence of images taken during this test, which show how the precipitation evolved at end face of the porous medium.

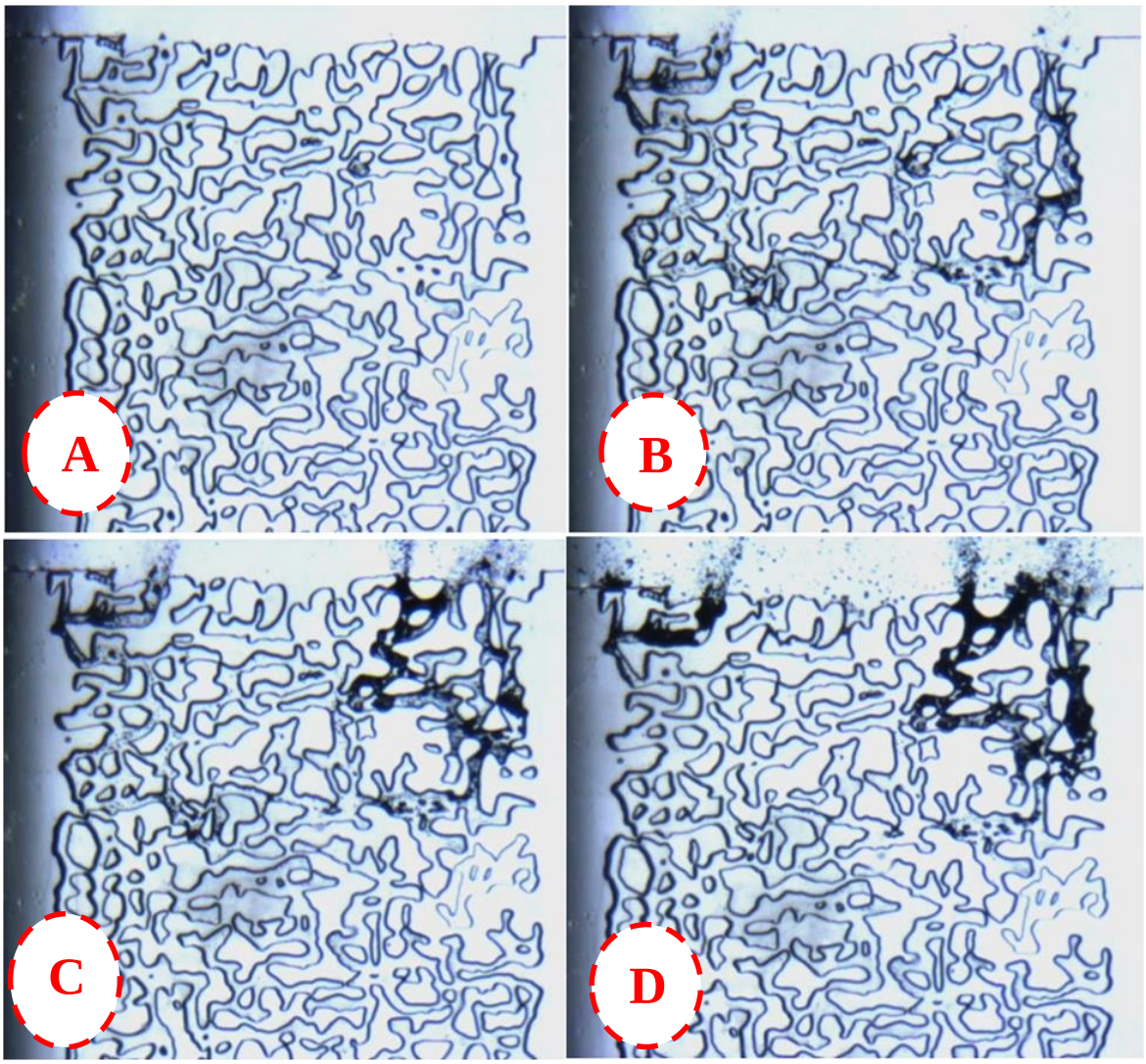

Figure 3-24: leaking at 1900 psig; (A) initial state of the micromodel before leakage, (B) start of particle formation, (C) particle precipitation, and (D) full blockage.

Very similar mechanisms of particle precipitation and blockage formation, which were observed in the previous test with HWS-2, were identified for the lower DP in this test as well. The blockage is more concentrated in terms of amount of solute formed in the flow path. The concentrated clogging bodies are attributed to the concept of larger particle formation near the critical supersaturation point and consequently, less precipitation is required to prevent leakages.

Experiment 10: HWS-2 with pressure drop of 900 psig

After successfully blocking the leakage in the previous test using HWS-2 at the pressure drop of 1000 psig, another test was carried out using HWS-2 and pure CO_2 at lower pressure drop (DP) of 900 psig. Testing with lower DP is of interest because it shows sensitivity of the leakage prevention process to small leaks.

Figure 3-25 shows the stages of the development of the blockage as a result of solid particle precipitation. Lower degree of supersaturation (or DP) was required for formation of particles using HWS-2 compared to that of HWS-3. The mechanism of precipitation and build-up of the plug was quite similar to the previous tests in terms of formation of large particles in the leakage flow path. A complete blockage of the leak was observed, however, unlike the previous tests, the blockage in this test was not very durable.

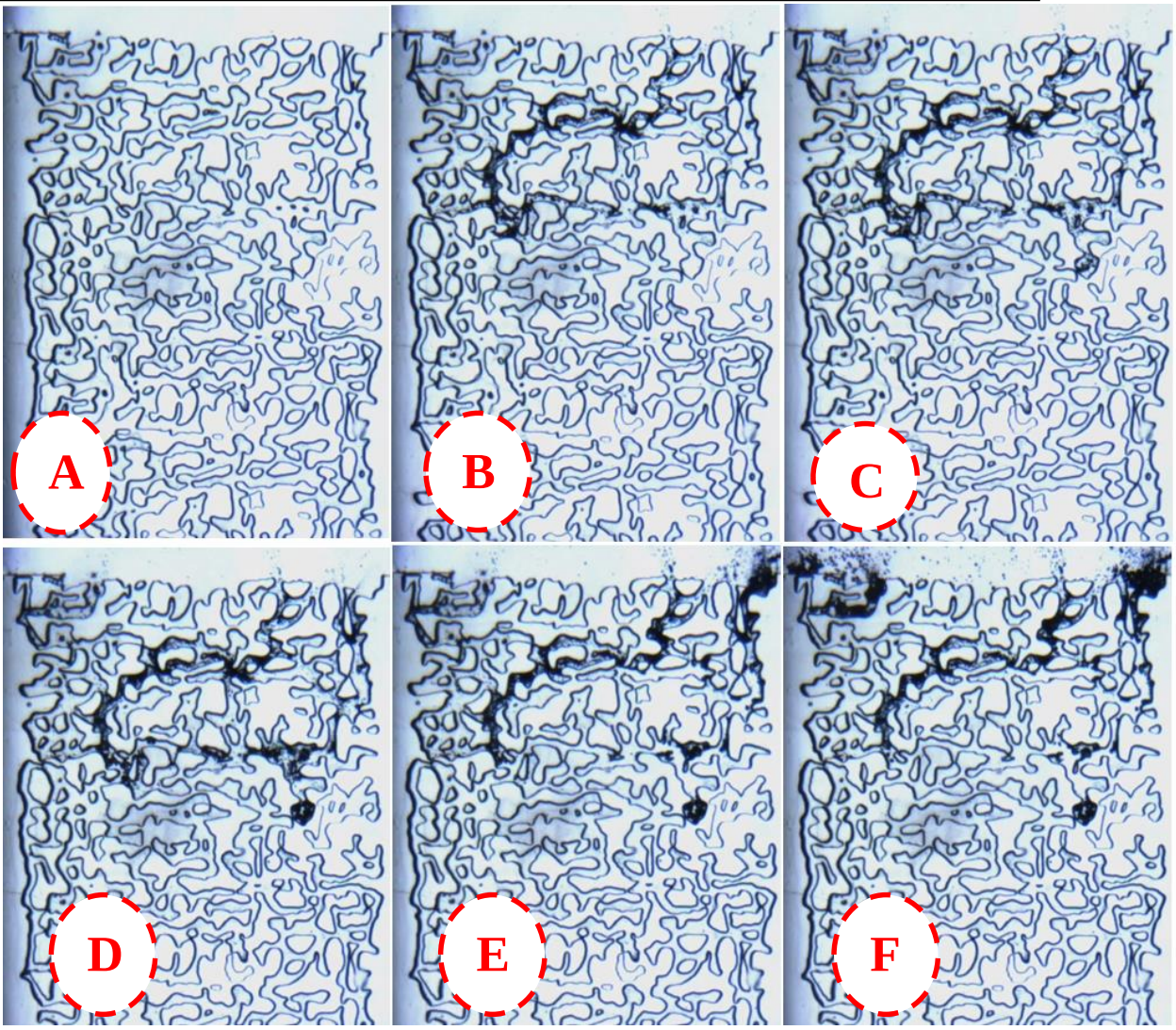

Figure 3-25: Micromodel test with HWS-2 from 2905 (storage pressure) to 2000 psig (leakage pressure). (A) Initial state of micromodel at the start of the test, (B) Start of particle nucleation during leakage. (C) Partial plugging, (D) Successive accumulation of particles in other flow path at right side of micromodel, (E) Solute precipitation at left side of micromodel, and (F) Full blockage against the flow path.

Obviously, the durability of the blockage is the one the main issues in application of this leakage prevention technique. To analyse the durability and strength of the blockage, the pressure discontinuity between the two ends of the blocked region was measured and recorded. In this experiment, the blockage opened up after sometime and hence pressure continuity was re-established. The sequence of the three images shown in Figure 3-26 shows the removal of the blockage from some of the previously blocked locations.

However, it should be noted that the sizes of the pores in micromodels are typically much larger than what would be expected in a real reservoir rock and therefore the removal of the plug observed for the condition of this experiment may not take place in a real reservoir rock. To verify these observations, similar experiments must be carried out in cores in order to test the stability of the blockage under various conditions.

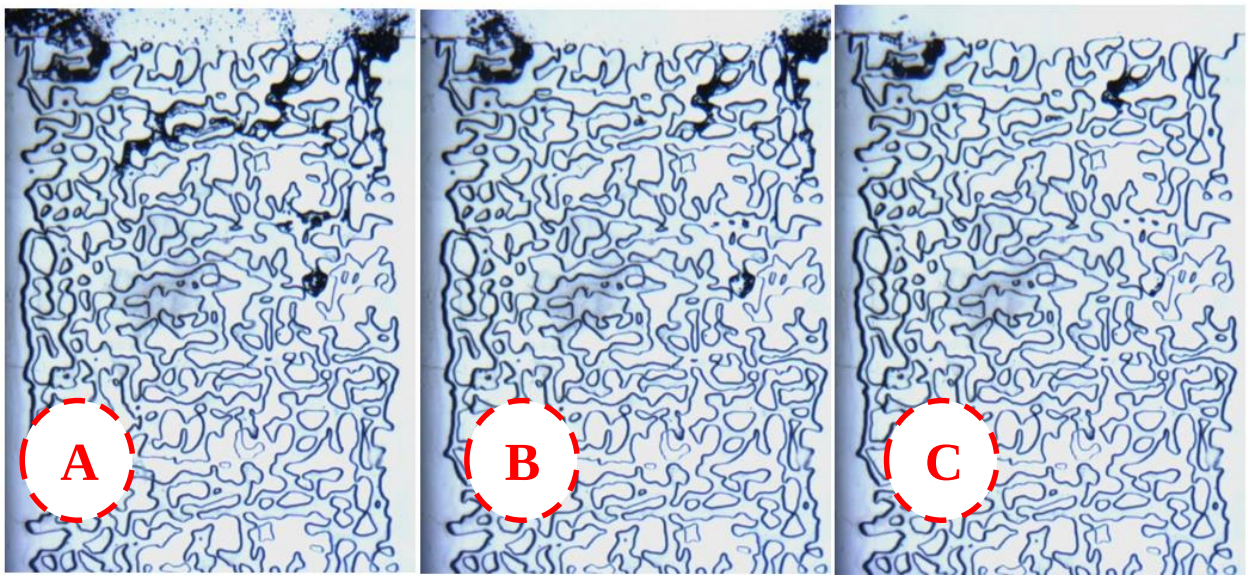

Figure 3-26: Reestablishment of flow through the micromodel; (A) Full blockage of micromodel. (B) Disintegration of the plug, and (C) Flow through the micromodel re-established.

The tests carried out in micromodel using HWS-3 and HWS-2 demonstrated that every solute has its own response to pressure disturbance and formation of blockage. These two solutes have similar solubility at prevailing conditions of the tests but the results of micromodel experiments revealed that chemical structure of the solute has more profound impacts on the nucleation kinetics of the solid solutes compared to the degree of supersaturation (differential pressure). According to the results of the micromodel tests, HWS-2 nucleates in pure CO_2 solution faster than HWS-3 even though HWS-3 has higher supersaturation than HWS-2 in test conditions. However, the nucleation theory conceptualizes the supersaturation level as the main parameter in formation of a new phase for completely identical substances. In summary, to achieve a highly responsive solute or mixture of solutes, not only the solubility data is needed but also the parameters pertinent to nucleation kinetics (e.g., interfacial tension) have to be studied thoroughly.

In the next part of this chapter, the results of one sightglass test will be presented and discussed.

3.5 Marginally Soluble Solute (HWS-1)

Unit price of the solutes and their solubilities are important selection factors and therefore they have to be considered as parts of economic evaluation of the LPT. Based on the current market prices of HWS-1, the bulk price of this solute is only 0.21 $/kilogram which makes it very attractive compared to some other more expensive solutes that we have used in this study. The HWS-1 solubility is very low (Serin, et al., 2010) and the estimated cost of using HWS-1 in a storage reservoir with an average pressure of 2500 psig and temperature of 45^{o}C and based on 0.0003 mole fraction solubility is 0.04 $ per tonne of CO_2 stored. The favourable economy of HWS-1 could be a motivation to investigate its performance as a solute in the LPT.

Solubility Estimation

HWS-1 solubility at test temperature is not available and it needs to be measured or estimated from correlations. In this report, solubility profile is estimated via a widely used correlation for dilute solutions. Solution of solid solutes and CO_2 is categorized as a diluted mixture and hence, the solubility can be obtained using an expression in which solubility of a solute is controlled by solvent (CO_2) density, temperature and pressure.

Figure 3-27 demonstrates the correlation fitted onto experimental HWS-1 solubility at temperatures of 60^{o}C and 100^{o}C (Serin, et al., 2010). At test temperature of 45^{o}C, the resulting correlation can be used to estimate HWS-1 solubility variations with respect to pressure. Figure 3-28 illustrates the solubility profile as a function of pressure at isothermal conditions of 45^{o}C.

Having estimated the HWS-1 solubility in supercritical CO_2, various pressure drop values were imposed on the CO_2 + HWS-1 solution to investigate its response to different leakage scenarios. The micromodel experiments were designed to; firstly, detect the onset pressure of particle formation and secondly, visualise the formation of consequent blockages.

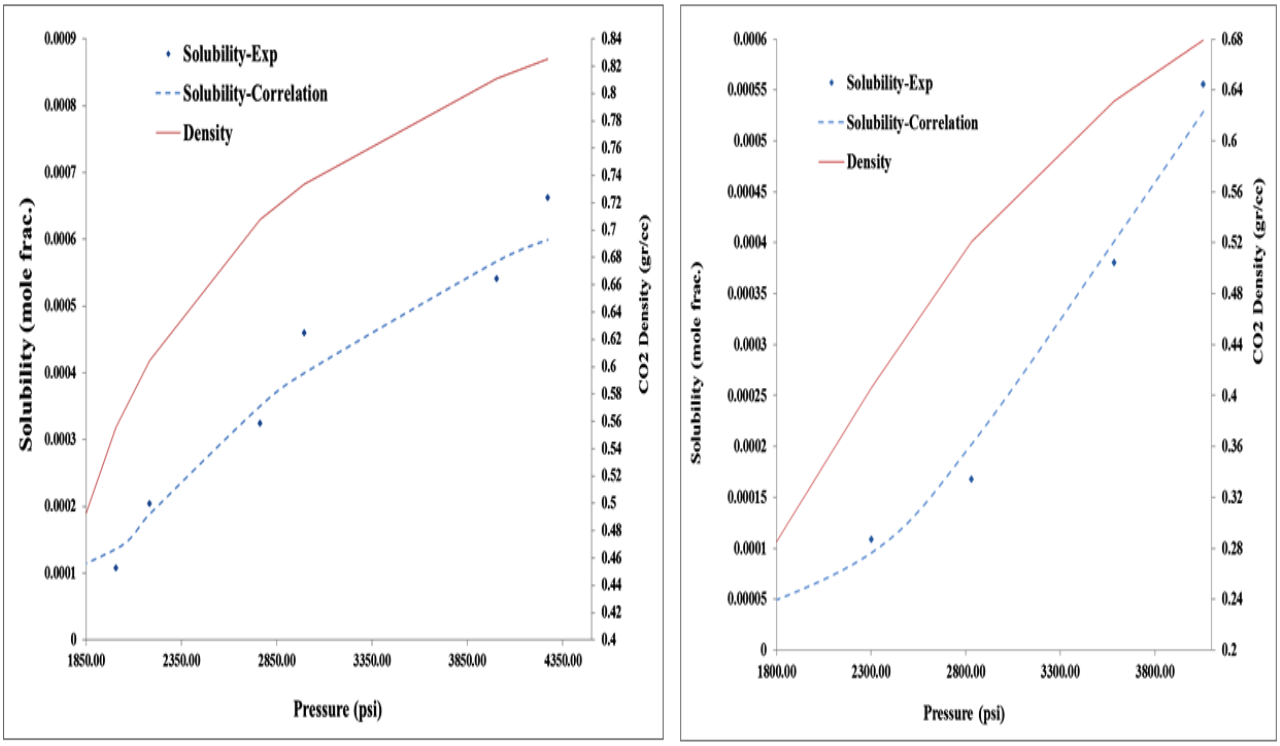

Figure 3-27: Isothermal HWS-1 solubility at temperatures of 60 ^{o}C and 100 ^{o}C extracted from literature.

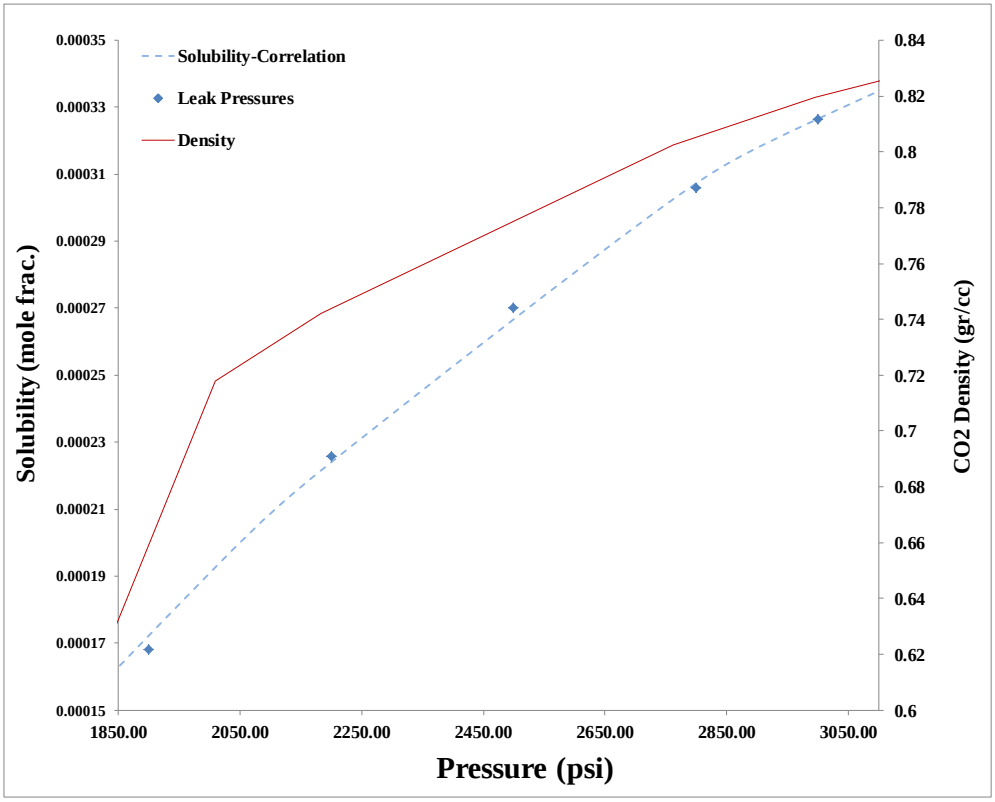

Figure 3-28: Isothermal HWS-1 solubility predicted by a correlation tuned to literature data to predict the corresponding value at micromodel tests temperature (45 ^{o}C).

Experiment 11: Detecting onset pressure of particle formation (2000 psig)

The onset pressure, at which a new phase is formed, should be determined for new solutes selected for our investigation. After saturating the micromodel with (gas-like) solution of HWS-1+CO_2 at pressure of 3000 psig and 45^{o}C, the micromodel pressure was reduced gradually by withdrawing the solution into the leak cell (Figure 3-1). The rate of pressure reduction was set at a low rate of 5 psig/min. Since the pore volume of the micromodel is around 0.01 cc, the particles formed in this porous medium can be easily carried away at higher flow rates and hence, this ultralow rate of pressure decline was chosen to allow settling the particles. Furthermore, lower pressure decline rate ensure a more accurate determination of the onset pressure for particle formation. The micromodel pressure was continuously recorded while the images of a selected section of it were taken to identify and capture the formation of micro-scale particles.

Figure 3-29 shows two images of the micromodel at the initial and the particle formation onset stages of this test. The HWS-1 particles started to appear when the micromodel pressure decreased to 2000 psig from the initial pressure of 3000 psig. Solid HWS-1 can be seen in the form of small dark spots. That is, the solution should experience 1000 psig of pressure drop to see HWS-1 particles as a separate phase. In field application terms, if the solution (HWS-1 + CO_2) is to be stored at 3000 psig and 45^{o}C, the HWS-1 particles will be formed along a leakage path under a pressure drop of 1000 psig.

Another feature of Figure 3-29 is the size and the number of the particles in the micromodel. The size of the formed HWS-1 particles is less than 10 micron, which is much smaller than previously used solutes (HWS-2, HWS-3, HWS-5). Figure 3-30, is a magnified image of the micromole which shows the size of the HWS-1 particles. The smaller size of the HWS-1 particles would have two impacts (in opposite directions) on the efficiency of the blockage; firstly, they would be packed easier, which could potentially lead to a firmer blockage. Secondly, smaller particles would have higher tendency to stay in the suspension form compared to larger granules. However, our visualization experiments show that the HWS-1 particles tend to deposit, rather than stay as suspension. The relatively small number of solid particles, which were formed at this pressure drop, can be attributed to ultralow solubility of this solute.

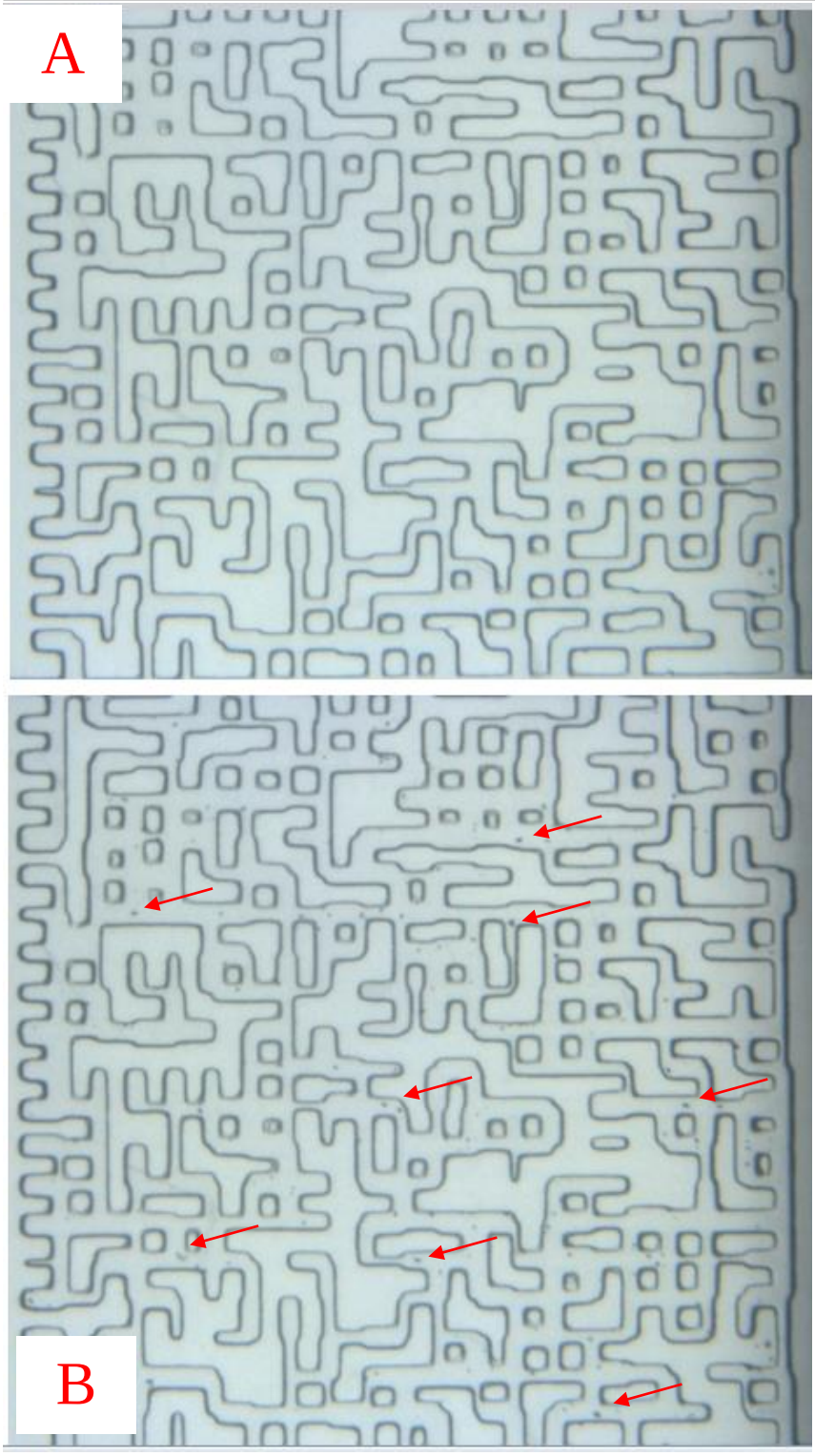

Figure 3-29: A magnified sections of the miromodel demonstrating the formation of HWS-1 particles at the leak pressure of 2000 psig; (A) the top image shows the initial clean state of the micromodel, (B) the bottom image taken from the same location of micromodel illustrates the appearance of dark spots, i.e. HWS-1 particles when leakage was applied.

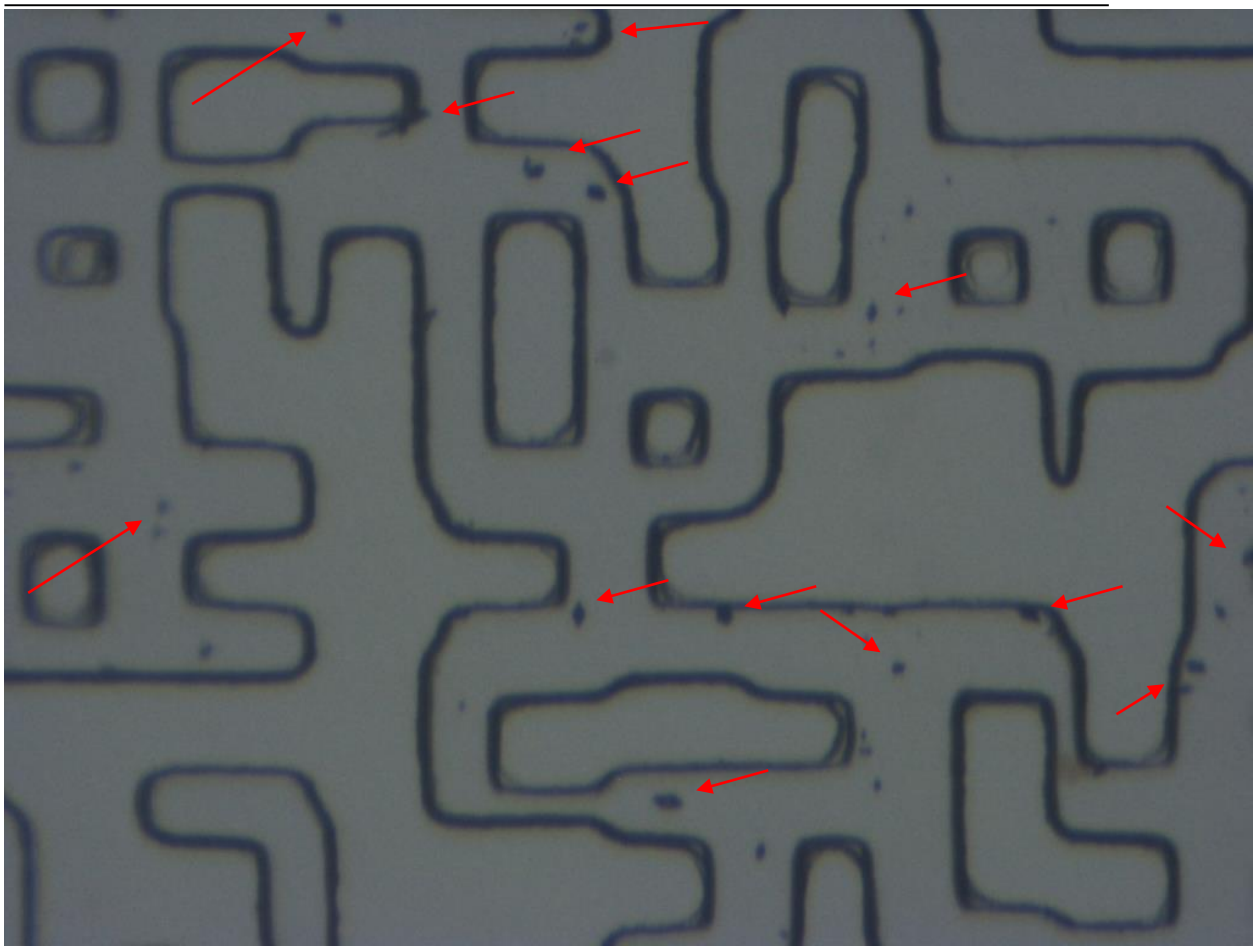

Figure 3-30: A highly magnified section of the micromodel image shown in Figure 3-29 with dark spots represents HWS-1 particles. Their sizes are less than 5 microns.

Experiment 12: HWS-1, Leak pressure of 2000 psig (no blockage)

After detecting the onset pressure of particle formation as described above, the inlet and outlet of micromodel were set at constant pressure of 3000 and 2000 psig, respectively. Any changes in flow properties can be identified through the flow (leakage) rate. After flowing 300 cc of the saturated solution through the leakage path, no changes in flow occurred indicating no effective precipitation of HWS-1 through the path. In addition to very high flow rates across the micromodel, which is unfavourable for particle precipitation, the pressure distribution across the leakage path and in particular in the micromodel is the other main reason behind the non-blocking behaviour. Figure 3-31 illustrates that due to the small size of the flow path the pressure in the micromodel is slightly higher than 2000 psig, which undermines formation of HWS-1 particles. Therefore, in the next experiment the pressure of the leakage cell was reduced further.

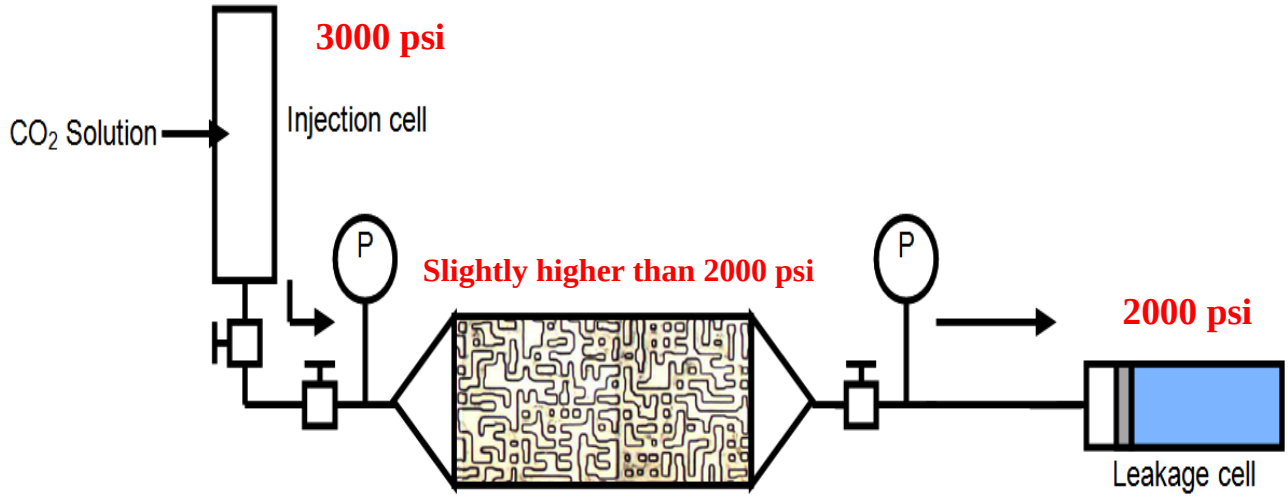

Figure 3-31: The pressure distribution in the micromodel setup. The pressure inside the micromodel is slightly higher than 2000 psig (onset pressure of particle formation) that explains why precipitation of particles was not observed at the leak pressure of 2000 psig.

Experiment 13: HWS-1, Leak pressure of 1900 psig (non-durable blockage)

The leak pressure of 1900 psig was selected for this test, i.e. the micromodel inlet and outlet pressures were 3000 psig and 1900 psig, respectively. In this case, the pressure in the porous medium (micromodel) is less than the onset pressure (2000 psig) and hence HWS-1 particles would be formed due to the imposed pressure drop. The solubility of HWS-1 at the original and the current outlet conditions are 0.0003 and 0.0002 mole fraction, which applies a supersaturation degree of $\frac{0.0003}{0.0002} = 1.5$. Similar to the previous test, changes in flow rate profile was considered as the main indication of the effective precipitation of solid particle along the leakage path.

Figure 3-32 demonstrates the final image of micromodel at the end of this experiment. It can be observed that HWS-1 particles were formed at the outlet of the porous medium rather than in the porous pattern of the micromodel. In other words, particles tend to favourably form near to the outlet (leakage conditions) where the pressure is lower leaving the inlet (storage conditions) unaffected.

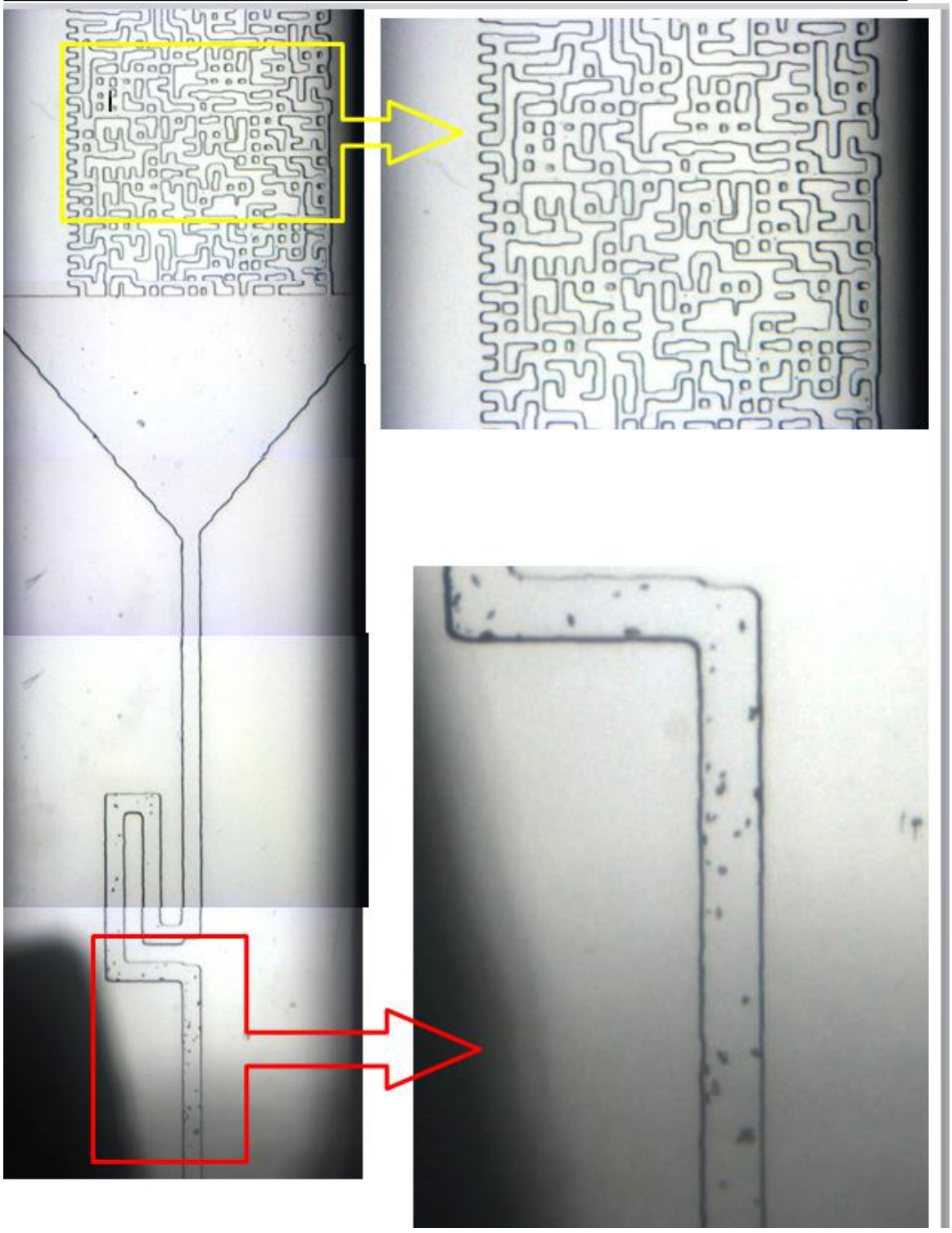

Figure 3-32: The outlet end of the micromodel showing the precipitation of HWS-1 particles in the pipes at the end of porous part of the micromodel at the leak pressure of 1900 psig. No precipitation took place in the porous pattern part of the micromodel. The blockage was formed in this outlet port of the micromodel.

Moreover, the precipitation in the port indicates that particle formation would lead to precipitation rather than being carried away in the form of suspension flow. Another feature of Figure 3-32 is the size of the particles compared to those formed in the previous test shown in Figure 5. This comparison shows that the size of the particles is notably larger in the current test. This can be attributed due to the aggregation of HWS-1 particles. Given that, compared to the previous test, there is a higher imposed pressure gradient of 1100 psig, a higher flow rate is expected. In this experiment, the leakage (flow) rate across the leakage path significantly dropped due to effective precipitation of the HWS-1 particles. However, it was also noted that after sometime the precipitants were mobilised and the high flow rate re-established. Figure 3-33 illustrates the profile of flow rate and pressure drop during the test. The decline in the flow rate from 180 to 10 cc/hr was noted at the early stage of the experiment but, later the precipitation is removed and the initial flow rate of 180 cc/hr is re-established.

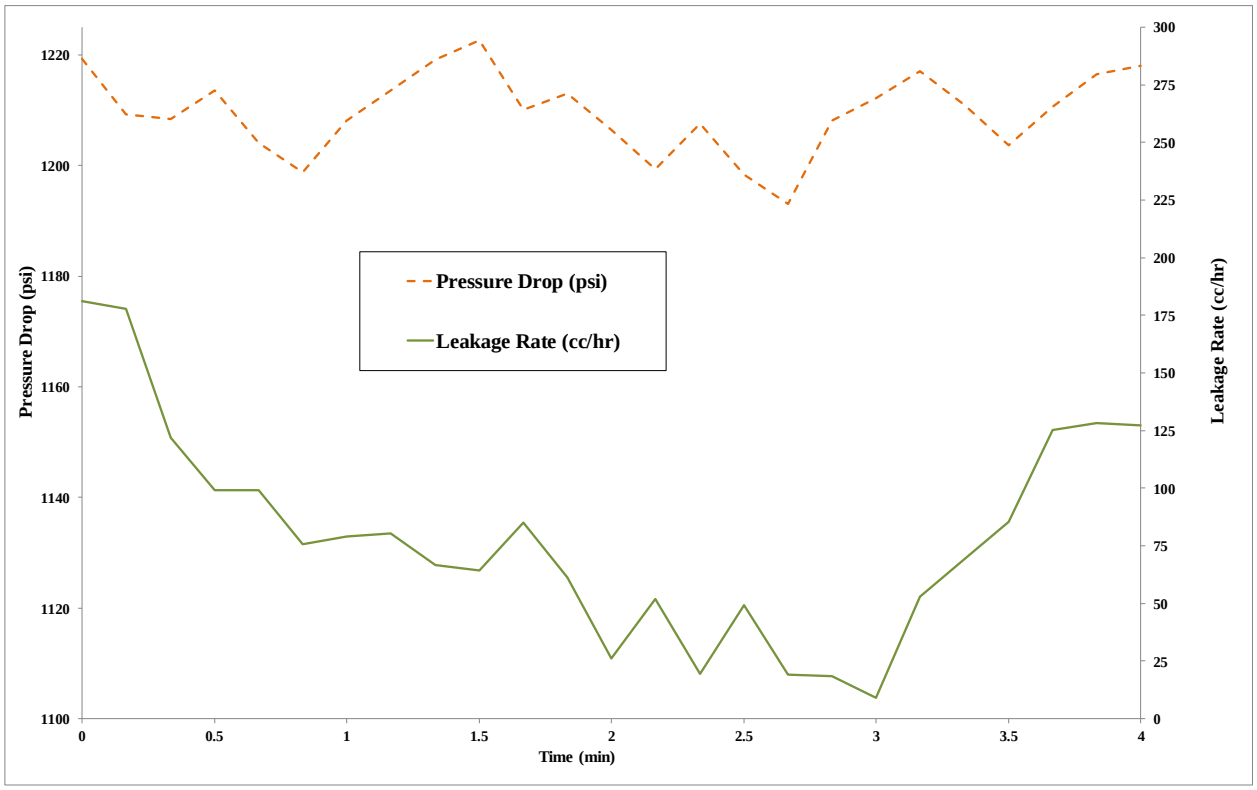

Figure 3-33: Profiles of the pressure drop and leakage rate during the test conducted at the leak pressure of 1900 psig. The leakage rate was significantly reduced from 180 cc/hr to 10 cc/hr but the blockage was not durable and the initial flow rate was re-established after 3 minutes.

Experiment 14: HWS-1, Leak pressure of 1700 psig (blockage)

In this experiment, the outlet pressure of the micromodel was further reduced to 1700 psig and the inlet pressure was kept the same as the previous tests. This resulted in a pressure drop of 1300 psig applied to the LPT solution in the micromodel. Figure 3-34 shows the formation of HWS-1 particles in the vicinity of outlet port of the micromodel. In terms of particle properties, HWS-1 was formed in smaller sizes resembling powder-like solid phase as opposed to previous HWS-1 particles with larger dimensions. A greater number of particles were formed in the porous pattern, which would be favourable in building up the blockage body. According to nucleation kinetics, smaller particles in higher population is to be formed at higher supersaturation degrees (higher pressure drops), which is in line with what we observed in this experiment. Furthermore, packing of the finer particles can endure higher pressure drops across the blockage body.

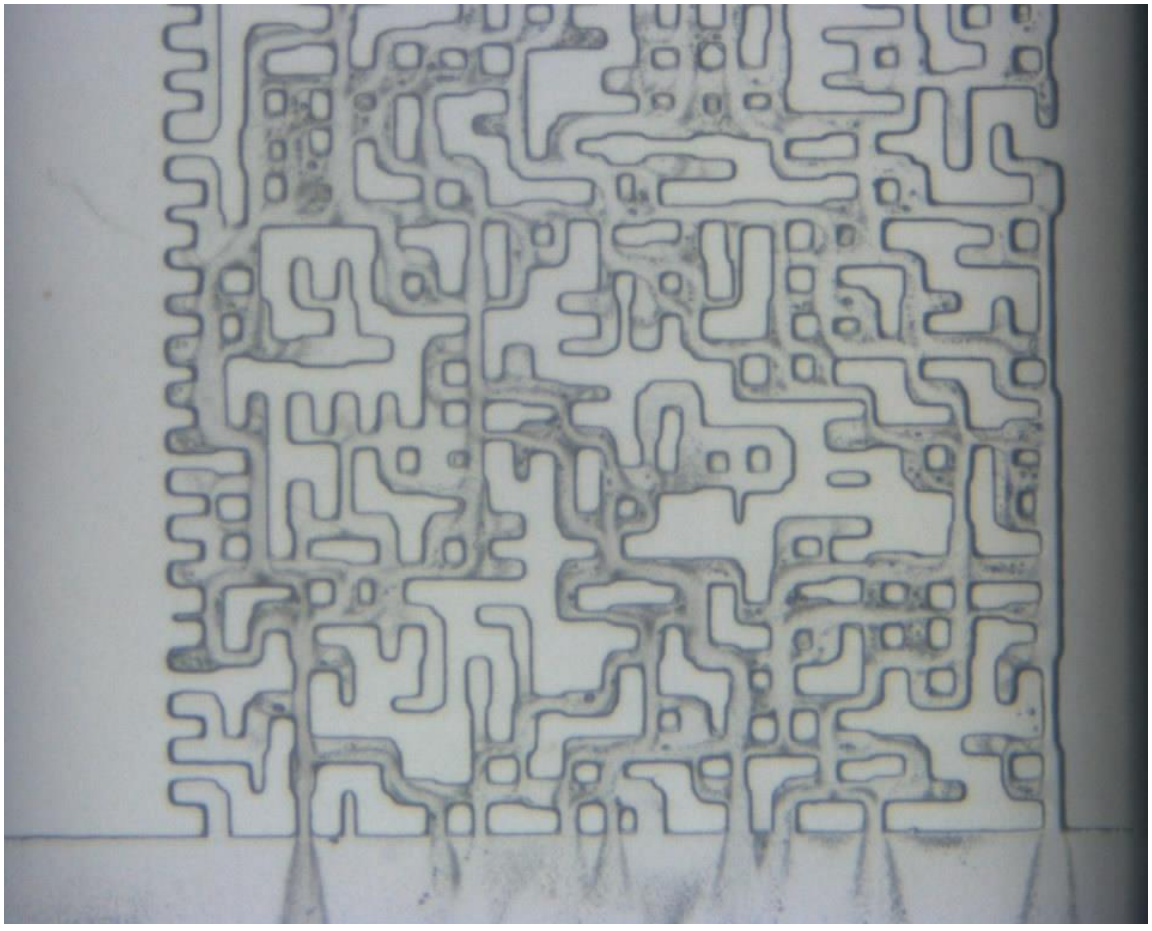

Figure 3-34: A magnified section of the micromodel demonstrating that at the leak pressure of 1700 psig, finer HWS-1 particles were formed in the micromodel leading to the formation of a stable blockage.

In terms of flow properties as the main indication of occurrence of a blockage, Figure 3-35 shows the pressure drop and the profile of flow (leakage) rate observed in the test. It can be seen that initially a high flow rate of 210 cc/hr was established in the micromodel but as the test proceeded, the leakage rate dropped abruptly from 210 cc/hr to 50 cc/hr which is attributed to a significant reduction in permeability of the leakage path. After 5 min of flow (120 cc cumulative flow of the solution), further reduction in the flow rate was noted and finally the leakage rate was stabilised around 0-5 cc/hr. In line with final stabilisation of the flow rate, the pressure drop (which was imposed by the pumps at both ends of the leakage path) became more stable, i.e. less oscillation, to keep the pressures constant and deliver the flow rate, which was another indication of effective stable precipitation and blockage formation. That is, unlike the previous test (leak pressure of 1900 psig), the blockage could withstand the pressure drop of 1300 psig for a prolong period of time, which indicates the durability of the blockage formed by HWS-1 particles. In other words, the significant reduction in the outlet flow rate (99% of the original value) and stabilised pressure readings over a long period of time is attributed to formation of a firm blockage.

In summary, HWS-1 was used in in the visualisation micromodel experiments. This solute has responded to the imposed leakage scenarios positively although micromodel tests were conducted in relatively high flow rates.

Having identified the onset pressure of 2000 psig (1000 psig pressure drop) and the formation of a durable blockage at pressure drop of 1300 psig (1700 psig outlet leakage pressure), the next aim was to formulate a LPT solution with higher sensitivity and response to lower pressure drops than those tested in micromodel tests. In chapter 7, the impact of adding a liquid co-solvent on the performance of the leakage prevention technique, was investigated for other solutes. The results clearly demonstrated a better performance of a two-component LPT solution (solid solute + liquid solute) by responding to lower pressure drops.

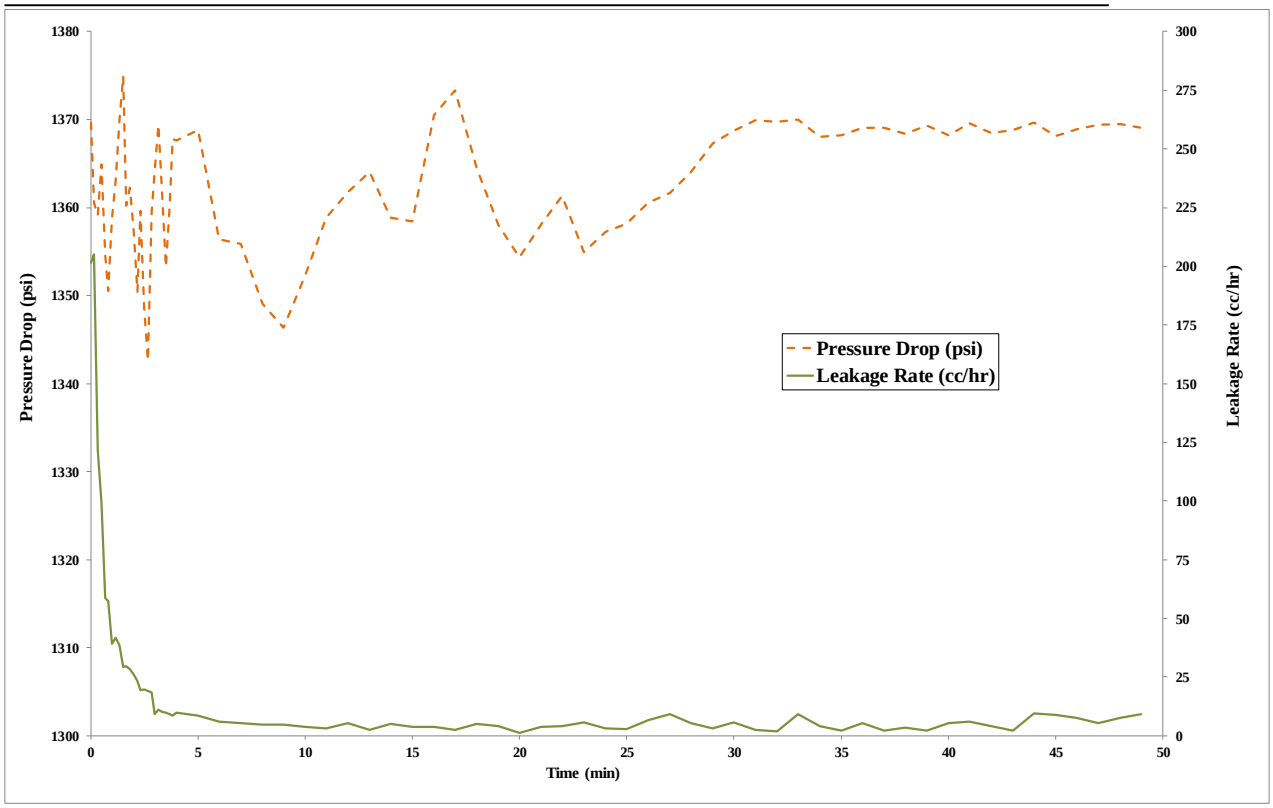

Figure 3-35: Profiles of the pressure drop and leakage rate during the test conducted at the leak pressure of 1700 psig. The leakage rate was sharply reduced to below 5 cc/hr from the initial value of 210 cc/hr leading to a successful blockage that could endure the imposed 1300 psig pressure drop.

3.6 Effect of Impurity

In the preceding sections, it was reported the visualisation results of tests performed with HWS-3. In those tests, pure CO_2 was saturated with HWS-3 at 2820 psig and 45 C and a maximum pressure drop of 1000 psig resulted in instantaneous nucleation of solute. In this section, the impact of insignificant amount of Nitrogen in CO_2 has been tested. It is expected that the CO2 stream injected and stored in geologic reservoirs will always have a small amount of impurities originated from combustion or leaked into the stream from air. Therefore, the influence of impurities should be taken into account when designing and implementing our proposed leakage prevention technique.

A sample composition taken from an industrial power plant (Kanniche, et al., 2010) was considered as a representative CO2 composition from an Oxyfuel power plant. The main operating principle for Oxyfuel is that combustion takes place in an atmosphere of pure oxygen instead of air. In this way, a CO_2 rich flue gas is produced. Other components present in the flue gas are mainly water, N_2, Ar, SO_x, NO_x and trace metals.

Table 3-2 presents the composition of CO_2 stream which has been used as the basis of the composition utilized for the test on an impure sample. As can be seen from Table 3-2, 3.9% of the total 5% impurities is made up of N_2, Ar and O_2, which have a similar effect of CO_2 phase behaviour and the remaining 5000 ppm is made up of a number of compounds. In the test performed with an impure CO_2, we lumped all the impurities into 5% N_2. Therefore, the overall composition of the CO_2 stream used in the test was 95% CO_2 and 5% N_2.

Table 3-2: Stream composition considered for investigating the impact of impurities.

Component	**Stream composition (mole frac.)**
CO_2	> 95 %
N_2+Ar+O_2	< 3.9 %
H_2O+CO+NO+SO_2+NH_3+NO_2	< 5000 ppm

Prior to performing the test with impure CO_2, we first ran a compositional simulator to check whether or not this 5% nitrogen would have any significant impact on physical properties of CO_2. Figure 3-36 shows the reduction in density of the sample as a result of addition of N_2 compared with the 100% CO_2 case. For instance, density of the impure sample at 2966 psig, i.e. test pressure, is 0.738 gr/cc which is significantly less than 0.817 gr/cc for pure CO_2 at the same conditions of pressure and temperature. The observed significant decrease in the density of CO_2 with addition of a small amount of nitrogen is expected to affect solvent power of super-critical CO_2.

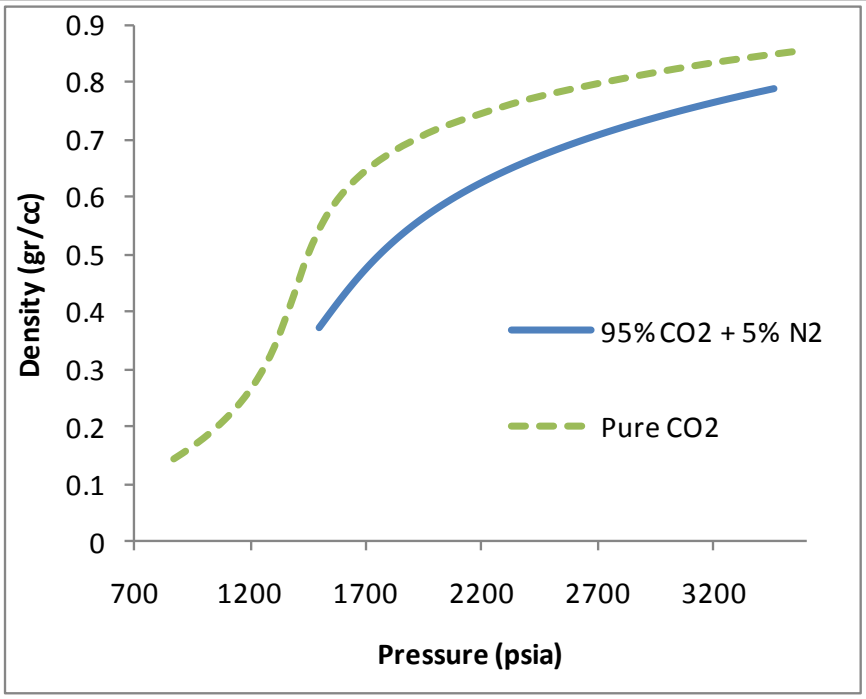

Figure 3-36: Density of pure and impure CO_2 streams as a function of pressure at 45°C.

3.6.1 *HWS-5*

Having made up the solution with *HWS-5* at pressure of 2966 psig and 45°C, three visualisation experiments were performed using the impure CO_2 sample. In the first attempt, a leakage was introduced in the system at 2600 psig. The leak was very quickly sealed as judged by the loss of pressure communication between the inlet and outlet ports of the porous medium. The system with 5% N_2 seemed to be more responsive and sensitive to pressure drop than the pure CO_2. The blockage happened in the connecting lines. Figure 3-37 depicts the accumulation of the precipitants in the entry valve of the micromodel resulted from exposing the solution to the pressure drop.

In the next attempt with impure CO_2, a leakage was introduced at 2700 psig. Again the leak was sealed very quickly by blocking the leakage lines instead of the micromodel.

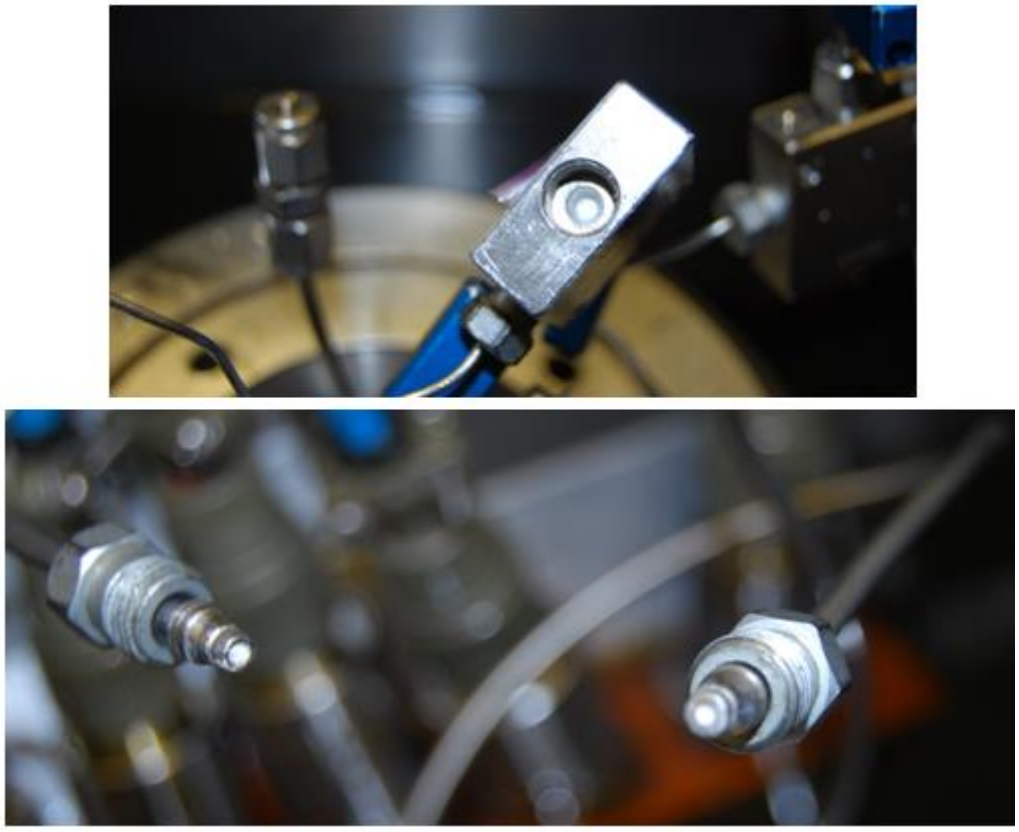

Figure 3-37: Accumulation of particles (white packs at the tip of lines) in the entry valve conducted outlet leakage pressure values of 2600 and 2700 psig, i.e. 366 and 266 psig pressure drop respectively.

In the third test of this series, a leak was introduced at 2800 psig which represented a small pressure drop of only 166 psig which was the lowest pressure drop tested so far. The leakage was very efficiently sealed by formation of solid blockages in the micromodel. Figure 3-38 shows a sequence of pictures taken from one spot of the micromodel during the leakage test with impure CO_2 with a pressure difference of only 166 psig. In these images time increases from left to right and from top to bottom.

Figure 3-38 shows how the particles were formed and accumulated around a single collector in the middle of the micromodel. Based on this figure, the mechanism of particle deposition in this test appeared to be the high aspect ratio pore-throat configuration at the upper right of the images in Figure 3-38. This geometry acted like a shower to generate the dispersed particles that were then precipitated at the adjacent pore, which acted as

spherical collector. The test resulted in complete sealing of the leak. The blockage strength was checked by maintaining the pressure for about 12 hours without reopening,

A very interesting observation regarding the impact of N2 was observed after the test. The mixture of the impure CO_2 and solute used in the above experiment had been made by saturating the solution with *HWS-5* at the test conditions of 2966 psig and 45^{o}C. 35.5 gr of *HWS-5* had been placed inside the cell but after the test when the cell was examined; surprisingly 33 gr of solute was still in the cell. This means that only 2 gr of the solute had been actually dissolved in the solution.

Therefore, the addition of nitrogen has significantly reduced the dissolution of the solute in CO_2 and yet more effectively sealed the leaks. This represents a significant achievement since it shows that for a more realistic CO_2 composition used in the field, the amount of solute required for dissolving in CO_2 would be less than the pure CO_2 yet the system becomes more efficient and more responsive to a potential leakage of CO_2.

In summary, based on the results of the above tests, addition of 5% nitrogen had some favourable impacts on the performance of the process by reducing supersaturation and making the fluid more sensitive and responsive to a reduction in pressure. The leaks were quickly sealed even at a small pressure drop of only 100 psig. Secondly, the solubility of the solute was significantly reduced in impure CO_2 compared to that of pure CO_2. This improves economy of the leakage prevention method as much less solid solute is required for obtaining an effective seal.

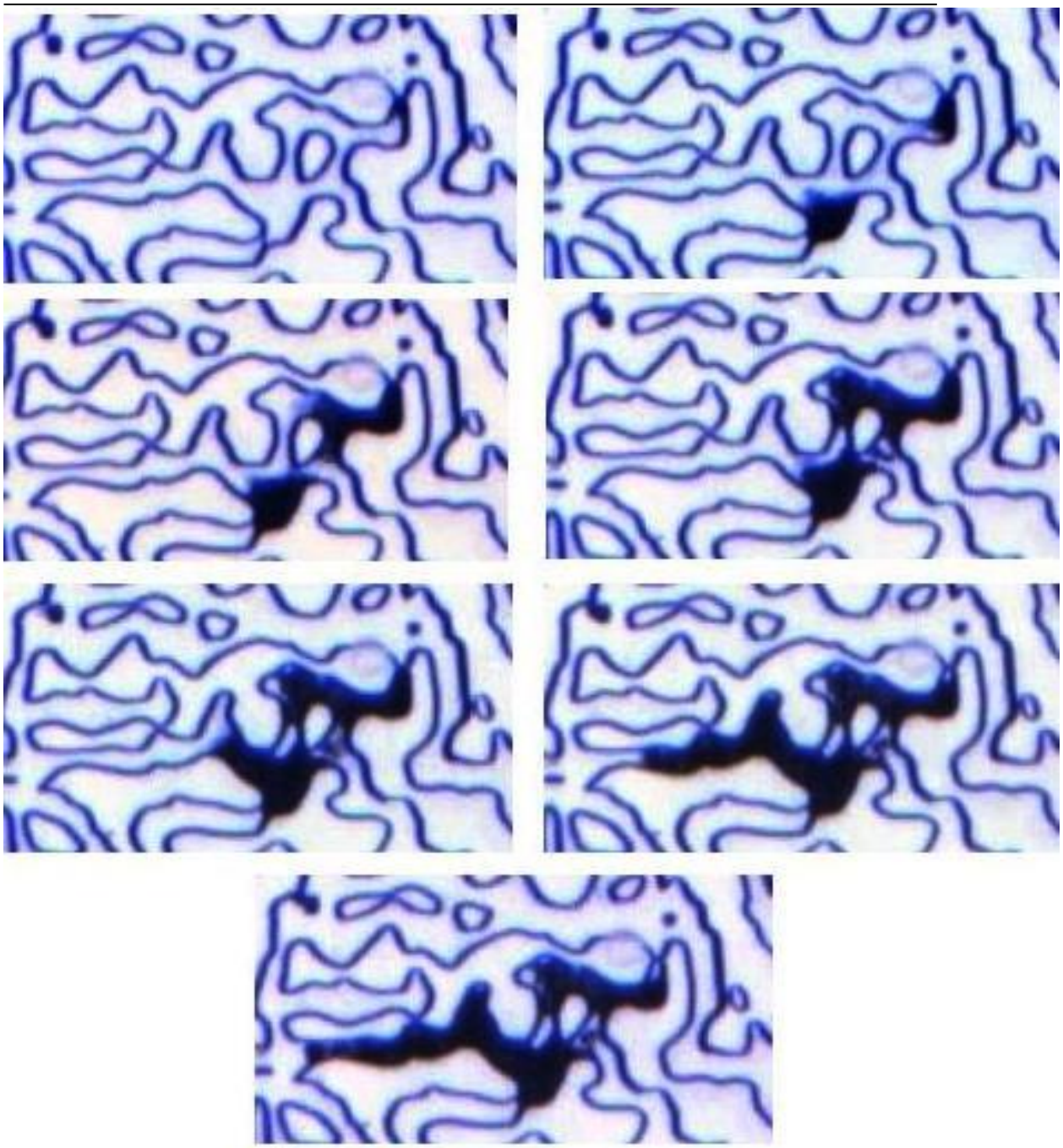

Figure 3-38: sequences of evolution and retention of particles using impure CO_2 stream during sample experiment 8 conducted under the pressure drop of 166=2966-2800; the upper left is the start of particle generation, upper right explains the particle precipitation, middle sections demonstratees the growth of the precipitants near the particle formation point, and the bottom image shows the last stage of deposition near the collector.

3.6.2 HWS-3

Figure 3-39 illustrates the solubility of HWS-3 in CO_2 as a function of pressure and at 45 °C. As expected, at a constant temperature, solubility increases as pressure increases. This figure also shows the change of density with pressure at the same temperature. As can be seen, there is a direct relationship between CO_2 density and its solvent power. The use of experimental data on CO_2 density is known as the most applicable method for correlating solubility data (Gupta & Shim, 2006). Studies on correlating the solubility in CO_2 with its density and temperature and pressure have resulted in the following correlation;

$$\ln(y_2 P) = \left(\frac{1}{T}\right)\left(-7270 + 136700\rho_{CO_2} + 14.59T\right) \qquad \text{Eq. 3-4}$$

Where y_2 is the solubility in mole fraction, P is the pressure in bar, and T is temperature in Kelvin. It should be pointed out that the density of carbon dioxide (in mole/cc) plays a major role in the Eq. 3-4.

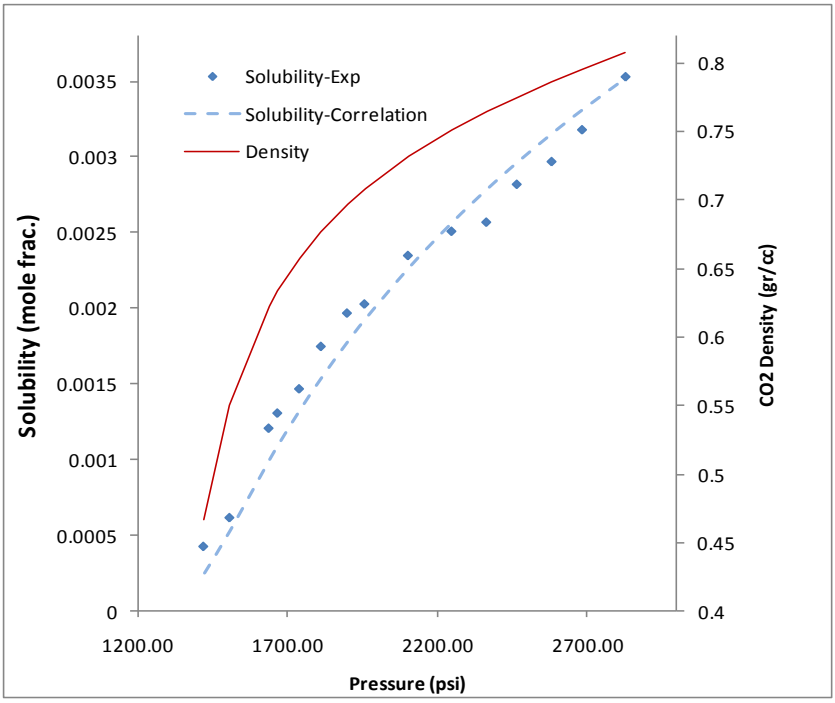

Figure 3-39: Isothermal solubility of HWS-3 and density of CO_2 at 45 °C (Gupta & Shim, 2006).

Addition of Nitrogen (N_2) to CO_2 reduces significantly the density of CO_2 and hence its solvent power. Strictly speaking, the above Equation (Eq. 3-4) is not applicable to

mixtures of CO_2 and N_2 and there is no experimentally measured data on solubility of solutes in mixtures of CO_2 and nitrogen. However, since our main concern in these experiments is to investigate the response of the solute-saturated CO_2 solution to pressure drop, we have added excess amount of solutes in the mixing cell to ensure that the solution is saturated.

HWS-3 with pressure drop of 820 psig

In this experiment the sample was made up in a 300 cc high-pressure cell with 95% CO_2 and 5% Nitrogen (as an impurity) and 5gr of HWS-3 (as a solute). The solution was brought to thermodynamic equilibrium at 2820 psig and 45^oC by shaking for about 24 hours. The initial state of the micromodel was set at 2000 psig which was 200 psig higher than the onset pressure for precipitation of HWS-3 in pure CO_2 under the same conditions. Then, to simulate a CO_2 leakage from the storage cell, the cell containing the mixture of CO_2, N_2 and the solute HWS-3 was connected to the micromodel from the bottom port. As a result of the differential pressure that existed between the storage cell and the micromodel (820 psig), the CO_2 solution flowed through the micromodel but it was observed that a solid phase was formed which eventually blocked the flow of the CO_2 stream.

Figure 3-40 shows the final state of the micromodel after formation of the blockage in this test where the dark area shows the blocked pores. The main outcome of this test is that, as it was observed in the tests performed by *HWS-5*, presence of Nitrogen as a lean gas contaminant facilitates and enhances nucleation of solid particles at lower pressure drops (compared to pure CO_2). In other words, Nitrogen (and probably other lean gases) makes the leakage prevention technique more sensitive to pressure drop compared to pure CO_2. In terms of particle precipitation, most of the precipitation occurred and accumulated at the end face of the porous medium where the highest pressure drop occurs. Regarding the underlying physics for having an effective blockage, this test demonstrates that the main parameter controlling the efficacy of leakage prevention technique is the formation of particles rather than the actual mechanisms by which the formed particles would be deposited building up the consequent blockage (i.e., whether particles attach to the surface of the porous medium or pack the pore space).

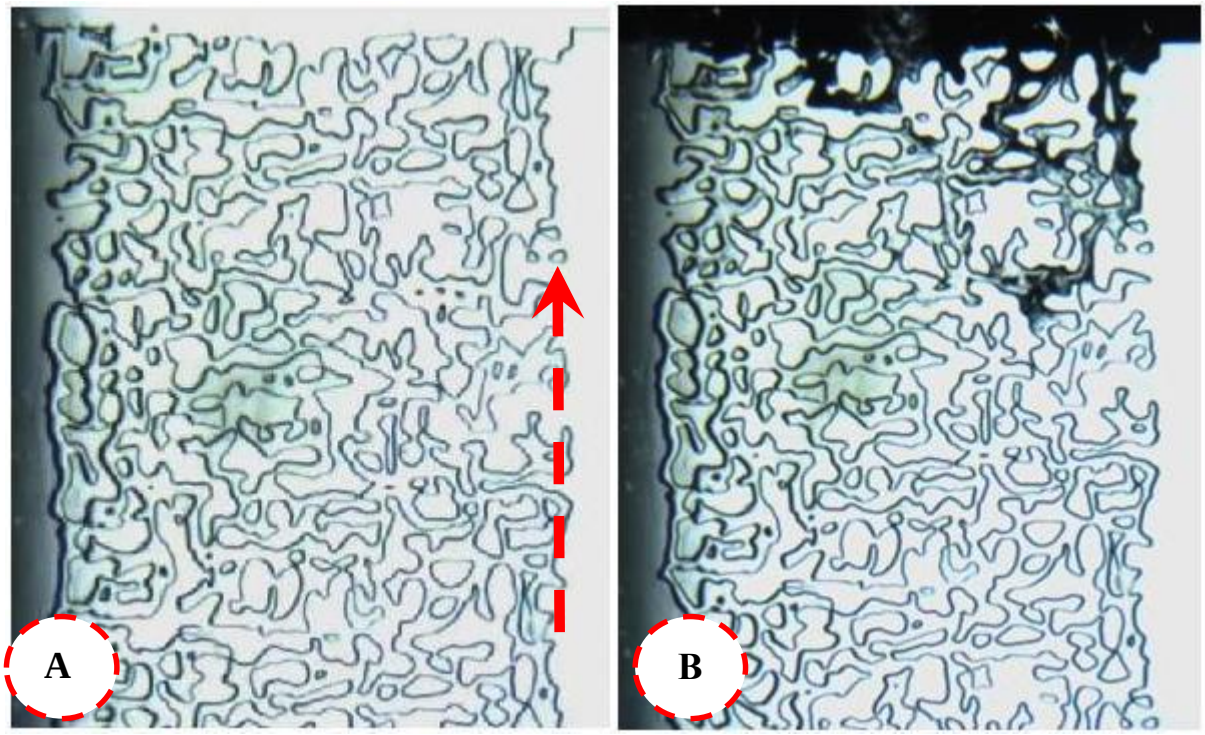

Figure 3-40: Leakage from 2820 psig to 2000 psig. (A) Initial state of the micromodel, (B) Final state of micromodel after blockage, red arrow shows the flow direction.

HWS-3 with pressure drop of 620 psig

After successful blockage in the previous test, the leakage pressure increased to 2200 psig (lower differential pressure) to test the efficiency of the technique at a lower pressure drop of 620 psig (compared to 820 psig in the previous test). Figure 3-41 shows two main steps in during the visualisation test, which resulted in full blockage occurred in the leakage flow paths. First, particle formation was observed within the pores experiencing pressure drop at the end of the micromodel (Figure 3-41, left). Second, firm and concentrated plugging were formed at places with the highest differential pressure and the complete sealing of the leak took place (Figure 3-41, right).

To interpret the left image in Figure 3-41, two main sections have been highlighted with red circles as the places were nucleation of the solid particles was initiated (nucleation). These areas have been identified with either high pore/throat aspect ratio or highly chaotic flow resulted from interception of flow streamlines. Therefore, there would be high probability of local pressure drops in vicinity of these circles. Regarding the jet-like flow at the end face of the micromodel, particles have a considerable tendency to depart from their accumulated colony due to low population of particles at this time of the test. Thus,

particles of HWS-3 have minimal affinity to attached to the surface of the pores walls and the main precipitation mechanism is believed to be coagulation of the particulates. The coagulation mechanism of precipitation is more likely to happen in water-wet rocks. In water-wet porous media, since water film would be present on the surface of the rock, it would be more difficult for the particles to adhere to the surface of the rock.

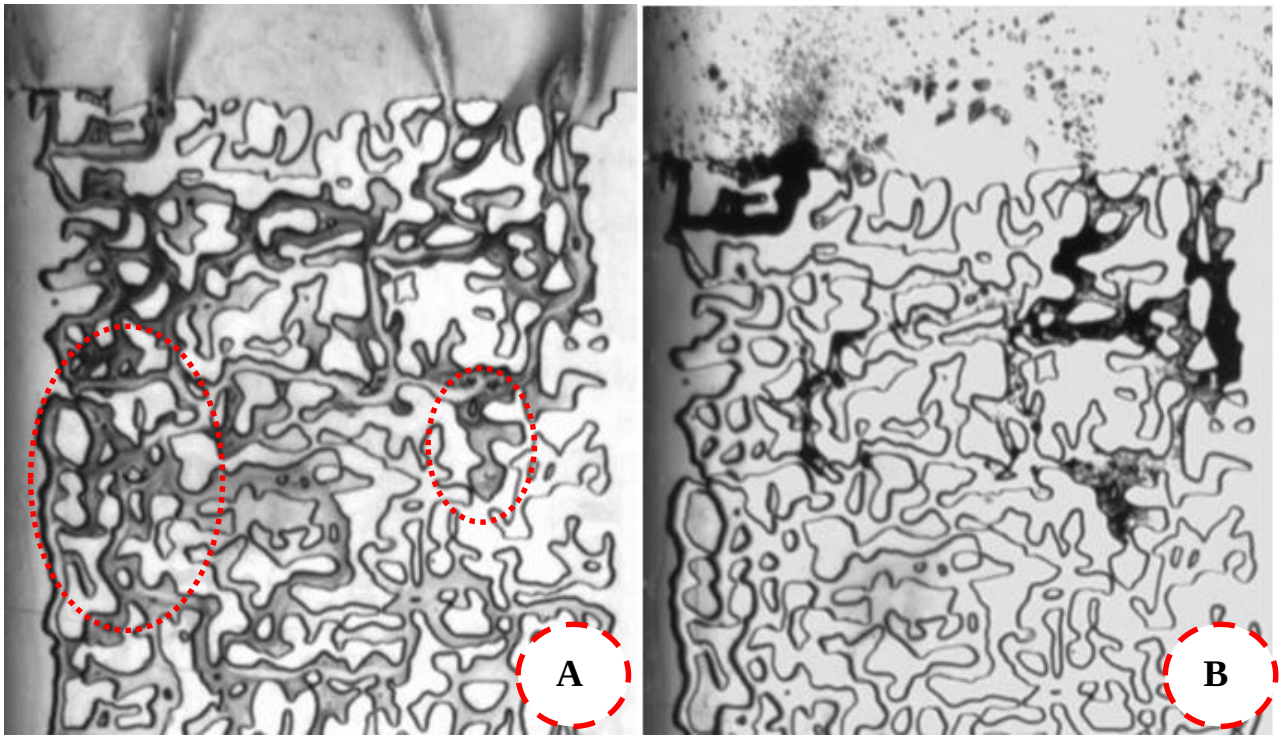

Figure 3-41: Leakage from 2820 psig to 2200 psig. (A) Potential sites for particle formation, (B) firm plugs forms in flow paths.

The right image in Figure 3-41 exhibits the final state of the micromodel after blockage. Compared to previous test, the precipitations were concentrated at the main flow paths at pore scale rather than bulk precipitation in the end face of the micromodel. Thus, one can infer that the particles are larger in this test. This behaviour indicates an important aspect of nucleation kinetics; the closer the leakage pressure of the test to the critical superstation of the solution, the larger the produced particles.

It should be noted that concentrated blockage inside porous media would form as a result of two reasons; first, due to the attachment of particles to the surface of the walls of the pores in the porous medium and, second, due to formation of large or coagulated particles and their trapping in smaller geometries. In this experiment, the second reason is the

dominant one since larger particles were generated as result of the leakage pressure being close to critical supersaturation.

3.7 Impact of presence of water

All geologic formation considered for CO_2 storage will contain some water, therefore, the impact of water on the performance of the leakage prevention method has to be investigated. The eminent role of water in porous media can be attributed to the wetting characteristic compared to gaseous-like CO_2. Normally, interstitial water has strong affinity to adhere to the surface of the porous media in systems of gas and water (Green & Willhite, 1998). As a result, during CO_2 injection, when CO_2 displaces resident water in the aquifer or reservoir, water layers remain behind covering the surface of the pores. The effect of these wetting layers on the precipitation of solid solutes and sealing of the leak will need to be investigated. The potential adverse impact of water can be categorized into two issues (1) undermining attachment of particles and (2) restricting further particle growth subsequent to the critical nuclei.

Figure 3-42 depicts the state of the micromodel which was initially fully saturated by water and was subsequently flooded with CO_2. Blue bodies and layers represent residual water saturation after invasion of CO_2. As can be seen, water retains its presence through water films across the porous medium and accumulated bodies in dead-end and narrow pores. Figure 3-42 shows the initial state of the micromodel fully saturated with water (top) and the image of the micromodel after the injection of CO_2 (bottom) which resulted in the displacement of bulk of water from the porous medium leaving behind water layers on the surface of the pores as well as in the dead-end pores.

In this visualisation experiment, the role of water on performance of LPT was investigated by performing a leak prevention test in micromodel initially fully saturated with water. The test was carried out at CO_2 storage pressure of 2820 psig and a leakage pressure of 1400 psig using HWS-3 (marginally soluble solute).

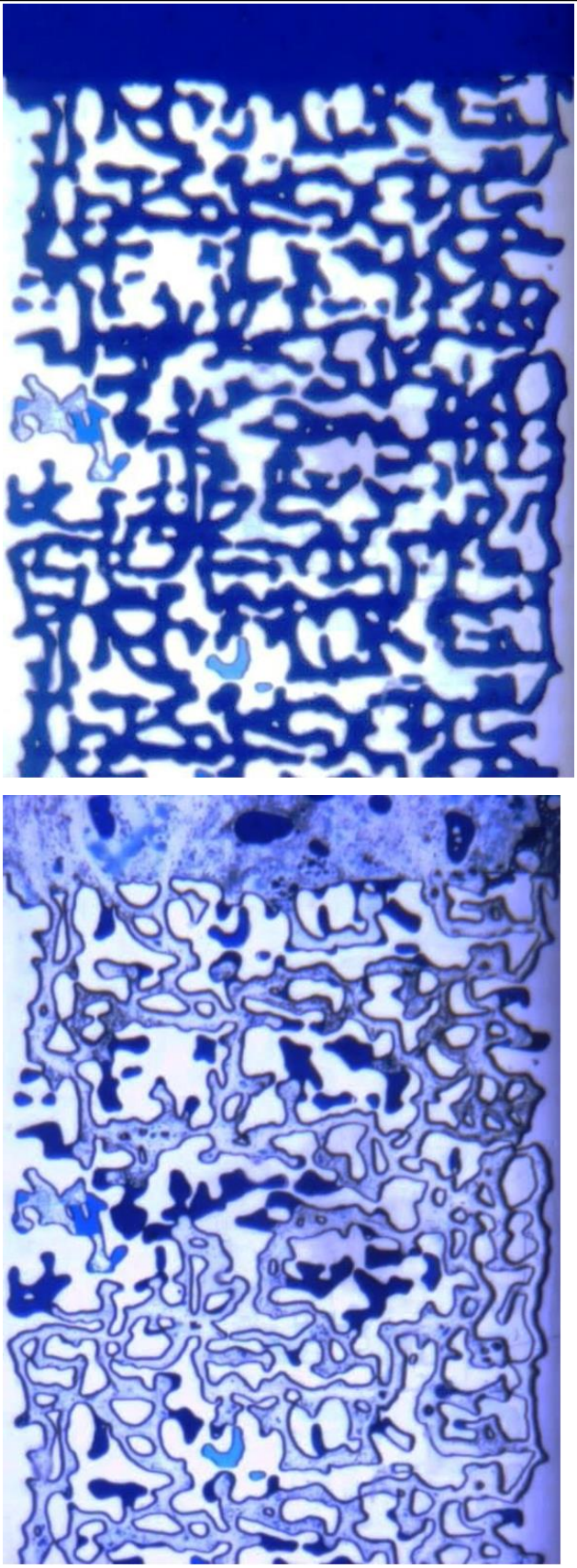

Figure 3-42: Top image is the initial state of 100% water saturated and bottom image shows the micromodel after the injection of CO_2 where bulk of water has been displaced but water layers and some water in the dead-end pores remain.

Having established the initial water saturation in forms of water layers and trapped in dead-ends, CO_2 leakage stage was then started. Figure 3-43 depicts a sequence of images taken during the leakage state which shows the activation of the leakage prevention mechanisms and the onset and precipitation of the solute. Due to the high velocity of particles (caused by high pressure drop), the main mechanism of particle retention was observed to be "inertial impaction" and "interception". The main parameter that controls the plugging in this retention mechanism is the population of particles as can be seen from the increasing density of the dark parts around the end face of the micromodel (Figure 3-43b). Another feature of Figure 3-43b and c is that although the particles have been formed all over the porous medium, they have accumulated at the end face of the micromodel, therefore, particle movement as a result of suspension flow has been enhanced as water acts like a layers on the surface of the micromodel, This phenomenon can be attributed to the lubricating effect of the water layers at high velocity of the leak, which would weaken the deposition of particles.

Complete blockage of the leak was attained which was verified both visually (Figure 3-43d) and by examination of the pressure discontinuity between the inlet and outlet of the micromodel which was completely lost due to the formation of the blockage in the micromodel. The sealing of the leak occurred by high population of particles which plugged the leak at the interface between the porous medium and the leakage path.

The main difference between this test (with water) and the previous tests (without water) was some delay which was observed in precipitation and building up the blockage. This can be attributed to the slight adverse effects of the water layers present on the surface of the porous medium which delays attachment of the particles to the surface of the rock and formation of a solid plug. Lubricating effect of water layers may also delay evolution of a blockage. Nevertheless, this delay was short and the complete sealing of the leak took place in only 10 minutes in the test with water.

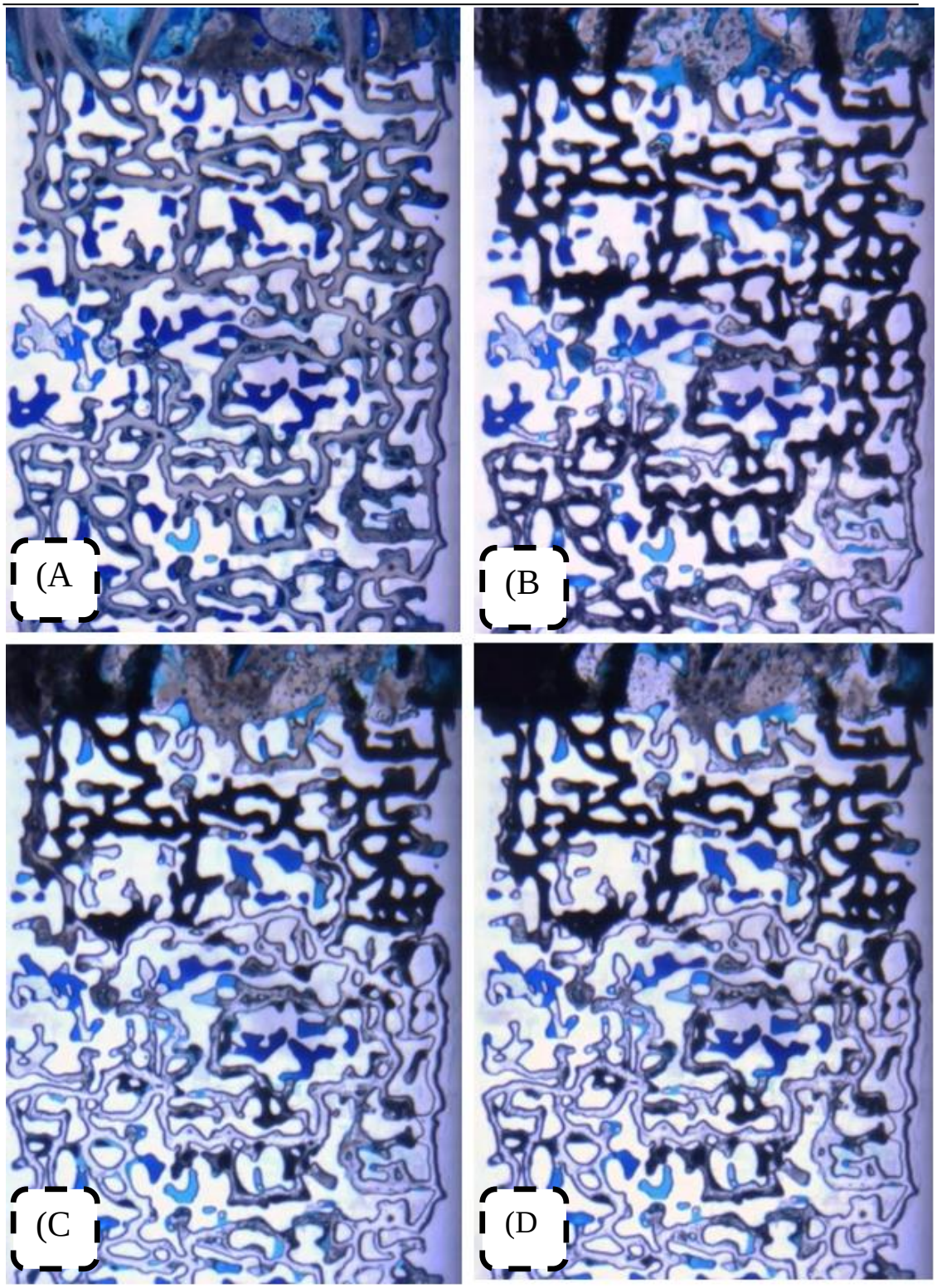

Figure 3-43: sequence of blockage evolution; a) particle formation started b) increasing population of particles, c) inertial impaction resulted in higher density in end face, and d) blockage occurred.

After testing the blockage stability for around 1 hour, the CO_2 injection pressure was increased to 2900 psig which was 100 psig higher than the initial CO_2 storage pressure to examine the response of the system to an increase in pressure that may happen subsequent to formation of a blockage. Figure 3-44 shows a sequence of magnified images showing the spot at which the blockage had happened during the subsequent increase in CO_2 pressure. As the pressure increased, the CO_2 was observed to press against the blockage (Figure 3-44a) and eventually opened a path between the blockage and the surface of the pore and established the leakage flow path again (Figure 3-44b). As soon as the leakage began again, it was observed that the precipitation of solute started (Figure 3-44c) and a new blockage was formed which resulted in sealing the leak again. This exercise proved that if as a result of increasing pressure or for any other reason the blockage is opened and the leak is established again, the leak prevention mechanism is activated again until the leakage sealed.

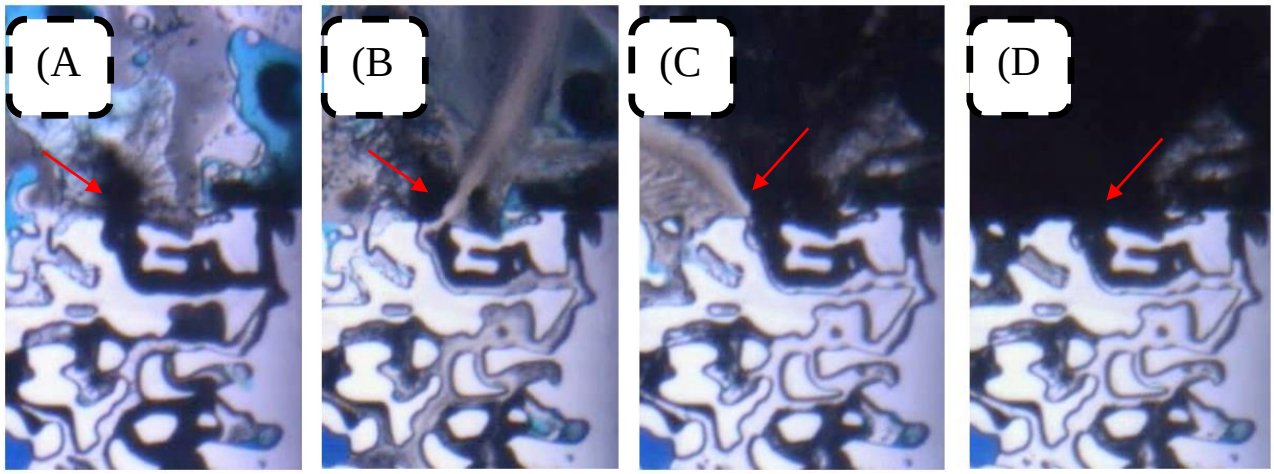

Figure 3-44: Reopening and resealing of a CO_2 leak during pressurization of CO_2 subsequent to formation of a blockage in the experiment with water. a) Pressurization, b) Reopening of the plugged leak, c) formation of a new blockage, d) re-plugging and self-healing.

3.8 Viewing Cell (Sightglass) Test

In a different set of experiments performed in a sightglass setup, two types of visualisation tests were performed in which, (i) nucleation kinetics and induction time of the particle formation were observed and (ii) mutual interactions between a brine and a solution made up with solid-solute + CO_2 was investigated . Mixtures of HWS-3 and pure CO_2 were taken into a visual cell (sightglass) to investigate the onset pressure of instantaneous particle formation and also the induction time needed at a pressure drop of 520 psig.

Nucleation and precipitation of solid solutes in supercritical CO_2 is one of the main principals of the leakage prevention technique and plays a crucial role in the performance of the method. To quantify the parameters in nucleation theory (see Chapter 1), the time necessary for the formation of the first batch of particles in the form of a distinct phase has to be measured in different supersaturation (Dp) values. Also to evaluate the efficiency of method in various leakage scenarios, the induction times for a particular solute needs to be measure. In real reservoirs, the required time for the CO_2 front to deposit the particles under the leakage conditions can be taken as the induction time which is the time between the onset of the particles to the time they precipitate. For instance, if it takes 10 hours for a solute to nucleate under a particular supersaturation, it is necessary to retain the solution for at least 10 hours in the leakage location at the corresponding supersaturation to ensure that the particles precipitate and block the leaking path.

The study of particle induction time and the impact of pertinent parameters on it can be done in a high-pressure viewing cell (sightglass), which is shown in Chapter 2 schematically. The glass windows in this high pressure cell allow us to view the formation of solid particles and to measure induction time under different conditions.

3.8.1 HWS-3 from 2820 psig to 2300 psig

In this experiment a solution of HWS-3 and pure CO_2 was prepared at the pressure of 2820 psig and 45 °C which corresponds to a solubility of 0.00353 mole fraction of HWS-3 in supercritical CO_2. After equilibrating the solution in the storage cell, the sightglass was connected to the CO_2 storage cell and was slowly filled up with the CO_2 solution at a very low rate in a 24 hours period. The transfer of CO_2 solution from the storage cell to the sightglass takes place under constant pressure and temperature in order to avoid

formation of solid particles in the process of charging the visual cell. The next step was pressure reduction in the sightglass in order to simulate a leak. The sample inside the sightglass was brought to the desired pressure with a sudden reduction of pressure instead of gentle decrease in pressure.

Two images of the sightglass content during the test are shown in Figure 3-45. The top image in Figure 3-45 shows the initial state of the CO_2 inside the sightglass before reducing the pressure and the bottom one shows the particles formed during the pressure reduction and deposited on the bottom of the sightglass. The period during which these particles were formed was measured and still images were continuously taken. The initial pressure of the sightglass content was 2820 psig and the target pressure of the test was 2300 psig which was much above the highest blocking pressure occurred in micromodel for the system of HWS-3/CO_2. The supersaturation associated with pressure reduction of 520 psig in this test can be basically calculated by dividing the corresponding solubilities at the initial pressure of 2820 psig and at the final pressure of 2300 psig, which will results in a supersaturation value of 1.406.

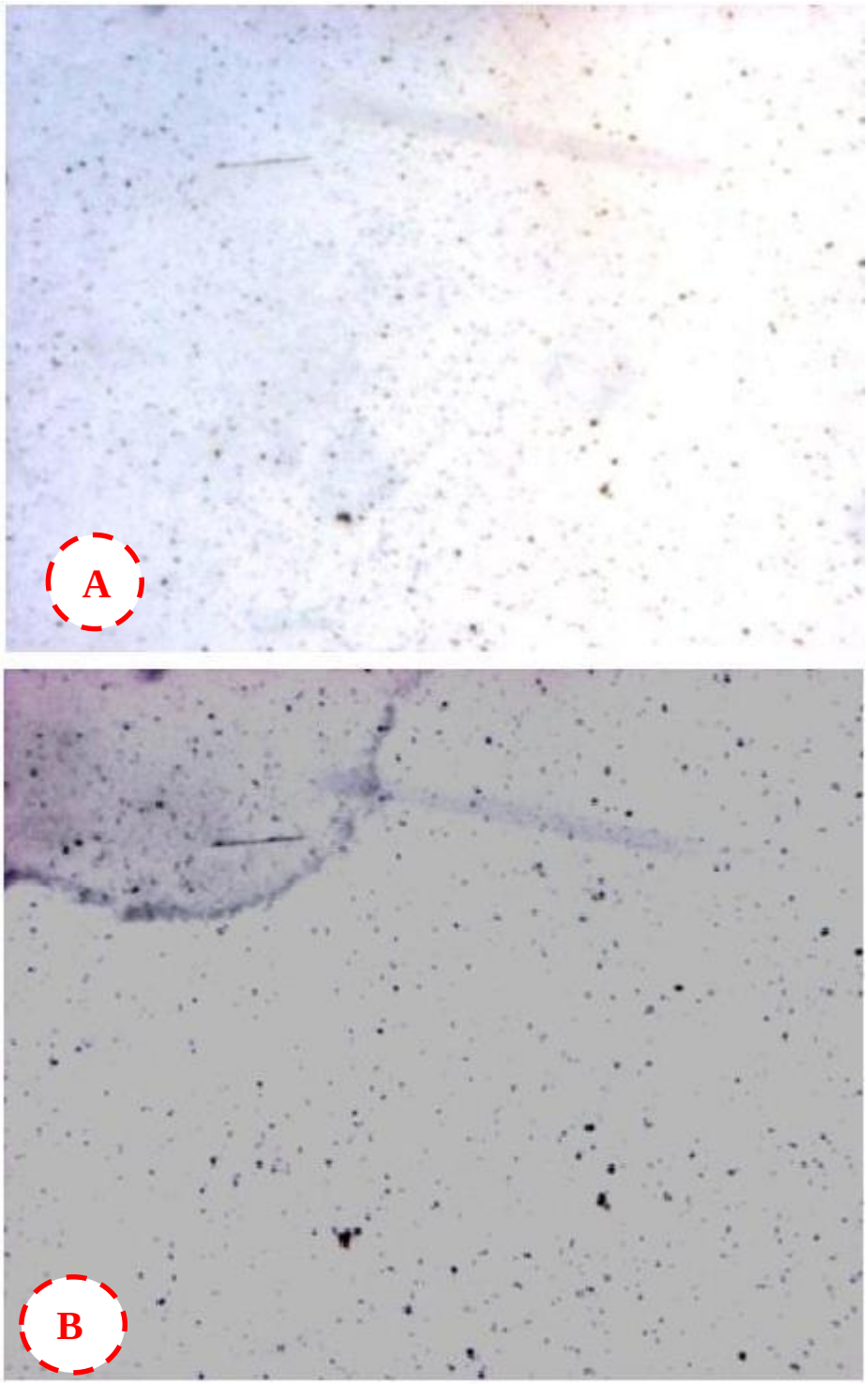

Figure 3-45: Visual observation of HWS-3 nucleation from 2820 to 2300 psig; (A) Initial state of sightglass with no solid particles, (B) Scattered particles across the visual cell and also aggregated particles at the left upper corner.

Based on the sightglass test, the induction time for HWS-3 to crystallize in supercritical solution as a distinct phase is about 4 hours and 52 minutes. Two important properties of the crystallization are the mean size of the particles and the number or mass of the solid phase but measuring these quantities by means the sightglass setup is difficult. Nonetheless, HWS-3 behaviour in micromodel was very promising and effectively blocked leakage if solid particles were nucleated and formed irrespective of their size and the population.

Although the induction time of 4 hours and 52 minutes obtained in this sightglass test seem to be a long time for the particles to appear, at reservoir scale this is not a long time. To put this in perspective, a typical velocity of fluids in the underground storage reservoirs is about 1 ft/D, consequently, it would take about 30 days for the front of the injected CO_2 to flow through a fracture on 10m caprock. In the next section, an analysis of the nucleation of HWS-3 in supercritical CO_2 is presented.

Nucleation studies

Two main relationships which control the kinetics of nucleation of a solute (e.g., HWS-3) in supercritical CO_2 are expressed by Eq. 3-5 and 3-6, in which S represents the supersaturation of the solution from the upstream solubility ($y^*(P_{up}, T)$) and downstream solubility ($y^e(P_{down}, T)$) conditions of the leakage path;

$$S = \frac{y^*(P_{up},T)}{y^e(P_{down},T)} \qquad \text{Eq. 3-5}$$

$$J = A.exp\left(-\frac{16\pi\sigma^3 v_m^2}{3k^3.T^3(\ln S)^2}\right) \qquad \text{Eq. 3-6}$$

Where k is the Boltzmann constant or the gas constant per molecule and T is the temperature in Kelvin. In the Eq. 3-6, J is the rate of nucleation, e.g. number of nuclei formed per unit time per unit volume and A is the constant of nucleation. It should be noted that σ is the interfacial tension between the solute nuclei and supercritical CO_2 and v_m is the molecular volume of the solute. By re-arranging the parameters in these equations, a general equation for induction time can be obtained as shown in Eq. 3-7.

$$ln\,\tau \propto [-ln\,A + \frac{16\pi}{3} \cdot \frac{\sigma^3 v_m^2}{k^3.T^3(ln\,S)^2}] \qquad \text{Eq. 3-7}$$

Thus a plot of $ln\,\tau$ (τ is the induction time is second) against $(ln\,S)^{-2}$ should yield a straight line if the interfacial properties of the new phase remains constant with respect to pressure which is a reasonable assumption for solid solutes. To get a sense of the induction time values, Table 3-3 presents the induction times for crystallization of water drops in saturated vapour.

Table 3-3: Induction time in super-cooled water as function of supersaturation degree.

Supersaturation, S	Time
1.0	∞
2.0	1062 years
3.0	10^3 years
4.0	0.1 s
5.0	10^{-13} s

Figure 3-46 shows the classical plot of induction times for the experiments performed with HWS-3. According to this graph, the slope is 5.736, which yields an interfacial tension of 12 dyne/cm using equation 4-7 with corresponding interfacial information of HWS-3. This measure is not in the range of the proposed value of 20-40 dyne/cm when solid solute nucleates in supercritical solutions (Türk, 2000). It should be noted that no generic value for interfacial tension of solid solutes and supercritical solutions can be considered since the chemical structure of each solutes would determine its nucleation characteristics. Another outcome of this analysis is prediction of induction times at various supersaturations assuming that primary nucleation would govern the particle formation and also the classical nucleation theorem can describe the kinetics of phase changes.

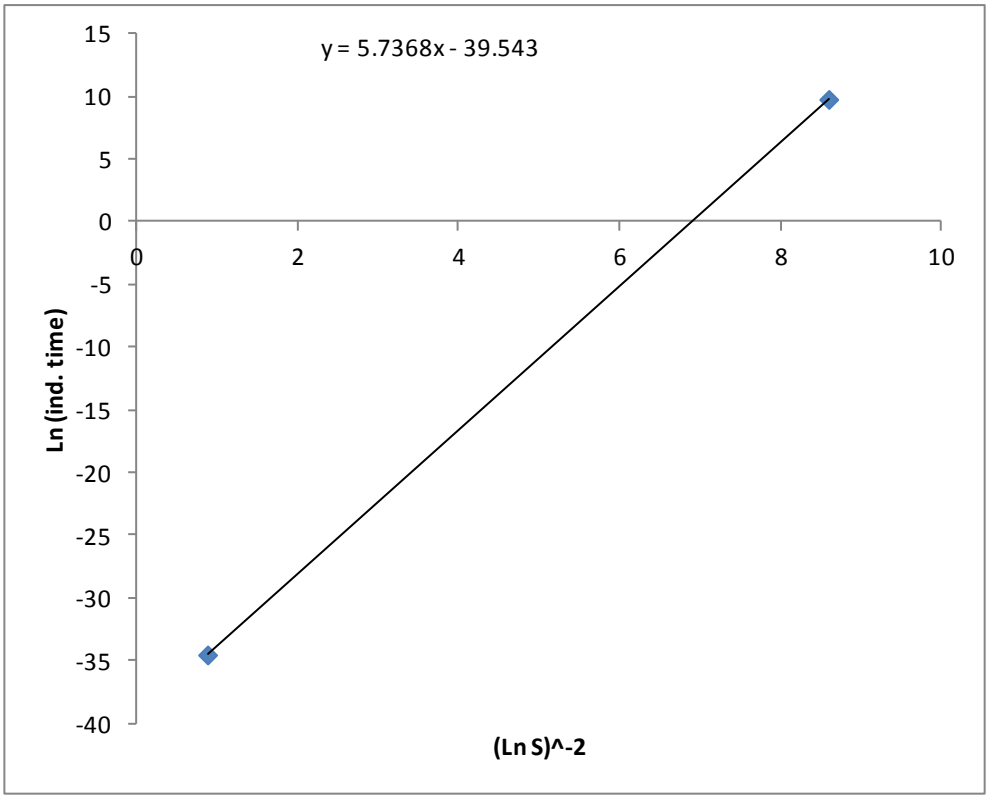

Figure 3-46: Classical induction time analyses to calculate interfacial properties of HWS-3.

3.8.2 Stability of solution in contact with water

Dissolution of CO_2 into reservoir brine is one of the important trapping mechanisms in the process CO_2 storage in underground reservoirs. Therefore, it is necessary to investigate the impact of CO_2 dissolution on the thermodynamic behaviour of CO_2 and solute mixture. Once the injected CO_2 mixes with in-situ fluids, some of the CO_2 molecules would dissipate from the solution to the reservoir brine. A sightglass test was carried out to study the long term mutual interaction between the fluids to ensure that the solution of CO_2 and solute remains stable during the dissolution of CO_2 in reservoir brine. In this experiment, distilled water was used to magnify the effects of CO_2 dissolution since salinity would decrease the CO_2 content of the brine. The procedure for doing the experiment is as follows; first, the sightglass was filled up with distilled water and pressurized to 2820 psig which is the saturation point of HWS-3 solution at 45 °C. Then, the mixture of solute (HWS-3) and CO_2 was injected into the sightglass at a very low rate of 1 cc/hr. During the flow of CO_2 solution into the sightglass, the interface between distilled water and CO_2 was followed by the camera to monitor the dynamic interaction between the phases.

As the CO_2 come in contact with the water in the sightglass dissolution of CO_2 in water begins and eventually the system achieves equilibrium whereby the water is saturated with CO_2 and likewise the CO_2 is saturated with water vapour. CO_2 solubility in distilled water at 2820 psig and 45 °C is about 5.4 weight percent (Duan & Sun, 2003).

Figure 3-47 shows a highly magnified image of the interface between CO_2 + solid-solute solution and distilled water in this test. Careful analysis of the image proved that no solid particles could be detected. Thus, the solution was not affected by the dissolution of CO_2 in water. The presence of salt in reservoir brine decreases the solubility of CO_2 into the brine. Therefore, the dissolution of CO_2 in brine during the injection and storage of CO_2 in aquifers is unlikely to cause any major issues for the leakage prevention technique.

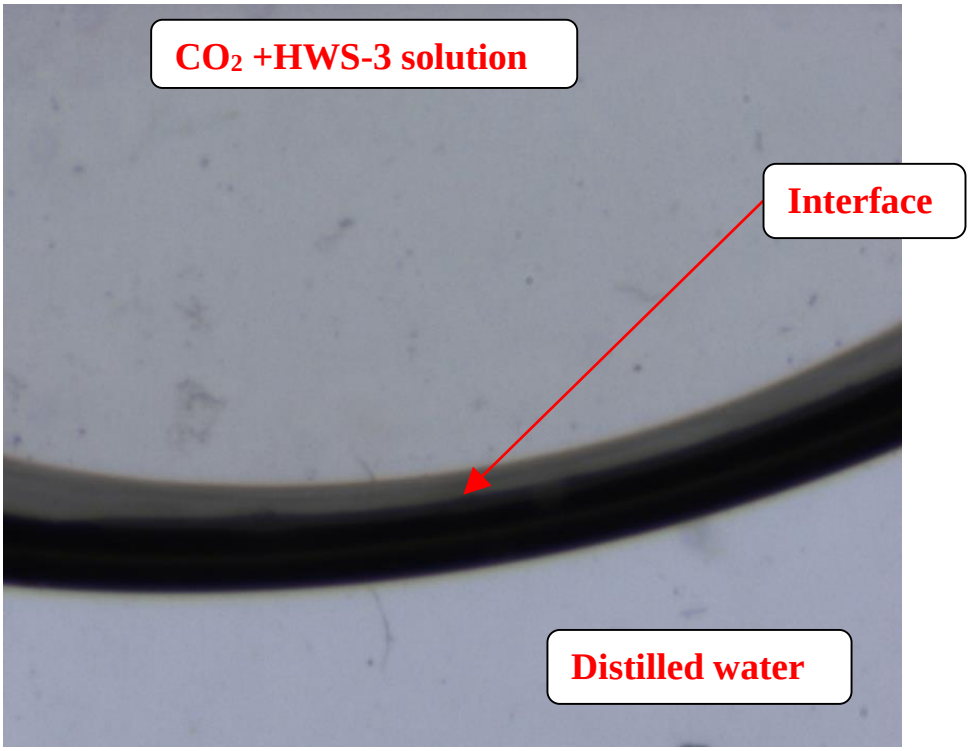

Figure 3-47: Mutual interaction of CO_2 solution and distilled water. No particle formed as a result of CO_2 dissolution in water.

3.9 Conclusions

For identifying the physics behind our proposed leakage prevention technique, a series of visualisation experiments was carefully designed to directly observe how the CO_2 + solid-solute solution would respond to simulated leakage path. Having performed theses micromodel visualisations, it was identified that the performance of leakage prevention technique is controlled by the dynamics behind nucleation and deposition of particles, which can be mainly influenced by solute type, solute solubility, degree of pressure drop, and flow velocity. Following detailed conclusions can be drawn from the micromodel experiment:

1. All the solutes tested in this work successfully sealed the induced leaks. However, the behaviour and the mechanisms of sealing were completely different for various solutes. Therefore, our proposed leakage prevention technique can potentially tackle and cease any contingent leakages.
2. Durability of the formed blockages was checked by pressurising the system after sealing. In some cases, if the leak was reopened, it was quickly sealed again due to reactivation of the sealing mechanism.
3. Using a highly soluble solute, it was observed that *HWS-5* would respond positively to the physically simulated leak. It was observed that high degree of solubility would make this solute highly responsive to the pressure drop as it was expected from analogy with new phase formation physics. On the other hand, this solute showed high affinity for adhering to the micromodel surface, which would facilitate the process of blockage formation.
4. For moderately soluble solutes, HWS-3 and HWS-2 were used in visualisation tests. HWS-3 exhibited a tendency to form blockage by agglomeration of particles together and packing the end of the leakage point by particles. However, HWS-2 would form larger particles leading to building up a more concentrated blockage body.
5. HWS-1 has been put forward as a marginally soluble solute with very inexpensive cost for practical field scale purposes. A firm and durable blockage was formed in the physically simulated leakage path. Having experimentally measured the onset of particle formation, it was observed that a relatively large pressure drop was needed to cease the lab scale leak. Nonetheless, HWS-1 has got a remarkable potential for industrial scale implementation of our proposed leakage prevention technique.

6. It was revealed that precipitation of solutes from supercritical CO_2 is governed by nucleation kinetics which does not happen under thermodynamic equilibrium. As a result, supersaturation of the CO_2 with solutes should be taken into account. In addition to supersaturation, IFT (interfacial tension between solute and CO_2) and molecular volume of solutes also impact particle formation. These parameters should be carefully considered for designing suitable solutes for the CO_2 leakage prevention technique.
7. Higher IFT between critical nuclei and the solvent (CO_2 solution) requires more energy for nucleation (onset of precipitation) although the role of molecular volume and temperature have to be considered too.
8. It was identified that three main mechanisms for deposition of particle would control the efficiency of precipitation; inertial impaction, inception, and sedimentation. Significance of each mechanism depends on the velocity of the flow and particle size.
9. As micromodel experiments were carried out at relatively high flow velocities, inertial impaction (change in flow streamlines) would have the predominant influence on the particle depositions.
10. Effect of impurities on the leak prevention technique was tested by adding 5% nitrogen to the CO_2 stream. It was observed that presence of nitrogen can improve the performance of the leakage prevention technique in two ways. First, it made the system more sensitive and responsive to drop in pressure and hence the system responded more quickly to leak. In one of the tests with nitrogen, the CO_2 injection pressure was 2966 psig and the blockage of the leak was achieved at 2800 psig (only 166 psig drop), which indicated significant progress in the design and effectiveness of the process. Second, while improving performance, it also reduced solubility of solutes in CO_2 meaning that less solute was required. Reduced solubility results in lower cost of field implementation of the leakage prevention technique.
11. The impact of presence of connate water on the performance of the leak prevention mechanism was investigated. The results showed that a relatively large leak was still effectively sealed by the process and in the presence of connate water. The main difference between the experiments with water with those without water was that the sealing process took place with some delay mainly caused by the presence of water layers on the surface of the porous medium.

12. In sightglass experiment, using HWS-3, the time required for particle formation under a definite pressure drop was measured, i.e. 4 hours and 52 minutes at pressure drop of 520 psig, and hence the relevant equations for nucleation kinetics was tuned to obtain the interfacial tension between HWS-3 particles and supercritical CO_2.
13. In another sightglass experiment, the mutual interactions between distilled water and the solution of CO_2 + HWS-3 were investigated to examine whether dissolution of CO_2 into the water would disturb the equilibrium in the solution and hence premature particle formation happens. Based on the observation, no HWS-3 particle was formed due to CO_2 dissolution and hence integrity of the solution would be preserved as it flows through the storage reservoir.

CHAPTER 4 Performance of Leakage Prevention Technique in Sandpack and Reservoir Rocks

4.1 Introduction

In previous chapter, the efficiency of the proposed CO_2 leak prevention technique was visually investigated in micromodel experiments, which provided a better understanding of the pore-scale mechanisms of formation of particles and their deposition at the leakage point. Various types of solutes, in terms of their solubility in supercritical CO_2, have been utilised in the micromodel experiments to produce the fundamental physics, which controls the kinetics of particle formation and precipitation. The majority of the micromodel experiments were performed at a relatively high pressure drop for which effective and durable blockage was formed. The interfacial properties of solid solutes and supercritical CO_2 have been recognised as an important pertinent parameter in generating solid phase in the solution.

In this chapter, two different porous media were utilised and the performance of the proposed leakage prevention technique was aimed to be investigated at various leakage rates and reservoir conditions. Provided that micromodel visualisations are very cumbersome to conduct, in the first set of experiments in this chapter, a long pipe packed with very fine grains of sand was used as a tool to evaluate the response of the CO_2 + solid-solute solutions to high leakage rates. Therefore, these experiments not only would shed some light on the performance of leakage prevention technique at high rates but also,

it would demonstrate whether Sandpack setup can be used as a simple yet robust screening tool to examine different solutes at various storage and leak conditions.

In a separate set of experiments, a number of coreflood experiments were carefully designed and carried out using real reservoir rocks. To better represent the realistic leakage paths with relatively large dimensions (length) coreflood experiments have been performed to investigate the effect of test conditions on our results. Also, the response of a CO_2-solute solution to low pressure drop (supersaturation) has been investigated to cover a wide range of supersaturations (low and high) that might take place in a real leakage scenario under reservoir conditions. Six coreflood experiments have been conducted to physically simulate precipitation of solutes in real porous media. Two different approaches were employed to prepare the CO_2 + solid-solute solution; (i) surface mixing where solid solute and CO_2 mixed in a cell prior to injection and (ii) bottomhole mixing in which, a pack of solid solute was placed in the lines connecting the CO_2 cell to the physically simulated leakage path and hence the injection CO_2 would become saturated with solid-solute as it flows through the solute pack. Using these designs, the results of the coreflood experiments can reveal whether a durable blockage would be formed in the core in response to a pressure drop and the flow (leakage) of CO_2 can be effectively sealed.

4.2 Sand-Pack Experiments (High Leakage Rates)

Sandpack facility was used in this study to quantify the pressure response of the solution and also as a reliable tool for fast screening of the solutes suitable for a particular application. The main feature of the sandpack experiments is its capability to determine the pressure at which the blockage can form in a rather short period of time. Sandpack setup is also equipped with a sightglass enabling us to visualize the influence of the suspension flow and particles size, which can be very helpful to study the kinetic of the precipitation process. In the next section, the experimental design and setup of the Sandpack rig is discussed. After that, basic properties of the solutes used in the test performed using this experimental set-up are given. Then, the results of series of the sandpack experiments performed using different solutes at different prevailing conditions are presented.

4.2.1 Experimental design

In this experimental set-up, a high pressure CO_2 + Solute cell represents the CO_2 storage reservoir at the prevailing conditions of CO_2 storage. This cell is connected to a simulated leakage path (sandpack) which has been set at a relatively lower pressure. This lower pressure drop is applied by another cell which acts as destination site for the leaked CO_2. The sandpack porous medium is considered as a crucial element of the interface between these two cells. Glass beads with very fine mesh size (350-400mesh size) were packed into a pipe to physically simulate a one dimensional flow conduit representing a leakage path in a CO_2 storage reservoir. The permeability of the sandpack (leakage path) is considerably high and therefore would not introduce considerable pressure drop across the sand pack. In all of the sandpack experiments, the leak has been applied in the form of a constant lower pressure at the outlet by setting the corresponding pump pressure.

In the sandpack experiments, the CO_2 and Solute have been brought into equilibrium at the test conditions to ensure that the resulting solution is at the saturation point. Subsequently, the pressure of the sandpack is adjusted to the leak conditions. It should be pointed out that the abrupt pressure difference between CO_2 + Solute cell and the sandpack (leakage path) allows us to have a preliminary investigation of the solute response to a pressure drop in a relatively short period of time prior to conducting the rigorous and cumbersome coreflood experiments. Therefore, the results of sandpack experiments can be used for screening potential solutes. In other words, once a solute successfully blocks the sandpack as the leakage path, it would be employed for further analysis using our coreflood or micromodel facilities.

This Sandpack facility is housed in a constant temperature oven. Similarly to the other experimental setups such as micromodel and coreflood experiments, the temperature of the oven has been set to 45^{o}C as the prevailing conditions of the leakage prevention experiments studied here. However, it should be mentioned that the temperature of leaking CO_2 would be decreasing as it flows upward and this reduction in temperature as a result of geothermal gradient is small and is expected to facilitate the precipitations favourably. Furthermore, it should be noted that there could be additional temperature drop because of the Joule-Thompson effects of CO_2 flow across the leakage path, which can be important for these experiments with more sudden pressure drop. However, as mentioned before, if the performance of a solute has been verified at isothermal

conditions, its blocking efficiency is expected to be higher in a real case with declining temperature.

4.2.2 Solutes

In this study, five different solutes have been used to test the efficiency of our proposed leakage prevention method for tackling CO_2 leakage in the sandpack. The criterion for classifying the solid solute solubility level is that if the maximum solubility of the isotherm is (i) above 0.01 (ii) between 0.01 and 0.001 or (iii) below 0.001, in mole fraction, the solid solute is a highly, moderately or marginally soluble solute, respectively. The main advantage of marginally soluble solutes is economic considerations since the very low concentration of the solute results in reduction of the cost of the proposed leakage prevention method by reducing the required amount of the solute. In the subsequent chapter, a method is proposed and verified experimentally for improving the efficiency of marginally soluble solute.

The moderately soluble solutes are considered as the main solutes that can be applied at the field scale. HWS-2 and HWS-3 that were investigated in micromodel and coreflood experiments have also been employed here in these sandpack tests.

4.2.3 Marginally soluble solutes

HWS-4

The melting point of HWS-4 is 218 ^oC which is in the form of solid particles at most storage conditions. This solute is insoluble in water, which makes it suitable to be applied in aquifers. Generally speaking, HWS-4 can be considered as a very-low soluble solute for storage purposes. Figure 4-1 shows the measured isothermal solubility of HWS-4 in supercritical CO_2 at 45 ^oC, which is the prevailing working temperature of the experiments reported here. The experimental procedure and steps for measuring the solute solubility are explained in details. It is obvious that in the test conditions HWS-4 dissolves into supercritical CO_2 at a very small quantity, i.e. 0.00008 mole fraction at 3000 psig as the storage pressure of the experiments reported here.

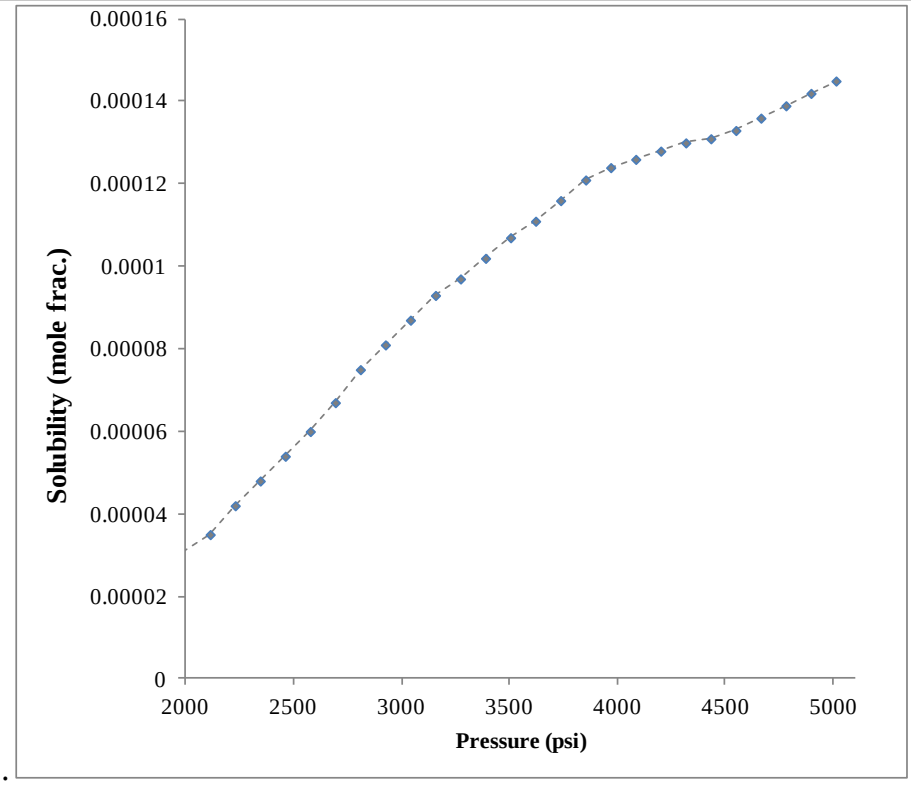

Figure 4-1: Isothermal solubility of HWS-4 in supercritical CO_2 at 45 ^oC.

HWS-1

HWS-1 can be produced in abundance as one of the by-product of processing the natural gas. The melting point of the solute is 115 ^oC and it is insoluble in water. Figure 4-2 illustrates the isothermal solubility of HWS-1 in supercritical CO_2 at 60 ^oC. Although the solubility of HWS-1 is higher than HWS-4, the range of the solute solubility falls into the category of marginally soluble solutes. The low cost of HWS-1 makes it economically attractive for using in our proposed leakage prevention method. Nonetheless, the efficiency of HWS-1-rich solution in tackling leakages has not been well-studied before.

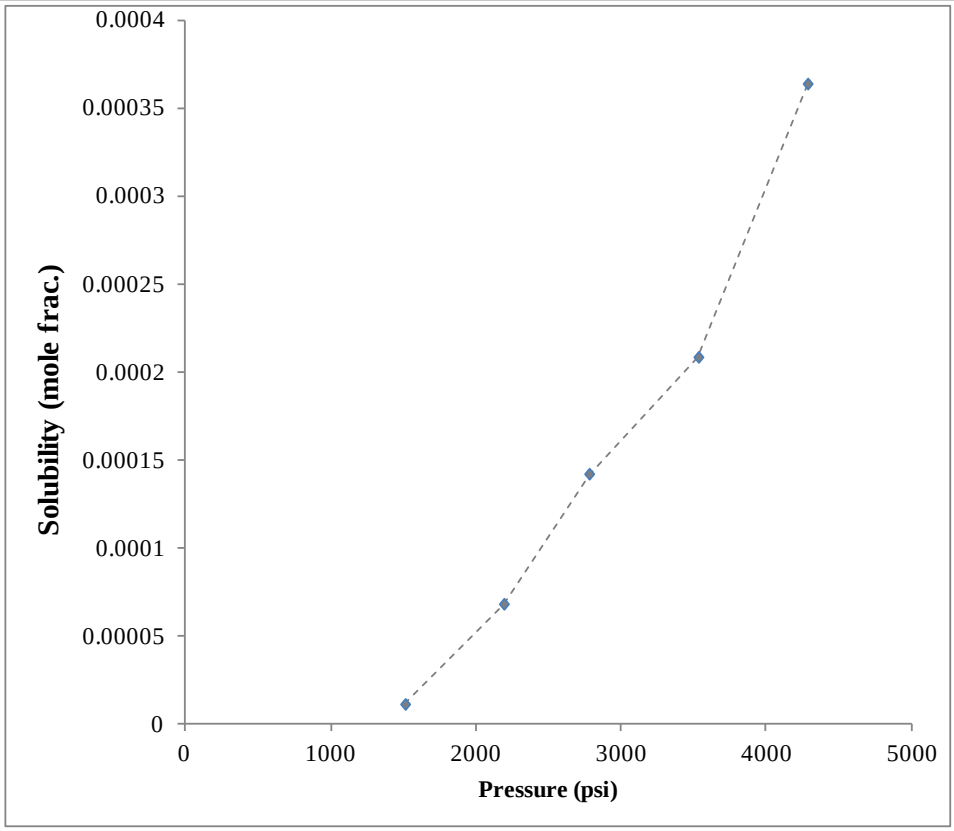

Figure 4-2: Isothermal solubility of HWS-1 in supercritical CO_2 at 60 ^oC.

4.2.4 Moderately soluble solutes

HWS-2

HWS-2 has a melting point of 270^oC, which makes it applicable in deep reservoirs. The solute is insoluble in water; therefore resident water cannot dissolve the blockage formed. Figure 4-3 shows the solubility profile of HWS-2 in supercritical CO_2 at constant temperature of 45 ^oC. HWS-2 (with around 0.00265 mole fraction solubility at 3000 psig and 45 ^oC) is categorized as a moderately soluble solute. This solute has been used extensively in micromodel and coreflood experiments.

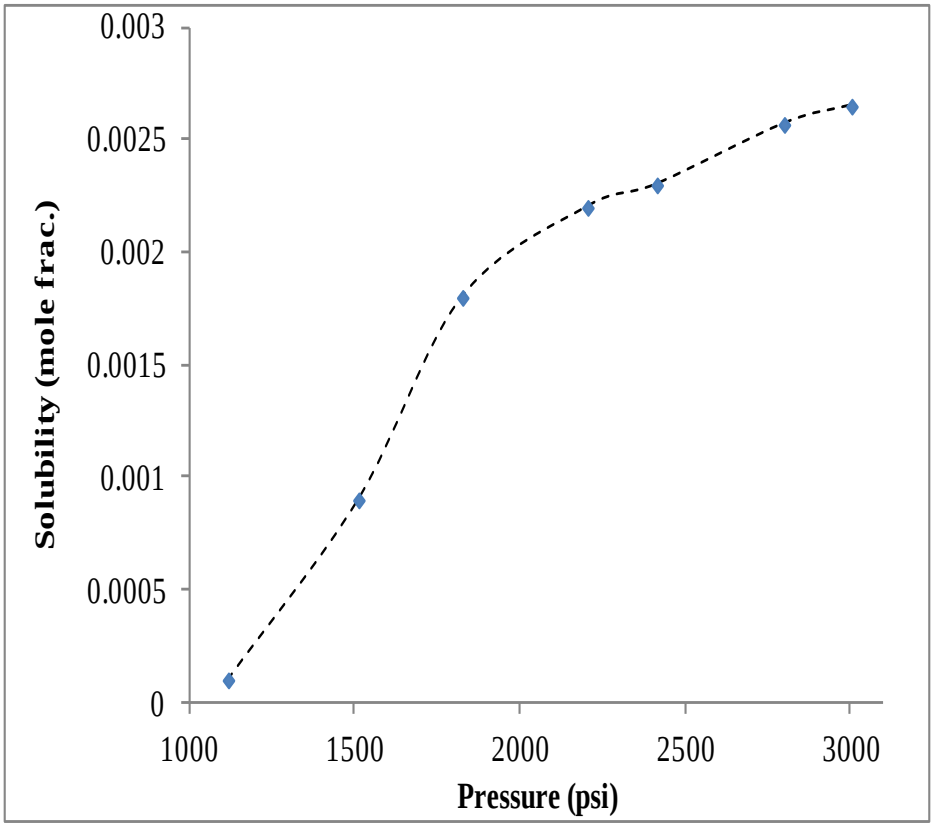

Figure 4-3: Isothermal solubility of HWS-2 in supercritical CO_2 at 45 ^oC.

HWS-3

HWS-3 (with around 0.0035 mole fraction solubility at 3000 psig), similar to HWS-2, dissolves moderately in supercritical CO_2. The melting point of this solute is 83^oC, which makes it suitable for prevailing conditions of not very deep reservoirs and perhaps aquifers. Figure 4-4 illustrates the solubility of the HWS-3 as a function of pressure. HWS-3 has been tested in several of our micromodel and coreflood experiments.

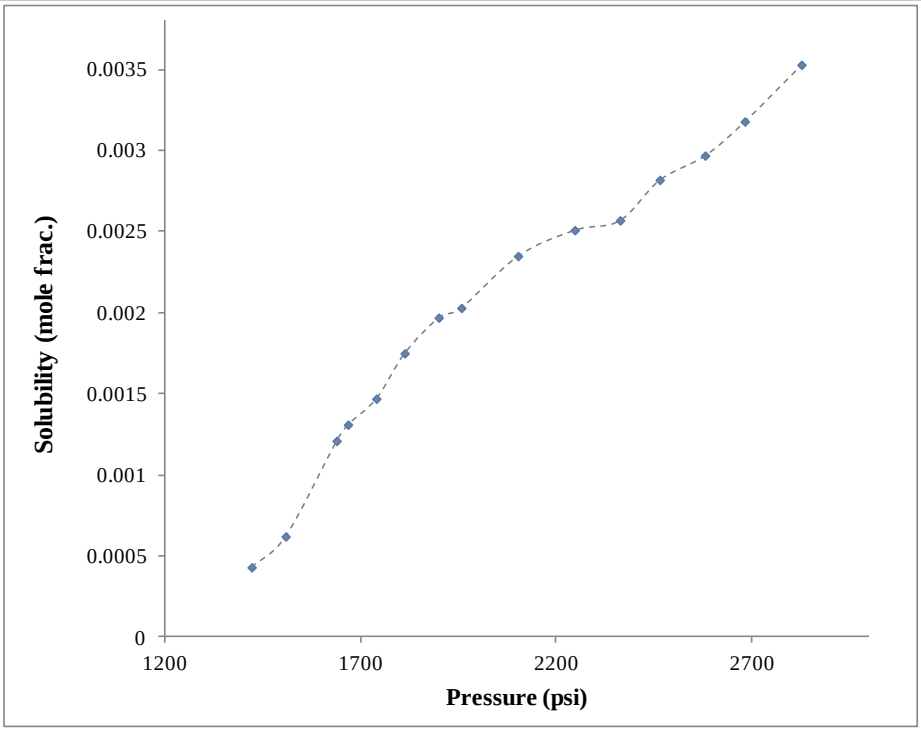

Figure 4-4: Isothermal solubility of HWS-3 in supercritical CO_2 at 45 ^oC.

4.2.5 Sandpack Test No. 1&2 (HWS-4)

Test conditions and results

In the following tests with HWS-4, the solution was prepared at 3000 psig and 45 ^oC. Initially, 5 gr of HWS-4 was place in the cell and 300 cc of high pressure CO_2 (3000 psig) was injected into the cell to prepare the solution, which was shaken intermittently to ensure that the mixture is in equilibrium. Based on the measured solubility of HWS-4, the weight required for having the solution at its saturation point is about 0.8 gr and hence the amount of solid solute in the cell (5 gr) is enough to ensure that the supercritical CO_2 is fully saturated with this solid solute. First trial test with HWS-4 was performed at the leak pressure of 2000 psig to investigate the behaviour of the solution when it undergoes the relatively high pressure drop of 1000 psig.

The solubility of the HWS-4 at the inlet (i.e. 3000 psig and 45 ^oC) and outlet (i.e. 2000 psig and 45 ^oC) conditions of sandpack are 0.00008 and 0.00003 mole frac., respectively, which corresponds to the supersaturation of 0.0008/0.0003=2.66 at leakage conditions. The pumps maintain the inlet and outlet pressures at 3000 and 2000 psig while CO_2

saturated solution passes through the simulated leakage path. Usually the flow of the supercritical CO_2 continues until the leak is blocked or significant precipitation is identified. At first trial with HWS-4, 280 cc of the injection cell volume was injected but no sign of a blockage (e.g. pressure discontinuity) was recognised by the transducers and the pumps and hence, it was concluded that HWS-4 saturated solutions could not block the simulated leakage in the sandpack. Figure 4-5 demonstrates the entrapment of HWS-4 particles in the sightglass which indicates that solid solute was formed in the sandpack but the amount was not sufficient to form a full blockage.

After the test was finished, the sandpack was disconnected from the rig and toluene was injected into the porous medium to recover the amount of solute precipitated. Then, the effluent was dried out. The residual solid solute represents HWS-4 produced from the sandpack. The weight of the recovered solute was 0.04 gr. In an ideal scenario, 0.06 gr of HWS-4 would be precipitated in sandpack as a result of the imposed pressure drop. The 0.02 gr difference from the ideal case can be attributed to the suspension flow of the particles carrying away the solid solute, which was observed in sightglass, and also the delay in nucleation of the HWS-4 particles.

After analysing the response of HWS-4 saturated solution to the imposed pressure drop of 1000 psig, Second test was performed at the leak pressure of 1800 psig. The condition at which CO_2 + Solute solution was prepared was identical to the first test. Therefore, the only difference in this test is the 200 psig higher pressure drop. Similar to the previous test, no blockage was formed after 280 cc of the solution flowed through the sandpack. In terms of the particles property in the sightglass, the images were similar to Figure 4-5 showing the presence of HWS-4 particles in the sightglass indicating the formation of the solid solute which was not adequate to block the flow of CO_2.

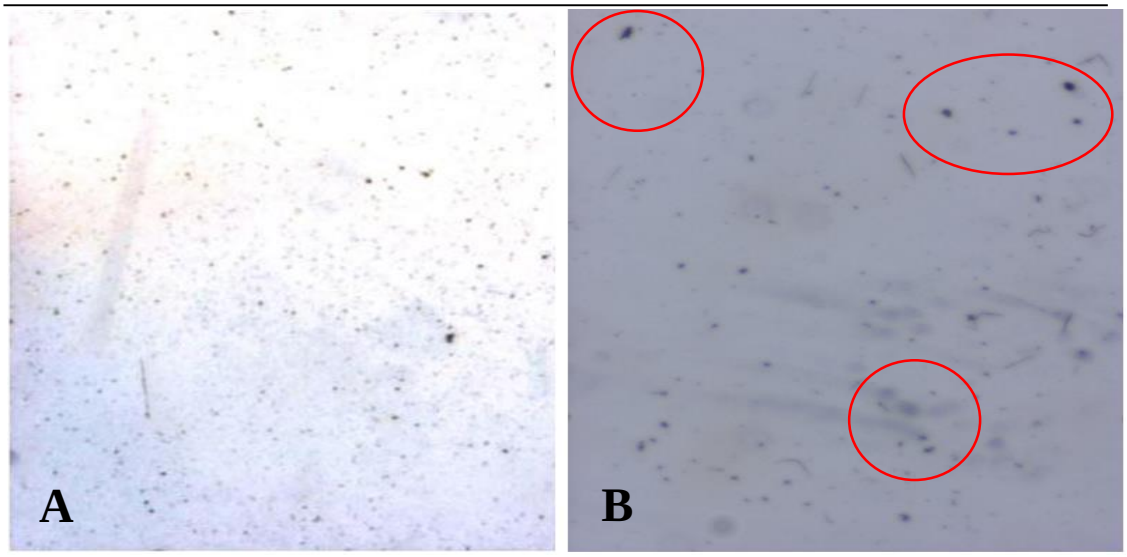

Figure 4-5: The states of sightglass during the test with HWS-4; A: initial sightglass image with no HWS-4 particles, B: HWS-4 particles (highlighted with red coloured circles) are observed in the sightglass image as a result of suspension flow.

Similar to the first test, the precipitated solute was recovered by injecting toluene into the sandpack. The resulting HWS-4 recovered was 0.04 gr, which is equal to the first test. Ideally, the precipitated solute should be 0.065 gr since the pressure drop is 1200 psi, i.e. 200 psig higher than the first test, but the recovered solid was the same. This happened because of more pronounced suspension flow when the pressure drop was increased. Therefore, if the formed solid particles are not enough to precipitate locally, the particles tend to be carried with CO_2 in the form of suspension flow.

4.2.6 Sandpack Test No. 3&4 (HWS-1)

HWS-1 as a marginally soluble solute was used to investigate the consistency and reliability of the results of the sandpack experiments using HWS-4 also with very low solubility power. In order to have a sound comparison between HWS-4 and HWS-1, the test conditions were exactly the same, i.e. the solution was prepared at 3000 psig and 45 ^{o}C. At equilibrium conditions, 1 gr of HWS-1 would be dissolved into the 300cc of supercritical CO_2 at these conditions (i.e. 3000 psig and 45 ^{o}C). To ensure having solution at saturation point, prior to perform the experiments, 5 gr of HWS-1 was placed in the cell to make up the CO_2 + Solute solution..

Test conditions and results

The first test using HWS-1 was carried out at the leak pressure of 1800 psig (Test No 3). After flow of 280 cc of the solution, no indication of significant precipitation or full blockage was identified. After completing the test, toluene was injected into the sandpack to wash out the solute precipitated in the porous medium. 0.032 gr of solute was recovered from the sandpack. Nonetheless, the amount of precipitated HWS-1 was not sufficient to form a blockage in the simulated leakage path in both tests.

Similar test conditions and procedure as those of Test No 3 were followed to perform Test No. 4 with the only difference being the leak pressure which was 1500 psig (as opposed to 1800 psig in Test No.3), which corresponds to the pressure drop of 1500 psig. After flow of 280 cc of the solution through the sandpack, significant precipitation and a consequent blockage were formed which identified from the pressure and rate gauges. Although the blockage formed, the precipitation failed in durability test; the inlet pressure increased by 200 psig and the precipitation was removed. Figure 4-6 illustrates the state of the sightglass during the flow of the solution through the sandpack which demonstrates the presence of the HWS-1 particles in the visualization cell. The existence of particles in the outlet of the sandpack again indicates the impact of suspension flow in carrying the formed particles. The solubility and supersaturation degree of HWS-1 in supercritical CO_2 is higher than that of the HWS-4 but the amount of particles in the sightglass is less in the case of HWS-1 which indicates weaker suspension flow, i.e. the HWS-1 particles have higher tendency to attach to the porous medium.

Similar to the HWS-4 experiments, toluene was injected for cleaning and recovering the solute particles precipitated in the sandpack. The effluent was dried out of toluene and the resulting HWS-1 was weighted to be 0.05 gr. Figure 4-7 shows the recovered HWS-1 in the beaker, the colour of which confirms the purity of the recovered solute.

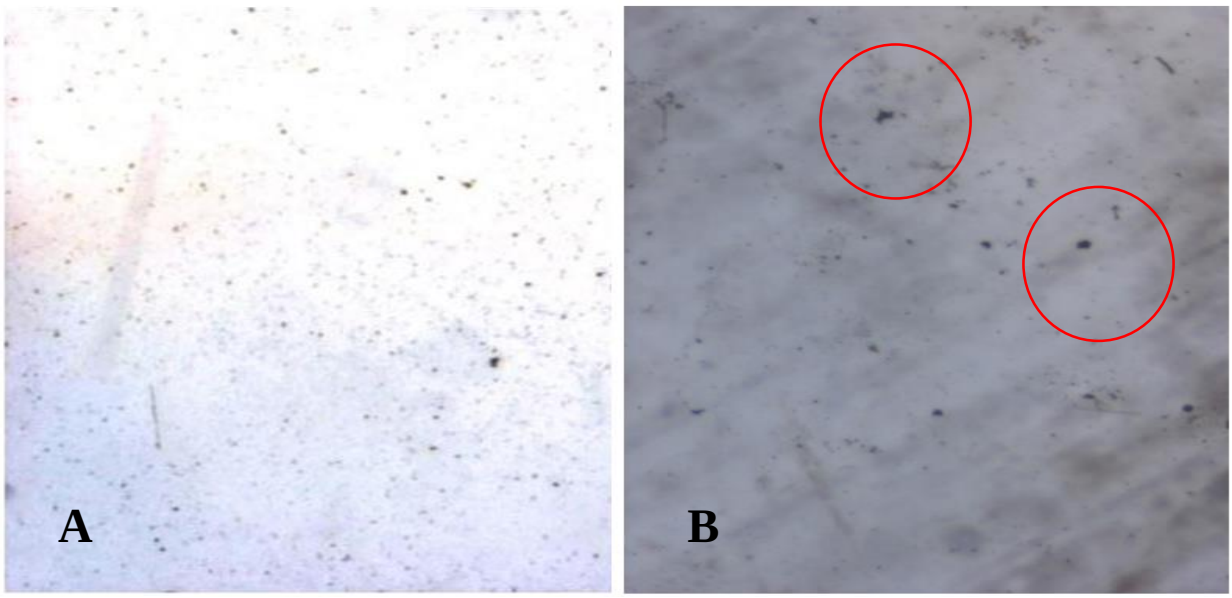

Figure 4-6: The states of sightglass during the test with HWS-1; A: initial sightglass image, B: HWS-1 particles (highlighted with red coloured circles) are observed in the sightglass image as a result of suspension flow.

Figure 4-7: HWS-1 precipitant produced from the sandpack.

4.2.7 Sandpack Test No. 5 (HWS-2)

HWS-2 as a moderately soluble solute was used in this test. Previously, HWS-2 had been used successfully in the micromodel and coreflood experiments making it a good candidate for applying in the CO_2 leakage method. However, the lowest leak pressure at which HWS-2 particles would come out of the solution and precipitate has not been determined in previous tests. As described before, sandpack facility has been used to

assess the solute behaviour in the case of sudden leakages. For Test No.5, 6 gr of HWS-2 was placed in the CO_2 + Solute cell and pure CO_2 was injected into the cell to pressurize it to 3000 psig. The test temperature was set at 45 ^oC. The solubility of HWS-2 at the injection cell is 0.00265 mole fraction. Although several tests at various leak pressures were performed, the highest leak pressure at which a successful blockage was formed is presented here.

Test conditions and results

The leak pressure was set at 2250 psig, which corresponds to the pressure drop of 750 psig across the sandpack. After flow of 70 cc of the solution through the sandpack, a firm and durable blockage was formed in the porous medium. The pressure discontinuity and no-flow condition between two ends of the sandpack indicated that HWS-2 particles precipitated and sealed the leakage path. Figure 4-8 shows the presence of HWS-2 particles in the sightglass at two stages; first (B), in the middle of the test, and, second, (C) at the end of the flow. Evidently, HWS-2 particles have a strong tendency to be attached to each other and form larger particulates as the test proceeds, which is favourable for our leakage prevention method. Because of observation of these particles in the sightglass, it can be concluded that, suspension flow exists in these sudden leakage scenarios regardless of the occurrence of blockage.

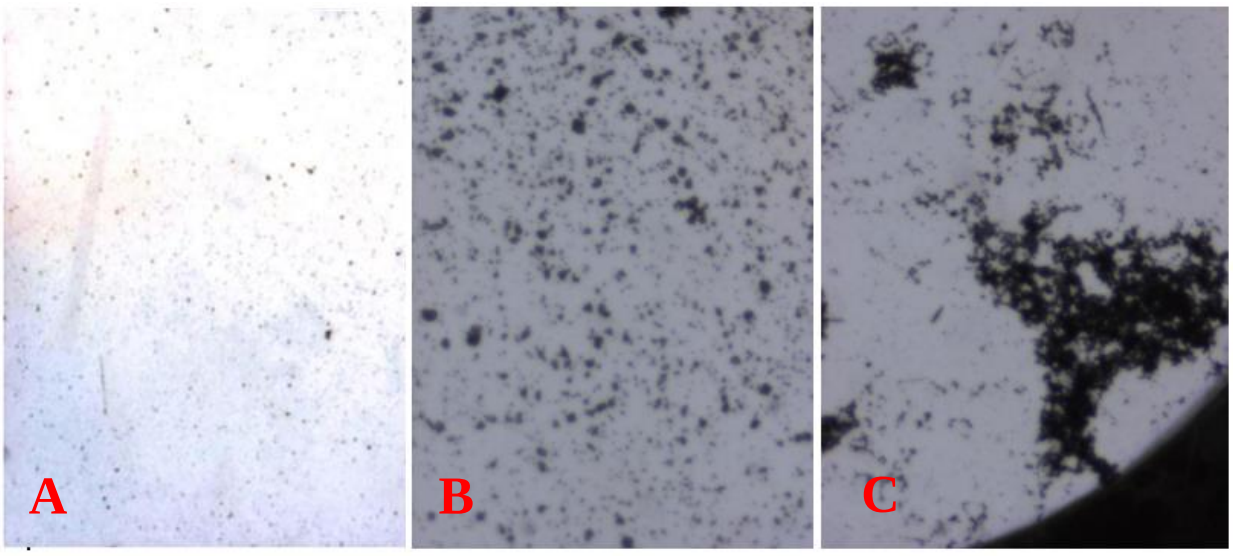

Figure 4-8: The states of sightglass during the test with HWS-2; A: initial sightglass image, B: HWS-2 particles are observed during the test as a result of suspension flow, C: aggregation of the HWS-2 particles to form larger particulates at the end of the test.

We can compare HWS-2 with HWS-4 and HWS-1. The measured solubility of HWS-2 in supercritical CO_2 at 2250 psig and 45 ^oC is 0.001951 mole fraction which gives a supersaturation degree of 1.36 for the solution at the leakage site. This supersaturation degree is much lower than that of HWS-4 and HWS-1, which indicates its less precipitation tendency. However, it seems that the magnitude of solubility is a crucial parameter for having an efficient blockage. After stabilization of the blockage, the inlet pressure was increased to 3500 psig to check the durability of the blockage, which was successful in that the blockage did not open. Subsequently, a mixture of Methanol/Acetone was injected to clean the sandpack and to recover the precipitated solid solute. The effluent was dried out and the weight of the residual HWS-2 was measured as 0.1 gr. This small amount of precipitated solute in the sandpack reveals that the blockage is concentrated locally and effectively and that to stop the leak at a relatively high pressure drop of 750 psig, there is no need to have massive precipitation, which is a confirmation of our theory that our CO_2 leak prevention technology would efficiently block the actual pores that are involved in the leakage.

4.2.8 Sandpack Test No. 6 (HWS-3)

To have a better understanding of the role of solubility in the formation of the blockage, HWS-3 was considered as another moderately soluble solute. Like HWS-2, 5 gr of HWS-3 was placed in the CO_2 + Solute cell and the cell was pressured to 3000 psig with pure CO_2 at 45 ^oC. The solution cell was shaken to achieve thermodynamic equilibrium. 280 cc of supercritical CO_2 dissolves 3 gr HWS-3 to become saturated with HWS-3 therefore the 5 gr HWS-3 available in the cell was sufficient to have a fully-saturated solution. The main purpose for performing experiments with HWS-3 was to compare the highest leak pressure at which the blockage would form with the corresponding pressure of HWS-2. Hence, several tests were carried out at various pressures to determine the highest leak pressure.

Test conditions and results

In this test, the outlet pressure of the sandpack (leak pressure) was set to 2100 psig, which corresponds to the pressure drop of 900 psig across the porous medium. 80 cc of HWS-3 saturated CO_2 solution flowed through the sandpack when the blockage was formed.

Observation of no-flow conditions at the pumps was the main indication of the formation of the blockage in the sandpack. Figure 4-9 illustrates the entrapment of HWS-3 particles in the sightglass, which again shows suspension flow. By a preliminary and qualitative comparison between Figure 4-8 and Figure 4-9, it can be seen that the particulate size of the HWS-2 is larger than HWS-3, which is due to two possible reasons; either the single particles of HWS-2 is larger than that of HWS-3 or the formed HWS-2 particles have more tendency to coagulated and form larger particulate.

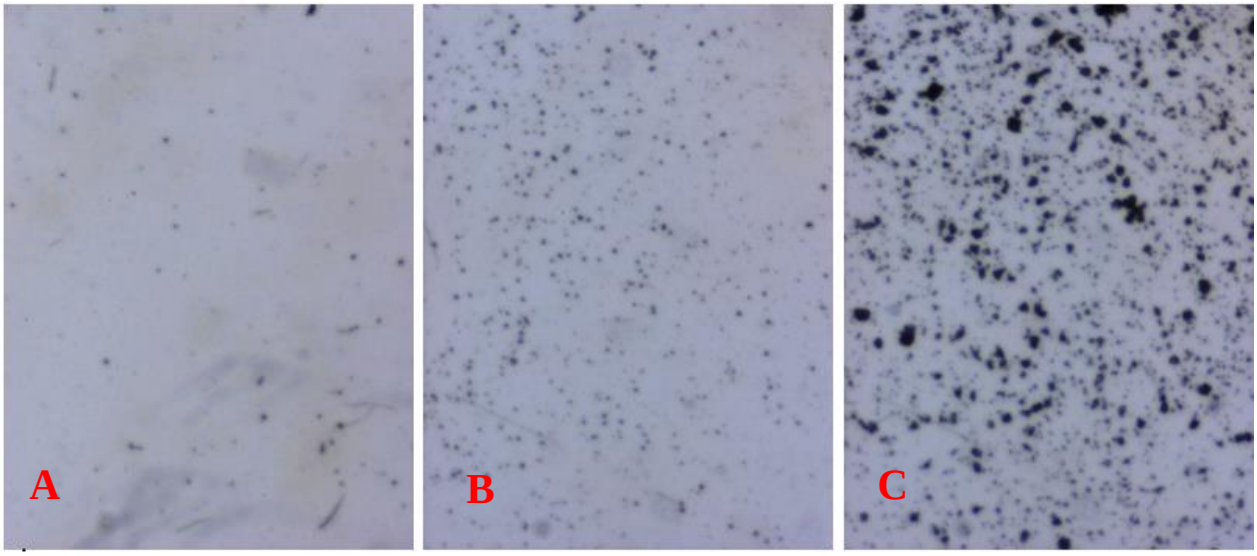

Figure 4-9: The states of sightglass during the test with HWS-3; A: initial sightglass image, B: HWS-3 particles are observed during the test as a result of suspension flow, C: aggregation of the HWS-3 particles to form larger particulates end of the test. HWS-3 forms smaller particles compared to HWS-2.

After formation of blockage, the inlet pressure was increased to 3500 psig to investigate the durability of the blockage. No indication of flow re-establishment was identified from the pressure and flow gauges. Therefore, the blockage was considered to be firm and durable. When the test finished, Acetone was used for cleaning the sandpack and the effluent was dried to recover the precipitated HWS-3. The weight of the solid solute was 0.11 gr which was consistent with the same relatively low value measured for HWS-2. Thus, it can be concluded that similar to the previous test using HWS-2, the HWS-3 blockage also occurred in a very concentrated form and without a need for large amount of precipitation.

Having analysed the results of the sandpack experiments with HWS-2 and HWS-3, it is noted that the highest pressure at which the blockage is formed s between 2100-2250 psig

which corresponds to the pressure drop of 750-900 psig. It should be noted that lower pressure drops, e.g. 500 and 600 psig, were tested but no successful blockage was formed against the simulated leakage. The need for relatively high pressure drop in these tests would undermine the efficiency of the leakage prevention method to some extent. In the next section, an idea for improving the efficiency of the leakage prevention method will be discussed when the results of the sandpack experiments using a secondary solute are presented.

4.3 CORE FLOOD EXPERIMENTS

We have so far investigated the proposed leakage prevention method using direct visualisation (micromodel) and sandpack experiments.

The micromodel tests were designed to analyse the response of the method to leakages associated with relatively high pressure drops. The results of micromodel visualisation experiments also visually demonstrated mechanism of the solid solute precipitation out of the CO_2 -solute solution. The outcome of the micromodel experiments showed that there is a time lag in the formation of solid solute after a pressure drop has been imposed on the system. This time lag mainly depends on the flow characteristics of the simulated leakage path such as supersaturation (pressure drop), flow rates, type of solute, and thermodynamic properties. These observations were verified using three different solutes. Moreover, it was identified that the precipitation takes place locally in concentrated forms rather than fully packing the leakage path. This would have an important implication that a small amount of solid solute is required to smartly target the main leaking paths and cease any contingent leakage.

In this section, coreflood experiments are mainly carried out for two purposes; first, to simulate slow rate of leakage and, second, to apply leakage prevention method in real porous rocks. As the primary trials, three core experiments with HWS-2 and HWS-3 saturated solutions were performed, which revealed that HWS-2-saturated solution is able to effectively seal the leakage path with concentrated precipitation of the solute provided there is sufficient pressure drop and optimum flow rate. Therefore, the occurrence of blockage depends on the flow properties and experimental conditions.

However, the delay in particle formation, which is controlled by nucleation kinetics have led into unfavourable behaviour of the method in two of the experiments. In Experiment No. 4 using HWS-2, the length of the high permeable core was not sufficient and the particles were not formed in the porous medium. In Experiment 6 using HWS-3 as the solute, either high pressure drop was required to seal the leak or the flow rate was needed to be notably lower. It should be noted that these core flood experiments are time consuming and optimising the test conditions can be a lengthy process.

4.3.1 Experimental Design

The behaviour of the system (CO_2 + solute) needs to be evaluated in real porous media (rocks) which are better able to replicate the real conditions of storage sites. Although the micromodel and sandpack experiments have revealed many of the controlling factors and mechanisms including the solution (CO_2 + solid solute) resistance to particle formation in response to pressure drops. In the previous experiments (micromodel and sandpack) the rate of CO_2 flow was high when the solutions were exposed to high pressure drops. The average velocity of CO_2 front flowing through the micromodel in response to a high pressure drop could be as high as 10^3 meter/day (based on Darcy's law) which is much higher than a typical velocity of fluids in reservoirs. Despite the high rate, the micromodel experiments revealed visually some essential and fundamental mechanisms at pore level. The experiments with high rate of flow were also useful as they simulated the conditions where a sudden release of the stored CO_2 takes place.

Coreflood experiments, on the other hands, allow us to get closer to the real conditions at which CO_2 is stored in geological formations. Figure 4-10 demonstrates a leakage scenario that has been used as the basis of our core flood experiments. In this scenario CO_2 leaks from the storage formation through a leakage path, e.g. fracture, into an upper formation which is not targeted for CO_2 storage. The thickness of the caprock is assumed to be 20 metre with a differential pressure in the range of 200 to 500 psig through a fracture. The frontal velocity of the leaked CO_2 is assumed to be very low and in the range of 0.1-10 metre/day.

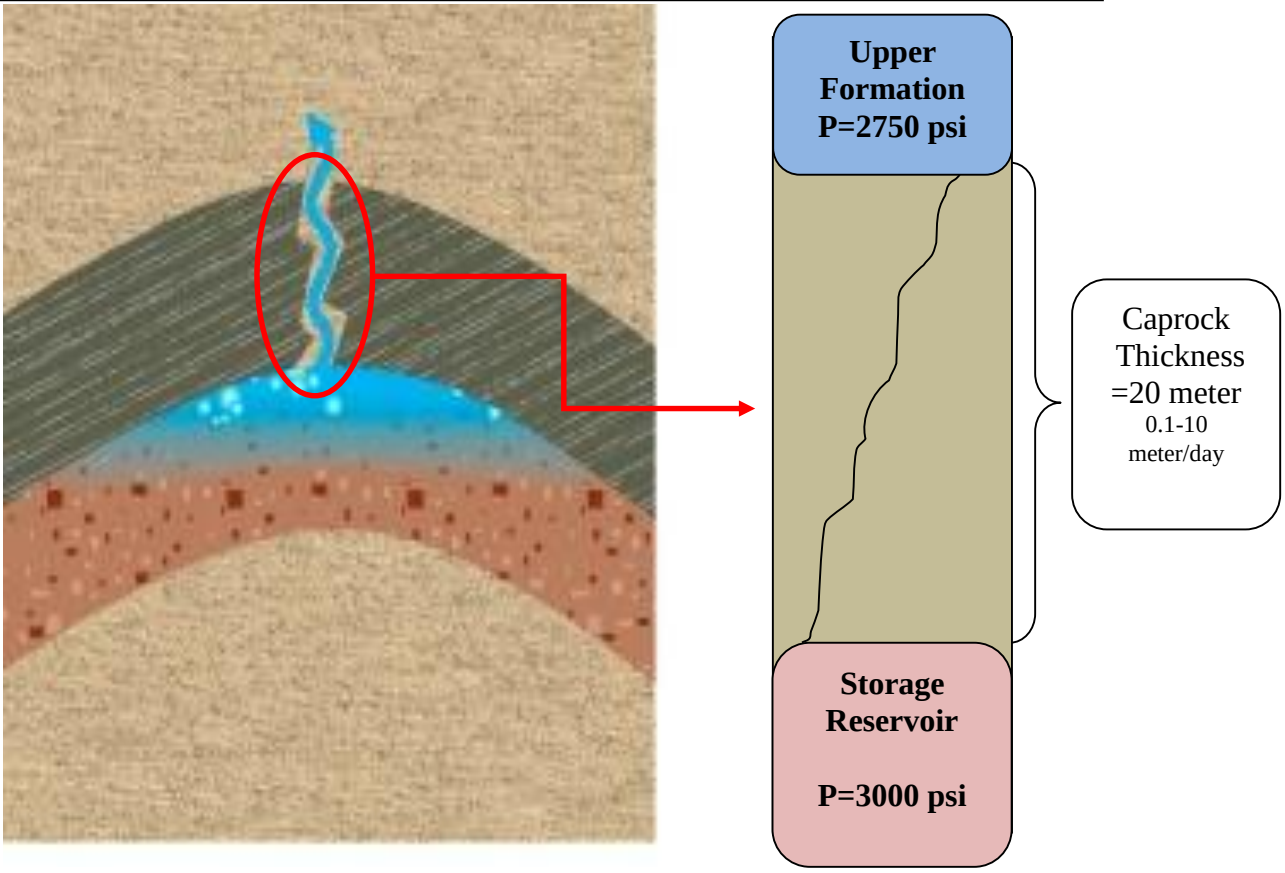

Figure 4-10: Schematic flow behaviour of a leakage from a caprock with thickness of 20 meter to a ground water formation. The storage pressure is 3000 psig and pressure of the overlying formation is assumed to be 2800-2750 psig.

The predominant behaviour of CO_2 flow within a fracture-like leakage path has been used as the rationale in designing the coreflood experiments. Therefore, in the coreflood tests, the pressure drops (DP) across the core was maintained in the range of 200-500 psig while the frontal velocities were kept in the range of 0.1-10 m/d (metre/day).

To achieve these conditions, a composite core made up of a low permeability core and a high permeability core was used. The combination of the two cores used in the composite core resulted in a low flow rate and high DP. This design would allow us to replicate the leak condition in lab scales.

Figure 4-11 shows the experimental setup of the rig which has been used for conducting the coreflood experiments. Two high pressure cells one filled with CO_2 + solute solution and the other with pure CO_2 are placed in the temperature-controlled oven near the inlet side of the coreholder. Two pressure transducers have been employed to accurately measure the pressure of both ends of the core. Two pumps are connected to the cells in

order to flow the fluids at high pressure. In these experiments, no back pressure regulator (BPR) utilised since the precipitation in BPR would block the flow lines.

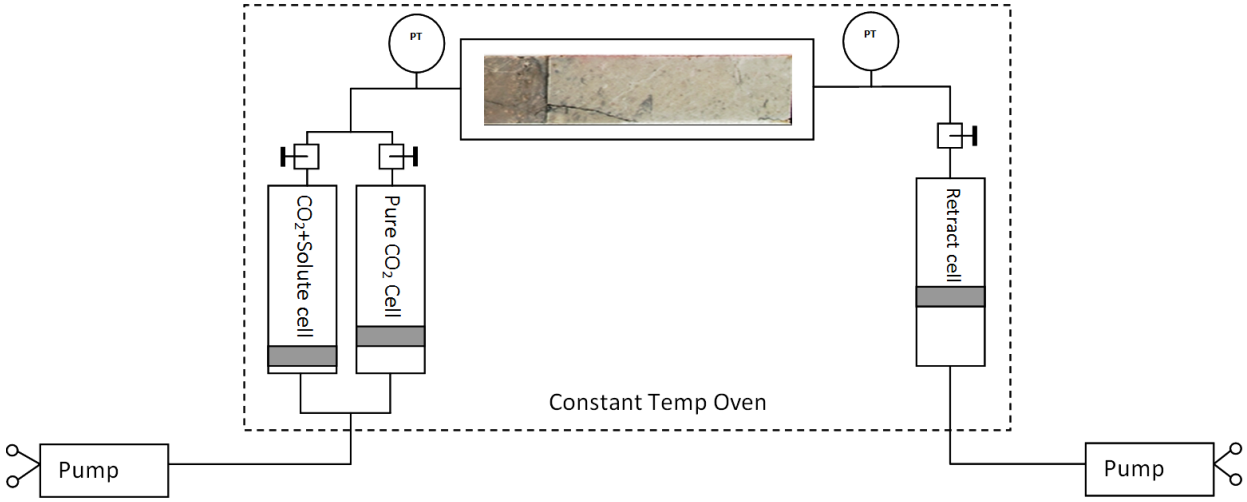

Figure 4-11: Experimental setup of the coreflood rig; the solution cell and CO_2 cell are located in inlet side of the coreholder.

Two leak types, (i) constant pressure and (ii) constant flow rate, were considered in these experiments. That is, in the first test, the leak was applied in the form of constant leakage rate but, in the second test, the outlet of the core was set to remain at constant pressure mode. However, in order to have a more consistent and fixed analysis of the solute solubilities at the inlet and outlet conditions, coreflood experiments (except first test) have been conducted at the constant pressure mode at both core ends to give us fixed solubility values.

Two methods for preparing the solution were utilised. (i) Surface mixing: the method for preparation of the solution (CO_2 + Solute) was based on mixing the supercritical CO_2 and the solid solute in a high pressure cell which simulates the process of surface mixing in the field. However, sometimes due to unfavourable thermodynamic behaviour of injected CO_2, surface mixing of the solute and CO_2 may not be a suitable option for applying the leakage prevention method in the field. Therefore, another approach was used in the coreflood experiments 4-6, i.e. (ii) downhole mixing: The modified setup represents a downhole mixing process in which the solute is added to the injected CO_2 stream at the bottom-hole conditions of an injection well. In the experiments 4-6, the solute is added to CO_2 as it travels into the core. That is, pure CO_2 picks up the amount of solute that it can

dissolve as it travels through the solute batch. For this purpose, a ¼" pipe with length of 80 cm, which was filled with the solute, was placed just before to the core inlet. Figure 4-12 illustrates the modified setup of the coreflood rig that is used for Test 4, Test 5, and Test 6. It should be pointed out that two filters have been placed at either ends of the pipe to prevent free flow (suspension flow) of the solute particles through the porous media. The solution at the end of the pipe (or inlet of the core) is assumed to be fully saturated with the solute.

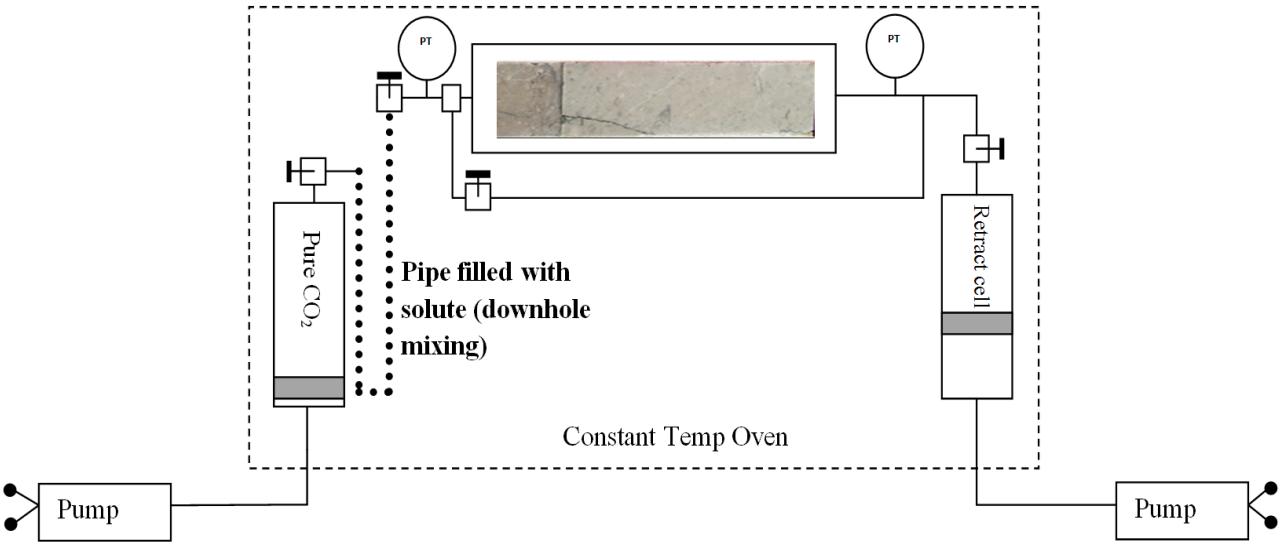

Figure 4-12: Experimental setup of coreflood experiments, which has been modified to simulate downhole mixing technique for delivering the solute into storage reservoir.

The procedure for coreflood test 4-6 with downhole mixing is as follows; first the injection and retract (leak) cells are pressurized up to test conditions. The pipe filled with a solute (HWS-2 or HWS-3) is placed between the "Pure" CO_2 cell and the inlet of the core. The pressure of the core is increased by injection of supercritical CO_2 from the retract cell. After stabilizing the pore pressure in the core, CO_2 (from CO_2 cell) starts to flow through the pipe and into the core to begin a leak test. In this type of mixing, prolonged duration of contact is needed to have the CO_2 stream saturated with the solute. It should be noted that a low flow rate of CO_2 injection is needed in these coreflood experiments to ensure the injection stream is fully saturated with the solute. Since the pumps are set to keep the inlet and the outlet pressure constant, the injection and retract (leak) flow rates are recorded as the main indication for detecting the solid solute

precipitation and blockage of the outlet path during the flow of the solution through the core.

It should be noted that the core plugs used in the tests are thoroughly cleaned with appropriate solvents after each test to be re-used. The composite core assembly is composed of two distinct types of rocks; tight (ultra-low permeable) and high permeable core plugs. The tight part is mainly composed of a dolomitic carbonate rock whereas the high permeable part has quartz (sandstone) as the main constituent. Carbon dioxide can react with carbonate rocks as it flows through the porous carbonates. Depending on the history of the contact between CO_2 and the carbonate rock, CO_2 may excavate or re-mineralize in this type of rock. To evaluate the extent and the impact of possible reactions between the resident fluid and the carbonate rock, a more in-depth investigation is needed. However, a general trend has been identified in the dolomitic carbonate rock which demonstrates an increase in rock permeability when the same plug is repeatedly used in several tests. This increase in permeability makes it more difficult to block the flow path and also to exactly repeat the same experiment again.

4.3.2 Solute used in coreflood experiments

Up to this stage, five solutes have been tested in micromodel and sandpack experiments; *HWS-5*, HWS-3, HWS-2, HWS-1, and HWS-4. The results of micromodel experiments revealed that every solute has its own precipitation characteristics. For instance, *HWS-5* particles have a high tendency to attach to the surface of the porous medium which is considered as an unfavourable phenomenon in aquifer with water wettability characteristics. The results also showed that supercritical solutions of HWS-3 and HWS-2 response similarly to a pressure reduction. However, the micromodel observations indicated that HWS-2 forms relatively larger particles and also the particle formation triggers at lower pressure drops which means HWS-2 is more responsive compared to HWS-3. Nonetheless, both solutes start to generate solid particles at relatively high supersaturation. Therefore, based on the visual observations made in the micromodel experiments, using HWS-2 is preferred over HWS-3 for coreflood experiments.

Figure 4-13 illustrates the isothermal solubility of HWS-2 with respect to pressure at constant temperature of 45^{o}C. As a moderately soluble solute, the trend of solubility clearly shows gradual decrease where pressure falls from 3000 psig to 1800 psig. However, from 1800psig down to 1000psig, the solubility of HWS-2 in supercritical CO_2 reduces sharply.

In the following coreflood tests, CO_2 will be saturated with HWS-2 at equilibrium conditions of 3000 psig and 45 ^oC to obtain a solution with solute concentration of 0.00265 mole fraction.

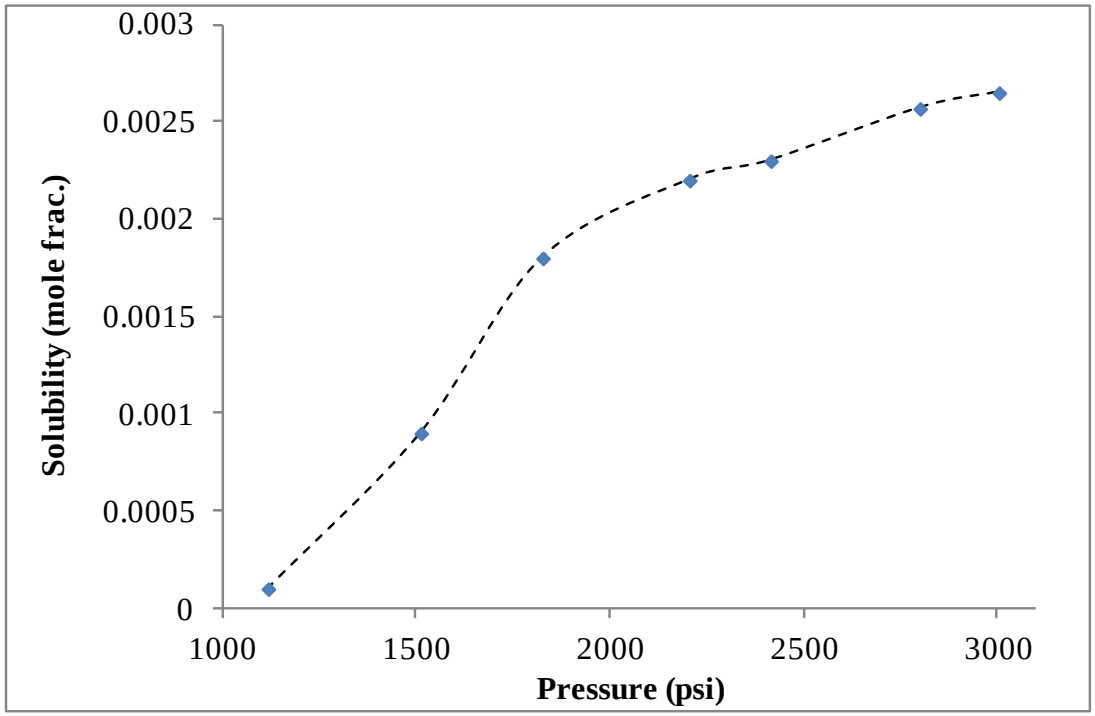

Figure 4-13: Isothermal solubility profile of HWS-2 with respect to pressure at temperature of 45 ^oC.

4.3.3 First coreflood experiment

Experimental procedure

Solid particle formation can be derived from nucleation of solid solutes out of the saturated CO_2 solution. To simulate the kinetics of particle formation, two core plugs with completely different characteristics have been employed; a tight (low permeability) core and a highly-permeable core.

Table 4-1 lists the basic properties of the core plugs which have been put together in order to form the composite core. The function of the tight core is to create the pressure drop while the rate is kept moderately low whereas the high permeable core is used for providing a suitable medium to trigger the precipitation of solute. During the experiment, after flowing through the tight core, the supersaturated solution enters the high-permeable core. This configuration would reduce the time scale of the nucleation kinetics compared to real conditions of CO_2 storage with low supersaturation of solute in supercritical CO_2.

Figure 4-14 shows the schematics configuration of the plugs in the composite core. The tight core is always placed on the inlet side of the composite core to impose the target pressure drop (200-500 psig) while the flow rate is controlled at around typical flow rates in a real storage reservoir. The design of the composite core represents a leakage scenario that may take place in a real reservoir in which supercritical CO_2 is stored.

Experiment 1 has been designed to simulate a leakage with constant rate which flows through the rock. After setting up the experiment and increasing the pressure and temperature of the core to the desired values, supercritical CO_2 containing the solute was injected through the core at a constant rate. During the test, the values of the pressure at both ends of the core were monitored and recorded. The behaviour of the pressure would reflect the state of flow through the core and possible building up and precipitation of the solute and consequent permeability reduction of the core.

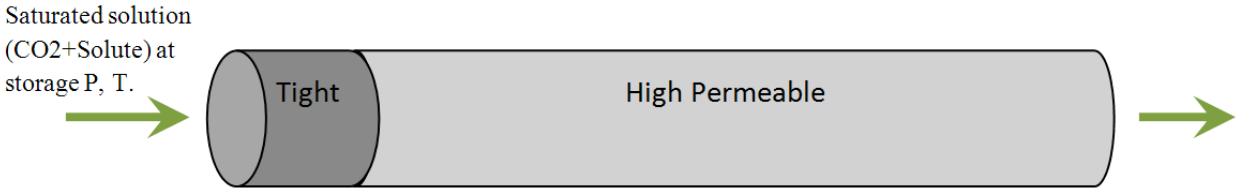

Figure 4-14: the configuration of the plug in the composite core; the tight core is in the inlet side in all tests.

Table 4-1: Basic properties of the plugs; T1 and H1 represent the tight and high-perm cores respectively.

Core ID	Length (cm)	Diameter (cm)	Weight (gr)	Porosity (fraction)	Permeability (md)
T1	3.44	2.59	48.683	0.038	0.003
H1	13.81	2.54	143.762	0.163	225

Coreflood experiment-1

In Experiment 1, the core plugs are assembled into the coreholder and the composite core is cleaned with Toluene and then with Methanol to remove any debris or residues remained after the coring process. During the cleaning stage, the colour of producing effluent is monitored and the solvent injection is continued until the effluent is totally clear. Then the plugs were removed from the core holder and were put in an oven to dry. Then, the plugs were weighed separately to establish the initial weight of the cores. Keeping an accurate record of the weight of the cores is crucial since any precipitation of solid solute during leak prevention experiments can be evaluated through the changes in the weight of plugs and hence the location of blockage can be detected.

Having cleaned the plugs thoroughly, the composite core was assembled and loaded in the core holder. The first step in preparation for the test involves applying the overburden pressure on the core while the system is being heated up to the working temperature which is 45^{o}C in this test. After stabilizing the overburden pressure at 3500psig at 45^{o}C, the rig is pressurized to the experiment pressure of 3000 psig by injecting high pressure CO_2 in the core. The injection and flow of CO_2 into the composite at the pressure and temperature of the experiment was continued in order to measure the permeability of the core and the flow characteristics of the system. The injection of CO_2 was conducted at a constant flow rate of 0.5 cc/hr and the outlet pressure has adjusted to 2900 psig. The injection (inlet) pressure was monitored during the injection of CO_2 and finally the pressure stabilised at 3395 psig which gives a DP of 495 psig.

Figure 4-15 shows the pressure distribution profile of the composite core which has been simulated with a commercial reservoir simulator (CMG-GEM). The graph depicts the pressure behaviour of the system and the role of each plug in replicating the leakage condition; the tight plug (T1) imposes the pressure drop from 3400 psig to 2900 psig and the subsequent high permeability plug maintains the flow condition.

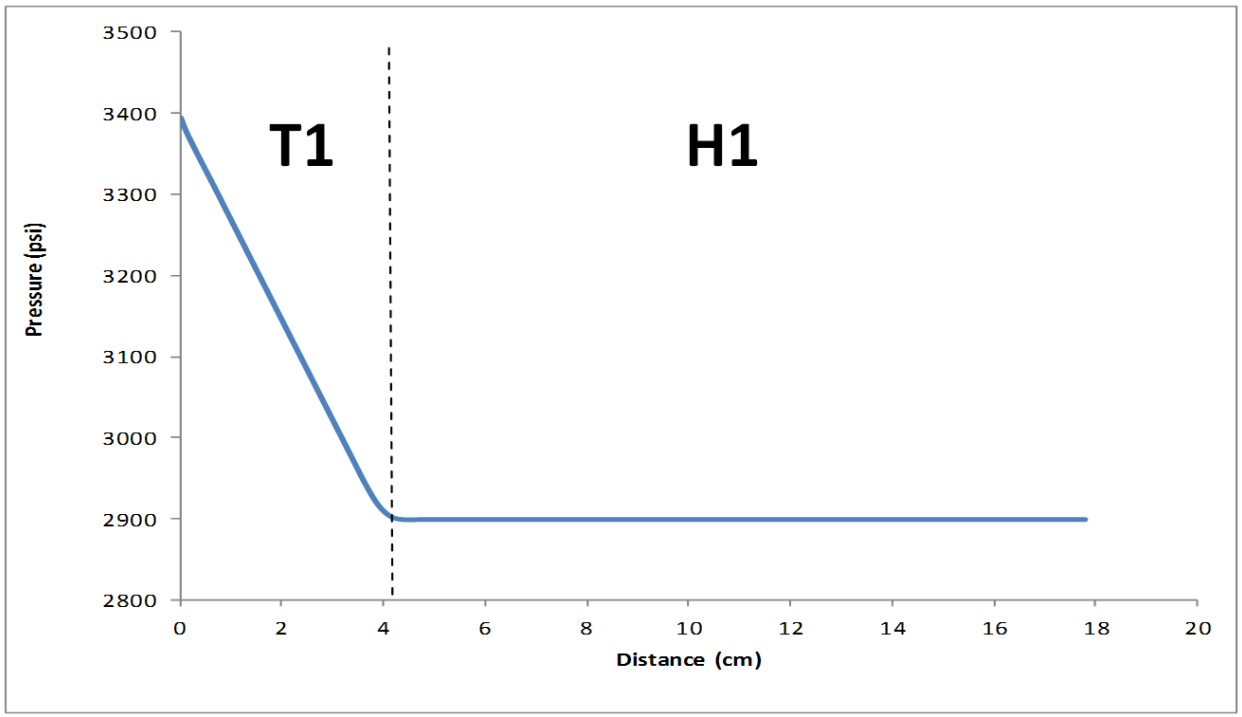

Figure 4-15: Pressure distribution along the composite core; T1 (tight) plug impose the pressure drop and flow rate, H1 (high-permeable) plug keeps the pressure roughly constant for nucleation.

After saturating the core with pure CO_2, the solution (CO_2+HWS-2) is injected into the core to displace the pure CO_2 out of the core. The solution was prepared at 3000 psig and 45^oC with a solubility of 0.00265 mole fraction. The inlet pressure of the core was maintained at 3400 psig and the outlet pressure was 2900 psig. Therefore, the solution was undersaturated at the core inlet and slightly supersaturated at the outlet. The plumbing of the rig allows the displacement of the in-situ pure CO_2, with the solute-loaded CO_2 solution by switching the injection fluid from pure CO_2 to the solution without disturbing the stabilised flow condition. The injection rate for displacing the pure CO_2 was adjusted at 1 cc/hr. The injection of solution was continued for about 1 pore volume (PV) and we assumed that the pure CO_2 would be displaced completely after injecting one pore volume of the solution. No change in pressure behaviour of the core has identified during injection of the solution which is a good indication of having no precipitation during the displacement. After this stage, while the injection pump was injecting the CO_2-solute solution at a constant rate of 0.5 cc/hr, the outlet pressure of the core was adjusted to 2800 psig. This condition of injecting at very low rate of 0.5 cc/hr while the outlet pressure is kept at constant value of 2800 psig is considered as the start of the test. In the next section, results of this coreflood experiment are presented and discussed.

Results-1

The main objective of this coreflood test is to analyse the response of the solute-loaded CO_2 solution to a pressure drop at a low super-saturation. Therefore, the results would show the kinetics of particle formation where the super-saturation (leakage) is imposed. The pressures at both ends of the core, the injection and production rates can be logged during the experiments. These types of data will reveal the occurrence of particle accumulation in response to an imposed pressure drop (leakage) which eventually yields a full blockage and stops the leak. In this experiment, the leakage scenario is based on the constant injection rate and if any precipitation is triggered and evolved, the core inlet pressure is expected to increase accordingly.

Figure 4-16 shows the complete log of pressure at the inlet and outlet of the core during the experiment. This record of pressures and their variation can be used to explain indirectly the phenomena taking place during the flow of the CO_2 solution through the composite core. Several events can be inferred from the pressure log. The green curve in Figure 4-16 represents the process of core preparation and pressurisation. The injection rate of 1 cc/hr was continued for 17 hours which corresponds to about 1 pore volume of the core. After that, the injection rate was reduced to 0.5cc/hr which resulted in slight decrease in the inlet pressure. After a couple of hours, the inlet condition stabilised at the target pressure of 3386 psig which means the flow behaviour of the CO_2-solute solution is similar to that of the pure CO_2 and hence, no significant precipitation of the solute had been occurred during the displacement of the pure CO_2 with the CO_2-solute solution. At this stage of the test, the outlet pressure had settled at 2800 psig. It should be emphasised that the solute solution inside the cell had been equilibrated at 3000 psig and 45^oC, i.e. at 3400 psig (core inlet pressure) the solution will be undersaturated and no precipitation will take place. Detail analysis of test results of this test will be discussed in Figure 4-17.

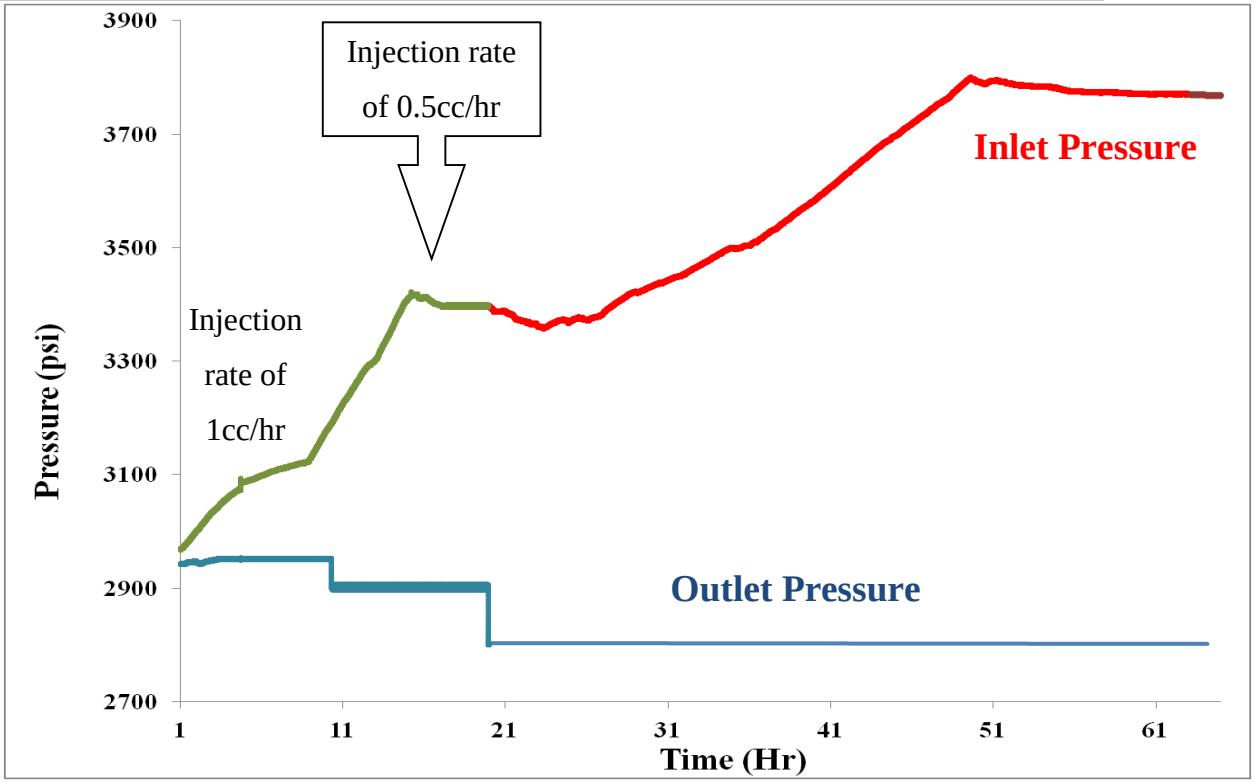

Figure 4-16: Complete log of the pressure at both ends of the core during the test. Blue curve represents outlet pressure. Green curve shows the inlet pressure before adjusting the outlet pressure to 2800psig. Red curve shows the inlet pressure during the main test (rising trend of inlet pressure indicates precipitation of particles).

Figure 4-17 shows the pressure versus time during the CO_2-solute injection period when the outlet pressure had been adjusted to 2800 psig. At early stage of the displacement (when the outlet pressure is reduced to 2800psig), the inlet pressure has slightly reduced as highlighted by the orange oval. This reduction of the core outlet pressure in response to the reduction in the injection rate clearly shows that there is good connectivity inside the core and between the inlet and the outlet i.e., no blockage or particle precipitation. However, after a period of time (10 hours), the inlet pressure starts to rise which is a clear sign of permeability reduction due to particle precipitation. Particle formation and precipitation continues as can be identified from the increasing trend of the pressure of the core inlet.

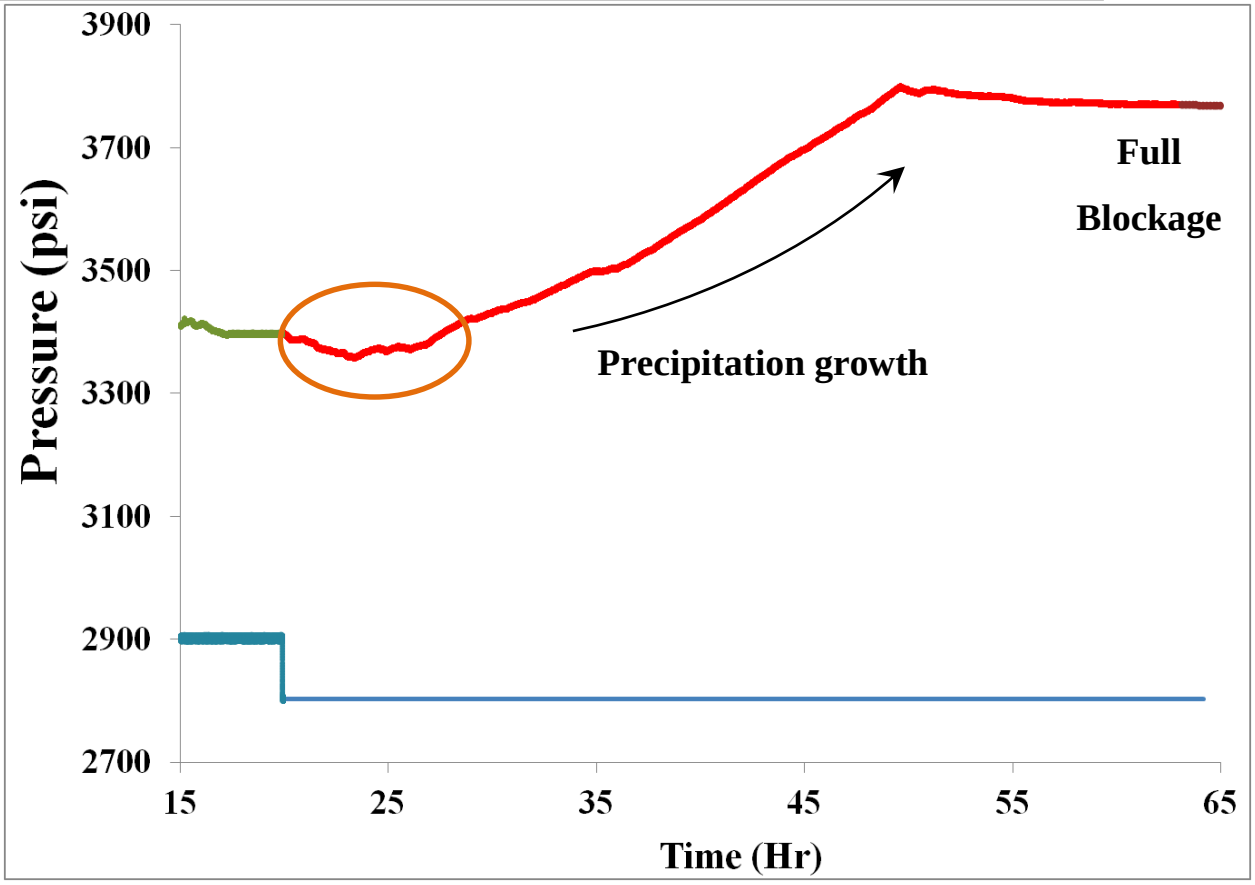

Figure 4-17: Detailed analysis of the pressure behaviour during the test; the orange oval indicates the connectivity between inlet and outlet. The rise in pressure shows the precipitation and eventually the blockage at latter stage of the test can be identified.

The growth of precipitation has been taken place in a long period of time and the blockage is eventually formed. It should be pointed out that the exact time of complete blockage cannot be determined by means of pressure profile since the core is a very low permeable core and hence the response of the core to any permeability change would not be instantaneous whereas in high permeable media, such as micromodel and sandpack, the response of the pressure to formation of blockage is very quick and can be detected on pressure profile immediately. But, indeed, the change of the trend of the core inlet pressure from decreasing to increasing clearly indicates the onset of the particle precipitation and occurrence of a blockage. The confining pressure on the composite core during this experiment was kept at 4000psigg which limits the maximum pressure of inlet pressure to 3800psig. Therefore, the injecting pump was switched off when the inlet pressure reached 3800psig. For the rest of the test, the inlet pump remained switched off. If there was any connection between the inlet and outlet of the core, the inlet pressure would gradually drop after switching off the injection pump.

For the leakage prevention technique to be effective, in addition to formation of blockage durability of it is also vital and has to be verified against the flow. We have tested the stability and durability of the blockage formed in the core by, first, by checking if the blockage can sustain the existing pressure drop of 1000 psig, and, second, if the blockage can take a higher pressure without failing.

At later stages of the test in Figure 4-17 where the pump is off, the inlet pressure remains almost constant, although negligible decline in pressure is observable which can be attributed to negligible change in oven temperature or pressure equilibration across the core. However, the durability of the blockage should be verified during a prolonged period of time. To evaluate the strength of the blockage, the outlet pressure of the core was substantially reduced from 2800psig to 1800psig. This increases the differential pressure across the core significantly. Figure 4-18 depicts the durability part of the test at which the out let pressure (blue line) was reduced to 1800 to bring about an overall pressure drop of 2000 psig across the core. As can be seen, despite doubling the differential pressure across the core, the inlet pressure stayed constant which proves the existence of a stable and firm blockage in the core.

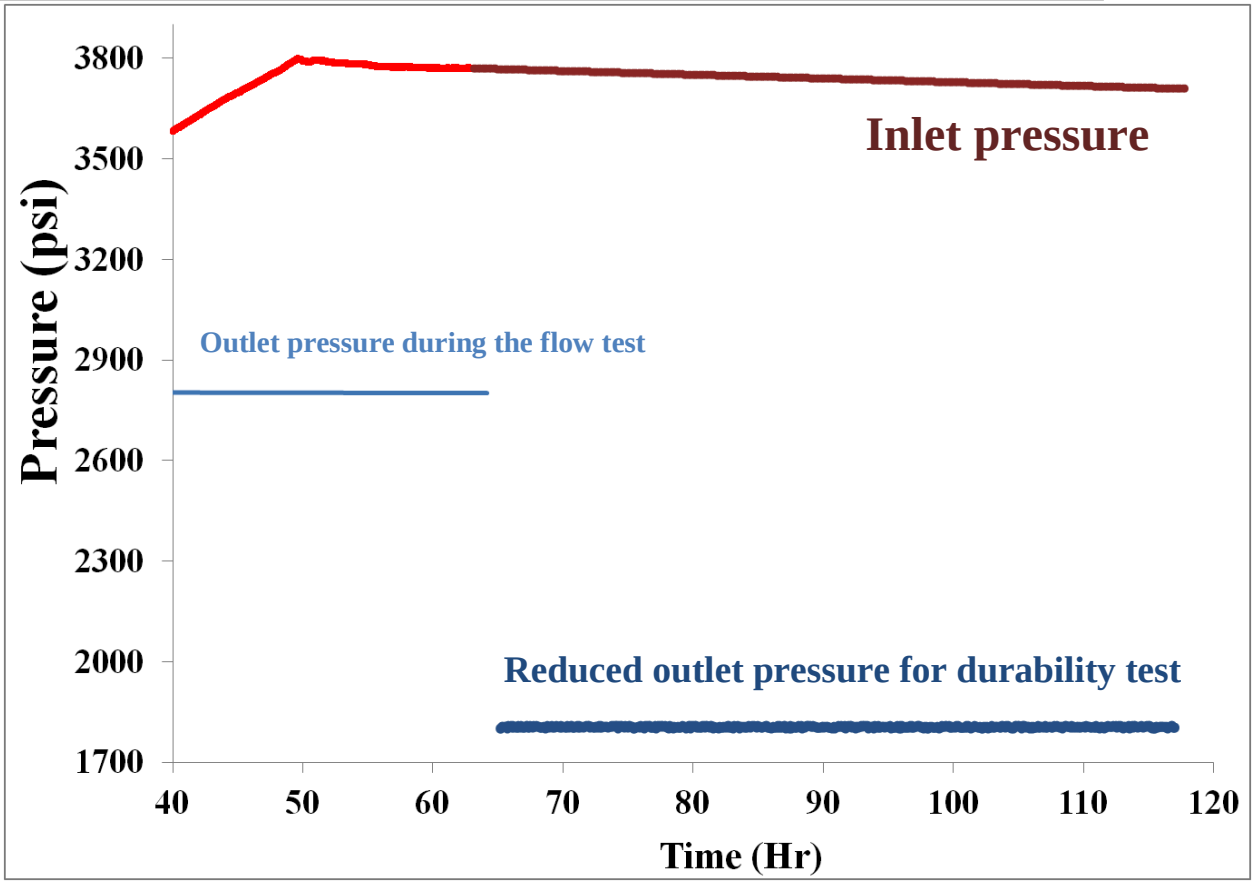

Figure 4-18: Durability test of the blockage; prolonged monitoring the inlet pressure verifies the occurrence of firm blockage.

Discussion-1

For the leakage scenarios involving sudden release or high supersaturation, precipitation, blockage, and durability of the leakage prevention method have been already verified in micromodel and sandpack experiments. As opposed to high supersaturation level, the precipitation in relatively low pressure drops (low supersaturation) needs comparatively high duration of flow. This coreflood test has been designed to cover some of the essential aspects of the particle formation and precipitation in the leakage cases involving low pressure drop of 200 psig. After ascertaining the existence of a blockage in core during the core flood test, we need to further investigate the particle precipitation and blockage formation from different angles, e.g., where the blockage took place and how much solute deposited in the composite core. To find out answers to these questions, after the experiment, the composite core was taken out of the coreholder in order to analyse each core plug separately. After dismantling the coreholder, the two plugs were checked for any marks on the exterior surfaces of them. Figure 4-19 shows a picture of the two plugs

after the test which does not show any visible signs of precipitation on the external surfaces.

Figure 4-19: Composite core after first core flood test. No sign of precipitation can be detected. The left plug is the tight one.

Next step is to weigh the core plugs separately to identify the location of the blockage. The initial weight of the tight core plug (T1) was 48.683 gr which remained the same after the test. Therefore, no precipitation occurred in the inlet core (T1). For H1 (high permeability) plug, the weight was increased from 143.763 gr to 144.635 gr. The difference in the weight clearly demonstrates that the precipitation has taken place in high-permeable (H1) plug. The mass of precipitated solute is calculated from the difference between the two weights which is 0.872 gr. Given that the blockage has been verified form pressure data, if we assume that the precipitation is locally concentrated, the thickness of the blockage can be determined by using the value of the porosity of the plug. By a simple calculation, the blockage thickness was calculated to be 1.009 cm.

In order to confirm the results of mass analysis of the blockage formed in the core, we attempted to clean the plug in to remove and recover the solute. The liquid solvent for dissolving HWS-2 is the mixture of Acetone/Methanol/Hexane. The cleaning procedure was performed at temperature of 60^{o}C to enhance the solubility of HWS-2 in the solvent. First, the plug T1 was cleaned. The initial sign of producing the precipitated material from the core was the darker colour of the effluent since HWS-2 would darken the solvent. The effluent of T1 plug produced the solvent with original colour which means no solute precipitated in T1 plug (consistent with the weight analysis of the two core plugs). Likewise, H1 plug was cleaned. The core effluent was collected in several test tubes for the analysis. Figure 4-20 illustrates the spectrum of the effluent colour from a dark fluid to a clean solvent. The dark fluid produced in the early stage of the cleaning (left image)

indicates the high contamination of the solvent with precipitated solute (HWS-2) whereas during the cleaning the colour of the solvent gradually got lighter (middle image) which is attributed to reduction in HWS-2 content of the solvent.

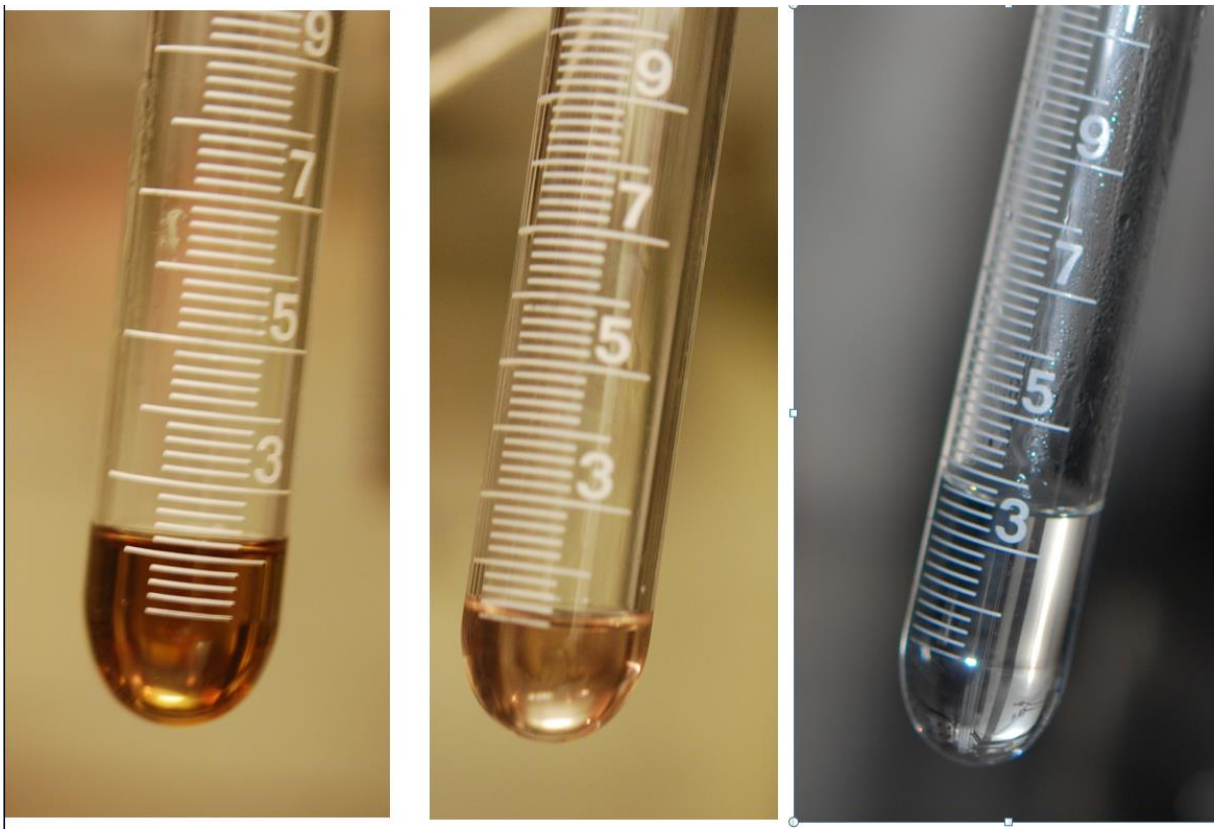

Figure 4-20: Change of colour of produced fluid during the cleaning of the plug H1. The left tube represents the early stage of cleaning (high contamination with HWS-2). The middle image indicates a lower content of HWS-2 in solvent. The right picture shows the clean solvent production at later stages of cleaning.

The cleaning process was continued until the core effluent became as bright as the original solvent at the injection face of the core plug. The right image of Figure 4-20 shows the final state of the core cleaning with no contamination. The produced liquid during the entire process of cleaning was collected in a beaker to analyse the amount of the solute that has been recovered. Figure 4-21 demonstrates the amount of residues of HWS-2 in the beaker after evaporating the solvent. The collected solute was weighed to cross-check the results of weighing the plug before the cleaning. 0.882gr of HWS-2 was recovered from the cleaning process. The slight difference in the weights is due to entrapment of solvent inside HWS-2 crystals. In summary, analysis of the results of first coreflood

experiment using different methods supports precipitation of the solute and formation of a blockage in the high permeability (H1) plug.

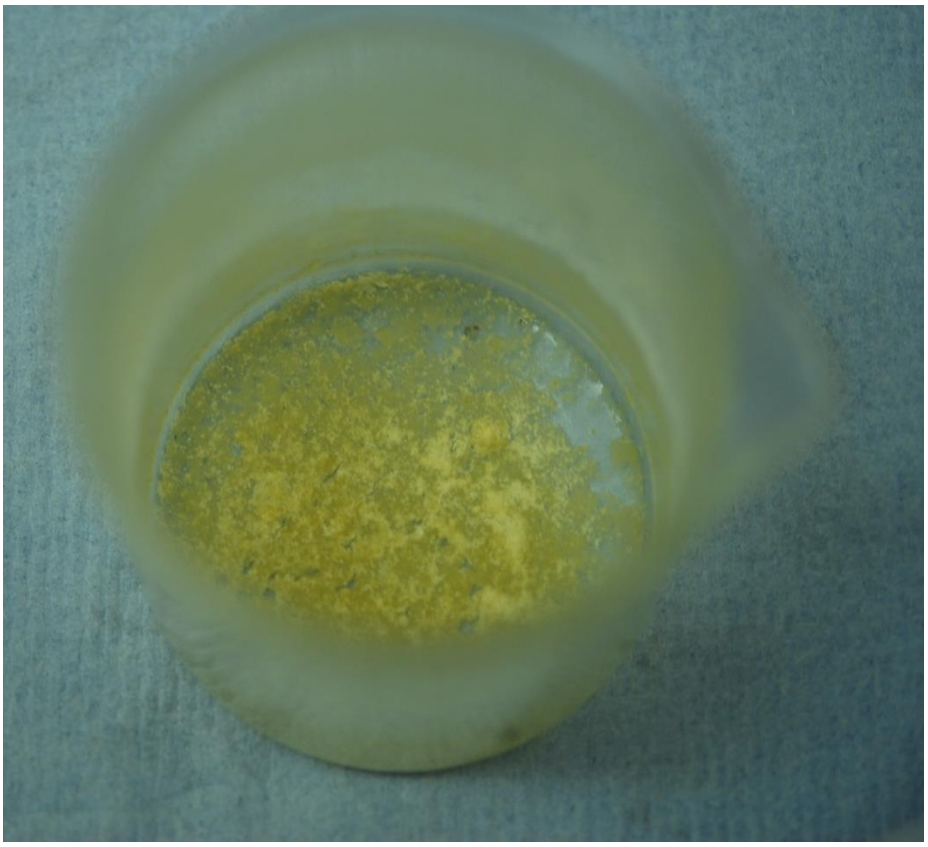

Figure 4-21: Recovered HWS-2 at the end of the test.

4.3.4 Second coreflood experiment

Experimental design-2

After successful blockage of the composite core in the first test, the second coreflood test was designed with a different tight core plug to study the effect of flow velocity on the nucleation kinetics. Table 4-2 shows the base properties of the core plugs which have been used in making up the composite core for the second coreflood test. The tight core plug of the composite core in this test is more permeable compared to the first test and has almost 10 times higher average permeability. Similarly to the first test, the tight plug (T2) was placed on the inlet side of the composite core. The solution of CO_2 and solute (HWS-2) was prepared at pressure of 3000 psig and 45 ^{o}C and with the corresponding solubility of 0.00265 mole fraction.

Table 4-2: Properties of the plugs in second coreflood test.

Core ID	Length (cm)	Diameter (cm)	Weight (gr)	Porosity (fraction)	Permeability (md)
T2	3.43	2.59	48.592	0.042	0.0028
H1	13.81	2.54	143.762	0.163	225

The second test was designed to investigate a different leakage scenario compared to the first test. In the first core flood test, the leak was considered to happen at a constant flow rate of 0.5 cc/hr, whereas in the second test, the leak was designed to happen in constant pressure mode. As a result of this difference, the data that was collected during the second test was injection rate instead of injection pressure which was the case in the first core flood test. A drop in injection rate during the test would indicate formation of a blockage in the core. In the next section, the procedure that was followed for performing the second core flood test will be described.

Experimental procedure-2

The procedure that was followed in the second test was similar to the previous test except the inlet and outlet pressures that were set at 3000 and 2800 psig respectively. The workflow for performing the second test can be explained as follows; first, the core holder oven temperature was set to 45^{o}C in order to heat up the equipment inside the oven. Then, a confining pressure of 3500 psig was put on the composite core. The core was then saturated and pressurized to 3000 psig with pure CO_2 to prepare the system for further flow. In the next step the core outlet pressure was adjusted to 2800 psig (test pressure) while the inlet pressure was kept constant at 3000 psig. Under these conditions CO_2 was injected in the core until steady state conditions were achieved and the permeability of the system could be calculated. The flow of pure CO_2 in the composite core was simulated with a commercial reservoir simulator (CMG-GEM) in order to estimate the pressure distribution along the core. Figure 4-22 presents the results of the simulation at steady state condition of flow and demonstrates the role of each core plug in the pressure behaviour of the composite core. As can be seen, most of the pressure drop has taken

place in the tight core plug (T2) and high permeability core (H1) has created a suitable porous medium for establishing the supersaturation (200 psig pressure drop).

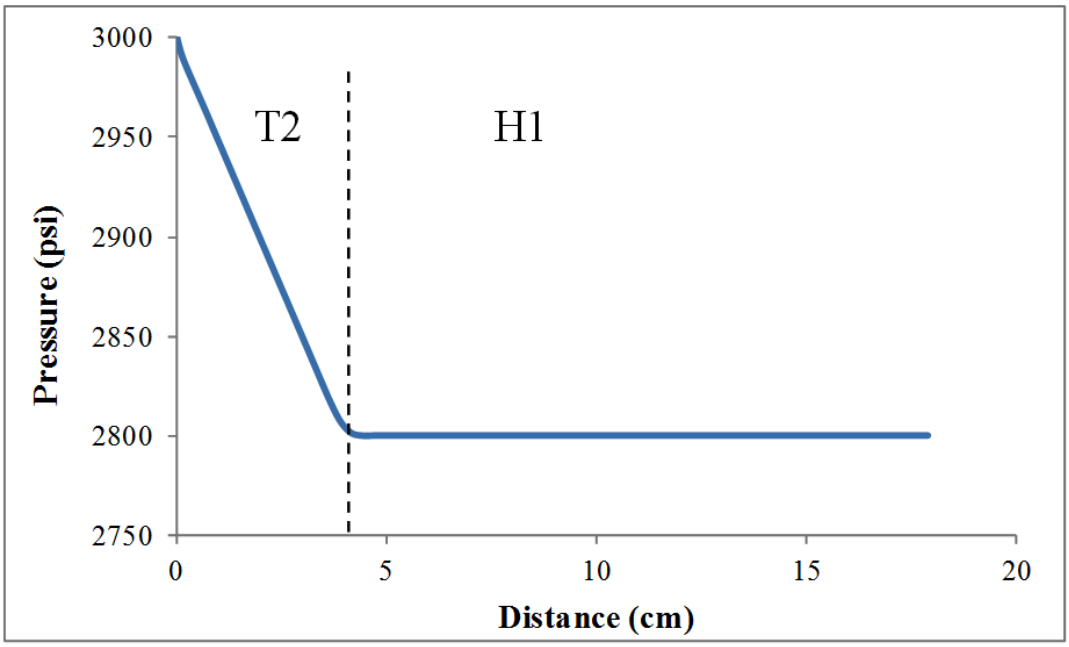

Figure 4-22: Pressure distribution along the composite core; T2 (tight) and H1 (high-permeable) were put together to form the composite core.

Having established steady state conditions in the core by injecting pure CO_2, the injection fluid was switched from pure CO_2 to the solution of CO_2 and solute (HWS-2). The CO_2-solute solution was injected through the core in order to displace the in-situ pure CO_2 from the core. During this stage of the test, the pressure at the outlet of the core was maintained constant at 2800 psig (as opposed to the first test in which the core was saturated with the CO_2-solute solution first and then subsequently the target supersaturation was applied). The condition of 200 psig pressure drop (the difference between 3000 psig at the inlet and 2800 psig at the outlet of the core) was maintained to investigate if the a blockage is formed. However, if the flow could not be ceased or no precipitation occurred, the outlet pressure would be reduced to a lower pressure in order to determine the onset pressure at which the leak would be stopped. In the following part, the results of the test will be presented.

Results-2

Figure 4-23 shows the detailed log of the injection and production volumes of the pumps during this core flood test. It should be noted that the pumps (both injection and production pumps) were working on constant pressure mode of 3000 and 2800 psig, respectively. Figure 4-23 illustrates the cumulative volume of the injection and the retract cells. During the early stages of the test (A), 80 cc of the CO_2-solute solution was injected into the core and approximately the same volume of the solution was retracted (withdrawn) into the producing cell.

5 pore volume (PV) of the solution flowed through the core and no indication of precipitation could be identified since the rate of fluid flow was almost constant and unaffected. Therefore, the outlet pressure was reduced from 2800 to 2500 psig (section B in Figure 4-23) in order to promote particle formation of HWS-2. Since the pressure drop was increased from 200 psig to 500 psig, the rate of fluid flow through the composite core proportionally raised which is expected if no reduction of the core permeability takes place. In this stage of the test, no blockage took place against the flow of CO_2 in the core and hence we decided to apply further pressure reduction at the outlet face of the core. The outlet pressure was reduced to 2300 psig which corresponds to a pressure drop of 700 psig (section C in Figure 4-23). It should be emphasised that the inlet pressure was being kept at 3000 psig which is the saturated condition of the solution and the corresponding solubility remained at 0.00265 mole fraction during the entire set of the imposed outlet pressures.

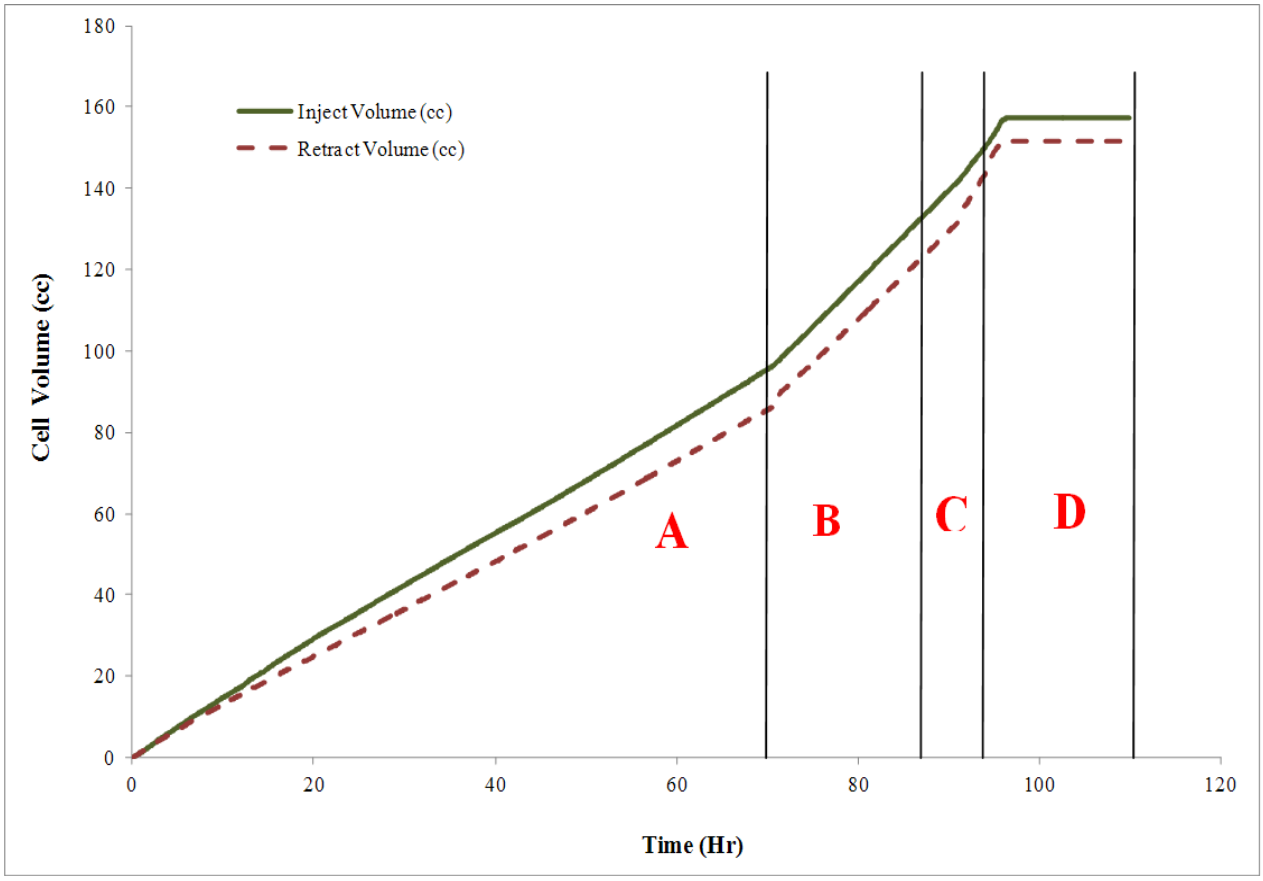

Figure 4-23: Logs of the injection and retraction volume into the corresponding cells; red labels show (A) outlet pressure of 2800psig, (B) outlet pressure of 2500 psig, (C) outlet pressure of 2300psig, and (D) outlet pressure of 2100 psig.

The outlet pressure of the core was reduced in three steps from 2800 to 2300 but no sign of a blockage was observed. Then, the pressure at the producing face of the core was reduced to 2100 psig which is very close to the pressure at which instantaneous nucleation had been observed in micromodel experiments reported in previous chapter. Shortly after reducing the inlet pressure to 2100 psig a blockage happened in the core. This is shown by section D in Figure 4-23 in which the rate of injection and production has become zero and, therefore, the cumulative production and injection volumes in the cells have become constant which is indicative of an effective precipitation against the flow and hence blockage of the leakage path. Sealing the leak at pressure of 2100 psig demonstrates the important role of nucleation kinetics in particle formation.

Discussion-2

Particle formation and precipitation are mainly controlled by the kinetics of nucleation. Therefore, a combination of suitable flow rate (time dependent parameter) and pressure drop (target supersaturation) can result in favourable precipitation and consequently blockage of the leakage path. In the second coreflood test, with producing (outlet) pressure of 2800 psig, the flow rate was 3 times higher compared to the first coreflood test which caused no precipitation in the core. From Figure 4-11, it can be seen that next to the coreholder, the outlet of the core is connected to the retract cell (production) which facilitates the nucleation of particles inside the cell instead of precipitating in the core. This phenomenon was also observed in outlet pressures of 2500 psig and 2300 psig.

However, at the outlet pressure of 2100 psig, particle precipitation occurred inside the core and the simulated CO_2 leakage was stopped. At the end of the test, the coreholder was dismantled for further analysis of the each plug. Figure 4-24 shows the outlet face of the composite core which clearly shows the presence of precipitation at the outlet face of the high permeable core plug. It should be pointed out that the precipitation was formed deeper than the outlet face of the core and inside the core which is not visible.

The amount of the precipitated HWS-2 can be obtained by weighing the plugs. The tight core (T2) was weighed which was the same as the original weight of the plug and hence, no precipitation had taken place in the tight core plug. However, the weight of high permeable core (H1) had been increased from 143.762 gr to 144.354 gr which shows a gain of 0.592 gr. If the precipitation is assumed to be form in the cylindrical shape, the corresponding thickness of the cylinder would be 0.6855 cm. Comparing to the thickness of blockage in the first coreflood test (1.009 cm), the thickness of blockage body was reduced notably which can be attributed to higher rate of concentrated precipitation and more rapid blockage in second test (outlet pressure of 2100 psig).

Figure 4-24: Outlet face of the composite core; the precipitation of HWS-2 can be seen.

After quantifying the amount of precipitated HWS-2 in the high permeable core, the core was put into the coreholder for cleaning purposes. The same solvent was used with mixture of Acetone, Methanol, and Hexane. The produced effluent of the core was collected in a beaker and was placed in a fume cupboard in order to evaporate the solvent and collect the solid solute. Figure 4-25 shows the residue of HWS-2 after drying the solvent out of the collected sample. The recovered HWS-2 was then weighed to double check the weight difference of the cores. 0.616 gr of HWS-2 was produced by cleaning the high permeable core which is in agreement with the results of the weight difference of the core. However, a negligible excess weight was observed in the recovered HWS-2 which can be attributed to the trapped solvent between the aggregated crystals of HWS-2 during the evaporation process.

In this test, because of the constant pressure mode of flow of CO_2, the CO_2 rate was changing during the test. The flow rate increased (as the pressure difference between the inlet and outlet of the core increased) and hence, the particles of the solute could not deposit and form a blockage at low supersaturation. Nonetheless, the blockage was successfully achieved at 100 psig less supersaturation compared to the micromodel tests.

Figure 4-25: Recovered HWS-2 after second test.

4.3.5 Test No. 3

Test conditions

The pressure conditions of the third test were similar to the first test as the aim was to investigate the repeatability of the observed blockage of a leak when the flow characteristics of the system are similar to the first test. As mentioned above, due to an increase in the carbonate rock permeability, it would be difficult to exactly replicate the same results. Since the permeability of the tight plug was changed in the first test, new plugs from the same rock type were used in the current test (Test No. 3). Three core plugs have been used in this test; two tight and one high-permeable. Table 4-3 shows the basic properties of the core plugs used; T1 is the same core as H1 that was used in the first coreflood test (after being thoroughly cleaned), but T2 is a new tight core plug included in the composite core used in this test. It should be noted that the permeability of T1 increased after cleaning from the initial value of 0.003 to 0.0038.

Table 4-3: Basic properties of core plugs; T1, T2, and H1 representing tight and high-permeability cores.

Core ID	Length (cm)	Diameter (cm)	Weight (gr)	Porosity (fraction)	Permeability (mD)
T1	3.44	2.59	48.683	0.038	0.0038
T2	4.01	2.56	57.661	0.037	0.0033
H1	13.81	2.54	143.762	0.163	225

Figure 4-26 illustrates the configuration of the composite core used in the third test. For the "Tight" part, the T2 core plug is placed at the inlet of the core before T1 and H1. A high permeability core plug was used at the outlet end of the composite core to accommodate suitable medium for particles to form and precipitate.

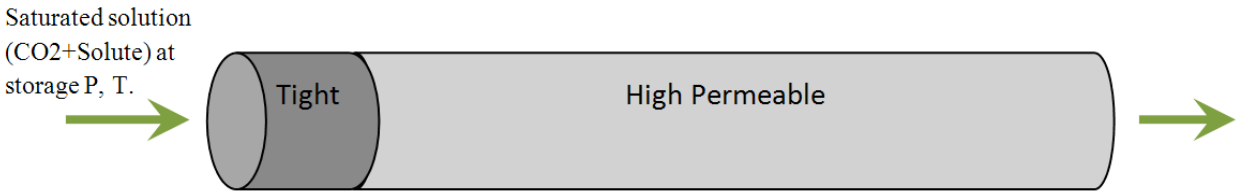

Figure 4-26: The configuration of the core plugs in the composite core; the tight core is on the inlet side in all tests.

To prepare the solution in a high pressure cell, the solute (HWS-2) is placed in the cell and high pressure CO_2 is injected into the cell to pressurize it up to 3000 psig. The cell is kept in an oven at constant temperature of 45 ^oC. The cell is shaken intermittently for two days in order to achieve saturated solution of HWS-2 and supercritical CO_2. The experiment is carried out in constant pressure mode. The inlet pressure of the core is set to 3000 psig and its outlet pressure is adjusted at 2750 psig. This results in a pressure drop of 250 psig across the composite core assembly. At these pressures, the corresponding solubilities at the inlet and outlet of the core were 0.00265 and 0.002395 mole fraction, respectively, which result in the supersaturation of 0.00265/0.002395=1.11.

Since the pressures were kept constant by pumps, the main indication of the blockage due to solid precipitation was reflected in the changes recorded in the injection and retraction flow rates of the pumps. Therefore, during the experiment, the flow rate was recorded and continuously monitored to identify any changes in the permeability of the core which could directly be linked to the solute's precipitation, build up and blockage of the core.

Results and discussion

Figure 4-27 demonstrates the full log of the injection and the retract flow rates with respect to time during the experiment. The injected fluid (CO_2 + HWS-2) flows through the composite core assembly at an average rate of 0.028 cc/min. There are some small fluctuations at the early stage of the test before flow is stabilized at 500 minutes after the start of injection. After this period of time, two distinct dominant flow behaviours can be identified (Figure 4-27). Initially, and for a long period of time during the experiment, the injection and retract flow rates remain almost constant which can be interpreted as an indication of no change in the rock's permeability or significant solid precipitation in the rock. After 8000 minutes, the flow rates begin to demonstrate significant fluctuations. These fluctuations are also associated with an obvious reduction in the flow rates. The steep declining trend of the flow rate indicates severe permeability reduction in the core as a result of the solid solute (HWS-2) precipitation that eventually stopped the flow of CO_2 through the leakage path.

The log of the flow rates can be used for detail analysis of the blockage evolution. We have shown in previous tests that the blockage forms in the high-permeable core whilst the highest pressure gradient happens in the tight part of the composite core assembly. Since the permeabilities of the core plugs are distinctly different and also they have been configured in series, the flow rate is controlled by the permeability of the tight core plug. Thus, if the high-permeable core plug (the target for the precipitation) is to influence the flow through the composite core assembly, its permeability must be drastically reduced. The observed significant reduction of the permeability of high permeable core plug corresponds to the gradual precipitation and accumulation of the solid solute in it. This slow process of solid solute accumulation is consistent with the low super-saturation of 1.11 that we had in this test. Hence, the prolonged period of the constant flow rates before 8000 minutes (at which blockage formed) can be attributed to the gentle and gradual build-up of the solid solute precipitation as the CO_2 passing through the core plugs. After

8000 minutes, sufficient amount of precipitation is attained and as a result a decrease in the flow rate is observed. The fluctuations in rate at this stage of the experiment are due to two reasons; (i) the response of the pump trying to keep the pressure constant at both ends of the core and, more importantly, (ii) the instability of blockage against the incoming flow of solution which results in periodic blockage and opening (removal of the precipitation) of the flow restriction. However, the average trend (green descending arrow in Figure 4-27) shows a declining flow rate which is attributed to dominant trend of solid precipitation over the outflow of deposited particle leading to a complete blockage, which occurs after 10000 minutes.

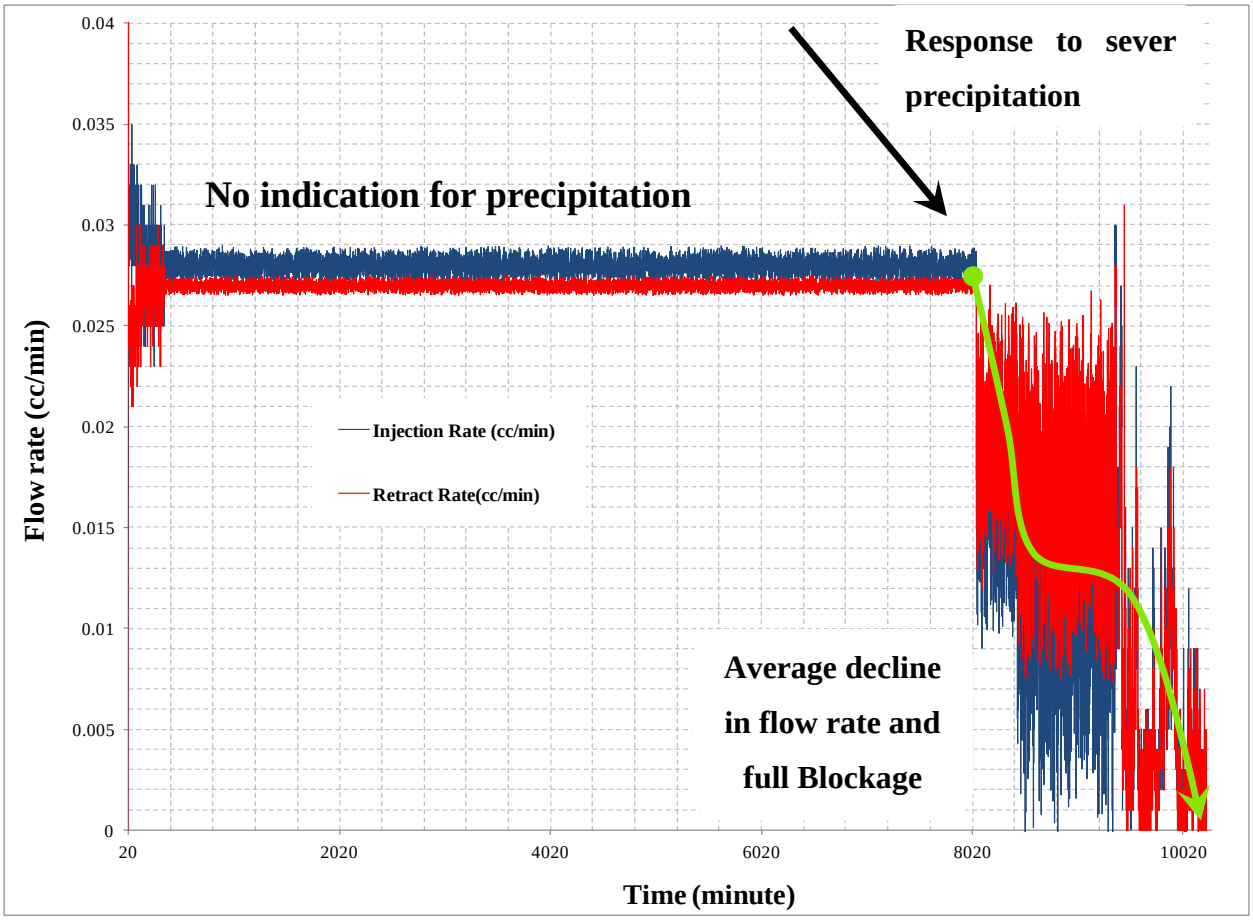

Figure 4-27: Log of the injection and the retract flow rates during Test No 3 coreflood experiment; after a period of flow, after some time the flow rates began to drop and eventually the blockage was established.

After the leak had stopped, the durability of the blockage was tested. The retract pump was set at 2750 psig during the leak test but, in the durability test, the pressure at the outlet of the core was reduced to 2000 psig to impose a higher pressure drop of 1000 psig for two days. No indication of flow re-establishment (or failure of the blockage) was detected from the transducers or the pumps. Therefore, it can be concluded that the blockage is highly durable and firm. Subsequently, the composite core assembly was taken out of the coreholder to analyse any changes to the core plug properties. Figure 4-28 shows the picture of the core plugs showing no apparent sign of precipitation externally, which in turn indicates the occurrence of precipitation in the interior pore spaces. Then, the plugs were weighed to detect where the blockage had happened. It was noted that the weight of the tight plugs was unchanged but the high-permeable core plug had gained 0.883 gr, which was attributed to the precipitation of the solute in the high permeability core and its blockage.

Figure 4-28: The image of the blocked core plugs after the test which exhibits no apparent indication of solid solute precipitation on the core surface.

The high-permeability core plug was cleaned with solvents (mixture of Methanol/Hexane/Acetone) to dissolve and remove the precipitated solute. The weight of the precipitated solute was determined to be 0.798 gr, which is in an acceptable agreement with the increase in the weight of the core after the test.

In summary, the leakage path with a pressure drop of 250 psig was effectively sealed with the solution of CO_2 and HWS-2. The full blockage occurred after more than 10000 minutes (7-8 days). This rather long period of time is in agreement with the low supersaturation level and hence a gradual precipitation of the solute within the high-permeability core plug. The durability of the blockage was confirmed by increasing the differential pressure across the rock from 250 to 1000 psig which did not opened the blockage. These results are in agreement with those of Test 1, reported previously.

4.3.6 Test No. 4

Test conditions

After successful blockage of the simulated leakage path in the previous test, in Test No. 4 mixing of the solute and injected CO_2 was performed in a different manner in an attempt to simulate downhole mixing. Figure 4-12 shows the modified setup for simulating the downhole mixing in the laboratory. Pressure conditions at the ends of the core were similar to those of the previous test, which was 3000 psig and 2750 psig at inlet and outlet, respectively. The experiment was also performed at constant temperature of 45 ^{o}C. The core plugs used in this test were the ones that had been used in the previous test but with one difference; the high permeable core was cut into two pieces to identify more specifically the location of the precipitation in the high permeable part. Table 4-3 shows the core properties. However, as it was mentioned previously, the permeability of the tight carbonate plugs might have changed due to possible reactions between rock and CO_2, which could results in having different flow rates in test 4 compared to test 3.

10 gr of HWS-2 was packed in the pipe that was connected to the inlet of the core holder. With the current range of the flow rates, i.e. between 0.01 to 1 cc/min, there was sufficient amount of solute for the injection CO_2 to become saturated with the solute (HWS-2) when it passed through the pipe. Similarly to the previous experiment, the main indication of

significant precipitation or blockage is the changes in the flow rates since the experiment is carried out in the constant pressure mode.

Results and discussion

Figure 4-29 demonstrates the full log of the flow rates during the test. The average flow rate through the composite core assembly is recorded as 0.044 cc/min, which is nearly two times higher than that in the previous test. Since the same plugs were used, the rise in flow rate confirms an increase in the permeability of the tight carbonate core plugs possibly due to reaction with supercritical CO_2 in previous test.

It is noted that apart from some small fluctuations in the log of the flow rates during the stabilised flow period, the general trend of Figure 4-29 is similar to that of the previous test. The period of constant rate at the early stage of the experiment can be attributed to solute precipitation and build up in the high-permeable core plug. After 2700 minute, the flow rates begin to fall considerably as a result of effective precipitation of the solute and consequently, the blockage is formed at around 3000 minute. Compared to the previous test, the blockage was formed in a shorter time which is in agreement with having a higher flow rate in this test. When the injection flow rate increases, the amount of the solute precipitated becomes more and overcome the particle removal rate. There is also a requirement of having the particles to be formed within the porous medium, which has been met at this higher rate.

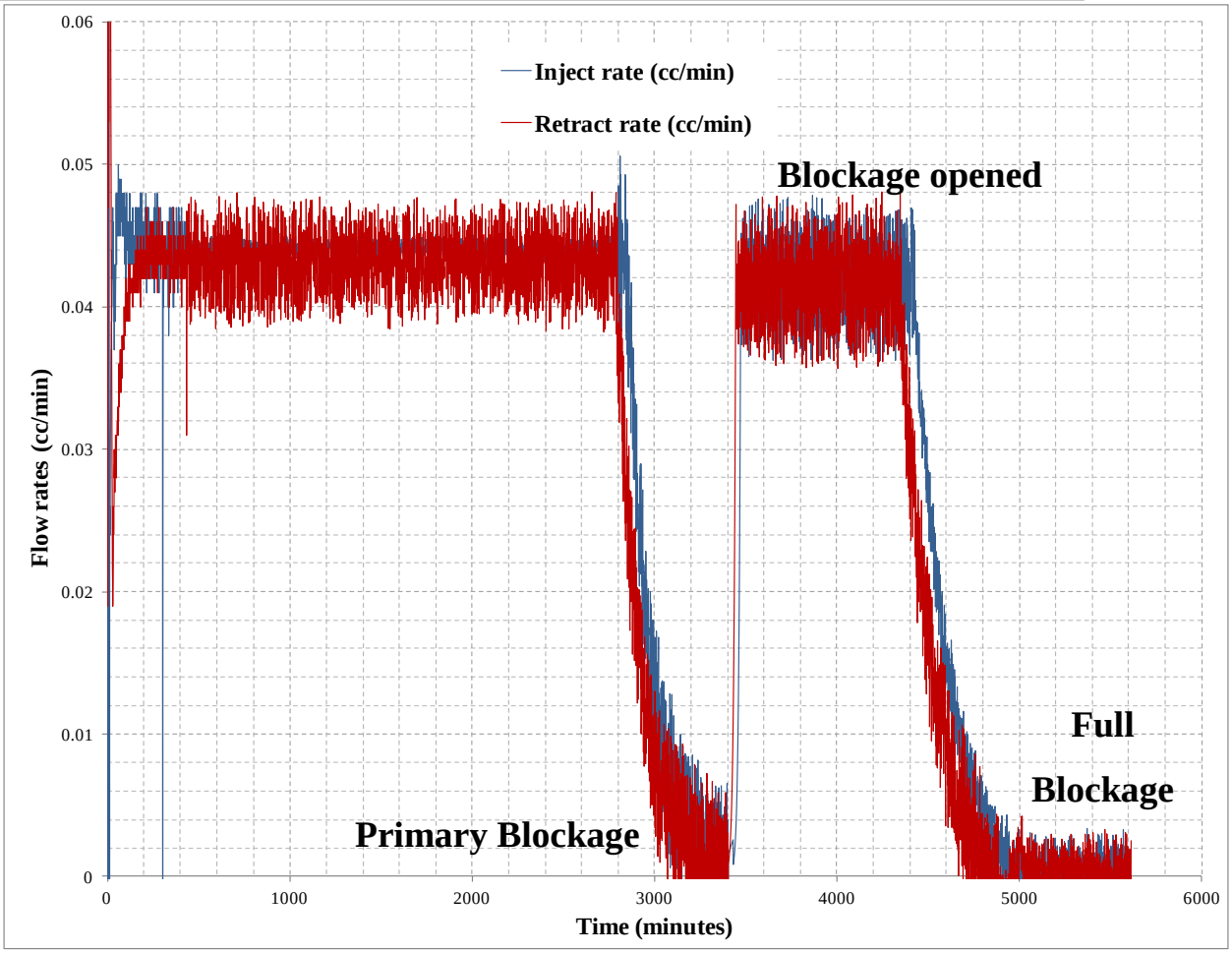

Figure 4-29: Log of the injection and the retract flow rates during the 4th coreflood experiment; after 3000 minutes, primary blockage formed but it was not durable. However, full blockage took place at the end of the test.

After confirming the occurrence of the blockage, the experiment was continued for several hours in order to stabilize the pressure distribution across the system. But, after 400 minutes, the blockage opened and the flow was restored through the core due to particle remobilization. Despite the very gradual evolution of the blockage, its opening seems to have occurred in relatively shorter period of time. The flow of the HWS-2-saturated CO_2 was continued for another 1000 minutes.

As the test continued, the flow rates started to decline again, which was the indication of the solid solute precipitation that eventually blocked the cores again. Two explanations for the repeated blockage can be given; first, building up a new blockage site and, second, repairing the former blockage site (Primary Blockage in Figure 4-29). Since the duration of the second flow period is much less (i.e. 1000 minutes compared to 2700 minutes for the first blockage), building up a completely new blockage site is unlikely. Thus, it can

be concluded that as the flow continued, the opened blockage site was repaired, which is an encouraging event for CO_2 leakage prevention method. That is, based on the observations made in this test, it can be concluded that if the blockage integrity is compromised and it is re-opened, the solution diagnoses the problem and the blockage is re-established. This phenomenon was previously reported for a high flow rate leakage occurring during the conducted micromodel tests.

The durability of the test was also performed for this coreflood experiment, and like the previous test, the retract pressure was reduced to 2000 psig (i.e. imposing 1000 psig pressure drop across the system). After two days, no indication of blockage re-opening or flow restoration was identified from the transducers or the pumps, which demonstrate the strength of the blockage.

When the test finished, the core was taken out to weigh the amount of precipitated solute. Like the previous test, the weight of the tight plugs (T1 and T2) was unchanged but the high-permeable core plugs had some weight gain due to precipitated HWS-2. As mentioned before, in this test, the high-permeable core plug (H1) had been cut into two pieces to more specifically identify the solute precipitation location. As shown in Figure 4-30, they are named H11 (closer to the inlet) and H12 (closer to outlet). The weight gain due to solute precipitation in H11 was 0.158 gr whereas H12 gained 0.748 gr. Therefore, it can be concluded that the blockage was formed in H12, which was closer to the outlet of the composite core.

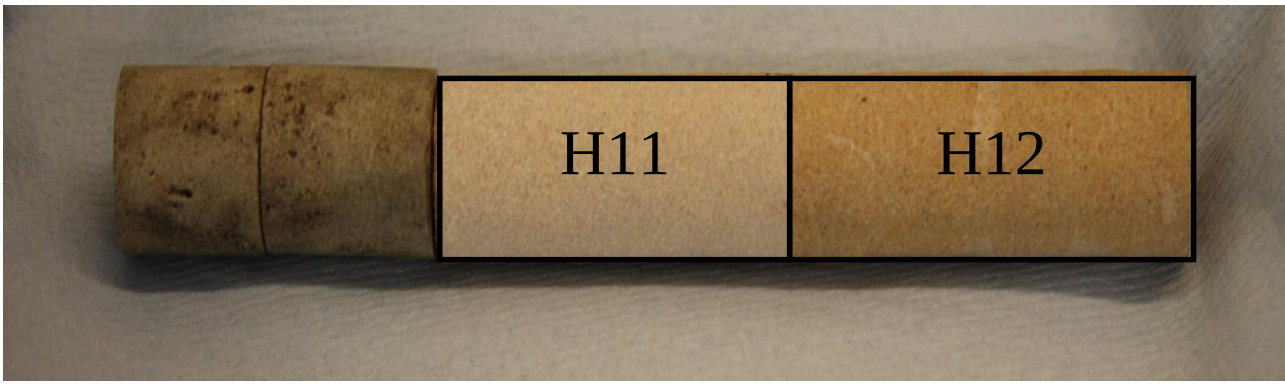

Figure 4-30: The configuration of core plugs in the 4th coreflood experiment; two identical core plugs (H11 and H12) with high permeability are used.

In summary, the successful blockage in the 4th coreflood experiment demonstrates that the injected CO_2 has been saturated with HWS-2 on its way into the core leading to an efficient solid solute precipitation and blockage. This blockage took place in the core plug which was closer to the outlet face of the composite core. This proves that the downhole mixing can be considered for applying our proposed leakage prevention method. In addition, the re-blocking of the simulated leakage path revealed that the solution is capable of repairing the blockage if its integrity is compromised. That is, if the particles are remobilised for any reason, the precipitation is re-established to form the blockage at the same precipitation site.

4.3.7 Test No. 5

Test Conditions

The pressure and temperature conditions of the 5th test were exactly similar to those of the 4th test (pressure drop of 250 psig and temperature of 45 °C). However, in this test the applied pressure drop was altered during the test. The same experimental set-up for mixing the same solute (HWS-2) and CO_2 was used. However, a different composite core assembly was used to investigate the impact of core properties on the blockage formation. Table 4-4 lists the basic properties of the core plugs used in the 5th coreflood test. The total length of the core used here is less than the one used in previous tests. In the fourth test, the total length of the high-permeable core plugs (H11 and H12) was 13.5 cm but, in the fifth test, only one of the two high permeable plugs (H11) was employed in the composite core assembly. Furthermore, in this test, T3 as a tight core plug was used to reduce the flow rate, which favours a more stabilised equilibrium conditions between the solute and solvent (supercritical CO_2).

Table 4-4: Basic properties of the core plugs used in the 5th coreflood experiment.

Core ID	Length (cm)	Diameter (cm)	Weight (gr)	Porosity (fraction)	Permeability (mD)
T2	4.01	2.56	57.661	0.037	0.0037
T3	2.98	2.61	42.044	0.037	0.0032
H11	7.01	2.54	72.963	0.163	225

Results and discussion

Figure 4-31 depicts the log of the injection and the retract flow rates during this experiment. As it can be seen, two imposed pressure drop scenarios were considered. Initially and up to 4000 minutes into the test, the pressure drop was similar to the previous tests and was set at 250 psig. However, because no sign of blockage was noticed, the pressure drop was increased to 450 psig, which also did not result in a blockage. With the pressure drop of 250 psig, the solution passed through the core with an average flow rate of 0.022cc/min. The rate was increased to an average value of 0.037cc/min applying pressure drop of 450 psig. A relatively steady and stable flow rate is noted in Figure 4-31 at both applied pressure drop which demonstrates that no significant precipitation of the solute took place against the simulated leakage path during the test. The main reason for these unfavourable results can be attributed to having a shorter high-permeability core part at the end of the composite core assembly.

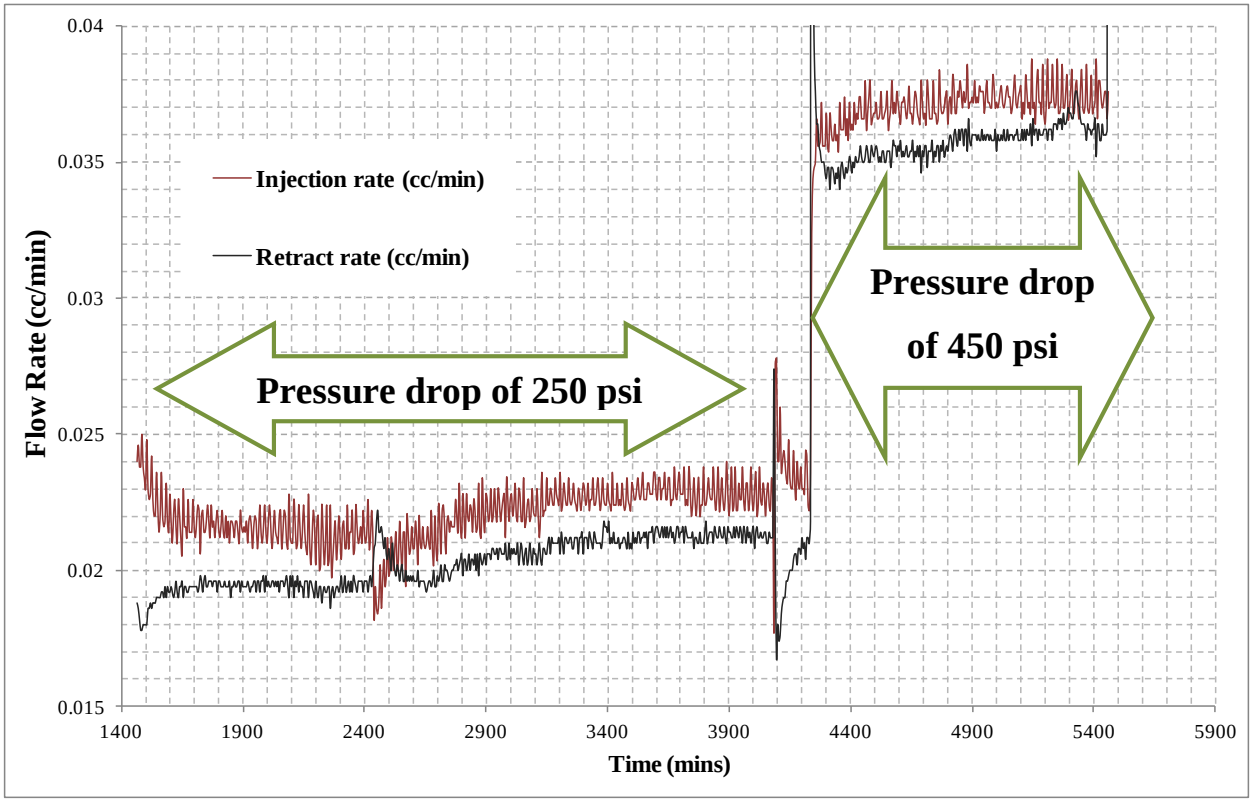

Figure 4-31: Log of the injection and the retract flow rates during the 5th coreflood experiment; no indication of significant precipitation or blockage is inferred.

It seems that the shorter high-permeability core plug, the less the probability of the precipitation and nucleation of particles. All conditions of the test were similar to those of the previous test (apart from increasing pressure drop in the second part of the test). To overcome the delay of particle formation, a longer high permeable core plug at the outlet face of composite core is needed to provide the sufficient core length for the solute to be nucleated and precipitate. However, in this test because we have a shorter core plug (H11) by a factor of two compared to the two previous tests, the formation of particles did not take place within this porous medium.

After continuing the experiment for about 5500 minutes, no indication of blockage was noted and hence, the core holder was dismantled to take out the core plugs for further analysis. It was noticed that the tight core plugs had their original weights but the high-permeability core plug gained slight weight of 0.151 gr due to slight precipitation of solid solute that was not sufficient to form a blockage.

The results of this fifth coreflood experiment revealed that the occurrence of significant precipitation and subsequent blockage is not guaranteed for every case of the simulated leakages at the laboratory scale. Most of the unfavourable results observed here are because of the experimental artefact, which in turn stem from scaling down the real process. In a real leakage scenario in a real geologic formation, the length of a high permeability leakage path through the caprock could be more than 20 metres, which provides the required length for precipitation and blockage.

4.3.8 Test No. 6

Test conditions

In this test HWS-3 was used as the solute to evaluate the effect of solute type on the blockage formation. HWS-3 has a melting point of 80 ^{o}C, which makes it solid when it comes out of the solution at the test temperature of 45 ^{o}C. The initial pressure conditions of the 6th test were exactly similar to the 4th test (i.e. pressure drop of 250 psig with inlet and outlet pressures of 3000 and 2750 psig, respectively). The solubility of HWS-3 is similar to HWS-2 at the prevailing conditions of the coreflood test. The approach for saturating the injected CO_2 with HWS-3 was similar to the previous test and was based

on the simulated downhole mixing. About 5.5 gr of HWS-3 was placed in the ¼" pipe connected to the inlet of the composite core assembly.

The core plugs were also similar to those of the 4th test. Table 4-5 shows the basic properties of the individual core plugs that were used in the 6th coreflood experiment. It is noted that the permeability of the tight core plug has considerably increased as a result of the reaction between the dolomitic carbonate and supercritical CO_2 taking place in the earlier testes

Table 4-5: Basic properties of the core plugs used in the 6th coreflood experiment.

Core ID	Length (cm)	Diameter (cm)	Weight (gr)	Porosity (fraction)	Permeability (mD)
T1	4.01	2.56	57.661	0.037	0.025
T2	2.98	2.61	42.044	0.037	0.021
H11	7.01	2.54	72.963	0.163	225
H12	6.13	2.54	63.529	0.163	225

Results and discussion

Figure 4-32 illustrates the log of the injection and the retract flow rates during this coreflood experiment. At first glance, two distinct flow behaviours can be identified; the quasi-steady flow during the course of applied 250 psig pressure drop and the significant variation of flow rates when the pressure drop was increased to 900 psig. The average flow rate at the early stage of injection with 250 psig pressure drop was about 0.2cc/min, which is higher by almost a factor of 5 compared to test No. 4 with HWS-2.

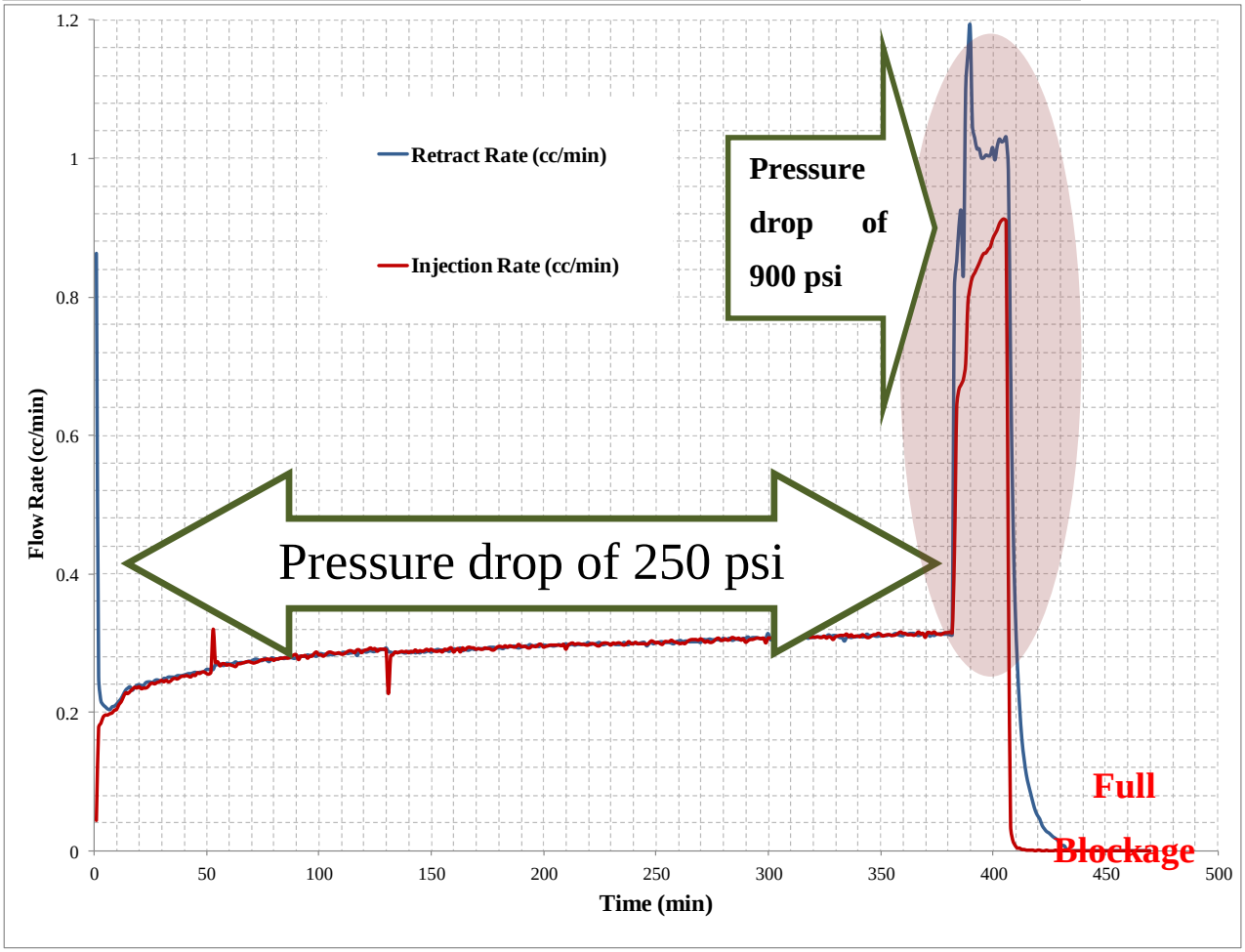

Figure 4-32: Log of the injection and the retract flow rates during the 6th coreflood experiment; a steady flow rate for 370 minutes indicates no-blockage behaviour. After significant fluctuations in flow rates for the applied pressure drop of 900 psig, full blockage was established

According to Figure 4-32, no indication of significant precipitation of the solute can be identified after 370 minutes of continuous flow of the solution. The relatively high flow rate of CO_2 solution can be considered as the main reason for non-blockage behaviour of the experiment during the low pressure drop of 250 psig. Thus, it can be concluded that to capture the precipitation in these porous media, the flow rates should be adjusted according to the imposed supersaturation (pressure drop) and the configuration of the composite core assembly (permeability and length of used core plugs). At this stage, the applied pressure drop was increased to 900 psig, which is close to the blockage pressure of micromodel tests reported in previous chapter and sandpack experiments which will be discussed in the second part of this report. The fluctuations of the flow rates, which were noted after imposing this higher pressure drop, imply that significant precipitation

occurred. It seems that after a short period of flow, the blockage was formed in the simulated leakage path. At this stage, the core was taken out for further evaluation of blockage properties. Figure 4-33 shows the outlet of the composite core assembly, which demonstrates the precipitation of HWS-3 particles in the outlet face of the core.

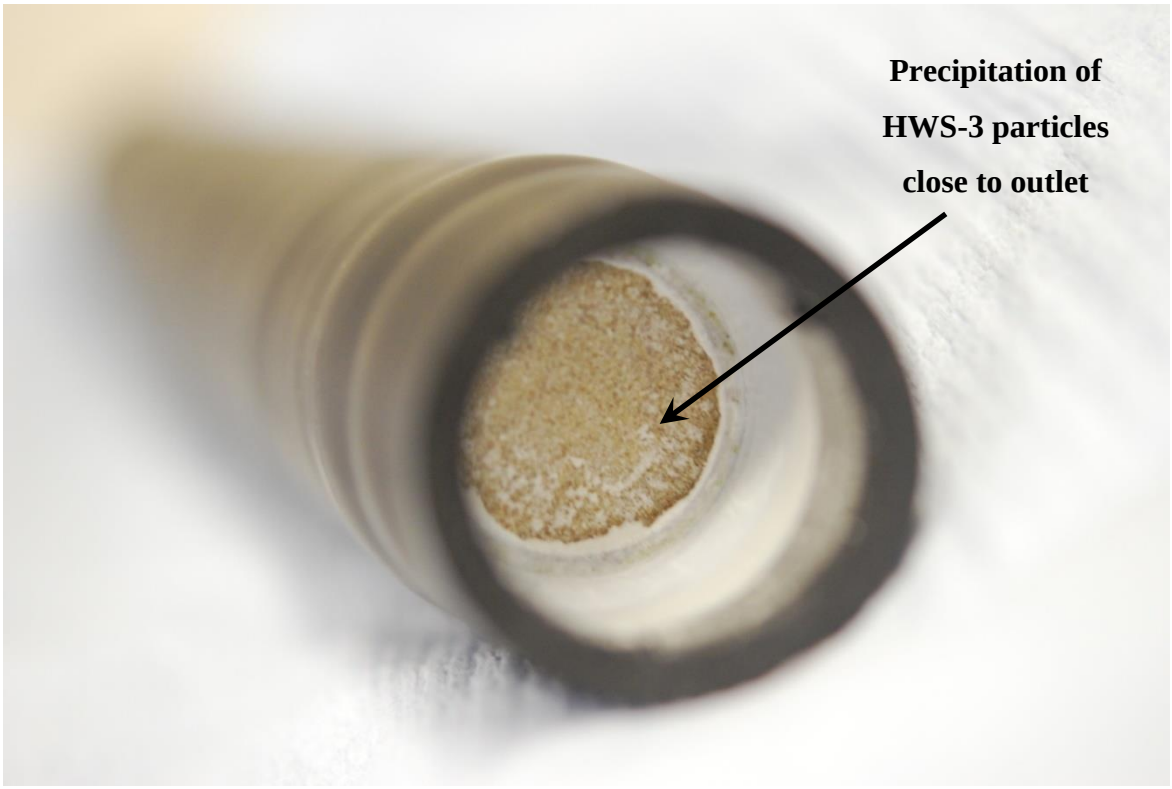

Figure 4-33: Image of the outlet face of the high permeable plug in the composite core assembly, which indicates the HWS-3 precipitation after imposing 900 psig pressure drop.

Massive precipitation of HWS-3 particles is not present at the outlet face of the core, but unlike the previous tests where blockage occurred within the core at low applied pressure of 250 psig, a clear indication of presence of HWS-3 at the core outlet is evident after imposing 900 psig pressure drop. The formation of precipitation at the end of the core reveals the importance of the flow regime (flow rate and pressure drop) on the location of the precipitation. Moreover, the particles remained attached to the core, which indicates the strength of the blockage when it was formed. At this stage, the core holder was dismantled to weigh the individual core plugs. Similarly to the previous tests, the weight of the tight core plugs was not changed but that of the H12 high-permeable core plug was increased by 1.245 gr, which is significantly higher than that reported in Test 4 using HWS-2 with 0.748 gr weight gain for the same high permeability core plug. It should be

pointed out that, in micromodel experiments, the amount of HWS-3 precipitation was qualitatively higher than HWS-2 which is in good agreement with the findings of coreflood tests reported here. This difference between the solutes precipitation stems from the mechanism of coagulation of particles. That is, HWS-2 particles have high tendency to be agglomerated and form larger particulates whereas the HWS-3 particles precipitates separately and hence more HWS-3 particles are needed to block the leakage.

Similar to the previous tests, the composite core assembly was then cleaned by injection of Acetone (strong solvent of solid HWS-3) to dissolve the precipitated HWS-3. Then, the effluent was dried out of the Acetone to recover the solid solute, as shown in Figure 4-34. The weight of the solid HWS-3 in the beaker is 1.313 gr, which is in good agreement with weight increase of the H12 core plug.

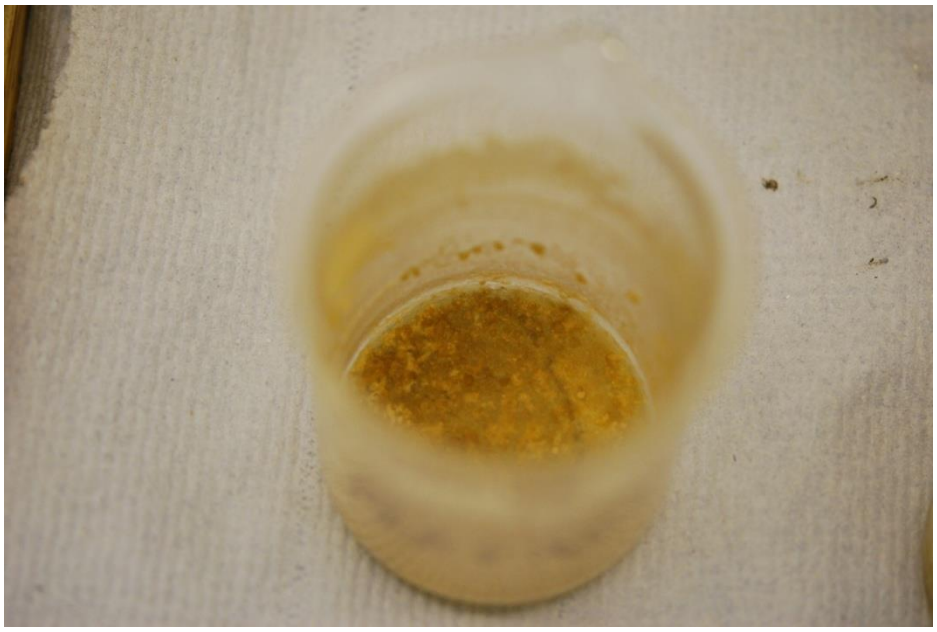

Figure 4-34: Recovered HWS-3 from the high-permeable H12 core plug in 6th coreflood experiment.

4.3.9 Discussion

Simulation of a real leakage path as those of storage site with exact characteristics (flow rate, pressure, permeability, and length) in the laboratory is not possible. Coreflood experiments have been conducted to investigate the efficiency of the leakage prevention method in real reservoir rocks and with conditions which are close to the possible leakage paths found in the storage sites. In most of the tests conducted with HWS-2, the simulated leakage paths in the laboratory scale were tackled and significant precipitation of the solid solute resulted in a firm and durable blockage. Based on the coreflood tests, the conditions

of experiment at which the blockage is formed, nonetheless, depend on the design of the composite core assembly and the length of the simulated leakage path.

Two mechanisms control the evolution of the blockage; particle formation (nucleation kinetics) and filtration of the solid particles (suspension flow). It seems that in these experiments the impact of suspension flow in prevention of blockage was not significant particularly tests 3 and 4. This can be explained noting that the cores are consolidated rocks and can be considered as proper barrier to entrap the formed particles. In other words, the flow of suspended formed particles cannot adversely affect the process of blockage build up.

However, the time lag for formation of the particles seems to be the main mechanism that brings about unfavourable results in some of the coreflood experiments. Its adverse effect was observed clearly in Test No.5, where the solution did not have sufficient time in the porous media to drop out the particles and block the leakage path.

In the case of HWS-3, the coreflood experiment results showed that, with increased flow rate (five times higher than that of test 4 using HWS-2), no significant precipitation was detected, which highlights the dominant effect of the time lag in particle formation. Qualitatively speaking, the significance of the time lag was also observed to be higher for the HWS-3-saturated solution compared to HWS-2- saturated solution in the micromodel experiments at which the HWS-3 particles became visible at higher pressure drop. Therefore, it is reasonable to conclude that HWS-3 requires higher supersaturation (pressure drop) to nucleate, which highlights the impact of solute type in this process. The solution using HWS-3 blocked the leakage path at a relatively pressure drop of 900 psig, which can represent special real cases with a thick caprock. These results highlight that, the design of the proper solution depends on the type of solutes and conditions of the particular storage reservoir.

The results of all these core flood experiments can be encapsulated in one general conclusion; the probability of having a durable blockage is high, but in some conditions there is not sufficient precipitation of solid solute to block the leak primarily due to the existing delay in the formation of particles as a result of nucleation kinetic of the process. Consequently, the leakage prevention method needs to be modified further to reduce the delay in particle formation for such cases. A modification has been proposed to improve the response of the solution at various leaks, which is described in next chapter.

4.4 Flow through storage reservoir

In order to design an efficient leakage prevention technique, integrity of the CO_2 + solid-solute solution in the storage reservoir should not be compromised due to its interaction with in-situ fluids, e.g. brine. To investigate the dynamic interactions between the solution and in-situ brine and rock, two different coreflood experiments were performed to identify the behaviour of the solution in the storage reservoir; (1) in the adsorption test, we aimed at evaluating the amount of adsorbed solute on the rock surface when the solution flows through the core, which represents the storage reservoir. It should be noted that adsorption of solutes reduces the solid content of the solution and hence it can undermine the efficiency of LPT. (2) Another core test was designed to investigate the possibility of premature precipitations due to the solution and resident brine interactions in the storage reservoir. Therefore, the experiments were designed to further investigate the practical issues around implementing the LPT in the field.

4.4.1 Adsorption experiment

One of the main concerns in the large scale implementation of the LPT is the adsorption of solutes on the rock surface as it flows though the storage reservoir. Any adsorption of solutes can adversely reduce the solute content of the injected CO_2 which would in turn decrease the efficiency of the solution when it meets leakages. Therefore, it is vital to investigate the tendency of the solid solute to be adsorbed on the rock surface, which should be measured experimentally. The coreflood setup was used to perform the test however; the inlet and the outlet conditions are different compared to previous tests. In the adsorption test, slight pressure drop (5 psig) was imposed across the porous medium and the weight change of the core before and after the test would be measured to detect possible adsorptions. Table 4-6 lists the basic properties of the core plugs used for adsorption experiment. The core plugs at the inlet should be high permeability to adjust the pressure distribution in favour of keeping the solute in the solution in the core because solute precipitation must happen due to adsorption not particle formation.

Table 4-6: Basic properties of core plugs used in adsorption experiment.

Core ID	Permeability (mD)	Porosity (frac.)	Length (cm)	Diameter (cm)	Weight (gr)	Lithology
Ad1	225	0.167	13.21	2.55	143.637	Sandstone
Ad2	225	0.167	10	2.55	112.841	Sandstone
Ad3	0.023	0.152	5	2.56	55.05	Sandstone

The procedure was similar to the previous coreflood experiments; solvent (pure CO_2) flows through a pipe filled up with HWS-2 and the resulting solution enters the core assembly. During the test, the pressures of inlet and outlet were kept constant at 3000 and 2995 psig, respectively and the flow rates were recorded for detecting the permeability change due to adsorption or precipitation. According to Figure 4-35, the injection flow rate is constant and steady during the experiment, which indicates no detectable change in the permeability of the system after injecting 160 cc of the saturated solution of CO_2 and HWS-2. Nonetheless, the weight of the core plugs should be analysed for identifying amount of adsorbed solute since the accuracy of weight measurement is much better than recoding the rates.

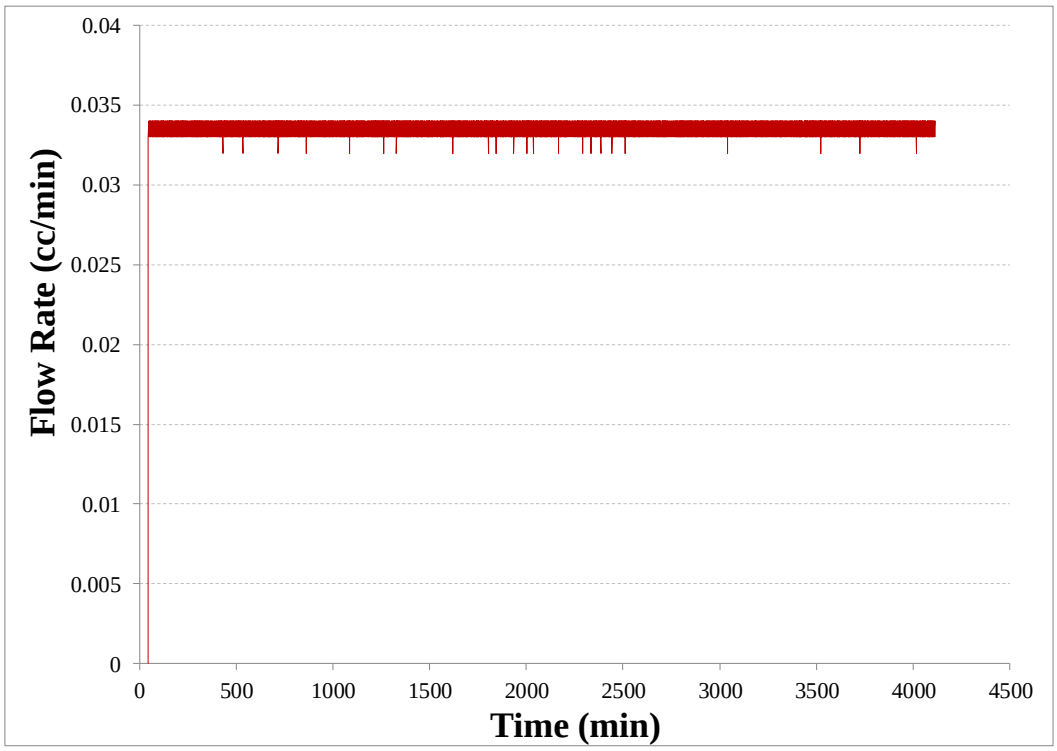

Figure 4-35: The injection flow rate during the adsorption experiment. No indication of permeability reduction can be identified.

At the end of the adsorption experiment, two source of information can be considered to measure the adsorbed solute; (i) the weight change of the core plugs and (ii) the produced HWS-2 in the retract cell. The changes in core weights were in the range of instrument error (±0.005 gr), which implies no adsorbed solute on the rock surface in the experimental conditions. Also, the amount of HWS-2 in the retract cell was recovered

and it was 0.987 gr, which is very close to the solid content of saturated solution (0.978 gr). Therefore, it can be concluded that the solid solutes has no or negligible tendency to be adsorbed on the rock surface. Given that water/oil can exist in real storage reservoirs, it should be pointed out that in-situ wetting phase (water/oil) would coat the rock surface protecting the porous medium from the contact with the injecting CO_2 and hence, the resident fluids would act as a barrier for any possible adsorption of solute. However, in the experiment, it was verified that no solid-solute was adsorbed on the rock surface.

4.4.2 Flow assurance test through storage reservoir

Premature particles precipitation in the storage reservoir can undermine the practical implementation of the LPT since it may adversely affect the reservoir permeability. On the other hand, highly under-saturated concentration of the solute could reduce the effectiveness of the technique significantly. Therefore, the behaviour of the proposed technique under the prevailing conditions of the storage reservoir has to be experimentally investigated. The experiment has been designed to simulate the conditions of an aquifer in which the solution is injected continuously with the aim of analysing the interaction between the resident fluid (water) and the injection solution. One possible interaction is the dissolution of CO_2 in the water, which may jeopardise the equilibrium conditions in the solution resulting in a premature precipitation of the solid particles in the reservoir. It should be noted that the salinity of aquifer brines has an influential role on the amount of CO_2 dissolution in brine; the higher the salinity of in-situ brine, the lower the amount of CO_2 dissoluble in the water phase. In other words, distilled water can have maximum uptake of CO_2 compared to other saline systems. Consequently, if no premature precipitation occurs due to interaction between distilled water and the solution (CO_2 and HWS-2), then it can be concluded that solution will not drop out any solid particle in more saline fluid systems. Considering the distilled water as the resident fluid, the porous media is saturated with distilled water and then the solution will be introduced to displace the resident water. The injection continues for 600 cc of solution and the flow rates are monitored for detecting the precipitation.

To measure the residual water saturation in the core after flooding with the solution, it is necessary to collect the producing fluid. However, the producing effluent of the coreflood cannot be collected for two reasons; (i) due to safety and laboratory limitations, the setup should be operated in closed form to prevent any release of solid-solute and CO_2 in the

lab. Also, back pressure regulator cannot be put in the setup because the precipitation blocks it at early stage of the test. Therefore, the flow test should be conducted differently; firstly, the core is saturated with distilled water and pure CO_2 is then injected into the porous medium to displace the water. After that, the core is taken out of the coreholder to be weighed for determining the residual water saturation. Secondly, after cleaning and drying the core, it is put in the coreholder again and saturated with distilled water but, at this stage, the solution (CO_2 + HWS-2) is injected into the composite core. When the injection is finished, the core plugs are taken out to be weighed. Considering the residual saturation of water measured in the first part of the test, any additional change of weight can be attributed to the premature precipitation of the solid solute.

Table 4-7 shows the list of the core plugs used for the flow test. The main purpose for selecting the core plugs was to achieve reservoir flow velocity (1 ft/day) while finite pressure drops of 30 psig applied across the composite core. The experiment was performed in constant pressure mode; the inlet and outlet were kept at 3000 and 2970 psig respectively. It should be emphasised that the objective of performing the flow test is to investigate the flow assurance in storage reservoir not in the vicinity of wellbore or leakage paths.

Table 4-7: Basic properties of core plugs used in the flow test.

Core ID	Permeability (mD)	Porosity (frac.)	Length (cm)	Diameter (cm)	Weight (gr)	Lithology
Ken2	0.11	0.09	5.0	2.56	55.050	Sandstone
AB	1.25	0.12	13.8	2.55	143.637	Sandstone
AB11	1.25	0.12	10.0	2.55	112.841	Sandstone

First cycle of gas injection (pure CO_2) was carried out to evaluate the residual water saturation and also, in the case of no precipitation in the core, comparison of the information from two cycles can be used to check the repeatability of the flow test. The residual water saturation in first (Ken2), second (AB) and third (AB11) core plugs are 41%, 34% and 26%, respectively. The water saturations were determined by weighing the cores after the first cycle (pure CO_2 injection). Afterwards, the composite core was put in the coreholder and the solution (CO_2 + HWS-2) was injected into the core. Figure 4-37 exhibits the injection flow rates during the first and the second cycles. The flow rate

during the early period of the test has a rising trend since the distilled water was displaced with the injection fluid (CO_2 or the solution). After 500 minutes, the injection flow rate became stabilised at the constant value of 0.14cc/min (disregarding the fluctuation in the recording of flow rates). Apart from the negligible drift between the curves, it is obvious that the results of the first cycle were repeated in the second cycle in terms of the injection flow rate. Analysing the flow rates recorded in both cycles indicates that no or negligible precipitation took place in the composite core since no identifiable difference between the first (pure CO_2) and the second (the solution) cycles exists. However, the weight of the core plug at the end of the test would be more reliable than flow rate data. The core plugs were weighed after the second cycle and the change of plug weight was in the range of the instrument's error (±0.005 gr) and hence, no precipitation can be identified through the measurement of core weights.

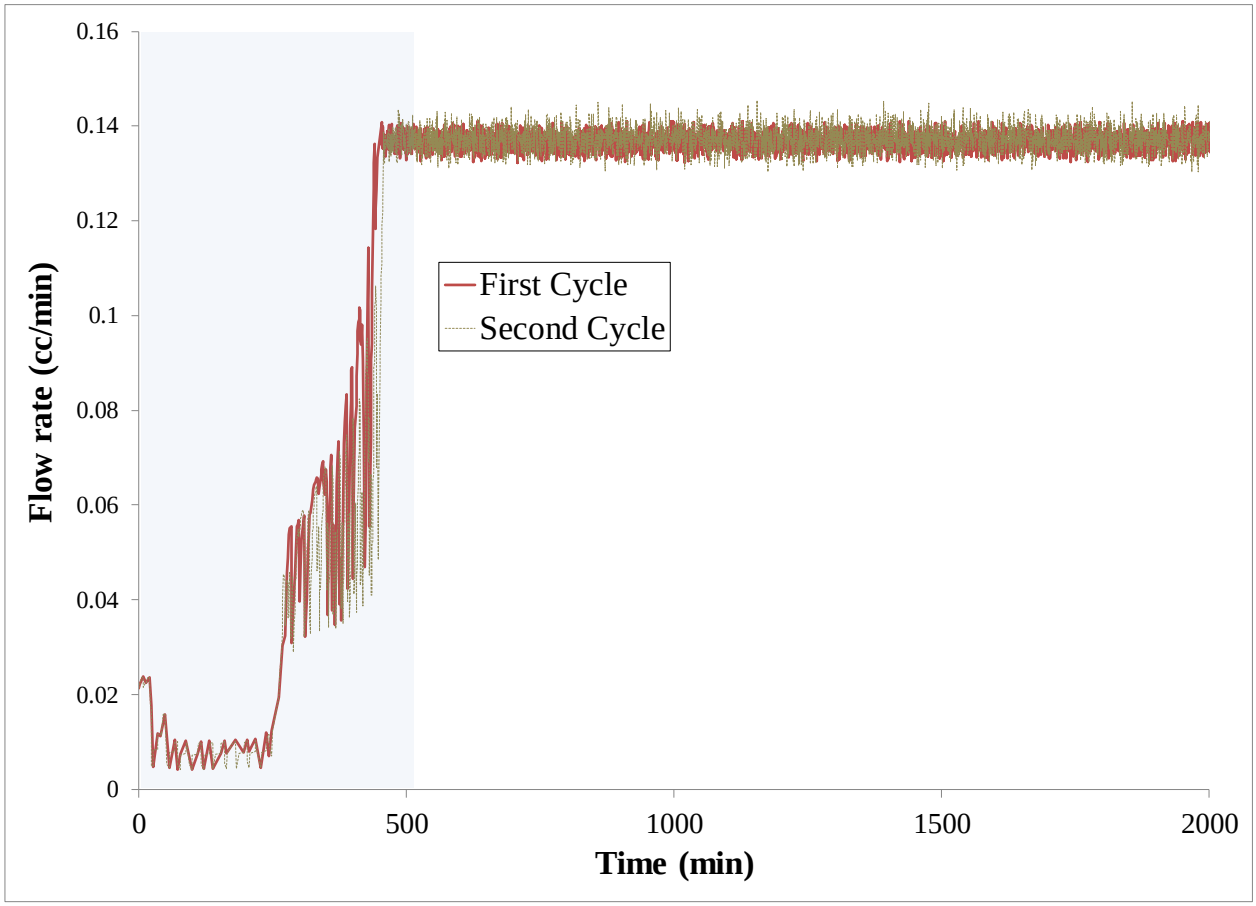

Figure 4-36: The flow rates during the flow assurance experiment for two cycles. The behaviour in the early stage of the test can be attributed to the two displacement of water by the gaseous like injection phases (pure CO_2 in the first cycle and the solution in the second cycle).

Having detected no premature precipitation under reservoir flow conditions, it would be worth evaluating the flow velocity during the flow test by performing simulation studies. Figure 4-37 demonstrates the flow velocity distribution along the core produced by CMG simulator. Although the flow velocity is not constant across the core, it is limited between 1.052 and 1.056 ft/day, which is close to prevailing typical flow velocity (1 ft/day) in real reservoir conditions.

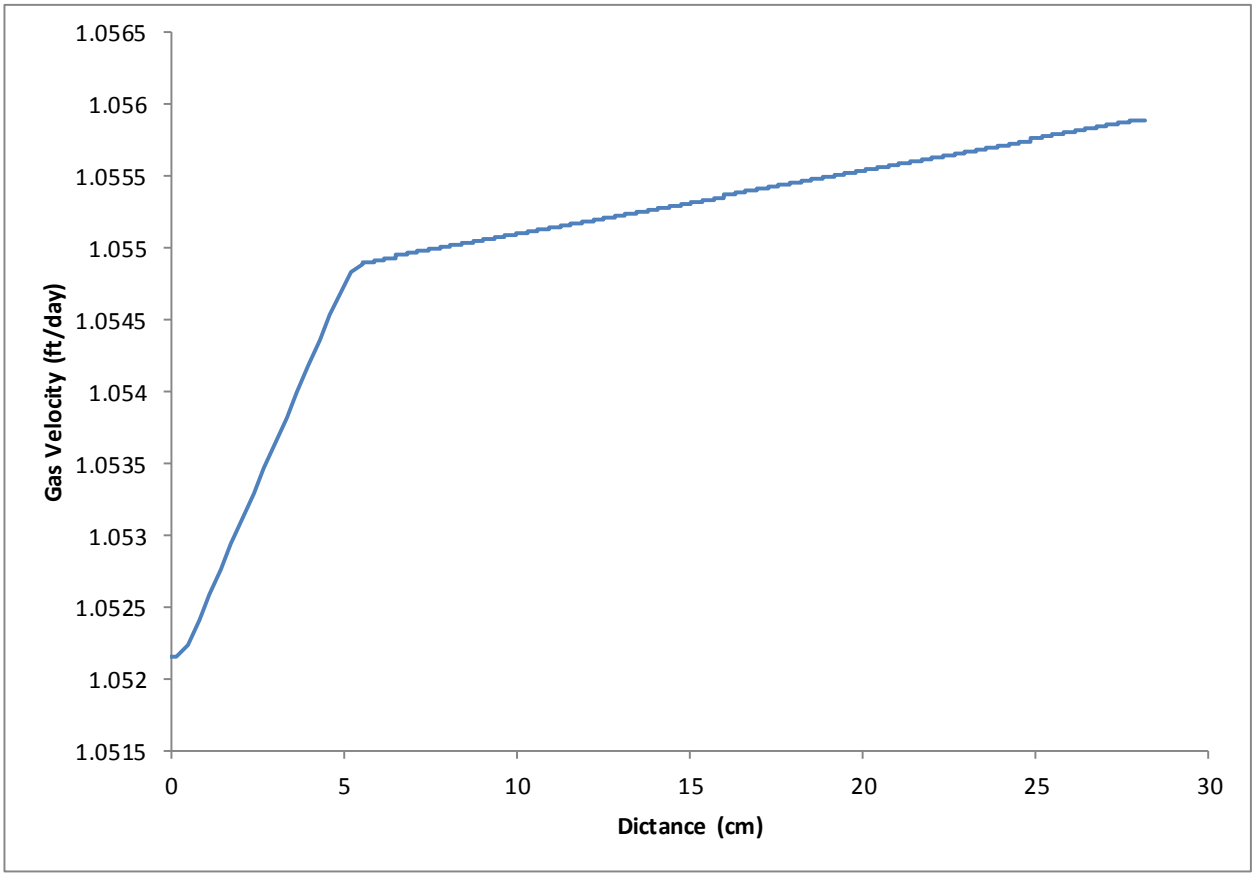

Figure 4-37: The flow velocity along the composite core simulated by CMG software.

4.5 Conclusions

Sandpack experiments were performed to quantify the lowest pressure drop (highest leakage pressure) at which the blockage stops the leakage in a relatively short period of time. This experimental facility serves as a reliable tool for fast screening of the solutes suitable for a particular application. It should be noted that the flow rates in the sandpack

experiments are high and corresponds to a sudden release of CO_2. The sandpack facility is equipped with a sightglass to evaluate the impact of suspension flow on our proposed leak prevention process. Five different solutes (HWS-4, HWS-1, HWS-2, HWS-3, and HWS-7) were used in the sandpack experiments. The sandpack results demonstrated that HWS-1 with very low solubility can be suitable for our purpose as it could block whereas, HWS-4 performed poorly. HWS-2 and HWS-3 were capable of producing a strong and durable blockage when pressure drop of 750 and 900 psig, respectively, were imposed on the system.

For analysing the response of the solution (CO_2 +Solute) in relatively low supersaturations, 6 coreflood experiments have been carefully designed and performed to investigate the behaviour of the solution in physically simulated leakage paths. Two types of core plugs were used; a tight one to impose the desired pressure drop while the flow rate was in the range of real reservoir flow, and a high permeable core to facilitate the precipitation of particles in the porous medium. The core plugs were put together to make up a composite core in order to achieve a flow behaviour that can represent CO_2 leakage from caprock. In the first coreflood test, a constant rate (0.5 cc/hr) of CO_2 flow was considered and 250 psig of pressure drop (supersaturation) was imposed on the solution. A complete blockage was identified by analysing the profile of injection pressure at the inlet of the core. Durability of the blockage was tested by applying the pressure drop of 2000 psig (two times higher than the original pressure drop) across the blockage body for 24 hours and no indication of CO_2 flow (reopening of the seal) was detected. Then, by weighing the plugs, an estimation of the location of the leakage blockage was detected which was in the high permeable core plug. The corresponding thickness was of the blockage was estimated to be 1.009 cm. The results of the weighing were confirmed by cleaning the core with a solvent. Although the weight of recovered solute in the process of cleaning was slightly different from what was obtained from weighing the core plug, they confirmed the estimated location of the precipitation which was in high permeable plug.

However, in the second coreflood test, the blockage did not occur at the supersaturations of 200, 500, and 700 psig since the velocity of CO_2 in the composite core in this test was 3 times higher compared to the first test. Nevertheless, the core was plugged at a pressure of 2100 psig which was 100 psig above the onset pressure of solute nucleation in previous micromodel test. Therefore, for having particle formation triggered in the rock, the velocity of CO_2 flow and the degree of supersaturation should be properly designed. The

precipitated amount of solute has been determined by weighing the plug; no precipitation was detected in the tight core but 0.592 gr of the solute (HWS-2) had been precipitated in the high permeability core plug. Compared to first test, the precipitation mass decreased in the second core flood test since, at higher supersaturation (second test), the particle nucleation would be more localized and faster which results in less cumulative precipitation of solute.

In the third coreflood experiment, it was aimed to repeat the first coreflood test by imposing similar conditions. In the first test, the constant flow rate was applied at the inlet whereas, the third test was carried out in constant pressure mode at either ends of the composite core. The outcome of the test showed the formation of complete blockage. The durability of the formed blockage was successfully checked. The amount of the precipitations was very close to first coreflood experiment, which indicates an acceptable degree of consistency between the tests.

The results of core flood experiments performed using the new experimental set-up (downhole mixing) showed that the blockage was successfully achieved in the high permeable core plug. The leak was effectively sealed by efficient use of solid solute through formation of a concentrated blockage at the exact location of the leak. It was also demonstrated that if the integrity of the blockage was compromised and the particles forming the blockage were remobilised by any means, the precipitation process would re-occur and the primary blockage be repaired and eventually a permanent blockage is formed. The above coreflood tests were designed and performed to simulate as a low rate leakage type. However, the delay in particle formation, which is controlled by nucleation kinetics have led into unfavourable behaviour in two of the experiments, i.e. tests 4 and 6. In experiment No. 4 using HWS-2, the length of high permeable core was not sufficient and the particles were not formed in the porous medium. In Experiment 6 using HWS-3 as the solute, either high pressure drop was required to seal the leak or the flow rate was needed to be notably lower. It should be noted that performing these experiments are time consuming and therefore optimising the test conditions can be a lengthy process. The results of coreflood experiments can be further utilised to develop a mathematical model and train the model

In a separate direction, the dynamic interactions between the CO_2 +solid-solute solution and constituents of storage reservoir (rock and brine) were investigated using coreflood setup. A coreflood experiment was performed for evaluating the adsorption of solid-

solute on the rock surface. It was identified that the adsorption of the solute would be negligible or out of the instrumental sensitivity for detecting the precipitation. This finding would indicate that the solution would not be adversely become under-saturated by solute adsorption. In another coreflood experiment the interactions of the solution and resident brine was investigated. The results showed that the dissolution of the CO_2 into the in-situ brine would not compromise the integrity of the solution and it would be unlikely to see premature particle formation in the storage reservoir as the solution forms the CO_2 plume.

CHAPTER 5 Controlling response of technique for various conditions

5.1 Introduction

So far, the performance of our proposed LPT (leakage prevention technique) has been extensively investigated by deploying various experimental techniques and setups. Two-dimensional (2D) micromodel visualisation experiments have revealed the mechanisms involved in precipitation of solid solutes albeit at relatively high flow rates. Coreflood experiments have been carried out, which highlighted the impact of flow rate and pressure drop on the blockage formation for a more realistic three-dimensional (3D) porous media (reservoir and outcrop rocks). Six different solutes were used in the experiments performed in previous chapters in order to investigate the impact of solute type on the performance of the LPT.

One observation made in some of the previous experiments was that a time lag exists in formation of solid blockage when only solid solute had been dissolved in the CO_2 solution. Therefore, to better control and speed up the onset of blockage formation, we would suggest using appropriate liquid solutes (co-solvent) in the solution. Using a liquid solute (co-solvent) enables us to adjust the sensitivity of the LPT solution (CO_2+solutes) based on the operational requirements. However, the mechanisms under which liquid solutes enhance the performance of the solution should be investigated visually through micromodel experiments to directly identify how the liquid co-solvent can adjust the response of the solution to different leakage scenarios. Therefore, in this chapter, our aim

has been to examine the impact of the liquid co-solvent by designing and performing micromodel visualisation tests. Before that, a series of sandpack experiments were designed and performed as the preliminary tool for fast screening and sensitising the impact of co-solvents on the performance of our leakage prevention technique. Having identified the influence of co-solvent (liquid solute), coreflood experiment were carefully designed and performed to investigate the improved responses of our proposed technique. In addition, the impact of presence of water on the precipitation process has been taken into account to physically simulate the effect of co-solvent under realistic conditions.

5.2 Rationale for Secondary Solute

The basic concept of the leakage prevention method is to add a small amount of an appropriate "solid" solute to supercritical CO_2. This solid solute should precipitate in the vicinity of the leakage path in response to a pressure drop. Up to this stage, we have investigated the response of a variety of solutes to different forms of leakage scenarios. It was shown that to have a successful blockage in lab scales, we need either a relatively high pressure drop or very slow leakage rates. The requirement of having high pressure drop for cases in which this can result in delays in particle formation is not desirable. The source of the delay in the formation of the solid solute relates to the kinetic of the process when the solid solute comes out of the solution. Our proposed idea for enhancing the efficiency of leakage prevention method is based on adding another (secondary) solute to the previous system of fluids (CO_2 + a primary solid solute).

The secondary solute should have two main characteristics; first, its solubility in supercritical CO_2 should be low and, more importantly, it must be in liquid state at reservoir conditions to reduce the delay time in precipitation of primary solid solute. It should be pointed out that the secondary solute is used only to facilitate the process of blockage and the primary solute is the main solid solute for precipitation and for sealing the leak.

Most liquid solutes, in the supercritical CO_2, are formed relatively immediately when the solution becomes supersaturated irrespective of the degree of supersaturation. In other words, for liquid solutes, (unlike solid solutes) there is no considerable delay in the formation of a new phase. Therefore, if there is a pressure drops in the vicinity of leakage path, the secondary solute will come out of the solution much quicker than its solid counterpart. It should be noted that the presence of a secondary liquid solute can also favourably promote the solubility of the primary solute in supercritical CO_2. As an

example, acetone or methanol is used as strong co-solvent in CO_2 extraction units to increase the amount of solute uptake in the supercritical CO_2 [1].

In terms of improving efficiency of the precipitation of the primary solute, the secondary (liquid) solute possesses two main impacts on the response of the solid solute. Firstly, as was mentioned, adding an appropriate secondary solute to supercritical CO_2 increases the solubility of the primary solute, which in turn results in an excess supersaturation degree in the vicinity of the leakage path where the liquid secondary solute is formed. This excess supersaturation degree facilitates the formation of the primary solid solute. The extent of this effect can be obtained by measuring the solubility of the primary solute in presence of the secondary liquid solute.

Secondly, the instantaneous formation of the liquid phase in the vicinity of the leakage path imposes an additional flow barrier, which either increases the pressure drop or reduces the flow rate of the leakage. In other words, formation of a new phase (secondary liquid solute) results in reduction in relative permeability of CO_2 in the vicinity of the leakage path and hence it creates more favourable conditions for nucleation of the primary solid solute. It should be emphasised that the new liquid phase would not block the leakage path but will facilitate formation of the blockage as explained above.

One issue with using the secondary solute is magnitude of primary solute solubility enhancement which would affect the required amount of the primary solute. Another important consideration is its cost. These issues should be considered when the new fluid system for a particular storage application is designed.

The significance of each mechanism for improving efficacy of the proposed leakage prevention method has not been fully investigated yet. Here, a number of sandpack and micromodel experiments were designed using HWS-7 and HWS-8 as the secondary solutes. The sandpack experiments would show the impact of liquid solute without conducting very cumbersome and costly micromodel and coreflood experiments. Subsequently, in a series of visualisation tests, the instantaneous nucleation of the secondary solute was observed by means of a visualization cell. The second set of tests was carried out in micromodel setup with the secondary solute added to the previous fluid system. The third type of experiments was the coreflood tests performed with the addition

[1] *Gupta, R.B. and Shim J., Solubility in Supercritical Carbon Dioxide, CRC Press (2007)*

of a secondary liquid solute to previous solution made with HWS-2. Similarly to the previous tests, the test temperature was 45 ^{o}C for all these tests.

5.3 SandPack

5.3.1 Secondary (liquid) Solute-HWS-7

For improving the efficiency of leakage prevention method, a new type of solute is considered which comes out of the solution in liquid form when the pressure drop is imposed. HWS-7 with melting point of 40 ^{o}C has been used to enhance the pressure response of the leakage prevention method by reducing the time required for particle formation. Figure 5-1 shows the solubility profile of HWS-7 versus pressure at constant temperature of 45 ^{o}C. The solute is relatively high soluble in the supercritical CO_2, but the experiments with HWS-7 is only performed to verify our proposed idea for having more responsive solution. It should be noted that, as our understanding evolves, naturally more practical and costly-effective secondary solutes would be identified.

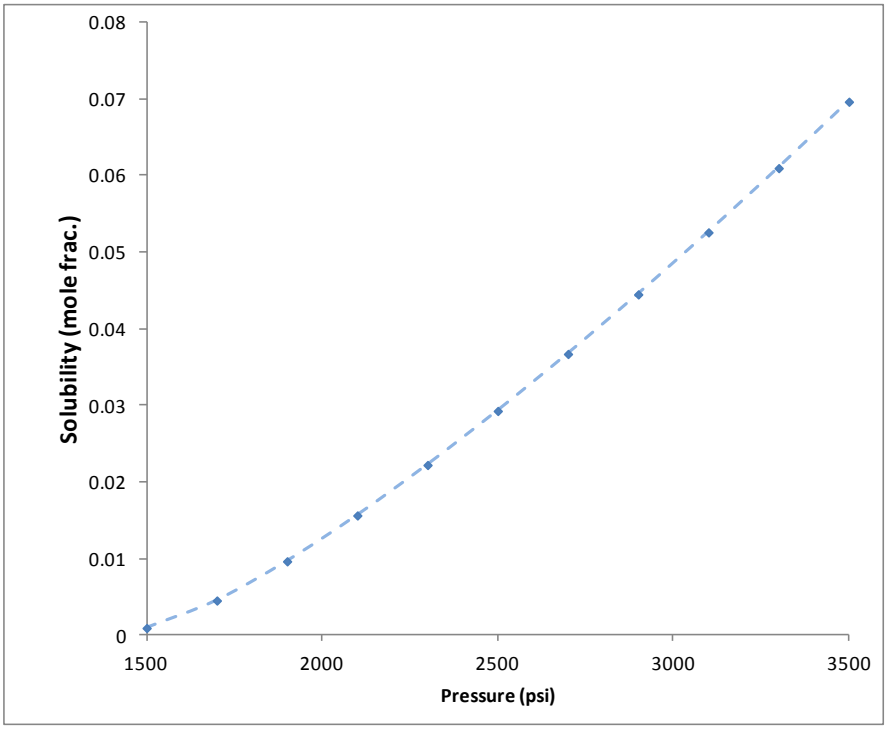

Figure 5-1: Isothermal solubility of HWS-7 in supercritical CO_2 at 45 ^{o}C.

5.3.2 Test No. 7 (HWS-7)

HWS-7, the secondary liquid solute, is used in the 7th experiment in the visualization cell (sightglass) to observe the nucleation of the new phase when pressure drops. The volume of the sightglass of the sandpack set-up used here is 2 cc, which makes it suitable for withdrawal tests to detect the formation of new phases. 10 gr of HWS-7 was placed in the cell, which was pressurized up to 3000 psig by adding pure CO_2. The melting point of the solute is 40 ^oC which leads to having a liquid solute when it precipitates out at the test conditions.

Test conditions and results

To pressurize the sightglass, pure CO_2 was injected into the visualization cell until its pressure reached 3000 psig. Then, 100 cc of HWS-7-saturated CO_2 was injected into the cell to displace the pure CO_2 at the constant pressure of 3000 psig to ensure that the in-situ fluid was the CO_2 + Solute solution. After allowing the fluid inside the sightglass to stabilise, the leak cell (explained in chapter 2, Figure 2-7) was set to retract the resident fluid from the visualization cell. While the fluid was being pulled back, the camera recorded the images of the sightglass continuously. Once the fluid inside the sightglass became cloudy, it was concluded that the phase change occurred and the corresponding pressure was recorded as the onset of the instantaneous nucleation. It is difficult to detect the exact value of the pressure

Figure 5-2 demonstrates the cloudy state of the sightglass near 2950 psig, which indicates only 50 ± 10 psig is needed for the new phase formation. This highlights how sensitive the solution is to a small reduction in pressure. This visualization test confirms that the secondary solute is formed with slight supersaturation.

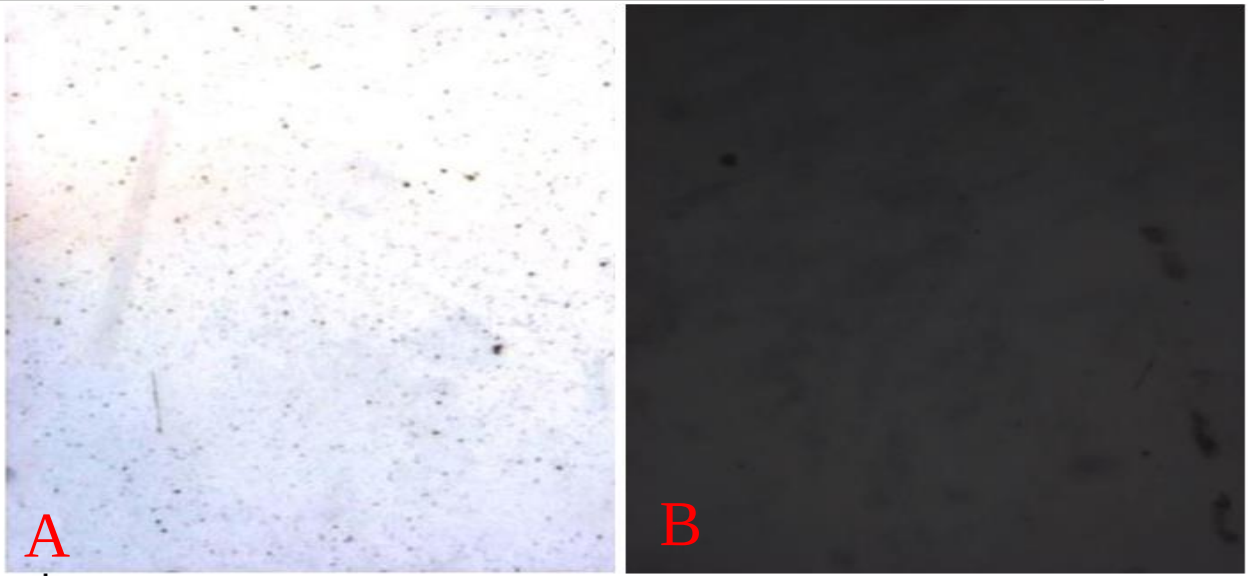

Figure 5-2: Formation of new phase with pressure drop of 50 psig in the case of using HWS-7; A: initial state of the sightglass, B: cloudy state of visualization cell which demonstrates the formation of HWS-7 liquid phase.

5.3.3 Test No. 8 & 9 (HWS-2 + HWS-7)

These tests were designed similar to tests chapter 5 and were performed with only the primary solute. Previous tests were successful to block the leakage path when the leak pressure was reduced to 2250, i.e. 750 psig pressure drop. The main aim of this test was to evaluate whether addition of liquid solute could result in a successful blockage. To investigate the impact of secondary liquid solute, several experiments with sandpack with leakage pressure varying between 2000 and 2600 psig were conducted. However, the test at which successful blockage was achieved at highest pressure is presented.

As explained before, the secondary solute is expected to enhance the solubility of the primary solute, therefore, when the secondary solute is added to the previous system with 5 gr of HWS-2, the solution is not fully saturated with HWS-2, which in this case, severely undermined the efficiency of leakage prevention method, i.e. no blockage was formed within the tested pressure range. The outcome of the test confirmed that adding a liquid solute to the solution increases the solubility of the primary solute and consequently the system cannot respond to the imposed leakage effectively.

The next test was performed by increasing the concentration of HWS-2, as the primary solute, to 10 gr (from the previous 5 gr) to ensure that the solution is fully saturated with HWS-2. It should be pointed out that, at this stage of the investigation, the thermodynamic properties of the three-component fluid system (supercritical CO_2, primary solid solute, and secondary liquid solute) and hence the amount needed to fully saturate the system is not well-understood yet but it was assumed that 10 gr of HWS-2 was sufficient to fully saturated the system.

Test conditions and results

The leak pressure was adjusted at 2500 psig, i.e. 500 psig pressure drop. The solution was prepared at 3000 psig and 45 ^oC with 10 gr of HWS-2 and 10 gr of HWS-7 placed in the 280 cc of the high pressure CO_2. After 110 cc of the solution passed through the sandpack, the discontinuity of flow and pressure between the inlet and outlet of the sandpack was observed, which was a strong indication of a blockage occurring in the leakage path. As was mentioned earlier in chapter 4 (Section 4.2.7), the two-component solution (HWS-2 + CO_2) formed a blockage at a leak pressure of 2250 psig. Here, in this test, the blockage formed at 2500 psig using the new solution, which means 250 psig improvement in the response of the solution. Figure 5-3 demonstrates the state of the sightglass during the test, which reveals the presence of the two solutes formed in the sightglass. The sequence of stages of the blockage formation process starts with appearance of the secondary solute (HWS-7) in the sightglass in the form of a cloudy phase followed by appearance of HWS-2 particles in the visualization cell. Then, we have the full blockage of the leakage flow path within the sandpack porous medium.

After having a stable blockage for two hours, the inlet pressure was increased to 3500 psig to test the durability of the blockage, which was successful, i.e. the blockage remained in place even at the higher pressure. In the micro-scale, a question may be raised that adding a liquid solute could have an adverse lubricating effect on the solid particles which may weaken the firmness of the solid particles precipitated. Clearly this was not the case here.

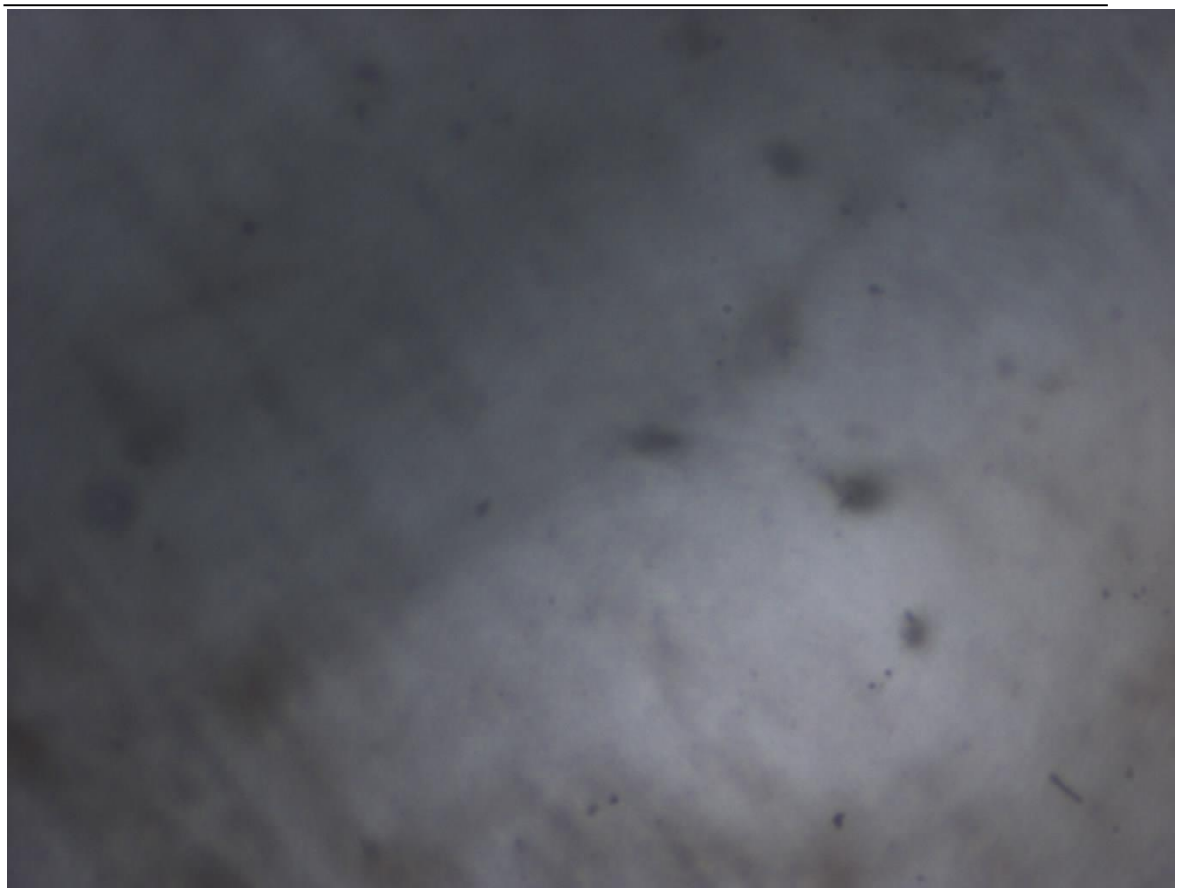

Figure 5-3: An image of the sightglass showing that when HWS-2 and HWS-7 are dissolved in the solution together; HWS-2 particles and the cloudy state of the sightglass are observed which demonstrates that both solutes were formed as a result of the imposed pressure drop.

It is believed that liquid solutes have a significantly lower nucleation time lag and hence, it was preliminary verified here to use a liquid solute (as a secondary solute) to improve the efficiency of the leakage prevention method. Two main benefits of adding a secondary (liquid) solute (HWS-7) are;

a. It increases solubility of the primary (solid) solute. This means that when the secondary solute comes out of the solution, additional supersaturation is imposed on the solution, which should make it more responsive, i.e. faster deposition of the primary solute.

b. It creates additional flow barrier, higher local pressure drop, for the leaking CO_2 as a result of a reduction in CO_2 relative permeability. This should also make the solution more responsive. .

Furthermore, it should be noted that the new liquid phase would not block the leakage path but would facilitate the process. The test was performed using HWS-7 with a melting point of 40 ^{o}C. The results demonstrated that: The solution with HWS-7 and supercritical CO_2 was observed to form a HWS-7 cloud immediately when a small pressure drop of 50 psig was applied to the systems.

To sum up, the addition of HWS-7 into a new solution consisting of supercritical CO_2, HWS-2, and this solute improved the response of the solution considerably. The highest pressure, at which the blockage was obtained, was 2500 psig corresponding to a pressure drop of 500 psig, which is 250 psig less than that required when CO_2 solution was only saturated with HWS-2 (without the secondary solute). However, these results should be verified for other combinations of primary solid and secondary liquid solutes and by performing core flood experiments.

5.4 Micromodel Visualisations

In this section, the experimental work mainly consists of micromodel visualisation to investigate two important factors; (i) impact of liquid co-solvent on the blockage efficiency of the LPT solution (ii) the impact of water on the formation of the blockages. HWS-1 as an inexpensive solute has been tested. The impact of a liquid solute (HWS-8) on the response of the HWS-1 has been investigated. This exercise demonstrated considerable improvement in the response of HWS-1 when the co-solvent was used. The visualisation results were used to verify the mechanisms under which the liquid co-solvent impacts the process. The efficiency of the LPT in micromodels was first tested without water. Then, distilled water was used as the aqueous phase to partially saturate the micromodel and identify the impact of water on the blockage evolution. These visual results are very useful and reveal the impact of liquid solute and water directly as opposed to the indirect results often obtained by coreflood experiments.

5.4.1 Impact of liquid solute

HWS-8

HWS-8 has been used for micromodel experiments with similar solubility compared to HWS-7. This ensures that our visual observations are not significantly affected by this

change of the liquid co-solvent. HWS-8 has a melting point of -1 ^{o}C . Figure 5-4 shows the isothermal solubility of HWS-8 with respect to pressure at temperature of 50^{o}C.

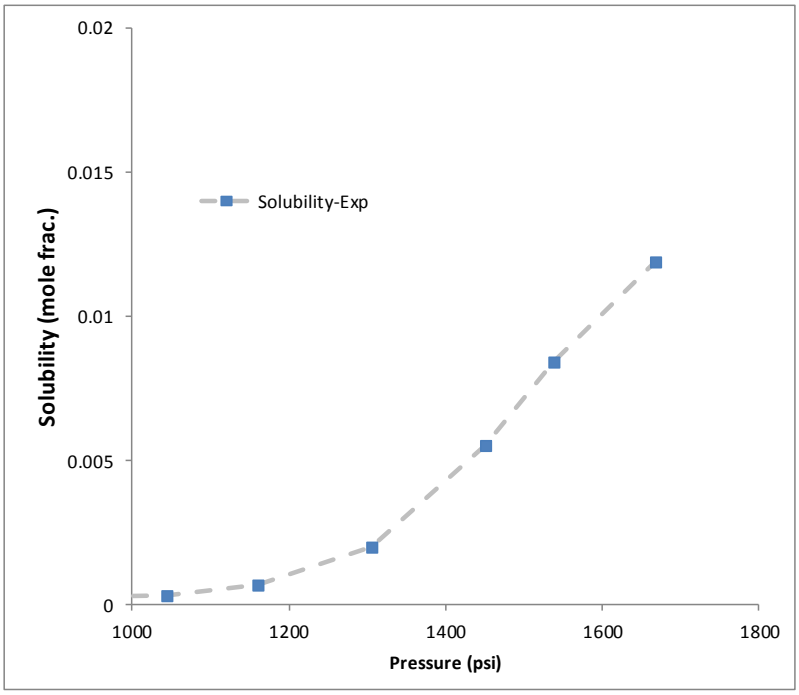

Figure 5-4: HWS-8 solubility versus pressure at a temperature of 50^{o}C.

Onset pressure of liquid formation (2900 psig)

The onset pressure, at which a new phase is formed, should be determined experimentally for the new solutes selected for our investigation. Similarly to the determination of onset pressure for the solution saturated with HWS-1, a solution made up of *HWS-8* and CO_2 was pre-equilibrated at 3000 psig and 45^{o}C. After saturating the micromodel with the prepared solution, the pressure of the micromodel was set at the lower pressure, e.g. 2900 psig, while images of a selected section of the micromodel were recorded. Figure 5-5 demonstrates the formation of the liquid phase in the micromodel when the micromodel pressure was set at 2900 psig (100 psig pressure drop).

One important aspect of the liquid phase formation is the location where HWS-8 would be accumulated in the leakage path. Figure 5-6 illustrates the full scan of micromodel highlighting the relative location of the liquid phase in the leakage path. It can be observed that the inlet of the micromodel was filled with the liquid phase whereas the porous pattern close to the outlet remained dry. This observation is in agreement with the rationale explained earlier for adding the co-solvent, i.e. liquid solute forms close to inlet

of leakage path. It should be pointed out that this experiment was carried out under static conditions when the solution was exposed to the applied leak pressure without any flow of the solution. Therefore, it would not possible to comment on the liquid phase flow properties. In the subsequent section, the flow properties of the liquid phase will be examined.

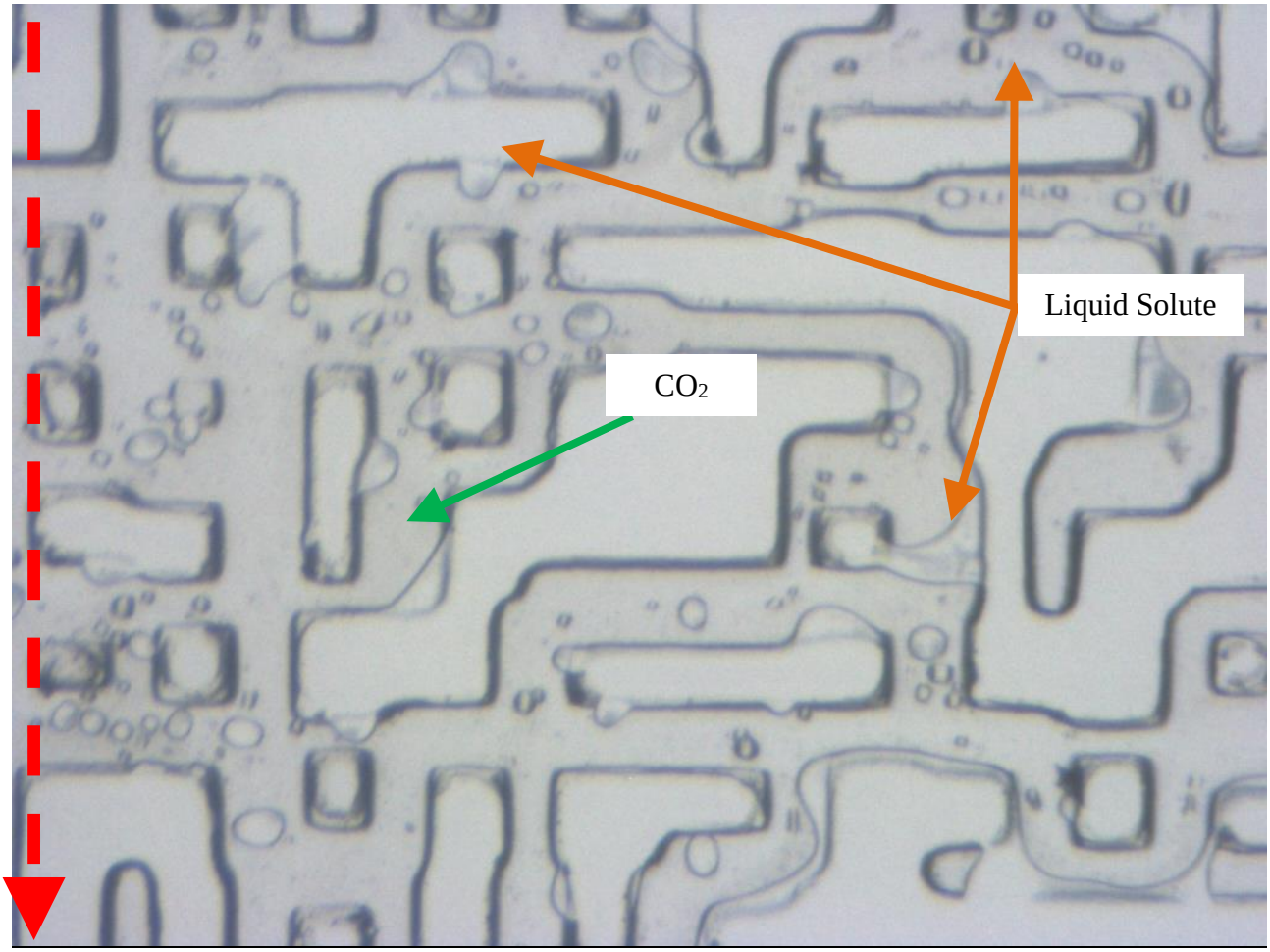

Figure 5-5: A magnified section of the micromodel demonstrating the formation of liquid solute in the inlet of the micromodel at the leak pressure of 2900 psig. CO_2 and liquid solute were mixed when the liquid phase was formed. The green arrow points to the liquid phase and the orange arrows highlight the presence of supercritical CO_2 solution mixed with the liquid.

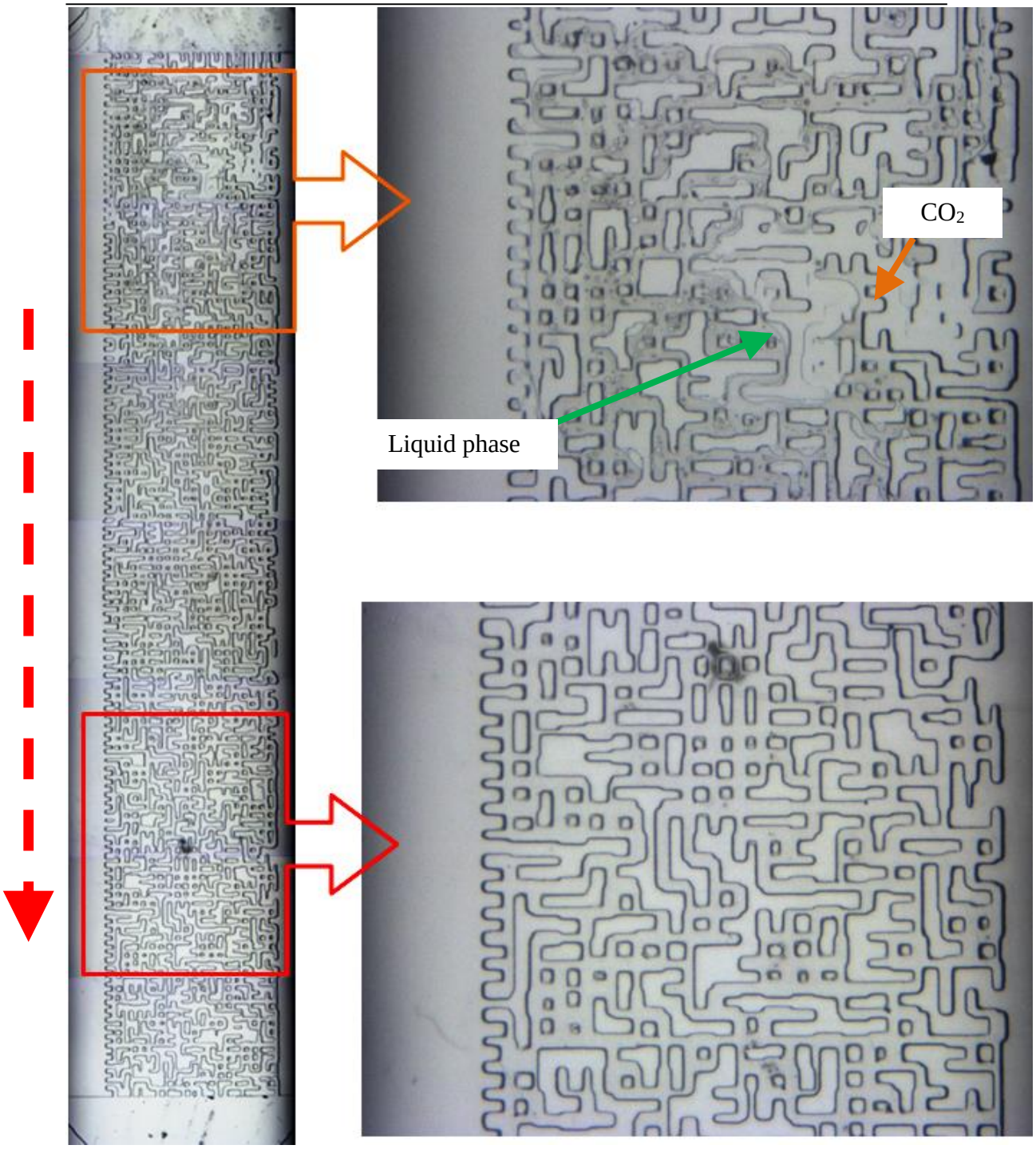

Figure 5-6: Full scan of the micromodel after exposing the solution to the leak pressure of 2900 psig. The top right image represents the inlet part occupied with the liquid phase. The bottom right image illustrates a part of micromodel close to the outlet where no liquid phase can be detected. The liquid phase was accumulated in the inlet of micromodel indicating likelihood of having liquid phase formed in the vicinity of inlet of leakage path.

Liquid formation at 2500 psig

Continuous formation of the liquid phase can result in flow of the liquid phase through the leakage path. This phenomenon has two consequences; (i) simultaneous flow of solid and liquid solutes can weaken the formation of blockage due to the lubricating effect of the liquid solute. (ii) Some of solid particles can be trapped in the liquid solute phase that reduces number of active particles for blockage. Therefore, the response of liquid solute at pressures below the 2900 psig onset pressure, under which the possibility of formation of large amount of liquid and its flow exists, should be studied. Therefore, the prepared solution at 3000 psig and 45^{o}C was exposed to a leak pressure of 2500 psig.

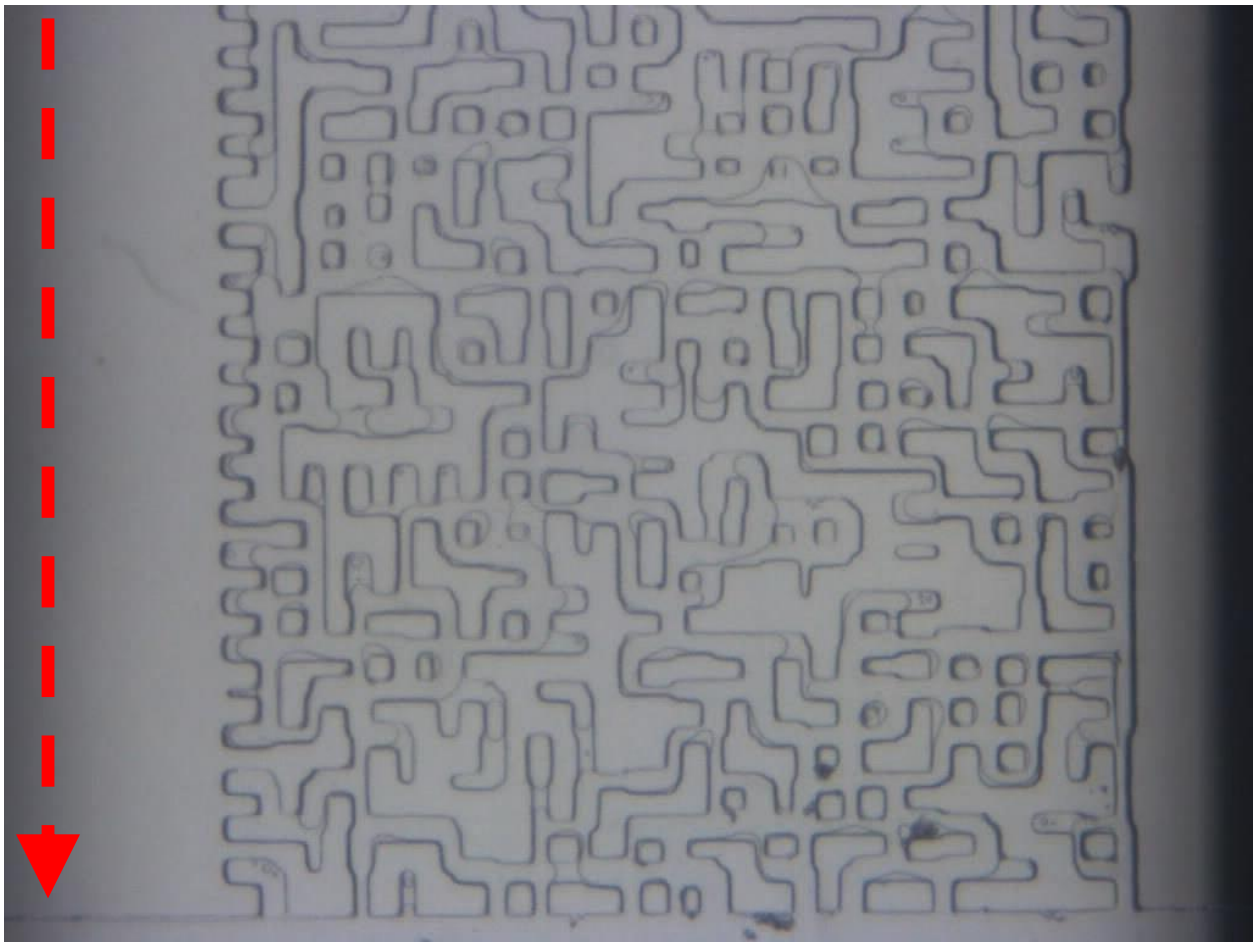

Figure 5-7: A magnified section of the micromodel demonstrating that at the lower leak pressure of 2500 psig, the liquid co-solvent started to flow towards the outlet.

Figure 5-7 demonstrates the presence of the liquid phase at the outlet of micromodel. The main cause of the appearance of the liquid phase in the outlet is the flow of HWS-8 from the inlet (location of liquid formation) towards the outlet. This two phase flow resulted in

reduction of the overall flow rate from 63 cc/hr to 51 cc/hr. In other words, the formation of liquid phase through the leakage path can decrease the leakage rate, but it should be noted that the precipitation of solid particles (not added to the solution here) is necessary for forming a blockage and stopping the CO_2 leak. The simultaneous effect of presence of these two solutes will be discussed in the next section.

Liquid formation at 2200 psig

The main purpose of this test is to analyse the flow of liquid phase at lower pressures, i.e. higher pressure drops. Compared to the previous test, the leak pressure was reduced to 2200 psig (from 2500 psig) and the continuous flow of the LPT solution (prepared at 3000 psig) was recoded. Figure 5-8 shows the flow of the newly formed liquid phase along the leakage path. The streamlines of the flow can be clearly seen.

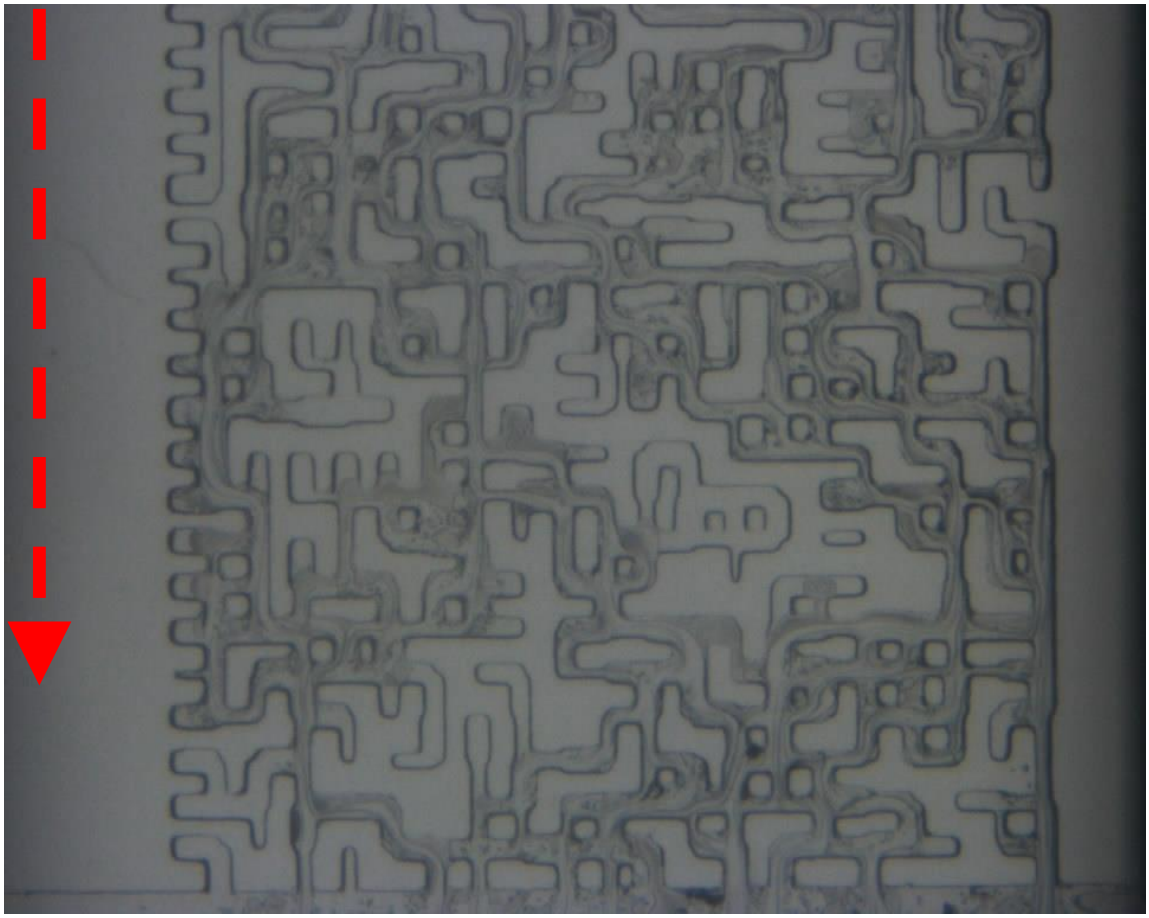

Figure 5-8: A magnified section of the micromodel demonstrating the flow of the liquid co-solvent at the leak pressure of 2200 psig.

5.4.2 HWS-1 + Co-solvent (*HWS-8*)

Leak pressure 2700 psig

In this test a leak pressure of 2700 psig was selected for visualising the impact of presence of co-solvent (HWS-8) and solid solute (HWS-1) added to the CO_2 solution. As mentioned above, at this pressure the formation of liquid phase was confirmed. Furthermore, this pressure is much higher than the 2000 psig onset pressure for formation of solid particles (HWS-1) when no liquid solute was present. It should be noted that here the aim was to investigate the simultaneous impact of presence of both the liquid and solid solutes.

Figure 5-9 illustrates two images from inlet and outlet of the micromodel. The top image shows the inlet of the micromodel, which clearly indicates the flow of liquid HWS-8 in the form of fine droplets. This simultaneous movement of two phases at 2700 psig leak pressure verifies that the presence of HWS-1 in the solution has not adversely affected by that of the liquid solute (co-solvent). It can be observed that the liquid phase has a high tendency to flow in suspension form and hence, at inlet, i.e. the liquid does not need to reach to a certain saturation to flow. In the bottom image of Figure 5-9, showing the outlet of micromodel, no clear sign of liquid phase, at least in the suspension flow for, can be seen. This can either be the liquid has become immobile on its way to the outlet or there small liquid layers formed on the surface of the porous medium.

Among all the aforementioned characteristics of the liquid phase flow, the delay in the flow of the solution can contribute to the formation of the solid phase. The presence of the liquid phase reduced the leakage rate from 47 (corresponding to the lowest rate at this leakage pressure when only solid solute was deposited) to 39 cc/hr. This reduction rate would favour formation of solid solutes. That is, previously, it was highlighted that a certain period of time (induction time), during which the solution is supersaturated, is needed before the solid solute starts to nucleate. This delay in the flow of the solution caused by the co-solvent can provide additional time to overcome the induction time. However, it seems this has not been sufficient for formation of solid solute to be seen in this test. It should be highlighted that this process cannot be fully captured in micromodel experiment due to its small length (7 cm). It should also be noted that the more measurable improvement in the performance of our LPT performance due to adding a co-solvent can be visually investigated if the leak pressure is adjusted to achieve a firm blockage due to

precipitation and accumulation of solid solutes an exercise performed with results described in the following sections.

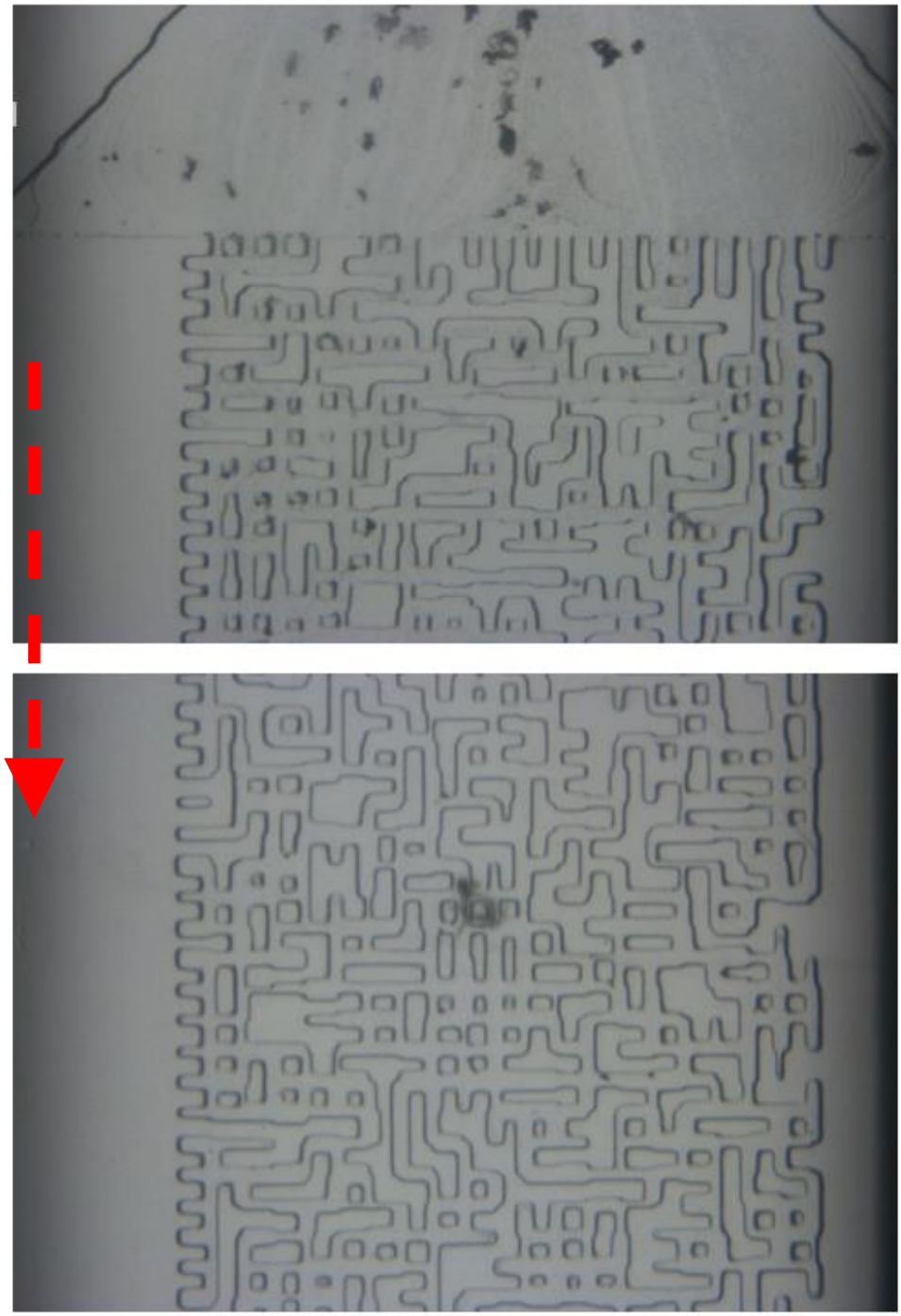

Figure 5-9: Magnified sections of the micromodel demonstrating that at the leak pressure of 2700 psig, the liquid co-solvent was formed in the inlet of the micromodel (top image), the outlet of the micromodel seems to remain dry (bottom image).

Leak pressure of 2450 psig

In this test, similar to previous tests, the solution with solutes (HWS-1 + HWS-8) and CO_2 was prepared at 45^oC and 3000 psig. After pre-equilibrating the solution, the micromodel pressure was set at 2450 psig and the solution was allowed to flow through the simulated leakage path while the inlet and outlet pressures were kept constant at 3000 and 2450 psig, respectively. This leakage pressure is also much higher than the 2000 psig, which is the onset pressure for formation of solid particles when no liquid solute was present. The camera was fixed at the outlet of the micromodel which is the most likely location to capture the formation of blockage due to solid particles precipitation and accumulation.

Figure 5-10 demonstrates an image of the micromodel outlet during this test. It is noted that, dark HWS-1 particles have been formed. In addition, the flow of liquid HWS-8 can be observed in the outlet of the micromodel, which has been highlighted with orange coloured circles in Figure 5-10. Considering visual observation of their behaviour, we have confirmed that the dark colour represents the solid particles whereas the liquid HWS-8 has appeared in form of a bright liquid. One important feature of this figure is the higher intensity of dark colour compared to previous experiments where HWS-1 was dissolved as a single solute (Figure 5-10 and Figure 3-34) and when the imposed pressure drop was much higher. This higher intensity of dark coloured particles can be interpreted as the higher amount of precipitated HWS-1 particles in the micromodel. This can be linked to considerably higher HWS-1 solubility in the presence of co-solvent (HWS-8), which resulted in higher HWS-1 concentration at the outlet of micromodel. It should also be noted that this test has clearly and very favourably demonstrated the formation of solid particles at a leakage pressure much lower than its onset pressure when liquid co-solvent was not present. In other words, the solution has responded to a leakage at much lower imposed (leakage) pressure drop.

Another important observation inferred from Figure 5-10 is the simultaneous flow of liquid and solid phase through the leakage path, which adversely affects the formation of a firm blockage. However, the leakage path was blocked at the end of the test due to precipitation of solid solute, as verified by the flow rate profile shown in Figure 5-11.

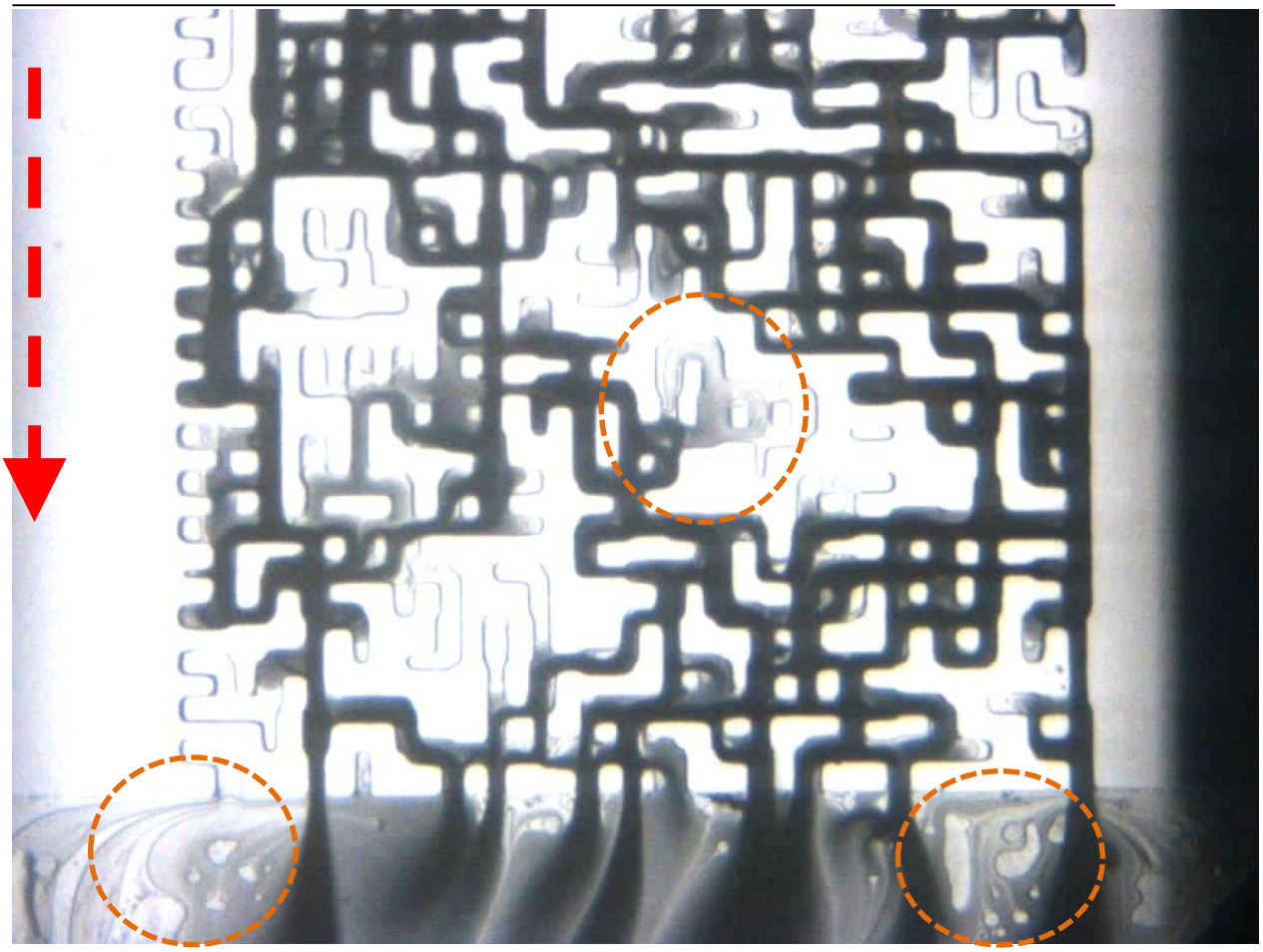

Figure 5-10: A magnified section of the micromodel demonstrating the formation of HWS-1 particles in the outlet of the micromodel at the leak pressure of 2450 psig. Compared to the single HWS-1 solution test shown previously, here higher dark intensity indicates higher amount of precipitated HWS-1 due to the presence of liquid co-solvent. The orange circles highlight the flow of the liquid solute, albeit with some solid HWS-1 content, towards the outlet. Also, some HWS-1 particles became mixed with the liquid solute, which can be seen in the orange circle in the middle of the image.

Furthermore, it should be noted that this adverse effect of flow of liquid and solid has been exaggerated in the high flow rates of the micromodel experiments. The main mechanism of precipitation in high flow rates is inertial impact, which would be significantly weakened in the presence of the two-phase flow of liquid and solid solutes. Under lower flow rate conditions, however, other precipitation mechanisms such as gravity segregation and interception can actively play a role in deposition of solid particles, which have not been captured here. In other words, we should have a more favourable performance of solid-liquid-CO_2 solution in the core experiments performed under lower rates.

Figure 5-11 shows the profile of pressure drop and leakage rate during this micromodel test. It is noted that the initial leakage rate has been around 81 cc/hr and then dropped to less than 5 cc/hr after 10 minutes of flow, i.e. 200 cc of the solution passed through the path. This is a valuable achievement and shows that adding a co-solvent (liquid solute) the response of the solution was significantly improved. That is, the solution with a single solute (HWS-1) stopped the leakage at a pressure of 1700 psig whereas a two component solutes system sealed the simulated leakage path at 2450 psig, which is 750 psig improvement in the response of the solution. Thus, appropriately selected and designed co-solvents can be effectively used to control and improve the performance of our LPT. In other words, liquid solutes can be used to adjust the pressure at which the solution is activated leading to a successful blockage. Comparing experimental information corresponding to the test with co-solvent and single-HWS-1 solute under 1300 psig pressure drop shows that the decline in the leakage rate is apparently more gradual here in the case with co-solvent despite the fact that "more" HWS-1 particles were formed in this experiment. This behaviour can be attributed to lower tendency of the formed particles to precipitate and form the blockage in the presence of liquid solute. However the difference in the pressure drop imposed across these systems (i.e. 550 versus 1300 psig) should also be considered.

In terms of blockage location, the HWS-1 particles precipitated in the converging part of the micromodel outlet port due to accumulation of solid particles. In the next section, the mechanism under which liquid solute can improve the response of the solution is further verified.

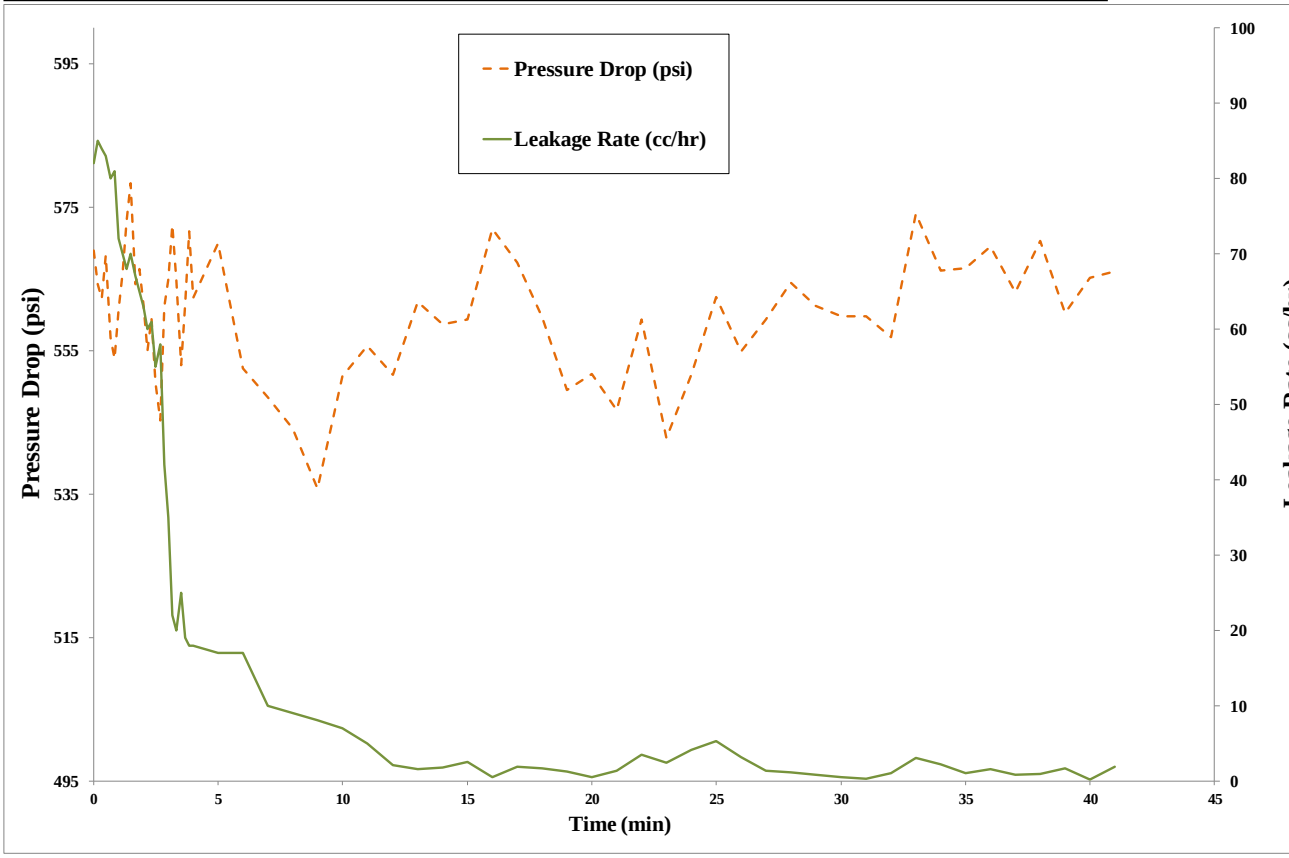

Figure 5-11: Profiles of the pressure drop and leakage rate during the test conducted at the leak pressure of 2450 psig. The decline in the leakage rate was relatively gradual with high fluctuation, which can be linked to the competition between the particle precipitation and their flow with the liquid solute. A stable blockage was eventually formed that could endure the 1300 psig applied pressure drop.

Verifying the proposed mechanism

Adding a co-solvent can result in an excess supersaturation degree in the vicinity of the leakage path where the liquid solute is formed. This excess supersaturation degree facilitates the formation of the primary solid solute. This was inferred from better response of the solution in the previous coreflood experiments however, it needs to be directly confirmed in visualisation studies. The basis of the proposed impact of liquid solute is the formation of co-solvent near the inlet of the leakage paths resulting in additional supersaturation on the solid solute in the solution. This notion was confirmed in the micromodel experiments discussed above where liquid solute was formed much sooner and lower onset pressure.

Figure 5-12 illustrates the full scan of micromodel during the test with a leakage pressure of 2450 psig. The images from inlet and outlet of the micromodel were enlarged to identify the mechanisms involved in the formation of blockage. In the enlarged image of the inlet, the formation of liquid phase can be clearly observed highlighted with green coloured circles. When looking at the full scan of the micromodel, the solid dark particles formed from the middle of the micromodel with apparent increase in dark colour intensity from top to bottom. In other words, the formation of HWS-1 at lower imposed pressure drops (550 psig) is due the deposition of the liquid co-solvent leading to a solution, which is super-saturated with the solid solute. In other words, the formation of the liquid phase in the vicinity of micromodel inlet triggered the HWS-1 nucleation as the solution flows toward the outlet, which resulted in significant improvement of the solution response to the imposed pressure drop.

It should be noted that, in the test with a leak pressure of 2700 psig the formation of the liquid phase was observed but no precipitation of solid solute was identified. Thus, by considering the results of these two tests (at 2700 psig and 2450 psig), it can be concluded that the addition of the liquid solute cannot completely eliminate the induction time (which would lead to instantaneous deposition of the solid solute for a slight super-saturation) but rather it reduces the time lag depending on the test conditions. Another feature of Figure 5-12 is that the liquid co-solvent can coexist with the solid solute at the outlet end of micromodel as highlighted by the green coloured circle. As mentioned above, this has the potential to negatively affect the blockage formation, but again we can conclude that its impact was insignificant.

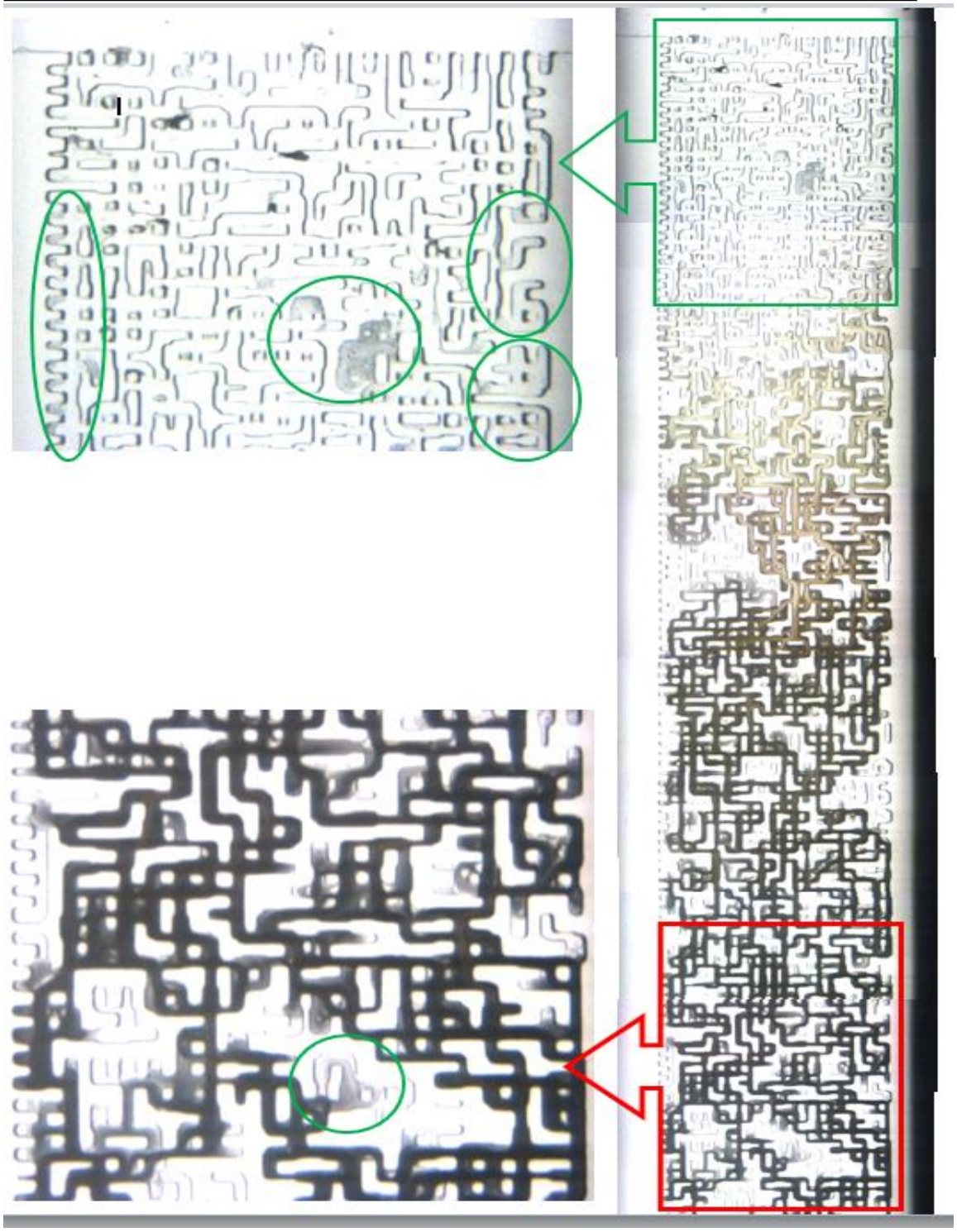

Figure 5-12: Full scan of the micromodel during the experiment at the leak pressure of 2450 psig. The top left image shows the formation of the liquid phase without any sign of having HWS-1 formation. As the solution travels towards the outlet, the HWS-1 particles appear. That is, early formation of the liquid phase has resulted in additional supersaturation improving the sensitivity of the HWS-1 to the applied pressure drop.

In summary, the visualisation experiments verified that liquid solutes have an overall positive impact on the performance of our leakage prevention technique because;

1. Formation of liquid co-solvent in the inlet of leakage paths generates additional supersaturation (driving force for nucleation of new phase) and hence HWS-1 particles can be formed at considerably lower pressure drops.
2. Liquid co-solvent formation in the vicinity of inlet of micromodel decreases the leakage rate notably, which accommodates a delay for the solution as it flows through the leakage paths. This delay can be beneficial to meet the required induction time.
3. The response of the solution to pressure drops (leakage scenarios) can be controlled based on the amount of liquid co-solvent added to the solution. This characteristic allows designing a solution for each storage conditions according to desired response to different pressure drops.

The drawbacks identified from micromodel tests are;

1. Liquid co-solvent covering the surface of the porous medium can reduce the possibility of the blockage.
2. Some of the solid particles can be present in the liquid, which decrease the amount of particles available for the blockage.

Although the significance of these effects depends on the test conditions, it seems that in these test, the overall effect is that the positive impact is more pronounced. Hence, it can be concluded that the response of the solution to pressure drops (leakage scenarios) can be controlled and adjusted based on the amount of liquid co-solvent added to the solution. This characteristic allows designing a solution for each storage conditions according to desired response to different pressure drops.

5.4.3 Response of solutions in presence of Water (Distilled Water)

Water can be present in bulk as aquifers or coexists with oil and gas in the form of irreducible water saturation. If CO_2 is injected into the aquifer, CO_2 displaces resident water in the aquifer or reservoir leaving water in the form of residual with layers covered the surface of the pores. Therefore, the impact of water should be investigated as an important parameter that can affect the behaviour of our proposed LPT. The dominant role of water in porous media is its wetting characteristic compared to CO_2. Water tends to adhere to the surface of the porous media in systems of oil/gas and water. This may

adversely affect the blockage formation and hence, the performance of the LPT. In this section, the result of our investigation on the impact of presence of water on the performance of CO_2/HWS-1 and CO_2/HWS-1+HWS-8 solutions is presented. In these tests, the solution displaces the resident water (or distilled water) at a slow rate of 0.01 cc/hr to establish irreducible water saturation (Swi) and its distribution in the micromodel. The pressure of the micromodel is then reduced, i.e. the solution is subjected to a leak.

Figure 5-13 shows full-length images of micromodel at two states; the left image shows the micromodel fully saturated with water representing an aquifer and the right hand side image represents the water distribution after CO_2 flooding. It can be seen that CO_2 has targeted most of the pore space of the micromodel leaving small water saturation behind. This water saturation distribution was established after 10 hrs of injection. In these two images, no particle formation was detected when the solutions (CO_2+HWS-1 or CO_2+HWS-1+HWS-8) came into contact with the resident water, which indicates no obvious adverse effect of water on the LPT solution. In the next section, the results of the test when the pressure of the micromodel is reduced to the desired leak pressure are presented.

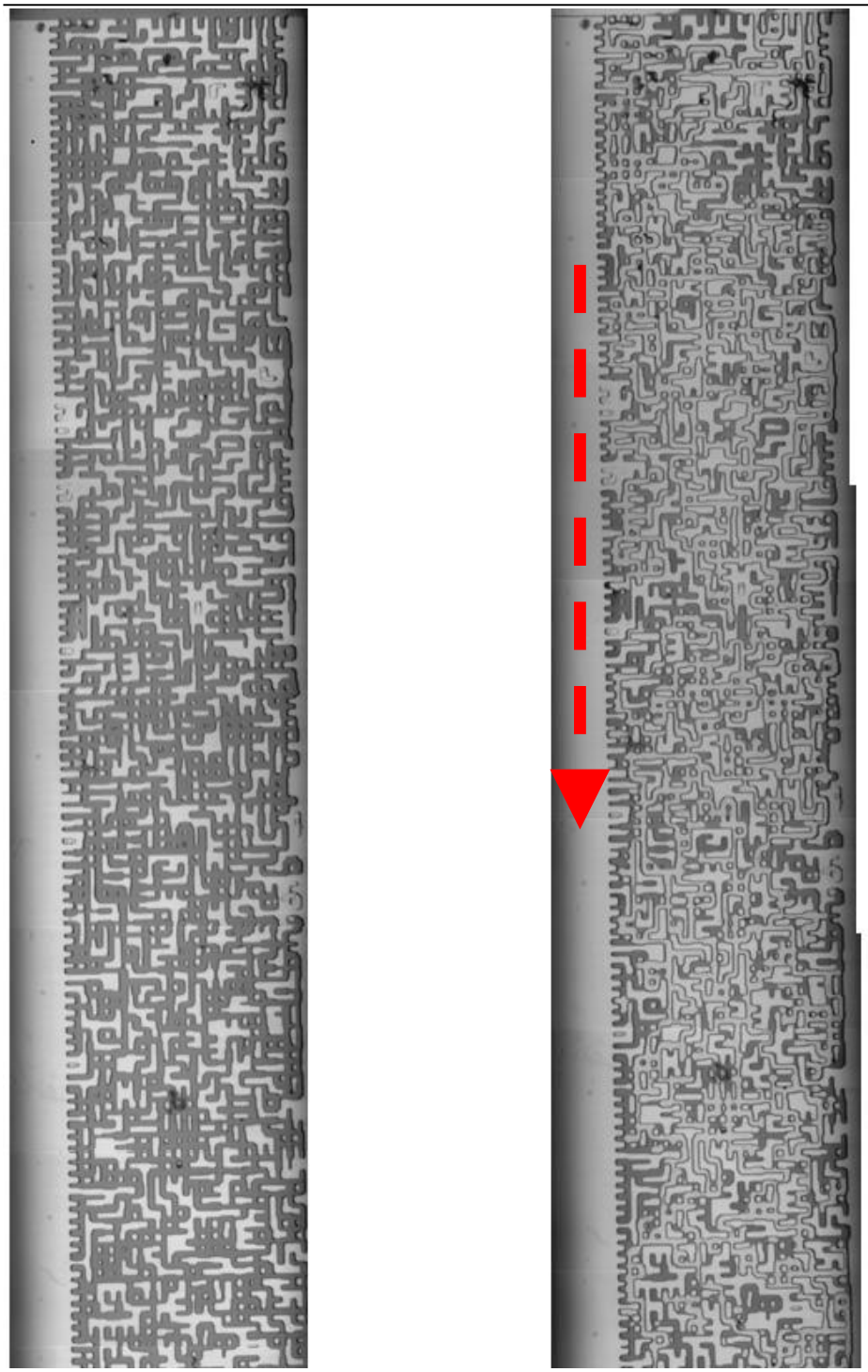

Figure 5-13: Left image illustrates a full scan of the micromodel fully saturated with distilled water. The right image demonstrates water distribution after CO_2 solution displaced the resident water. Relatively low water saturation obtained in this image indicates high displacement efficiency of the CO_2 injection. No solid particle was formed due to contact between resident water and the solution.

HWS-1; Leak pressure of 1500 psig

The CO_2 solution with HWS-1, similarly to the tests carried out in the absence of water, was prepared at 3000 psig and 45°C and used in these tests in order to be able to compare the results of these two sets experiments. In the experiments performed in dry micromodel, the pressure at which HWS-1 blocked the simulated leak was 1700 psig. The test was repeated in the presence of water but an effective blockage was not formed. Hence, the pressure was further reduced to 1500 psig. The test at 1500 psig leak pressure demonstrated successful formation of a firm blockage.

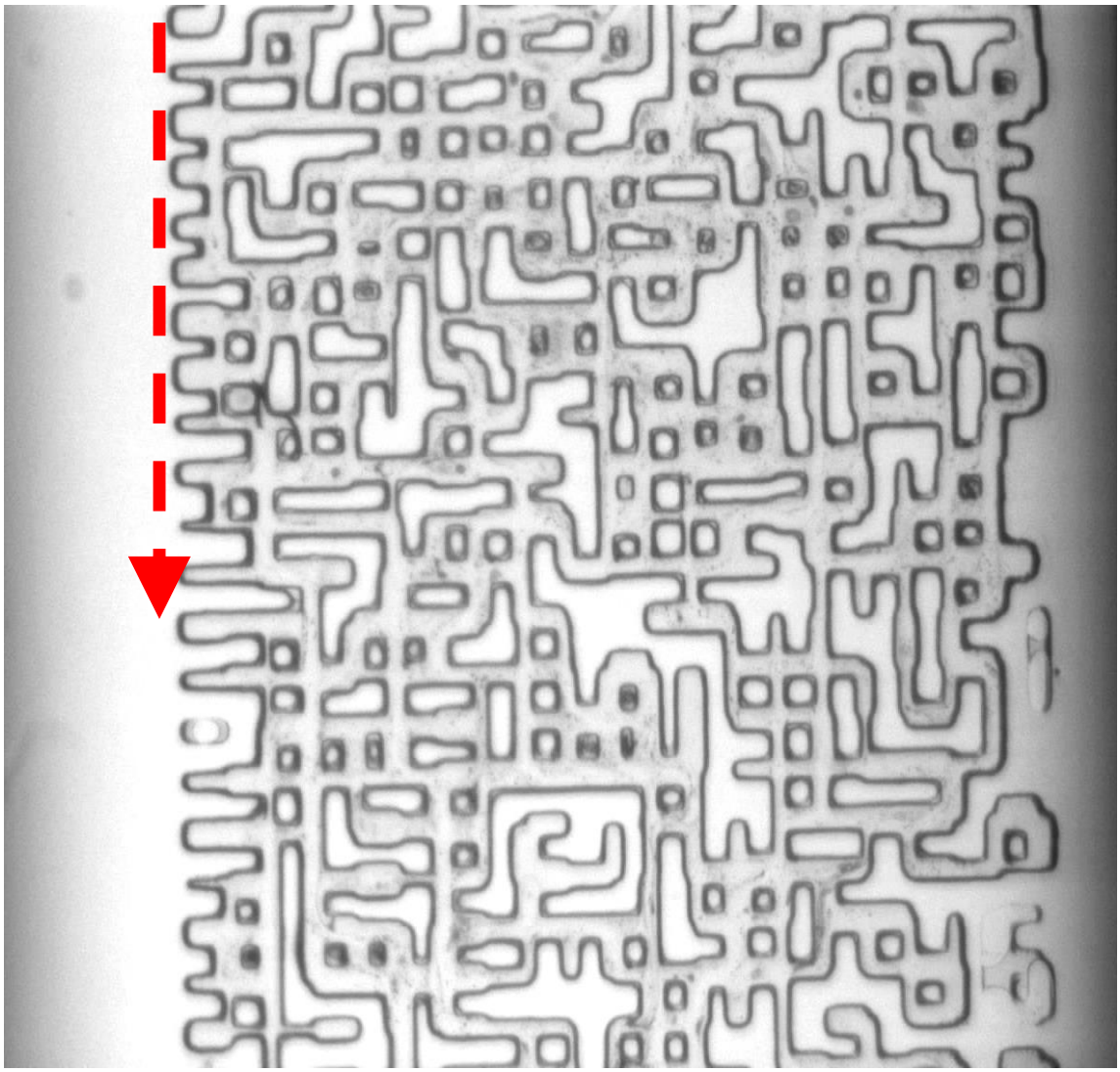

Figure 5-14: A magnified section of the micromodel demonstrating the formation of finer HWS-1 particles at the lower leak pressure of 1500 psig.

Figure 5-14 illustrates the state of micromodel at pressure of 1500 psig showing the formation of very fine HWS-1 particles. Although a higher pressure drop (1500 psig) was

needed to block the leakage path when water was present, less volume of solution passed through the micromodel before the leak was stopped. In the dry micromodel test, 120cc of solution was required to see notable reduction in the leakage rate whereas 65 cc of solution was enough for formation of blockage in the presence of water. Figure 5-15 shows the pressure drop and leakage rate profiles recorded in this experiment. Higher degree of fluctuations can be seen in this test and the leak was stopped after 10 minutes of flow.

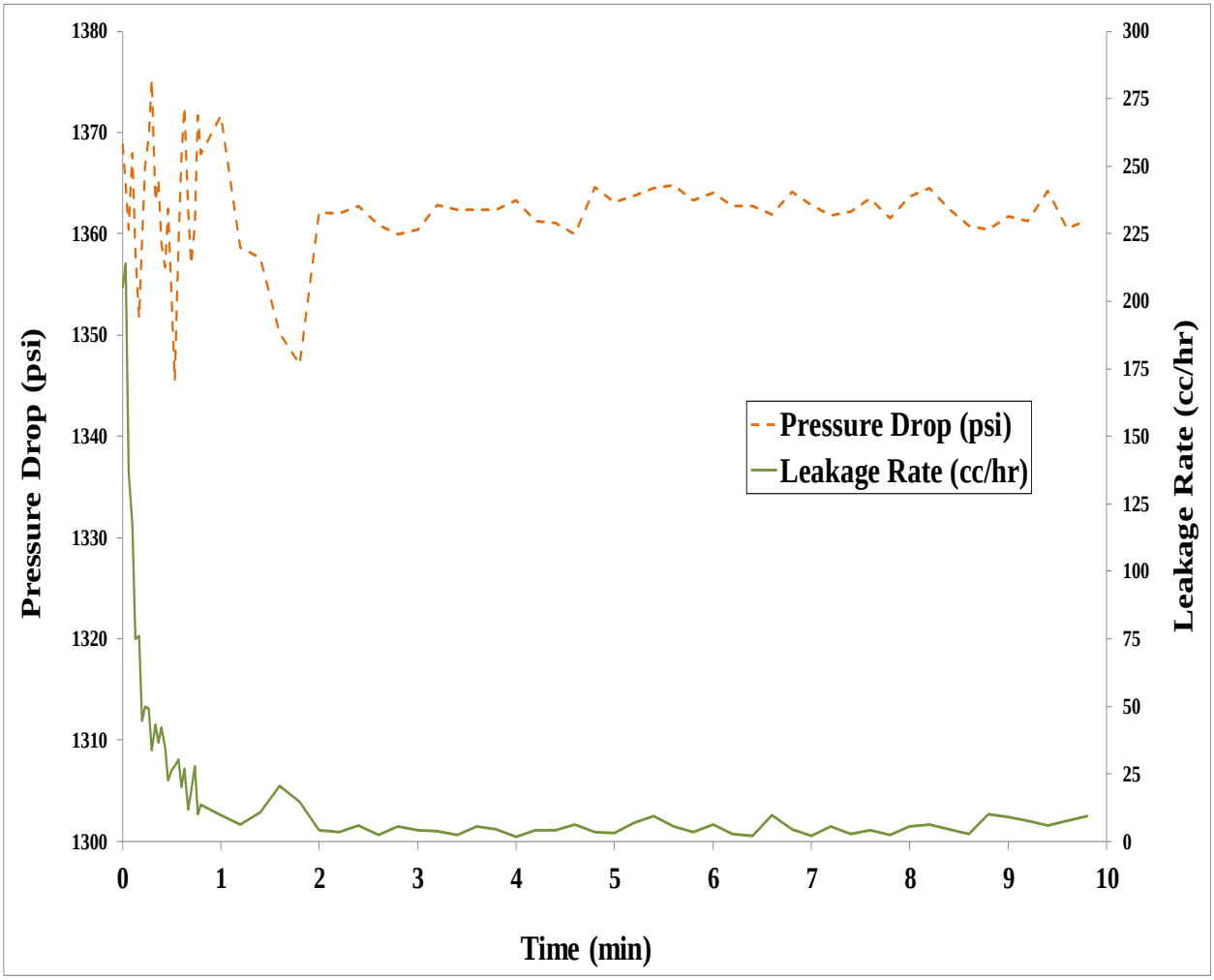

Figure 5-15: Profiles of the pressure drop and leakage rate during the test conducted at the leak pressure of 1500 psig carried out with HWS-1 as a single-component solute. The duration of test was significantly decreased and the leakage rate dropped sharply. At very low leak pressure, finer particles were formed which lead to more durable blockage.

HWS-1 + HWS-8

The behaviour of the liquid solute in the presence of water is investigated in this test. Onset pressure of liquid co-solvent (without the presence of HWS-1 solid solute) in the presence of connate water was first measured in this test. Figure 5-16 depicts the formation of a separate liquid phase at the onset pressure of 2850 psig. The liquid co-solvent appeared in two forms; bright separate phase (green circle in the right) and emulsion-type coexistence of water and HWS-8 (green circle in the left). It also caused redistribution of the resident water. Comparing the value obtained for the onset pressure in tests with that without water, it is noted that the presence of water has decreased the onset pressure of the HWS-8 formation by 50 psig.

It should be noted that these approximate onset pressures values were obtained visually, which is not very accurate. Hence, we conclude that the observed difference is not significant and within the error of measurements. In the next section, the performance of the LPT solution at the leak pressure of 2400 will be discussed.

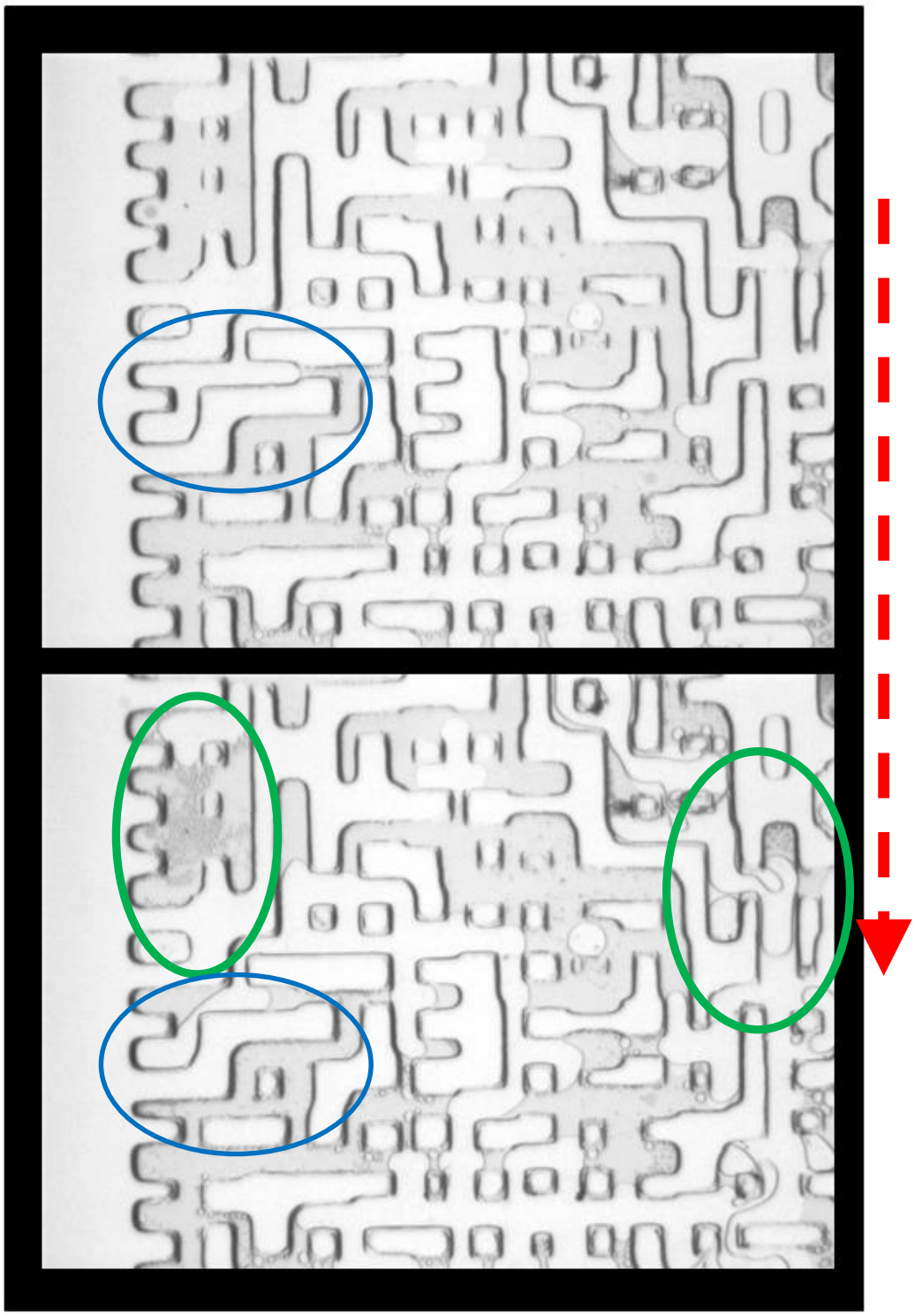

Figure 5-16: Two magnified sections of the micromodel. The top image illustrates the initial state of the micromodel prior to pressure reduction. The bottom image shows the formation of liquid HWS-8 at the leak pressure of 2850 psig. Green circles highlight the appearance of the new liquid phase. The blue circle indicates the water saturation re-distribution as a result of the liquid HWS-8 formation.

Leak pressure of 2400 psig

In this experiment, the CO_2 solution with HWS-1 + HWS-8 was prepared at 3000 psig and 45^oC. The solution in the micromodel was then subjected to a leak pressure of 2400 psig, i.e. 600 psig pressure drop was imposed on the solution. Figure 5-17 exhibits the formation of HWS-1 particles throughout the micromodel. Since the water phase was coloured with blue dye, the criterion for detecting very fine HWS-1 particles is the appearance of dark spots in the HWS-8 or CO_2 phase. The red coloured circles in Figure 5-17 highlights the pore spaces where HWS-1 particles were formed and deposited.

Figure 5-18 demonstrates that the HWS-1 particles were formed in the vicinity of micromodel outlet and a firm and stable blockage was formed. Comparison of Figure 5-18 and Figure 5-10 indicates that the behaviour of the solution is quite similar to what was observed in the test without water. In other words, the presence of the irreducible water in the dead-end pores, has not adversely affected the behaviour of the solution. The pressure drop and the leakage rate profiles of this test are presented in Figure 5-19. Comparison of these data with the corresponding data for the test without water shows minimal differences in the trends, i.e., the leakage rates are in fairly good agreement indicating that the presence of distilled water did not affect the performance of the solution.

It should be noted that the leak pressure of this test with the corresponding test without water (both lead to complete blockage) differ by 50 psig, i.e. 2450 for the without water 2400 psig for the with water experiments. Similar to what was mentioned above, this difference can be considered small and in the range of experimental error. Thus, it can be concluded that the presence of water did not have a significant adverse effect on the behaviour of the solution.

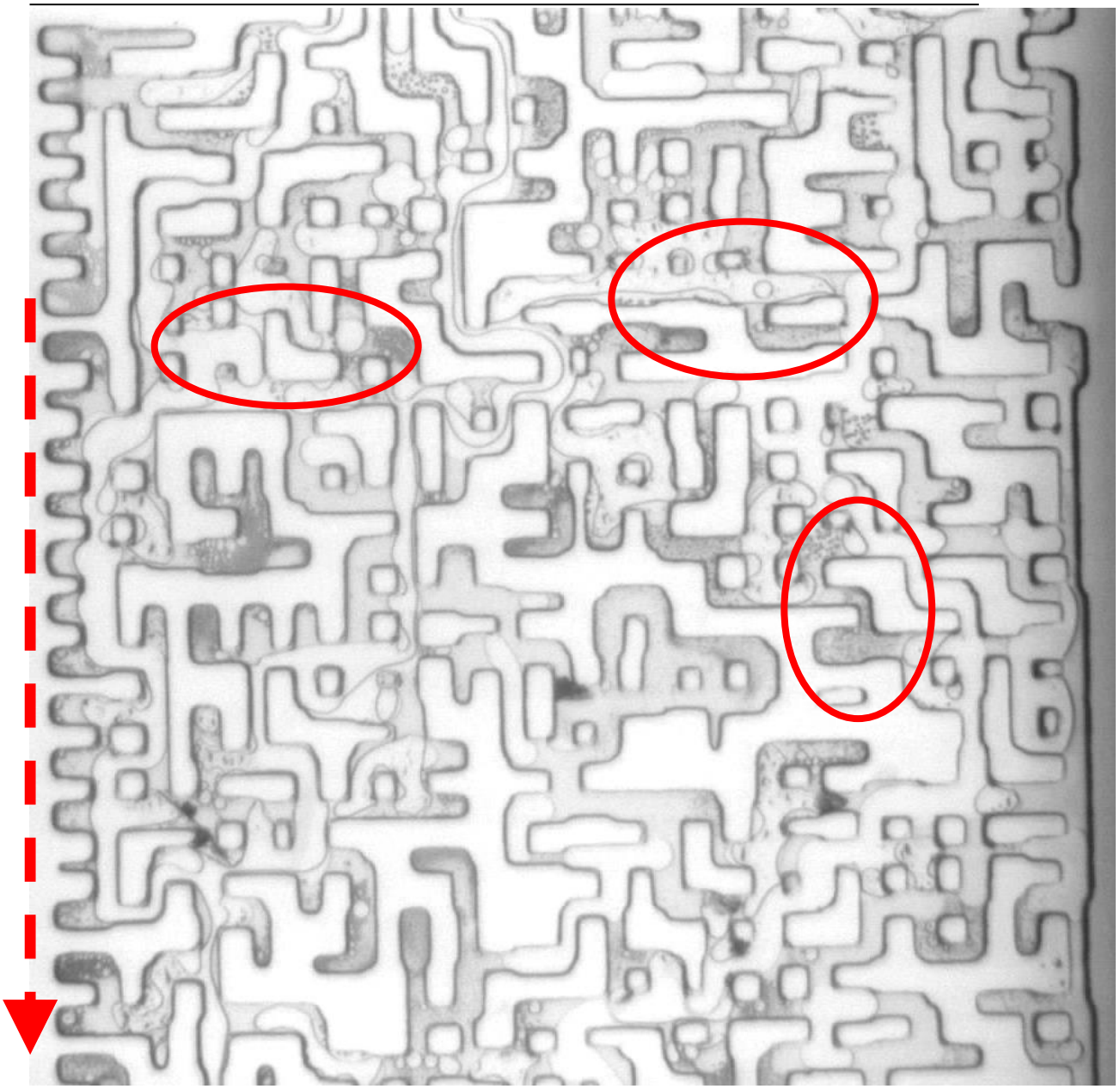

Figure 5-17: A magnified section of the micromodel demonstrating the formation of HWS-1 particles at the leak pressure of 2400 psig. Red circles indicate appearance of dark HWS-1 particles throughout the micromodel.

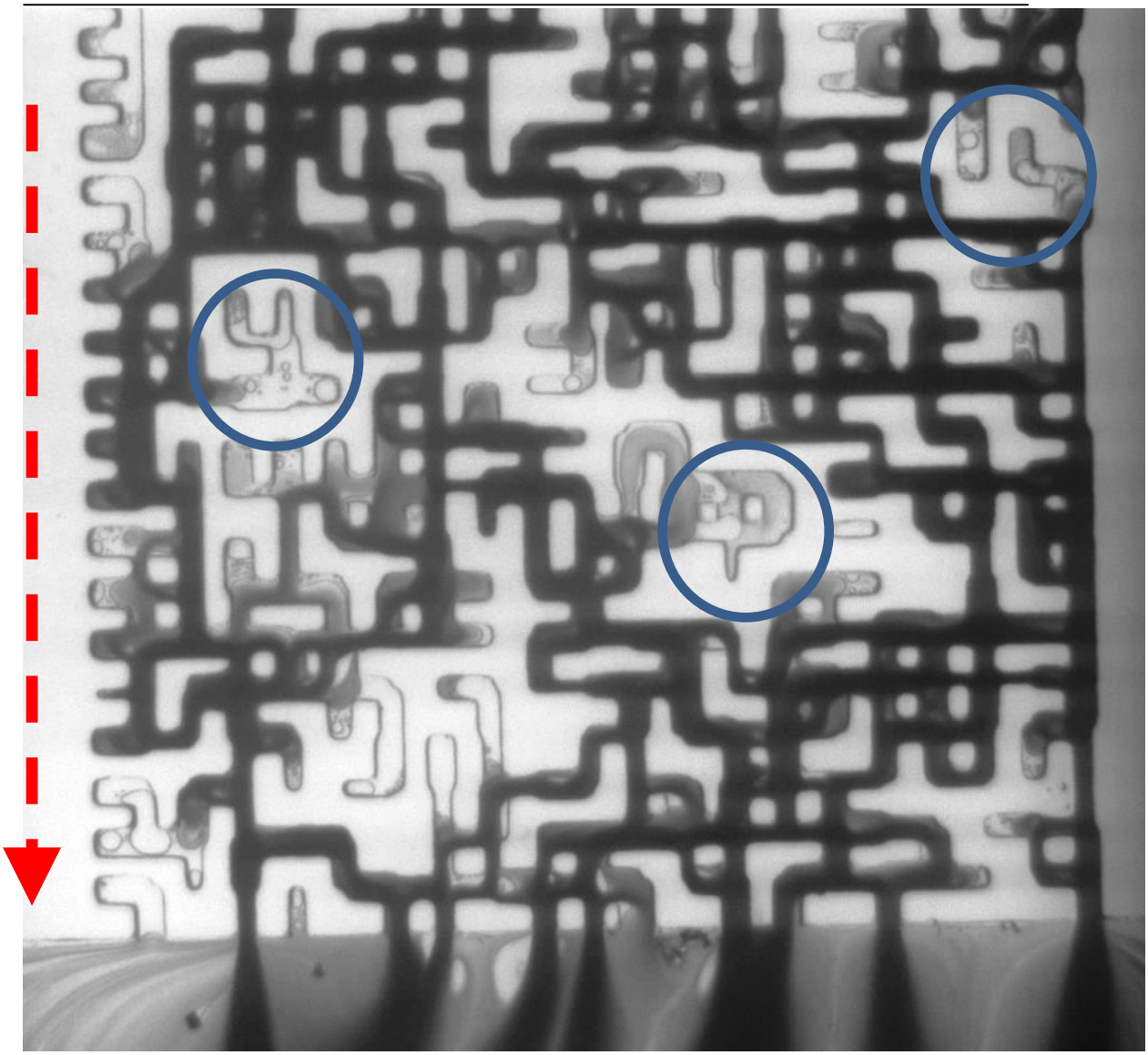

Figure 5-18: A magnified section of the micromodel demonstrating the formation of HWS-1 particles in the outlet of micromodel at the leak pressure of 2400 psig. Blue circles show the presence of water in the dead-end pores during the test. It was inferred from this test that water would not adversely affect the performance of the solution due to the presence of the liquid co-solvent.

In summary, the presence of water has adversely affected the performance of the single-solute CO_2 solution of HWS-1, i.e. 200 psig higher pressure drop was needed to have a firm blockage. However, the two component solute system (HWS-1+HWS-8) responded to the leak pressure similarly in both with and without water tests. This latter behaviour can be linked to the role of the liquid co-solvent, which can alleviate any possible adverse effect from the presence of water in the system. It should be noted that water layers on the surface of the rock might have a more pronounced effect in longer leakage paths and

at lower flow rates than what was observed here in the micromodel tests with higher flow rates. Consequently, these micromodel experiments have to be performed in reservoir rocks with more realistic flow conditions to be able to confirm the conclusions of this study.

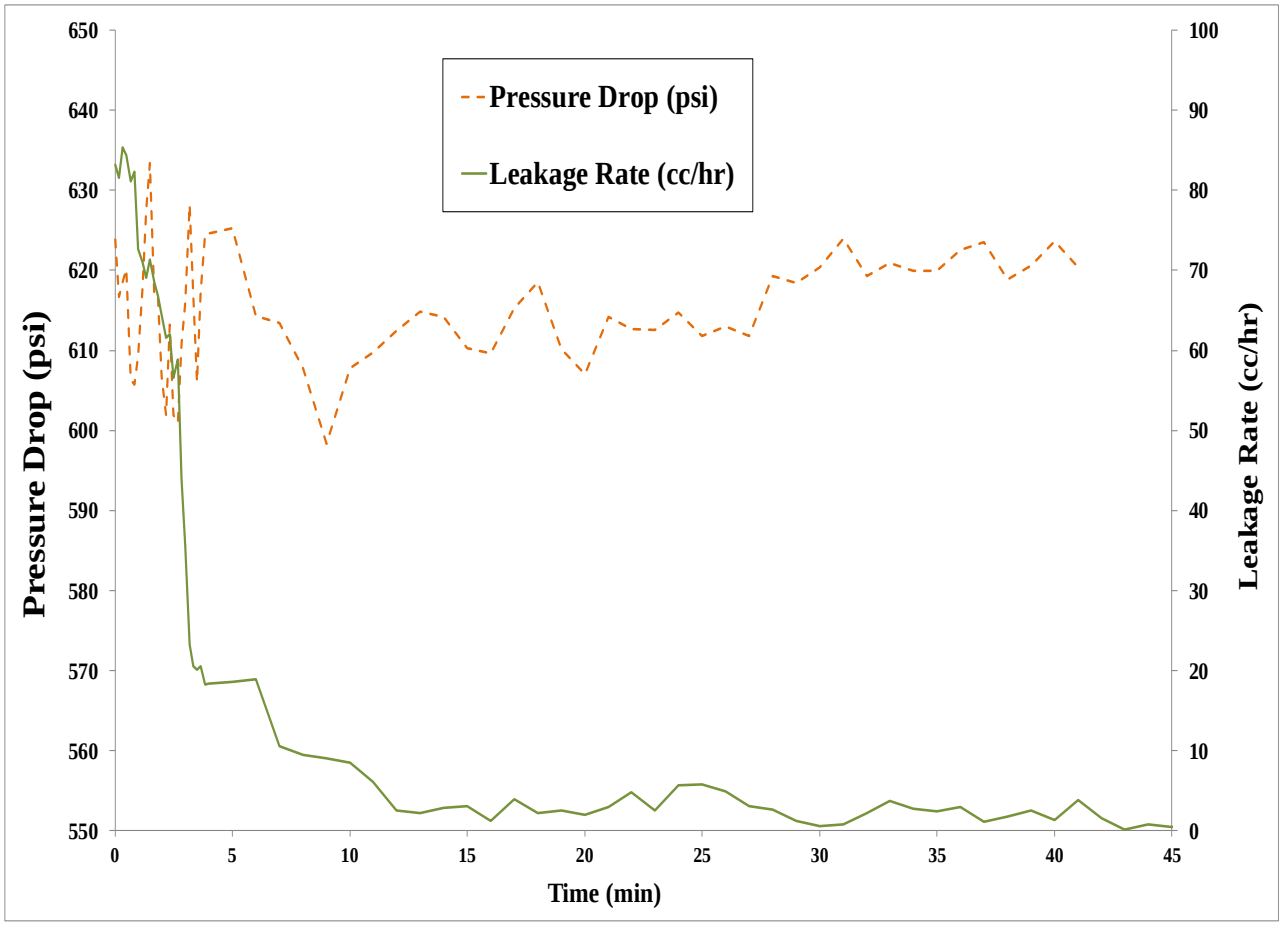

Figure 5-19: Profiles of the pressure drop and leakage rate during the test conducted at the leak pressure of 2400 psig. The trends are similar to the test performed in the dry micromodel without connate water. A stable blockage took place after 10 minutes of the flow.

5.5 Coreflood experiments

The coreflood tests in this section focused on: how can the response of the solution be controlled for various leak types?

Two tests were designed similar to previous coreflood experiments but the liquid solute was added to the injection stream to improve the response of the solution. In the first test, an amount of HWS-7 (liquid solute) was adjusted in order to inhibit the formation of liquid solute in the core. In the second test, higher amount of liquid solute was added to the solution to investigate the role of liquid solute when it is dropped out of the solution in the core.

5.5.1 First Test; partially saturated with co-solvent

In the first coreflood experiment with co-solvent, the test was carried out to investigate the role of adding small quantities of HWS-7 to the injection CO_2 to make the injecting fluid partially saturated with the liquid solute. Table 5-1 lists the basic properties of the core plugs used in the experiment. Like the previous coreflood tests, tight core plugs were put at the inlet of the composite core to impose low flow rates while high pressure gradients applied across the core. Five core plugs were used in the composite core enabling us to estimate the location of possible precipitation in the core by weighing each plug before and after the test.

Table 5-1: The basic properties of the core plugs used in 7th coreflood experiment.

Core ID	Permeability (mD)	Porosity (frac.)	Length (cm)	Diameter (cm)	Weight (gr)	Lithology
A11	0.011	0.047	5	2.57	71.947	Vuggy Dolomite
Cu3	0.023	0.08	10	2.54	121.522	Sandstone
Ch1	300	0.23	5	2.55	49.367	Chalk
C11	225	0.167	5	2.54	52.846	Sandstone
B11	225	0.167	5	2.56	51.665	Sandstone

The procedure used for preparing the solution replicates the mixing process in the previous chapter. The solution of CO_2 and HWS-7 is prepared in a 600 cc cell by placing 20 gr of liquid solute, which makes the solution under saturated (37 gr of HWS-7 is needed to have the saturated solution) and the cell is pressurized up to 3000 psig at 45^oC with pure CO_2. It should be pointed out that HWS-7 content of the CO_2 is adjusted to inhibit the formation of liquid solute in the core. The rationale for making up an undersaturated solution is to investigate the role of liquid solute amount on its performance. For the solid solute, HWS-2 powder was packed into a pipe fitted between the solution cell and the inlet of the core to provide a suitable space where the solution can pass through and become saturated with the solid solute. The pipe is filled with 15 gr of HWS-2 to ensure that sufficient solid solute is available for the flowing solution (5 gr of HWS-2 is needed to saturate 600 cc of CO_2 at test conditions). Therefore, the injection CO_2 is saturated with solid solute but undersaturated with liquid solute.

The experimental conditions are similar to the previous coreflood tests in chapter 5 (Test No. 3, No. 4, and No. 5); the inlet and the outlet pressures are kept constant at 3000 and 2750 psig, respectively. The flow rates are recorded continuously during the experiment to detect solute precipitations.

The pressure distribution in the core assembly would indicate the flow behaviour and the solubility profile of the solution as it flows through the porous medium. A reservoir simulator can be utilised to estimate the pressure profile in the core since the permeability of each plug has been determined in separate flow tests. Figure 5-20 shows the pressure distribution simulated by CMG reservoir simulator showing different pressure regimes; (i) sharp pressure drop of 150 psig in the first 5 cm of the porous medium, (ii) moderate pressure drop of 100 psig in next 10 cm of the core and (iii) the flat pressure profile in the rest of the core assembly. Generally speaking, this pressure profile is similar to previous coreflood tests.

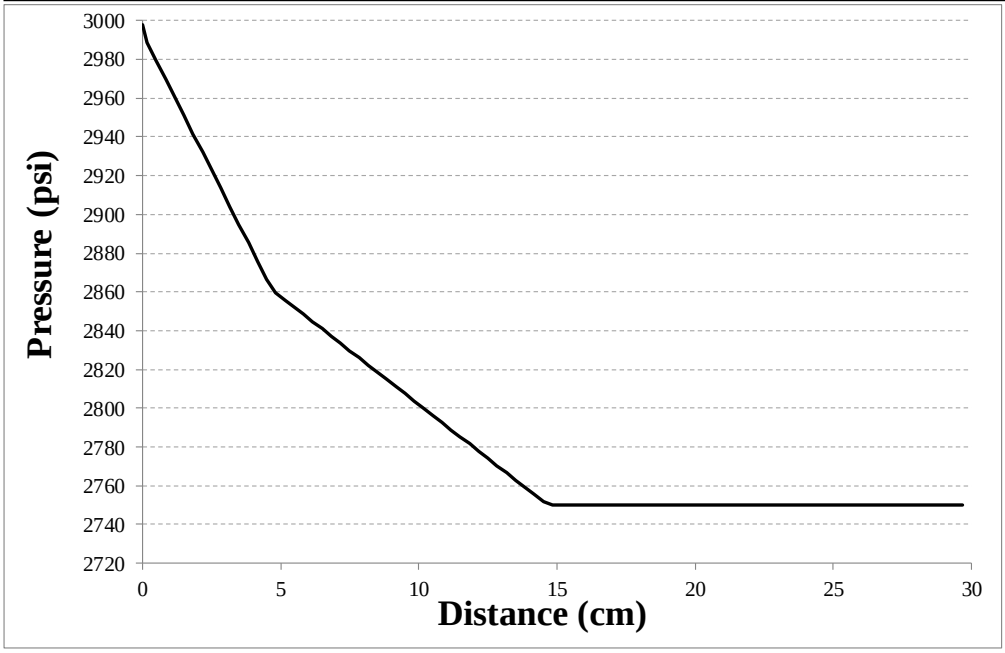

Figure 5-20: Simulated pressure distribution in seventh coreflood experiment. Three pressure regimes can be identified in the distribution.

Figure 5-21 demonstrates the injection and the production rates during this coreflood test. Generally, the rates fluctuated between 0.08 to 0.09 cc/min, which was 2 or 3 times higher than the rates that had been observed in the 3rd and 4th tests, respectively. Although the flow rates were steady for 4500 min, the precipitation continued and the flow rates started to be affected by the precipitations by showing notable drop in the flow rates. The steady flow part of the test is similar to previous tests where the constant flow rate was interpreted as the continuous precipitation in the core assembly. However, the rates dropped relatively sharply and full blockage formed against the physically simulated leakage path indicating formation of a blockage somewhere in the system. Therefore, given the rate of flow in this test was 2 or 3 times higher than the previous test, it can be concluded that adding liquid solute to the injection CO_2 can improve the response of the LPT.

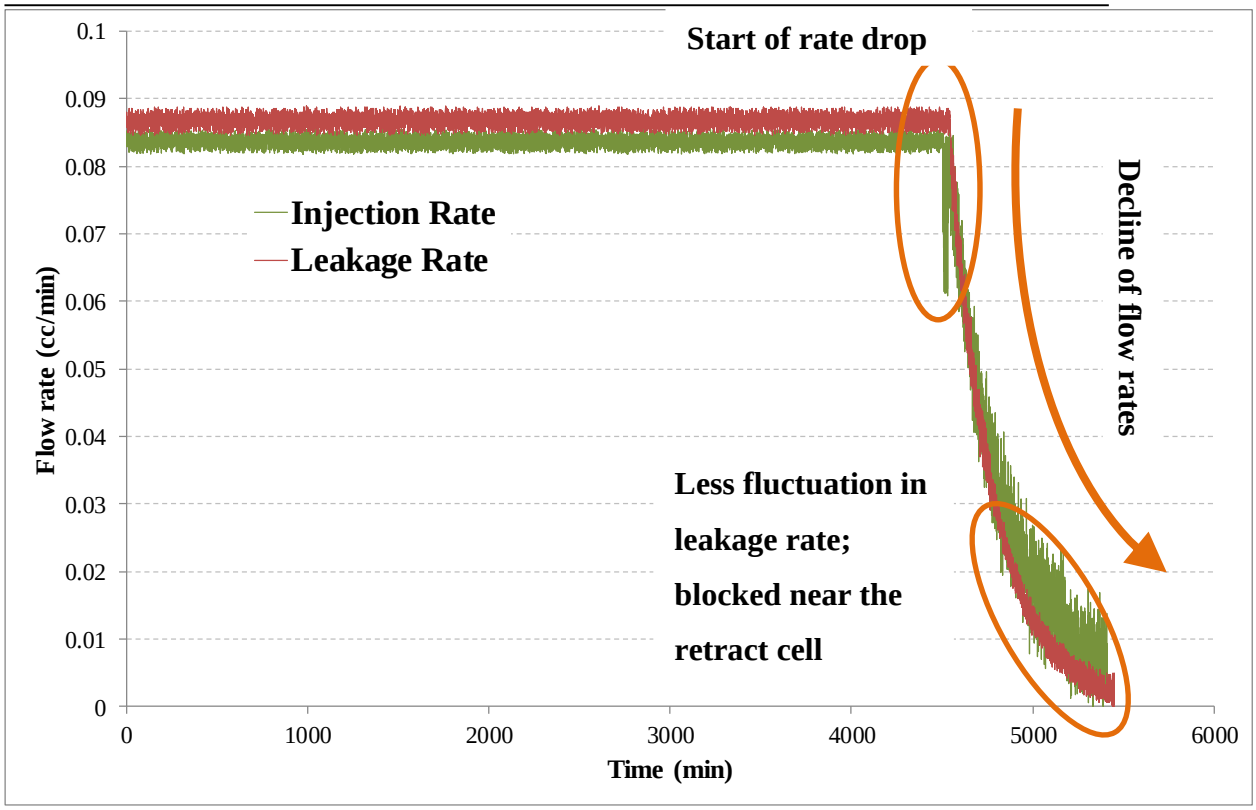

Figure 5-21: The profile of the leakage and injection rates during the coreflood experiment. The rates started to drop after 4500 mins. High degree of fluctuation in the injection rate indicates the competition between the particles to be precipitated.

One important feature of Figure 5-21 is the apparent difference in the fluctuation of the injection and the production rates at the late stages of the experiment, which is another indication of having a blockage very close to the production face. The information from pressure transducers can be used detect the location of blockage more precisely. Figure 5-22 illustrates schematically the recorded pressures at different transducers used in the experimental setup which can be used to identify the location of the pressure discontinuity as the main sign of the blockage. As it has been highlighted in Figure 5-22, the blockage formed in the line between the outlet of the core and the retract cell.

The rationale for performing the experiments has been explained thoroughly in chapter 5, which is aimed at physically simulating the conditions of a storage reservoir in the injection cell and conditions of a leak in the retract cell and a porous medium representing the connection between these conditions. Unless the precipitation takes place near the injection face, which has the pressure level close to the storage conditions, the rest of the flow path can be considered as the simulated leakage path including the lines at the outlet

part of the setup. Therefore, it can be concluded that if the core could be longer, then the precipitation would occur in the core instead of the lines. It should be noted that no porous medium exists in the lines to capture the formed particles and hence the process of precipitation would be prolonged due to the weak tendency of the particles to be precipitated in the pipes. Finally, the precipitation cannot be characterised quantitatively since the blockage body could not be recovered.

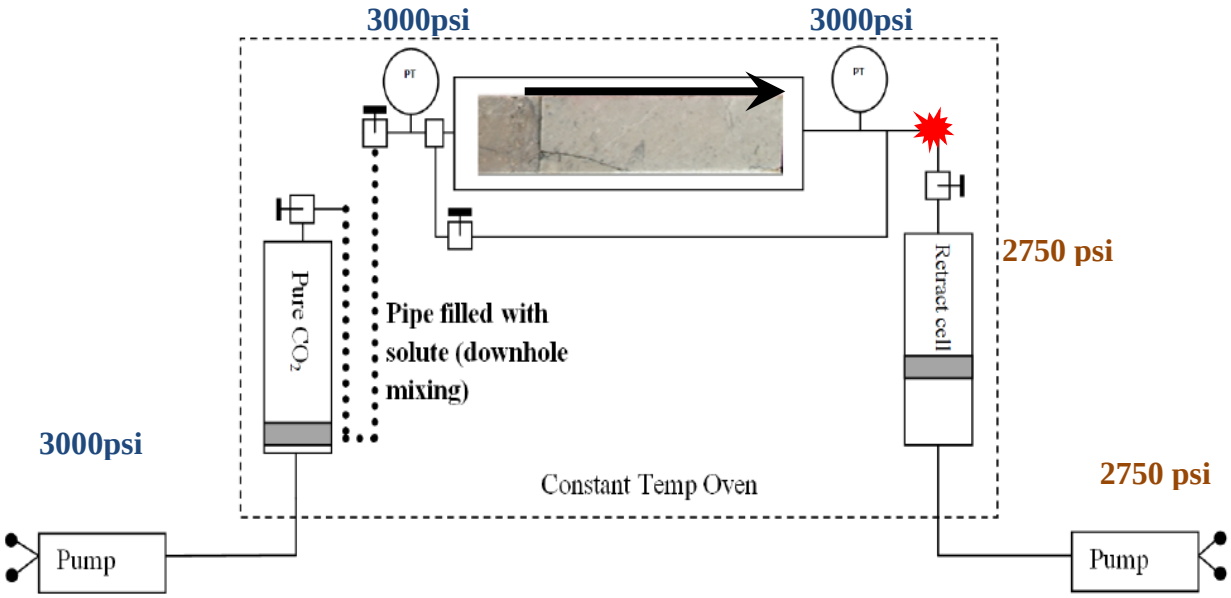

Figure 5-22: The recorded pressures at different locations of the coreflood setup to detect the location of pressure discontinuity and formed blockage. The red asterisk body represents the blockage formed in lines. The black arrow shows the flow direction.

To summarize the main findings of this coreflood experiment;

1. HWS-7 was added to CO_2 but it was presumed that no liquid formed in the core.
2. The firm blockage was formed against the simulated leakage, which stopped the escape of CO_2 from the leak.
3. The blockage happened despite the flow rate being higher than the previous tests, which means adding the liquid solute (co-solvent)increased the sensitivity of the leak prevention solution to the pressure drop, although the content of liquid solute was adjusted to inhibit the formation of liquid phase in the system.
4. It can be concluded that adding different amounts of liquid solute results in better control of the response of the solution to a leakage. In the next experiment, a

higher amount of liquid solute will be added to the solvent to investigate the role of liquid solute content.

5.5.2 Second Test; higher content of secondary solute

After successfully blocking the leak in previous experiment, it is needed to test the impact of the amount of liquid solute to investigate the role of HWS-7 in controlling the response of the proposed leakage prevention technique. In this experiment, the objective is to adjust the liquid solute content in order to have it dropped out in the core. The inlet and outlet conditions were identical to those in the last coreflood test. Therefore, the system of three phase flow (gaseous like CO_2, liquid solute, and solid solute) is to form in the coreflood experiment.

Supercritical CO_2 and liquid solute are mixed to prepare a saturated solution, which drops its liquid at 2750 psig (the outlet conditions). 40 gr of HWS-7 is placed in the solution cell to fulfil the desired conditions in the coreflood test. Table 5-2 lists the basic properties of the core plugs used in this test. Six core plugs were put together to form a composite core, which can be subsequently taken apart to identify the location of possible precipitations by weighing each individual core plug. Like the previous tests, two tight core plugs were placed in the inlet of the composite core to impose low flow rates while the pressure is dropped 250 psig across the core.

Table 5-2: The basic properties of the core plugs used in the eighth coreflood test.

Core ID	Permeability (mD)	Porosity (frac.)	Length (cm)	Diameter (cm)	Weight (gr)	Lithology
Cu11	0.023	0.08	5	2.54	60.695	Sandstone
Cu12	0.023	0.08	5	2.54	61.138	Sandstone
Sc1	5.014	0.098	5	2.55	55.949	Limestone
Le1	30.1	0.11	5	2.55	55.967	Limestone
C11	225	0.167	5	2.54	52.846	Sandstone
B11	225	0.167	5	2.56	51.665	Sandstone

Figure 5-23 shows the pressure distribution produced by CMG reservoir simulator simulating the pressure behaviour and supersaturation degrees along the core assembly.

As can be seen, the pressure drop of 250 psig occurs in first two plugs and the rest of the porous medium maintains the supersaturation imposed in the preceding core plugs, which would accommodate suitable environment for the precipitation to be formed.

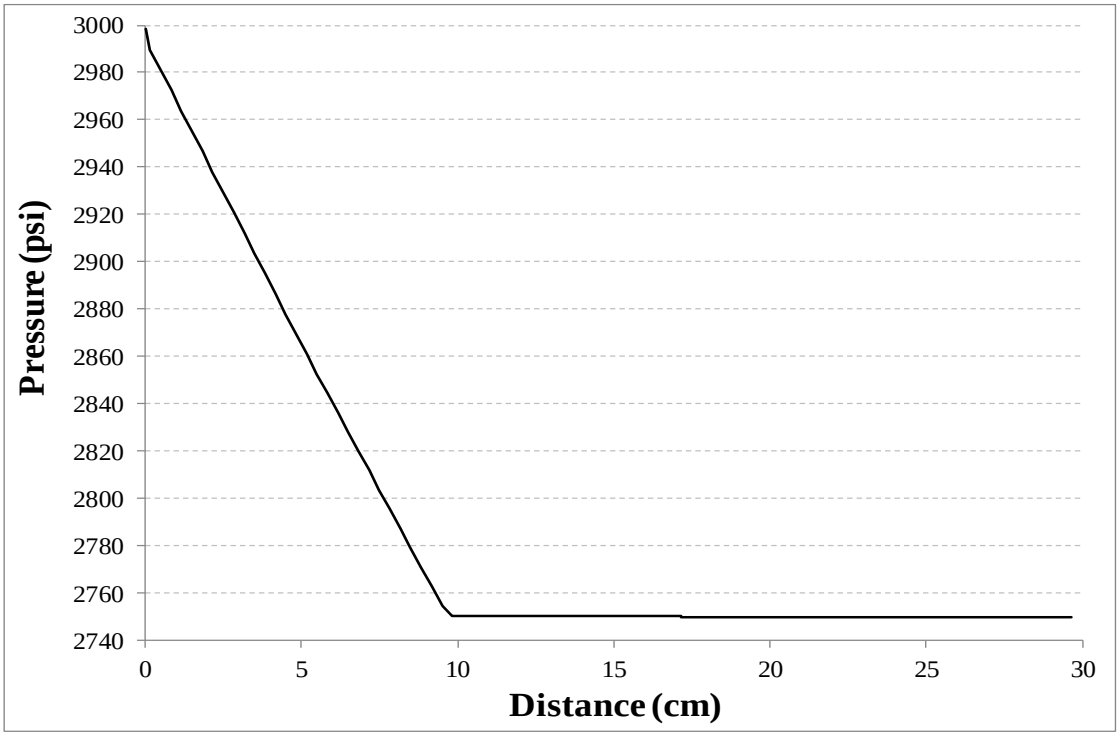

Figure 5-23: The pressure distribution along the composite core in the coreflood experiment.

Figure 5-24 demonstrates the injection rate and leak rate during the coreflood experiment. Several features can be identified from the rates to characterise the behaviour of the solution;

1. At a very early stage, steady flow rate of 0.17cc/min was established at the inlet of the core, which is almost 6 times higher than the tests with the pure CO_2 and single solid solute.
2. After that, the flow rates started to decline very gently, which is a clear indication of the formation of liquid solute throughout the $\frac{2}{3}$ of downstream of the composite core where the pressure distribution is flat.
3. After 500 cc of the solution had passed through the core, high degree of fluctuations was identified at inlet and outlet of the core. This fluctuating trend continued with notable decline in the flow rates of the injection and leak sides. Like the previous coreflood test, less fluctuation in the leak rate indicates the

formation of blockage very close to outlet face. However, further evidence will be put forward to detect the location of precipitation.

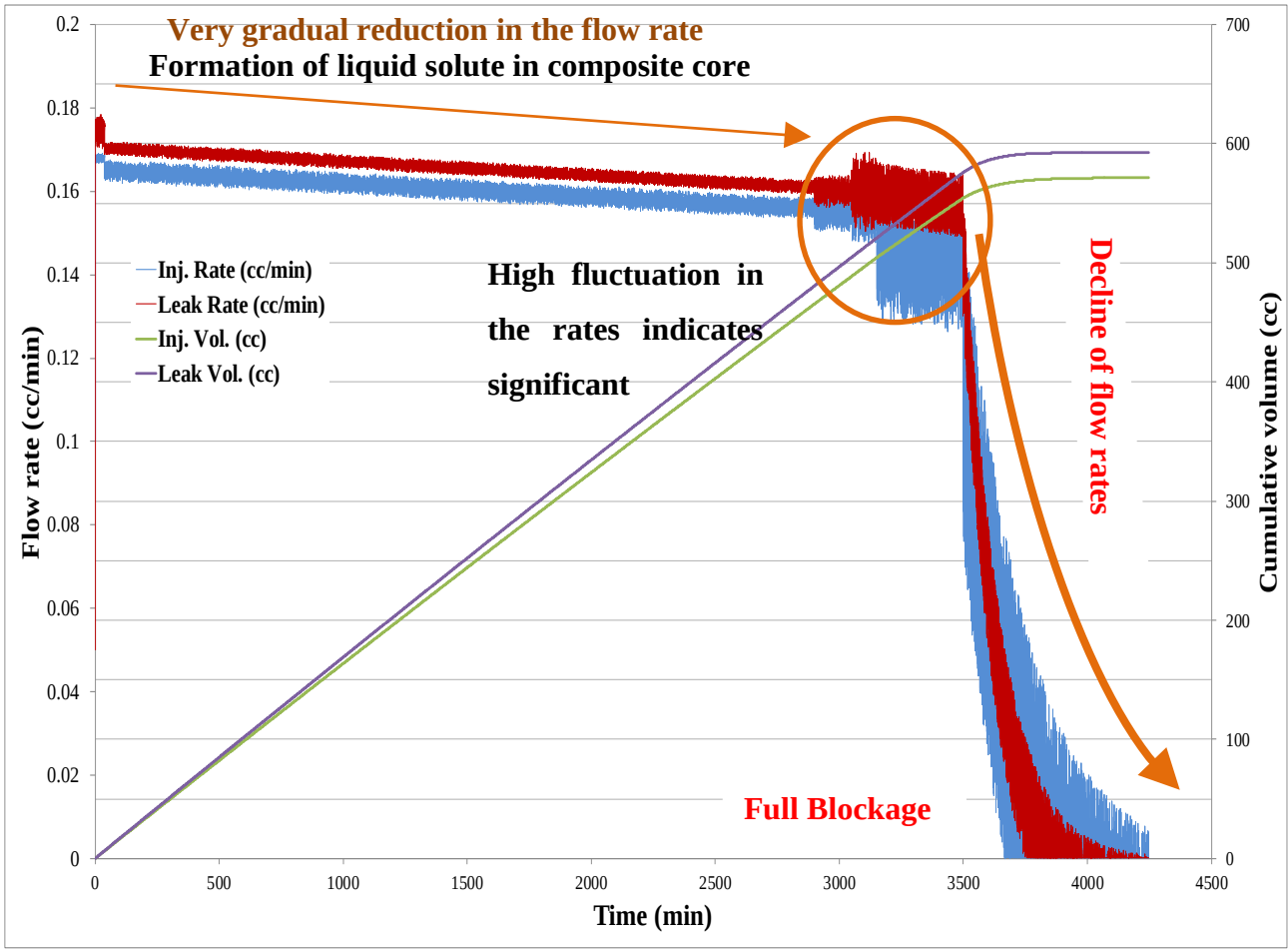

Figure 5-24: The profile of injection and leak flow rates during the coreflood experiment. After almost 600 cc passed through the core, the rates stopped and the blockage formed. The notes on the figure expalins different flow regimes during the test.

After identifying the formation of a blockage, the blockage should be characterised in terms of location and amount of precipitants. The location of blockage can be easily identified by detecting the pressure discontinuity at the end of experiment. Figure 5-25 illustrates schematically the pressures at different transducers in the experimental setup, which clearly indicates the occurrence of the precipitation in the core rather than the lines.

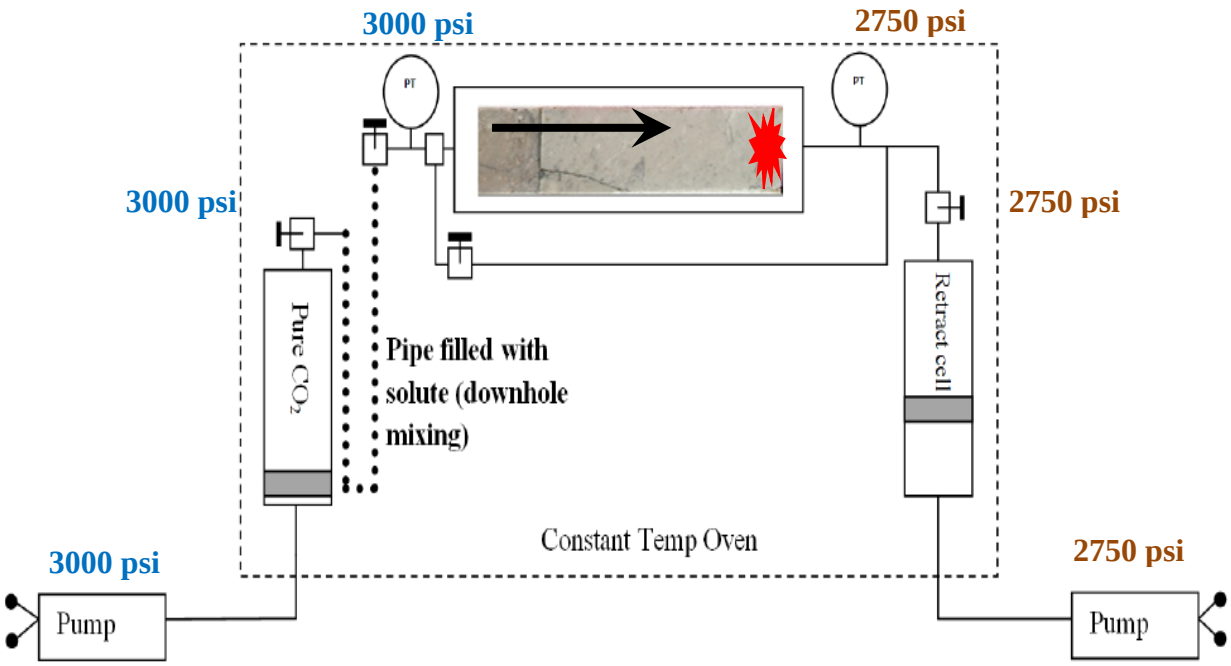

Figure 5-25: The recorded pressures at different locations of the coreflood setup to detect the location of pressure discontinuity and formed blockage at the end of the experiment. The red asterisk body represents the blockage formed in lines. The black arrow shows the flow direction

Another source for characterising the precipitation is the analysis of weight of the each core plug. Table 5-3 presents the weight of the core plugs before and after the coreflood experiment. The weights of the first two plugs are intact indicating no precipitation however; the changes take place from the third core plug. The results of weight change demonstrates the presence of liquid solute in the third core plug (Sc1) and its quantity was 0.551 gr. The presence of liquid solute is highlighted in Figure 5-26-A. By comparing the change in the weight of fourth (Le1) and fifth (C11) plugs, it can be inferred that clear reduction in the formation of liquid solute happened in the subsequent core plugs. Therefore, the changes of plug weights in Le1 and C11 can be attributed to two possible mechanisms; either the solution did not drop out all the liquid solutes in the third plug and the rest of liquid solutes formed in the other plugs, or the formed liquid solutes in third plug became mobile and moved to the adjacent plugs (although it is possible to have both mechanisms active concurrently).

Having identified the behaviour of the liquid solute in three core plugs (Sc1, Le1, and C11), the changes in the last core plug is the highest, which indicates the precipitation of

solid solute. The amount of precipitation (1.233 gr) is in agreement with the weight of the blockage body measured in the previous coreflood tests, which demonstrated high degree of consistency between the coreflood experiments. Figure 5-26 shows the state of core plugs at the end of the experiment, which verifies the occurrence of the precipitation in the last core plug (Figure 5-26-C). In addition, the presence of liquid solute can be seen in Figure 5-26-A (red circle).

Table 5-3: The changes in the core plugs weight due to solute precipitation.

Core ID	Before test	After test	Change
Cu11	60.695	60.691	-0.004
Cu12	61.138	61.135	-0.003
Sc1	55.949	56.5	0.551
Le1	55.967	56.144	0.177
C11	52.846	52.869	0.023
B11	51.665	52.898	1.233

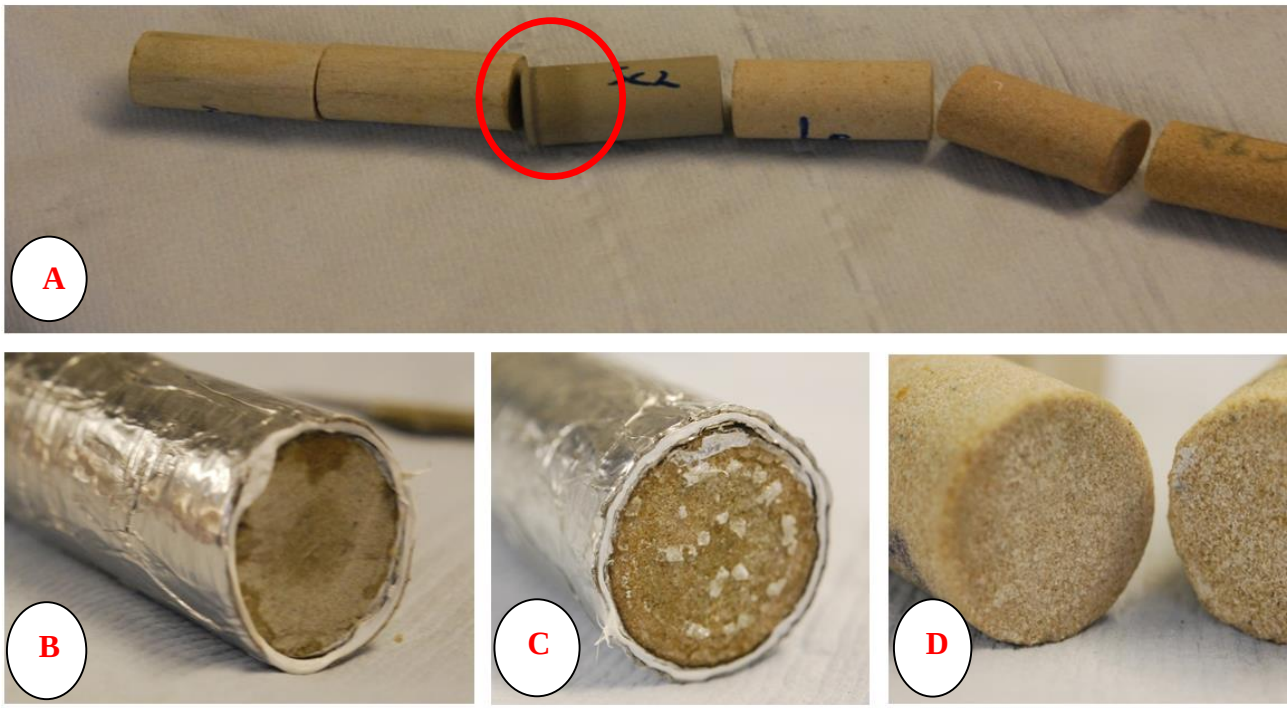

Figure 5-26: The state of the core plugs after the coreflodd experiment; (A) showing all core plugs; the red circle highlights the existence of liquid solute in the tird plug. (B) showing the inlet of the composite core with no precipitation. (C) the outlet of the of the composite core, showing the precipitants at the core end face. (D) the interface between C11 and B11 core plugs, which indicates the presence of small amount of solute.

In summary;

1. Mixing higher amount of HWS-7 with CO_2 results in having more responsive solution to the imposed pressure drop since the flow rate was 5-6 times higher than previous coreflood tests with pure CO_2.
2. The liquid solute was formed as soon as the pressure dropped below 2760 psig. The amount of liquid solute in the subsequent plugs reduced considerably verifying the immediate formation of liquid solute in the third core plug.
3. 1.233 gr of HWS-2 was precipitated in the last core plug to build up the blockage body and stop the leakage path.

5.6 Discussion and Conclusions

The viability of adding a secondary liquid solute to improve the efficiency of our proposed leak prevention method was evaluated through sandpack, micromodel visualisation and coreflood experiments. It is believed that liquid solutes have a significantly lower nucleation time lag and hence, can improve the solute-loaded solution's response time by (i) increasing the solubility of the primary (solid) solute, which would results in higher supersaturation degree when the secondary liquid solute is deposited quickly and under a small imposed pressure drop and (ii) creating additional flow barrier, higher local pressure drop, for the leaking CO_2 as a result of a reduction in CO_2 relative permeability. It should be noted that the new liquid phase would not block the leakage path but would facilitate the process of sealing the leak. The results demonstrated that addition of HWS-7, which when deposited at the test temperature of 45 ^oC is in liquid form, into a new solution consisting of supercritical CO_2, HWS-2, and this secondary solute improved the response of the solution considerably. It reduced the required pressure drop for a durable blockage from 750 psig to 500 psig, which is 250 psi less than that required when CO_2 solution was only saturated with HWS-2. However, these results should be verified for other combinations of primary solid and secondary liquid solutes by performing core flood experiments.

In the visualisation experiments, another co-solvent (secondary liquid solute) was used and HWS-1 was added to supercritical CO_2 as the primary solid solutes. The direct visualisations revealed how liquid solute would improve the response of our proposed leakage prevention technique and verified the hypothetical idea behind addition of the co-

solvent. The liquid solute would form much quicker than solid solutes, which would in turn bring about notably higher supersaturation degrees facilitating formation of solid particles. It was observed that the formation of liquid solute in the inlet of micromodel would cause significantly better response of HWS-1-saturated solution.

In line with sandpack and micromodel experiments, two coreflood experiments were designed and carried out to evaluate the role of co-solvent at low rates in real rocks. The outcome of the coreflood experiments showed a notable improvement in the response of the solution in terms of the required pressure drop and leakage rate to stop the leakage in lab scales. Like micromodel visualisations, the formation of liquid solute could be seen near the inlet of composite core. From weighing the individual core plugs, it was inferred that the main precipitation leading to blockage was formed close to outlet of the composite core. Therefore, addition of insignificant amount of co-solvent would empower the solid solute to tackle leakages with much lower rates. It should be pointed out that these conclusions were inferred from the findings attained from lab-scale experiments and it would be conceivable to see adequate effectiveness for solid-solute + CO_2 solution. However, at this stage of proving the concept of our proposed leakage prevention technique, it is necessary to be able to control and improve the response of our technique based on any desired storage/leakage conditions.

CHAPTER 6 Mathematical Modelling and Simulation of LPM

6.1 INTRODUCTION

Having identified the underlying mechanisms behind the precipitation and the consequent blockage, modelling and simulation of particle formation and blockage evolution would accommodate another pertinent tool for practical implementation of our leakage prevention technique. A reliable model that can adequately reproduce the laboratory results would be a big step for large scale employment of the leakage prevention technique. The performance of LPT should be sensitised at different spatial and time scales before any field trails and the reliable model would enable us to predict the outcome of experiments and field trials, which are cumbersome and costly to carry out. On the other hand, newly identified solutes should be tested for various conditions and covering the full possible ranges of the solute usage is not feasible. However, an examined simulator would a powerful tool to check the response the new solutes. Therefore, the model would have two valuable advantages; (i) it would enable us to up-scale the laboratory results to examine the performance of LPT at real conditions of CO_2 storage and also (ii) a reliable tool would reduce the number of experiments needed for identifying and evaluating the performance of new solutes.

Two lines of study were considered for modelling the processes under which the precipitation and blockage would occur; (i) using commercial simulators and (ii)

developing an in-house model with pertinent physics built in. If the commercial simulators with some manipulations could be able to capture the underlying mechanisms, it would provide an option to simulate performance of LPT in large scales. The phase behaviour and particle formation should be considered/treated as the core of any simulation study and the new phase (particle) formation is solely governed by instantaneous thermodynamic equilibrium in commercial simulators. In other words, in conventional simulators, as pressure drops even in very small degrees, the new phase (solid particles) forms based on the solubility-vs.-pressure relationship. However, as identified in laboratory experiments, there exists a time lag in the formation of solid particle out of the CO_2+Solute solution. Therefore, there may be an inadequacy in commercial simulators to reproduce the laboratory outcomes.

In the first part of this chapter, a commercial simulator was utilised and the required modifications was put in place to replicate how our proposed leakage prevention technique would work. Simulation of particle precipitation and blockage is not a straightforward task and some parameters should be manipulated. In this simulation exercises, the CO_2+solute solution was analogised with a retrograde gas-condensate system in which the pressure reduction would trigger formation of a new phase (condensate) out of the main gaseous phase. A leaky storage reservoir was used and LPT was applied. The results would demonstrate how the commercial simulator can be employed to simulate our proposed leakage technique. However, it should be pointed out that, based on our preliminary analyses, the commercial simulators would not be able to reproduce the laboratory findings. In the coreflood experiment, the time and location of blockage could not be simulated in commercial simulator with the assumption of instantaneous formation of particles.

The desire to capture the kinetics and time dependency of particle formation has prompted the mathematical modelling of the mechanisms involving in particle formation and precipitations. It has been aimed at developing a reliable tool which can capture the observed mechanisms in laboratory experiments and match the results of the flow/blockage tests. It was attempted to develop a simple yet sophisticated set of equations that would not introduce high degree of complexity to the simulations, which may make the model practically unusable for large scale cases.

The results of these two simulation and mathematical works would provide the tools required for simulating LPT in any scales.

6.2 Simulation of LPM Using Commercial Simulators (FLOW OF SOLID SOLUTE-CO_2 SOLUTION IN A RESERVOIR WITH A PREFERENTIAL LEAKAGE PATH)

In this part of the study, CMG compositional reservoir simulator (GEM) has been used to capture the impact of pertinent parameters when CO_2 is stored into an aquifer with a preferential leakage flow path. In general, synthetic homogenous geological models would inherit less dependent variables and hence leading to a simpler simulation process. That is, by assigning typical reservoir property values for a synthetic model, the complexity of underground flow in porous media would be minimised and at the same time the results would be more generic. A realistic reservoir model, on the other hand, would be case dependent due to specific characteristics of the reservoir it represents. In the following simulation exercises, a storage reservoir with homogeneous properties was considered. Table 6-1 lists the main parameters of the 2D synthetic underground storage site shown in Figure 6-1, which has been considered in this study. Some of the reservoir data has been extracted from an example of a CO_2 storage project albeit with the initial pressure and temperature of the reservoir changed to suit the application of HWS-3 as the solid solute that will be dissolved in the stored CO_2. In this model, CO_2 is injected for 25 years through a well, which operates at constant rate of 100 cuft/day. Therefore, the cumulative CO_2 injection will be 21270 tonne. The leakage flow path leads to a surface reservoir (overlying formation) with a controlled pressure of 2850 psi, i.e. the pressure of the overlying formation kept constant since it was assumed to be connected to a constant pressure source such as a ground water reservoir. This condition was established throughout the shallow reservoir by a set of wells operating at the constant pressure of 2850 psi. Therefore, if the pressure of this formation increases due to flow of the fluids from storage reservoir, the wells would be activated to withdraw the excess fluids and stabilize the pressure at 2850 psi. For initializing the target deep reservoir pressure, the pressure of the top grid of the storage reservoir was set to 2850 psi. Other grid pressure would be initialised based on hydrostatic head of column of water. This results in a pressure of 2822.5 psig at the end of the leakage path leading to the shallow depth reservoir. Thus, initially the pressure of the overlying reservoir will be less than 2850 psig. Typical Corey type kr data with exponents of 2 and 3 for CO_2 and brine, respectively, were used. The immobile brine and residual gas saturations were assumed to be 0.2 and 0.15, respectively.

Initially we assume that pure CO_2 will be injected into the storage site. It should be noted that deep storage reservoir has experienced a leakage flow path connecting it to the shallow surface reservoir. In this part a number of methods that are conventionally applied to address the leakage will be investigated. Then HWS-3 is added to CO_2 to investigate the impact of application of our technique to this process. Prior to this exercise, we describe a new modelling technique for describing the relevant phase behaviour of the system using the CMG commercial reservoir simulator.

Table 6-1: Basic input data of the geological storage site.

	Value	Comment
X dimension (ft)	3000	100 grids
Y dimension (ft)	30	1 grid
Z dimension (ft)	720	60 grids
Top of Reservoir (ft)	7500	
Permeability (mD)	100	
Porosity (fraction)	0.13	
Reservoir Temperature (F)	113.59	Based on HWS-3 data
Initial Pressure (psig)	2850	Based on HWS-3 data
Caprock Thickness (ft)	60	
Fault Permeability (mD)	20	

6.2.1 Pure CO_2 Injection

Figure 6-1 illustrates a 2-D view of the water saturation in the reservoir after a certain period of pure CO_2 injection for a base case scenario. It is noted that at this time, CO_2 has reached to the leakage flow path and starts to leak.

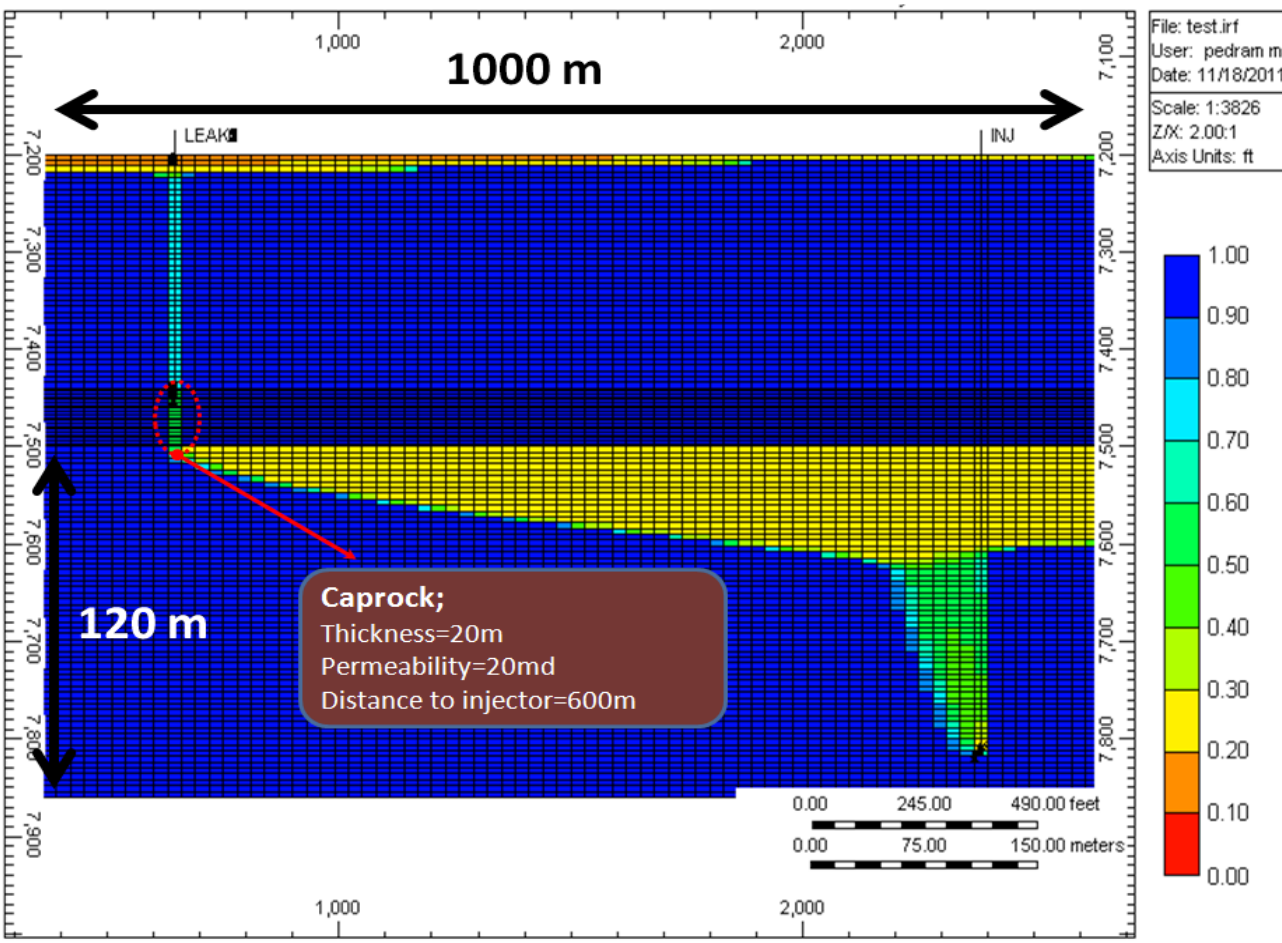

Figure 6-1: 2D cross section of both the shallow and deep reservoirs showing the distribution of water saturation due to CO_2 injection.

Some of the uncertain properties and operational constraints have been selected for more thorough analyses. These parameters have been selected to investigate the impact of the leakage rather than the storage capacity of the sector. First, the effect of solubility of CO_2 in the resident brine on the amount of CO_2 stored was considered. The main motivation for this investigation was to demonstrate its minimal impact on the fate of solute mixture dissolved in CO_2 solution for implementation of our leakage prevention scenario. It should be noted that the main difficulty of integrating of the impact of CO_2 solubility for our purpose is the uncertainty in the phase behaviour of ternary system of CO_2, solid solute, and reservoir brine. Based on the results of this sensitivity this option was excluded from the other sensitivities conducted in the rest of this report. The two last sensitivities conducted in this part evaluate the impact of distance of leakage path from the injection point and that of injection rate on the fate of injected pure CO_2.

Effect of CO_2 Solubility in Brine

CO_2 dissolution in aquifer brine has been known as one of the main mechanism of the CO_2 storage in the CCS processes. Saturation of reservoir brine with carbon dioxide would increase the density of in place brine in the favour of downward flow of the CO_2 saturated brine and hence the convective flow of reservoir brine might take place, which in turn increases CO_2 trapping as a result of dissolution. It should be noted that this convective flow would be taken place in long geological time scales. In this section we quantify the impact of this mechanism in terms of the amount of leaked and stored CO_2. In this simulation study, solubility of the CO_2 into the reservoir brine was estimated by Harvey correlation for Henry's constants (Harvey, 1996).

Figure 6-2 exhibits the trend of the CO_2 in the reservoir in the form of separate gas phase and dissolved form during a period of 2500 years. It is noted that initially the amount of CO_2 stored increases with time but then decrease when CO_2 reaches to the leakage point. From the 21270 tonne of injected CO_2, 2370 tonne would be stored via dissolution into the brine comparing to 5100 tonne of stratigraphic trapping of CO_2 and 13800 tonne of CO_2 leaked from the leakage path to the overlying layer. That is, only 11 percent of the injected CO_2 will be remained inside the reservoir in the dissolved form. Therefore, it can be concluded that the storage capacity of this mechanism for the cases considered here is minimal. Thus, for the rest of the simulations, the dissolution of CO_2 into the reservoir brine will be ignored.

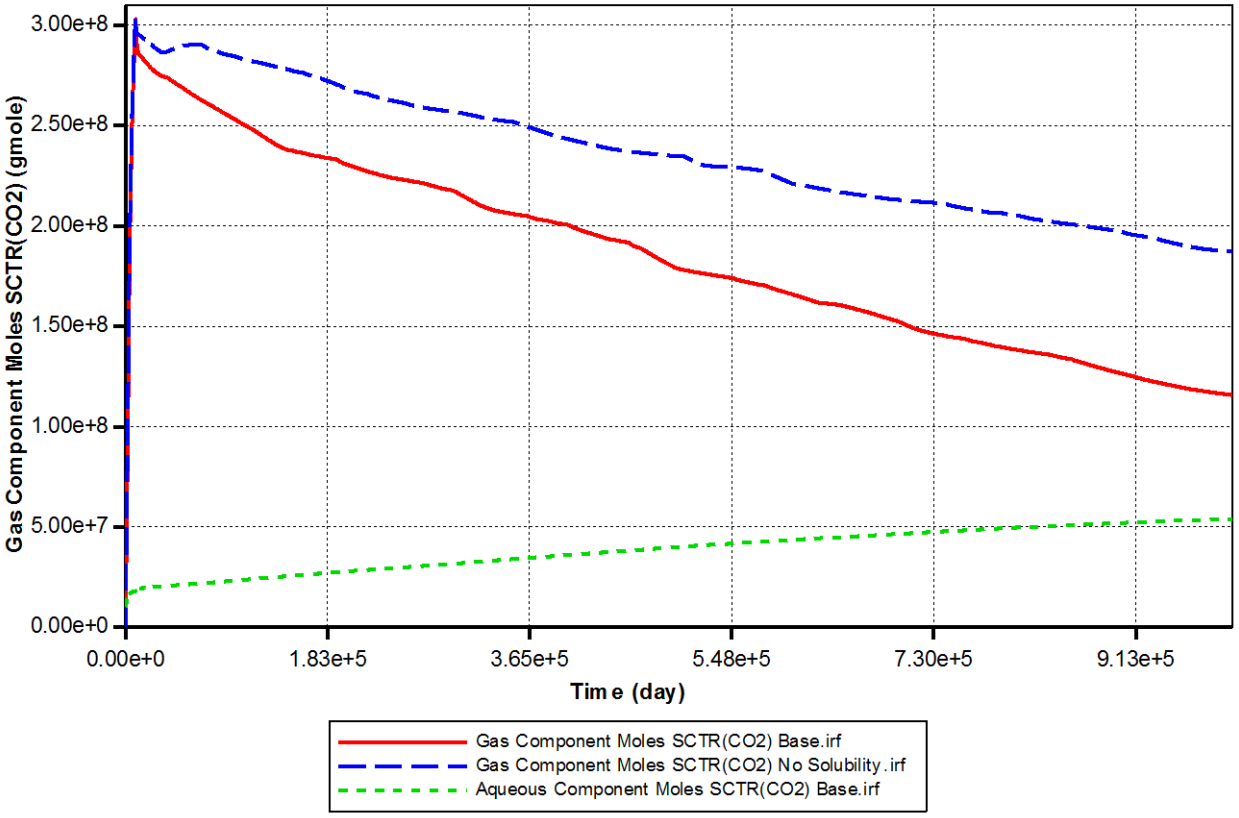

Figure 6-2: Profile of cumulative moles of CO_2 as (i) a separate phase in the solubility included case (solid red line), (ii) a separate phase in No-solubility case (dashed blue line), and (iii) dissolved CO_2 in solubility included case (dotted green line).

Effect of Location of Leakage Path

Location of the leakage path is considered as one of the most uncertain parameter in natural and man-made geological CO_2 storage sites. Detection of fractures and faults across the caprock of the storage site by seismic modelling is associated with high level of uncertainty unless the CO_2 phase enters the conduit and magnifies the density contrast in the geological anomalies. To investigate the impact of leakage location, two cases were studied; first one is the base case reported previously with 600 metres distance between injection point and leakage path. In the second case this distance has been increased to 200 meters.

Figure 6-3 shows the average reservoir pressure response to the pure CO_2 injection. The trend exhibits three main behaviour; (1) the sharp increase in pressure which indicates the impact of added volume of stored CO_2 under the sealing part of the caprock within the reservoir, (2) decline in the pressure when the CO_2 front reaches the leakage path, and (3)

the sudden pressure drop when CO_2 injection is ceased. Comparing two pressure graphs reveals that the ultimate pressure of the reservoir does not significantly depend on location of the leakage path.

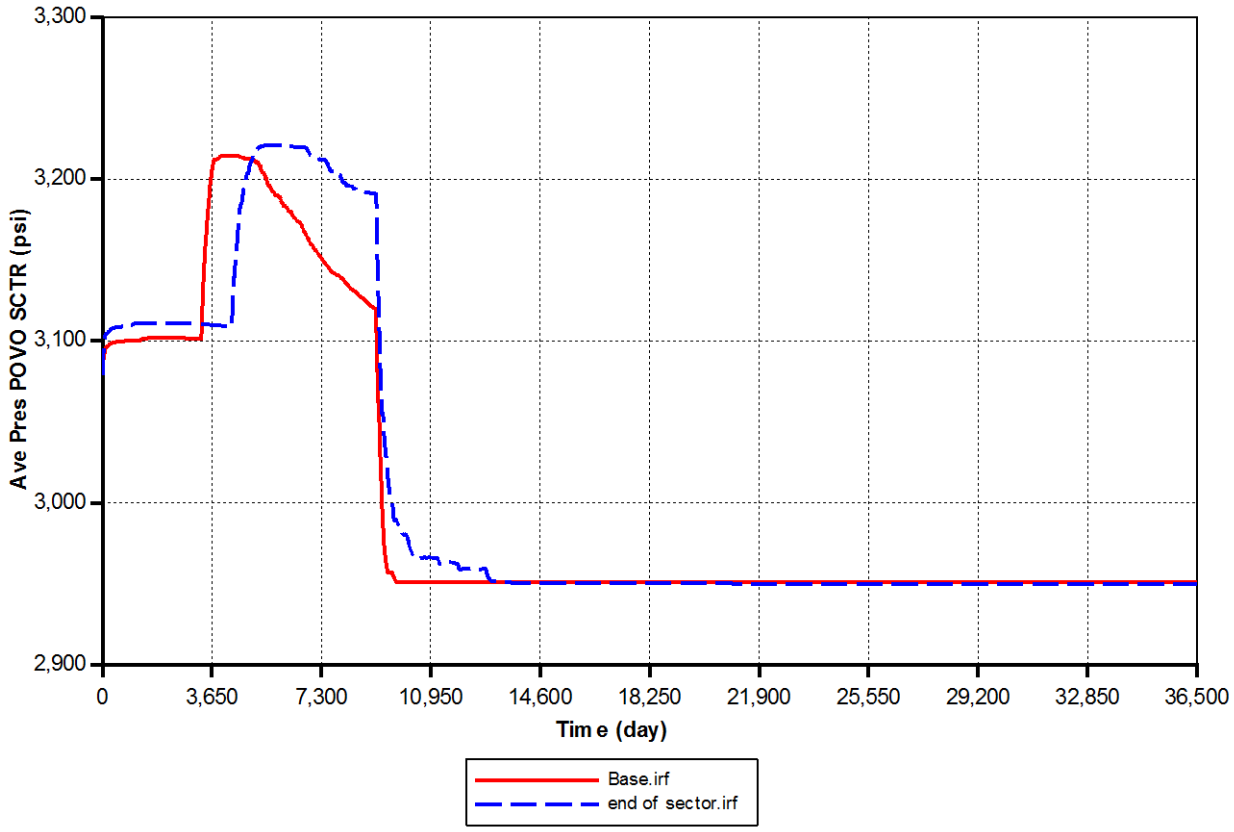

Figure 6-3: Average reservoir pressure for two distances between injector and leakage path; 600 m (solid red line), 800 m distance (dashed blue line).

After analyzing the impact of leakage location on the average reservoir pressure, mass of stored CO_2 for the two assumed leakage location was investigated. Figure 6-4 shows the short term CO_2 storage profile whereas the Figure 6-5 demonstrates the long term effectiveness of CO_2 storage for these two cases.

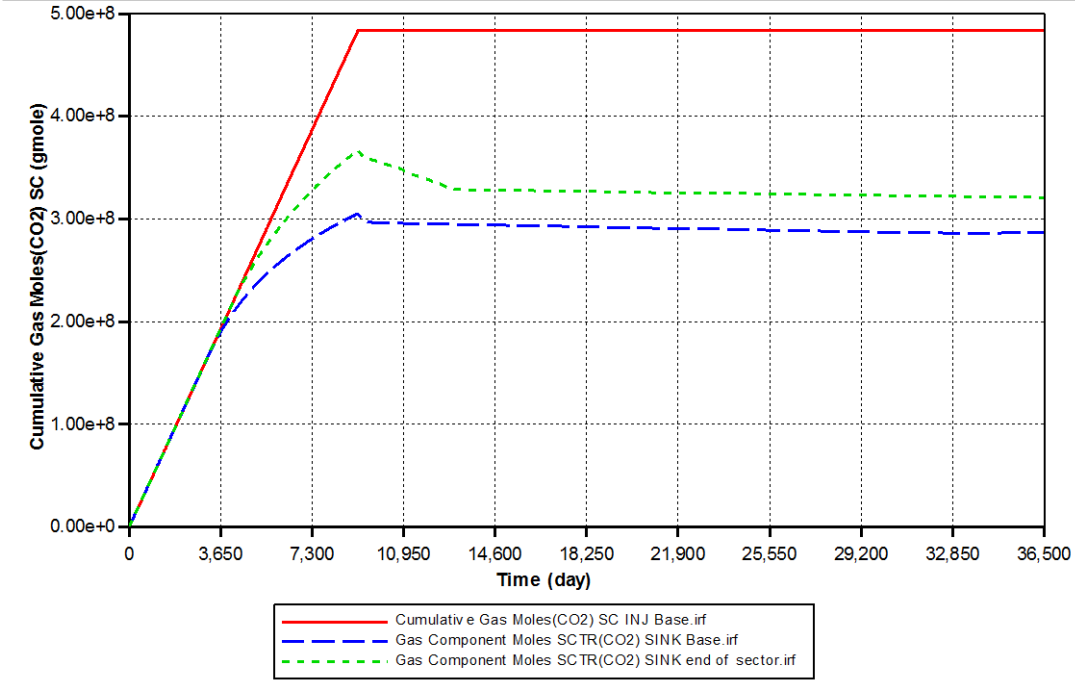

Figure 6-4: Short term profile of cumulative moles of CO_2; injected CO_2 (solid red line), stored CO_2 as a separate phase with 600 m distance between the injector and leakage path (dashed blue line), stored CO_2 as a separate phase when this distance is increased to 800 m (dotted green line).

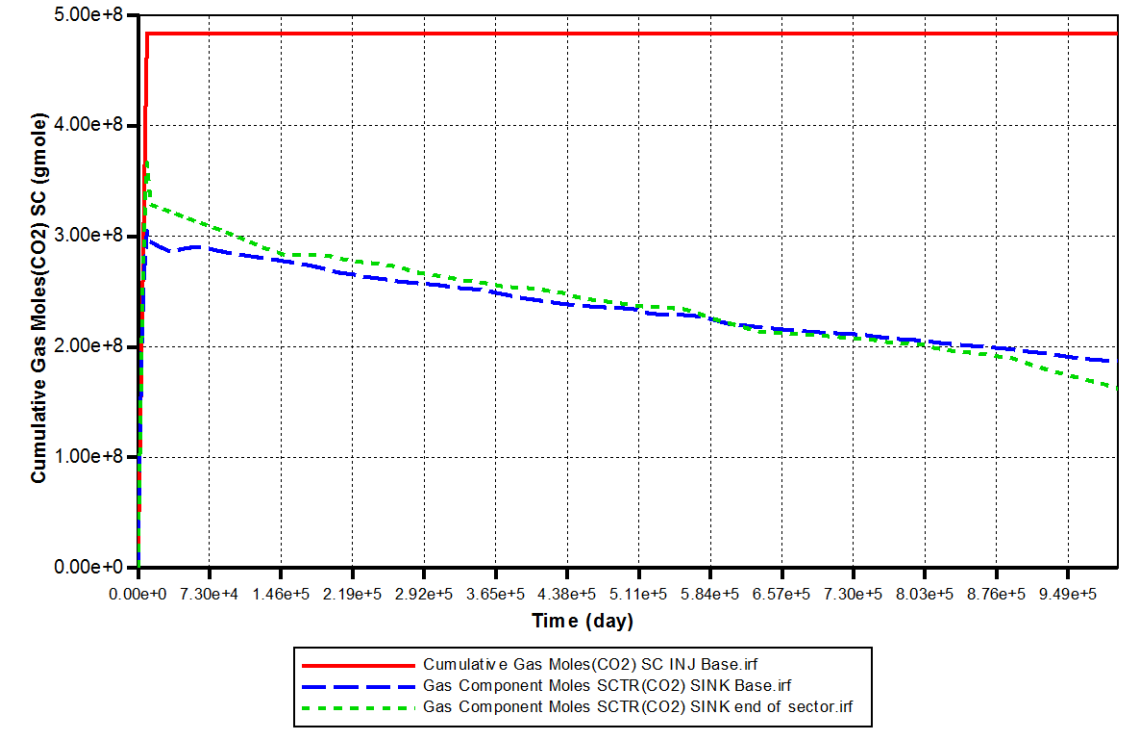

Figure 6-5: Long term profile of the cumulative moles of CO2; injected CO2 (solid red line), stored CO2 as a separate phase with 600 m distance between the injector and leakage path (dashed blue line), stored CO2 as a separate phase when this distance is increased to 800 m (dotted green line).

In the short term, the reservoir with higher distance between injection well and the leakage path would retain more CO_2 but in the long term, fate of the CO_2 in both cases is more similar highlighting the fact that in this geological storage project, location of leakage will not significantly affect the final amount of CO_2 in the reservoir. This simulation would also questions the relevance of discussions around the lateral extend of the CO_2 plume.

Effect of Injection Rate

Injection rate is the main operational constraint that would be optimized according to the reservoir capacity, fracturing pressure of the formation and economic issues. Herein, the fracturing pressure has not been included in the simulation and the main objective of performing sensitivity analyses is to assess the amount of leaked CO_2 at various rates. Three different rates were taken into account to investigate the resultant impact on the average reservoir pressure and stored CO_2. The base rate of 100cuft/day at bottomhole conditions were reduced to 50 and 25 in two separates simulations. In all these three simulation the total amount of injected CO_2 was kept constant by increasing the CO_2 injection duration for the low injection rate scenarios.

According to Figure 6-6, average reservoir pressure depends strongly on the injection rate. It is noted that the pressure of high rate injection is higher but it decreases shortly after CO_2 injection is stopped. It should be noted that in this model the pressure at the surface shallow reservoir is constant and the flow of water through the leakage flow path before CO_2 reaches the leakage path and that of water and CO_2 afterwards continues based on the resultant pressure gradient till the whole system pressure stabilizes.

The reason behind the trends of the pressure response to injection rate can better be explained by the data of Figure 6-7 which presents the shape and extend of the CO_2 plume. It is noted that at the injection rate of 100cuft/day (the image on the left), the plume invaded more area in the horizontal direction compared to the rate of 25cuft/day. This is because at lower rates the CO_2 pressure and hence its density will be lower enhancing the gravitational segregation of the reservoir brine and CO_2.

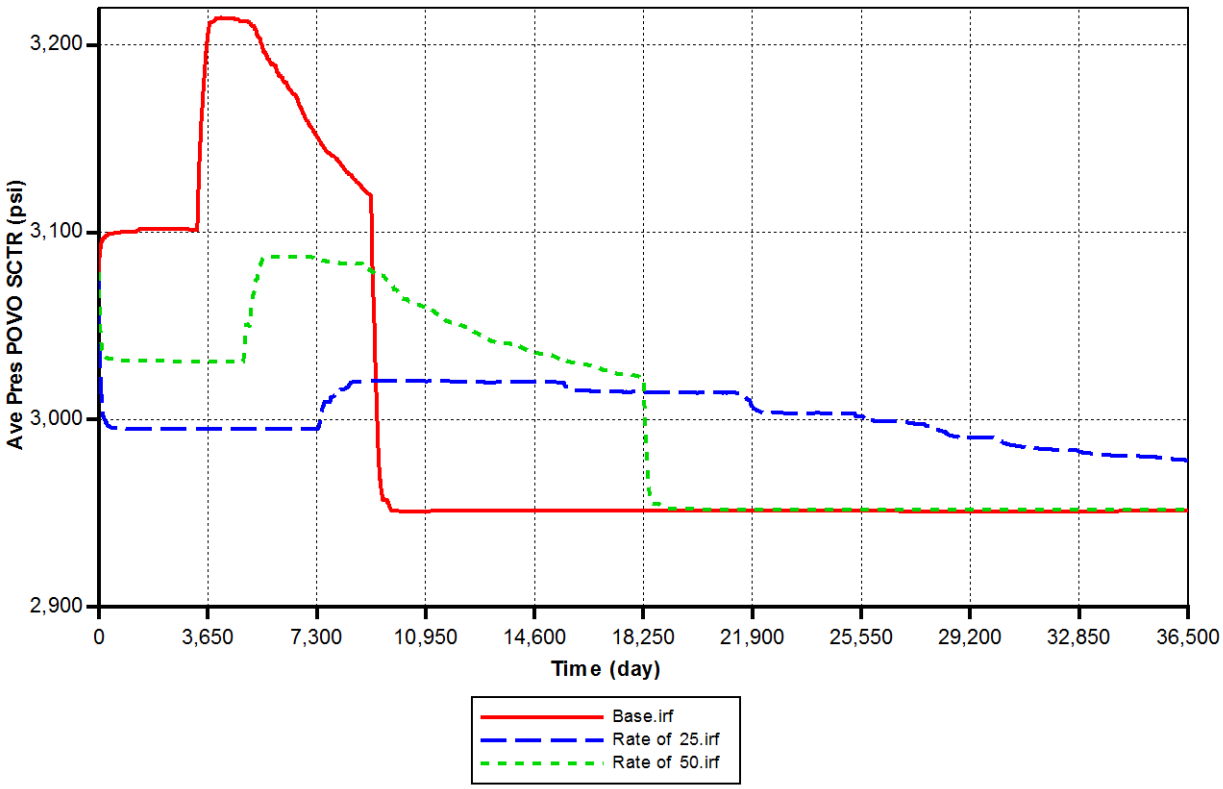

Figure 6-6: Average reservoir pressure for three injection rate cases: 100 (solid red line), 50 (dotted green line), and 25 cuft/day (dashed blue line).

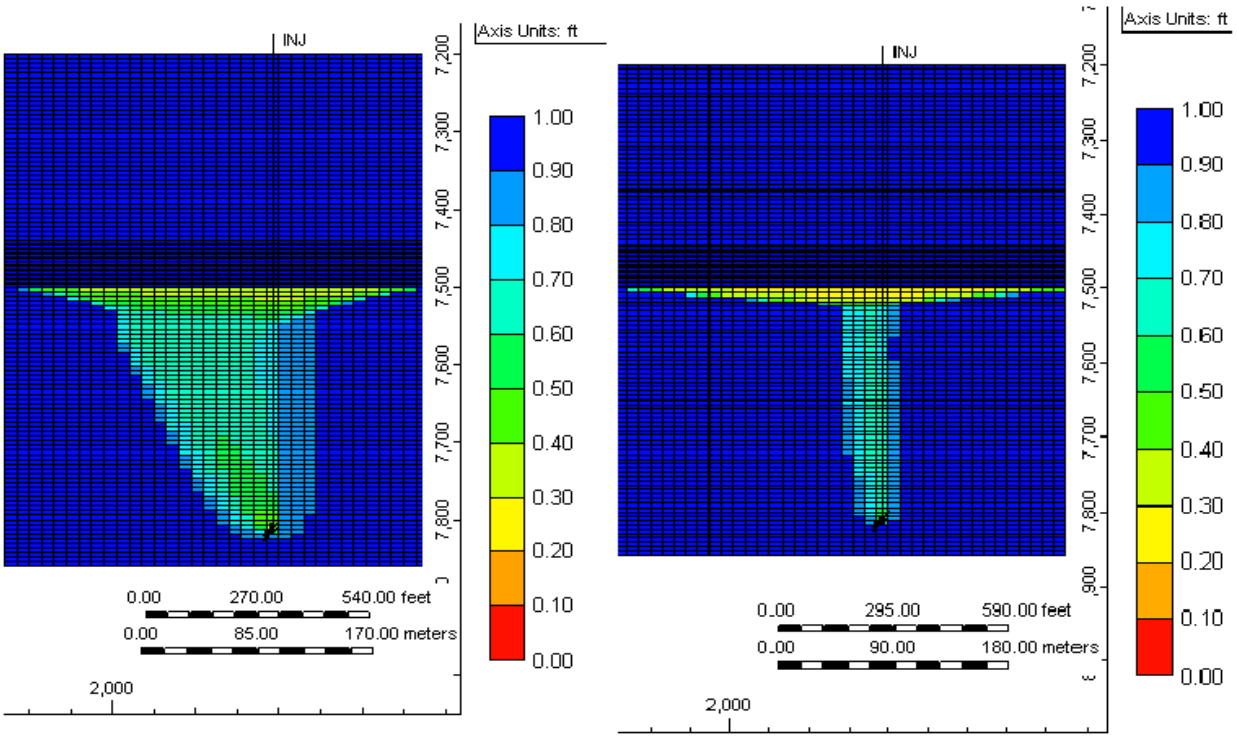

Figure 6-7: Extension of plume in two different cases with two CO_2 injection rate of 100 (left image), and 25 cuft/day (right image).

Figure 6-8 shows the behaviour of the reservoir in terms of the amount of stored CO_2 at different injection rates. It is noted that at higher rates the amount of leaked CO_2 would be significantly less than that of the lower rates because of more laterally distributed CO_2 plum which results in higher trapped CO_2, Figure 6-7. That is, the intesified vertical segregation of the fluids at lower rates allows more rapid advancement of the CO_2 front to the leakage path.

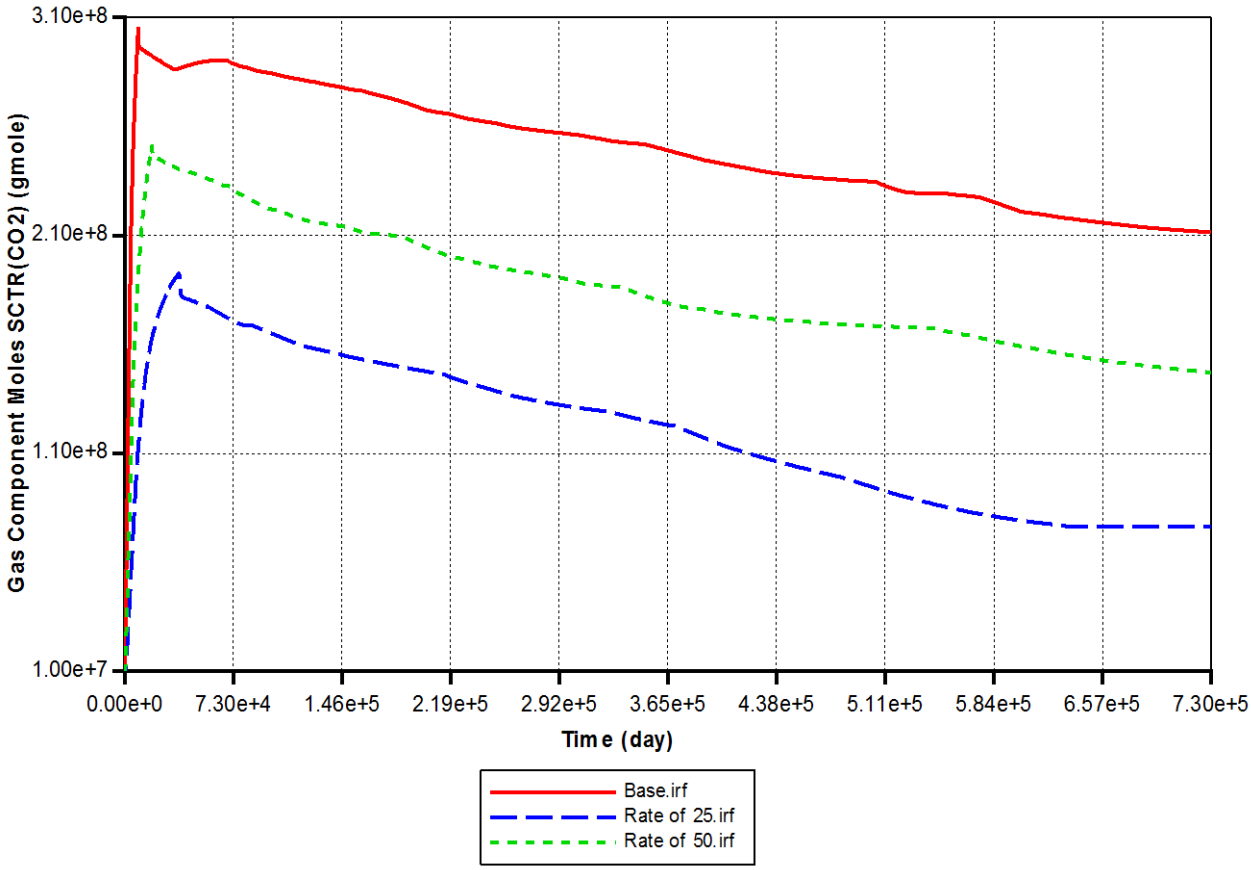

Figure 6-8: Cumulative moles of stored CO_2 for the three injection rate cases: 100 (solid red line), 50 (dotted green line), and 25 cuft/day (dashed blue line).

6.2.2 Application of Conventional Mitigation Strategies

In this study three types of mitigation strategies has been deployed to tackle the leakage from the reservoir; first, drilling a new well at the vicinity of the leaking conduit to pressurize the overlying layer, second option is to drill a production well to produce CO_2 from the plume and prevent propagation of leakage to the surface. The third option is to deploy our Leakage Prevention Technique from the beginning of injection.

Pressurizing Overlying Formation

One method to minimise the leakage rate from the leaky reservoir is to drill an injection well in the overlying formation to pressurize the system with water injection and reduce the migration of CO_2 from the storage site. The main obstacle in applying this method is the intrinsic uncertainty in detection of underground leakage path within the reservoir, which impacts the location of the injection well. There is also the duration of injection and economical consideration of such an operation. In the particular case studied, the mitigation well was placed 100 meters away from the leakage path. The water injection period was for the whole 2500 years of simulation period. The time of water injection commencement has been selected right after CO_2 reached the leakage path. Figure 6-9 demonstrates the amount of stored CO_2 for the two cases without and with pressurizing the overlying formation. It is noted that pressurising the overlaying formation has decreased the leakage rate but it has not completely stopped it as the amount of stored CO_2 decreases with time for this case as well.

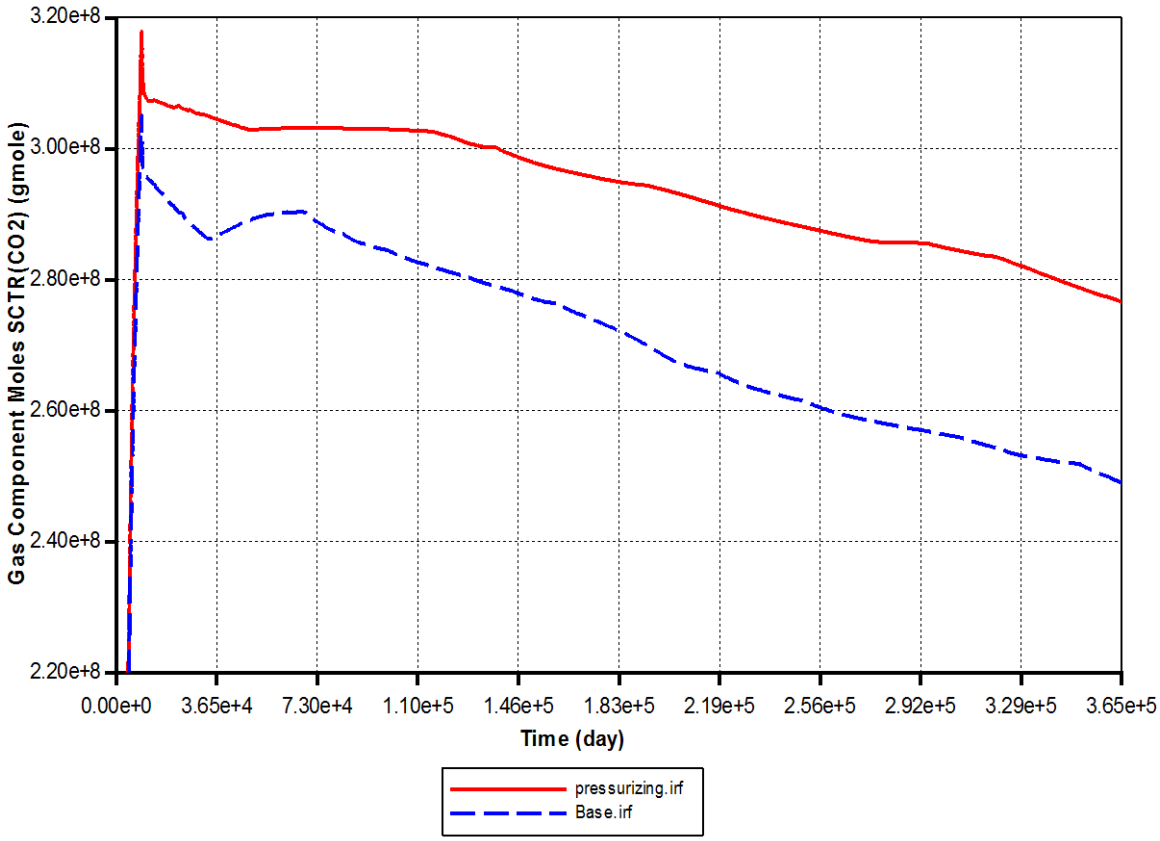

Figure 6-9: Cumulative moles of stored CO_2 for two cases; drilling a well to pressurize the overlying layer (solid red line), and without deploying any mitigation method (dashed blue line).

Producing from CO_2 Plume

Another method to reduce the emission of stored CO_2 from a leaky reservoir is to produce CO_2 from the stored CO_2 plume. The same logistic and economic considerations that were mentioned for the previous case also apply here. In our simulation we have used the same well location as that used for CO_2 injection but instead of injecting at the bottom of the storage reservoir, the well perforation was altered to the top of the storage reservoir and altered the control mode from CO_2 injection to CO_2 production. The production rate was equal to the injection rate with the start time right at the moment that CO_2 reached the leakage path. The production continued till the end of the simulation but the effective period during which majority of production stream was CO_2 was limited to first two years of applying the mitigation method. This is shown in, by the flat trend of the dashed blue line corresponding to the amount of CO_2 produced. The flat trend of the stored CO_2 red curve in Figure 6-10 demonstrates that producing from the plume can reduce the adverse impact of CO_2 leakage from the storage site. However this curve is below that without implementation of this strategy due to the 1420 tonne cumulative amount of produced CO_2. The cumulative injected CO_2 is 21270 tonne, stored CO_2 mass is 8550 tonne and consequently less than 11300 tonne has leaked from the sink.

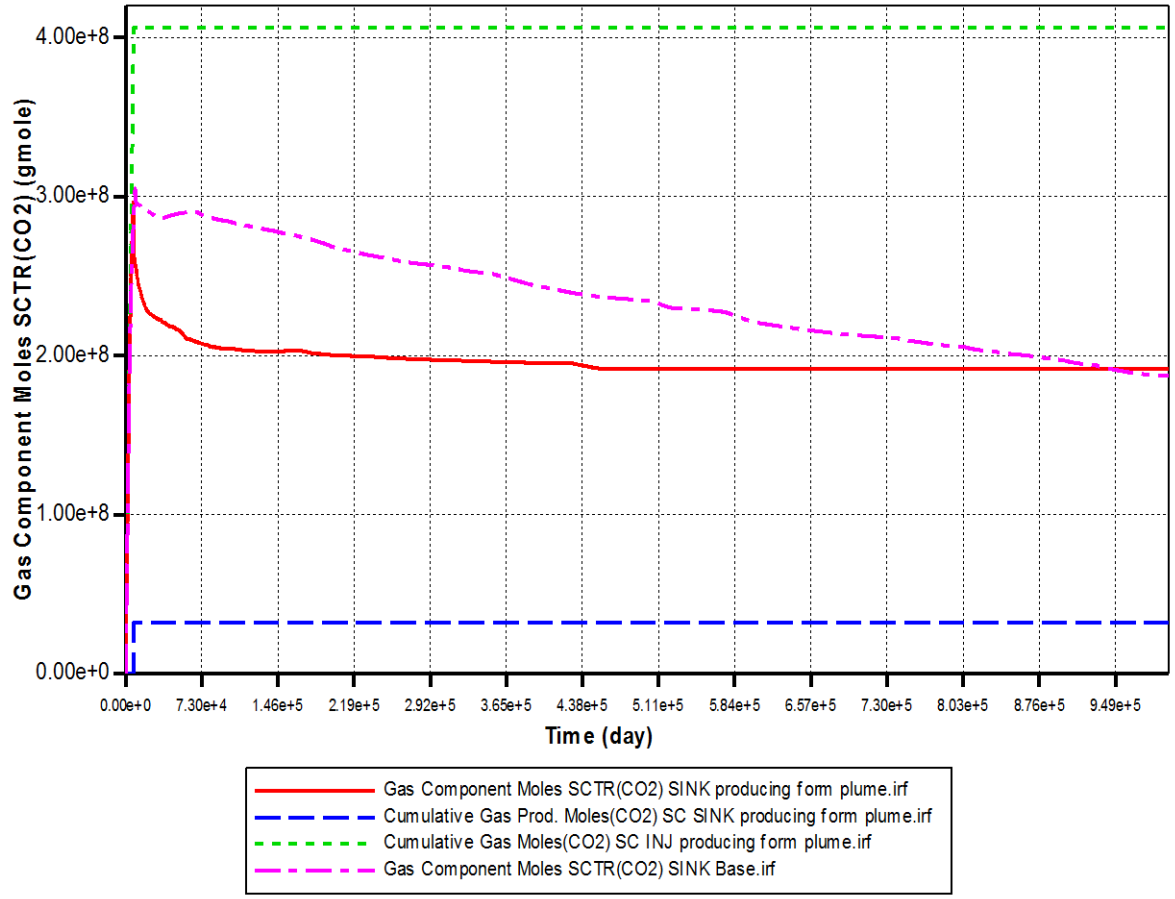

Figure 6-10: Cumulative moles of CO_2; dotted green line represents injected CO_2, the dashed pink line shows stored CO_2 in the reservoir without mitigation and solid red line is for the case with CO_2 production from the plume, and the dashed blue line shows the produced CO_2 for the mitigation case scenario.

6.2.3 Simulation Technique for HW Leak Prevention Technique Using Conventional Commercial Reservoir Simulators

Conventional reservoir simulators solve the multiphase flow equations but no particular option is available for defining solid phase in the gaseous solution. Therefore, some manipulation of the available options and parameters is needed to capture the main physics governing our leakage prevention mechanism. In this process it is assumed that solid particle formation takes place at saturation point and not above it. Moreover, the solute particles have negligible flow element when they solidify, i.e. they precipitate as immobile phase as soon as they are formed at the saturation pressure. The general workflow of the leakage prevention technique resembles the behaviour of gas-condensate reservoirs. Thus, by taking advantages of analogy between gas-condensate and CO_2-

solute systems, the thermodynamic behaviour of the system would be modelled. The final point is to set the relative permeability of the solid solute (or condensate phase) to zero. In short, a gas-condensate system has the representative phase behaviour of our system with zero relative permeability for the condensate phase all representing the precipitation of immobile solid particles. It should be noted that the following main assumptions have been made:

1. Instantaneous nucleation of particles at any super-saturation.
2. No suspension flow of the generated particles.

Phase Behaviour of Solid Solute

Phase behaviour of the CO_2+solid solute system controls the efficiency of the technique. In this study HWS-3 was used as the solid solute. Including the solute in the PVT model as a single component would lead to severe numerical instability in the phase behaviour calculation mainly because of significant contrast between the solid solute and supercritical CO_2 mixture properties.

To overcome this modelling artefact, the HWS-3 component was split by internal splitting subroutine of the Winprop (CMG) into four components. The sub-pseudo components were adjusted to maintain the overall properties of the HWS-3. The highest composition was assigned to the most analogous components among the pseudo-components. Table 6-2 lists the compositions and the critical properties of the pseudo-components which results in HWS-3 properties if grouped into a single component. It can be deduced that the "Solute1" component with the highest composition and closest HWS-3-like properties has the most dominant effect on the phase behaviour of this system. The critical properties of the pseudo-components were produced by tuning them to match HWS-3 solubility in CO_2 (Gupta & Shim, 2006).

Table 6-2: Thermodynamic properties of pseudo-components which represent HWS-3 when grouped.

	Composition (mole frac.)	Pc (atm)	Tc (K)	Acentric factor
Solute1	0.0025	32.45	736.83	0.49
Solute2	0.0009	28.06	496.96	0.30
Solute3	0.0001	24.35	628.88	0.39
Solute4	0.0001	17.04	707.24	0.63

Figure 6-11 shows the acceptable agreement between the experimental solubility data and EOS modelling after the tuning process. In the tuning process, a weight factor of 50 was assigned to the saturation pressure of the HWS-3 and CO_2, i.e. 2820 psig at temperature of 45C, to ensure that precipitation would occur at this pressure. It should be noted that the Y-axis in the Figure 6-11 is in volumetric unit compared to the mole fraction in solubility curve presented before.

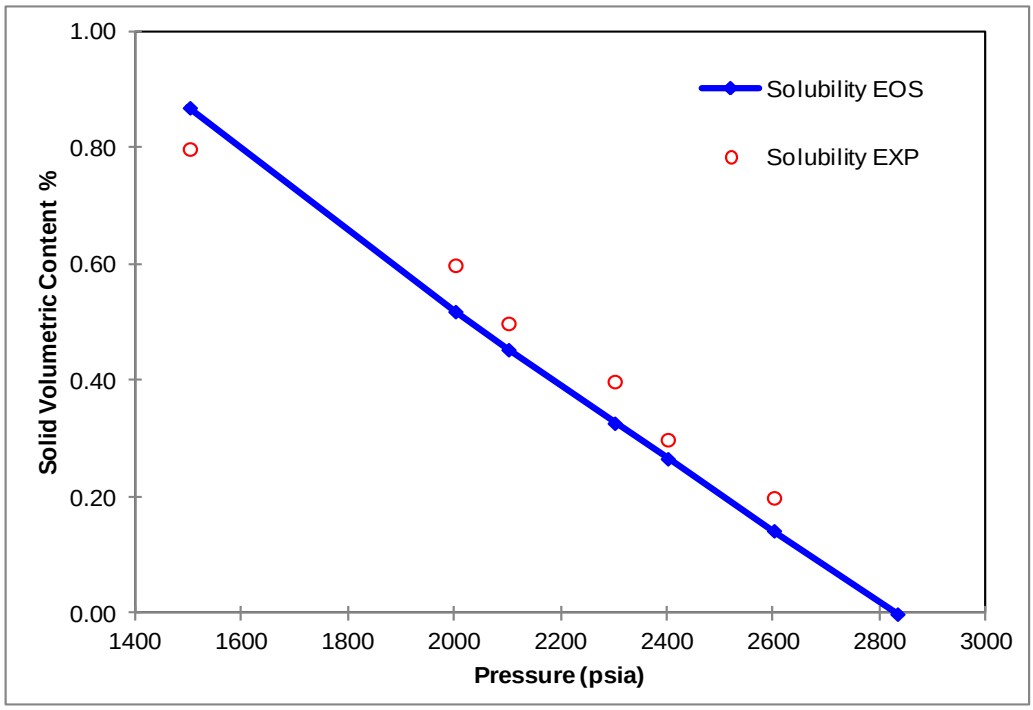

Figure 6-11: Experimental and EOS modelling data for volumetric solid solubility of the solution.

Simulation Results

The main objective of performing the simulation reported in this part is to investigate the effectiveness of the technique. Two cases were considered: (i) the case with pressure at the top of the leakage path and bottom of the shallow reservoir being 2850 psig which is above the saturation pressure of 2820 psig and corresponds to no precipitation of the solute in the leakage path which is identical to previous cases except the presence of the solute in the injection stream and (ii) the case with the corresponding pressure reduced to 2550, which allows the precipitation of solid solute. The initial deep storage site reservoir pressure was set to 2900 psig, which is 80 psig above the saturation pressure of the injection stream. Other simulation parameters are similar to the case described in the previous section.

Figure 6-12 and Figure 6-13 show the short term and long term responses of the leaky reservoir. In the first case, the reservoir behaves very similar to the previous simulations. However, according to Figure 6-12, the leakage in the second case has been significantly reduced immediately after the solution reached to the leakage path. Although the technique has stopped the leakage from the reservoir, certain amount of leakage is inevitable since the precipitations would be built up gradually. This delay in complete ceasing the leakage path corresponds to 2000 tonne of the CO_2 escape from the reservoir, which is relatively small compared to first case with 13800 tonne for the same simulation period.

One of the issues is the durability of the blockage because the average reservoir pressure increases with increased amount of injected CO_2 after the precipitation blocked the leakage path. Figure 6-13 shows that there is negligible difference in the amount of stored CO_2 in 2500 years, which is quite distinct compared to the gradual reduction of this quantity with time for the base case. In short, the technique efficiently ceases the leakages if the pressure of the leakage path falls below the saturation pressure with small amount of leaked CO_2 prior to complete blockage of the path, which is durable for a long period of time.

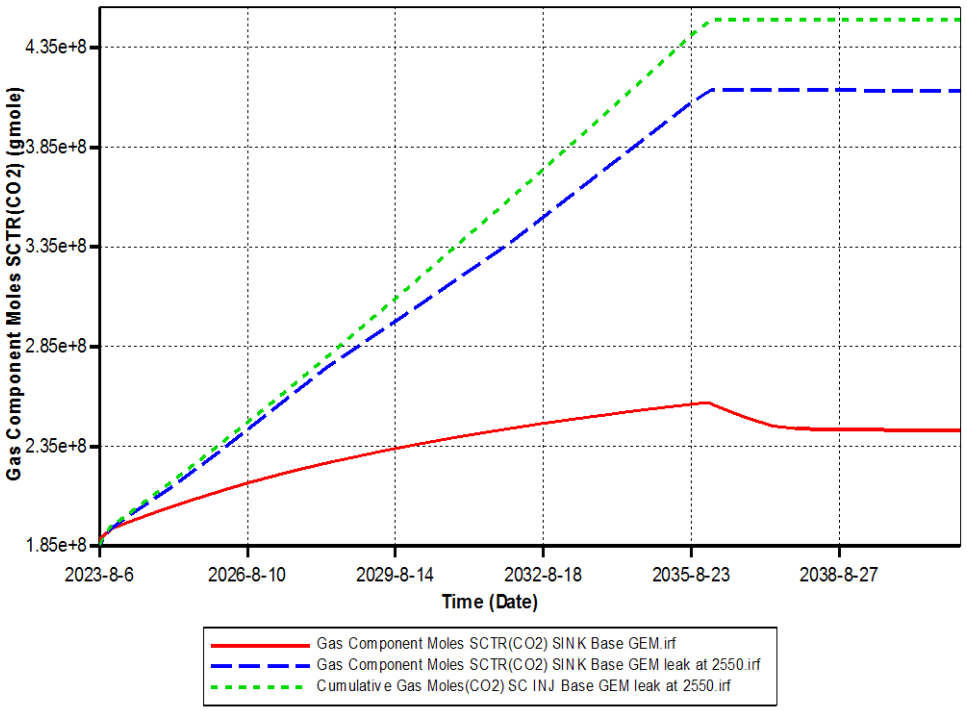

Figure 6-12: Short term cumulative moles of CO_2 as a separate phase; injected CO_2 (dotted green line), stored CO_2 without precipitation (solid red line), and stored CO_2 with solid precipitation resulting in stopping the leakage path (dashed blue line).

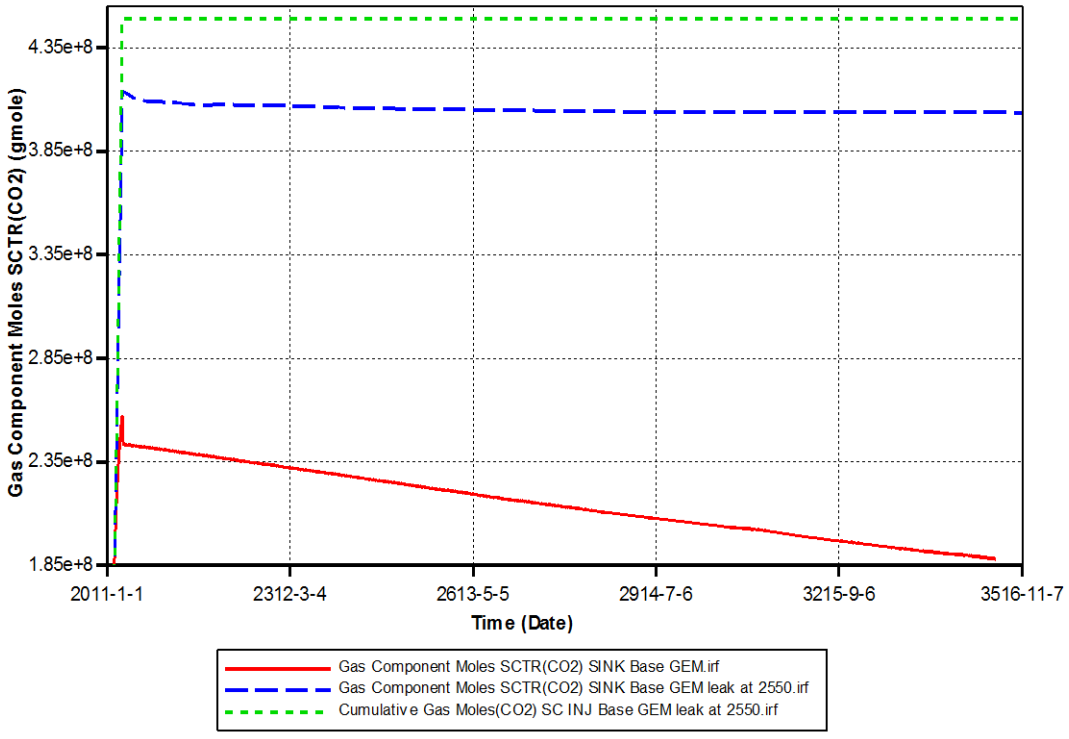

Figure 6-13: Long term cumulative moles of CO_2 as a separate phase; injected CO_2 (dotted green line), stored CO_2 without precipitation (solid red line), and stored CO_2 with solid precipitation resulting in stopping the leakage path (dashed blue line).

Effect of Leakage Path Permeability

The leakage path permeability is the key parameter affecting the leaked flow rate and pressure drop from the deep storage reservoir site to the overlying formation. Therefore we investigated the efficiency of the method at various conduit permeabilities by decreasing the leakage path permeability by a factor of 5 from 20 mD to 4 mD. In this exercise a no leakage case was also simulated to compare its results with these cases.

According to Figure 6-14, there is minimal difference between the total amount of CO_2 stored in both the 20 mD and the low permeability 5 mD cases. However, Figure 6-15 depicts that the pressure response to different leakage path permeability is different. In should be noted that for data shown in these two figures no solid solute was dissolved in the CO_2 solution.

In another sensitivity study we compared the pressure response of the low permeability leakage with that of a no leakage simulation case. The results shown in Figure 6-16 demonstrate the minimal differences in bottomhole pressure of the injection well (about 6 psig) between the low permeability leakage path and no-leakage cases. These results suggest that in such a low leakage rate case it is practically difficult to detect the leakage by recording the downhole pressure data.

Figure 6-17 compares the pressure behaviour of the base and low permeability cases when our leakage prevention technique has been implemented. The curve for the case of injection pure CO_2 solution without any solid solute dissolved in it has also been included. It should be noted that the main criterion for identifying the start of precipitation is the distinct rise in average pressure of the reservoir. Thus, it would be more appropriate to analyse the pressure curves rather than the cumulative amount of stored CO_2 in the reservoir. From Figure 6-17, three main trends can be identified; (i) initially the curves follow almost the same trend prior to the CO_2 reaching the leaking path (ii) they gradually diverge from each other indicating different precipitation rate of solute particles in the leakage path (iii) finally the pressure stabilises at a constant value. It is noted that for the cases with solid solute the pressure stabilise at a high value demonstrating the durability of the blockage. Furthermore, this pressure value is less for the low permeability case demonstrating more gradual blockage of the leakage path.

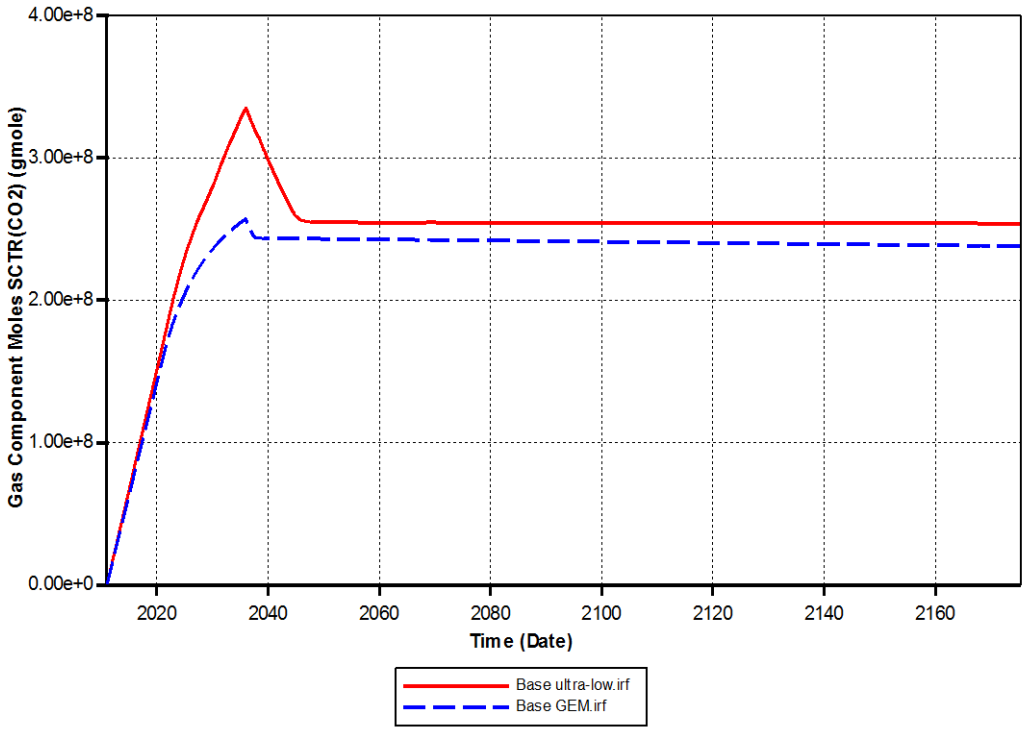

Figure 6-14: Cumulative moles of CO_2 stored without utilizing solute in two cases; low permeability 5 mD leakage path (solid red line), moderate permeability 20 mD leakage path (dashed blue line).

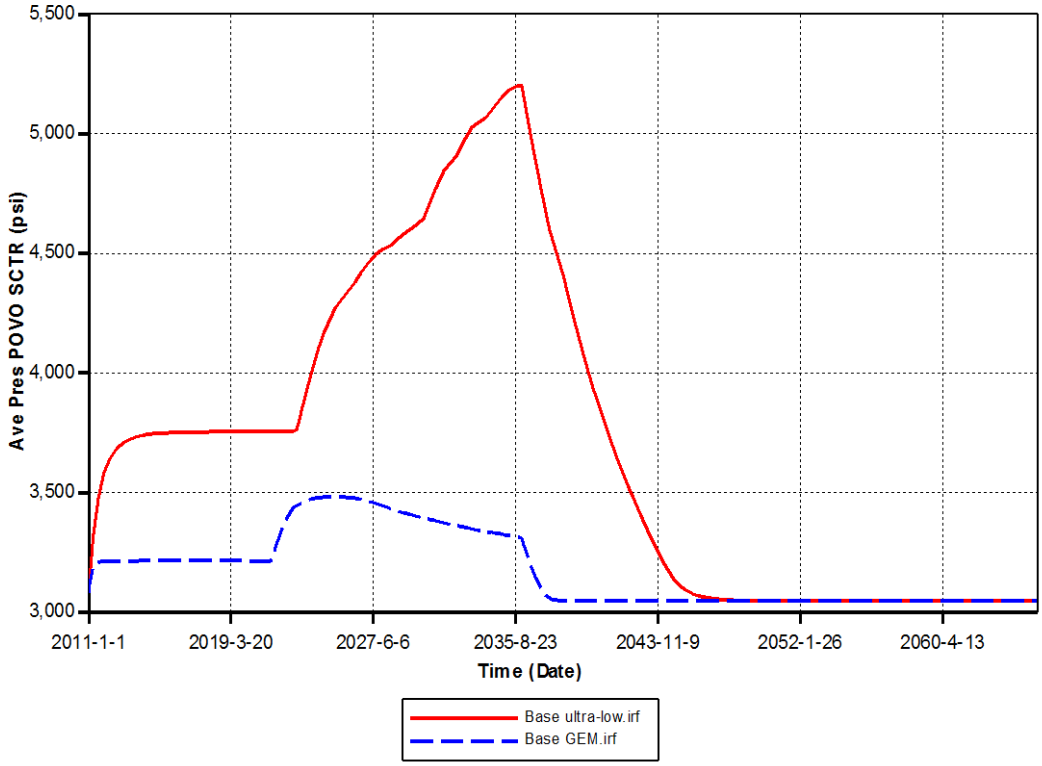

Figure 6-15: Average reservoir pressure without utilizing solute in two cases; low permeability 4 mD leakage path (solid red line), moderate permeability 20 mD leakage path (dashed blue line).

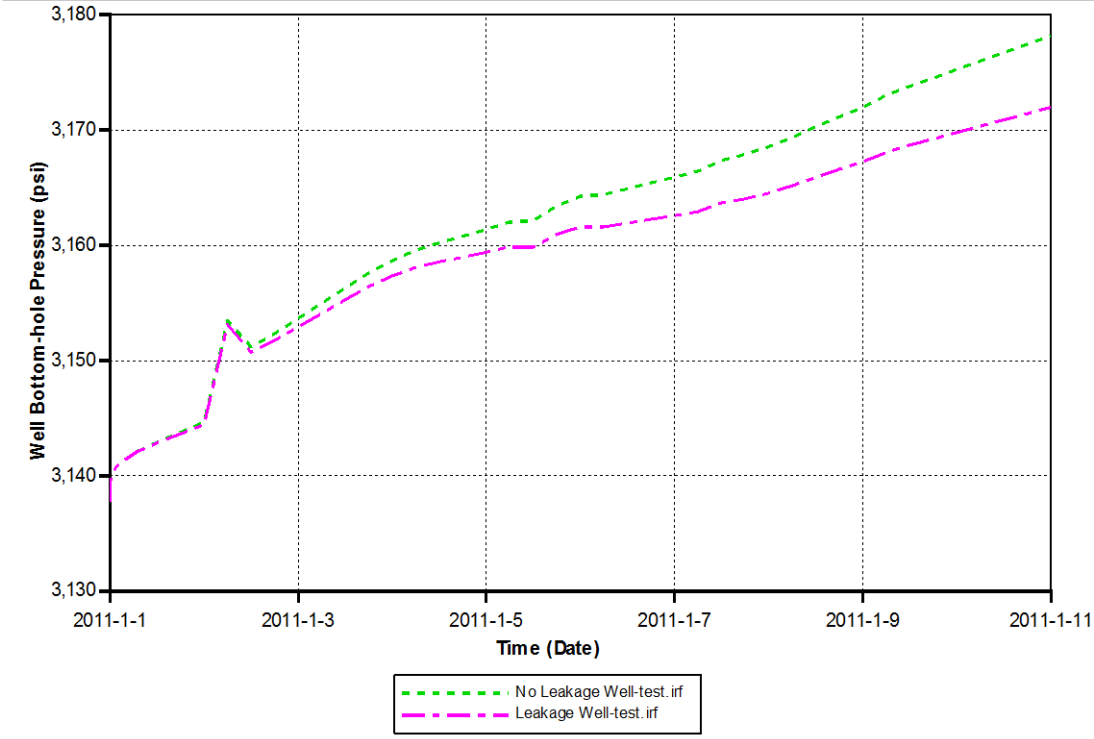

Figure 6-16: Bottomhole pressure of the injection well in two cases; the low 4 mD permeability leakage path (dotted pink line), and the no-leakage storage reservoir (dashed green line).

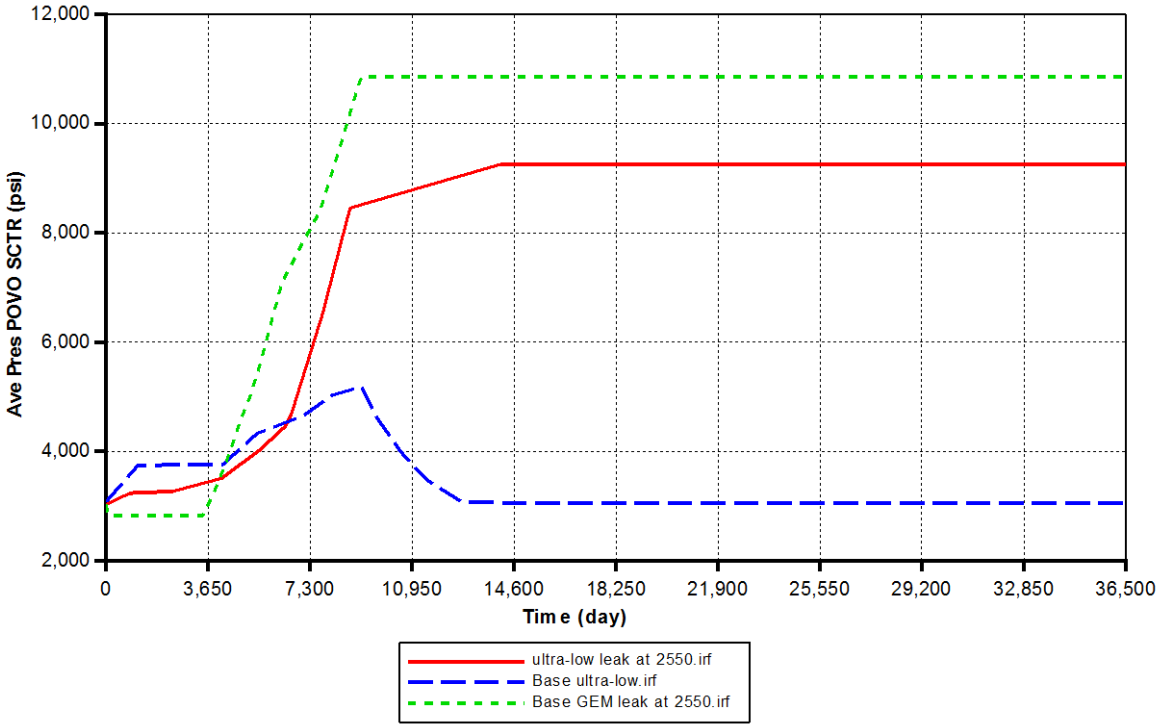

Figure 6-17: Average reservoir pressure in three cases; without deployment of the leakage prevention method (dashed blue line), deploying the leakage prevention technique for the low 5 mD permeability leakage path case (solid red line), and that for the base 20 mD permeability case (dotted green line).

In the modelling section, to simulate the process, gas-condensate system in conventional reservoir simulators can be used with essential manipulation in phase behaviour and flow properties of phases although we are not able to include some of the main physical characteristics of the technique such as nucleation kinetics and filtration mechanism.

6.3 Mathematical Modelling of LPT

6.3.1 Introduction

In the visualisation experiments, the solute particles were dropped out rather rapidly at relatively high pressure drops (~1000 psig). This finding has been confirmed in the sandpack experiments where their flow rates were in the same range of the micromodel tests. However our core experimental results have revealed that there is a relatively long transient period before solid particle is formed and precipitated out leading to the blockage of flow path especially at low supersaturation (solution containing more of the solute that it can dissolve under thermodynamic equilibrium conditions) degrees. In other words, the resistance for the formation of a solid particle at the given test temperate and supersaturation conditions can be interpreted by the time lag (induction time) for nucleating the solid embryos. This time primarily depends on the relatively high interfacial tension between the solid solute and supercritical CO_2. It should be noted that the formed particles would also tend to flow with the carrier gas ($SCCO_2$) in the suspension form. However, our visualization experiments and coreflood tests have verified that the contribution of suspension flow is small. That is, solid particles, amount of which determined by the nucleation rate expression, precipitate as soon as they are formed.

Considering these observations, it was decided to adopt a mechanistic modelling approach that accounts for proper modelling of the solid precipitation primarily based on the nucleation kinetics. The precipitated solid decreases the porous medium porosity and more importantly its permeability, which would consequently lead to blockage of the leak. The proposed sets of equations describing the kinetics of solid solute precipitation and porosity and permeability reduction have been linked to the Computer Modeling Group (CMG-GEM) reservoir simulator, which solves the flow equations. The coupled flow/precipitation equations are solved simultaneously in an explicit approach. The calculation continues till the permeability reduction is reached to a pre-defined level indicating the blockage of the leak.

Applying the nucleation kinetics would account the majority of the permeability reduction observed in experimental results. In our analyses, we found out that 98% of permeability reduction can be explained through employing the nucleation kinetics. However, to reach to the full blockage, it was identified that another mechanism should be put in place. This complementary physics was inferred from the visualisation

information in which, we observed a process becoming activated in later stage of the blockage formation, i.e. particle remobilisation. Basically, at late stage of precipitation, the flow velocity would be increased due to lower permeability. As a result, precipitated particles started to mobilise building up a more concentrated and localised blockage.

In this part of *Chapter 6*, firstly, the mechanisms involved in the leakage prevention technique (LPT) will be described. Then, the developed governing equations are introduced. Subsequently, the results of coreflood experiments are discussed and the main findings are highlighted. Next, the modelling results of an exercise (Coreflood-1) performed to evaluate sensitivity of pertinent parameters of the nucleation kinetics are discussed. This task was in particular aimed at reducing the number of parameters that should be tuned during the history matching of the experimental core flood data. Afterwards, the model is further fine-tuned to capture particle remobilisation as a complementary mechanism and a core flood experiment was then simulated. In the last two parts, the predictive capability of the simulator is tested and the results of an exercise for examining large scale leakage paths are given.

6.3.2 Mechanisms involved in LPT

Particle Formation

The process of nucleation and precipitation of a solute from a solution is a dynamic process that requires supersaturation (solution containing more of the solute that it can dissolve under thermodynamic equilibrium conditions). This dynamic process has to be considered as a time-dependent mechanism rather than an instantaneous thermodynamically equilibrated process. Theoretically, based on the condensation of a vapour to a liquid, the phase change occurs by minimisation of the Gibbs free energy (G) with Equation 1 describing the critical nucleus size.

$$r^* = \frac{2\sigma v_m}{k.T.\ln(Ss)} \qquad \text{Eq. 6.1}$$

Where σ is the interfacial tension, T is the temperature, v_m is the molecular volume, k is the Boltzmann constant. Ss represents the supersaturation, which is defined based on the assumption of ideal solution as follows:

$$Ss = \frac{y^*(P_{up},T)}{y^e(P_{down},T)} \quad \text{Eq. 6.2}$$

In this Equation y^* is the solute mole fraction at the upstream pressure conditions of P_{up} and y^e is defined as the solubility at the downstream pressure condition of P_{down}.

This has been adopted for the present case, which involves formation and deposition of solid particles from a gas stream. It should be noted that the above definition of supersaturation can be extended to non-ideal conditions by including the fugacities at each relevant mole fraction. However, for the present case, the assumption of ideal solution is acceptable due to the solute low solubility.

The rate of nucleation, *J*, the number of nuclei formed per unit time per unit volume, can be expressed by the following equation:

$$J = A.exp\left(\frac{-\Delta G}{k.T}\right) \quad \text{Eq. 6.3}$$

In Equation 6.3, the constant A is a characteristic of the solute. As a generic approximation it can vary between 10^{20} and 10^{27}. However, this constant can be estimated for each particular solvent and solute pairs using the following Equation (Türk, 2000):

$$A = \theta\alpha_c v_m N^2 \left[\frac{2\sigma}{k.T}\right]^{0.5} \quad \text{Eq. 6.4}$$

θ = non-isothermal factor (θ=1 for isothermal conditions)

α_c = condensation coefficient (α_c = 0.1 for crystallization process)

$N = \rho_{mixture} * y_e * N_a$ (N_a = 6.023*10^{23})

Substituting the expression of the critical nuclei size (Eq. 6.1) into the Eq. 6.3 gives the formula for predicting the rate of nucleation in terms of solute properties and working conditions;

$$J = A.exp\left(-\frac{16\pi\sigma^3 v_m^2}{3k^3.T^3(\ln(Ss))^2}\right) \quad \text{Eq. 6.5}$$

According to this equation, three main variables control the kinetics of nucleation; *temperature, degree of supersaturation and interfacial tension*. Supersaturation degree has the dominant critical influence on the nucleation rate. It can be considered as the driving force for the particles to be formed, i.e. a higher rate of nucleation for a particular

solution occurs at higher degree of supersaturation. Based on the Classical Nucleation Theory (CNT), interfacial tension between $SCCO_2$ and solid solute has a significant role on the formation of particles; i.e. at higher interfacial tensions, the rate of the particle formation is drastically reduced, which indicates the importance of determining this controlling parameter. IFT between HWS-2 and $SCCO_2$ was measured and reported in Chapter 3 as 0.008 dyne/cm for the solution depressurized from 3000 psig to 2750 psig at 45 ^{o}C.

Another important feature of nucleation kinetics is the existence of time lag (induction time) in initiation of particle formation for low supersaturation degrees. This phenomenon implies a delay in the solidification of solute embryos corresponding to the degree of supersaturation. Equation 6.6 expresses the relationship between induction time and supersaturation (*Ss*) under stationary conditions (Mullin, 2001);

$$Ln(t_{ind}) = \left[-Ln(A) + \frac{16\pi}{3}.\frac{\beta^3 v_m^2 \sigma^3}{k.T(Ln(Ss))^2}\right] \qquad \text{Eq. 6.6}$$

If the saturated solution of the $SCCO_2$+HWS-2 solution at 3000 psig and 45^{o}C, experience a finite pressure drop of 250 psig, no precipitation is formed at the inlet but as the solution flows through the path and after certain induction time, the particles start to form and precipitate. Hence, the concept of induction time should be considered to control/determine the precipitation location. In the governing equations section, the relevant term for induction time under non-stationary conditions will be discussed.

6.3.3 Particle Precipitations

Inertial Impaction

After particles have been formed, they are required to precipitate to cause blockage. One of the main mechanisms of particle precipitation for particles with diameter greater than 1μm is inertial impaction. In this process, the fluid streamlines closer to the point of precipitation (collector) begin to change direction, as shown in Figure 6-18. These streamlines as they turn away from the spherical collector, in order to conserve the no-slip flow conditions, cause a change of velocity which in turn results in deposition. In other words, because of their inertia and deviation from the corresponding streamline, some of the particle trajectories may intersect with the collector surface leading to

deposition. The discussion here is qualitative and aimed at understanding of the physical significance of the inertial impaction.

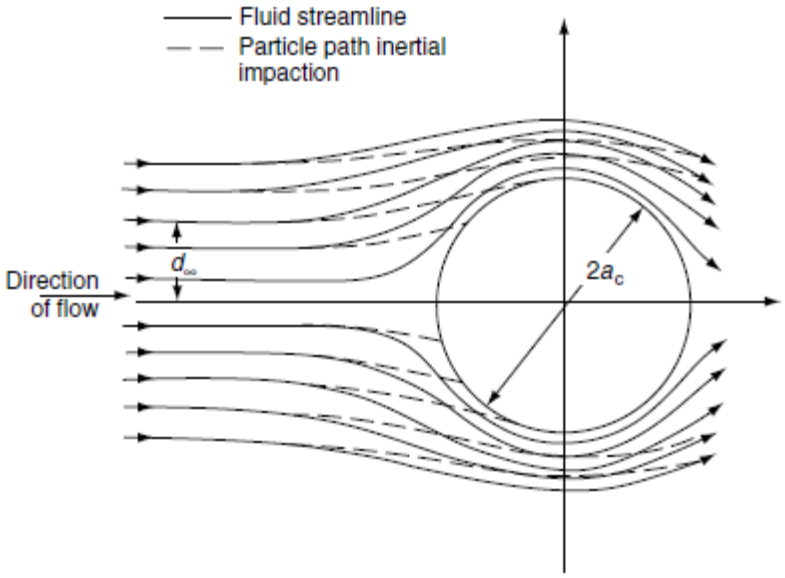

Figure 6-18: Particle deposition by inertial impaction.

The parameter which governs the extend of the inertial impaction is the Stokes number, N_{st}, defined as;

$$N_{st} = \frac{2\rho_p \bar{U} a_p^2}{9\mu a_c} \qquad \text{Eq. 6.7}$$

Where a_p is the particle radius; a_c the characteristic length of the collector; $\bar{U}$ the average velocity of the flow; and ρ_p particle density and μ is the fluid viscosity. The physical meaning of the Stokes number can be explained as the ratio of the inertial force to the drag force, which can be further expressed as the particle's stopping distance if it was multiplied by the characteristics length of the collector.

Sedimentation

In the presence of density difference between the particle and carrier fluid, the gravitational force causes the particles to settle down. The speed of the sedimentation in dilute suspension of solid particles with diameter (a_p) can be approximated by the Stokes law:

$$V_t = \frac{2}{9}\frac{a_p^2 g \Delta\rho}{\mu} \qquad \text{Eq. 6.8}$$

Consequently the single collector efficiency can be described by

$$\eta_G = \frac{2a_p^2 g \Delta\rho}{9\mu\bar{U}} = N_G \qquad \text{Eq. 6.9}$$

Equation 9 implies that for sedimentation to take place, either large particles (large density difference) or low superficial velocity would be needed. The influence of the direction of the velocity would modify the efficiency of capturing the particulates by sedimentation.

In the prevailing flow conditions of the underground storage reservoirs, the particles would be deposited by the sedimentation mechanism due to large density difference and low gas velocity (~1 *ft/day*). Therefore, it is assumed that the particles would precipitate once they are formed. However, it is conceivable to assume that the particles may be transported for short distance before precipitation if the CO_2 velocity increases.

6.4 Mathematical Modelling (governing equations)

The amount of solute formed can be described by the nucleation rate. Therefore, the location and magnitude of precipitation can be modelled by relevant expressions derived from nucleation kinetics. Including the induction time in the formation of the new phase (solid solute) is another crucial part for modelling the location of precipitations. For simulating induction time, the concept of travelling time has been introduced. Travelling time is defined as the time that elapses when an elemental volume of fluid flows between two points in a porous medium. Although the flow is continuous in the leakage path, the leaking CO_2 can be assumed in the form of separate elemental volumes. Therefore, if an elemental volume enters the leakage path, the solid solutes would form when its travelling time exceeds the induction time.

Next part explains the details of the relevant equations. It should be highlighted that, as mentioned before at this stage, suspension flow is ignored, i.e. solid particles, amount of which is determined by the nucleation rate expression, precipitate as soon as they are formed.

6.4.1 Nucleation Kinetics

To the best of our knowledge, there is no method available for modelling of flow of low supersaturated solution of $SCCO_2$ and solid solute through porous media. Therefore, it was required to develop the governing equations in-house. The proposed approach utilises the effective parameters mentioned in the literature such as the supersaturation degree and the concentration of the solution (Debenedetti, 1990).

Induction time

Assuming a one dimensional flow in the leakage path, the cumulative travelling time of each elemental volume, which has flowed from the inlet grid (*i=1*) to n^{th} grid, can be described by the following equation;

$$(t_{travel})_n = \sum_{i=1}^{n} \left(\frac{\Delta x * A}{q}\right)_i \qquad \text{Eq. 6.10}$$

Where t_{travel} is the travelling time. Δx, A, and q are the length, cross sectional area, and flow rate of each grid, respectively. It is necessary to include the parameters pertinent to the history of nucleation kinetics, i.e. what has happened to the solution when it travelled through the preceding grids. Accordingly, the supersaturation degree and the concentration of the solute in each grid block are used as weight factors for the travelling time. To have a more general solution, appropriate dimensionless numbers (Equations 6.11 and 6.12) were defined to be included in the induction time expression (Eq 6.13).

$$S_i = \frac{Ss_i}{Ss_{max}} \qquad \text{Eq. 11}$$

$$W_i = \frac{\omega_i}{\omega_{max}} \qquad \text{Eq. 12}$$

$$(t_{travel})_n = \sum_{i=1}^{n} (C_{11} * {S^N}_i + C_{12} * {W^M}_i) \left(\frac{\Delta x * A}{q}\right)_i \qquad \text{Eq.13}$$

Where S and W are dimensionless supersaturation and concentration groups respectively and C_{11}, C_{12}, N, and M are the coefficients and exponents, which are required to be tuned based on history matching of some experimental data. The expressions in the first bracket describing the effect of supersaturation and concentration are called *hysteresis* terms. In Equation 6.13, four constants were considered for the preliminary analysis of the process

since the effect of each parameter in controlling the induction time was not well-understood. However, as described below and our understanding evolved, it was noted that fewer constants would suffice for proper modelling of the particle formation. Generally speaking, the main criterion for particle formation is the difference between the stationary induction time of each grid cell and the cumulative travelling time.

$$I = (t_{ind})_n - \sum_{i=1}^{n}(C_{11} * S^N + C_{12} * W^M)\left(\frac{\Delta x * A}{q}\right)_i \qquad \text{Eq. 6.14}$$

Where t_{ind} is the induction time for n^{th} grid in the leakage path (equation 6.6). That is, based on Equation 6.14 the process of particle formation initiates in the n^{th} grid if '*I'* becomes negative.

Nucleation

When this criterion is met, it has been proposed to estimate the amount of the solute to be deposited based on the nucleation kinetics including the effect of imposed supersaturation in the preceding grids, i.e. the *hysteresis* effect, using Equation 6.15.

$$J = (\sum_{i=1}^{n}(C_{21} * S^a + C_{22} * W^b)) * (J)_n \qquad \text{Eq. 6.15}$$

$(J)_n$ is the nucleation rate in the stationary conditions (Equation 6.5). Like the induction time equation, four parameters (2 coefficient and 2 exponents) have been considered that should be tuned based on history matching of some experimental data.

Material Balance

However, the equation for nucleation rate must have a constraint to limit the amount of particle formation to that obtained by material balance (i.e. weighting the core before and after the test) at the end of experiment. This constraint is based on the maximum amount of solid solute that the solution can drop out in any grid block at any time step, which is obtained from thermodynamic equilibrium conditions (Equation 6.16);

$$J_{max} = \left(\frac{\phi * \Delta x * A * \rho_{CO_2}}{MW_{CO_2}}\right)(\omega_i - \omega_{eq}) \qquad \text{Eq. 6.16}$$

Where ω is the concentration in supersaturated (*i*) and equilibrium (*eq*) conditions. The first bracket gives the mole of CO_2 in each grid while the second one shows the maximum deriving force for the particle formation, i.e. the difference in the concentrations.

Equations 6.14 and 6.15 are used to control the entire process of particles formation. Equation 6.14 (induction time) controls the location of the precipitation. Equation 6.15 (nucleation rate) determines the amount of precipitation. Equation 6.16 is used as an upper limit of Equation 6.15 and primarily for the purpose of matching the total amount of precipitated solute within the core at the end of experiment, i.e. if nucleation rate cannot be higher than that predicted by Equation 6.16 in any grid block and at any time step. That is, solution of Equation 6.15 should not exceed calculated value of Equation 6.16. It will be shown that we use Equation 6.16 is sufficient for the present work.

Porosity and Permeability Reduction

As solid solute precipitates it reduces porosity and more importantly the permeability of the porous medium, which leads to blockage of the leakage path. A power law function was used to relate the porosity to permeability as expressed by Eq. 6.17a. (Nelson, 1994)

$$k = c * \phi^n \qquad \text{Eq. 6.17a}$$

Where *k* and ϕ are absolute permeability and porosity respectively.

This equation has been widely used in the petroleum industry due to its simplicity and flexibility albeit with different constants and exponent values. To reduce the uncertainty of contribution of the constant, we can write it for two states to eliminate *c* and relate the variation of porosity to that of permeability. Therefore

$$k_{i+1} = k_i \left(\frac{\phi_{i+1}}{\phi_i}\right)^n \qquad \text{Eq. 6.17b}$$

Where *n* is a constant, which controls the rate of permeability reduction to that of porosity reduction, which can easily be linked to the amount of precipitated solid solutes.

6.4.2 Implementing the equations

Solution technique

The above sets of Equations are solved in an excel based platform. These calculations have been linked to Computer Modelling Group (CMG-GEM) reservoir simulator, which solves the corresponding two-phase flow equations for flow of fluids through a core, with fixed length and cross-sectional area. The number of grids in the constructed CMG-GEM based model has initially been selected 100, which ensures minimum numerical dispersion. It is assumed that the solute content of $SCCO_2$ at the inlet of the leakage path is fixed and equal to the solid solubility at equilibrium conditions. Initial distribution of porosity and permeability are assigned for this porous medium. These properties change subsequently as a result of precipitation of solid solute. In fact, CMG-GEM is run for one time step and the resulting pressure distribution and the flow rates are extracted to be used in the nucleation and permeability reduction equations, which are then used for the flow calculation by CMG-GEM in an explicit mode.

These equations are solved numerically to describe and investigate the role of pertinent parameters on the formation of the blockage. The corresponding algorithm , which consists of consecutive use of flow equations in CMG-GEM and kinetic nucleation and permeability reduction equations in our code are described as below;

1) At the end of each CGM-GEM time step the pressure of each grid is used to calculate the equilibrium solubility. Then, the degree of supersaturation is obtained by dividing actual solid content to the equilibrium solubility.
2) The flow rates obtained from the CMG-GEM simulation and the calculated supersaturation is then used to evaluate the travelling time (Equation 6.13).
3) The static induction time of each grid is calculated by Equation 6.6.
4) The "*I*" factor in Equation 6.14 is determined for each grid to evaluate when the particle formation commences, which is when its value is negative.
5) If *I* becomes negative, the particles are formed and immediately afterwards precipitation takes place according to the nucleation rate expression (Equation 6.15). If *I* is negative for a cell, it is negative for subsequent cells too, i.e. precipitation starts from the first upstream cell with negative *I* and continues in all subsequent cells.
6) At the end of each time step, the volume of precipitated solute is calculated to reduce the porosity. The resulting porosity is then used for updating the

permeability based on Equation 6.17b. It should be noted that in Equation 6.17b the subscript (*i*) represents two consecutive time steps.

7) The concentration of solute in the solution is updated according to the loss of solute due to precipitation. It should be noted that the, assumption of perfect mixing between the in-situ and influx solutions is made for adjusting the concentration of solid solute in each grid block.
8) When the porosity and permeability of each grid are updated, the input data of the (CMG-GEM) reservoir simulator will be set up with the new values and the flow calculation for the subsequent time step is performed and the program returns to step 1.

6.5 Experimental investigation and findings

Identifying the roles and significance of underlying mechanisms requires designing and performing a limited number of experiments in which the dynamics of particle formation and precipitations would be accounted along with CO_2 flow. Visualisation of flow through porous media is a valuable tool enabling us to contemplate directly the process of particle formation and blockage evolution. Using a glass micromodel, which accommodates a see-through capability, a number of visualisation experiments were designed and carried out to investigate the role of pertinent parameters on the performance of leakage prevention technique. It should be noted that the findings obtained from these observations can be later used in analysing the modelling parameters. Figure 6-19 shows the setup that was used for visualisation experiments in which, the blue porous pattern represents the physically simulated leakage path and the CO_2 + solute solution is allowed to flow through.

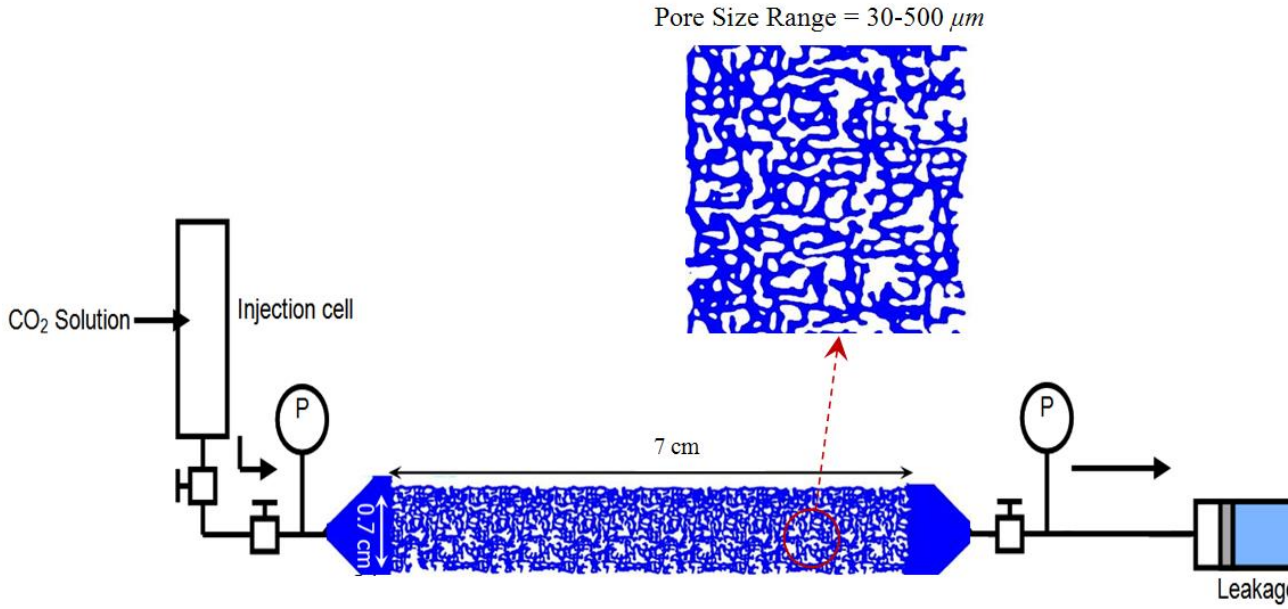

Figure 6-19: Experimental setup of the micromodel illustrating the basic dimension of the porous medium. On the magnified section of the micromodel, the pore size distribution range is shown. Two cells in the both ends of the micromodel establish the pressure conditions across the leakage path.

Following visualisation experiments were performed to observe the formation of particles and consequent precipitations (28 experiments in total);

7. Using different solutes (5 solutes)
    a. 18 different scenarios of pressure drop were imposed.
8. Impact of impurities (Nitrogen)
    a. Using 2 solutes at 3 different pressure drop regimes.
9. Impact of presence of Water
    a. 1 pressure drop scenarios were applied.

Figure 6-20 demonstrates an example of blockage formation occurred in one of visualisation experiments where a solution with composition of 95% CO_2 and 5% N2 was brought into equilibrium with a solid solute and the impact of CO_2 stream impurity was investigated. Here, two main events should be highlighted for utilising in modelling exercises; (i) very concentrated precipitation formed at very end of leakage path, which is used in correlating the change in porosity with the change in leakage path permeability and (ii) particle reconfiguration towards the end of the experiment, which is considered as the basis for particle remobilisation employed in later for modelling the 100%

permeability reduction. Furthermore, the particle formation would trigger close to the path outlet, which can be directly linked to the presence of the induction time concept (time lag in particle formation) that is the foundation of this mathematical modelling.

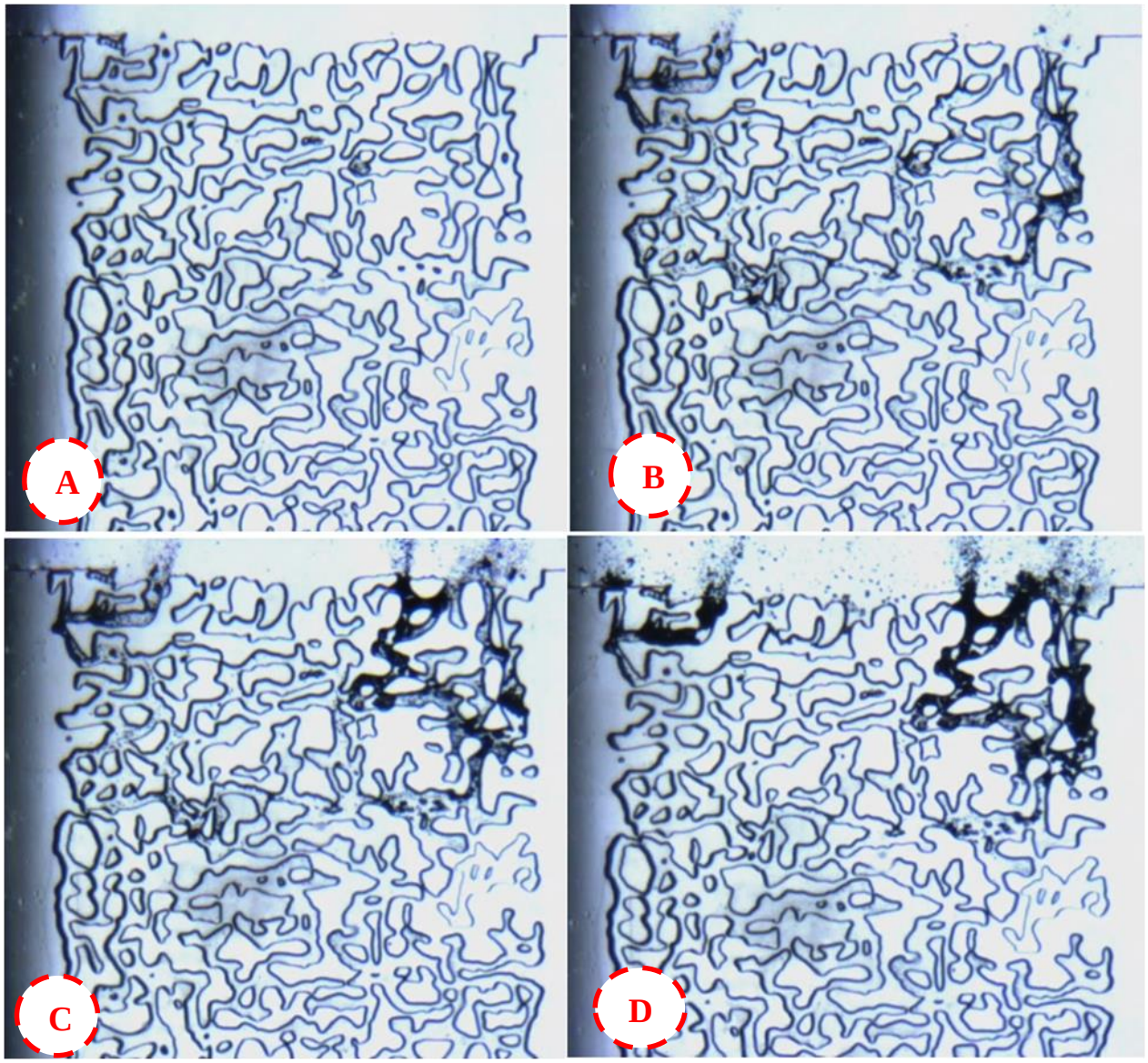

Figure 6-20: leaking at 1900 psig; (A) initial state of the micromodel before leakage, (B) start of particle formation, (C) particle precipitation, and (D) full blockage.

Apart from the visualisation experiments, which were performed to identify the underlying mechanisms, developing and verifying the mathematical model requires conducting flow experiments in rocks (core plugs). Hence, two types of flow experiments were conducted; capillary tube and coreflood tests which can also highlight the role of porous medium in the precipitation process. In capillary tube experiment, the solid solute

and supercritical CO_2 were brought into equilibrium and then, the resulting solution was flowed through the capillary tube with one end exposed to atmosphere pressure. A durable blockage was formed. However, it should be pointed out that the results indicated a sudden pressure release, which is not applicable to transient process of particle formation occurring in slow flow rates of real CO_2 storage conditions. Therefore, a number of core experiments were performed with more realistic flow rate conditions. These flow/precipitation experiments was carried out by the below procedure followed;

1. A clean set of core plugs was put together to construct the composite core. Core plugs were carefully selected and aligned to be able to control the pressure drop and flow rates. This experimental design would enable us to physically simulate real long leakage paths in lab scales.
2. Having established the working temperature (45^{o}C), the composite core was pressurised to the desired pressure (3000 psig) by injecting plain CO_2.
3. The resident CO_2 was displaced with our solution (CO_2 + solid solute).
4. The target pressure drop, e.g. 250 psig, was imposed across the composite core by injecting (inlet) and retracting (outlet) at constant pressures of 3000 and 2750 psig, respectively. The solution was allowed to flow in the imposed pressure drop for the extended period of time (6-10 days).
5. All the pertinent indicators of flow/precipitation were recorded, i.e. injection/retraction flow rates and inlet/outlet pressures.

Five coreflood tests were performed aiming at identifying time-dependency of particle formation and precipitation. Flow rate and length of the leakage path were considered as the main variables for designing the coreflood experiments. Increasing the flow rate would reduce the time during which the solution would undergo the pressure drop. On the other hand, changing the length of composite core (leakage path) would shed some light on the location of precipitation. Therefore, the experimental results would produce sufficient insights on how the kinetics of particle formation affects the blockage evolution, which can in turn lead to development of the relevant mathematical model. Figure 6-21 shows the composite core designed for our coreflood experiments in which a low and high permeable core plugs would enable us to physically simulate different types of leakage paths.

Figure 6-21: Composite core after first core flood test indicating the arrangement of tight and high permeable core plugs.

Table 6-3 summarises the details of experiments performed to investigate the evolution of blockage in our leakage prevention technique. In this table, the prevailing conditions of the experiments were described along with the main objective and the condensed findings attained from the experimental results. In Coreflood-1 to 5, HWS-2 was used as the solid solute at identical pressure and temperature conditions. The flow rate at Coreflood-1 is ultralow and successful blockage was obtained. After the test finished, the precipitants in the core was cleaned and the blockage mass was weighed, which was less than 1 gr. Therefore, the precipitation has occurred in a concentrated manner. However, for Coreflood-2 and 3, various flow rates were imposed by utilising different core plugs.

For performing the coreflood experiments, two approaches were employed for delivering the solid solute into the solution; surface mixing and downhole mixing. In the surface mixing, the solute and solvent (CO_2) was brought to equilibrium in a cylinder prior to injection into the core. In the downhole mixing, the solid solute was packed into a pipe, which was placed before the core inlet, and the CO_2 was flowed through the packed bed and the resultant CO_2 would become saturated with the solute. Occurrence of blockage in both cases would demonstrate high efficiency of the leakage prevention technique irrespective of solute transport method. Coreflood-4 and 5 were carried out utilising downhole mixing approach. A firm and durable blockage was formed in Coreflood-4 confirming the effectiveness of leakage prevention technique regardless of how the solution was prepared.

In Coreflood-5, the length of the core was reduced by one third to identify the exact location of the precipitation. No blockage was formed revealing that the previous blockages were built up near the core outlet. In Coreflood-6, HWS-3 was used instead of HWS-2 while other parameters were kept identical. The leak was stopped but at higher pressure drop. The experimental results indicated a different response for HWS-3 which

highlights the role of solute characteristics in response to imposed pressure drop and hence, each particular solid solute has its own behaviour when a leak occurs.

Table 6-3: Details of core experiments performed to capture the undelying mechniams controlling the precipitation and blockage formation.

Test ID	Solute, Temperature (C), Pressure (psig)	Objective	Findings
Coreflood-1	HWS-2 45C, 3000 psig	• First trial. • Ultralow flow rates.	• The leakage path was blocked firmly. • 1 gr of precipitation suffice ceasing the leakage path. • The blockage body was formed locally. • In lab scales, there is an induction time required to have precipitation started.
Coreflood-2	HWS-2 45C, 3000 psig	• Initially 10 times higher flow rate (with respect to Coreflood-1). • Investigating the rate (time) & DP dependency of the precipitation process.	• Initially no effective precipitation occurred. • 4 times higher pressure drop resulted in full blockage. Higher DP reduces induction time is reduced significantly ensuring formation of blockage within the core. • Clear dependency between flow rate and length of leakage path was identified.

Coreflood-3	HWS-2 45C, 3000 psig	• 3 times higher flow rate (with respect to Coreflood-1) by replacing a tighter core plug with a more permeable one. • Identifying the role of flow rate on the formation of blockage. (what is the differnc between 2 &3)	• A firm and durable blockage formed. • Blockage was formed locally. • In lab scales, flow rate and length of leakage path are important in formation of effective blockage.
Coreflood-4	HWS-2 45C, 3000 psig	• Imposing similar conditions (Coreflood-3), but downhole mixing method was employed as an alternative against surface mixing.	• Initially a blockage was formed but it was not firm enough. • After reopening of the first blockage, another firm and durable blockage was formed subsequently. • Downhole mixing method is a conceivable approach for solute transport.
Coreflood-5	HWS-2 45C, 3000 psig	• Imposing similar conditions (Coreflood-4), length of leakage path was reduced to investigate the role of experimental design in lab scales.	• No effective blockage was formed. • Experimental design is a crucial step in investigating the effectiveness of our leakage prevention method. • This experiment highlight that the importance of scale of leakage path should be considered.
Coreflood-6	HWS-3 45C, 3000psig	• Employing similar conditions (Coreflood-4), another solute was used (HWS-3). HWS-3 and HWS-2	• Compared to HWS-2, blockage was formed at higher pressure drop (i.e. DP=450, 200 psig higher

		have similar solubilities in supercritical CO2.	than those of above). • In addition to solute solubility, other solute characteristics are in play in particle formation and precipitation.

In summary, two distinct features should be inferred from the core experiments, which need to be considered in any modelling investigation; (i) time lag in particle formation and (ii) localised and concentrated precipitation. The time lag in particle formation can be expressed through nucleation kinetics while the form of precipitation can be captured through the combination of nucleation kinetics and particle mobilisation. These crucial mechanisms cannot be modelled in conventional simulator and it is necessary to develop the relevant equations expressing the time-dependent processes.

6.6 Modelling Results (based on Coreflood-1 experiment)

At this stage a sensitivity analysis was performed to evaluate the impact of pertinent parameters and in particular assess the possibility of reducing the number of constants, which based on Equations 6.14, 6.15 and 6.17b are 9. The results demonstrated that, the *hysteresis* terms (second term on the RHS) in Equations 6.14 and 6.15 can be combined into one term that would sufficiently characterise the precipitation process. This required defining a new dimensionless number, which is the product of supersaturation and concentration numbers;

$$Hyst_i = (S_i) * (W_i) \qquad \text{Eq. 6.18}$$

Therefore, instead of Equations 6.14 and 6.15, we have two new equations for the induction time and nucleation rate;

$$I = (t_{ind})_n - \sum_{i=1}^{n}\left(C_{11} * {Hyst_i}^N\right)\left(\frac{\Delta x * A}{q}\right)_i \qquad \text{Eq. 6.19}$$

$$J = \left(\sum_{i=1}^{n}\left(C_{21} * {Hyst_i}^B\right)\right) * (J)_n \qquad \text{Eq. 6.20}$$

This reduced the total number of the parameters (coefficient and exponent) to be tuned to 5; four (C_{11}, C_{12}, N, and B) for nucleation kinetics and one (n) for correlating permeability change with porosity reduction.

Having modified the number of constants in the equations, the performance of the model was investigated using the some of the reported coreflood data. For this purpose, two different coreflood tests with distinct features have been selected. The Coreflood-1 experimental data were used to tune the values of these five constants. The other ones will be used for assessing the predictive capability of the proposed model

6.7 Modelling Coreflood-1 experiment

The properties of the core plug used in Coreflood-1 experiment are listed in Table 6-4. It should be pointed out that HWS-2 was used as the solid solute and the solution was injected at a constant rate and the outlet pressure was fixed at 2750 psig.

Table 6-4: Basic properties of core plugs; T1, and H1 representing tight and high-permeability cores.

Core ID	Length (cm)	Diameter (cm)	Weight (gr)	Porosity (fraction)	Permeability (md)
T1	3.44	2.59	48.683	0.038	0.002
H1	13.81	2.54	143.762	0.163	225

Based on the micromodel visualisations, the precipitation and the blockage took place in several locations in the form of concentrated bodies targeting the main flow path in the porous media. Figure 6-22 depicts the magnified image of the micromodel showing these locations for this solution. It is noted that selective sections of the micromodel that has been contributing to the fluid mobility are blocked. This suggests that a small change in the overall porosity results in a large reduction in permeability, i.e. blockage of the flow path. This observation would help identifying the "n" exponent in the correlation of permeability and porosity (Equation 6.17b). In line with this, our simulation runs have suggested that the exponent should be between 25 and 30, i.e. small porosity reduction should result in large permeability reduction. For simulation of the current experiment a value of 30 has been selected. This value should not be linked to the values found in the

literature that relates naturally occurring porosity and permeability with n varying in the range of 3-5.

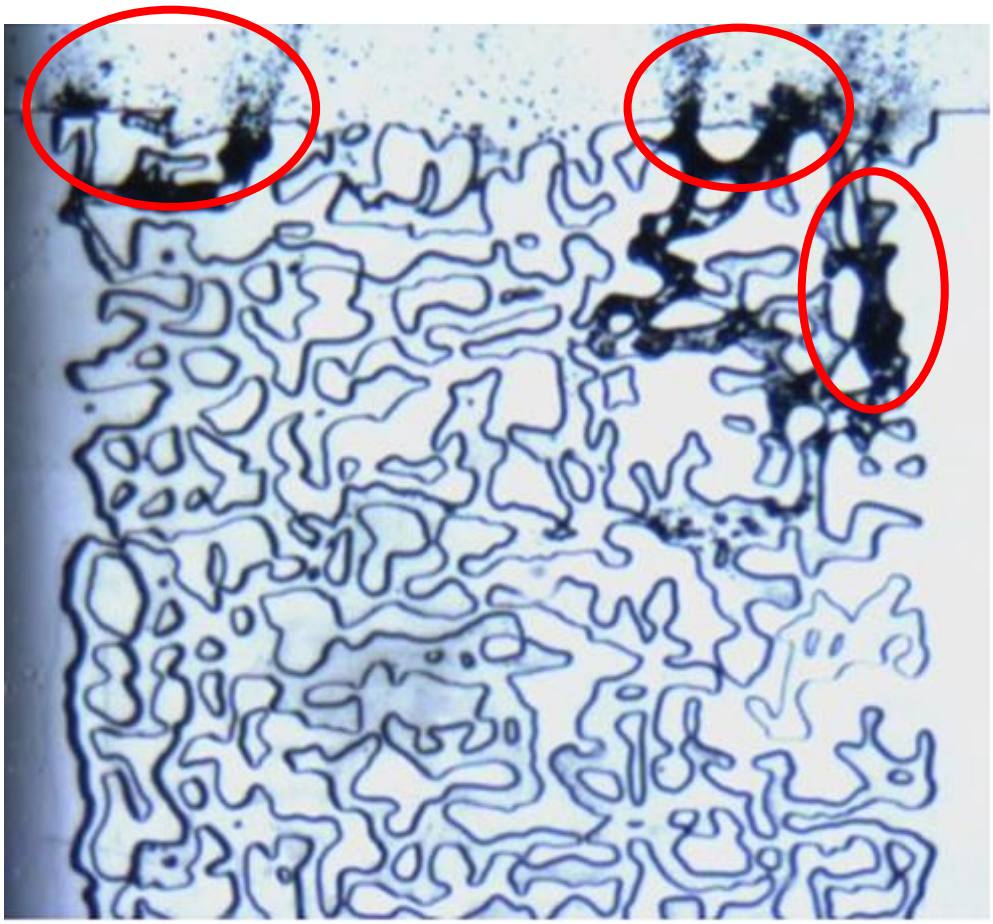

Figure 6-22: Localised precipitation observed in the micromodel experiments indicating the relationship between amount of precipitation and permeability reduction; that is, permeability is reduced significantly with small amount of precipitation or small reduction in porosity.

One of the main findings from coreflood experiments was the approximate location of the precipitation and blockage shown to be close to the end face of the porous media. In fact in one of the core flood experiments it was demonstrated that the most likely region for the precipitation was 7-10 cm away from the outlet face of the core. Therefore, in our simulation the location of precipitation is chosen to be somewhere after 70^{th} grid, i.e. no precipitation between first and 70^{th} grid (a condition imposed, verified with experiments). The induction time expression (Equation 6.19) is solely responsible for determining the location where formation of solid particles and their precipitation starts. Therefore, the relevant exponents (C_{11} and N) need to be tuned according to the flow behaviour in the grids with precipitation. It should be noted that in this process the first upstream cell with

negative *I* plays a big part particularly in determination of these coefficients. In fact it will be shown that C11 is determined by constraining the model to start the precipitation process in the 70th grid block.

To understand the behaviour of the model it is useful to study the trend of its results when C_{11} and *N*, as the two parameters of the super saturation hysteresis term (first term of the first bracket in Equation 6.14), are individually varied. Figure 6-23 illustrates the variation of C_{11} during the optimisation process at different hysteresis exponent (*N*). It is noted that, for different N values of 1, 2 and 5, the overall trend of C_{11} variation is similar. Based on these results, it was concluded that C_{11} can sufficiently control the precipitation process and hence the value of the exponent (*N*) can be fixed at unity.

Furthermore, based on the data of Figure 6-23, it is noted that generally C_{11} remains constant for first 300 time steps. However, after 300 time steps, C_{11} starts to increase sharply, which as explained below is due to the pressure build up in the grids prior to the 70th grid block.. That is, when the pressure starts to build up, there would be a rise in the equilibrium solute solubility value and hence a reduction in supersaturation (Equation 6.2,), which is the driving force for the precipitation.

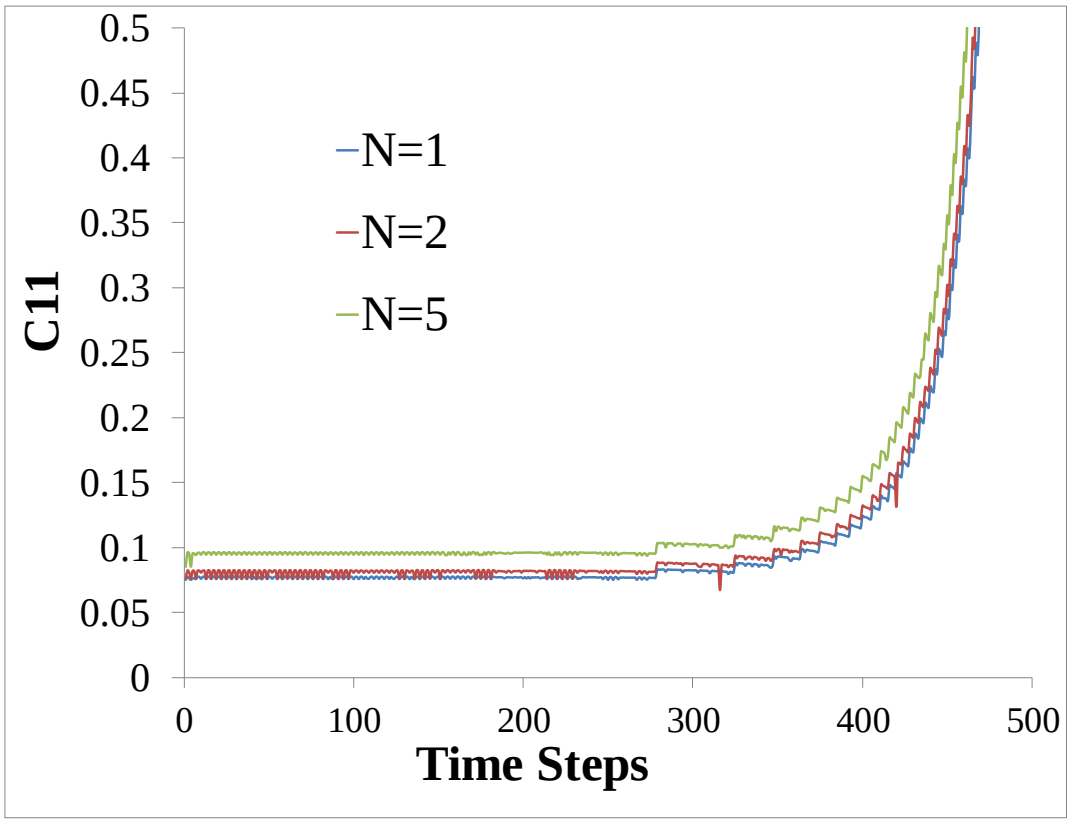

Figure 6-23: Variation of C11 coefficient during the optimization process of the simulated core experiment.

At this stage, another sensitivity was run to evaluate if C11 should vary during the simulation process (particularly after 300 time steps in Figure 6-23) or a constant value (which is observed during the first 300 time steps in Figure 3) can produce an acceptable match. Two different sets of simulations were performed with constant and variable C11 and the impact on the final permeability profile was studied as shown in Figure 5. The constant C11=0.08138 is an average value for C11 corresponding to the first 300 time steps of the blue curve (with N=1) in Figure 6-23. The variable C11 case corresponds to the whole blue curve of Figure 6-23. It is noted that the permeability of the high-permeable plug shown in Figure 6-24 reaches to zero only if the coefficient of the hysteresis term varies with time.

In the case of contact C11, the nucleation equations predict a permeability reduction from 225 md to 5 md, which is about 98% decrease in the permeability. As it was described earlier, the variable coefficient cannot realistically describe the process of nucleation kinetics. Therefore the non-blocking behaviour of the constant coefficient can be attributed to the simplifying assumptions made particularly lack of suspension flow of the particles, which needs to be investigated further. In other words, the rest of the permeability reduction should be modelled with another mechanism, which can be the transport of solid particles by suspension flow. As described above in Section 6.3.3, the suspension flow is mainly controlled by velocity of carrier gas ($SCCO_2$) and the weight of each particle. Assuming constant size of particles precipitated, the velocity of the flowing CO_2 would increase as the precipitation builds up. This change in micro-scale CO_2 velocity occurs due to the resultant flow restriction stemmed from the precipitation. This will results in some of the particles transported in suspended form, which can be deposited in the subsequent grid blocks leading. In other words, it is expected that the suspension flow would result in the accumulation of particles more locally leading to the full blockage. However at this stage and for the rest of the report, the results with constant C11 would be acceptable, which gives over 98% reductions in the original permeability.

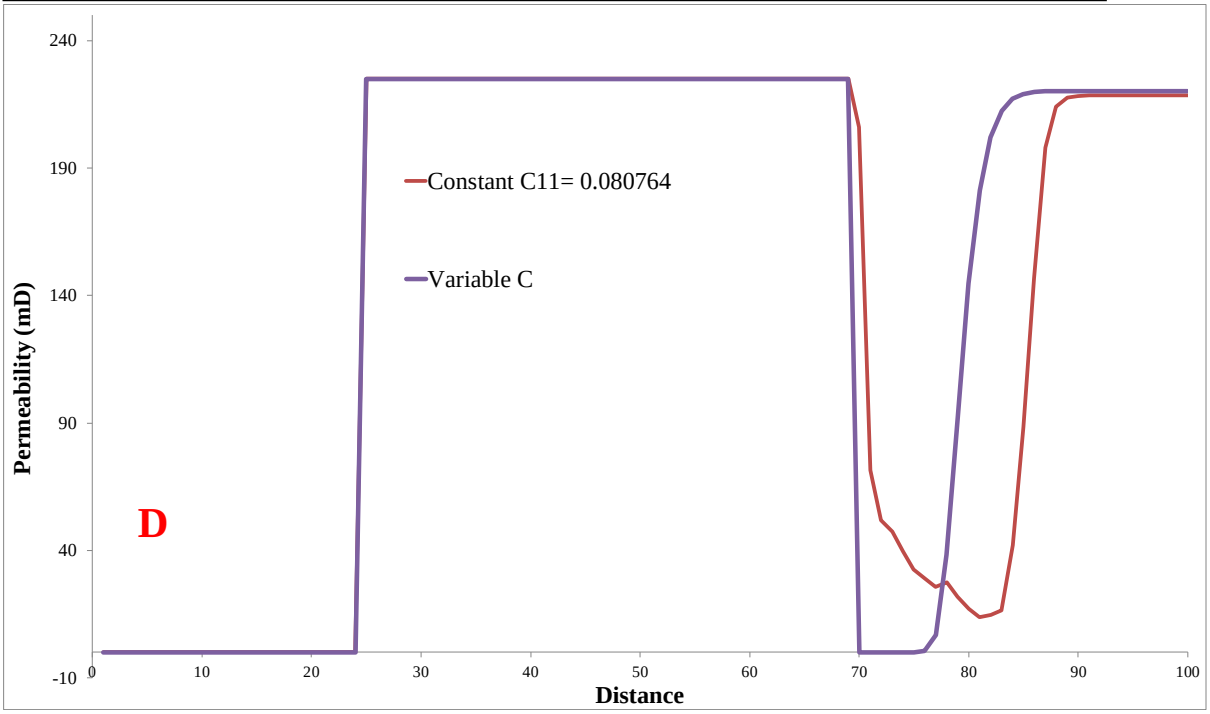

Figure 6-24: Permeability distribution at end of the simulation run with a variable or constant value of remaining unknown coefficient of induction time, i.e. C11. No precipitation took place in the inlet side and the permeability of tight core (close to inlet) is 0.002 mD which has been highlighted.

The depth of penetration for precipitating the particles, which is defined as the number of the grids from the target grid until the precipitation becomes negligible, depends essentially on two factors; firstly, the advancement of the solid solute precipitation frontal (i.e. first grid block in which precipitation commences) for each time step and secondly, the rate of nucleation (Equation 6.20). In simulating this Coreflood-1 experiment, the depth of penetration for effective precipitation during each time step was approximately 5 grid blocks, e.g. in a time step the precipitation occurred between 70-75 grids. However it should be noted that overall precipitation occurs within 20 adjacent grid blocks. Figure 6-25 exhibits the index of the first grid before which there is no precipitation at each time step. It should be noted that as mentioned before precipitation does not occur in any grid block prior to the 70^{th} grid block. It is noted that the index of this target grid varies between 70^{th} and 85^{th}, which means the entire precipitation area was between 70-90 grid blocks due to the 5 grid block penetration depth.

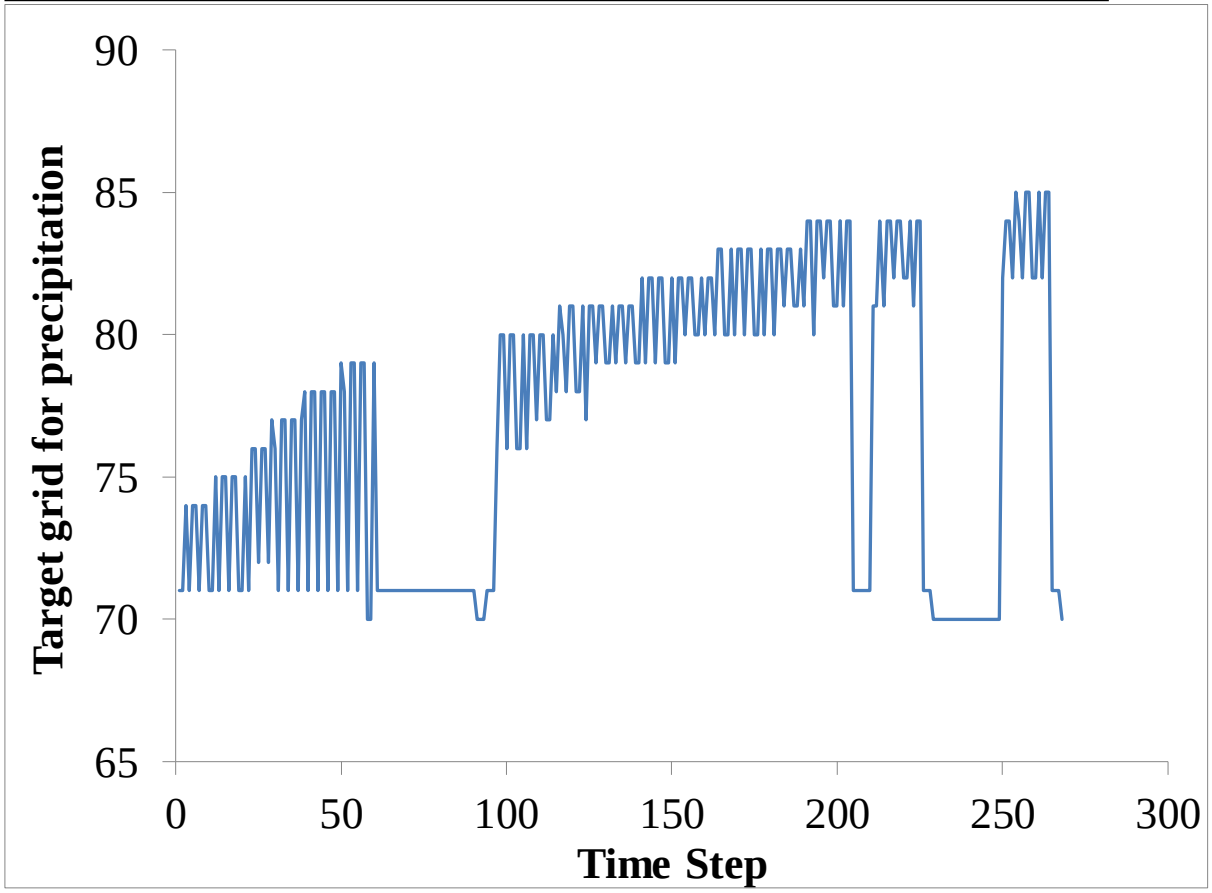

Figure 6-25: The index of the first grid before which there is no precipitation at each time step.

The other two parameters that should be tuned are the coefficients of nucleation rate, i.e. C_{21} and B in Equation 6.20. In the Coreflood-1 experiment, the precipitation rate with time was not measured. Therefore, it was not possible to determine these by matching the profile of the precipitation. However, the final amount of solid precipitated in the core is known (i.e. 0.872 gr), which can be used for tuning the nucleation rate parameters. In this process, it was noted that the tuned values of C_{21} and B in Equation 6.20 give *J* values that are equal to its maximum values as stated by Equation 6.16. As it was mentioned above, this suggests that Equation 6.16 can replace Equation 6.20 and there is no need for additional tuning (this should be mentioned above). In other words, Equation 6.16 do not have any unknown coefficients and hence, tuning of "induction time" parameters in Equation 6.19 automatically honours the mass balance obtained by weighting the core before and after the experiment. Figure 6-26 shows the precipitation profile which was simulated using tuned parameters. The curve of the cumulative precipitation has a steady trend indicating strong dependency between the rate of precipitation and the rate of CO_2 flow in the experiment. However, in the model, the incremental precipitation rate (dashed

green line in Figure 6-26) fluctuates around the average value of 0.001 gr per time step of simulation, which is roughly equivalent to 0.0045gr/hr. The fluctuation in the incremental precipitation happens mainly due to variable time steps selected by the CMG-GEM simulator. It should be noted that we plot the cumulative precipitation, which has a reasonably acceptable smooth trend.

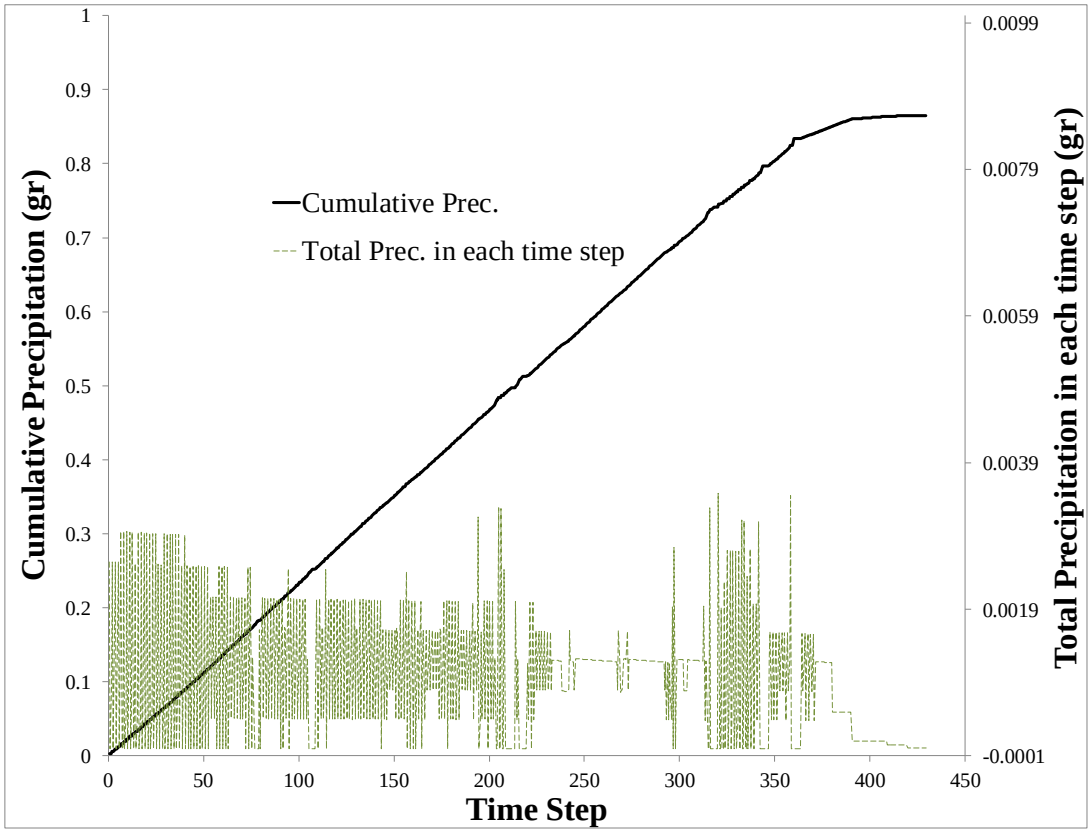

Figure 6-26: Cumulative and incremental amount of solid solute precipitated during the simulation of the core experiment.

6.8 Discussion for implementing particle remobilisation

In this modelling approach, the equations are solved numerically through coupling the nucleation kinetics and the flow through porous media. The results revealed that implementing the nucleation kinetics cannot fully address the occurrence of blockage in the coreflood experiments. 98% of the blockage was simulated when the corresponding tuning parameters were matched to the one of the coreflood experiment. However, to capture the remaining 2% needed to obtain complete blockage, other mechanisms had to be included to the model.

We have investigated this issue and concluded that the deposition of the particles that were deposited upstream and then mobilised in the form of suspension flow is the mechanism that should be captured to have 100% blockage during simulation of a core flow experiment. In this part of the report, the conditions under which this mechanism can be dominant will be discussed. That is, the conditions under which the initial deposition of particles occurs, the particles start to be mobilised in the suspension form this location and finally they deposit further downstream where the blockage is occurring, are highlighted. A description of the governing equations that have been developed and implemented in the software is given. Finally, the developed model is used to complement the previous simulation exercise carried out on the Coreflood-1 experiment.

6.9 Particle mobilisation

Figure 6-24 (red curve) shows the permeability distribution obtained in our previous simulation attempt, which included only the nucleation kinetics. Based on this result, the precipitation has targeted about 20 grid blocks, which is equivalent to 3.45 cm of the core length (one fifth of the whole core). The area targeted by the precipitation was not determined experimentally. However from the micromodel experiments, the observation was that the blockage was formed in less than on tenth of the leakage path as shown in Figure 6-22. Therefore, if we assume that the analogy between micromodel and coreflood experiments is valid, the area of precipitation predicted by the simulator should be less in order to produce more realistic simulation. In other words, a modification is needed to be put in place for implementing this reduced precipitation area, which would also address lack of achieving 100% blockage.

Since, in the previous simulation exercise, the simulated amount of precipitation matched the experimental information, the modification in the area of precipitation should not be associated with further particle generation. Thus, the amount of particles formed as a result of nucleation kinetics as captured by the model, is sufficient. However, our observations of the dynamic process of blockage evolution indicated that the nucleated particles would undergo two possible phenomena; (i) growth/coagulation of the particles and (ii) mobilisation of the precipitants. Growth/coagulation of particles is a highly complex process in which molecular forces should be taken into account. Furthermore, the mobilisation of particles was observed to be a more dominant phenomenon compared to growth/coagulation of particles. That is, particles will start to mobilise sooner than they

coagulate. The mobilisation of solid precipitants should also capture the reduction in the precipitation area discussed above. It should also be noted that as described below the movement of precipitants can be explicitly included in the simulator without significant modification in the original model. Nevertheless, the dynamics of the process needs to be captured properly.

It is believed that mobilisation of precipitants needs to be triggered by a disturbance in flow properties such as pressure profile or local flow rates. Previously, it was identified that the nucleation kinetics mechanism slows down considerably when the supersaturation distribution started to reduce. The build-up of the precipitated particles is accompanied by changes in pressure profile and hence the flow properties. The main driving force for mobilising the particles is the drag force exerted on the precipitants, which highlights the importance of local velocity of the flowing phase, i.e. CO_2 solution. Figure 6-27 shows the flow velocity distribution between 30th and 100th grid blocks during the same simulation run mentioned above. The velocity has been calculated by applying Darcy law for flow through porous media using the following equation;

$$u = \left(\frac{k}{\phi}\right) * \left(\frac{A^2}{l}\right) * \Delta P \quad \text{Eq. 6.21}$$

Where, u and ΔP are the flow velocity of carrier fluid (CO_2 solution) and local pressure drop between the grids, respectively. k, ϕ, A, l are permeability, porosity, cross-sectional area and length of the grid cells. According to Figure 6-27, the flow velocity increases from 68th to 88th grid blocks as simulation proceeds.

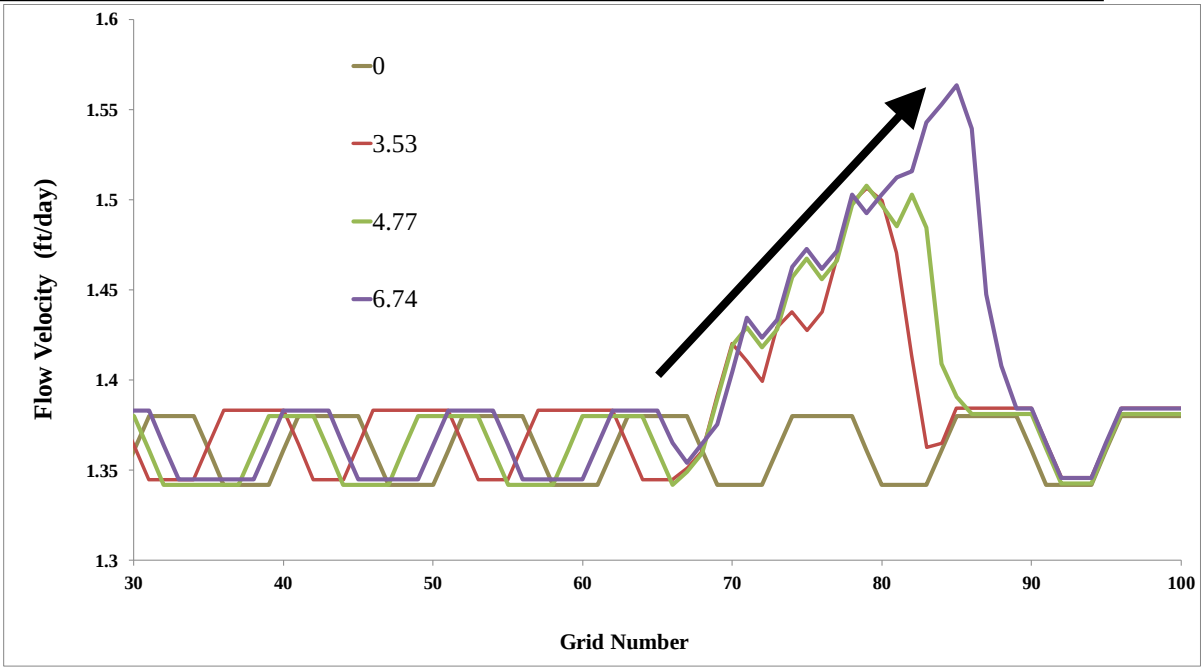

Figure 6-27: Distribution of flow velocity in the leakage path at 0, 3.53, 4.77, and 6.74 days. The black arrow indicates the jump in the velocity occured between 68th to 88th grid cells.

The sharp increase in flow velocity (i.e. significant flow disturbance) happens, in the area targeted by the precipitation. Therefore, the foundation for implementing the particle mobilisation is the disturbance in the flow velocity caused by the precipitation. In other words, a fraction of the precipitants can be detached and mobilised (in the form of suspension flow) and carried over the flowing phase. The significance of particle mobilisation is assumed to be proportional to the degree of the velocity disturbance. Another crucial step in this process is the definition of a constraint under which the mobilised particles would be re-deposited. Based on one of the precipitation mechanisms, i.e. inertial impaction, the suspended solids would reside in the areas where the highest velocity occurs. Based on this notion, the mobilised particles would remain in suspension and would be deposited downstream around the grid block with the highest velocity. In the subsequent section, the corresponding equations developed to capture this concept and the algorithm for implementing the governing equations will be discussed.

6.9.1 Algorithm of particle mobilisation

1. The coupled equations of nucleation kinetics and flow through porous media are solved to calculate pressure distribution and solid precipitation.

2. At the first stage of simulation, the velocity distribution is determined and the maximum velocity is considered as the base value to be compared with the corresponding values in the subsequent simulation steps.
3. At any other stage of simulation, the maximum velocity in the determined velocity profile is identified. The ratio of this velocity and that obtained in step two is considered as a criterion for mobilisation of solid particles as per Equation 6.22. (where u_{max}-base (initial before k starts to drop, it is constant)

$$U_{TF} = \frac{(u_{\max})_i}{(u_{max})_{base}} \qquad \text{Eq. 6.22}$$

4. Once the selected velocity threshold factor is reached, a fraction of mass of the precipitated particles is mobilised based on Equation 6.23.

$$(m_{mob})_i = \theta * \left(\frac{u-u_b}{u}\right)_i * \left(m_{perc}\right)_i \qquad \text{Eq.6.23}$$

Where, θ is the tuning constant for particle mobilisation, $m_{perc}$is the total mass of precipitated particles in each grid block, at any simulation time step.

5. The mobilised particles are carried over with the flowing CO_2 solution.
6. The suspended mobilised solid particles are precipitated if during the simulation time steps they arrive to either the grid cell with highest velocity, or one adjacent to it on either side. The suspended particles passing the block with the highest velocity or that after it, is considered to have left the system
7. Porosity and permeability of each grid cell are updated according to the magnitude of particle mobilisation and re-precipitation.

6.10 Implementing the proposed process (simulating Coreflood-1 experiment)

Basically, two tuning parameters were introduced in the equations; (i) threshold for activation of the particle mobilisation, i.e. U_{TF} (please see above) as expressed by Equation 6.22, and (ii) the fraction of precipitated solutes that is remobilised, i.e. the θ coefficient in Equation 6.23. It should be pointed out that these parameters cannot be directly measured, however experimental results are used to tune them experimentally.

6.10.1 Sensitivity analysis

The threshold, beyond which the precipitants start to be mobilised, depends mainly on the applied drag force and the size and bonds between particles. At this stage of the project, the change in the velocity is the primary factor included in the threshold factor (i.e. U_{TF} expressed by Equation 6.22), which represents the change in the drag force. Based on a sensitivity exercise, the threshold U_{TF} defined for activating the process of particle mobilisation controls the time that the full blockage occurs. Figure 6-28 demonstrates the relationship between the threshold U_{TF} value and the blockage time. The time to have full blockage during the experiment is around 5.8 to 6 days. Based on this range, a threshold U_{TF} value of 1.112 can be considered as the tuned value.

Having tuned the threshold parameter, it is required to tune the other crucial parameter of the particle mobilisation, i.e. the θ coefficient in Equation 6.23, which reflects the fraction of precipitated solutes that is remobilised. Figure 6-29 illustrates the permeability distribution in the vicinity of the area targeted by the precipitation at three different θ. Zero value for θ represents no particle mobilisation as the reference case. Generally speaking, the implementation of the particle mobilisation resulted in the more concentrated precipitation and hence smaller blockage body.

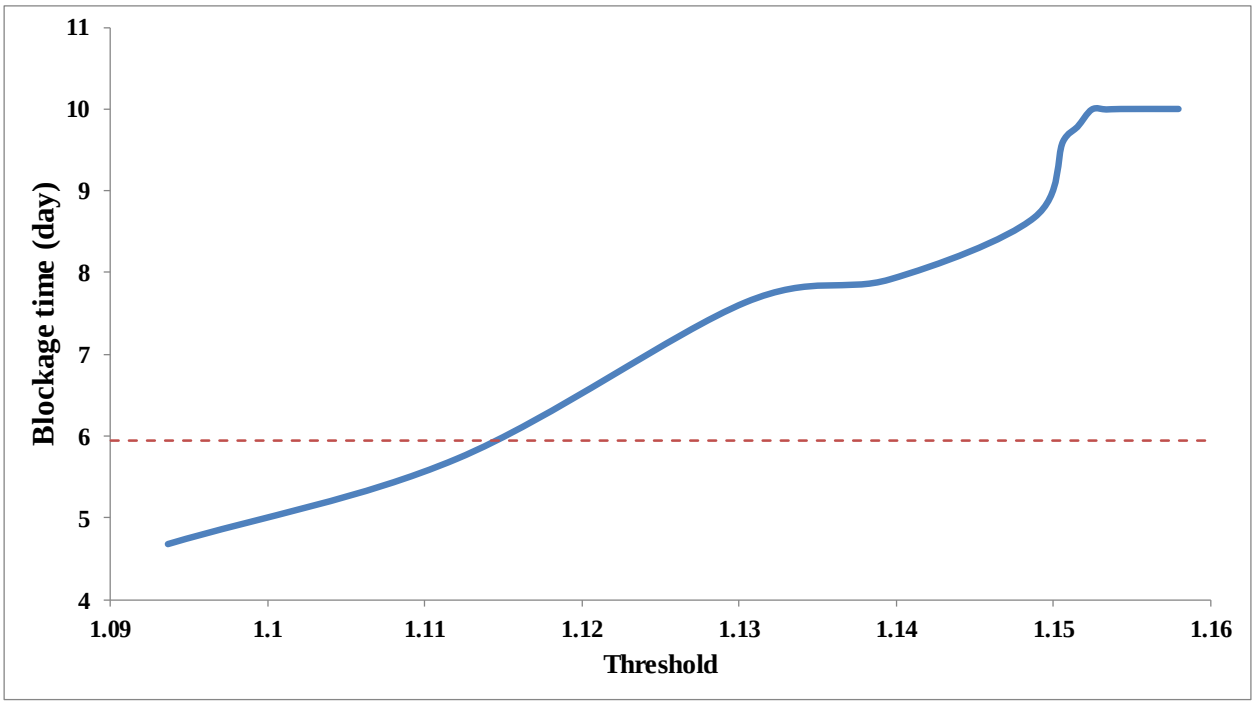

Figure 6-28: Variation of the blockage time with respect to the threshold factor (i.e. U_{TF} expressed by Equation 6.2) for particle mobilization. The red dashed line represents the approximate blockage time measured during the first test in our laboratory.

Two θ values were selected in order to clarify the role of this parameter. At a smaller value of θ = 0.00001, additional particle formation took place close to the outlet of the core since the very gradual particle mobilisation favoured re-activation of nucleation kinetics, which in turn invalidate the cumulative amount of simulated precipitation matching the experimental data based on the first and more dominant mechanism of nucleation kinetic. As it was mentioned before, the approach proposed here is based on the assumption that nucleation kinetic accounts for precipitation of particles dissolved in the solution as matched by the mass balance. In other words, during the process of re-mobilisation and precipitation we only move some of the particles from one to another participation site. This also leads to an unrealistic reduction of permeability after the blockage site. However, at a larger value of θ=0.001, we have trends more consistent with our understandings of the process and our simulation approach. Therefore, this value (θ=0.001) is the tuned coefficient for the particle mobilisation.

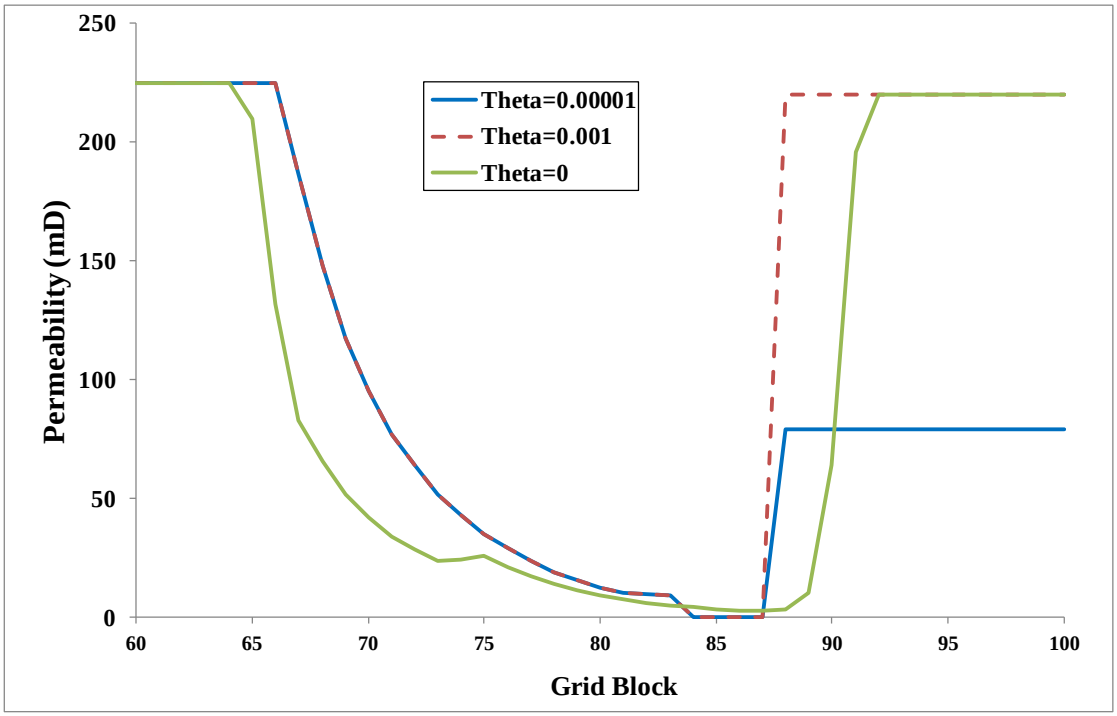

Figure 6-29: Permeability distribution in the vicinity of the area targeted by precipitation. For θ= of 0.00001 (blue solid line), an unrealistic permeability reduction at the end of the core was obtained. With θ=0.001, the blockage was simulated adequately and the particles precipitated mass balance between the measured and simulated values obtained during the previous stage of simulation was preserved. θ in Equation 6.23 controls the fraction of precipitated solutes that is remobilized.

6.11 Prediction of the results of Coreflood-3 experiment

Having tuned the pertinent parameters of our numerical model based on Coreflood-1 experiment, the predictive capability of the resultant model should be assessed by employing the outcome of a similar coreflood experiment. Coreflood-3 was performed in similar conditions (compared to Coreflood-1), i.e. HWS-2 used at 3000 psig and 45^{o}C. Like Coreflood-1, pressure drop of 250 psig was imposed across the core. The differences between these two coreflood experiments are the flow rate and length of the composite core, i.e. higher flow rate and higher length of the composite core in Coreflood-3. Table 6-5 shows the properties of each core plugs used in Coreflood-3.

Table 6-5: Basic properties of core plugs; T1, T2, and H1 representing tight and high-permeability cores.

Core ID	Length (cm)	Diameter (cm)	Weight (gr)	Porosity (fraction)	Permeability (mD)
T1	3.44	2.59	48.683	0.038	0.0038
T2	4.01	2.56	57.661	0.037	0.0037
H1	13.81	2.54	143.762	0.163	225

In this experiment a firm and durable blockage was formed against the leak. Approximately 6 days of solution (CO_2 + solute) flow was elapsed till the precipitation could be effectively detected. The reason behind expressing the blockage time in approximate form is the nature of low flow rate of gaseous flow through porous media where gaseous-like compressibility of CO_2 would make any response in flow to be inexact. However, we consider 6 days as the blockage time with an acceptable tolerance band of ±0.5 day. Three important sources of data can be considered for evaluating the predictive capability of the mathematical model: occurrence of blockage, amount of precipitation, time of blockage occurrence.

Figure 6-30 illustrates the permeability distribution of composite core obtained from the simulation results of Coreflood-1 and Coreflood-3, which indicates a significant drop in the original permeability from 225 to 10^{-5} mD. It should be noted that the simulation

results of Coreflood-3 is a prediction utilising the corresponding tuning parameters obtained from Coreflood-1. In the Coreflood-3 experiment, the full blockage was observed and the simulation outcome has predicted the occurrence of blockage satisfactorily. Therefore, based on the simulation results, one source of experimental data was successfully matched in this predictive exercise.

However, comparatively speaking, particle precipitation has targeted a wider area in Coreflood-3. Also, the blockage was formed closer to the core outlet in Coreflood-3, which can be attributed to the higher flow rate established in this experiment. Furthermore, the pattern of the precipitation is similar in both simulations with a difference in target area, which is in line with experimental information, i.e. a high degree of similarities exist between the experiments.

In terms of blockage time, the simulation of Coreflood-3 did predict that blockage would occur at 6.19 day. Compared to experimental information, which is 6±0.5 day, the simulation outcome has exhibited a reasonable quality of match between the experiment and prediction. The difference between the experiment and simulation can nevertheless be linked to inaccurate identification of blockage time as explained above.

When the Coreflood-3 experiment finished, the composite core was cleaned by injecting a suitable solvent to recover the precipitated solute in the core to obtain another source of information, i.e. precipitation mass. The weight of precipitated HWS-2 was 0.884 gr. From the simulation results, the total amount of precipitation mass is 0.841 gr. Hence, a relative error of 4.8% exists between the experiment and the prediction ($\frac{0.884-0.841}{0.884} = 0.048$). This less than 5% error for this predictive estimation of a complex and transient process can be considered insignificant.

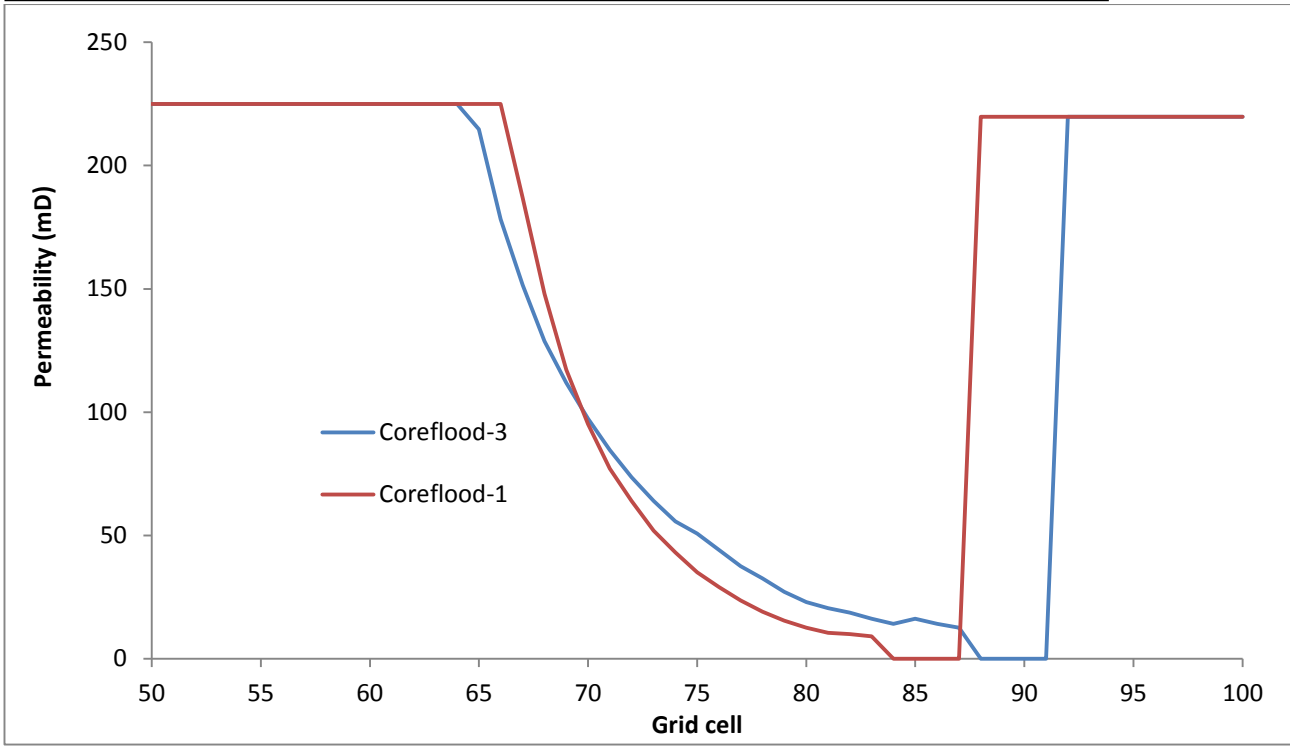

Figure 6-30: Final simulated absolute permeability distribution of the composite core in Coreflood-1 and Coreflood-3 experiments, which indicates permeability reduction from the original value of 225 mD to 10^{-5} mD. This permeability reduction can be interpreted as an acceptable prediction for Coreflood-3.

In summary, the predictive analysis of this modelling exercise has revealed that the developed mathematical model can satisfactorily estimate the performance of our leakage prevention technique in companion scenarios. In other words, if the tuning parameters of nucleation kinetics and particle mobilisation for a solute are adjusted based on a core experiment, the resultant model would be confidently utilised in similar scenarios in different scales.

6.12 Prediction in large scales

At this stage the model with its tuned parameters was used to investigate the performance of our leakage prevention technique in a leakage path with uniform permeability. In other words, the response of our model was evaluated for an equivalent homogeneous medium replicating the precipitation process occurred in the Coreflood-1 experiment simulated in the previous section. In Coreflood-1 experiment, two core plugs with two distinct permeability were incorporated which may not represent some of the leakage paths. The high permeable core (with k=225 mD) represented the main flow path whilst the very low permeable core (with k=0.002 mD) was used to create the required pressure drop. It may

be suggested that, a leaky flow path is likely to have a homogenous permeability throughout. However; it is expected that a long porous medium of such nature is required to simulate this leakage path, which is not feasible to have in the laboratory. Nevertheless, the tuned model would be a useful tool to conduct this investigation. Therefore, in this exercise, we aim at evaluating the equivalent length of a homogeneous leakage path (with the high permeability of 225 mD) which results in the same flow performance as that in the first core flood experiment simulated above., The inlet and outlet flow rate and pressure values, were those of the experimental conditions of Coreflood-1 test. The simulation results showed that a length of 450-500 ft for this 1D leakage path is necessary to have significant precipitation, which would lead to the same blockage as that of the two core assembly case.

Figure 6-31 shows the permeability distribution along the leakage path at the end of this simulation run. It is noted that the permeability of last 8 grid blocks in the leakage path has been affected by the continuing precipitation of the solid solute. The permeability of the last grid (100th grid), has dropped to 5.190 mD from the initial value of 225 mD. This simulation took 70 days (simulation time) to reach to this state.

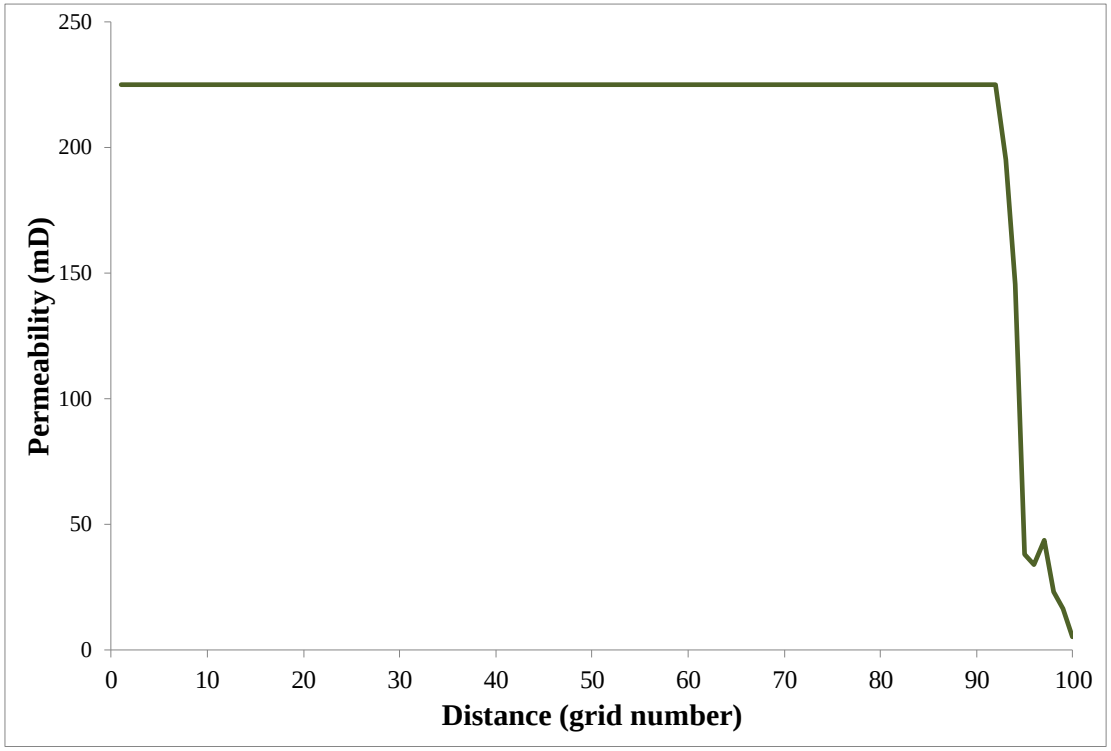

Figure 6-31: Permeability distribution at the end of simulation of the homogeneous leakage path with k=225 mD. The required length to have the significant permeability reduction is 450 ft highlighting the need to include the very low permeable core (k=0.002 mD) for the experiment conducted in the laboratory.

The pressure distribution along the leakage flow path reveals the influence of the precipitation on its rate of increase as shown in Figure 6-32. In this Figure, the pressure profile along the leakage path at the end of the simulation run has been compared with that at the start of simulation. It is noted that, the pressure before 92th grid block, which is the first grid block with solid precipitation, has increased considerably, which confirms our previous discussion that based on the incorporated mechanism in the model precipitation rate should decrease, which may explain why permeability it did not reach a desired zero value.

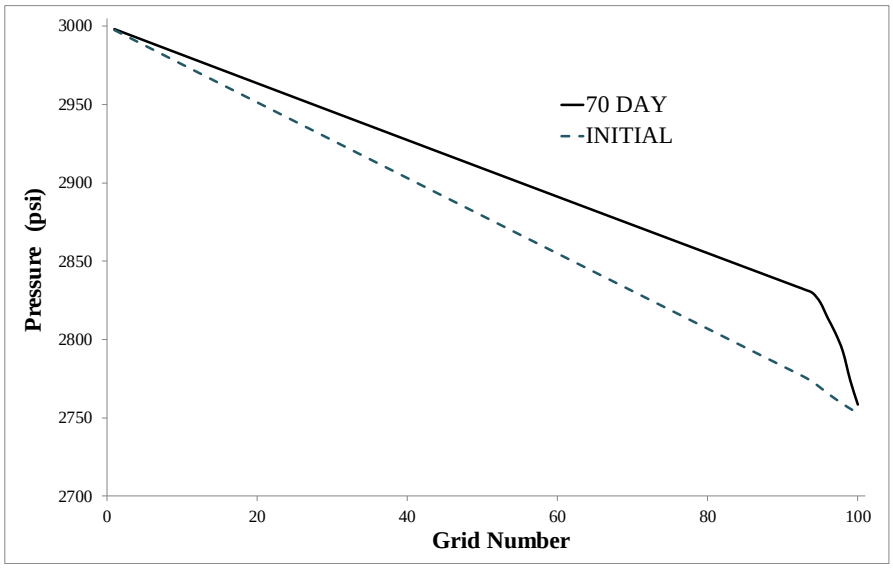

Figure 6-32: Pressure distribution at the beginning and end of simulation of the homogeneous leakage path with k=225 mD; the pressure build-up close to the outlet of the porous medium highlights the role of the supersatuation, precipitation and suspension flow.

6.13 Limitations of developed mathematical model

The successful outcome of the developed mathematical model demonstrated that the process of dynamic precipitation of solid particle can be simulated by coupling the transient phenomenon of nucleation kinetics with flow in porous media. The results could capture the trends and reproduce the main observations, i.e. blockage time and mass of precipitation as compared with the experimental results. It was assumed that in each time step, the flow equations are solved by CMG simulator and the pressure and flow velocity outputs in each grid cell are used in nucleation kinetics to calculate the hysteresis parameters and nucleation equations, which would determine the consequent precipitation. This method of coupling flow and nucleation is defined as an explicit solution. Although the outcome of the mathematical modelling could satisfactorily

capture the performance of leakage prevention technique, two minor discrepancies were identified in the simulation results. In Figure 6-27, the flow velocity shows a non-smooth behaviour which would not reflect the real flow characteristics of single phase flow in porous medium. Also, in Figure 6-31, the permeability reduction due to precipitation occurred in a non-monotonic fashion, which would be in contrary of concentration profile that would have a decreasingly monotonic profile from inlet to outlet of the leakage path. Therefore, these issues should be addressed in order to highlight sources of errors, which may enable us to improve the simulation results.

Despite the promising results of the simulation attempts, there are a number of limitations stemmed mainly from how the equations were implemented; firstly, it was assumed that the nucleation kinetics would be solved in an explicit manner and secondly, finite difference method would inherit a degree of errors from truncation and roundoff assumptions. The explicit formulation would dictate that the results of nucleation kinetics would not affect the flow equation at a single time step. In other words, no iterative approach was considered to solve nucleation and flow equations. This assumption would bring about an insignificant degree of error to the profiles of flow and precipitation. There could be another approach (which was not used in this work) to implement an iterative algorithm in which the precipitation can change the rock properties such as porosity and permeability, which would in turn affect the flow properties such as pressure and velocity and at each time step, the iteration of the parameters would continue till precipitation and flow properties become unchanged due to iteration. Implicit formulation may reduce the slight fluctuations and non-monotonic behaviour seen in the solutions but on the other hand, this marginal improvement can increase the computation cost at each time step. Hence, for the cases considered in this investigation, the explicit formulation would adequately capture the performance of leakage prevention technique with reasonable computation cost. Also, it should be noted that there are other sources of errors such as truncation and roundoff which are generated in the reservoir simulator (solving the flow equations) and it may propagate in nucleation kinetics. However, this latter source of error could not be managed considerably since the access to the commercial reservoir simulator (CMG) formulation is restricted.

6.14 Discussions and Conclusions

Two lines of study were carried out for simulating and modelling of the leakage prevention technique; in the first part, a method was proposed to implement the leakage

prevention technique in commercial simulators (CMG-GEM) and in the second part, it was attempted to include the underlying mechanisms identified in the experiments into a mathematical model, which enabled us to fundamentally investigate the role of pertinent parameters in history-matching of the experimental results.

Using a conventional simulator with assumptions of instantaneous equilibrium (no time dependency in particle formation), a series of simulation exercises was performed to demonstrate how the leakage prevention technique can be simulated in commercial simulators by analogy between the gas-condensate systems with that of our CO_2+solute solution. It was assumed that solid solute would behave like condensate phase and would be dropped out as the pressure fall below the saturation pressure (dew point). For simulating the precipitation process, the relative permeability of the solid particles (condensate phase) was set at zero. The results of simulations showed that the LPT can stop/alleviate the leakage effectively. The precipitation and consequent blockage would be accumulated around the leakage path due to the local pressure drop. Therefore, the proposed method to manipulate the input data can capture the general behaviour of LPT. However, it is not feasible to capture the time dependency and nucleation of particles in simulators as observed in the experiment. This necessitated to develop a mathematical model in order to simulate the coreflood experiments.

Our preliminary use of commercial simulators have demonstrated a need for a more sophisticated mechanistic modelling approach that captures main mechanisms dominating the process involved in our leakage prevention method. It was discussed that based on the experimental results of the micromodel visualizations and coreflood tests the governing equations describing the time depending nucleation of solid solutes dissolved in the CO_2 stream that is flowing through a leakage path was developed. The proposed sets of equations describing the kinetics of solid solute precipitation and porosity and permeability reduction have been linked to the Computer Modelling Group (CMG-GEM) reservoir simulator, which solves the corresponding flow equations. The calculation continues till the permeability reduction is reached to a pre-defined level indicating the blockage of the leak. During this process, we benefited from the following findings:

1) The location of the precipitation can be controlled by including the relevant equations for induction time, which is defined as an initiation of particle formation for low supersaturation (solution containing more of the solute that it can dissolve

under thermodynamic equilibrium conditions) degrees. Hysteresis effect (effect of the supersaturation and concentration throughout the leakage path and in the grid block prior to the block where nucleation occurs) was taken into account for developing the induction time terms.

2) In the induction time and nucleation rate equations, suitable dimensionless numbers were proposed for the supersaturation and concentration of the solution to have a more general solution.
3) The micromodel visualization results were considered for qualitative investigation of permeability-porosity correlation. That is, it was noted that small amount of precipitation, i.e. porosity reduction, results in significant reduction in permeability. This was incorporated with high exponent of the power law function that relates porosity to permeability.
    a. The data of the Coreflood-1 experiment were used for optimising the tuning parameters.
4) Initially and without suspension flow, the solid particles precipitate where they are formed, the mathematical model predicted 98% permeability reduction (from 225 mD to 5 mD), but the software was unable to achieve zero permeability (i.e. the full blockage). This was attributed to the simplifying assumption made and in particular lack of acknowledging the contribution of suspension flow of the particles, in the implemented equations.
5) Mobilisation of precipitants and re-precipitation of these particles were considered as the complementary mechanism to capture suspension flow achieve the full blockage. A model was developed that adequately captures the process of particle mobilisation, suspension flow, and re-precipitation.
6) From the visualisation experiments, it was inferred that the area targeted by precipitation should be small, i.e. smaller than what the model without suspension flow predicted. The inclusion of this new mechanism also helps us to achieve this.
7) The governing equations were implemented in the model introducing two new parameters to be tuned based on the available experimental data; (i) the threshold velocity beyond which the particle mobilisation process is activated, i.e. U_{TF} expressed by Equation 22 and (ii) the fraction of precipitated solutes that is remobilised, the θ coefficient in Equation 23.
8) U_{TF} controls the blockage time with an approximate value of 1.112 matching the observed blockage time of the first experiment.

9) A Larger value of θ would produce results more consistent with our understanding of the process and incorporated assumptions in the model. In particular, it reduces the precipitation target area. The simulation results of the First experiment indicated that the optimised value for θ is 0.001.
10) The results of this modelling exercise are very encouraging as it captures the main dominant underlying mechanisms and predicts Coreflood-3 was carried out with same solute and pressure/temperature conditions but the flow rate and length of leakage path differed. The simulation results demonstrated an acceptable degree of match between the experiment and our model highlighting a high level of predictive capability for the model.
11) The tuned model was also used to estimate the length of an equivalent homogenous leakage path if we had only the high permeable core plug. This length was 450 ft for the core experiment performed highlighting the need to include the very low permeability core (k=0.03 md) for the experiment conducted in the laboratory.

CHAPTER 7 Solubility Measurements and Modelling Solubility Profile along Injection Wellbore

7.1 Introduction

One of the key issues in application of our self-diagnosing and self-sealing technique is safe transfer of the solute in the dissolved state into the storage site. That is, application of the proposed leakage prevention technique necessitates the investigation of bulk flow of the solid solute- CO_2 solution from the surface down to the sandface and throughout the storage site. The first main issue, in terms of practical and operational aspects is that the solute is transferred to the sandface without premature precipitation. The design and solubility level of the solute at the sandface should also be in line with the requirement that the injected fluid remains dissolved in the reservoir and solid particles released efficiently in the case of a leakage scenario.

Two feasible methods can be considered for delivery of CO_2-solute solution to the storage site; downhole and surface mixing. In the case of downhole mixing, the solute and carrier fluid (supercritical CO_2) will be mixed in the sandface of the injection well. This technique is associated with considerable operational complexities and uncertainties, which make downhole mixing technically very undesirable. On the other hand, surface mixing provides more flexibility in terms of operational issues since the surface facilities are practically more manageable compared to the downhole mixing. However delivering the solute from surface to the sandface involves some engineering considerations with the

main one being that the solute should remain dissolved in the CO_2 as the solution travels through the well experiencing the changes in pressure and temperature with depth. The level of solid solubility when it reaches to the storage site at the bottomhole conditions, which affects the efficiency of this leakage prevention technique, is another important aspect in this process.

In order to address these, the solute content of the solution must be designed according to the solubility profile along the wellbore. Therefore, the principal objective of this part of the study was to determine the solubility profile of a number of selected solutes screened for our specific purpose along the wellbore. In this exercise we targeted the prevailing conditions of Goldeneye, which is regarded as a leading potential site for CO_2 storage within the UK. However, the information from this study is applicable not only to Goldeneye but also to other storage sites with similar prevailing conditions. If the storage sites temperature and pressure conditions are significantly different, then it would require extrapolation of measured data well beyond their measurement conditions in which case, new measurements should be carried out and included in the developed software to obtain more realistic solubility profile.

The studies' objectives were achieved by conducting laboratory experiments and mathematical modelling. In the experimental part, solubility tests were conducted to generate solubility data for a number of solutes selected based on a set of screening criteria. These criteria include the proper solution response to a leakage scenario during the performed flow visualisation tests as well as cost and environmental considerations and stability and durability of solid solute at the pressure and temperature storage conditions. In the theoretical directions, excel based program was developed that determines the solubility profile for a selected solute along the wellbore as it travels from the surface to the sandface. The program estimates the temperature, pressure, CO_2 density and solid solute solubility profiles using the appropriate incorporated equations for the given solid solute, thermal gradient, surface temperature and reservoir pressure. It can also perform sensitivity on the solute type and changes in wellhead injection pressure.

7.2 Solutes used in solubility measurement

7.2.1 HWS-4

HWS-4, compared to the previous solutes, is a low soluble solute that does not dissolves considerably into the supercritical CO_2.

One can argue that a low soluble solute requires less amount of solute, which favourably reduces the cost However, at the same time; the issue would be that it may not generate sufficient particles to stop the leakage. It should be pointed out that the leakage prevention method never aims to block the entire leakage path but it rather seals the interface between storage site and leakage path by local precipitation. Therefore, a low soluble solute could also be a good candidate. Another relative advantage of a low soluble solute is their lower risk of precipitation within the storage site due to any unforeseen circumstances.

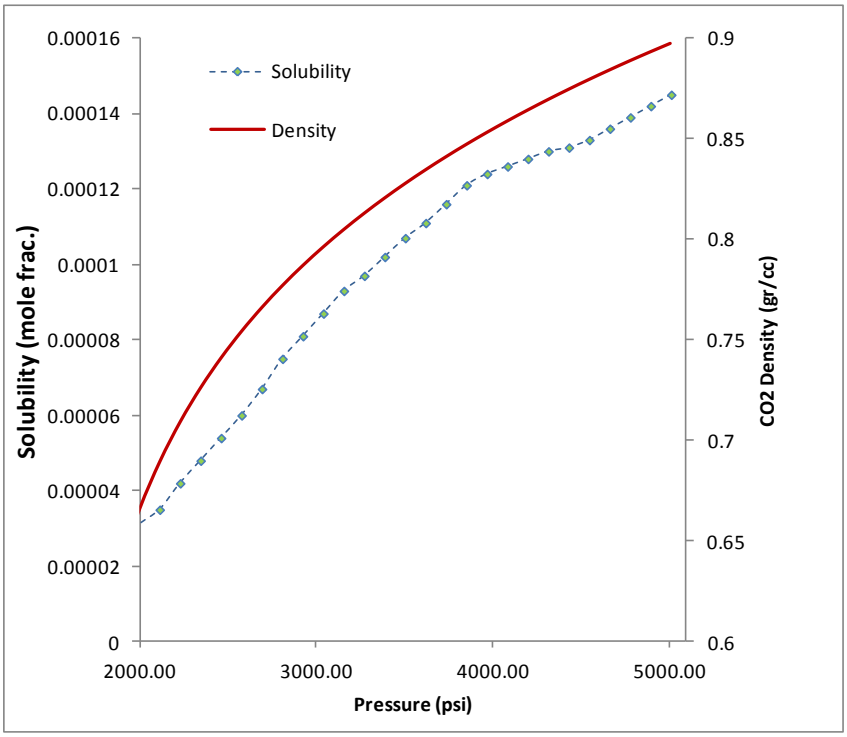

Figure 7-1: Solubility of HWS-4 and density of CO_2 at 50C.

HWS-4 has several promising characteristics such as inexpensive bulk price and high melting point of 218^{o}C, which makes it thermally stable at higher temperatures. Moreover, the published data in literature on the solubility of HWS-4 in supercritical CO_2 at various temperatures is abundant. Figure 7-1 shows the solubility of HWS-4 and CO_2 density with respect to pressure at 50^{o} C. No micromodel test was performed for this solute but considering similarity of the trend of its solubility with the previous two cases, it is expected that similar promising results would be achieved.

7.2.2 *HWS-5*

Up to this part of the report, we examined the appropriate candidates which are technically viable solutes. *HWS-5*, on the other hand, falls into the category of unsuitable solutes

because its precipitation mechanism undermines the efficiency of the leakage prevention method. Figure 12 shows the solubility of the *HWS-5* at supercritical CO_2 and CO_2 density at constant temperature of 45^o C. According to Figure 7-2, the solubility of the *HWS-5* (with around 0.05 mole fraction solubility at 2500 psig) is one order of magnitude higher than those of HWS-3 and HWS-2.

The behaviour of *HWS-5* and, in particular, its tendency to attach to the surface of the porous medium is of great importance and interest since this characteristic directly affects the required concentration of the solute. In these experiments, the pressure of the stored CO_2 cell and micromodel were 2960 and 2400 psig, respectively, giving a pressure drop of 560 psig. The solute concentration was 0.0383 mole fraction.

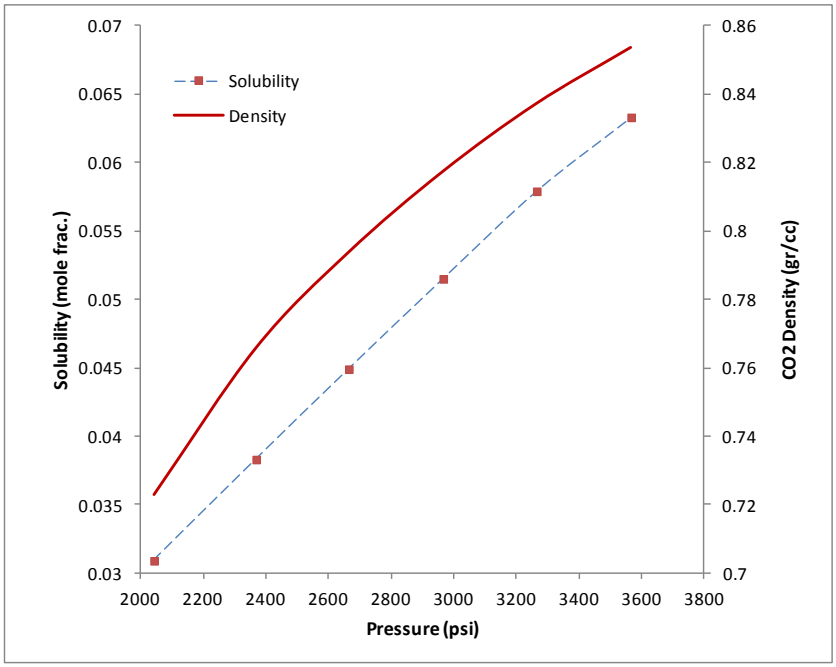

Figure 7-2: Solubility of *HWS-5* and density of CO_2 at 45C.

During this test, it was noted that as a result of the leakage and the activation of the leakage prevention mechanism, precipitation of the solute took place in some of the pores. One very obvious and interesting observation was that the precipitation of HWS-4 was more scattered.

Figure 7-3 shows a sequence of images of one section of the micromodel taken during this experiment. In this sequence of images, time increases from left to right and from top to bottom, which can be identified from the evolution of the dark spots as the precipitation progresses. As can be seen, the size of the blockages formed during the experiment

increased with time till the leak was completely sealed. However, it is noted that the solid solutes are attached to the surface.

It is well-accepted that injected CO_2 as the non-wetting phase tends to occupy the bigger pores whilst the resident liquid phase adheres to the surface of the pore-throat as the wetting phase. Therefore, in terms of pore-scale phenomena, surface of the porous rock is not available for such substances to attach to. Thus, to have efficient precipitation, the solutes with high tendency to adhere to the pore surface, as opposed to the solutes with the particle coagulation mechanism, should be excluded from the list of the potential solutes. Consequently, *HWS-5*, which demonstrated profound affinity to attach to the pore surface, was not considered a suitable candidate for our purpose.

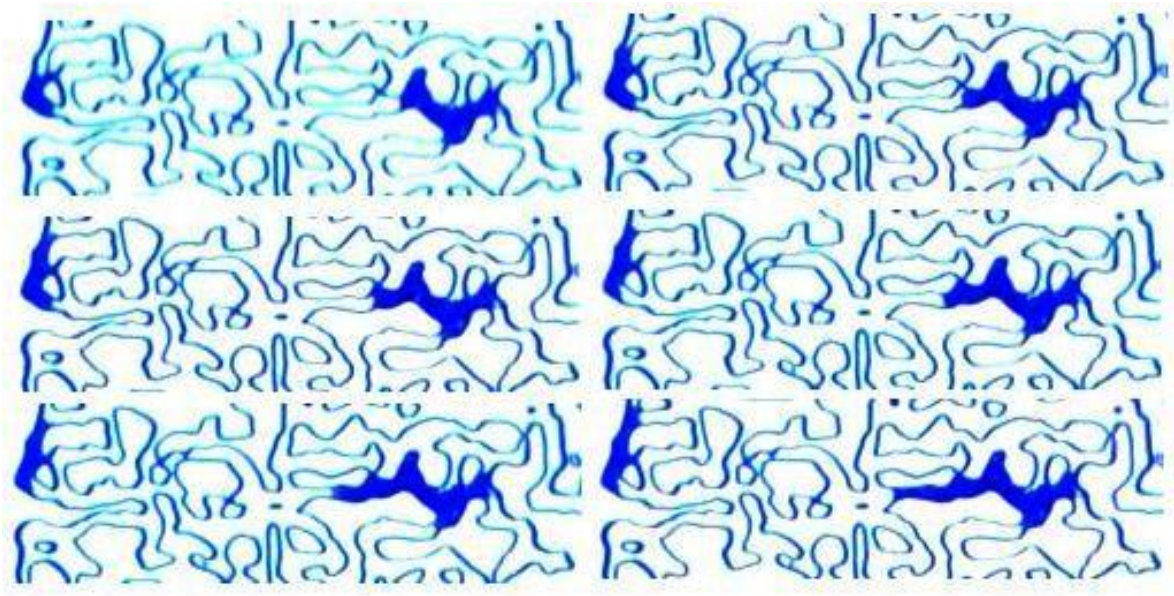

Figure 7-3: Process of sealing the leakage under 560 psig pressure drop using HWS-5.

7.2.3 HWS-6

HWS-6 with a solubility of 0.36 mole fraction at test temperature and high pressure of 2500 psig is categorized as a highly soluble solute. It has a melting point of 175 C, which makes it a suitable candidate for this study. Furthermore, because of its high solubility variation due to a change in pressure, it was expected that it would be more responsive to a pressure drop. However the results of micromodel experiments demonstrated that no particle nucleation was observed even at a very high pressure drop of 1200 psig. This pressure drop is the highest pressure drop that can be imposed in our in micromodel facility before its integrity is compromised. It should be noted that the experimental procedure was like those of the previous solutes. This behaviour was attributed to

undesirable interfacial properties between this solute and CO_2. Therefore due to its poor precipitation characteristics in the micromodel, this solute was not considered as a suitable solute for our purpose.

7.3 SOLUBILITY MEASUREMENTS

As mentioned above, two feasible methods can be considered for delivery of CO_2-solute solution to the storage site; downhole and surface mixing. Surface mixing provides more flexibility in terms of operational issues since the surface facilities are practically more manageable compared to the downhole mixing.

Considering the low critical temperature (31.1°C, 87.8 °F) and critical pressure (72.9atm, 7.39 Mpa, 1070 psig) of CO_2, practically speaking, at surface temperature, injected CO_2 will be at either vapour or liquid state depending on the injection pressure and local temperature conditions. Due to the solubility dependency to density (i.e. minimal solubility is when CO_2 is at it vapour state) and to increase the mass of injection fluid, CO_2 would be injected at its liquid state by increasing the injection pressure. However, solubility data of most solid solutes in the literature are limited to supercritical region and hence there is a gap in solubility of solid solutes in liquid CO_2. Furthermore, as solid solute solution is travelling from the surface to the sandface, it experiences pressure and temperature variation with depth, which might not be covered by the available solubility data in the literature. Therefore, solubility measurements were designed to produce sufficient data for modelling the solubility profile along the wellbore, if our leakage prevention method were to be implemented by mixing the solute at the surface, whilst benefiting from data available in the literature.

To achieve this purpose, the isothermal (constant temperature) solubility data of selected solutes (HWS-3, HWS-2, and HWS-4) was measured at 4 to 6 pressures. A lower temperature limit of 19^{o}C, which is 12^{o}C lower than that of the supercritical condition (31^{o}C) was selected. As mentioned previously, at this temperature, CO_2 can be either liquid or vapour depending on the working pressure. The minimum pressure value in the solubility tests was selected as 840 psig to ensure CO_2 is in the liquid state even at this low pressure value. An upper pressure limit of 3000 psig pressure was selected based on the target injection pressure of the Goldeneye storage reservoir. An upper temperature of 85^{o}C, which is reservoir temperature of the Goldeneye storage prospect, was also considered.

For HWS-3, measurements were carried out at 19^{o}C. In the case of HWS-2, the experiments were conducted at 19^{o}C and 45^{o}C. For HWS-4, the test was done only at 19^{o}C. Total of 20 solubility points were measured for these four isotherms. A correlation was also fitted to these data to interpolate and generate solubility profile along the wellbore. It should be noted that due to complexity of solubility measurements at higher temperatures, which required modification to our rig that could not be achieved during the short period of this project, solubility data were not measured at high temperature, instead, we only relied on the extrapolation of the correlation, which fitted nicely to the measured data as described in the following sections. In the following sections, before presenting the results of the solubility measurements a brief description of experimental setup and procedure are given.

7.3.1 Experimental Setup

In this study, the general methodology of solubility measurement is based on depressurizing a finite volume of saturated solution in a closed system and measuring the content of dissolved solid solute. This involves three steps (i) equilibrating the solid solute and CO_2 at the prevailing conditions, (ii) displacing a pre-determined volume of the solution to a secondary cell and (iii) the displaced fluid is depressurized to allow nucleation of solute particles and hence the solid content can be measured. Figure 7-4 illustrates the schematic setup of the rig, which was used for the solubility measurement. Two cells, which were connected to two automated pumps, and one pressure transducer was mounted in an oven. Porserve cells along with the Quisix pumps enabled us to work at high pressure covering the entire range of injection pressure. Although the pumps were equipped with pressure transducers, a highly accurate Quartzdyne transducer was considered for logging the working pressure during each test. A number of similar set-ups were mounted to perform a series of experiments simultaneously.

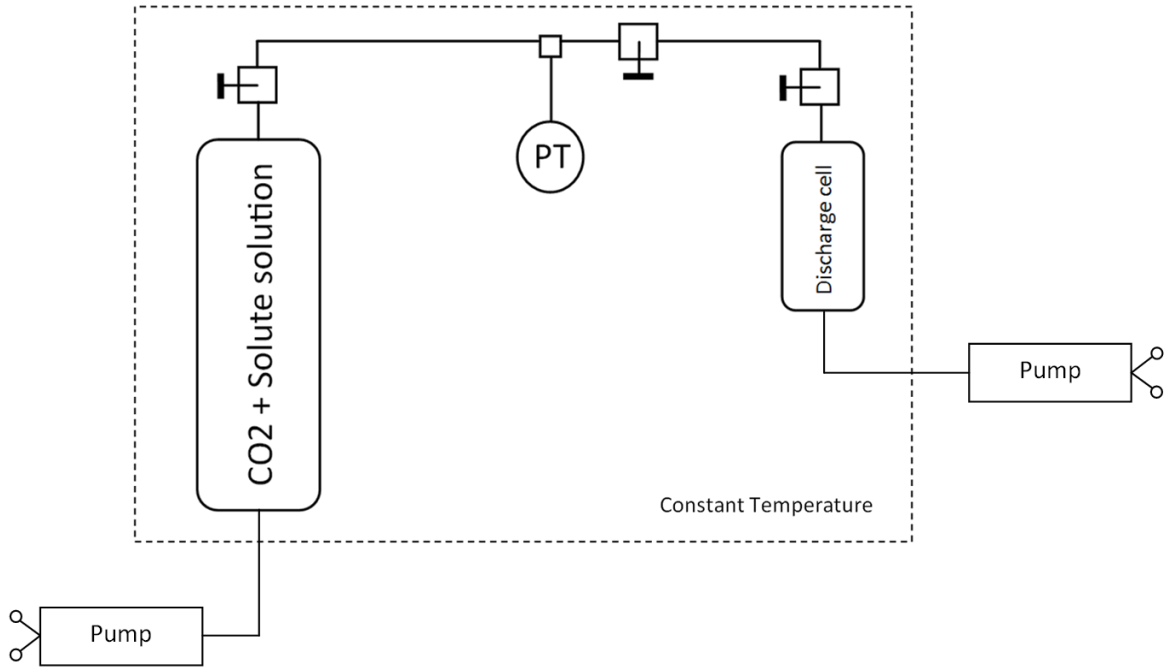

Figure 7-4: Experimental setup of the solubility measurement rig.

7.3.2 Experimental Procedure

In order to prepare the saturated solution of CO_2 and solute, an overestimated value for solid solubility was assumed and added into a cell. Then, the cell is filled with CO_2 up to the desired pressure of the test. To establish the equilibrium conditions between CO_2 and solute, the solution was allowed to mix for 10 hours at constant pressure and temperature. Then a second cell was connected to the solution cell to extract a sample of saturated CO_2 solution. The process of filling up the second cell was carried out at constant pressure to ensure thermodynamic equilibrium conditions were maintained. Next the pressure of the second cell with known finite volume of saturated solution of CO_2 and solute was reduced till all solid is precipitated out of the solution at the base of the cell due to gravitational segregation. This occurred when CO_2 was in the vapour state with minimal solvent power. Finally, vapour CO_2 was purged and the residue solid was weighted and its solubility in CO_2 was calculated.

7.3.3 Experimental Error

Considering the experimental procedure described above, the main source of error is the recovery of the solute particles residing in the cell. This error is expected to depend on the solubility, i.e. it would be higher at lower solubility. To ensure this experimental error is minimal in our tests, two points from previously measured and published solubility data of a solute were selected and measured using our procedure. Solubility of HWS-3 at

pressure of 2820 psig and 45°C reported as 0.00353 in mole fraction was considered as the first data point. The measured solubility at these conditions was 0.00375 mole fraction. This value is slightly overestimated, compared to the published value, with 6.4% deviation, which is acceptable. The second point was considered at a different working pressure. Generally speaking, solubility varies monotonically with changes in pressure. At lower pressure of 1985psig, the reported solubility of HWS-3 is 0.00203mole-fraction, which is one order of magnitude less than the previous one. The measured value for the solubility at 45°C and 1985 psig in our experiment was 0.00218 with corresponding deviation of 7.4%. Figure 7-5 demonstrates negligible discrepancies between the measured data and the previously published ones, confirming the integrity of our procedure and reliability of generated data.

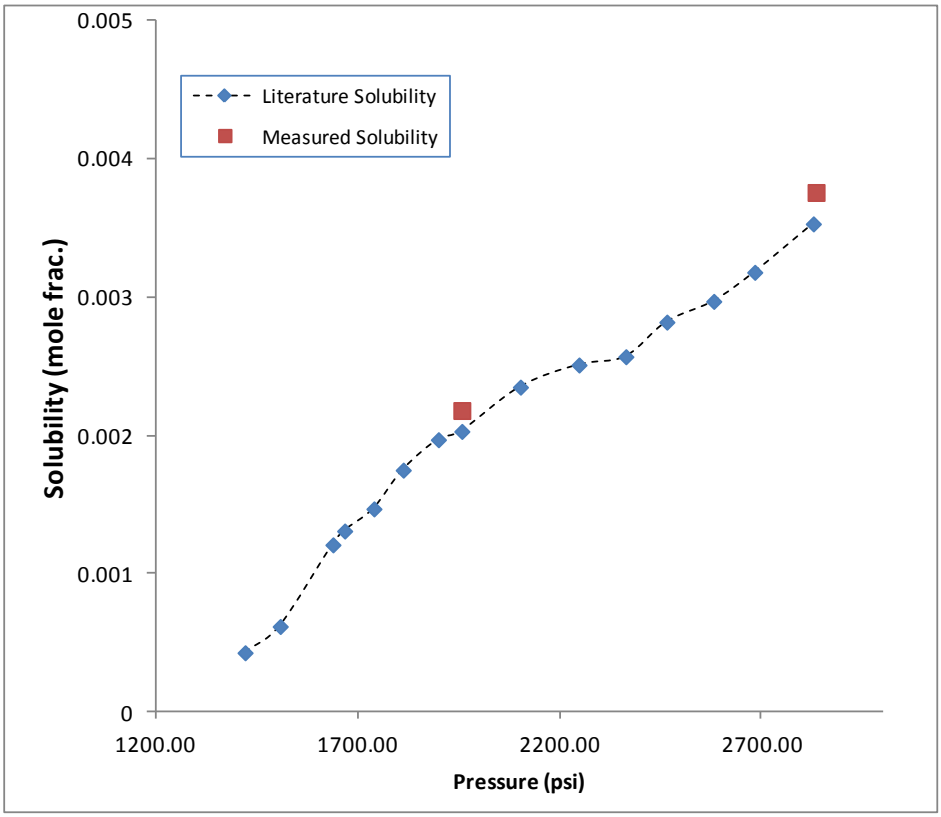

Figure 7-5: Comparison of solubility data measured during this study with data reported in the literature.

7.3.4 Extension of Experimental Data

Solubility of a particular solute in CO_2 depends mainly on pressure and temperature. Theoretically speaking solubility can be modelled by means of an equation-of-state.

However solution of solid solutes and CO_2 is categorized as a diluted mixture and hence, the solubility can be obtained using an expression in which solubility of a solute is controlled by solvent (CO_2) density, temperature and pressure. Equation 7.1 expresses the proposed formulation for such dilute solutions.

$$\ln(y_2 P) = \left(\frac{1}{T}\right)\left(A + B\rho_{CO_2} + CT\right) \qquad \text{Eq. 7.1}$$

Where, y_2 represents the molar solubility of the solute in CO_2 and A, B, and C are constants. This correlation is often used to interpolate the limited experimental data with constants A, B, and C used to tune its prediction for a particular solute. In this exercise, P and T are pressure in bar and temperature in Kelvin and ρ_{CO2} is the CO_2 density of in mole/cc. The same correlation and units would be applied for the solubility correlation used throughout this chapter.

Broadly speaking, CO_2 density has the highest impact on the solubility of the solvent with the corresponding constant B (in Equation 7.1) expressing the extent of solubility variation with this thermodynamic property. As mentioned above, at higher temperatures, we only relied on the extrapolation of the correlation, which fitted nicely to the measured data as described in the following sections.

7.3.5 HWS-3 Solubility Data

Figure 7-6 shows the measured solubility data for HWS-3 at a temperature of 19^o C. In all such Figures presented in this chapter, CO_2 density has also been included in the same graph for comparison purposes. Using these data to obtain A, B, and C of Equation 7.1 gives:

$$ln(y_2 P) = \left(\frac{1}{T}\right)\left(-7270 + 158404\rho_{CO_2} + 12.59T\right) \qquad \text{Eq. 7.2}$$

Figure 7-7 shows the close agreement between the predicted data by Equation 7.2 and the corresponding measured data.

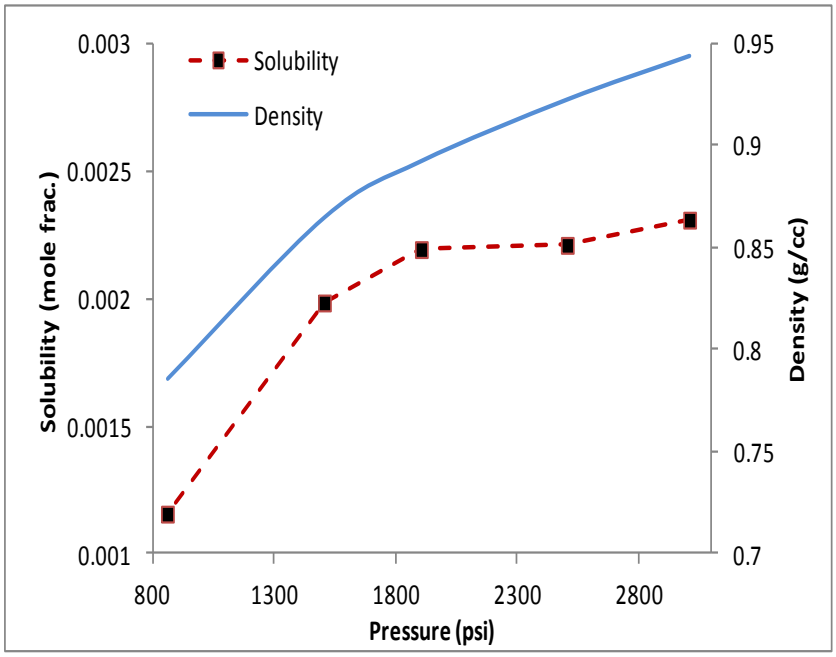

Figure 7-6: Measured solubility data for HWS-3 at 19 °C.

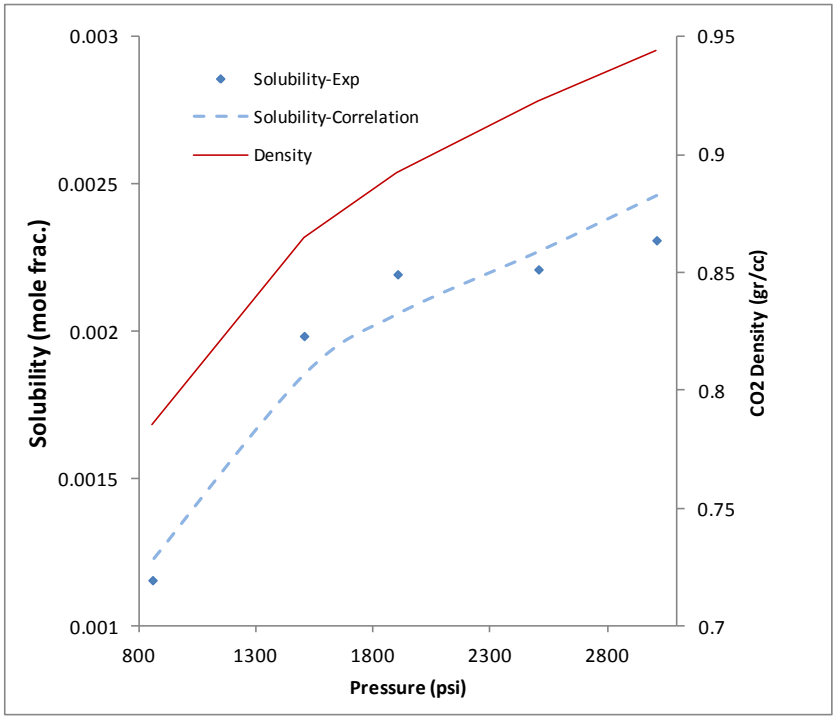

Figure 7-7: Comparison of measured data with those predicted by Equation 7.1, HWS-3, 19 °C.

7.3.6 HWS-2 Solubility Data

Experiments using HWS-2 were carried out at two different temperatures of 19 °C and 45 °C. Figure 7-8 and Figure 7-9 show the measured solubility data for HWS-3 at these temperatures, respectively. Using these data to obtain A, B, and C of Equation 7.1 gives:

$$ln(y_2 P) = \left(\frac{1}{T}\right)\left(-10266 + 162040\rho_{CO_2} + 21.13T\right) \qquad \text{Eq. 7.3}$$

$$ln(y_2 P) = \left(\frac{1}{T}\right)\left(-10066 + 96154\rho_{CO_2} + 25.42T\right) \qquad \text{Eq. 7.4}$$

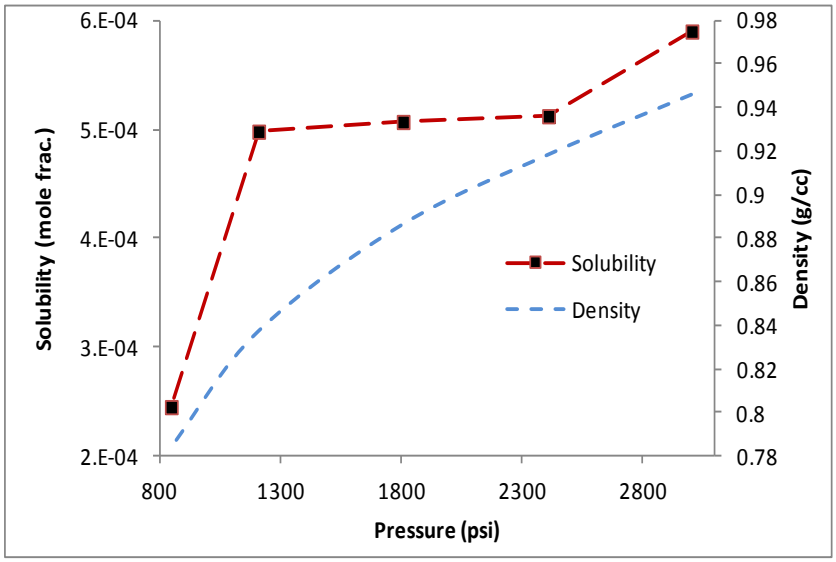

Figure 7-8: Measured solubility data for HWS-2 at 19 °C.

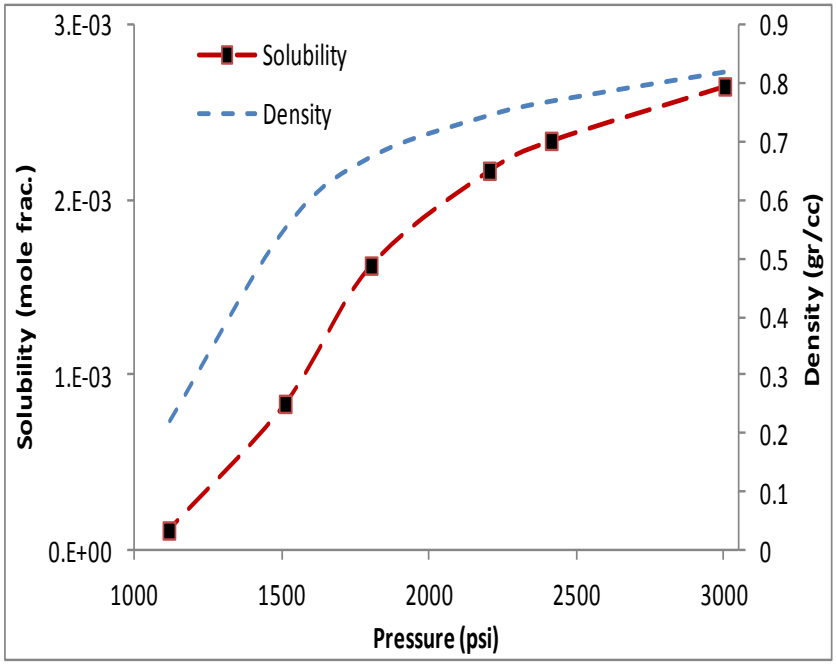

Figure 7-9: Measured solubility data for HWS-2 at 45 °C.

7.3.7 HWS-4 Solubility Data

The experiment using HWS-5 was carried out at a temperature of 17 °C. Figure 7-10 shows the measured solubility data for HWS-5, which were used to tune A, B, and C coefficients of Equation 7.1 to give:

$$ln(y_2 P) = \left(\frac{1}{T}\right)\left(35486 + 143298\rho_{CO_2} + 138T\right) \qquad \text{Eq. 7.5}$$

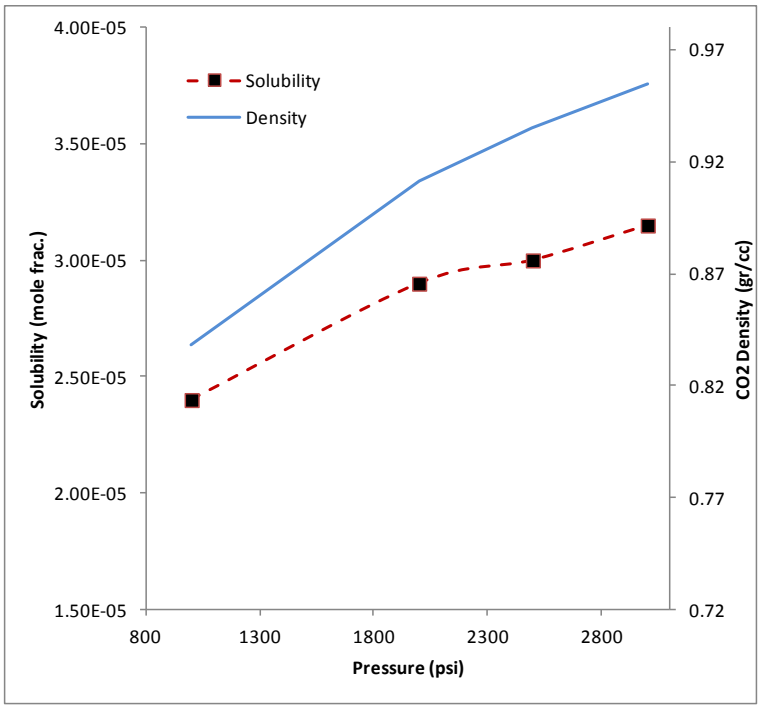

Figure 7-10: Measured solubility data for HWS-5 at 17 ºC.

7.4 Modelling Solubility Variation Along Wellbore

As mentioned previously, the main objective of this investigation was evaluation of transport of solid solute that is added to the injected CO_2 stream. If the assumption of thermodynamic equilibrium prevails, transport of solid solute from surface to sandface is mainly controlled by the solute solubility in CO_2, which depends on pressure and temperature for a given solute. Temperature profile along the wellbore obeys the geothermal gradient of the region and hence, this parameter is controlled by regional constraints, consequently, injection pressure is the only operational parameter. With these in mind, excel based program was developed to determine the solubility profile along the wellbore from the surface to the sandface. The program includes the solubility data for three solutes selected in the experimental sections. It also allows the user to define a solute of his/her choice. The program provides temperature, pressure and solid solute solubility profiles for the given solid solute, thermal gradient, surface temperature and injection pressure. The software is also capable of performing sensitivity on the solute type and changes in wellhead injection pressure.

The software, which includes the corresponding equation required to perform the calculations, was developed in the Excel Microsoft VBA platform. The coded algorithm

is composed of four main parts; (i) First the program calculates the temperature profile within the wellbore by knowing the local geothermal gradient and upstream ambient temperature. (ii) Then it estimates the pressure profile assuming a gravity controlled flow (hydrostatic equilibrium which varies only with fluid density) and with known injection pressure. In this calculation, density of CO_2 at different pressure and temperature is read from a very large data bank incorporated in the program in tabular from. (iii) The solute solubility profile, as the main output of this study, is then estimated using the experimentally measured solubility data and generated temperature and pressure profiles. In this part an interpolation technique has been incorporated to cover the full range of pressure and temperature variations. (iv) The last part consists of an option for the user to perform sensitivities on the solute type or changes in wellhead injection pressure. Below a more detailed description of these four parts is given followed by a field example using these four software capabilities.

7.4.1 Temperature Profile Determination

The temperature profile along the wellbore is dictated by the geothermal gradient of the injection site, which relates the subsurface temperature to the penetration depth by a linear relationship as described by Equation 7.6.

$$T_{i+1} = T_i + G_{th_i}(z_{i+1} - z_i) \qquad \text{Eq. 7.6}$$

Where T_{i+1} and T_i are the temperature at the depth corresponding to point i and i+1 and G_{th_i} (λ_i in Figure 7-11) represents the relevant geothermal gradient between depths of z_{i+1} and z_i.

It is believed that a single geothermal gradient is not a well-defined representative of the real temperature profile. Therefore the calculation in the program can be performed based on multiple geothermal gradients (maximum of three). Figure 7-11 exhibits a schematic example of the temperature variation with depth along a well drilled in a reservoir with three geothermal gradients.

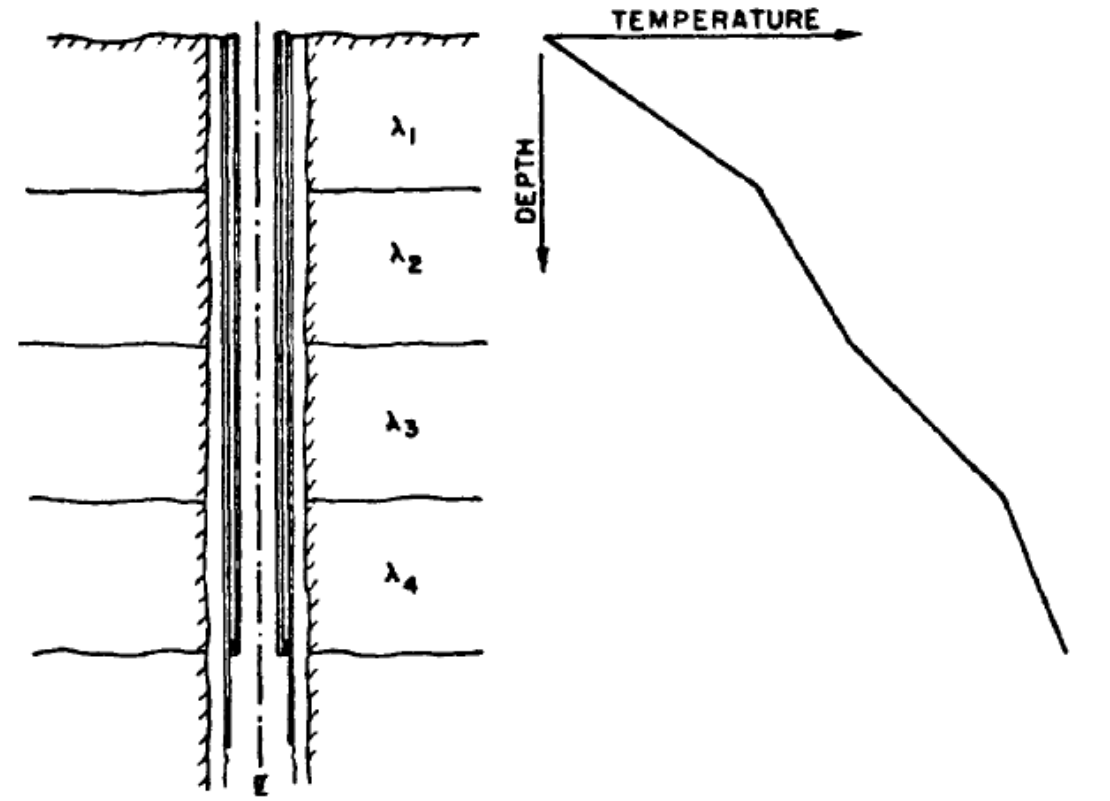

Figure 7-11: Geothermal model with three geothermal gradients.

7.4.2 Pressure Profile Determination

After determining the temperature profile, the next step involves modelling the hydro-static pressure profile within the wellbore which depends on the fluid density. It should be noted that theoretically speaking, density variation with pressure and temperature can be modelled by means of an equation-of-state. However because, the thermodynamic state of CO_2 from surface to the sandface alternates between liquid and supercritical it is very difficult, if not impossible, to have an stable equation of state expressing the variation of CO_2 density with pressure and temperature. Therefore, in this study, to cover a wide range of pressure and temperature variations, a large data bank of CO_2 density was sourced, from available data in the literature and incorporated in the program in Tabular form.

Considering that both temperature and pressure varies with depth, a computer code was developed to estimate density along the wellbore and calculate the incremental pressure rise as expressed by Equations 7.7 and 7.8.

$$dP = \rho g \, dz \qquad \text{Eq. 7.7}$$

$$P_{i+1} = P_i + \int_{z_i}^{z_{i+1}} (\rho g) dz \qquad \text{Eq.7.8}$$

Where P and ρ are the pressure and density of CO_2 at corresponding depth of z. Equation 7.8 is solved numerically to generate pressure versus depth profile.

7.4.3 Solubility Profile Determination

As described in Section 7.3.4, Equation 7.1 expresses the solubility of a solute in CO_2, which depends on density, temperature and pressure. This correlation is often used to interpolate between the limited experimental data with constants A, B, and C used to tune its prediction for a particular solute.

The dependency of solubility on temperature suggests that tuning the constants of Equation 7.1 necessitates incorporating two isothermal solubility data with respect to pressure, i.e. the correlation cannot be used for a single isothermal solubility-pressure curve. Therefore, in our software and for known temperature, pressure, and CO_2 density (T_i, P_i, and $\rho_{CO_{2i}}$, respectively) the program searches for two adjacent existing isothermal solubility data, i.e. $T_1 \leq T_i \leq T_2$, to tune the constants of the correlation and then T_i, P_i, and $\rho_{CO_{2i}}$ are used in the tuned equation to calculate the corresponding solubility.

7.4.4 Sensitivity of Operating Injection Pressure

For CO_2 storage purposes and with our leakage prevention technique, two main operational parameters that can be optimised are wellhead pressure and solute type. To evaluate the optimum wellhead pressure for CO_2 injection, two factors should be considered; first, injecting CO_2 must not be in the form of vapour state, which has low density and reduces the amount of injected CO_2. Second, solute solid content of the injected CO_2 solution should be at its optimum value. Therefore, the software is capable of performing sensitivity on the solute type and changes in wellhead injection pressure. That is, either pressure for a selected solute is sensitised or the impact of solute type for a selected injection pressure is evaluated. This feature of the program is described in more detail by an example in the next section.

7.4.5 Case Study Example

As it was mentioned previously this study targets the prevailing conditions of Goldeneye, whereby CO_2 is to be stored in a depleted gas-condensate reservoir. Therefore, for this part the program was used to perform a sensitivity study on the operational conditions of

this project. The basic reservoir data are given in Table 7-1. It should be noted that "initial reservoir pressure" refers to the reservoir pressure prior to commencing production from this gas-condensate reservoir. This pressure is regarded as the target storage site pressure to avoid fracturing the reservoir rock, that is, the bottomhole injection pressure is limited to 3600 psig.

Table 7-1: General properties of the depleted gas condensate reservoir used for CO_2 storage.

Depth (ft)	8500
Surface temperature (^oF)	54
Reservoir temperature (^oF)	185
Initial reservoir pressure (psig)	3600
Current reservoir pressure (psig)	2500
Average Regional geothermal gradient (^oF/100ft)	1.54

As mentioned before, the integration and iteration of equations are performed numerically within a set interval from surface to sandface, which in this example is discritized to 100 sections (grids) within the wellbore. The initial step is determination of the temperature profile along the wellbore for the given input data, which is obtained using the first Tab of this Microsoft excel based program entitled "Temperature Profile", Figure 7-12. In the first Table on the top left hand corner of Figure 7-12, with the heading of "Initialisation", the well name, reservoir depth, surface temperature and number of sections within the wellbore, should be given. The input data for the second Table are depth and the corresponding temperature gradient, which includes one row of data for this example. As mentioned above a maximum of three gradients can be defined. After entering the input data and pressing the "Estimate Temperature Profile" Tab a pop-up window appears reminding the user that the required information should be input in the corresponding data fields. Then the user confirms the number of thermal gradients defined in the second Table before observing the temperature profile. The output data include depth in foot (ft) and meter (m) and the corresponding temperature data at three different units of Fahrenheit (F), Kelvin (K) and centigrade (C).

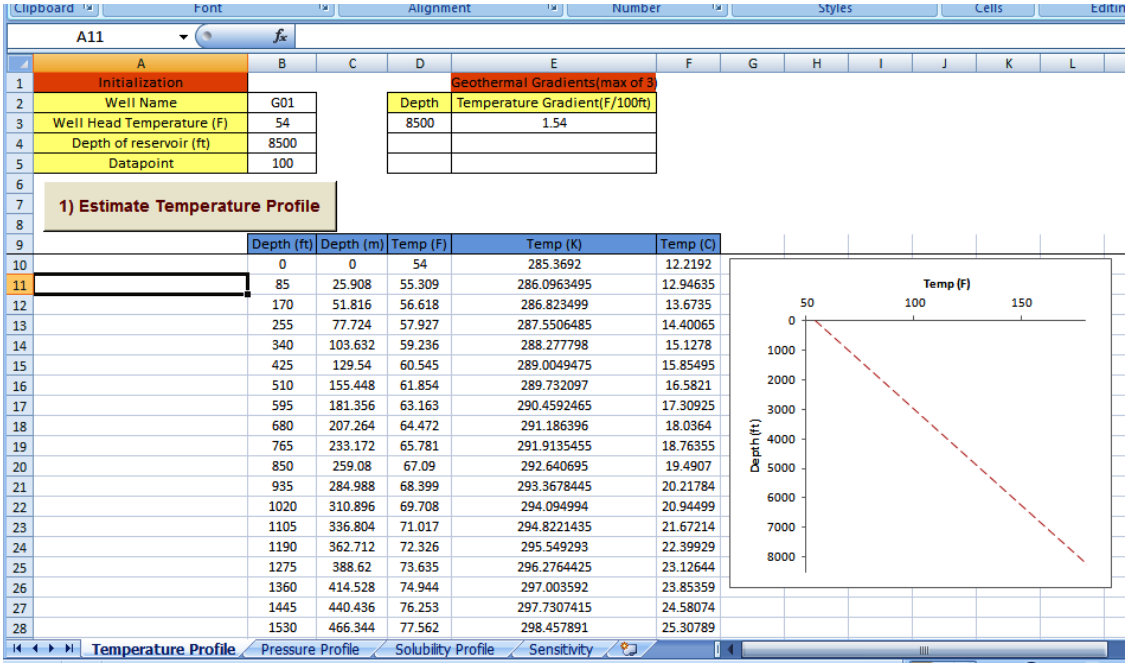

Figure 7-12: Software interface for the temperature profile calculation.

Next Tab, entitled Pressure profile, corresponds to the pressure profile calculations, which requires the surface injection pressure as the main input data given in the first Table on the top left hand corner of Figure 7-13. In this exercise, the wellhead pressure of the wellbore was adjusted to ensure that the injection pressure at the sandface of the reservoir is below the initial reservoir pressure, i.e. 3600psig. This is required to ensure that there is no risk of fracturing the reservoir and hence, integrity of the reservoir is preserved. In order to maintain the injection pressure at around 3600 psig, the wellhead pressure was set to 725 psig.

It should be noted that this injection pressure is lower than the CO_2 critical pressure of 1070 psig, but because the surface temperature (54 °F) is well below CO_2 critical temperature (88 °F) at this pressure CO_2 is still in its liquid state. The stream pressure reaches to critical pressure at a depth of around 1000 ft at which point the temperature is around 70 °F, which is still below its critical temperature.

As noted in the drop down menu in the second Table of Figure 7-13, there are two choices for pressure integration of Equation 7.8, i.e., trapezoidal and Simpson rules. The trapezoid al method is faster for large number of data points along the wellbore but for less number of data points (for instance 20), the Simson's rule would generate more rigorous result of pressure profile. In this example there was minimal difference between the results of these two. The number of discritized data points along the wellbore was 100 corresponding to

the Simpson's numerical integration method as shown in Figure 7-13. After entering the input data and pressing the "Estimate Pressure Distribution" Tab a pop-up window appears asking the user to confirm the injection pressure after which the pressure profile is estimated. The output data include depth in foot (ft) and meter (m) and the corresponding temperature data at two different units of Fahrenheit (F), and Kelvin (K), pressure data in pounds per square inch (psig) and bars (bar) and CO_2 density in pounds per cubic feet (lb/ft^3) and kilogram in cubic meter (kg/m^3). According to Figure 7-13, the pressure profile resembles a linear trend with depth indicating approximately constant density of CO_2 throughout the wellbore.

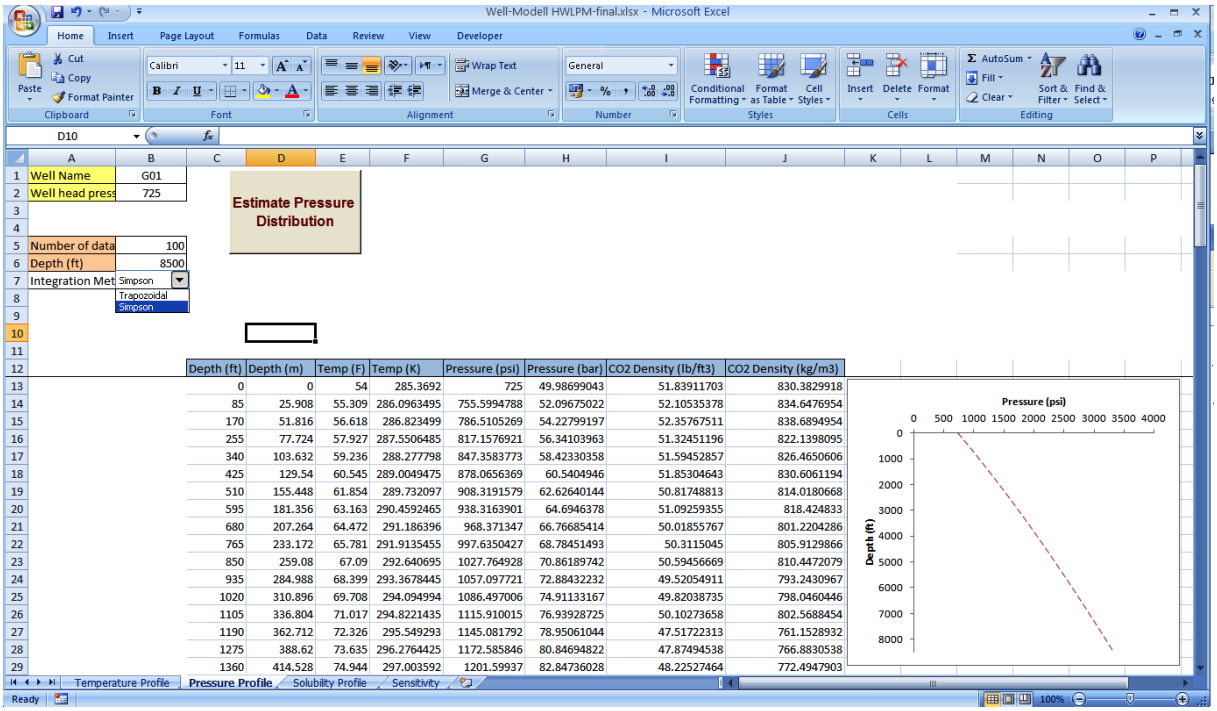

Figure 7-13: Software interface for the pressure profile calculation.

The next Tab, entitled Solubility Profile, corresponds to the solubility profile calculations. Here the user can select the solute type form the dropdown menu shown in Figure 7-14. After selecting the solute type and pressing the "Estimate Solubility Profile" Tab the solubility profile is estimated. The output data include depth in foot (ft) and the corresponding temperature data in centigrade (C), pressure data in pounds per square inch (psig), CO_2 density in gram per cubic centimetre (g/cc) and solubility in mole fraction.

It is noted that the solubility profile of HWS-2 shown in Figure 7-14, stays almost constant at around 0.0001 up to a depth of around 2000 ft and then it increases with depth. It should be noted that according to the solubility correlation (Equation 7.1), the main controlling parameter for solubility variation is the CO_2 density, which here decreases

monotonically suggesting a decrease in solid solubility with depth. However, the trend shown in Figure 7-15 highlights the role of state of CO_2, which in particular depends on the temperature. That is, as mentioned above at a depth of 1000 ft the stream pressure is equal to the CO_2 critical pressure but its temperature is still below the critical temperature, i.e. the solution is in liquid state up to the depth of around 2200 ft. Up to this depth the solubility stays almost constant. For the supercritical CO_2 at higher depth the solubility increases, as expected, because of further increase in temperature.

This trend suggests that if at the surface, the solution is at its saturation point, it would be under-saturated as it travels down the well with higher degree of under saturation at higher depth. The associated adverse effect of this trend is that the solution will be undersaturated within the reservoir. However, this behaviour ensures that during the injection, there is no premature precipitation of solute along the wellbore.

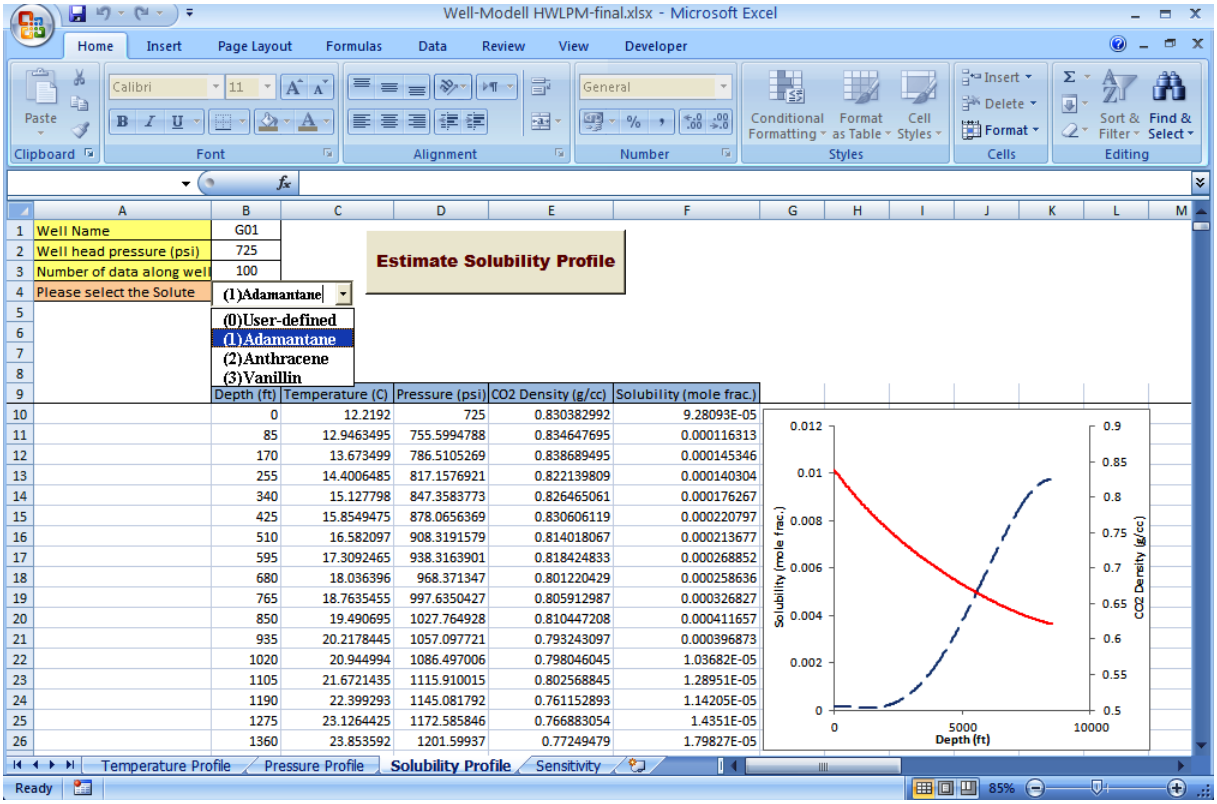

Figure 7-14: Software interface for the solubility profile calculation, HWS-2.

Figure 7-15 shows the solubility profile of HWS-3 and CO_2 density along the wellbore. In this case there is a non-monotonic solubility trend. That is, for HWS-3, the solubility on the surface condition is around 0.0026 mole fraction. This value decreases as the depth (i.e. temperature) increases up to around 3000 ft below the surface at which point the

minimum solubility of 0.0016 mole fraction is achieved. Then the solubility increases with depth to 0.0032 mole fraction at the sandface.

This trend suggests that if at the surface the solution is at its saturation point, the solute would prematurely precipitate out of the solution on its way down till depth of 3000 ft. In order to overcome such premature precipitation problem, the solid content of the solution must correspond to the minimum solubility of this solute along the wellbore. In other words, based on the solubility profile in Figure 7-15 for HWS-3, the solid content should be adjusted to be around 0.0016 mole fraction. This suggests that the solution would be under-saturated at the surface as well as reservoir conditions.

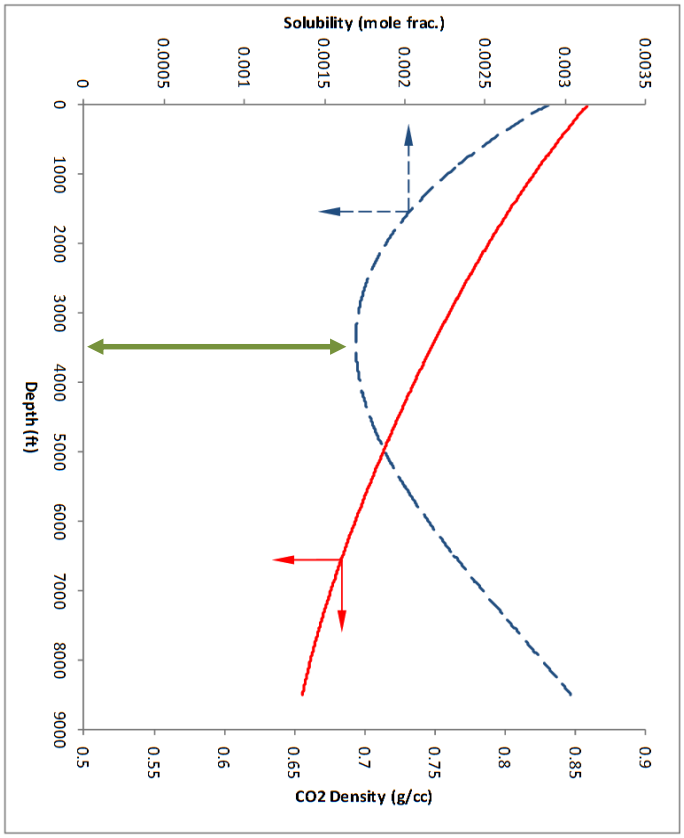

Figure 7-15: Solubility of HWS-3 and CO_2 density along the wellbore. The green arrow shows the optimum solid content of the solution.

7.5 Discussions and Conclusions

These results suggest that, to avoid premature particle formation while the solution travels down to the sandface, the solid content of CO_2 has to be adjusted according to its minimum solubility along the wellbore. According to this, the optimum solid content at

the surface for these particular solutes would yield an undersaturated solution inside the storage reservoir, which raises questions on the effectiveness of the proposed leakage prevention technique. That is, the pressure drop along the leakage path triggers the precipitation only when the solution experience a pressure at which it is oversaturated (i.e. the solid content is more than its solubility level) and if the solution is undersaturated inside the reservoir then the precipitation is delayed, which is unfavourable for ceasing the leakage within the reservoir. Under such conditions and when a leakage path (e.g. abandoned wells) is extended from reservoir to surface, the leakage prevention method is activated within the leakage path but not in the desired location. That is, as highlighted in Figure 7-16, the desired blockage location is immediately above the storage reservoir and within the caprock. However, having an under-saturated solution inside the reservoir postpones the precipitation to a lower depth where the pressure is lower than the corresponding saturation pressure. This is going to be an issue if the leakage path, on its way to the surface, branches into several leakage paths, which would increase the amount of CO_2 leakage before they are fully blocked. However, as mentioned above, injection of an under-saturated solution ensures that the solution does not experience a premature precipitation along the wellbore. Furthermore, an under-saturated solution ensures that the solution within storage site is stable without premature precipitation as it travels within the site in response to small pressure fluctuations.

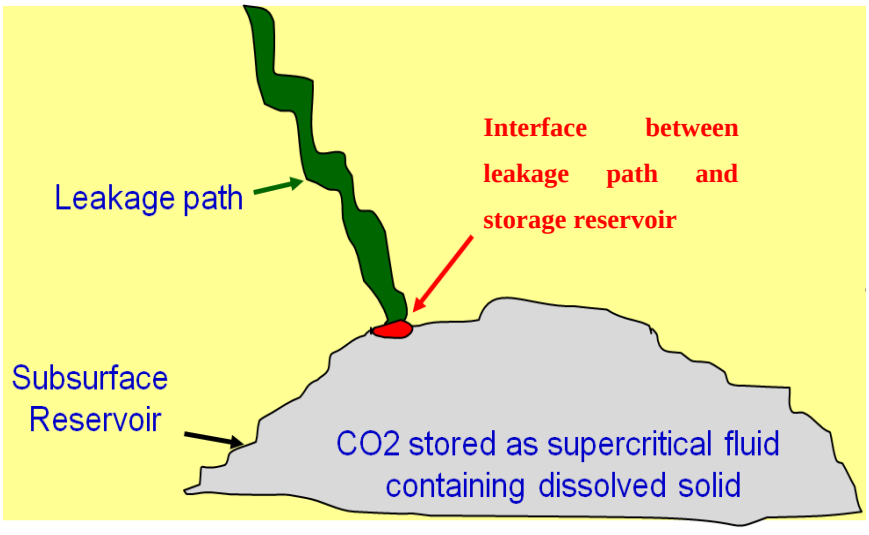

Figure 7-16: Schematic representation of a leakage path.

As it was mentioned above the software is capable of performing sensitivity on the solute type and changes in wellhead injection pressure. For the results presented here, the

wellhead injection pressure was sensitised when using HWS-2 as the solid solute dissolved in the CO_2 stream. From the input data in the first Table on the top left hand corner of Figure 7-17, it is noted that the base or reference wellhead pressure was set to 750 psig for HWS-2. As shown in the second Table the number and amount of pressure change steps were selected as 2 and 250 psig, i.e. the calculation is performed for three wellhead pressures. The data for the third Table, which corresponds to the solubility type, is not used because from the drop down menu in the last row of the first Table, the Sensitivity Parameter was selected to be wellhead pressure. In this exercise, the software performs the calculations for each wellhead pressure in two steps, i.e. it first calculates the pressure profile and then solubility profile. Figure 7-18 shows the results of wellhead pressure sensitivity of the case under study at three pressure values with pressure step size of 250 psig.

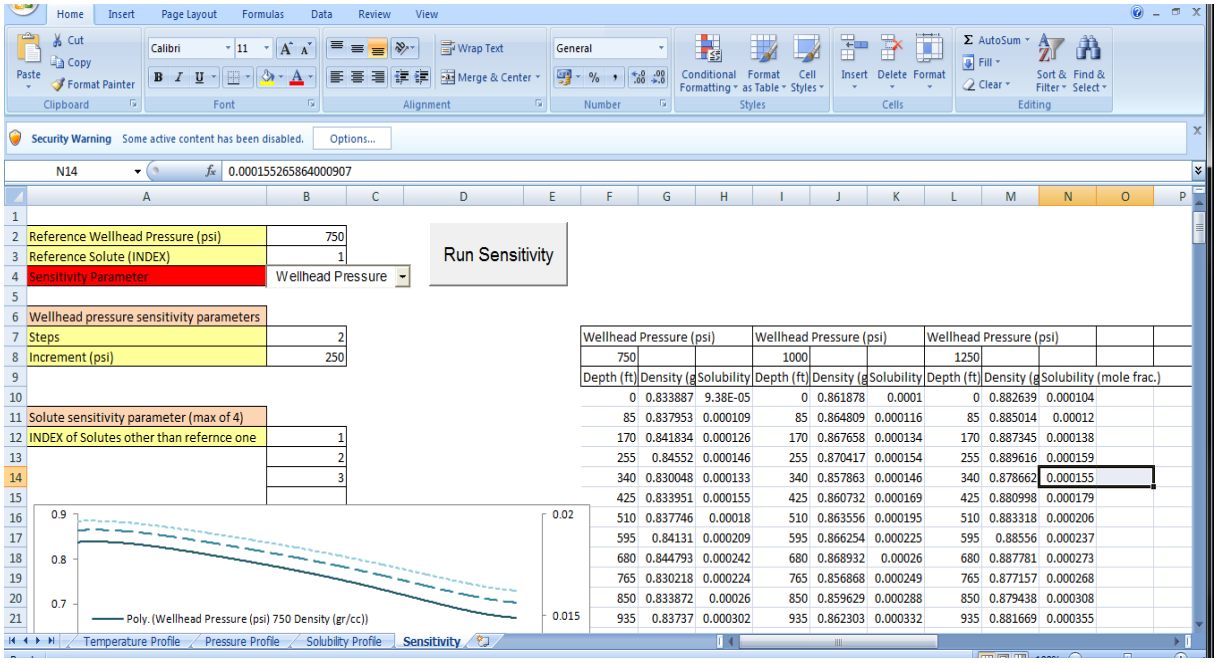

Figure 7-17: Software interface for sensitivity on wellhead pressure, HWS-2.

According to Figure 7-18, despite the considerable increase in wellhead pressure the solubility profile would not significantly change especially from the surface up to the depth of 3000 ft, through which CO_2 is in the liquid state. In other words, although the density profile has reacted to the abrupt changes in wellhead pressure, the solubility of HWS-2 responded negligibly where the injected CO_2 is in the liquid state. However, at higher depth and when CO_2 is in the supercritical state, the solubility curves start to diverge to some extent highlighting the sensitivity of solid solubility for supercritical CO_2

solutions. Similar calculations can be repeated for other solutes. Sensitivity can also be performed on the solute type if it is selected as the sensitivity parameter from the drop down menu in the last row of the first Table. In this case the solubility profile calculation is estimated for the calculated pressure profile based on a given wellhead pressure and for up to three solutes as defined in the third Table of Figure 7-17.

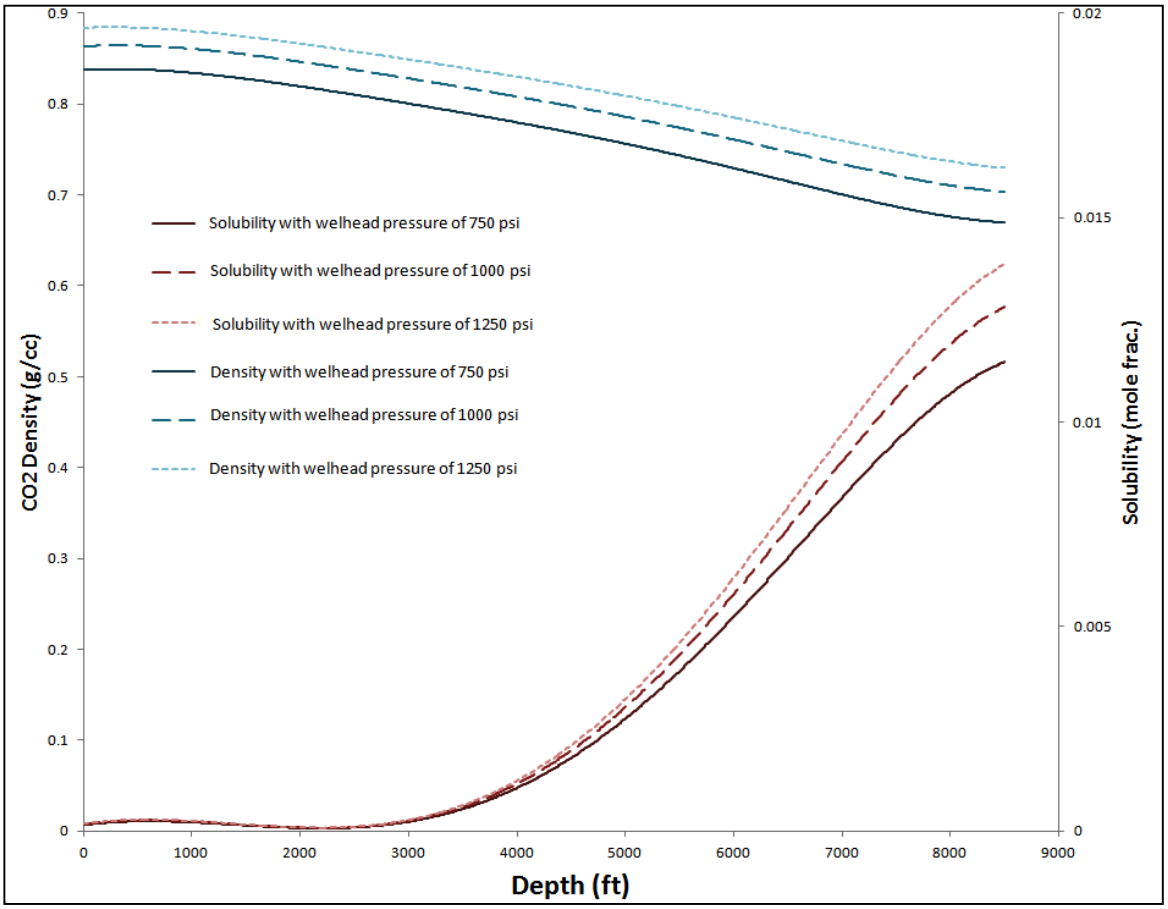

Figure 7-18: Sensitivity of wellhead pressure on CO_2 density and solubility profiles of HWS-2 along the wellbore.

Dissolution of solid solute into the injected CO_2 stream for the leakage prevention purposes at the surface, compared to downhole mixing, is preferable due to less operational complexities and uncertainties. In this study, 17 potential solutes were initially screened based on their compatibility with the temperate and pressure conditions, environmental considerations, and cost. In other words, the melting point of the solutes should be higher than the prevailing reservoir condition. Second, the substances to be injected into subsurface should fulfil certain environmental criteria. Moreover, proper solutes should not add considerable amount of cost to the storage expenditure, which

would undermine the application of the proposed leakage prevention method in CO_2 storage projects. After preliminary screening of the solutes, five shortlisted solutes were tested to evaluate the response of the CO_2-solute solutions to a simulated leakages scenario during micromodel (visualisation) experiments. Three solutes responded to the leakage efficiently by blocking it for extended period of time. The precipitation of one of the two other solutes was considered unfavourable since it tended to attach to the surface of the porous medium, which in real reservoir conditions is covered by water, hence, not available for the solute to accumulate and block the leakage path as it did during the micromodel experiments. The other solute, despite its high solute concentration, did not precipitate to block the leakage path even at a high pressure drop applied across the micromodel. These results highlighted the importance of participation mechanisms for these solutes.

Solubility data were then measured for the three selected solutes using a new experimental set-up. The integrity of our experimental procedure and reliability of information and data generated was confirmed by reproducing solubility data for one of the solute at conditions at which published data were available. The error of measurements was calculated which was in the range of 6% to 7%, which is acceptable.

Considering that the solubility data of solutes in CO_2 in open literature is only limited to the supercritical state of CO_2, we attempted to fill this gap and we generate isothermal solubility at various pressures for all these three solutes in liquid CO_2. Solubility of HWS-2 in supercritical CO_2 at a temperature of 45 ^oC was also measured to generate sufficient data to establish its full solubility profile along the wellbore. The parameters of a correlation suitable for dilute solution were tuned to these measured data with acceptable accuracy. The measurements and correlations revealed that the constants of the correlation for supercritical CO_2 cannot be used for liquid CO_2. Nonetheless, the data of solute solubility in liquid CO_2 obeys the trend in dilute correlation.

The solubility data (both measured and those collected from the published data available in open literature) and corresponding equations have been included in an Excel-based software, developed during the course of this exercise, to achieve a complete set of required data to estimate temperature, pressure and solubility profiles. In order to establish the solubility profile along the wellbore (in the field), the simultaneous variation of both pressure and temperature are taken into account. For temperature profile determination, three sets of geothermal gradients can be included. The pressure profile, which affects the CO_2 density and hence solid solubility, is estimated based on hydrostatic equilibrium conditions. The solubility profile is estimated based on the known pressure

and temperature profiles and using the incorporated correlation suitable for dilute mixtures.

The software is also capable of performing sensitivity on the solute type and changes in wellhead injection pressure. That is, either injection pressure, as the main flexible operational parameter, for a selected solute is sensitised or the impact of solute type for a selected injection pressure is evaluated.

It was shown with an example that depending on the local atmospheric temperature and solid solute type, the solubility could either remain almost constant or slightly decrease as the state of CO_2 solution changes from liquid at the surface to supercritical conditions at higher depth. Further increase in temperature and pressure with depth would result in a monotonic increase in solubility. It was discussed that if the minimum solubility value along the wellbore is selected for the injected solution at the surface, it avoids premature precipitation of the solutes along the wellbore. The associated adverse effect of this trend is that the response to the pressure drop in the vicinity of leakage path is delayed for an under-saturated solution, which could adversely affect the effectiveness of the technique by delaying the response time and shifting the location of precipitation to lower depth rather than the desired location of the leakage storage site interface. Furthermore, considering that the leakage flow path is expected to be relatively small compared to the stored CO_2 volume, it is expected that a smaller concentration of solute would not significantly impact its performance. However this should be considered for the specific geological storage site under study.

The generated experimental data and the Excel based computer program serve as a valuable source of information on the application of the proposed self-sealing technique and safe storage of CO_2.

CHAPTER 8 SUMMARY, CONCLUSIONS AND RECOMMENDATIONS

To the best of our knowledge, no practically viable techniques existed for prevention of CO_2 leaks from unknown leakage paths. Our technique is based on in-situ precipitation of an appropriate solute dissolved in the stored super-critical CO_2. Supercritical CO_2 ($SCCO_2$) has a distinct characteristic that its density changes from gaseous-like to liquid-like monotonically and uniformly. This allows $SCCO_2$ to act as manageable solvent for various solid solutes. Thus, once the solution of $SCCO_2$ + solid solutes departs from the equilibrium conditions, the solute will appear in the form of crystallized particles. Based on this unique behaviour of the supercritical solutions, we have developed a novel technique for tackling contingent CO_2 leakage from storage sites as a preventive method. The sealing process takes place in-situ at the exact location of the leak without the need for identifying the leak target area and the exact nature of the leak.

The broad objective of this investigation is to examine a preventive technique proposed to tackle contingent leakages and develop the necessary tools for large scale implementation of the Leakage Prevention Technique (LPT). These objectives were attempted to achieve by conducting a comprehensive set of flow visualisation experiments, core/sand pack flow studies, numerical modelling and simulation. The approach is to conduct flow visualization studies in the transparent micromodels to investigate pore scale mechanisms controlling the efficiency of our leakage prevention technique. The micromodel observations are used to design and perform representative core and sand-pack flow studies. The quantitative results from coreflood tests will be used in an in-house mathematical model to check if the experimental results can be properly reproduced. The results obtained from pore scale and core scale experiments can be utilised to help defining the pertinent parameters of the in-house model and tuning of the parameters. Eventually the trained simulator will be used for scaling-up purposes and prediction of the performance of the developed LPT at larger scales.

This thesis reports the findings attained from the experimental and theoretical works performed to identify fundamentally the phenomena taking place in the developed leakage prevention technique. The main focus was on the process taking place as our solution passes through the interface between the leakage path and the storage reservoir, which is highlighted with a red colour in Figure 8-1. Hence, it has been aimed to stop the leakage in the interface although the original concept was conceived for a very long leakage path from the reservoir up to the surface. In other words, our developed leakage

prevention technique was conceptually suggested according to significant reduction in solute solubility in the CO_2 critical point (which would occur near the surface) but, as our understanding evolved, the target for ceasing the leakage was altered to the interface, which required careful designing of experiments and solute selections. Nonetheless, the experimental results (particularly coreflood experiments) revealed that our leakage prevention technique is able to stop the upward escape of CO_2 at low rates.

The central achievement of this investigation was to find an efficient solid-solute for stopping leaks at reasonable costs. Also, a tool should be developed in order to simulate the performance of LPT in large scales based on the laboratory findings. Furthermore, a method was put forwards to control/enhance the performance of solid-solutes at different leakage scenarios, which would enable us to design practical strategies for specific storage reservoir conditions. Various solid-solutes were used and they were classified base on their solubility and blockage efficiency.

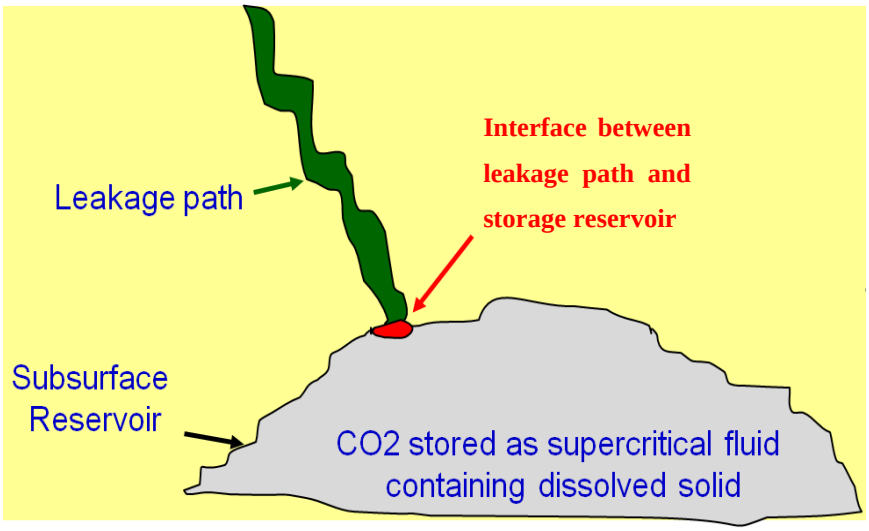

Figure 8-1: Schematic representation of a leakage path.

For identifying the physics behind our developed leakage prevention technique, a series of visualisation experiments was carefully designed to directly observe how the CO_2 + solid-solute solution would respond to simulated leakage path. Having performed theses micromodel visualisations, it was identified that the performance of leakage prevention technique is controlled by the dynamics behind nucleation and deposition of particles, which can be mainly influenced by solute type, solute solubility, degree of pressure drop, and flow velocity. Following detailed conclusions can be drawn from the micromodel

experiment. Almost all the solutes tested in this work successfully sealed the induced leaks. However, the behaviour and the mechanisms of sealing were completely different for various solutes.

Durability of the formed blockages was checked by pressurising the system after sealing. In some cases, if the leak was reopened, it was quickly sealed again due to reactivation of the sealing mechanism. Therefore, it was visually verified that removal of blockage body (for whatever reason) would lead to building up another blockage body. This occurrence was also seen in coreflood experiments, which indicates the high degree of consistency between the observations obtained in different sets of experiments.

Using a highly soluble solute, it was observed that *HWS-5* would respond positively to the physically simulated leak. It was observed that high degree of solubility would make this solute highly responsive to the pressure drop as it was expected from analogy with new phase formation physics. On the other hand, this solute showed high affinity for adhering to the micromodel surface, which would facilitate the process of blockage formation. For moderately soluble solutes, HWS-3 and HWS-2 were used in visualisation tests. HWS-3 exhibited a tendency to form blockage by agglomeration of particles together and packing the end of the leakage point by particles. However, HWS-2 would form larger particles leading to building up a more concentrated blockage body. HWS-1 has been put forward as a marginally soluble solute with very inexpensive cost for practical filed scale purposes. A firm and durable blockage was formed in the physically simulated leakage path. Having experimentally measured the onset of particle formation, it was observed that a relatively large pressure drop was needed to cease the lab scale leak. Nonetheless, HWS-1 has got a remarkable potential for industrial scale implementation of our developed leakage prevention technique. From micromodel visualisations, it can be generally conclude that the each solute would have different behaviour and each solute should be experimentally investigated for at least one or two experiments.

It was visually revealed that precipitation of solutes from supercritical CO_2 is governed by nucleation kinetics which does not happen under thermodynamic equilibrium. As a result, supersaturation of the CO_2 with solutes should be taken into account. In addition to supersaturation, IFT (interfacial tension between solute and CO_2) and molecular volume of solutes also impact particle formation. These parameters should be carefully considered for designing suitable solutes for the CO_2 leakage prevention technique.

Effect of impurities on the leak prevention technique was tested by adding 5% nitrogen to the CO2 stream. It was observed that presence of nitrogen can improve the performance of the leakage prevention technique in two ways. First, it made the system more sensitive and responsive to drop in pressure and hence the system responded more quickly to leak. In one of the tests with nitrogen, the CO_2 injection pressure was 2966 psig and the blockage of the leak was achieved at 2800 psig (only 166 psig drop), which indicated significant progress in the design and effectiveness of the process. Second, while improving performance, it also reduced solubility of solutes in CO_2 meaning that less solute was required. Reduced solubility results in lower cost of field implementation of the leakage prevention technique.

The impact of presence of connate water on the performance of the leak prevention mechanism was investigated. The results showed that a relatively large leak was still effectively sealed by the process and in the presence of connate water. The main difference between the experiments with water with those without water was that the sealing process took place with some delay mainly caused by the presence of water layers on the surface of the porous medium.

Using larger scales, sandpack experiments were performed to quantify the lowest pressure drop (highest leakage pressure) at which the blockage stops the leakage in a relatively short period of time. This experimental facility serves as a reliable tool for fast screening of the solutes suitable for a particular application. The sandpack results demonstrated that HWS-1 with very low solubility can be suitable for our purpose as it could block

For analysing the response of the solution (CO_2 +Solute) in relatively low supersaturations, 6 coreflood experiments have been carefully designed and performed to investigate the behaviour of the solution in physically simulated leakage paths. The core plugs were put together to make up a composite core in order to achieve a flow behaviour that can represent CO_2 leakage from caprock. In the first coreflood test, a complete blockage was identified and durability of the blockage was tested. However, in the second coreflood test, the blockage did not occur at the supersaturations of 200, 500, and 700 psig since the velocity of CO_2 in the composite core in this test was 3 times higher compared to the first test. Nevertheless, the core was plugged at a pressure of 2100 psig which was 100 psig above the onset pressure of solute nucleation in previous micromodel test. Therefore, for having particle formation triggered in the rock, the velocity of CO_2 flow and the degree of supersaturation should be properly designed. Compared to first

test, the precipitation mass decreased in the second core flood test since, at higher supersaturation (second test), the particle nucleation would be more localized and faster which results in less cumulative precipitation of solute. In the third coreflood experiment, it was aimed to repeat the first coreflood test by imposing similar conditions. In the first test, the constant flow rate was applied at the inlet whereas, the third test was carried out in constant pressure mode at either ends of the composite core. The outcome of the test showed the formation of complete blockage. The durability of the formed blockage was successfully checked. The amount of the precipitations was very close to first coreflood experiment, which indicates an acceptable degree of consistency between the tests.

The results of core flood experiments performed using the new experimental set-up (downhole mixing) showed that the blockage was successfully achieved. It was also demonstrated that if the integrity of the blockage was compromised and the particles forming the blockage were remobilised by any means, the precipitation process would re-occur and the primary blockage be repaired and eventually a permanent blockage is formed (which is consistent to micromodel visualisations). In experiment No. 4 using HWS-2 in shorter core, the length of high permeable core was not sufficient and the particles were not formed in the porous medium. Therefore, to establish the blockage in lab conditions, a very meticulously designed experiments are required to replicate more realistic conditions.

In a separate direction, the dynamic interactions between the CO_2 +solid-solute solution and constituents of storage reservoir (rock and brine) were investigated using coreflood setup. It was identified that the adsorption of the solute would be negligible or out of the instrumental sensitivity for detecting the precipitation. This finding would indicate that the solution would not be adversely become under-saturated by solute adsorption. In another coreflood experiment the interactions of the solution and resident brine was investigated. The results showed that the dissolution of the CO_2 into the in-situ brine would not compromise the integrity of the solution and it would be unlikely to see premature particle formation in the storage reservoir as the solution forms the CO_2 plume.

Having identified a delay in the response of the solution, the viability of adding a secondary liquid solute to improve the efficiency of our developed leak prevention method was evaluated through sandpack, micromodel visualisation and coreflood experiments. It is believed that liquid solutes have a significantly lower nucleation time lag and hence, can improve the solute-loaded solution's response time by (i) increasing the solubility of the primary (solid) solute, which would results in higher supersaturation

degree when the secondary liquid solute is deposited quickly and under a small imposed pressure drop and (ii) creating additional flow barrier, higher local pressure drop, for the leaking CO_2 as a result of a reduction in CO_2 relative permeability. It should be noted that the new liquid phase would not block the leakage path but would facilitate the process of sealing the leak. In the visualisation experiments, a co-solvent (secondary liquid solute) was used and HWS-1 was added to supercritical CO_2 as the primary solid solutes. The direct visualisations revealed how liquid solute would improve the response of our developed leakage prevention technique and verified the hypothetical idea behind addition of the co-solvent. The liquid solute would form much quicker than solid solutes, which would in turn bring about notably higher supersaturation degrees facilitating formation of solid particles. It was observed that the formation of liquid solute in the inlet of micromodel would cause significantly better response of HWS-1-saturated solution.

In line with micromodel experiments, two coreflood experiments were designed and carried out to evaluate the role of co-solvent at low rates in real rocks. The outcome of the coreflood experiments showed a notable improvement in the response of the solution in terms of the required pressure drop and leakage rate to stop the leakage in lab scales. Like micromodel visualisations, the formation of liquid solute could be seen near the inlet of composite core. From weighing the individual core plugs, it was inferred that the main precipitation leading to blockage was formed close to outlet of the composite core. Therefore, addition of insignificant amount of co-solvent would empower the solid solute to tackle leakages with much lower rates.

Our preliminary use of commercial simulators have demonstrated a need for a more sophisticated mechanistic modelling approach that captures main mechanisms dominating the process involved in our leakage prevention method. It was discussed that based on the experimental results of the micromodel visualizations and coreflood tests the governing equations describing the time depending nucleation of solid solutes dissolved in the CO_2 stream that is flowing through a leakage path was developed. The developed sets of equations describing the kinetics of solid solute precipitation and porosity and permeability reduction have been linked to the Computer Modelling Group (CMG-GEM) reservoir simulator, which solves the corresponding flow equations. The calculation continues till the permeability reduction is reached to a pre-defined level indicating the blockage of the leak.

Hysteresis effect (effect of the supersaturation and concentration throughout the leakage path and in the grid block prior to the block where nucleation occurs) was taken into account for developing the induction time terms. Initially and without suspension flow, the solid particles precipitate where they are formed, the mathematical model predicted 98% permeability reduction (from 225 mD to 5 mD), but the software was unable to achieve zero permeability (i.e. the full blockage). Mobilisation of precipitants and re-precipitation of these particles were considered as the complementary mechanism to capture suspension flow achieve the full blockage. A model was developed that adequately captures the process of particle mobilisation, suspension flow, and re-precipitation based on the visualisations obtained in micromodel experiments. From the visualisation experiments, it was inferred that the area targeted by precipitation should be small, i.e. smaller than what the model without suspension flow predicted. The inclusion of this new mechanism also helps us to achieve zero permeability in the vicinity of blockage body.

The results of this modelling exercise are very encouraging as it captures the main dominant underlying mechanisms and predicts Coreflood-3 was carried out with same solute and pressure/temperature conditions but the flow rate and length of leakage path differed. The simulation results demonstrated an acceptable degree of match between the experiment and our model highlighting a high level of predictive capability for the model.

The tuned model was also used to estimate the length of an equivalent homogenous leakage path if we had only the high permeable core plug. This length was 450 ft for the core experiment performed highlighting the need to include the very low permeability core (k=0.03 md) for the experiment conducted in the laboratory.

Having investigated the performance of the LPT solution at various condition, the methods for delivering the solid solute into the storage reservoir should be addressed and examined. Two methods were considered; (i) surface mixing where the solid solute is mixed with CO_2 at surface conditions, i.e. liquid CO_2, and (ii) downhole mixing. These results suggest that, to avoid premature particle formation while the solution travels down to the sandface, the solid content of CO_2 has to be adjusted according to its minimum solubility along the wellbore. According to this, the optimum solid content at the surface for these particular solutes would yield an undersaturated solution inside the storage reservoir, which raises questions on the effectiveness of the developed leakage prevention technique. That is, the pressure drop along the leakage path triggers the precipitation only

when the solution experience a pressure at which it is oversaturated (i.e. the solid content is more than its solubility level) and if the solution is undersaturated inside the reservoir then the precipitation is delayed, which is unfavourable for ceasing the leakage within the reservoir. Under such conditions and when a leakage path (e.g. abandoned wells) is extended from reservoir to surface, the leakage prevention method is activated within the leakage path but not in the desired location. That is, the desired blockage location is immediately above the storage reservoir and within the caprock. Dissolution of solid solute into the injected CO_2 stream for the leakage prevention purposes at the surface, compared to downhole mixing, is preferable due to less operational complexities and uncertainties. However, it appears that downhole mixing would be the viable option for delivering the solid solute in the dissolved form into the storage reservoir.

Recommendations

Based on the finding attained in this study, the following recommendations can be put forwarded for further extension of the current work;

1. Changing the test temperature, the impact of temperature on the nucleation of solute particles should be investigated. Temperature is an influential parameter that can impact the significance of nucleation kinetics. Also, the geothermal gradient existing in storage reservoirs would play an important role in large scale implementation of LPT. Furthermore, CO_2 possesses an indispensable degree of Joule-Thomson effect that may affect the temperature locally in the vicinity of leakage paths. Therefore, a series of tests on the effect of temperature is advised to be performed.

2. CO_2 may be storage in depleted oil and gas reservoirs and hence, it would be interesting to physically simulate a depleted oil/gas reservoirs and apply the developed leakage prevention technique. The significant interactions between the solution (mainly composed of supercritical CO_2) and the resident oil/gas in depleted reservoir can impact the performance the LPT.

3. HWS-1 has demonstrated to be an economical and efficient solute to tackle contingent leakages. It can be interesting to select different co-solvents to be able to control the response of HWS-1 to various leaks. This can be done through

performing a series of coreflood experiment in which different co-solvents should be mixed with HWS-1-rich solution to investigate the solution performance. Also, the coreflood experiments should be coupled with a series solubility measurements to evaluate the impact of liquid co-solvent on HWS-1 solubility.

4. Using Sightglass setup, the nucleation kinetics of HWS-1 particles in supercritical CO_2 should be investigated for measuring the interfacial properties, which would be in turn used in designing coreflood experiments and mathematical modelling.

5. Downhole mixing of the solute should be investigated thoroughly as the most feasible method to deliver solid solute into the storage reservoir in the dissolved form.

6. On the modelling side, tuning of pertinent parameters of another solute should be interesting, i.e. hysteresis parameters of HWS-1. Also, including the impact of co-solvent can shed some lights on the tuning parameters of previously matched coreflood experiments.

7. At this stage, our developed leakage prevention technique has been verified to be tackling the physically simulated leakage in laboratory scales. Based on the findings and tools produced in this study, the LPT is ready to be implemented in pilot or demonstration trials to investigate its performance in a real storage site. It would be suggested to select a leaky natural analogue and inject the solution nearby a known leakage path and monitor the fate of CO_2. The outcome of this trial would add more confidence on the efficiency of the LPT.

REFERENCES

Arts, R. et al., 2008. Ten years' experience of monitoring CO2 injection in the Utsira Sand at Sleipner. *First Break: CO2 Sequestration,* Volume 26, pp. 65-72.

Bachu, S. & Bennion, B. D., 2009. Experimental assessment of brine and/or CO2 leakage through well cements at reservoir conditions. *International Journal of Greenhouse Gas Control,* 3(4), pp. 494-501.

Bachu, S. et al., 2007. CO2 storage capacity estimation: Methodology and gaps. *Int. Journal of Greenhouse Gas Control,* 1(4), pp. 430-443.

Beizaie, M., 1977. *Deposition of particles on a sigle collector.* Syracuse: Syracuse University, PhD Dissertation.

Boait, F. et al., 2011. Layer spreading and dimming within the CO2 plume at the sleipner field in the north sea. *Energy Procedia,* 4(GHGT-10), pp. 3254-3261.

Boyd, A. et al., 2013. Controversy in technology innovation: Contrasting media and expert risk perceptions of the alleged leakage at the Weyburn carbon dioxide storage demonstration project. *International Journal of Greenhouse Gas Control,* May, Volume 14, pp. 259-269.

Debenedetti, P. G., 1990. Homogeneous nucleation in supercritical fluids. *AIChE Journal,* 36(9), pp. 1289-1298.

Debenedetti, P. G. & Kumar, S. K., 1986. Infinite dilution fugacity coefficients and the general behavior of dilute binary systems. *AIChE Journal,* 32(8), pp. 1253-1262.

Duan, Z. & Sun, R., 2003. An improved model calculating CO2 solubility in pure water and aqueous NaCl solutions from 273 to 533 K and from 0 to 2000 bar. *Chemical Geology,* 193(3-4), pp. 257-271.

Eiken, O. et al., 2011. Lessons learned from 14 years of CCS operations: Sleipner, In Salah and Snøhvit. *Energy Procedia,* 4(GHGT-10), pp. 5541-5548.

Emeka Eke, P., Naylor, M., Haszeldine, S. & Curtis, A., 2011. *CO2 leakage technologies.* Aberdeen, UK, SPE Offshore Europe Oil and Gas Conference and Exhibition.

Grataloup, S. et al., 2009. A site selection methodology for CO2 underground storage in deep saline aquifers: case of the Paris Basin. *Energy Procedia,* 1(1), pp. 2929-2936.

Green, D. W. & Willhite, P. G., 1998. *Enhanced Oil Recovery.* Fourth ed. ISBN:978-1-55563-077-5: Society of Petroleum Engineers.

Gupta, R. B. & Shim, J.-J., 2006. *Solubility in Supercritical Carbon Dioxide.* 1 ed. Abingdon: CRC Press.

Ha-Duong, M. & Keith, D. W., 2004. Carbon storage: the economic efficiency of storing CO2 in leaky reservoirs. In: S. K. Sikdar, P. Glavic & R. Jain, eds. *Technological Choices for Sustainability.* Pittsburgh: Springer Berlin Heidelberg, pp. 165-182.

Harvey, A. H., 1996. Semiempirical correlation for Henry's constants over large temperature ranges. *AIChE Journal,* 42(5), pp. 1491-1494.

Hawkins, D. G., 2004. No exit: thinking about leakage from geologic carbon storage sites. *Energy,* 29(9-10), pp. 1571-1578.

He, M. et al., 2011. Risk assessment of CO2 injection processes and storage in carboniferous formations: a review. *Journal of Rock Mechanics and Geotechnical Engineering,* 3(1), pp. 39-56.

Kanniche, M. et al., 2010. Pre-combustion, post-combustion and oxy-combustion in thermal power plant for CO2 capture. *Applied Thermal Engineering,* 30(1), pp. 53-62.

Kirsch, K., Navarre-Sitchler, A. K., Wunsch, A. & McCray, J. E., 2014. Metal Release from Sandstones under Experimentally and Numerically Simulated CO2 Leakage Conditions. *Environmental Science & Technology,* 48(3), pp. 1436-1442.

Kvenvolden, K. A. & Cooper, C. K., 2003. Natural seepage of crude oil into the marine environment. *Geo-Marine Letters,* 23(3-4), pp. 140-146.

Lewicki, J. L., Birkholzer, J. & Tsang, C.-F., 2007. Natural and industrial analogues for leakage of CO2 from storage reservoirs: identification of features, events, and processes and lessons learned. *Environmental Geology,* 52(3), pp. 457-467.

Malik, Q. & Islam, M., 2000. *CO2 injection in the Weyburn field of Canada: Optimisation of enhanced oil recovery and greenhouse gas storage with horizontal wells.* Tulsa, Oklahama, SPE/DOE Improved Oil Recovery Symposium.

Mendez-Santiago , J. & Teja, A. S., 2000. Solubility of Solids in Supercritical Fluids: Consistency of Data and a New Model for Cosolvent Systems. *ndustrial & Engineering Chemistry Research,* 39(12), pp. 4767-4771.

Metz, B. et al., 2005. *Carbon dioxide capture and storage*. Cambridge: Cambridge University Press.

Monastersky, R., 2013. Seabed scars raise questions over carbon-storage plan. *Nature,* 19 December, 504(7480), pp. 339-340.

Mullin, J. W., 2001. *Crystallization.* Fourth ed. Oxford: Butterworth-Heinemann.

Nelson, C. et al., 2005. *FACTORS AFFECTING THE POTENTIAL FOR CO2 LEAKAGE FROM GEOLOGIC SINKS.* North Dakota: University of North Dakota, Energy & Environmental Research Center, PCOR Partnership.

Nelson, P. H., 1994. Permeability-porosity Relationships In Sedimentary Rocks. *The Log Analyst,* 35(03), pp. 38-62.

Paretsky, L. C., 1972. *Filtration of Aerosols by Granular Bed.* New York: The City University of New York, PhD Dissertation.

Payatakes, A. C., Tien, C. & Turian, R. M., 1974. Trajectory calculation of particle deposition in deep bed filtration: Part I. Model formulation. *AIChE Journal,* 20(5), pp. 889-900.

Pendse, H., 1979. *A study of certian problems concerning deep bed filtration.* Syracuse: Syracuse University, PhD Dissertation.

Pietzner, K. et al., 2011. Public awareness and perceptions of carbon dioxide capture and storage (CCS): Insights from surveys administered to representative samples in six European countries. *Energy Procedia*, 4(GHGT-10), pp. 6300-6306.

Queirós, A. et al., 2014. *Potential impact of CCS leakage on marine communities*, Plymouth Marine Laboratory: ECO2 Deliverable.

Riazi, M. et al., 2011. Visualisation of mechanisms involved in Co2 injection and storage in hydrocarbon reservoirsand water-bearing aquifers. *Chemical Engineering Research and Design,* 89(9), pp. 1827-1840.

Römer, F. & Kraska, T., 2010. Molecular dynamics simulation of the formation of pharmaceutical particles by rapid expansion of a supercritical solution. *The Journal of Supercritical Fluids,* 55(2), pp. 769-777.

Serin, J.-P.et al., 2010. Experimental studies of solubility of elemental sulphur in supercritical carbon dioxide. *The Journal of Supercritical Fluids,* 53(1-3), pp. 12-16.

Shik Han, W., McPherson, B. J., Lichtner, P. C. & Wang, F. P., 2010. Evaluation of trapping mechanisms in geologic CO2 sequestration: Case study of SACROC northern platform, a 35-year CO2 injection site. *American Journal of Science,* April, Volume 310, pp. 282-324.

Shipton, Z. K. et al., 2004. Analysis of CO2 leakage through 'low-permeability' faults from natural reservoirs in the Colorado Plateau, east-central Utah. *Geological Society,* 233(Special Publications), pp. 43-58.

The Canadian Press, 2011. *Alleged leak of CO2 at Sask. farm to be probed.* [Online] Available at: http://www.cbc.ca/news/technology/alleged-leak-of-co2-at-sask-farm-to-be-probed-1.1050056

The Globe and Mail, 2011. *Alleged leaks from carbon storage project questioned.* [Online] Available at: http://www.theglobeandmail.com/technology/science/alleged-leaks-from-carbon-storage-project-questioned/article562508/
[Accessed 19 Jan 2011].

Tien, C. & Ramarao, B., 2011. *Granular Filtration of Aerosols and Hydrosol.* second ed. ISBN: 978-1-85617-458-9: Elsevier Ltd.

TNS Opinion & Social at the request of Directorate-General for Energy, 2011. *Public Awareness and Acceptance of CO2 capture and storage,* Brussels, Belgium: TNS Opinion & Social (European Commision).

Tokushige, K., Akimoto, K. & Tomoda, T., 2007. Public perceptions on the acceptance of geological storage of carbon dioxide and information influencing the acceptance. *International Journal of Greenhouse Gas Control,* 1(1), pp. 101-112.

Türk, M., 2000. Influence of thermodynamic behaviour and solute properties on homogeneous nucleation in supercritical solutions. *J of Supercritical Fluids,* Volume 18, pp. 169-184.

van der Zwaan, B. & Gerlagh, R., 2009. Economics of geological CO2 storage and leakage. *Climatic Change,* 93(3-4), pp. 285-309.

Volmer, M. & Schultz, W., 1931. Kondensation an Kristallen. *Zeitschrift für Physikalische Chemie,* Volume 156, pp. 1-22.

Zhang, Y., 1996. Dynamics of CO2-driven lake eruptions. *Nature,* 379(6560), pp. 57-59.